Topological crystalline insulators and superconductors

Dissertation
zur Erlangung des Grades eines
Doktors der Naturwissenschaften

am Fachbereich Physik
der Freien Universität Berlin

vorgelegt von
Max Geier

Berlin 2020

Gutachter
Erster Gutachter: Prof. Dr. Piet Brouwer, Freie Universität Berlin

Zweiter Gutachter: Prof. Dr. Alexander Altland, Universität zu Köln

Datum der Disputation: 27.10.2020

Selbstständigkeitserklärung

Name: Geier
Vorname: Max

Ich erkläre gegenüber der Freien Universität Berlin, dass ich die vorliegende Dissertation selbstständig und ohne Benutzung anderer als der angegebenen Quellen und Hilfsmittel angefertigt habe. Die vorliegende Arbeit ist frei von Plagiaten. Alle Ausführungen, die wörtlich oder inhaltlich aus anderen Schriften entnommen sind, habe ich als solche kenntlich gemacht. Diese Dissertation wurde in gleicher oder ähnlicher Form noch in keinem früheren Promotionsverfahren eingereicht.

Mit einer Prüfung meiner Arbeit durch ein Plagiatsprüfungsprogramm erkläre ich mich einverstanden.

Datum: _____ Unterschrift: _____

Declaration of authorship

Name: Geier
First name: Max

I declare to the Freie Universität Berlin that I have completed the submitted dissertation independently and without the use of sources and aids other than those indicated. The present thesis is free of plagiarism. I have marked as such all statements that are taken literally or in content from other writings. This dissertation has not been submitted in the same or similar form in any previous doctoral procedure.

I agree to have my thesis examined by a plagiarism examination software.

Date: _____ Signature: _____

CONTENTS

List of publications

The main chapters of this thesis are based on the following two first author publications and one first author preprint. The author contributions are indicated below.

- Chapter 2: Max Geier, Luka Trifunovic, Max Hoskam, and Piet W. Brouwer, "Second-order topological insulators and superconductors with an order-two crystalline symmetry", Phys. Rev. B 97 205135 (2018) ©2018 American Physical Society,
  https://doi.org/10.1103/PhysRevB.97.205135
  The project was initiated and supervised by PWB. It is a follow-up project to a previous article by LT, PWB, and others [Phys. Rev. Lett. 119, 246401 (2017)]. MG, LT, and PWB developed the theoretical ideas and wrote of the manuscript. All authors worked out the central analytical results presented in tables V to XIII. The numerical simulations were carried out by MG, LT, and MH.

- Chapter 3: Max Geier, Ion Cosma Fulga, Alexander Lau, "Bulk-boundary-defect correspondence at disclinations in crystalline topological insulators and superconductors", arXiv:2007.13781 (2020) (preprint)
  https://arxiv.org/abs/2007.13781v2
  ICF initiated the project with the idea of considering the Volterra process in 2d and 3d second order topological phases. AL supervised the project. MG performed the topological crystal calculations and obtained the classifications presented in our tables. AL and MG performed the numerical simulations. MG and AL produced the figures of the manuscript. All authors contributed to developing and understanding the results and to writing the manuscript.

- Chapter 4: Max Geier, Piet W. Brouwer, and Luka Trifunovic, "Symmetry-based indicators for topological Bogoliubov–de Gennes Hamiltonians", Phys. Rev. B 101, 245128 (2020) ©2018 American Physical Society,
  https://doi.org/10.1103/PhysRevB.101.245128
  The project was initiated by MG. All authors contributed to developing the theoretical ideas, working out the examples, and to writing of the manuscript.

The following publications were completed in parallel. They are a result of a collaboration with Stefan Ludwig's group at the Paul Drude Institute, Berlin.

- Jaan Freudenfeld, Max Geier, Vladimir Umansky, Piet W. Brouwer, Stefan Ludwig, "Coherent Electron Optics with Ballistically Coupled Quantum

Point Contacts", arXiv:2002.12340 (2020) – accepted for publication with Physical Review Letters

- M. Geier, J. Freudenfeld, J. T. Silva, V. Umansky, D. Reuter, A. D. Wieck, P. W. Brouwer, and S. Ludwig, "Electrostatic potential shape of gate-defined quantum point contacts", Phys. Rev. B 101, 165429 (2020)

Abstract

Topological phases are quantum phases of matter that appear close to absolute zero temperature. In contrast to commonly known condensed phases of matter, such as a magnet or a superconductor, distinct topological phases may have the same symmetry. Instead, these phases are distinguished by the topology of the electronic wavefunction. Already the single-particle excitations described by band theory in an insulator or a metal or by Bogoliubov-de Gennes theory in a superconductor may have novel *anomalous* properties associated to their topology. This *topological band theory* is the subject of this thesis. We aim towards identifying the anomalous boundary and defect states associated to the topology of the band structure in crystalline insulators and superconductors. Furthermore, we determine criteria to easily identify the topological phases from the band structure of a given insulator or superconductor.

In Chapter 2 we show that crystalline topological insulators and superconductors may host anomalous gapless or in-gap excitations on corners of a two-dimensional crystal or hinges of a three-dimensional crystal. These topological phases are called "second-order" according to the codimension "2" of their anomalous boundary states. We discuss the precise conditions for their appearance and when they can be linked to the bulk topology. Our discussion includes mirror, twofold-rotation and inversion as crystalline symmetries.

In Chapter 3 we discuss the appearance of anomalous gapless or ingap states at defects in a crystalline insulator or superconductor. In particular, we link the existence of anomalous states at disclinations – lattice defects that violate a rotation symmetry only locally – to second-order topological crystalline phases. As a side product, we identify the possible contributions of other topological phases to the disclination anomaly. The results of this chapter allow to determine precisely how the disclination anomaly is linked to the bulk topology.

In Chapter 4 we present how to construct "symmetry-based indicators" for topological superconductors that admit a description within the Bogoliubov-de Gennes framework. Symmetry-based indicators are necessary criteria for a given Bogoliubov-de Gennes Hamiltonian to realize a topological crystalline phase with anomalous boundary exitations. These criteria are formulated in terms of data from a small set of high-symmetry momenta only. Our approach guarantees to extract the maximal information on the anomalous boundary exitations that can be extracted from a point-wise evaluation of the Bogoliubov-de Gennes Hamiltonian. In the limit of weak superconducting pairing, our criteria can be formulated in terms of data from the normal-state band structure alone.

Zusammenfassung

Topologische Phasen sind Quanten-Phasen, welche in Festkörpern nahe dem absoluten Temperatur-Nullpunkt auftreten. Im Gegensatz zu gewöhnlichen Phasen in Festkörpern, wie einem Magneten oder Supraleiter, können verschiedene topologische Phasen die gleiche Symmetrie haben. Stattdessen werden diese Phasen durch die Topologie der elektronischen Wellenfunktion unterschieden. Bereits Einteilchen-Anregungen, welche durch die Bandstruktur oder eine Bogoliubov-de Gennes Theorie in Supraleitern beschrieben werden, können aufgrund ihrer Topologie neue, anomale Eigenschaften haben. Das Ziel dieser Arbeit ist es anomalen Zustände an Ränder und Defekten zu identifizieren, welche mit der Topologie der Einteilchen-Anregungen in kristallinen Isolatoren oder Supraleitern assoziert sind. Ausserdem wird eine Methode vorgestellt, mit welcher sich einfache Kriterien für die Identifizierung der Topologie der zugehörigen Bandstruktur oder Bogoliubov-de Gennes Theorie aufstellen lassen.

In Kapitel 2 wird gezeigt, dass kristalline topologische Isolatoren und Supraleiter anomale Zustände an Ecken eines zweidimensionalen Kristalls oder an Kanten eines dreidimensionalen Kristalls beherbergen können. Diese topologischen Phasen werden "zweiter Ordnung" genannt, nach der Kodimension "2" ihrer anomalen Randzustände. Es werden die genauen Bedingungen für das Auftreten dieser anomalen Zustände diskutiert, so wie unter welchen Umständen sie mit der Topologie der Wellenfunktion im Kristall in Verbindung gebracht werden können. Unsere Diskussion umfasst Spiegel-, zweifache Rotation-, sowie Inversionssymmetrie.

In Kapitel 3 wird das Auftreten von anomalen Zuständen an Defekten im Kristall diskutiert. Insbesondere wird gezeigt, dass die Existenz von anomalen Zuständen an Disklinationen – Gitterdefekte welche eine Rotationssymmetrie nur lokal verletzen – mit der Präsenz einer topologischen Phase zweiter Ordnung verbunden ist. Ausserdem werden alle möglichen Beiträge von anderen topologischen Phasen zur Anomalie an der Disklination identifiziert. Mit den Ergebnissen aus diesem Kapitel lässt sich der genaue Zusammenhang zwischen der Anomalie an der Disklination und der Topologie des Kristalls bestimmen.

In Kapitel 4 werden "Symmetrie-basierte Indikatoren" für topologische Supraleiter vorgestellt, welche sich durch einen Bogoliubov-de Gennes (BdG) Hamiltonians beschreiben lassen. Symmetrie-basierte Indikatoren sind notwendige Kriterien damit ein gegebener Einteilchen-Hamiltonian eine topologische Phase mit anomalen Randzuständen realisiert. Für diese Kriterien ist die Kenntnis des BdG Hamiltonian an einer kleinen Menge von Hochsymmetrie-Impulsen ausreichend. Unsere Methode garantiert, dass die maximale Information über die anomalen Randzustände des topologischen Supraleiters gewonnen wird, welche sich aus einer punktweisen Evaluation des BdG Hamiltonians extrahieren lässt.

INTRODUCTION

Topology is the mathematical study of global properties of objects that remain invariant under continuous deformations. An illustrative example is the topology of shapes of two-dimensional surfaces in three-dimensional space. Here, roughly speaking, a deformation of a shape is continuous as long as one does not rip or punch holes in the shape. With these rules, one can continuously deform a cup into a bagel. However, the bagel can not be deformed into a ball. This is because both the bagel and a cup have a single hole while the ball does not – and punching holes is forbidden by our rules for continuous deformations. Thus, one says that the cup and the bagel are *topologically equivalent*, where the equivalence relation is provided by the continuous deformation. One approach to identify the distinct topological equivalence classes of objects is to find and define a quantity that distinguishes the equivalence classes. These quantities are called *topological invariants*. In our example of shapes, such a quantity is the number of holes in the shape.

The idea of classifying objects can be applied to condensed matter physics, where the physical systems are described by a Hamiltonian. Here, one considers gapped Hamiltonians and equivalence is defined with respect to continuous deformations for which all excitations remain gapped, i.e. require a finite energy cost

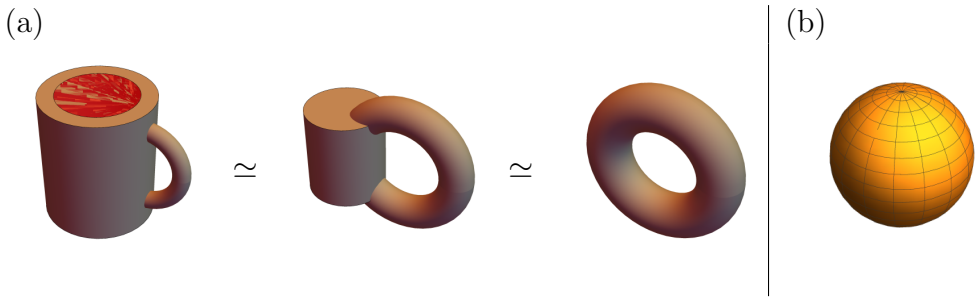

Fig. 0.1: (a) A mug can be continuously deformed into a bagel. However, it can not be deformed into a ball, depicted in (b). Figures were created with Wolfram Mathematica and Ref. 1.

at all times during the deformation. The most famous example where distinct topological equivalence classes appear is a two-dimensional electron gas with an applied perpendicular magnetic field. At low enough temperatures, this setup exhibits a quantized Hall conductivity [2]. A quantized Hall conductivity of the form $\sigma_{xy} = \nu\frac{e^2}{h}$ with ν integer can already be explained with a single-particle Hamiltonian [3]. In fact, it can be shown that the quantized Hall conductivity is a topological invariant for single-particle Hamiltonians [4]. A quantized Hall conductivity at fractional values of ν has also been observed [5] which requires an explanation in terms of a stongly interaction theory [6].

The different topological equivalence classes of Hamiltonians have been called *topological phases of matter* [7] due to their similarity to "conventional" phases of matter. A phase transition between topological phases of matter at absolute zero temperature is accompanied by the closure of the energy gap for extended excitations, leading to similar phenomenology as in conventional phase transitions [8]. However, topological phase transitions do not involve symmetry breaking, for which they lie outside the conventional Landau theory of phase transitions [9].

Many novel phenomena are associated to the topology of the Hamiltonian. For single-particle Hamiltonians, these most prominently include the appearance of gapless or in-gap anomalous states at boundaries or at defects of the sample. In the integer quantum Hall effect, the quantized Hall conductivity is carried by a number of one-dimensional chiral states (perfectly conducting channels in which current may flow only in a single direction) that are located on the sample boundary [10]. Topological phases in strongly interacting systems may furthermore host novel, *fractional* quasiparicles whose exchange statistics may be distinct from the exchange statistics of the relevant elementary particles composing the solid material [11, 12]. In the *fractional* quantum Hall effect, the measured quantized conductance plateaus at fractions of $\frac{e^2}{h}$ have been identified as a signature of quasiparticles with *fractional* electronic charge [13, 14, 15].

When studying topology in condensed matter, it is natural to include symmetries in the topological classification. On the one side, symmetries may prohibit some topological phases. For example, time reversal symmetry requires the Hall conductivity to vanish. On the other side, symmetries also constrain the allowed deformations, which gives rise to new, *symmetry protected* topological phases. Here, the prime examples are the quantum spin Hall effect [16, 17, 18] and the three-dimensional topological insulator[19] protected by time reversal symmetry which were experimentally verified [20, 21]. The topological properties of all of these examples have been described with a single-particle Hamiltonian. The study of the topology of single-particle Hamiltonian has been called *topological band the-*

ory.

Superconductors, too, can be described with an effective single-particle Hamiltonian, if the superconducting correlations are captured by an appropriate mean-field theory. Then, the elementary excitations in the superconductors behave as free fermionic particles and can be described by the Bogoliubov-de Gennes equation [22]. The corresponding Bogoliubov-de Gennes Hamiltonian is a single-particle Hamiltonian with an additional constraint that captures its inherent particle-hole symmetry. In superconductors, it has been suggested that fractional quasiparticles with non-abelian exchange statistics with the property of a self-conjugate "Majorana" fermion appear in connection with the topology of its Bogoliubov-de Gennes Hamiltonian [23, 24, 25].

In the presence of crystalline symmetries, the problem of classifying topological phases of matter, determining their phenomenology and finding criteria to identify the topological phases in a given material acquires a new level of complexity due to the large number of crystalline symmetry groups. To answer these questions within the framework of topological band theory is the central subject of this thesis.

The correspondence between the topology of Hamiltonian and the appearance of anomalous states on the sample boundary has been termed *bulk-boundary correspondence* [26]. The conditions under which this correspondence holds and how bulk topology and boundary anomaly are precisely related are well-established for topological phases protected by internal (i.e. non-crystalline) symmetries. In Chapter 2, we discuss the bulk-boundary correspondence in systems with a single crystalline symmetry of order two, such as mirror, twofold rotation or inversion symmetry. Furthermore, in Chapter 3, we discuss how the bulk topology is related to the occurrence of anomalous states at defects in crystalline systems.

Chapter 4 presents a constructive method to define *symmetry-based indicators* to identify crystalline topological phases in topological superconductors. Symmetry-based indicators are easy-to-compute topological invariants for topological crystalline phases whose original works [27, 28] contributed significantly to the discovery of new topologically insulating materials [29, 30, 31, 32, 33, 34, 35]. The presented approach contains the provably complete topological information that can be extracted from the Bogoliubov-de Gennes Hamiltonian evaluated at high-symmetry momenta in the Brillouin zone.

Not only do these invariants indicate the existence of isolated Majorana bound states or other gapless anomalous boundary excitations, but one can also identify its precise nature by comparing to a complete classification of topological crys-

talline phases up to an inherent ambiguity of this approach. While a few illustrative examples are discussed, the presented approach is algorithmic and can readily be applied to superconductors with any symmorphic space group. Assuming that the order parameter is small compared to typical energy scales of the normal-state Hamiltonian, all information required to compute our symmetry-based indicators can be extracted from the normal-state single-particle Hamiltonian and the symmetry of the superconducting order parameter.

Chapter 1 contains a technical introduction. It presents the topological classification of topological insulators and superconductors in terms of *topological K-theory*. Much of the unified understanding of topological insulators and superconductors is gained from this method. This method is applied in the following Chapters. From this perspective, we will introduce the bulk-boundary correspondence as a basic phenomenology of topological insulators and superconductors from a heuristic argument and an explicit calculation. We will discuss how these arguments need to be adapted in the presence of crystalline symmetries. This serves as a suggested starting point to study the bulk-boundary correspondence in crystalline topological insulators and superconductors which is part of Chapter 2. The following Chapter 3 shows how the bulk-boundary correspondence is related to a bulk-defect correspondence, where a topological bulk requires the existence of anomalous states at defects such as vortices, dislocations or disclinations.

Chapter 1 will show that the topological phases of the single-particle Hamiltonians of insulators and superconductors can be described with the same mathematical theory. However, in section 1.4 we discuss some aspects of topological superconductors that are uniquely associated to the superconducting correlations and do not have a direct analogue for insulators. This is particularly relevant for Chapter 4 in which we extend the theory of symmetry-based indicators from insulators to superconductors.

The introduction in Chapter 1 also serves to put the thesis into perspective, motivate the suggested approaches and provide an overview on relevant literature. The following principal Chapters 2 to 4 are largely self-contained and can be read individually. The references of each Chapter are included at its end. The conclusion summarizes the central results of each Chapter and contains an outlook on open research questions.

1. TECHNICAL INTRODUCTION

1.1 Topological classification of single-particle Hamiltonians

An elementary tool that is used throughout this thesis is the topological classification of single-particle Hamiltonians within *topological K-theory*. The restriction to the topological phases that can be described with single-particle Hamiltonians implies that we require that the relevant interaction effects have been treated by an appropriate mean field theory. In the mean-field approximation, the fermionic many body Hamiltonian is quadratic in the fermionic creation and annihilation operators. Such a theory is also called a *free fermionic* theory. We comment briefly on the effects of interactions on the topological classification in the conclusion.

In this Chapter we formalize the definition of topological equivalence for single-particle Hamiltonians. Based on this discussion, we motivate and illustrate the basics of topological K-theory with the goal to obtain a topological classification of a single-particle Hamiltonian in a given symmetry class.

Statement of the problem. We consider a translation symmetric, d-dimensional system described by a Bloch-single-particle Hamiltonian $H(\mathbf{k})$ subject to the symmetry group G. The symmetry group may contain unitary internal symmetries such as $SU(2)$ spin rotation symmetry, antiunitary internal symmetries such as time reversal symmetry $\mathcal{T}$, crystalline symmetries such as inversion $\mathcal{I}$ and the internal particle-hole antisymmetry $\mathcal{P}$ inherent to BdG-Hamiltonians. We say a symmetry element g is crystalline if it acts nontrivially on the real space coordinates $\mathbf{r} \in \mathbb{R}^d$ ($\exists \mathbf{r} \in \mathbb{R}^d$ such that $g\mathbf{r} \neq \mathbf{r}$). We say g is an internal symmetry if it act trivally on the real space coordinates ($g\mathbf{r} = \mathbf{r} \ \ \forall \mathbf{r} \in \mathbb{R}^d$).

Requiring that the Hamiltonian $H(\mathbf{k})$ is symmetric under the symmetry group G implies that there is a projective representation $U(g)$ for all $g \in G$ such that the Hamiltonian satisfies for g unitary

$$U(g)H(g\mathbf{k})U^\dagger(g) = c(g)H(\mathbf{k}) \tag{1.1}$$

where $c(g) = \pm 1$. The element g is said to be a symmetry (antisymmetry) if $c(g) = 1$ ($c(g) = -1$). For antiunitary elements $g \in G$, the Hamiltonian satisfies

$$U(g)H^*(-g\mathbf{k})U^\dagger(g) = c(g)H(\mathbf{k}). \tag{1.2}$$

The representations $U(g)$ define the "factor system"

$$\{z_{g,h} = U(gh^{-1})U(g)U(h) = \pm 1 \text{ for } g, h \in G\} \tag{1.3}$$

of the projective representation. The label "projective" applies to representations if there exists a pair $g, h \in G$ with $z_{g,h} \neq 1$. The representations of space group elements for spinful fermionic systems are projective in general, as a 2π rotation of a spinful particle shifts the phase of its wavefunction by π, such that $z_{\mathcal{R}_\pi,\mathcal{R}_\pi} = U(\mathcal{R}_\pi\mathcal{R}_\pi^{-1})U(\mathcal{R}_\pi)U(\mathcal{R}_\pi) = U(\mathcal{R}_\pi)^2 = -1$.

For physical systems in the absence of superconductivity, the projective representation and corresponding factor system is specified by the presence or absence of $SU(2)$ spin-rotation symmetry. In case $SU(2)$ spin-rotation symmetry is absent, the fermions transform under the corresponding spinful (double group) representation. In the presence of $SU(2)$ spin-rotation symmetry, the fermions in each subspace transform under the spinless representation. In the presence of superconductivity, the symmetry of the superconducting order parameter enters the factor system of the projective representation, as discussed in detail in Section II of Chapter 4.

The Bloch-Hamiltonian $H(\mathbf{k}) : T^d \to \mathfrak{M}[G_\mathbf{k}, z_{g,h}, N]$ is defined as a continuous map from the d-dimensional Brillouin zone torus T^d to the space of Hermitian matrices $\mathfrak{M}[G_\mathbf{k}, z_{g,h}, N]$ of rank N subject to the symmetry group G with projective representation $z_{g,h}$, where $G_\mathbf{k} \subseteq G$ is called the *little co-group* that contains all elements of G that leave the momentum $\mathbf{k}$ invariant, $G_\mathbf{k} = \{g \in G | g\mathbf{k} = \mathbf{k} \text{ mod } \mathbf{b}\}$, where $\mathbf{b}$ is a reciprocal lattice vector. For example, inversion symmetry relates $\mathbf{k} \to -\mathbf{k}$ which implies that the inversion symmetric momenta $\mathbf{k} = -\mathbf{k}$ mod $\mathbf{b}$ have a larger little co-group than the surrounding momenta.

Topological equivalence classes $[H(\mathbf{k})]$ can be defined defined for gapped Hamiltonians $H(\mathbf{k})$. Two Hamiltonians $H_0(\mathbf{k})$ and $H_1(\mathbf{k})$ are said to be *homotopy equivalent* $H_0(\mathbf{k}) \simeq H_1(\mathbf{k})$ if there exists a continuous path $H(\mathbf{k}; t)$, $t \in [0, 1]$ with $H(\mathbf{k}; 0) = H_0(\mathbf{k})$ and $H(\mathbf{k}; 1) = H_1(\mathbf{k})$ such that $H(\mathbf{k}; t)$ is gapped and is symmetric under G for all $t \in [0, 1]$.

We point out that the classification of gapped Bloch-Hamiltonians is equivalent to the classification of the vector bundle defined as the subspace of the Hilbert space spanned by the eigenstates with energy below the gap at each $\mathbf{k}$. This

connection is established by the projector $P(\mathbf{k})$ onto this subspace which can be defined either from the Bloch-Hamiltonian or from the respective eigenbasis. The Bloch-Hamiltonian $H(\mathbf{k})$ can be reconstructed from its projector up to homotopy equivalence as $H(\mathbf{k})$ is homotopy equivalent to its "spectral flattened" form $Q(\mathbf{k}) = \frac{1}{2}(1 - P(\mathbf{k}))$ where all eigenstates below (above) the gap have eigenvalues -1 $(+1)$. This equivalence is useful as it allows to approach the problem frow two different perspectives. The perspective in terms of vector bundles is common in the mathematical literature [36].

While homotopy equivalence yields the finest classification of gapped Bloch-Hamiltonians, the actual computation of the homotopy equivalence classes is very complex and in general does not follow a regular pattern [36] (see for example the nth homotopy groups of spheres, i.e. homotopy equivalence classes of maps $S^n \to S^m$). Furthermore, the classification depends on the number of bands of $H(\mathbf{k})$, i.e. matrices of different size can not be homotopy equivalent. A reasonable simplification is to require that the classification should not depend on the number of bands. Physically, this is motivated as many crystals possess a number of strongly bound bands far below the Fermi energy which should not influence the classification. Furthermore, there always exists an infinite number of bands at high energies above the Fermi energy.

Mathematically, this simplification is incorporated by considering *stable* homotopy equivalence [37, 38, 39, 40]. The central simplification of stable homotopy equivalence consists of two steps: (i) When checking for *stable* homotopy equivalence "$\sim$", one is allowed to augment the objects by a certain trivial objects Y, Y' as

$$H_1(\mathbf{k}) \sim H_2(\mathbf{k}) \text{ if } H_1(\mathbf{k}) \oplus Y \simeq H_2(\mathbf{k}) \oplus Y'$$

where "$\oplus$" denotes the direct sum of two matrices. In the classification of $d \geq 1$ dimensional topological phases, the trivial objects may take the form $Y = \sigma_3 \otimes \mathbf{1}_N$, $Y' = \sigma_3 \otimes \mathbf{1}_M$ [40] which may be interpret as an flat bands of strongly bound orbitals. Here "$\otimes$" denotes the tensor product of matrices. (ii) Stable homotopy equivalence classes are defined for pairs of Hamiltonians $[H(\mathbf{k}), H'(\mathbf{k})]$ where two pairs are said to be stably homotopy equivalent

$$[H_1(\mathbf{k}), H_1'(\mathbf{k})] \sim [H_2(\mathbf{k}), H_2'(\mathbf{k})]$$

if $H_1(\mathbf{k}) \oplus H_2'(\mathbf{k}) \sim H_2(\mathbf{k}) \oplus H_1'(\mathbf{k})$ are stable homotopy equivalent. A detailed and illustrative discussion can be found in Ref. 37. Special care needs to be taken in the stable classification of matrices (i.e. in case the base space is S^0). This case is discussed in detail in Section III of Chapter 4 and is essential for the discussion in this Chapter 4.

The set of stable homotopy equivalence classes $\{[[H(\mathbf{k}), H'(\mathbf{k})]]\}$ can be promoted to an abelian group K where addition and subtraction is defined using the direct sum,

$$\begin{aligned}[[H_1(\mathbf{k}), H_1'(\mathbf{k})]] + [[H_2(\mathbf{k}), H_2'(\mathbf{k})]] &:= [[H_1(\mathbf{k}) \oplus H_2(\mathbf{k}), H_1'(\mathbf{k}) \oplus H_2'(\mathbf{k})]] \\ [[H_1(\mathbf{k}), H_1'(\mathbf{k})]] - [[H_2(\mathbf{k}), H_2'(\mathbf{k})]] &:= [[H_1(\mathbf{k}) \oplus H_2'(\mathbf{k}), H_1'(\mathbf{k}) \oplus H_2(\mathbf{k})]].\end{aligned} \tag{1.4}$$

This construction is called the *Grothendieck group* construction [39, 40]. The abelian group of stable topological equivalence classes is said to be the K-theory of the vector bundle over the Brillouin zone torus T^d with symmetry group G and projective representation $z_{g,h}$. Throughout most of the literature it is denoted by the label K with some additional parameters to specify the dimension and symmetry class. Throughout this introduction, we use the notation $K[G, z_{g,h}, X]$ to denote the classifying group K of stable equivalence classes of maps $H(\mathbf{k}) : X \to \mathfrak{M}[G_{\mathbf{k}}, z_{g,h}]$, where we omit the argument N as stable equivalence allows to compare matrices with different number of bands.

One can define a set of topological invariants $\nu_i([H_1(\mathbf{k}), H_1'(\mathbf{k})])$ for the pair as

$$\nu_i([H_1(\mathbf{k}), H_1'(\mathbf{k})]) = \nu_i(H_1(\mathbf{k})) - \nu_i(H_1'(\mathbf{k})) \tag{1.5}$$

where $\nu_i(H(\mathbf{k}))$ is a quantity defined on non-contractible loops, surfaces etc. of the Brillouin zone torus. A common example of $\nu_i(H(\mathbf{k}))$ is the Chern number. The topological invariants identify the stable topological equivalence class $[[H(\mathbf{k}), H'(\mathbf{k})]] \in K$ the given pair corresponds to.

Formulating the topological invariants that identify a given (pair of) Bloch Hamiltonians to its stable homotopy equivalence class is a complicated task in general. For all topological phases protected by internal symmetries, a complete set of topological invariants has be defined [40]. However, these topological invariants are formulated in terms of derivatives of the occupied eigenstates of the Bloch Hamiltonian. This requires to diagonalize the Bloch-Hamiltonian for a sufficiently dense grid of momentum values $\mathbf{k}$ and choose a continuous gauge over the Brillouin zone, which is a complicated and numerically expensive procedure. In the presence of crystalline symmetries, a complete and explicit list of topological invariants does not exist to our knowledge at the time this thesis is written. Current approach to define topological invariants for topological crystalline phases are to find expressions in terms of the symmetry data at a few high symmetry momenta in the Brillouin zone [41, 42, 39, 43, 44, 45, 27, 28, 46, 47, 48], Wilson loops defined on one-dimensional lines in the Brillouin zone [49, 50, 51, 52, 53, 54, 55, 56, 57, 58, 59], or a generalization to higher dimensional manifolds [60].

The former approach, utilizing only the data from a few high symmetry momenta in the Brillouin zone, has been called *symmetry-based indicators* for band

topology [28] as it allows to only extract partial information on the topology of the single-particle Hamiltonian. In particular, the resulting topological invariants in general are only sufficient criteria for a specific topological phases, but in some cases may not be necessary. For example, in an inversion symmetric system, only the parity of the Chern number can be determined from the inversion parities at the inversion symmetric momenta [42, 39]. The formulation of this approach to general Bogoliubov-de Gennes Hamiltonians is subject of Chapter 4 of this thesis.

The difference between a classification of systems with internal symmetries based on homotopy and stable homotopy equivalence has been discussed in Refs. 61, 62, 63, 64. With internal symmetries, early examples where a difference between the homotopy and the stable homotopy classification is observed are the Hopf insulator [61, 65, 66] and the Hopf superconductor [66]. More recently, such topological phases that are non-trivial under a homotopy equivalence, but are trivial under stable homotopy equivalence have been called *fragile* topological phases [67, 68, 56]. They have been shown to occur in the presence of crystalline symmetries [69, 70, 57, 71, 72, 73, 58] and in strongly interacting systems [74].

Computation of the classifying groups. One approach to obtain the classification of the Bloch-Hamiltonian is to assume a description of the low-energy expansion of the Hamiltonian around a relevant momentum $\mathbf{k}_0$ in terms of a massive Dirac-Hamiltonian [61, 37, 40]

$$H_{\text{Dirac}}(\mathbf{k}) = \mathbf{k} \cdot \mathbf{\Gamma} + m\Gamma_0 \tag{1.6}$$

where $\mathbf{k} = (k_1, ..., k_d)$ is the momentum relative to $\mathbf{k}_0$ and $\mathbf{\Gamma} = (\Gamma_1, ..., \Gamma_d)$ are Dirac matrices that satisfy the Clifford relation $\Gamma_i\Gamma_j + \Gamma_j\Gamma_i = 2\delta_{ij},\ i, j = 0, 1, ..., d$. Here, the terms proportional to $\mathbf{k}$ are called the kinetic energy terms and the constant term is called a mass term. The mass term is responsible for the energy gap in the bulk. If the limiting behavior $\lim_{|\mathbf{k}|\to\infty} H(\mathbf{k}) = H_\infty$ is fixed, then the d-dimensional Bloch-Hamiltonian describes a map from the d-sphere S^d to the space of symmetric Hamiltonians $\mathfrak{M}[G_\mathbf{k}, z_{g,h}]$ (where the north pole corresponds to $\mathbf{k} = 0$ and the south pole corresponds to $|\mathbf{k}| = \infty$).

The computation of the classifying group $K[G, z_{g,h}, S^d]$ can now be mapped to the problem of identifying the stable homotopy equivalence classes of the mass term $m\Gamma_0$ [37, 40]. This result is based on the mathematical literature on K-theory [75, 76]. The stable homotopy equivalence classes can be determined from the *classifying space* of the mass term $m\Gamma_0$ [37, 40]. The classifying space is spanned by all matrices Γ_0 subject to all symmetry constraints imposed by $U(g),\ g \in G$ as well as the Clifford relation with to the kinetic energy terms. The procedure of identifying the classifying space is as follows.

The mass term is subject to the symmetry group G that may contain internal as well as point group symmetries, and must anticommute with all kinetic energy terms Γ_i. The kinetic energy terms can therefore be treated as additional unitary antisymmetries of the mass term M. We denote the group that contains all symmetries as well as the constraints from the kinetic energy terms as $G \otimes \mathbf{\Gamma}$. In the first step one block-diagonalizes the mass term M under the irreducible representations of the unitary symmetries of $G \otimes \mathbf{\Gamma}$. The remaining antiunitary symmetries/antisymmetries and unitary antisymmetries may relate different blocks and determine the *Cartan symmetric space*, also called *Cartan class*, of the individual blocks. The Cartan class is determined by the presence of antiunitary symmetries/antisymmetries or an antisymmetry in the individual block, as summarized in Table 1.1. Ref. 77 showed that there are in total ten distinct Cartan classes appearing in single-particle Hamiltonians of fermionic systems (see also Ref. 78 for an extensive discussion). The classifying spaces are determined by the Cartan classes [40]. The stable homotopy equivalence classes for each Cartan class are tabulated [37, 40] and shown in in Table 1.1.

				$K[G, S^d]$							
Cartan class	$\mathcal{T}$	$\mathcal{P}$	$\mathcal{C}$	$d=0$	1	2	3	4	5	6	7
A	0	0	0	$\mathbb{Z}$	0	$\mathbb{Z}$	0	$\mathbb{Z}$	0	$\mathbb{Z}$	0
AIII	0	0	1	0	$\mathbb{Z}$	0	$\mathbb{Z}$	0	$\mathbb{Z}$	0	$\mathbb{Z}$
AI	1	0	0	$\mathbb{Z}$	0	0	0	$\mathbb{Z}$	0	$\mathbb{Z}_2$	$\mathbb{Z}_2$
BDI	1	1	1	$\mathbb{Z}_2$	$\mathbb{Z}$	0	0	0	$\mathbb{Z}$	0	$\mathbb{Z}_2$
D	0	1	0	$\mathbb{Z}_2$	$\mathbb{Z}_2$	$\mathbb{Z}$	0	0	0	$\mathbb{Z}$	0
DIII	-1	1	1	0	$\mathbb{Z}_2$	$\mathbb{Z}_2$	$\mathbb{Z}$	0	0	0	$\mathbb{Z}$
AII	-1	0	0	$\mathbb{Z}$	0	$\mathbb{Z}_2$	$\mathbb{Z}_2$	$\mathbb{Z}$	0	0	0
CII	-1	-1	1	0	$\mathbb{Z}$	0	$\mathbb{Z}_2$	$\mathbb{Z}_2$	$\mathbb{Z}$	0	0
C	0	-1	0	0	0	$\mathbb{Z}$	0	$\mathbb{Z}_2$	$\mathbb{Z}_2$	$\mathbb{Z}$	0
CI	1	-1	1	0	0	0	$\mathbb{Z}$	0	$\mathbb{Z}_2$	$\mathbb{Z}_2$	$\mathbb{Z}$

Tab. 1.1: Definition of Cartan classes and periodic table of topological insulators and superconductors [37]. The first column denotes the Cartan label for the symmetry class determined by the antiunitary symmetry $\mathcal{T}$, antiunitary antisymmetry $\mathcal{P}$ and unitary antisymmetry $\mathcal{C}$ with $\mathcal{T}^2 = \pm 1$, $\mathcal{P}^2 = \pm 1$ as indicated in the following three columns. The entry "0" indicates the absence of the respective symmetry or antisymmetry. It is always possible to choose $\mathcal{C}^2 = 1$, if present, by a multiplication of the representations with a phase factor. The remaining columns denote the classifying group $K[G, S^d]$ of the d-dimensional, massive Dirac Hamiltonian in the respecitive symmetry class. The column $K[G, S^0]$ denotes the number of distinct stable homotopy equivalence classes of matrices in the respective Cartan class.

In the absence of crystalline symmetries, this procedure is nicely illustrated in section C of Ref. 40. We present an example on how the classification is obtained in the presence of inversion symmetry in section 1.3 below. This approach lead to the famous *periodic table of topological insulators and superconductors* [37] that summarizes the classifying group $K[G_{\text{Cartan}}, S^d]$ of d-dimensional massive Dirac Hamiltonians with symmetry group G_{Cartan} of internal symmetries corresponding to the ten Cartan classes.

The periodicity of the table is related to the *Bott periodicity* [36, 37, 40] of the classifying groups of maps from S^d into the Cartan symmetric spaces [1]. Furthermore, the periodicity of the classifying groups suggests the existence of a *diagonal map* or *dimension-raising and lowering map* that provides an isomorphism between the classifying groups in different dimension and symmetry class. This isomorphism has first been defined in terms of a map between massive Dirac Hamiltonians in Ref. 38 and has been discussed in the context of homotopy theory in Refs. 62, 64. The map has been extended to obtain a classification of crystalline topological phases in Refs. 79, 80. We will discuss and utilize the dimensional raising map in Appendix A.4 of Chapter 3. Another formulation of this isomorphism can be expressed in terms of the scattering matrix of a lead connected to the boundary of a topological insulator or superconductor [81]. An extension of the scattering matrix expression for the isomorphism for crystalline topological phases is discussed in Ref. 82 and in Chapter 2.

This approach has been extended to the symmorphic space group symmetries [83, 84] by realizing that the classification with space group symmetries is the same as with a corresponding set of internal symmetries. This *crystalline equivalence principle* was first established for interacting bosonic and fermionic symmetry protected topological phases in Ref. 85.

Notice that a necessary condition for the massive Dirac theory (1.6) to describe a topologically non-trivial phase is that once the Dirac matrices $\Gamma_i,\ i = 0, 1, ..., d$ are fixed there exists no additional 'mass term' $m_1\tilde{\Gamma}$ proportional to the Dirac matrix $\tilde{\Gamma}$ that anticommutes with all Γ_i. If such a mass term $m_1\tilde{\Gamma}$ exists, then the extension of $H_{\text{Dirac}}(\mathbf{k}) + m_1\tilde{\Gamma}$ onto the sphere S^d is homotopy equivalent to $m_1\tilde{\Gamma}$. One easily verifies that the anticommutativity of the Dirac matrices guarantees the homotopy equivalence. A momentum independent Bloch-Hamiltonian H_0 in

[1] In the mathematics literature [36], Bott periodicity was first established for maps from S^d into the Cartan symmetric spaces. In this scenario, each point of the sphere maps onto the same Cartan class. This is different from the setting of Bloch-Hamiltonians, because the antiunitary symmetries/antisymmetries act as an inversion on the momentum coordinates. Therefore, for Bloch Hamiltonians the general momentum $\mathbf{k} \neq -\mathbf{k}$ is in Cartan class A or AIII, depending on the presence of a unitary antisymmetry.

$d \geq 1$ is topologically trivial as the associated vector bundle is simply a direct product of the base space S^d or T^d with the Hilbert space of the bands below the gap of H_0.

In a band insulator or superconductor, the Bloch-Hamiltonian is defined on the Brillouin zone torus. On the torus, the classification is further refined as the Bloch-Hamiltonian along a non-contractible loop, surface etc. may itself be nontrivial [37]. The topological phases associated to these non-contractible loops, surfaces rely on the translation symmetry of the band insulator or superconductor and are called 'weak' topological phases [19]. In contrast, the topological phases arising from the d-dimensional manifold are called 'strong' topological phases. It has been proven in Ref. 63 that the classification of Bloch-Hamiltonians defined over the torus T^d can be decomposed into the classification over S^d and lower dimensional spheres corresponding to the non-contractible surfaces, loops etc of the torus T^d.

The labels 'weak' and 'strong' describe the stability of the topological phase towards perturbations that break translation symmetry. Weak phases are protected by translation symmetries and the weak topological invariants can be changed by a perturbation that breaks the translation symmetries. In contrast, strong phases do not require translation symmetries and remain invariant under a perturbations that break the translation symmetry. This is also discussed in more detail in section 3.4.2 in Chapter 3.

1.2 Bulk-boundary correspondence of topological insulators and superconductors with internal symmetries

A fundamental phenomenology of topological phases protected by an internal symmetry is the appearance of gapless, anomalous modes on the boundary of the crystal. This property directly follows from the Dirac-Hamiltonian description of the low-energy theory [61, 40]. Below we present a heuristic argument for the occurrence of gapless modes at the interface between two distinct topological phases.

Consider a system whose low-energy theory is described by a massive Dirac theory as defined in Eq. (1.6) with internal symmetries G. We introduce a boundary in the system by letting the mass term $m(\mathbf{r})\Gamma_0$ be spatially dependent. Furthermore, we assume that the variation of $m(\mathbf{r})$ is slow on any length scale of the microscopic Dirac Hamiltonian such that at every point $\mathbf{r}$, the low energy excitations are approximately described by a massive Dirac Hamiltonian with constant

mass $m = m(\mathbf{r})$. Next, we require that the system at two points $\mathbf{r}_0$ and $\mathbf{r}_1$ is in two distinct topological phases. This implies that the mass terms $m(\mathbf{r}_0)$ and $m(\mathbf{r}_1)$ are not stably homotopy equivalent under the symmetry group of internal symmetries G. As a consequence, the continuous mass term $m(\mathbf{r})$ must vanish at some point along any path connecting $\mathbf{r}_0$ and $\mathbf{r}_1$. The interface between the two topologically distinct phases is formed by the $(d-1)$-dimensional manifold along which the mass term vanishes. Therefore, the low-energy excitations at the interface should described by a $(d-1)$-dimensional gapless Dirac theory. Notice that this heuristic argument relied on the result of Ref. 37 that the classification of topological phases in terms of massive Dirac Hamiltonians can be reduced to the classificaion of the mass term.

The gapless boundary theory can be explicitly computed in an explicit example [61]. Consider a system whose low-energy theory is described by a massive Dirac theory as defined in Eq. (1.6) with internal symmetries G. We introduce a hard boundary in the system via a spatially dependent mass term $\text{sign}\,(x)m\Gamma_0$ (see also Section VI of Chapter 2 for a similar derivation in the presence of crystalline symmetries). The corresponding Dirac theory reads

$$H_{\text{Dirac}}(x, \mathbf{k}_\perp) = -i\hbar\partial_x\Gamma_1 + \mathbf{k}_\perp \cdot \mathbf{\Gamma}_\perp + \text{sign}\,(x)m\Gamma_0 \tag{1.7}$$

This Hamiltonian admits a zero-energy solution corresponding to states localized on the boundary whose spinor wavefunction satisfies

$$\partial_x\psi(x, k_\perp) = -\frac{i}{\hbar}m\text{sign}\,(x)\Gamma_1\Gamma_0\psi(x, k_\perp) \tag{1.8}$$

For an N-dimensional spinor, there are $N/2$ bounded solutions with a x-independent spinor structure. The projection operator onto the subspace of $N/2$ bounded solutions is

$$P_x = \frac{1}{2}[i\Gamma_1\Gamma_0 + 1]. \tag{1.9}$$

By projecting the massive Dirac Hamiltonian onto the subspace of bounded solutions, one obtains the $N/2$-band boundary Hamiltonian,

$$H_{\text{boundary}}(\mathbf{k}_\perp) = P_x H_{\text{Dirac}}(x, \mathbf{k}_\perp)P_x = \mathbf{k}_\perp \cdot \tilde{\mathbf{\Gamma}} \tag{1.10}$$

where $\tilde{\mathbf{\Gamma}} = (P_x\Gamma_1 P_x, ..., P_x\Gamma_d P_x)$ contains the projected Dirac matrices of rank $N/2$. The remaining terms of the bulk Dirac Hamiltonian are projected out as is directly verified from the commutation relations of the Dirac matrices.

The $(d-1)$-dimensional surface Dirac Hamiltonian is *anomalous* in the sense that it can not be realized by as the low energy theory of a $(d-1)$-dimensional

lattice model. For lattice models, it is clear that this implies that the low-energy theory can only be realized on the surface of a topological bulk, where the anomaly is canceled on the opposite surface. Furthermore, these anomalous surface theories are stable towards symmetric perturbations, i.e. they can not be gapped by perturbations that preserve the symmetries of the system [61]. Below, we illustrate these facts at a few examples.

In $d = 1$ dimensions, a topological BdG Hamiltonian in symmetry class D may host isolated zero-energy modes at its boundary. The eigenstates of a BdG Hamiltonians come in particle-hole symmetric pairs, implying that for each eigenstate at energy E, there is an eigenstate at energy $-E$. This implies that if a non-degenerate zero-energy state exist somewhere in the system, there must be another zero-energy state in the system such that they can be superposed as a particle-hole symmetric pair. Furthermore, the particle-hole antisymmetry of the BdG Hamiltonian pins the energy of an isolated zero-mode to zero energy. These zero-energy modes describe self-conjugate quasiparticles $\hat{\gamma} = \hat{\gamma}^\dagger$ with the properties of a Majorana fermion. Two Majorana fermions combine to an ordinary fermion $\hat{c} = \frac{1}{2}(\hat{\gamma}_1 + i\hat{\gamma}_2)$. It can be shown on general grounds that each physical fermionic state must allow a description in terms of a density matrix composed out of bilinears of Majorana fermionic operators while single Majorana fermion operators are forbidden. This fact is a consequence of the conservation of fermion number parity, which has been formulated as the *fermionic superselection rule* [86, 87, 88, 89].

In $d = 2$ dimensions, consider a topological insulator in class A hosting a single chiral mode at its surface with low-energy boundary Hamiltonion $H_{\text{boundary}}(k) = k$. This low energy theory corresponds to a single channel of fermions propagation only in one direction. A tight-binding model must satisfy periodicity $H_{\text{boundary}}(k) = H_{\text{boundary}}(k + 2\pi)$. In order to satisfy periodicity, the dispersion would need to cross zero energy at another momentum such that the low-energy theory necessarily would need to consist of right- and left-moving quasiparticles. Therefore the chiral low-energy boundary Hamiltonian can not be realized in a one-dimensional lattice model. A local perturbation on the boundary can move, but not remove the chiral hinge state, because back-scattering in these states is forbidden. This was first established as the one-dimensional *Nielsen-Nimoniya theorem* [90, 91, 92].

In $d = 3$ dimensions, consider a time-reversal symmetric topological insulator in class AII hosting a single Dirac cone at its surface with low-energy boundary Hamiltonion $H_{\text{boundary}}(\mathbf{k}) = k_x\sigma_1 + k_y\sigma_2$. One easily verifies that the Dirac cone can not be gapped out as long as time reversal symmetry $\mathcal{T} = i\sigma_2 K$ is preserved. By

a similar argument as for our two-dimensional example, one verifies that this low-energy theory can not be realized in a time-reversal symmetric, two-dimensional lattice model.

1.3 Bulk-boundary correspondence of crystalline topological insulators and superconductors

The gapless, anomalous boundary states in crystalline topological phases are subject of Chapter 2 of this thesis. For the purpose of the introduction, we show how the arguments of the previous section need to be modified in the presence of crystalline symmetries.

In the previous section, we presented a heuristic argument for the existence of gapless anomalous states at the interface of two topologically distinct regions by considering a smooth and slowly varying mass term $m(\mathbf{r})$. By definition, crystalline symmetry elements g have a non-trivial action on real space $g\mathbf{r} \neq \mathbf{r}$. Therefore, if a massive Dirac Hamiltonian is adiabatically evolved along a path $\mathbf{r}(t)$, the terms appearing in the adiabatic evolution should be constrained only by the crystalline symmetry elements g that leave the path itself invariant, $g\mathbf{r}(t) = \mathbf{r}(t)$. As a consequence, along a path $\mathbf{r}(t)$, $t \in [0,1]$ connecting two regions described by massive Dirac Hamiltonians $H_{\text{Dirac}}(\mathbf{k}, \mathbf{r}(0))$, $H_{\text{Dirac}}(\mathbf{k}, \mathbf{r}(1))$ that are stably homotopy inequivalent under the crystalline symmetry group G, a gap closing must exist only if the path itself is invariant under all crystalline symmetry elements. In particular, if the massive Dirac Hamiltonians $H_{\text{Dirac}}(\mathbf{k}, \mathbf{r}(0))$, $H_{\text{Dirac}}(\mathbf{k}, \mathbf{r}(1))$ are stably homotopy equivalent under the symmetry group of the path $G[\mathbf{r}(t)] := \{g \in G | g\mathbf{r}(t) = \mathbf{r}(t)\} \subset G$, then an adiabatic evolution between $H_{\text{Dirac}}(\mathbf{k}, \mathbf{r}(0))$ and $H_{\text{Dirac}}(\mathbf{k}, \mathbf{r}(1))$ along the path $\mathbf{r}(t)$ exists. This implies that the Hamiltonian $H_{\text{Dirac}}(\mathbf{k}, \mathbf{r}(t))$ remains gapped and therefore all excitations along the path $\mathbf{r}(t)$ may remain gapped.

In Chapter 2 we will discuss in detail the boundary theory of crystalline topological phases and its relation to the bulk topology. In particular, crystalline symmetries can protect higher-order topological phases, where a topological phase is said to be of nth-order if the gapless anomalous states are located on codimension n submanifolds of the boundary, for example a two-dimensional second-order topological phase has anomalous corner states. The emphasis of Chapter 2 is on second-order topological phases in systems with an order-two crystalline symmetry, such as mirror, twofold rotation or inversion symmetry. This work was extended in Refs. 93, 94 to higher-order topological phases and general point

group symmetries. An important connection between massive Dirac theories and the order of the topological phase was established in Ref. 93: The order of the topological phase is determined from the number of *crystalline symmetry breaking mass terms* M_i, which is the number of Dirac matrices that anticommute with the massive Dirac Hamiltonian that are allowed if all crystalline symmetry constraints are lifted. Furthermore, some crystalline topological phases do not have anomalous boundary states at all, as we show in the example below.

Furthermore, in Chapter 3 we will show that for crystalline topological phases, the appearance of gapless, anomalous boundary modes is directly linked to the appearance of gapless, anomalous modes at topological lattice defects, such as dislocations and disclinations. First-order topological phases protected by internal symmetries in certain symmetry classes may host anomalous states at defects such as vortices in topological superconductors [38]. Chapter 3 contains a general discussion on the types of defects that host anomalous states in topological phases, and clarifies the relation between bulk topology, anomalous boundary states and defect anomaly.

Example: One-dimensional insulator with inversion symmetry. Consider a one-dimensional insulator in Cartan class A with inversion symmetry. The classifying group of strong topological phases can be obtained by a classification of the mass term in the massive Dirac Hamiltonian as we show in the following. The massive Dirac Hamiltonian satisfies inversion symmetry $U(\mathcal{I}) = \sigma_3 \otimes \mathbf{1}_N$, $\mathcal{I}\mathbf{k} = -\mathbf{k}$, where σ_i are Pauli matrices and "$\otimes$" denotes the direct product of matrices. The massive Dirac Hamiltonian for the one-dimensional theory is written as

$$H_{\text{Dirac}}(k) = k\Gamma_1 + M. \tag{1.11}$$

where Γ_1 anticommutes with $U(\mathcal{I})$ and M commutes with $U(\mathcal{I})$. Thus, M is block diagonal in the eigenbasis of inversion symmetry where the two blocks $M_\pm$ correspond to inversion eigenvalues ± 1, respectively. Without loss of generality, we may choose $\Gamma_1 = \sigma_1 \otimes U_N$, where U_N is a unitary $N \times N$ matrix satisfying $U_N^2 = \mathbf{1}_N$. The condition that M anticommutes with Γ_1 implies that the two blocks of the mass term are related as $M_+ = -U_N M_- U_N^\dagger$. Each block itself is in Cartan class A. Therefore, the stable topological equivalence classes of the mass term M are determined by the stable topological equivalence classes of a single block which is in Cartan class A, such that we have $K[C_i, S^1] \simeq K[C_1, S^0]$. From the periodic table of topological insulators and superconductors, Table 1.1, we find that there are in total $K[C_1, S^0] \simeq \mathbb{Z}$ distinct stable homotopy equivalence classes (see Ref. 40 for an illustrative derivation of the stable homotopy equivalence classes of matrices in Cartan class A). This result is in agreement with literature [79].

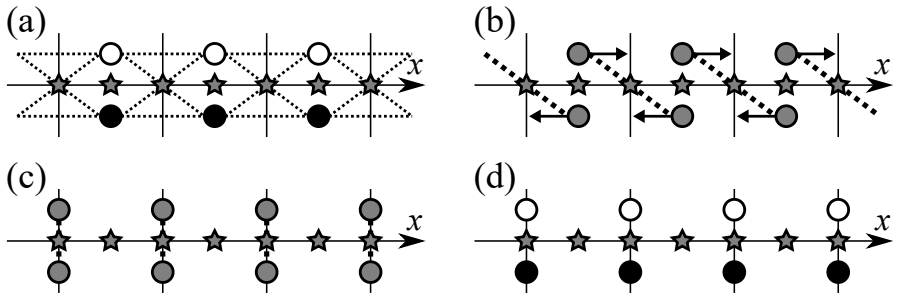

Fig. 1.1: Transformation of the regularized generator Hamiltonian (1.13) of the obstructed atomic limit in the one-dimensional, inversion symmetric insulator to a system of orbitals localized on the unit cell boundary. The gray stars denote the inversion centers. The unit cell is enclosed by the vertical lines. The hopping terms between orbitals are denoted by dotted lines. (a) Representation of the initial Hamiltonian (1.13) where filled and empty dots denote orbitals with inversion eigenvalues ± 1. (b) Basis transformation such that inversion symmetry exchanges the orbitals. The resulting orbitals are denoted by gray dots. (c) Transformation that moves the orbitals to the unit cell boundary. (d) Basis transformation back to the eigenbasis of inversion symmetry.

A generator for the classifying group $K_A[C_i, S^1]$ can be written in terms of the minimal massive Dirac theory

$$H_{\text{Dirac}}(k) = k\sigma_1 + m\sigma_3. \tag{1.12}$$

By introducing a boundary between two topologically distinct phases with opposite sign of the mass term $m\sigma_3$, Eq. (1.10) shows that this Dirac Hamiltonian binds a single, fermionic mode with zero energy at the interface. This zero-mode is merely an artifact of the simple form of the Dirac Hamiltonian (1.12), which has many additional accidental symmetries. In particular, the Dirac Hamiltonian (1.12) satisfies accidental antisymmetries, which ensure that the mode at the interface lies accidentally at zero energy. However, if sufficiently many symmetry-allowed perturbations are included (which break the accidental symmetries), the bound state may acquire an arbitrary energy or even disappear in the bulk bands. As inversion symmetry is broken locally at the interface, such a perturbation may for example be a local chemical potential, or a hybridization $m_1\sigma_2$. In other words, isolated fermionic modes are not anomalous in the absence of superconductivity which allows them to acquire an arbitrary energy. An extensive discussion of this example can also be found in Ref. 94.

It can be seen that the topologically non-trivial phases are obtained by a *hyridization transition* [27] between different configuration of atomic orbitals, also

called *atomic limits*. The topologically non-trivial atomic limits are also called *obstructed atomic limits*. To see this, consider the extension of the minimal massive Dirac theory onto the one-dimensional Brillouin zone

$$H(k) = \sigma_1 \sin k + \sigma_3 \cos k. \tag{1.13}$$

This model describes a pair of orbitals with opposite inversion parity located at the center of the unit cell. The orbitals are hybridized with their nearest neighbors. This system is depicted in Fig. 1.1 (a). A basis transformation $U = e^{i\pi\sigma_1/2}$ switches to a basis in which the orbitals are exchanged under the inversion symmetry, $UU(\mathcal{I})U^\dagger = \sigma_2$, as depicted in Fig. 1.1 (b). Next, one can move the orbitals symmetrical to the boundary of the unit cell, which is expressed by the operator $U_x = e^{ika\sigma_3/2}$, where a is the lattice spacing, as depicted in Fig. 1.1 (c). Finally, one switches back into the eigenbasis of inversion symmetry, such that the resulting Hamiltonian reads $H'(k) = \sigma_3$ with representation of inversion symmetry $U(\mathcal{I}) = \sigma_3 e^{ika}$, as depicted in Fig. 1.1 (d). In summary, this shows that this systems can be deformed to a pair of orbitals located at the boundary of the unit cell.

The existence of a description in terms of an atomic limit that presenves the crystalline symmetries and the absence of $(d \geq 1)$-dimensional gapless, anomalous boundary modes are in one-to-one correspondence to each other [27, 28]. As an atomic limit corresponds to an arrangement of localized orbitals, it can not have gapless, anomalous boundary modes. Conversely, if $d \geq 1$-dimensional gapless anomalous states exist on the boundary, then in a lattice model, there needs to be an extended bound state that connects the anomalous states on opposite surfaces. This is required in order to cancel the anomaly of the surface theories such that a lattice model can be defined (see our discussion on the anomalous surface states in the previous subsection). The necessary existence of extended bulk states implies that the bulk lattice model can not be deformed to an atomic limit (in which all bulk states can be exponentially localized). The above heuristic argument is a generalization of the original argument by Halperin in Ref. 10. More formal proofs have been established for individual cases by determining general criteria on whether an atomic limit can be constructed in terms of *exponentially localized Wannier functions* [2] [96, 97, 98, 99, 95].

[2] A Wannier function is a superposition of the Bloch eigenfunctions of a given band (more generally: set of connected bands) – expressed by the Fourier transformation of the Bloch wavefunction – such that the resulting superposition is localized in real space [95]. If a set of exponentially localized Wannier functions that preserves all symmetries of the system can be found, then it corresponds to an atomic insulator by construction [27]. This is because the Wannier functions of any atomic insulator are exponentially localized at the position of the atomic orbitals by definition.

The connection between the existence of an atomic limit and the appearance of anomalous boundary modes suggestes an alternative definition of 'topologically trivial' insulator: Each Hamiltonian that is adiabatically connected to an atomic limit is considered topologically trivial. This definition is used in Refs 27, 28 to define symmetry-based indicators for topological crystalline insulators with gapless, anomalous boundary states. Notice that, depending on the presence of time-reverrsal and spin rotation symmetry, insulators may correspond to the Cartan symmetry classes A, AI or AII. In these Cartan classes, the tenfold-way periodic table 1.1 shows that there exist only $d \geq 1$ dimensional anomalous states. Therefore, the above definition captures all topological insulators with anomalous boundary states.

All Cartan classes AIII, BDI, D, DIII, CII hosting zero-dimensional anomalous states may be realized in superconducting systems. In these Cartan classes, the definition of an atomic limit is more subtle as (i) the above connection between an absence of exponentially localized bulk states (Wannier functions) could only be established for topological phases hosting $d \geq 1$ dimensional anomalous states. In Section 1.4 below, we are going to show that for the one-dimensional topological superconductor in Cartan class D, all bulk states can be exponentially localized. This shows that exponential localization of the bulk states is not a sufficient criterion to determine the absence of anomalous boundary states in superconductors as it misses the possibility for isolated anomalous zero-energy states. Furthermore, (ii) the microscopic length scale associated to superconductors is the superconducting coherence length, which is typically of the order of 10^1 to 10^3 atomic lattice constants, suggesting a different physical interpretation of an atomic limit for superconductors [100].

In Chapter 4 we are going to show how an atomic limit for superconductors can be defined using the Grothendieck construction as used in the definition of stable homotopy equivalence. This allows to systematically construct all atomic limits for superconductors. Accordingly, we show how to define symmetry-based indicators for topological superconductors within the stable homotopy classification that also detect topological phases hosting anomalous, zero-dimensional zero-energy modes on the boundary.

1.4 Aspects of topological superconductors

The purpose of this section is to illustrate a few aspects of topological superconductors at the simplest example of a one-dimensional topological superconductor

in Cartan class D. We start from a general Bogoliubov-de Gennes Hamiltonian and show how its ground-state is constructed and give relevant definitions along the way. We show that the one-dimensional topological superconductor realized on a ring has an anomalous response with respect to a magnetic flux penetrating the ring. We show that this implies that its Cooper-pair wavefunction must decay algebraically in the topological phase. We emphasize which information the definition of an 'atomic limit' for a superconductor must contain in order to distinguish the topological phases of a one-dimensional topological superconductor.

1.4.1 Superconductors in Bogoliubov-de Gennes theory

This work focuses on the classification and phenomenlogy of topological insulators and superconductors in free fermion systems. By definition, free fermionic systems are desribed by a quadratic fermionic Hamiltonian whose general form in d dimensions is

$$\hat{H} = \sum_{\mathbf{r},\mathbf{r}'} \sum_{i,j} \hat{c}^\dagger_{\mathbf{r},i} h_{i,j}(\mathbf{r},\mathbf{r}') \hat{c}_{\mathbf{r}',j} + \frac{1}{2} \left(\hat{c}^\dagger_{\mathbf{r},i} \Delta_{i,j}(\mathbf{r},\mathbf{r}') \hat{c}^\dagger_{\mathbf{r}',j} - \hat{c}_{\mathbf{r},i} \Delta^*_{i,j}(\mathbf{r},\mathbf{r}') \hat{c}_{\mathbf{r}',j} \right) \quad (1.14)$$

where $\mathbf{r}, \mathbf{r}'$ are discrete real space coordinates, $\hat{c}^\dagger_{\mathbf{r},i}$ is a fermionic creation operator and $i = 1, ..., N(\mathbf{r})$, $j = 1, ..., N(\mathbf{r}')$ enumerates the local degrees of freedom at the position $\mathbf{r}, \mathbf{r}'$ such as a spin or orbital degree of freedom. The matrix $h_{i,j}(\mathbf{r},\mathbf{r}')$ is called the normal state Hamiltonian describing hopping of electrons and holes. The matrix $\Delta_{i,j}(\mathbf{r},\mathbf{r}')$ describes superconducting correlations and is called the superconducting order parameter. The superconducting order parameter is usually determined from a self-consistency relation involving the electron-electron interactions [22]. In this thesis we do not consider the self-consistency relation. Instead, we analyze the properties of the single-particle Hamiltonian with a superconducting order parameter prescribed by symmetry.

Introducing $\hat{\mathbf{\Psi}}_{\mathbf{r},j} = \begin{pmatrix} \hat{c}_{\mathbf{r},j} & \hat{c}^\dagger_{\mathbf{r},j} \end{pmatrix}^T$, the Hamiltonian is written in Bogoliubov-de Gennes form

$$\hat{H} = \frac{1}{2} \sum_{\mathbf{r},\mathbf{r}'} \sum_{i,j} \hat{\mathbf{\Psi}}^\dagger_{\mathbf{r},i} H^{\mathrm{BdG}}_{i,j}(\mathbf{r},\mathbf{r}') \hat{\mathbf{\Psi}}_{\mathbf{r}',j} \quad (1.15)$$

with the Bogoliubov-de Gennes Hamiltonian

$$H^{\mathrm{BdG}}_{i,j}(\mathbf{r},\mathbf{r}') = \begin{pmatrix} h_{ij}(\mathbf{r},\mathbf{r}') & \Delta_{ij}(\mathbf{r},\mathbf{r}') \\ -\Delta^*_{ij}(\mathbf{r},\mathbf{r}') & -h^*_{ij}(\mathbf{r},\mathbf{r}') \end{pmatrix}.$$

We require that both the normal state Hamiltonian $h_{i,j}(\mathbf{r},\mathbf{r}')$ and the pairing term $\Delta_{i,j}(\mathbf{r},\mathbf{r}')$ satisfy a discrete translation symmetry

$$h_{i,j}(\mathbf{r},\mathbf{r}') = h_{i,j}(\mathbf{r}+\mathbf{G}_\alpha,\mathbf{r}'+\mathbf{G}_\alpha) =: h_{i,j}(\mathbf{R}-\mathbf{R}',\tau,\tau')$$
$$\Delta_{i,j}(\mathbf{r},\mathbf{r}') = \Delta_{i,j}(\mathbf{r}+\mathbf{G}_\alpha,\mathbf{r}'+\mathbf{G}_\alpha) =: \Delta_{i,j}(\mathbf{R}-\mathbf{R}',\tau,\tau')$$

with the Bravais lattice vectors $\mathbf{G}_\alpha$, $\alpha = 1,...,d$ and $\mathbf{r} = \mathbf{R}+\tau$ where $\mathbf{R} = \sum_\alpha n_\alpha \mathbf{G}_\alpha, n_\alpha \in \mathbb{Z}$ is the position of the unit cell center and τ is the displacement of the orbital with respect to the unit cell center. Translation symmetric lattice models are conventionally analysed in Bloch basis which is expressed by a Fourier transformation with respect to the unit cell center as

$$\hat{c}_{\mathbf{R}+\tau_l,j} = \sum_{\mathbf{k}\in \mathrm{BZ}} e^{-i\mathbf{k}\mathbf{R}} \hat{c}_{\mathbf{k},\tau_l,j} \tag{1.16}$$

where the sum is performed over all $\mathbf{k}$ in the discretized Brillouin zone BZ such that the resulting Hamiltonian reads

$$\hat{H} = \frac{1}{2}\sum_{\mathbf{k}\in\mathrm{BZ}}\sum_{i,j} \hat{c}^\dagger_{\mathbf{k},i} H^{\mathrm{BdG}}_{i,j}(\mathbf{k}) \hat{c}_{\mathbf{k},j} \tag{1.17}$$

with $\hat{\mathbf{\Psi}}_{\mathbf{k},j} = \begin{pmatrix} \hat{c}_{\mathbf{k},\tau'(j),j} & \hat{c}^\dagger_{-\mathbf{k},\tau'(j),j} \end{pmatrix}^T$ and

$$H^{\mathrm{BdG}}_{i,j}(\mathbf{k}) = \begin{pmatrix} h_{i,j}(\mathbf{k}) & \Delta_{ij}(\mathbf{k}) \\ -\Delta^*_{ij}(-\mathbf{k}) & -h^*_{i,j}(-\mathbf{k}) \end{pmatrix}$$

where

$$h_{i,j}(\mathbf{k}) := \sum_{\mathbf{R}-\mathbf{R}'} e^{i\mathbf{k}(\mathbf{R}-\mathbf{R}')} h_{ij}(\mathbf{R}-\mathbf{R}',\tau(i),\tau'(j))$$
$$\Delta_{ij}(\mathbf{k}) := \sum_{\mathbf{R}-\mathbf{R}'} e^{i\mathbf{k}(\mathbf{R}-\mathbf{R}')} \Delta_{ij}(\mathbf{R}-\mathbf{R}',\tau(i),\tau'(j)),$$

and where we have redefined the indices $i,j = 1,...,\sum_\tau N(\tau)$ to enumerate all $N(\tau)$ local degrees of freedom of all orbitals with position τ within the unit cell. The BdG Hamiltonian satisfies an antiunitary antisymmetry $U(\mathcal{P})(H^{\mathrm{BdG}})^*(-\mathbf{k})U(\mathcal{P})^\dagger = -H^{\mathrm{BdG}}(\mathbf{k})$ due to the fermionic anticommutation relations with $U(\mathcal{P}) = \tau_1$ with τ the Pauli matrix in Nambu space. For local Hamiltonians ($H^{\mathrm{BdG}}_{i,j}(\mathbf{r},\mathbf{r}') \leq ae^{-\lambda|\mathbf{r}-\mathbf{r}'|}$ for some finite $a,\lambda>0$) the Bloch-BdG-Hamiltonian $H^{\mathrm{BdG}}(\mathbf{k})$ is smooth and periodic with the Brillouin zone.

The Bloch-BdG Hamiltonian is diagonalized as $U^\dagger(\mathbf{k})H^{\mathrm{BdG}}(\mathbf{k})U(\mathbf{k}) = \mathcal{E}(\mathbf{k})$ with

$$U_{i,j}(\mathbf{k}) = \begin{pmatrix} u_{i,j}(\mathbf{k}) & v_{i,j}(\mathbf{k}) \\ v^*_{i,j}(-\mathbf{k}) & u^*_{i,j}(-\mathbf{k}) \end{pmatrix} = \begin{pmatrix} |\phi_i(\mathbf{k})\rangle_j & \mathcal{P}|\phi_i(\mathbf{k})\rangle_j \end{pmatrix}$$

composed out of the single-particle eigenstates $|\phi_i(\mathbf{k})\rangle, \mathcal{P}|\phi_i(\mathbf{k})\rangle = \tau_1|\phi_i(-\mathbf{k})\rangle^*$ with energy $H^{\mathrm{BdG}}(\mathbf{k})|\phi_i(\mathbf{k})\rangle = E_i(\mathbf{k})|\phi_i(\mathbf{k})\rangle$ and $H^{\mathrm{BdG}}(\mathbf{k})\mathcal{P}|\phi_i(\mathbf{k})\rangle = -E_i(\mathbf{k})\mathcal{P}|\phi_i(\mathbf{k})\rangle$ such that $\mathcal{E}_{i,j}(\mathbf{k}) = E_i(\mathbf{k})\tau_3\delta_{i,j}$. Gapped superconductors have the same number N of bands with positive and negative energy throughout the Brillouin zone. This allows to choose by convention that $E_n(\mathbf{k}) > 0$ such that $\hat{\gamma}^\dagger_{\mathbf{k},n} = \sum_j u_{j,n}(\mathbf{k})\hat{c}^\dagger_{\mathbf{k},j} + v^*_{j,n}(-\mathbf{k})\hat{c}_{-\mathbf{k},j}$ for $n \leq N$ creates a particle with positive energy $E_n(\mathbf{k}) > 0$ and momentum $\mathbf{k}$. We focus on gapped superconductors below and apply this convention.

There is a gauge ambiguity in choosing the diagonalization $U(\mathbf{k})$: In case the spectrum is non-degenerate, the gauge ambiguity is the common U(1) gauge freedom of quantum mechanics: If $U(\mathbf{k})$ diagonalizes $H(\mathbf{k})$, then $\tilde{U}(\mathbf{k}) = e^{iD(\mathbf{k})}U(\mathbf{k})$, with $D(\mathbf{k})$ a diagonal matrix, diagonalizes $H(\mathbf{k})$. For $D(\mathbf{k}) = d(\mathbf{k})\tau_3$, the gauge transformed states satisfy $\mathcal{P}|\phi_j(\mathbf{k})\rangle = \tau_1|\phi_j(-\mathbf{k})\rangle^*$.

In diagonal basis, the Hamiltonian is written as, using Einstein sum convention and that unitarity of $U(\mathbf{k})$ implies $U_{i,m}(\mathbf{k})U^\dagger_{k,m}(\mathbf{k}) = \delta_{i,k}$,

$$\begin{aligned}
\hat{H} &= \frac{1}{2}\sum_{\mathbf{k}\in\mathrm{BZ}} \hat{\mathbf{\Psi}}^\dagger_{\mathbf{k},i} U_{i,m}(\mathbf{k})U^\dagger_{k,m}(\mathbf{k})H^{\mathrm{BdG}}_{k,l}(\mathbf{k})U_{l,n}(\mathbf{k})U^\dagger_{j,n}(\mathbf{k})\hat{\mathbf{\Psi}}_{\mathbf{k},j} \\
&= \frac{1}{2}\sum_{\mathbf{k}\in\mathrm{BZ}} \hat{\mathbf{\Gamma}}^\dagger_{\mathbf{k},m}\mathcal{E}(\mathbf{k})_{m,n}\hat{\mathbf{\Gamma}}_{\mathbf{k},n} \\
&= \frac{1}{2}\sum_{\mathbf{k}\in\mathrm{BZ}} \hat{\gamma}^\dagger_{\mathbf{k},n}E_n(\mathbf{k})\delta_{n,m}\hat{\gamma}_{\mathbf{k},m} - \hat{\gamma}_{-\mathbf{k},n}E_n(-\mathbf{k})\delta_{n,m}\hat{\gamma}^\dagger_{-\mathbf{k},m} \\
&= \sum_{\mathbf{k}\in\mathrm{BZ}} \hat{\gamma}^\dagger_{\mathbf{k},n}E_n(\mathbf{k})\hat{\gamma}_{\mathbf{k},n}
\end{aligned} \tag{1.18}$$

where $\hat{\mathbf{\Gamma}}_{\mathbf{k},n} = \begin{pmatrix}\hat{\gamma}_{\mathbf{k},n} & \hat{\gamma}^\dagger_{-\mathbf{k},n}\end{pmatrix}^T := U^\dagger_{j,n}(\mathbf{k})\hat{\mathbf{\Psi}}_{\mathbf{k},j}$ such that

$$\hat{\gamma}_{\mathbf{k},n} = \sum_j u^*_{j,n}(\mathbf{k})\hat{c}_{j,\mathbf{k}} + v_{j,n}(-\mathbf{k})\hat{c}^\dagger_{j,-\mathbf{k}} \tag{1.19}$$

$$\mathcal{P}\hat{\gamma}_{\mathbf{k},n} = \hat{\gamma}^\dagger_{-\mathbf{k},n} = \sum_j v^*_{j,n}(\mathbf{k})\hat{c}_{j,\mathbf{k}} + u_{j,n}(-\mathbf{k})\hat{c}^\dagger_{j,-\mathbf{k}} \tag{1.20}$$

Using the commutation relations of fermionic opertors, one shows that $[\hat{H}, \hat{\gamma}^\dagger_{\mathbf{k},n}] = E_n(\mathbf{k})\hat{\gamma}^\dagger_{\mathbf{k},n}$. The system in the ground state should not be able to gain energy by removing particles. Thus, the ground state can be constructed as the state that is annihilated by all quasiparticle operators that remove a particle with positive energy,

$$|\mathrm{GS}\rangle = \frac{1}{\mathcal{N}}\prod_{\mathbf{k}}\prod_n \hat{\gamma}_{\mathbf{k},n}|\mathrm{vac}\rangle \tag{1.21}$$

where the product runs over all n with $E_n(\mathbf{k}) > 0$, $\mathcal{N}$ is a normalization factor, and $|\text{vac}\rangle$ is the vacuum of original fermions $\hat{c}_{i,\mathbf{k}}|\text{vac}\rangle = 0$. For superconductors, this definition is equivalent to the common description of the ground state as a coherent state as we illustrate below.

A closer look reveals that for superconductors, the ground state is composed out of pairs fermions with opposite momentum. For gapped superconductors with a single, spin-polarized band ($N = 1$), we can write

$$\begin{aligned}
|\text{GS}\rangle &= \frac{1}{\mathcal{N}} \prod_{\mathbf{k}' \in \{\mathbf{K}\}} \hat{\gamma}_{\mathbf{k}'} \prod_{\mathbf{k} \in \text{BZ}/\{\mathbf{K}\}} \hat{\gamma}_{\mathbf{k}} |\text{vac}\rangle \\
&= \frac{1}{\mathcal{N}} \prod_{\mathbf{k}' \in \{\mathbf{K}\}} \hat{\gamma}_{\mathbf{k}'} \prod_{\mathbf{k} \in \frac{1}{2}\text{BZ}/\{\mathbf{K}\}} \hat{\gamma}_{-\mathbf{k}} \hat{\gamma}_{\mathbf{k}} |\text{vac}\rangle \\
&= \frac{1}{\mathcal{N}} \prod_{\mathbf{k}' \in \{\mathbf{K}\}} \hat{\gamma}_{\mathbf{k}'} \prod_{\mathbf{k} \in \frac{1}{2}\text{BZ}/\{\mathbf{K}\}} u^*(-\mathbf{k}) v(-\mathbf{k}) \left(1 + \frac{v(\mathbf{k})}{u^*(-\mathbf{k})} \hat{c}^\dagger_{\mathbf{k}} \hat{c}^\dagger_{-\mathbf{k}}\right) |\text{vac}\rangle \\
&= \frac{1}{\mathcal{N}_c} \prod_{\mathbf{k}' \in \{\mathbf{K}\}} \hat{\gamma}_{\mathbf{k}'} \exp\left(\sum_{\mathbf{k}} g(\mathbf{k}) \hat{c}^\dagger_{\mathbf{k}} \hat{c}^\dagger_{-\mathbf{k}}\right) |\text{vac}\rangle
\end{aligned} \tag{1.22}$$

where

$$g(\mathbf{k}) := \frac{v(\mathbf{k})}{u^*(-\mathbf{k})}$$

is conventionally called the Cooper pair wavefunction, $\mathcal{N}_c$ is a redefined normalization factor, $\mathbf{k} \in \{\mathbf{K}\}$ are the inversion symmetric momenta in the Brillouin zone $\mathbf{k} = -\mathbf{k} \mod \mathbf{b}$ where $\mathbf{b}$ is a reciprocal lattice vector, and $\mathbf{k} \in \frac{1}{2}\text{BZ}/\{\mathbf{K}\}$ contains the momenta of only one half of the Brillouin zone after removing the inversion symmetric momenta.

These momenta play a special role as their presence in the ground state depends on the flux in the system. In section 1.4.2 we show that the fermion parity at these momenta and the associated behavior under flux insertion is directly related to the ground state topology. For single-band superconductivity, unitarity of $U(\mathbf{k})$ implies that $g(\mathbf{k}) = -g(-\mathbf{k})$ is an antisymmetric function as expected for wavefunctions describing a pair of fermions. A generalized expression can be derived straightforwardly for multi-band and/or spinful superconductivity.

1.4.2 A topological superconductor in one dimension

Consider a chain of spin-polarized fermions with nearest neighbor hopping elements t. In the normal state, the single-particle spectrum of the chain consists of a single band with band width $2t$. The system is metallic if the chemical potential resides within the band. The simplest superconducting pairing that can be induced in the system couples two neighboring fermions. The corresponding single-particle Hamiltonian reads

$$\hat{H} = \sum_x \mu \hat{c}_x^\dagger \hat{c}_x + \frac{t}{2}\hat{c}_{x+1}^\dagger \hat{c}_x + \frac{t^*}{2}\hat{c}_x^\dagger \hat{c}_{x+1} + \frac{\Delta}{2}\hat{c}_{x+1}^\dagger \hat{c}_x^\dagger - \frac{\Delta^*}{2}\hat{c}_{x+1}\hat{c}_x. \tag{1.23}$$

Using Eqs. (1.15) to (1.17), the Hamiltonian is expressed in Bloch-Bogoliubov-de Gennes form as

$$\hat{H} = \frac{1}{2}\sum_{k\in \mathrm{BZ}} \hat{\mathbf{\Psi}}_k^\dagger H_{\mathrm{BdG}}(k) \hat{\mathbf{\Psi}}_k \tag{1.24}$$

with $\hat{\mathbf{\Psi}}_k^\dagger = (c_k^\dagger, c_{-k})$ and

$$H_{\mathrm{BdG}}(k) = \begin{pmatrix} \mu + t\cos k & i\Delta \sin k \\ -i\Delta^* \sin k & -\mu - t\cos k \end{pmatrix}. \tag{1.25}$$

The spectrum of this Hamiltonian is

$$E(k) = \pm\sqrt{(\mu + t\cos k)^2 + |\Delta|^2 \sin^2 k}. \tag{1.26}$$

If $|\Delta| > 0$, the Hamiltonian has a gapped excitation spectrum everywhere except at $|\mu| = t$. In the following we show that this point separates two phases that are distinguishable by the topology of its ground state. First, we argue that the ground state within the parameter space $|\mu| < t$ is *topologically non-trivial* in the sense that it cannot be written as a state composed of a product of localized fermionic creation operators. We illustrate our conclusions for the parameters $\mu = 0$, $\Delta = t$ real and argue that they are general properties of the topological phase.

In this limit we have $E(k) = t$ and the Hamiltonian is brought into diagonal form as in Eq. (1.18),

$$\hat{H} = t\sum_{k\in \mathrm{BZ}} \hat{\gamma}_k^\dagger \hat{\gamma}_k$$

using the Bogoliubov quasiparticle operators

$$\hat{\gamma}_k = u^*(k)\hat{c}_k + v(-k)\hat{c}_{-k}^\dagger. \tag{1.27}$$

with the weights $u(k) = e^{ik/2}e^{i\pi/4}\cos k/2$ and $v(k) = -e^{ik/2}e^{i\pi/4}\sin k/2$.

When requiring translational symmetry, we implicitly assume the chain forms a ring. When connecting the two ends of the chain to form a ring, we can choose to apply periodic or antiperiodic boundary conditions. The latter corresponds to including a magnetic flux quantum in the ring. Below we assume that the ring contains an even number N of lattice sites. Similar conclusions apply also for a ring with an odd number of lattice sites.

The choice of boundary conditions determines the allowed values of the crystal momentum k. For N even and for periodic boundary conditions, the allowed momenta satisfy $e^{ikN} = 1$ and are given by

$$k \in \left\{ \frac{\pi n}{N} | n = 0, \pm 2, ..., \pm(N-2), N \right\}.$$

The ground state therefore is constructed as, using Eq. (1.22),

$$|\mathrm{GS}\rangle = \frac{1}{\mathcal{N}} \hat{\gamma}_\pi \hat{\gamma}_0 \prod_{0<k<\pi} \hat{\gamma}_{-\mathbf{k}} \hat{\gamma}_{\mathbf{k}} |\mathrm{vac}\rangle. \tag{1.28}$$

The Bogoliubov quasiparticle operators at the inversion symmetric momenta have the form

$$\hat{\gamma}_0 = e^{-i\pi/4} \hat{c}_0, \quad \hat{\gamma}_\pi = e^{-i\pi/4} \hat{c}_\pi^\dagger.$$

As $\hat{c}_0 \prod_{0<k<\pi} \hat{\gamma}_{-\mathbf{k}} \hat{\gamma}_{\mathbf{k}} |\mathrm{vac}\rangle = 0$, the ground state has to be constructed using only $\hat{\gamma}_\pi = e^{-i\pi/4} \hat{c}_\pi^\dagger$. This shows that if the fermion parity of the system is constrained to be even, the system cannot reach its ground state if the ring encloses an even number of flux quanta as it can always reduce its energy by accepting an additional fermion.

For N even and for antiperiodic boundary conditions, the condition $e^{ikN} = -1$ is satisfied by the momenta

$$k \in \left\{ \frac{\pi n}{N} | n = \pm 1, ..., \pm(N-1) \right\}.$$

In this case the inversion symmetric momenta $k = 0$ and π are not included in the construction of the ground state. The ground state

$$|\mathrm{GS}\rangle = \frac{1}{\mathcal{N}} \prod_{0<k<\pi} \hat{\gamma}_{-\mathbf{k}} \hat{\gamma}_{\mathbf{k}} |\mathrm{vac}\rangle \tag{1.29}$$

therefore has even fermion parity. This consideration shows that if the magnetic field is allowed to fluctuate, the ground state of the system on a large ring with even number of fermions encloses an odd number of flux quanta. Other boundary

conditions than periodic or antiperiodic are not allowed for a superconductor with a well-defined order parameter and no vector potential.

This response of the system with respect to a magnetic flux directly implies that the Cooper pair wavefunction is non-local as we show in the following. In our example, this is seen by rewriting the ground state as a coherent state using Eq. (1.22) as

$$\begin{aligned}|\mathrm{GS}\rangle &= \frac{1}{\mathcal{N}_c}\exp\left(\sum_{k\in\frac{1}{2}\mathrm{BZ}/\{\mathbf{K}\}}\frac{v(k)}{u^*(-k)}\hat{c}_k^\dagger\hat{c}_{-k}^\dagger\right)|\mathrm{vac}\rangle \\ &= \frac{1}{\mathcal{N}_c}\exp\left(\sum_{X\neq X'}g(X-X')\hat{c}_{X'}^\dagger\hat{c}_X^\dagger\right)|\mathrm{vac}\rangle\end{aligned}$$

using the inverse Fourier transformation to Eq. (1.16) with respect to the Bloch basis and introducing the real space profile of the Cooper pair wavefunction

$$g(X-X') = \sum_{k\in\frac{1}{2}\mathrm{BZ}/\{\mathbf{K}\}} e^{ik(X-X')}\frac{v(k)}{u^*(-k)} = -i\sum_{k\in\frac{1}{2}\mathrm{BZ}/\{\mathbf{K}\}} e^{ik(X-X')}\tan(k/2). \quad (1.30)$$

Numerical evaluation of the sum shows that the Cooper pair wavefunction decays algebraically at large distances as

$$\lim_{|X-X'|\to\infty}|g(X-X')| \propto |X-X'|^{-\frac{1}{2}}.$$

In general, the coefficients of a Fourier transformation of a discontinuous function decay at most algebarically. In fact, the Paley-Wiener theorem implies that the expansion coefficients decay exponentially only for analytic functions [101]. This algebraic decay of the Cooper pair wavefunction in the topological phase of a one-dimensional superconductor has also been shown in Refs. 102, 101. We point out that also the Cooper pair wavefunction in a two-dimensional $p_x + ip_y$ topological superconductor [23, 102] as well as a three-dimensional topological superconductor in class DIII [61] exhibits algebraic decay at large distances .

If the fermion parity at the $k = 0$ and π differs, the Cooper pair wavefunction has to be non-local. This follows by considering that unitarity of $U(k)$ for spin polarized single-band superconductors requires $g(k) = -g(-k)$. If $g(k)$ is continuous and periodic with the Brillouin zone $k \in (-\pi, \pi]$, then $g(0) = g(\pi) = 0$ which implies $u(0) = u(\pi) = 0$. In this case $\hat{\gamma}_K \propto \hat{c}_K$ for $K = 0, \pi$ and consequently the fermion parity of the ground state is even and independent of the magnetic flux through the ring. If $u(K) \neq 0$ for $K = 0, \pi$, then $g(k)$ can not be continuous and

periodic with the Brillouin zone. In this case the Paley-Wiener theorem guarantees that the expansion coefficients of the Fourier transformation decay at most algebraically. An extension of this argument to an arbitrary number of bands is found in Ref. [101].

Description in terms of exponentially localized Bogoliubov-quasiparticles. By superposition of the extended Bogoliubov quasiparticles $\hat{\gamma}_k$ which are the eigenstates of the translation symmetric Bogoliubov-de Gennes Hamiltonina, one can construct a set of localized Bogoliubov quasiparticles using the Fourier transformation with respect to the Bloch basis as

$$\begin{aligned}\hat{\gamma}_X^\dagger &= \sum_{k\in \mathrm{BZ}} e^{-ikX}\hat{\gamma}_k^\dagger \\ &= \sum_{k\in \mathrm{BZ}} \left[-\frac{1}{2i}e^{ikX}e^{i\pi/4}\left(e^{ik}-1\right)\hat{c}_{\mathbf{k}} + \frac{1}{2}e^{ikX}e^{-i\pi/4}\left(e^{ik}+1\right)\hat{c}_{-\mathbf{k}}^\dagger\right] \\ &= \frac{e^{-i\pi/4}}{2}\left(\hat{c}_{X+1}^\dagger - \hat{c}_{X+1} + \hat{c}_X^\dagger + \hat{c}_X\right) \\ &= \frac{e^{-i\pi/4}}{2}\left(\hat{a}_{X+1} + \hat{b}_X\right)\end{aligned} \tag{1.31}$$

where we introduced $\hat{a}_X = \left(\hat{c}_X^\dagger + \hat{c}_X\right)$ and $\hat{b}_X = i\left(\hat{c}_X^\dagger - \hat{c}_X\right)$ which satisfy the Majorana relation $\hat{a}_X^\dagger = \hat{a}_X$, $\hat{b}_X^\dagger = \hat{b}_X$ and combine into the original fermions as $c_X = \frac{1}{2}(a_X + ib_X)$. The operator $\hat{\gamma}_X^\dagger$ thus describes a fermion that is composed out of a pair of Majorana fermions of adjacent sites. The charge center of the fermion $\hat{\gamma}_X^\dagger$ is localized exactly in the center between two adjacent fermions $\hat{c}_X^\dagger$, $\hat{c}_{X+1}^\dagger$. This proves that all quasiparticle excitaitons of the one-dimensional topological superconductor can be exponentially localized. Notice that this is in contrast to our result for topological phases with $d \geq 1$ dimensional anomalous boundary states, where the boundary anomaly implied the necessary existence of extended bulk states.

The above calculation shows how the Majorana fermion operators $\hat{a}_X, \hat{b}_X$ arise naturally in the "dimerized limit" $\mu = 0$, $\delta = t$ of the one-dimensional topological superconductor. By rewriting the Hamiltonian (1.23) with the operators $\hat{a}_X, \hat{b}_X$, one verifies straightforwardly in the dimerized limit that it realizes isolated Majorana bound states at each end of the chain (see Ref. 102 for a detailed demonstration). In the original paper by Kitaev discussing the one-dimensional topological superconductor in Ref. 25, it has been shown that the appearance of Majorana end states is directly connected to the difference of the fermion parity at different parity of the number of enclosed magnetic flux quanta.

For insulators, a sufficient condition for the existence of gapless, anomalous boundary states is whether one can form a basis of exponentially localized states by superposition of the bulk eigenstates (Wannier functions) [27, 28], see Sec. 1.3 above. This condition is not sufficient to diagnose topological superconductivity, as the above example shows that it misses topological superconducting phases that host isolated Majorana bound states at its boundary. The above example suggests that one furthermore needs to require that the Cooper pair wavefunction can be exponentially localized [101]. Alternatively, one can include the position of the original fermions as additional data and require that the localization position of Bogoliubov quasiparticles (if exponentially localized) should coincide with the position of the original fermions. In Chapter 4 we extend the latter idea in order to define and construct atomic limits for superconductors within the framework of the stable homotopy classification. It has been suggested to extend the latter idea to formulate a criterion for higher-order topological superconductivity with isolated Majorana bound states on the boundary [100].

Bibliography

[1] S. M. Blinder, ""coffee mug to donut" from the wolfram demonstrations project," (2011), http://demonstrations.wolfram.com/CoffeeMugToDonut/ .

[2] K. v. Klitzing, G. Dorda, and M. Pepper, Phys. Rev. Lett. **45**, 494 (1980).

[3] D. J. Thouless, M. Kohmoto, M. P. Nightingale, and M. den Nijs, Phys. Rev. Lett. **49**, 405 (1982).

[4] M. Kohmoto, Annals of Physics **160**, 343 (1985).

[5] D. C. Tsui, H. L. Stormer, and A. C. Gossard, Phys. Rev. Lett. **48**, 1559 (1982).

[6] X. G. Wen and Q. Niu, Phys. Rev. B **41**, 9377 (1990).

[7] X. G. Wen, Int. J. Mod. Phys. B **04**, 239 (1990).

[8] J. M. Kosterlitz and D. J. Thouless, Journal of Physics C: Solid State Physics **6**, 1181 (1973).

[9] L. D. Landau, Zh. Eksp. Teor. Fiz. **7**, 19 (1937).

[10] B. I. Halperin, Phys. Rev. B **25**, 2185 (1982).

[11] V. Kalmeyer and R. B. Laughlin, Phys. Rev. Lett. **59**, 2095 (1987).

[12] X. G. Wen, F. Wilczek, and A. Zee, Phys. Rev. B **39**, 11413 (1989).

[13] R. B. Laughlin, Phys. Rev. Lett. **50**, 1395 (1983).

[14] R. de Picciotto, M. Reznikov, M. Heiblum, V. Umansky, G. Bunin, and D. Mahalu, Nature **389**, 162 (1997).

[15] L. Saminadayar, D. C. Glattli, Y. Jin, and B. Etienne, Phys. Rev. Lett. **79**,

2526 (1997).
[16] C. L. Kane and E. J. Mele, Phys. Rev. Lett. **95**, 146802 (2005).
[17] C. L. Kane and E. J. Mele, Phys. Rev. Lett. **95**, 226801 (2005).
[18] B. A. Bernevig and S.-C. Zhang, Phys. Rev. Lett. **96**, 106802 (2006).
[19] L. Fu, C. L. Kane, and E. J. Mele, Phys. Rev. Lett. **98**, 106803 (2007).
[20] M. König, S. Wiedmann, C. Brüne, A. Roth, H. Buhmann, L. W. Molenkamp, X.-L. Qi, and S.-C. Zhang, Science **318**, 766 (2007).
[21] D. Hsieh, D. Qian, L. Wray, Y. Xia, Y. S. Hor, R. J. Cava, and M. Z. Hasan, Nature **452**, 970 (2008).
[22] P. G. de Gennes, *Superconductivity Of Metals And Alloys*, 1st ed. (Westview Press, 1999).
[23] N. Read and D. Green, Phys. Rev. B **61**, 10267 (2000).
[24] D. A. Ivanov, Phys. Rev. Lett. **86**, 268 (2001).
[25] A. Y. Kitaev, Physics-Uspekhi **44**, 131 (2001).
[26] M. Z. Hasan and C. L. Kane, Rev. Mod. Phys. **82**, 3045 (2010).
[27] B. Bradlyn, L. Elcoro, J. Cano, M. G. Vergniory, Z. Wang, C. Felser, M. I. Aroyo, and B. A. Bernevig, Nature **547**, 298 (2017).
[28] H. C. Po, A. Vishwanath, and H. Watanabe, Nature Communications **8**, 50 (2017).
[29] Z. Song, T. Zhang, Z. Fang, and C. Fang, Nature Communications **9**, 3530 (2018).
[30] M. G. Vergniory, L. Elcoro, C. Felser, N. Regnault, B. A. Bernevig, and Z. Wang, Nature **566**, 480 (2019).
[31] F. Tang, H. C. Po, A. Vishwanath, and X. Wan, Nature **566**, 486 (2019).
[32] F. Tang, H. C. Po, A. Vishwanath, and X. Wan, Sci Adv **5**, eaau8725 (2019).
[33] F. Tang, H. C. Po, A. Vishwanath, and X. Wan, Nature Physics **15**, 470 (2019).
[34] T. Zhang, Y. Jiang, Z. Song, H. Huang, Y. He, Z. Fang, H. Weng, and C. Fang, Nature **566**, 475 (2019).
[35] D. Wang, F. Tang, J. Ji, W. Zhang, A. Vishwanath, H. C. Po, and X. Wan, Phys. Rev. B **100**, 195108 (2019).
[36] A. Hatcher, *Algebraic topology* (Cambridge University Press, 2002).
[37] A. Kitaev, AIP Conference Proceedings **1134**, 22 (2009).
[38] J. C. Y. Teo and C. L. Kane, Phys. Rev. B **82**, 115120 (2010).
[39] A. M. Turner, Y. Zhang, R. S. K. Mong, and A. Vishwanath, Phys. Rev. B **85**, 165120 (2012).
[40] C.-K. Chiu, J. C. Y. Teo, A. P. Schnyder, and S. Ryu, Rev. Mod. Phys. **88**, 035005 (2016).
[41] L. Fu and C. L. Kane, Phys. Rev. B **76**, 045302 (2007).

[42] T. L. Hughes, E. Prodan, and B. A. Bernevig, Phys. Rev. B **83**, 245132 (2011).
[43] C. Fang, M. J. Gilbert, and B. A. Bernevig, Phys. Rev. B **86**, 115112 (2012).
[44] J. C. Y. Teo and T. L. Hughes, Phys. Rev. Lett. **111**, 047006 (2013).
[45] W. A. Benalcazar, J. C. Y. Teo, and T. L. Hughes, Phys. Rev. B **89**, 224503 (2014).
[46] K. Shiozaki, (2019), arXiv:1907.13632 .
[47] A. Skurativska, T. Neupert, and M. H. Fischer, Phys. Rev. Research **2**, 013064 (2020).
[48] S. Ono, H. C. Po, and H. Watanabe, Sci Adv **6**, eaaz8367 (2020).
[49] A. Alexandradinata, X. Dai, and B. A. Bernevig, Phys. Rev. B **89**, 155114 (2014).
[50] A. Alexandradinata and B. A. Bernevig, Physica Scripta **T164**, 014013 (2015).
[51] A. Alexandradinata and B. A. Bernevig, Phys. Rev. B **93**, 205104 (2016).
[52] A. Alexandradinata, Z. Wang, and B. A. Bernevig, Phys. Rev. X **6**, 021008 (2016).
[53] Z. Wang, A. Alexandradinata, R. J. Cava, and B. A. Bernevig, Nature **532**, 189 (2016).
[54] T. Li, L. Duca, M. Reitter, F. Grusdt, E. Demler, M. Endres, M. Schleier-Smith, I. Bloch, and U. Schneider, Science **352**, 1094 (2016).
[55] W. A. Benalcazar, B. A. Bernevig, and T. L. Hughes, Science **357**, 61 (2017).
[56] A. Bouhon, A. M. Black-Schaffer, and R.-J. Slager, Phys. Rev. B **100**, 195135 (2019).
[57] Y. Hwang, J. Ahn, and B.-J. Yang, Phys. Rev. B **100**, 205126 (2019).
[58] J. Ahn, S. Park, D. Kim, Y. Kim, and B.-J. Yang, Chinese Physics B **28**, 117101 (2019).
[59] H. Li and K. Sun, (2020), arXiv:2004.05504 .
[60] K. Shiozaki, M. Sato, and K. Gomi, (2018), arXiv:1802.06694 .
[61] A. P. Schnyder, S. Ryu, A. Furusaki, and A. W. W. Ludwig, Phys. Rev. B **78**, 195125 (2008).
[62] R. Kennedy and M. R. Zirnbauer, Physica Scripta **T164**, 014010 (2015).
[63] R. Kennedy and C. Guggenheim, Phys. Rev. B **91**, 245148 (2015).
[64] R. Kennedy and M. R. Zirnbauer, Communications in Mathematical Physics **342**, 909 (2016).
[65] D.-L. Deng, S.-T. Wang, C. Shen, and L.-M. Duan, Phys. Rev. B **88**, 201105 (2013).
[66] R. Kennedy, Phys. Rev. B **94**, 035137 (2016).
[67] J. Cano, B. Bradlyn, Z. Wang, L. Elcoro, M. G. Vergniory, C. Felser, M. I.

Aroyo, and B. A. Bernevig, Phys. Rev. Lett. **120**, 266401 (2018).
[68] H. C. Po, H. Watanabe, and A. Vishwanath, Phys. Rev. Lett. **121**, 126402 (2018).
[69] B. Bradlyn, Z. Wang, J. Cano, and B. A. Bernevig, Phys. Rev. B **99**, 045140 (2019).
[70] H.-X. Wang, G.-Y. Guo, and J.-H. Jiang, New Journal of Physics **21**, 093029 (2019).
[71] S. Liu, A. Vishwanath, and E. Khalaf, Phys. Rev. X **9**, 031003 (2019).
[72] S. H. Kooi, G. van Miert, and C. Ortix, Phys. Rev. B **100**, 115160 (2019).
[73] J. Ahn, S. Park, and B.-J. Yang, Phys. Rev. X **9**, 021013 (2019).
[74] D. V. Else, H. C. Po, and H. Watanabe, Phys. Rev. B **99**, 125122 (2019).
[75] M. Karoubi, *K-Theory: An introduction*, 1st ed. (Springer-Verlag Berlin Heidelberg, 1978).
[76] M. F. Atiyah, Q J Math **17**, 367 (1966).
[77] A. Altland and M. R. Zirnbauer, Phys. Rev. B **55**, 1142 (1997).
[78] M. R. Zirnbauer, (2010), arXiv:1001.0722 .
[79] K. Shiozaki and M. Sato, Phys. Rev. B **90**, 165114 (2014).
[80] K. Shiozaki, M. Sato, and K. Gomi, Phys. Rev. B **95**, 235425 (2017).
[81] I. C. Fulga, F. Hassler, and A. R. Akhmerov, Phys. Rev. B **85**, 165409 (2012).
[82] L. Trifunovic and P. Brouwer, Phys. Rev. B **96**, 195109 (2017).
[83] E. Cornfeld and A. Chapman, Phys. Rev. B **99**, 075105 (2019).
[84] K. Shiozaki, (2019), arXiv:1907.09354 .
[85] R. Thorngren and D. V. Else, Phys. Rev. X **8**, 011040 (2018).
[86] C. Krumnow, *Detecting and Understanding Ecient Structures in Finite Fermionic Systems*, Ph.D. thesis, Freie Universitaet Berlin (2017).
[87] G. C. Wick, A. S. Wightman, and E. P. Wigner, Phys. Rev. **88**, 101 (1952).
[88] Z. Zimborás, R. Zeier, M. Keyl, and T. Schulte-Herbrüggen, EPJ Quantum Technology **1**, 11 (2014).
[89] M. Johansson, (2016), arXiv:1610.00539 .
[90] H. B. Nielsen and M. Ninomiya, Physics Letters B **105**, 219 (1981).
[91] H. B. Nielsen and M. Ninomiya, Nuclear Physics B **185**, 20 (1981).
[92] H. B. Nielsen and M. Ninomiya, Nuclear Physics B **193**, 173 (1981).
[93] L. Trifunovic and P. W. Brouwer, Phys. Rev. X **9**, 011012 (2019).
[94] L. Trifunovic and P. W. Brouwer, (2020), arXiv:2003.01144 .
[95] D. Vanderbilt, *Berry Phases in Electronic Structure Theory* (Cambridge University Press, 2018).
[96] T. Thonhauser and D. Vanderbilt, Phys. Rev. B **74**, 235111 (2006).
[97] C. Brouder, G. Panati, M. Calandra, C. Mourougane, and N. Marzari, Phys. Rev. Lett. **98**, 046402 (2007).

[98] A. A. Soluyanov and D. Vanderbilt, Phys. Rev. B **83**, 035108 (2011).
[99] D. Monaco, "Advances in quantum mechanics: Contemporary trends and open problems," (Springer, 2017) Chap. Chern and Fu–Kane–Mele Invariants as Topological Obstructions, pp. 201–222.
[100] R.-X. Zhang, J. D. Sau, and S. Das Sarma, (2020), arXiv:2003.02559 .
[101] F. Schindler, B. Bradlyn, M. H. Fischer, and T. Neupert, Phys. Rev. Lett. **124**, 247001 (2020).
[102] J. Alicea, Reports on Progress in Physics **75**, 076501 (2012).

2. Second-order topological insulators and superconductors with an order-two crystalline symmetry

2.1. INTRODUCTION

In comparison to conventional "first-order" topological insulators and superconductors, which combine a gapped bulk with topologically protected gapless boundary states,[1–3] the protected gapless states in a second-order topological insulator or superconductor exist in one dimension lower:[4] A two-dimensional second-order topological insulator or superconductor has zero-energy states at corners of the crystal[5–9] and a three-dimensional topological insulator or superconductor has gapless modes along crystal edges or "hinges".[4, 9–14] Second-order topological insulator and superconductor phases have been proposed to exist in a (first-order) topological insulator in three dimensions to which a suitable time-reversal-breaking perturbation is applied,[10, 11] in the superfluid ^{3}He-B phase,[12] or in crystals with rotation or mirror symmetries.[4–9, 13, 14]

A complete classification of first-order topological insulators and superconductors has been developed, accounting for the presence or absence of non-spatial symmetries (see also Chapter 1).[15–17] The three fundamental non-spatial symmetry operations time-reversal $\mathcal{T}$, particle-hole $\mathcal{P}$, and $\mathcal{C} = \mathcal{P}\mathcal{T}$, known as "chiral symmetry", define the ten Altland-Zirnbauer symmetry classes,[18] see Table 2.1. For each Altland-Zirnbauer class, the number and type of protected boundary states is uniquely rooted in the topology of the bulk band structure, so that topological classifications of gapped bulk band structure and gapless boundary states are essentially identical, a feature known as "bulk-boundary correspondence". Complete classifications for all Altland-Zirnbauer classes with additional spatial symmetries exist only for the order-two crystalline symmetries,[19] such as mirror symmetry,[20–22] order-two rotation symmetry, inversion symmetry,[23] and non-symmorphic order-two crystalline symmetries.[24] In parallel, a wealth of symmetry-based indicators has been identified for topological phases with other crystalline symmetries (see also Chapter 4).[25–36] With crystalline symmetries, the bulk-boundary correspondence — *i.e.*, the one-to-one correspondence between bulk topology and the number and type of gapless boundary states — only applies to boundaries which are invariant with respect to the crystalline symmetry operation; non-symmetric boundaries are generically gapped (see also Section 1.3 of Chapter 1).

In this chapter we consider the classification problem for second-order topological insulators. We identify the type and number of zero-energy states at corners or gapless modes at hinges and relate this classification of corner states and hinge modes to the topology of the bulk band structure. This program is carried out for all ten Altland-Zirnbauer classes with one additional order-two spatial symmetry, for which the classification of the bulk band structure is known.[19]

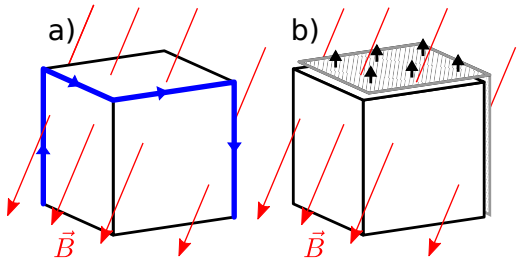

FIG. 2.1. Schematic picture of an "extrinsic" second-order topological insulator consisting of a three-dimensional topological insulator placed in a magnetic field in a generic direction, as proposed by Sitte *et al.*[10] (a). Each surface has a finite flux and there are chiral modes along hinges that touch two faces with opposite sign of the magnetic flux. The gapless hinge modes may be removed by exchange-coupling some of the crystal faces to a two-dimensional ferromagnetic insulator (b).

In contrast to first-order topological insulators, for which the number and type of protected boundary states depends on the topology of the bulk band structure only, the occurrence of zero-energy corner states or gapless hinge modes may also depend on properties of the boundary, *i.e.*, on the lattice termination. Correspondingly, the classification of corner states and hinge modes of second-order topological insulators and superconductors has to distinguish between termination-dependent and termination-independent properties of corner states and hinge modes. This naturally leads to an "intrinsic" topological classification, in which crystals that differ by a lattice termination only are considered topologically equivalent, and an "extrinsic" classification, which accounts for termination effects and defines topological equivalence with respect to continuous transformations that preserve both bulk and boundary gaps.

An example of an "extrinsic" second-order topological insulator is a three-dimensional topological insulator (without further crystalline symmetries) placed in a magnetic field in a generic direction, such that there is a finite magnetic flux through all surfaces,[10, 11] see Fig. 2.1. Such a crystal has chiral modes along hinges that connect faces with an inward and outward-pointing magnetic fluxes. The chiral modes are stable with respect to continuous transformation of the Hamiltonian that preserve bulk and surface gaps. They may be removed, however, upon exchange coupling the crystal faces with an inward magnetic flux to ferromagnetic insulating films, with a magnetization direction chosen such that the exchange field reverses the effect of the applied magnetic field.

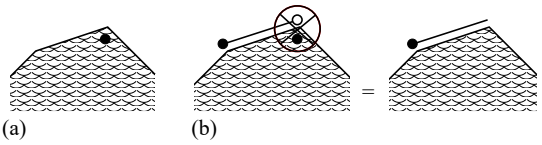

FIG. 2.2. (a) Schematic picture of a generic corner of a two-dimensional crystal. A generic corner may host a protected zero-energy state if and only if the corresponding Altland-Zirnbauer class in $d-1$ dimensions is nontrivial. (b) Zero-energy corner states in a generic corner can always be moved to a different corner by a suitable change of the lattice termination. For the example shown here, a one-dimensional topological insulator or superconductor with two end states is "glued" to one of the crystal faces adjacent to the top corner, such that its end state and the original zero-energy corner state mutually gap out. As a result, the corner state has moved to the corner on the left.

Cartan	(anti)symmetries	$d=2$	$d=3$
A	-	0	$\mathbb{Z}$
AIII	$\mathcal{C}$	$\mathbb{Z}$	0
AI	$\mathcal{T}^+$	0	0
BDI	$\mathcal{T}^+$, $\mathcal{P}^+$	$\mathbb{Z}$	0
D	$\mathcal{P}^+$	$\mathbb{Z}_2$	$\mathbb{Z}$
DIII	$\mathcal{T}^-$, $\mathcal{P}^+$	$\mathbb{Z}_2$	$\mathbb{Z}_2$
AII	$\mathcal{T}^-$	0	$\mathbb{Z}_2$
CII	$\mathcal{T}^-$, $\mathcal{P}^-$	$2\mathbb{Z}$	0
C	$\mathcal{P}^-$	0	$2\mathbb{Z}$
CI	$\mathcal{T}^+$, $\mathcal{P}^-$	0	0

TABLE 2.1. The ten Altland-Zirnbauer classes are defined according to the presence or absence of time-reversal symmetry ($\mathcal{T}$), particle-hole antisymmetry ($\mathcal{P}$), and chiral antisymmetry ($\mathcal{C}$). The superscript $\pm$ indicates the square of the time-reversal or particle-hole conjugation operation. The presence of chiral antisymmetry $\mathcal{C}=\mathcal{P}\mathcal{T}$ is automatic for Altland-Zirnbauer classes with both time-reversal symmetry and particle-hole antisymmetry. The third and fourth column give the classification of stable zero-energy states at generic corners of two-dimensional crystals ($d=2$) or hinges of three-dimensional crystals ($d=3$). This is an "extrinsic" classification, in the sense that the number of corner states or hinge modes at a generic corner or hinge is not a bulk property and can be changed by a change of the lattice termination. Its topological protection is with respect to all continuous transformations that preserve both bulk and boundary gaps.

An "intrinsic" second-order topological insulator or superconductor, for which the presence of corner or hinge states does not depend on the lattice termination, requires the presence of additional crystalline symmetries. Examples that have been identified in the literature include mirror-reflection symmetry,[4, 9] rotation symmetries,[4, 13, 14] or more general point group symmetries.[6, 7, 36] In these cases corner states continue to exist under continuous transformations of the Hamiltonian that close the boundary gap, provided the bulk gap is not closed and the lattice termination remains compatible with the crystalline symmetry.

In the presence of a crystalline symmetry, a classification of corner states and hinge modes must also distinguish between corners and hinges that are themselves invariant with respect to the crystalline symmetry, and generic non-symmetric corners or hinges. The classification of zero-energy states and gapless modes at a generic, non-symmetric corner or hinge (schematically shown in Fig. 2.2a) equals that of a generic codimension-one defect, which is the same as the regular classification of topological phases but with the dimension shifted by one,[37] see Table 2.1. This simple result also follows from the observation that the absence of gapless boundary states implies that the bulk is essentially topologically trivial, so that a corner or hinge may be seen as a junction between two "stand-alone" topological edges or surfaces.[9] Note that this classification of corner states or hinge modes at a generic corner or hinge is an *extrinsic* classification: Any corner state or hinge mode at a generic corner or hinge can be moved away from that corner or hinge by a suitable change of the crystal boundary, without affecting the bulk, see Fig. 2.2b.[4, 36] Hence, the *intrinsic* classification of corner states or hinge modes at a generic corner or hinge is always trivial.

A classification of zero-energy states and gapless modes at mirror-symmetric corners and hinges is given in Sec. 2.4. In addition to providing the intrinsic (termination-independent) and extrinsic (termination-dependent) classifications, we consider the effect of perturbations that locally break mirror symmetry at corners and hinges, to account for the experimental reality that corners and hinges are more prone to defects and disorder than crystal faces. The intrinsic classification of zero-energy states and gapless modes at mirror-symmetric corners and hinges coincides with the classification of bulk topological crystalline phases in two and three dimensions,[19–22] respectively, after removal of the first-order topological phases. This "corner-to-bulk correspondence" (or "hinge-to-bulk correspondence, for three-dimensional topological crystalline insulators and superconductors) not only confirms that every topological class of the bulk band structure is associated with a unique configuration of zero-energy corner states or gapless hinge modes, but also that for every possible configuration of mirror-symmetric zero-energy corner states or hinge modes, there is a topological crystalline phase that produces it.

With rotation or inversion symmetry there are no symmetry-invariant corners or hinges for two- and three-dimensional crystals, respectively. Hence, each corner or hinge in a crystal with rotation symmetry or inversion symmetry is a "generic" corner or hinge, described by the extrinsic classification of Table 2.1. Zero-energy corner states or gapless hinge modes at a given corner or hinge can always be removed by changing the lattice termination. Nevertheless, as we show in Sec. 2.5, the role of the bulk crystalline symmetry, combined with the requirement that lattice termination is symmetry-compatible, is to impose a $\mathbb{Z}_2$ *sum rule* to the total number of corner

or hinge states, which is an odd multiple of two for the nontrivial phases and an even multiple of two otherwise. (For Altland-Zirnbauer classes with a time-reversal or particle-hole symmetry squaring to -1 one should count pairs of corner states/hinge modes.)

In Refs. 4 and 9 is the construction of a nontrivial intrinsic second-order phase out of a nontrivial bulk mirror-reflection-symmetric phase made use of the bulk-boundary correspondence, according to which a nontrivial topological crystalline bulk phase implies a gapless boundary mode at a boundary that is left invariant under mirror reflection. The existence of protected corner states or hinge modes was then concluded upon noting that mass terms that are generated upon tilting the boundary away from the mirror-invariant direction have a different sign at mirror-related boundaries, such that a corner separating mirror-related boundaries represents a domain wall and, hence, hosts a zero-energy state or a gapless hinge mode. The same procedure can be applied to a three-dimensional crystal with a twofold rotation symmetry, because these, too, allow for symmetry-invariant faces. It fails, however, for a two-dimensional crystal with twofold rotation symmetry or a three-dimensional crystal with inversion symmetry, because these have no symmetry-invariant surface. To derive the existence of a second-order topological phase with zero-energy corner states in a two-dimensional crystal with twofold rotation symmetry or of gapless hinge modes in a three-dimensional crystal with inversion symmetry, we employ a dimensional reduction scheme, making use of the existence of symmetry-invariant faces for crystals with the same order-two crystalline symmetry in one dimension higher. Our results are consistent with nontrivial second-order topological phases predicted recently by Fang and Fu[14] and by Khalaf *et al.*[36] for three-dimensional inversion-symmetric crystals.

This chapter is organized as follows: In Sec. 2.2 we introduce the relevant symmetry classes for an order-two crystalline symmetry coexisting with time-reversal symmetry, particle-hole symmetry, or chiral symmetry and we review Shiozaki and Sato's classification of the crystalline bulk phases. The dimensional reduction map is outlined in Sec. 2.3. A classification of mirror-symmetric corners and hinges follows in Sec. 2.4; Section 2.5 discusses twofold rotation and inversion symmetry. A few representative examples of tight-binding models realizing second-order topological phases are discussed in Sec. 2.6. We conclude in Sec. 2.7. The appendices contain a detailed discussion of the dimensional reduction scheme as well as a brief discussion of all relevant crystalline symmetry classes that are not considered in the main text.

2.2. SHIOZAKI-SATO SYMMETRY CLASSES

We consider a Hamiltonian $H_d(\mathbf{k})$ in d dimensions, with $\mathbf{k} = (k_1, k_2, \ldots, k_d)$. In addition to the crystalline order-two symmetry, to be discussed in detail below, the Hamiltonian H_d possibly satisfies a combination of time-reversal ($\mathcal{T}$) symmetry, particle-hole ($\mathcal{P}$) antisymmetry, and/or chiral ($\mathcal{C}$) antisymmetries.[1] These take the form[39]

$$\begin{aligned} H_d(\mathbf{k}) &= U_{\mathcal{T}}^\dagger H_d(-\mathbf{k})^* U_{\mathcal{T}}, \\ H_d(\mathbf{k}) &= -U_{\mathcal{P}}^\dagger H_d(-\mathbf{k})^* U_{\mathcal{P}}, \\ H_d(\mathbf{k}) &= -U_{\mathcal{C}}^\dagger H_d(\mathbf{k}) U_{\mathcal{C}}, \end{aligned} \tag{2.1}$$

where $U_{\mathcal{T}}$, $U_{\mathcal{P}}$, and $U_{\mathcal{C}}$ are $\mathbf{k}$-independent unitary matrices. If time-reversal symmetry and particle-hole symmetry are both present, $U_{\mathcal{C}} = U_{\mathcal{P}} U_{\mathcal{T}}^*$. Further, the unitary matrices $U_{\mathcal{T}}$, $U_{\mathcal{P}}$, and $U_{\mathcal{C}}$ satisfy $U_{\mathcal{T}} U_{\mathcal{T}}^* = \mathcal{T}^2$ and $U_{\mathcal{P}} U_{\mathcal{P}}^* = \mathcal{P}^2$ and we require that $U_{\mathcal{C}}^2 = \mathcal{C}^2 = 1$ and $U_{\mathcal{P}} U_{\mathcal{T}}^* = \mathcal{T}^2 \mathcal{P}^2 U_{\mathcal{T}} U_{\mathcal{P}}^*$. Throughout we use the symbols $\mathcal{T}^\pm$ and $\mathcal{P}^\pm$ to refer to a time-reversal symmetry or particle-hole antisymmetry squaring to one ($+$) or minus one ($-$). The ten Altland-Zirnbauer classes defined by the presence or absence of three non-spatial symmetry operations $\mathcal{T}$, $\mathcal{P}$, and $\mathcal{C}$ are separated in two "complex" classes, which do not have antiunitary symmetries or antisymmetries, and eight "real" classes, which have at least one antiunitary symmetry or antisymmetry. Following common practice in the field, we use Cartan labels to refer to the ten Altland-Zirnbauer symmetry classes, see Table 2.1 (see also Chapter 1).

In addition to the non-spatial (anti)symmetries $\mathcal{T}$, $\mathcal{P}$, and $\mathcal{C}$, the Hamiltonian $H_d(\mathbf{k})$ satisfies an order-two crystalline symmetry or antisymmetry. The "spatial type" of the symmetry operation is determined by number $d_\parallel$ of spatial degrees of freedom that are inverted: Mirror reflections have $d_\parallel = 1$, twofold rotations have $d_\parallel = 2$, and inversion has $d_\parallel = 3$. (In two dimensions, the spatial operations of inversion and twofold rotation are formally identical. We will refer to this operation as a twofold rotation.) We will use the symbol $\mathcal{S}$ to denote a general unitary order-two crystalline symmetry, replacing $\mathcal{S}$ by $\mathcal{M}$, $\mathcal{R}$, or $\mathcal{I}$ for considerations that apply specifically to mirror reflection, twofold rotation, or inversion symmetry, respectively. For a general antiunitary symmetry, antiunitary antisymmetry, and unitary antisymmetry we use the composite symbols $\mathcal{T}^\pm\mathcal{S}$, $\mathcal{P}^\pm\mathcal{S}$ and $\mathcal{C}\mathcal{S}$, respectively, again replacing $\mathcal{S}$ by $\mathcal{M}$, $\mathcal{R}$, $\mathcal{I}$ when appropriate. Without loss of generality we may require that the symmetry operation $\mathcal{S}$ squares to one.[2] Following Refs. 19–21, to further characterize the (anti)symmetry operation, we specify the signs $\eta_{\mathcal{T},\mathcal{P},\mathcal{C}}$ indicating whether it commutes ($\eta = +$) or anticommutes ($\eta = -$) with time-reversal $\mathcal{T}$, particle-hole conjugation $\mathcal{P}$, or the chiral operation $\mathcal{C}$.

[1] Although $\mathcal{P}$ and and $\mathcal{C}$ are commonly referred to as "particle-hole symmetry" and "chiral symmetry", we will refer to these as antisymmetries, because they connect H to $-H$, see Eq. (2.1).

[2] For spin 1/2 electrons often spatial symmetries squaring to -1 are used. Multiplication by i then gives a symmetry operation squaring to 1. Note, however, that multiplication with i turns a symmetry that commutes with $\mathcal{T}$ or $\mathcal{P}$ into a symmetry that anticommutes with $\mathcal{T}$ or $\mathcal{P}$ and vice versa.

AZ class	s	t	symmetry operations	representative
A	0	0	${}_{+}U$	$\mathcal{S}$
AIII	1	0	${}_{\alpha}U_{+}$	$\mathcal{S}_{+}$
A	0	1	${}_{-}U$	$\mathcal{CS}$
AIII	1	1	${}_{\alpha}U_{-}$	$\mathcal{S}_{-}$

TABLE 2.2. Shiozaki-Sato equivalence classes of unitary symmetry and antisymmetry operations for the Altland-Zirnbauer classes A and AIII. The symbol ${}_{\sigma}U_{\eta\mathcal{C}}$ is used to denote unitary symmetry ($\sigma = +$) and antisymmetry ($\sigma = -$) operations that commute ($\eta_{\mathcal{C}} = +$) or anticommute ($\eta_{\mathcal{C}} = -$) with the chiral symmetry, if applicable. The last column lists a unitary crystalline symmetry $\mathcal{S}_{\eta\mathcal{C}}$ or the product of a unitary symmetry operation $\mathcal{S}$ and the chiral operation $\mathcal{C}$ as a crystalline symmetry operation representative of the Shiozaki-Sato class (s,t).

Unitary symmetry and antisymmetry operations $\mathcal{S}$ and $\mathcal{CS}$ are represented by unitary matrices $U_{\mathcal{S}}$ and $U_{\mathcal{CS}}$ (with $\mathcal{S}$ being replaced by $\mathcal{M}$, $\mathcal{R}$, or $\mathcal{I}$ as needed), respectively, such that

$$\begin{aligned} &H_d(k_1,\dots,k_{d_\parallel},k_{d_\parallel+1},\dots,k_d)\\ &= U_{\mathcal{S}} H_d(-k_1,\dots,-k_{d_\parallel},k_{d_\parallel+1},\dots,k_d) U_{\mathcal{S}}^{-1}, \end{aligned} \tag{2.2}$$

if H_d satisfies a unitary symmetry, and

$$\begin{aligned} &H_d(k_1,\dots,k_{d_\parallel},k_{d_\parallel+1},\dots,k_d)\\ &= -U_{\mathcal{CS}} H_d(-k_1,\dots,-k_{d_\parallel},k_{d_\parallel+1},\dots,k_d) U_{\mathcal{CS}}^{-1}, \end{aligned} \tag{2.3}$$

if H_d satisfies a unitary antisymmetry. The matrices $U_{\mathcal{S}}$ and $U_{\mathcal{CS}}$ satisfy $U_{\mathcal{S},\mathcal{CS}}^2 = 1$, $U_{\mathcal{S},\mathcal{CS}} U_{\mathcal{T}} = \eta_{\mathcal{T}} U_{\mathcal{T}} U_{\mathcal{S},\mathcal{CS}}^*$, $U_{\mathcal{S},\mathcal{CS}} U_{\mathcal{P}} = \eta_{\mathcal{P}} U_{\mathcal{P}} U_{\mathcal{S},\mathcal{CS}}^*$, and $U_{\mathcal{S},\mathcal{CS}} U_{\mathcal{C}} = \eta_{\mathcal{C}} U_{\mathcal{C}} U_{\mathcal{S},\mathcal{CS}}$. Similarly, antiunitary symmetry and antisymmetry operations $\mathcal{T}^{\pm}\mathcal{S}$ and $\mathcal{P}^{\pm}\mathcal{S}$ are represented by unitary matrices $U_{\mathcal{TS}}$ and $U_{\mathcal{PS}}$, with

$$\begin{aligned} &H_d(k_1,\dots,k_{d_\parallel},k_{d_\parallel+1},\dots,k_d)\\ &= U_{\mathcal{TS}} H_d(k_1,\dots,k_{d_\parallel},-k_{d_\parallel+1},\dots,-k_d)^* U_{\mathcal{TS}}^{-1}, \end{aligned} \tag{2.4}$$

if H_d satisfies an antiunitary symmetry, and

$$\begin{aligned} &H_d(k_1,\dots,k_{d_\parallel},k_{d_\parallel+1},\dots,k_d)\\ &= -U_{\mathcal{PS}} H_d(k_1,\dots,k_{d_\parallel},-k_{d_\parallel+1},\dots,-k_d)^* U_{\mathcal{PS}}^{-1}, \end{aligned} \tag{2.5}$$

if H_d satisfies an antiunitary antisymmetry. The matrices $U_{\mathcal{TS}}$ and $U_{\mathcal{PS}}$ satisfy the conditions $U_{\mathcal{TS},\mathcal{PS}}^2 = \pm 1$, $U_{\mathcal{TS},\mathcal{PS}} U_{\mathcal{T}}^* = \eta_{\mathcal{T}} U_{\mathcal{T}} U_{\mathcal{TS},\mathcal{PS}}^*$, $U_{\mathcal{TS},\mathcal{PS}} U_{\mathcal{P}}^* = \eta_{\mathcal{P}} U_{\mathcal{P}} U_{\mathcal{TS},\mathcal{PS}}^*$, and $U_{\mathcal{TS},\mathcal{PS}} U_{\mathcal{C}}^* = \eta_{\mathcal{C}} U_{\mathcal{C}} U_{\mathcal{TS},\mathcal{PS}}$.

As pointed out in Ref. 19, the characterization of unitary and antiunitary symmetry and antisymmetry operations by means of the signs $\eta_{\mathcal{T},\mathcal{P},\mathcal{C}}$ and the square (in case of antiunitary symmetries) is partially redundant, because symmetry operations that are characterized differently may be mapped onto each other using non-spatial symmetries of the Hamiltonian H_d. For example, if a time-reversal symmetric Hamiltonian H_d satisfies a crystalline unitary symmetry $\mathcal{S}$, then it also satisfies the antiunitary symmetry $\mathcal{TS}$. Using such equivalences, Shiozaki and Sato group the (anti)symmetries into 44 "equivalence classes", which, together with the Altland-Zirnbauer class of Table 2.1, are labeled by one integer s or by two integers s and t. These equivalence classes are defined in Tables 2.2–2.4 for the complex Altland-Zirnbauer classes with unitary symmetries and antisymmetries, the complex Altland-Zirnbauer classes with antiunitary symmetries and antisymmetries, and the real Altland-Zirnbauer classes. For each of these Shiozaki-Sato classes, the tables also list a representative (anti)symmetry operation, consisting of a unitary symmetry $\mathcal{S}$ squaring to one or a product of a unitary symmetry and one of the fundamental non-spatial symmetry operations $\mathcal{T}$, $\mathcal{P}$, or $\mathcal{C}$, with indices $\eta_{\mathcal{T},\mathcal{P},\mathcal{C}}$ specifying the fundamental commutation or anticommutation relations with the non-spatial symmetries $\mathcal{T}$, $\mathcal{P}$, and $\mathcal{C}$, if present. We implicitly assume that (anti)symmetry operations $\mathcal{T}$, $\mathcal{P}$, and $\mathcal{C}$ used for the construction of the representative (anti)symmetry operation commute with the crystalline symmetry operation $\mathcal{S}$. With these assumptions, the indicated square of $\mathcal{T}$ and $\mathcal{P}$ (in Table 2.3) and the commutation relations of $\mathcal{S}$ with $\mathcal{C}$ (in Tables 2.2 and 2.3) or with $\mathcal{T}$ or $\mathcal{P}$ (in Table 2.4) fix the algebraic properties of the representative (anti)symmetry operations $\mathcal{TS}$, $\mathcal{PS}$, and $\mathcal{CS}$. [3]

Following this scheme, Shiozaki and Sato have classified all insulators and superconductors with a single crystalline order-two unitary or antiunitary symmetry or antisymmetry.[19] Central to the classification of Ref. 19 is a set of isomorphisms between the groups $K^{\mathbb{C}}(s,t|d_\parallel,d)$, $K^{\mathbb{C}}(s|d_\parallel,d)$, and $K^{\mathbb{R}}(s,t|d_\parallel,d)$ classifying d-dimensional Hamiltonians in the Shiozaki-Sato symmetry class (s,t) or s and with $d_\parallel$ inverted spatial dimensions (these isomorphisms are also discussed and utilized

AZ class	s	symmetry operations	representative
A	0	${}_{+}A^{+}$	$\mathcal{T}^{+}\mathcal{S}$
AIII	1	${}_{\alpha}A^{+}_{+}$	$\mathcal{T}^{+}\mathcal{S}_{+}$
A	2	${}_{-}A^{+}$	$\mathcal{P}^{+}\mathcal{S}$
AIII	3	${}_{\alpha}A^{-\alpha}_{-}$	$\mathcal{T}^{-}\mathcal{S}_{-}$
A	4	${}_{+}A^{-}$	$\mathcal{T}^{-}\mathcal{S}$
AIII	5	${}_{\alpha}A^{-}_{+}$	$\mathcal{T}^{-}\mathcal{S}_{+}$
A	6	${}_{-}A^{-}$	$\mathcal{P}^{-}\mathcal{S}$
AIII	7	${}_{\alpha}A^{\alpha}_{-}$	$\mathcal{T}^{+}\mathcal{S}_{-}$

TABLE 2.3. Shiozaki-Sato equivalence classes of antiunitary symmetry and antisymmetry operations for the Altland-Zirnbauer classes A and AIII. The symbol ${}_{\sigma}A^{\pm}_{\eta\mathcal{C}}$ is used to denote antiunitary symmetry ($\sigma = +$) and antisymmetry ($\sigma = -$) operations that commute ($\eta_{\mathcal{C}} = +$) or anticommute ($\eta_{\mathcal{C}} = -$) with the chiral symmetry, if applicable, and square to ± 1. The last column lists the product of a unitary crystalline symmetry $\mathcal{S}$ ($\mathcal{S}_{\eta\mathcal{C}}$ for class AIII) and time-reversal $\mathcal{T}^{\pm}$ or particle-hole conjugation $\mathcal{P}^{\pm}$ as a crystalline symmetry operation representative of the Shiozaki-Sato class (s,t).

[3] The algebraic relations of the symmetry operations define the factor system as introduced in Section 1.1 of Chapter 1.

AZ class	s	t	symmetry operation	representative
AI	0	0	${}_{+}U_{\alpha}^{\alpha},\ {}_{+}A_{\alpha}^{+}$	$\mathcal{S}_{+}$
BDI	1	0	${}_{\alpha}U_{\beta,\beta}^{\beta},\ {}_{\alpha}A_{\beta,\beta}^{+}$	$\mathcal{S}_{++}$
D	2	0	${}_{+}U_{\alpha}^{\alpha},\ {}_{-}A_{\alpha}^{+}$	$\mathcal{S}_{+}$
DIII	3	0	${}_{\alpha}U_{\beta,\beta}^{\alpha\beta},\ {}_{\alpha}A_{\beta,\beta}^{-\alpha}$	$\mathcal{S}_{++}$
AII	4	0	${}_{+}U_{\alpha}^{\alpha},\ {}_{+}A_{\alpha}^{-}$	$\mathcal{S}_{+}$
CII	5	0	${}_{\alpha}U_{\beta,\beta}^{\beta},\ {}_{\alpha}A_{\beta,\beta}^{-}$	$\mathcal{S}_{++}$
C	6	0	${}_{+}U_{\alpha}^{\alpha},\ {}_{-}A_{\alpha}^{-}$	$\mathcal{S}_{+}$
CI	7	0	${}_{\alpha}U_{\beta,\beta}^{\alpha\beta},\ {}_{\alpha}A_{\beta,\beta}^{\alpha}$	$\mathcal{S}_{++}$
AI	0	1	${}_{-}U_{-\alpha}^{\alpha},\ {}_{-}A_{\alpha}^{-}$	$\mathcal{CS}_{-}$
BDI	1	1	${}_{\alpha}U_{\beta,-\beta}^{\alpha\beta},\ {}_{\alpha}A_{\beta,-\beta}^{\alpha}$	$\mathcal{S}_{+-}$
D	2	1	${}_{-}U_{\alpha}^{\alpha},\ {}_{+}A_{\alpha}^{+}$	$\mathcal{CS}_{+}$
DIII	3	1	${}_{\alpha}U_{-\beta,\beta}^{\beta},\ {}_{\alpha}A_{\beta,-\beta}^{+}$	$\mathcal{S}_{-+}$
AII	4	1	${}_{-}U_{-\alpha}^{\alpha},\ {}_{-}A_{\alpha}^{+}$	$\mathcal{CS}_{-}$
CII	5	1	${}_{\alpha}U_{\beta,-\beta}^{\alpha\beta},\ {}_{\alpha}A_{\beta,-\beta}^{-\alpha}$	$\mathcal{S}_{+-}$
C	6	1	${}_{-}U_{\alpha}^{\alpha},\ {}_{+}A_{\alpha}^{-}$	$\mathcal{CS}_{+}$
CI	7	1	${}_{\alpha}U_{-\beta,\beta}^{\beta},\ {}_{\alpha}A_{\beta,-\beta}^{-}$	$\mathcal{S}_{-+}$
AI	0	2	${}_{+}U_{-\alpha}^{\alpha},\ {}_{+}A_{\alpha}^{-}$	$\mathcal{S}_{-}$
BDI	1	2	${}_{\alpha}U_{\beta,\beta}^{-\beta},\ {}_{\alpha}A_{\beta,\beta}^{-}$	$\mathcal{S}_{--}$
D	2	2	${}_{+}U_{-\alpha}^{\alpha},\ {}_{-}A_{\alpha}^{-}$	$\mathcal{S}_{-}$
DIII	3	2	${}_{\alpha}U_{\beta,\beta}^{-\alpha\beta},\ {}_{\alpha}A_{\beta,\beta}^{\alpha}$	$\mathcal{S}_{--}$
AII	4	2	${}_{+}U_{-\alpha}^{\alpha},\ {}_{+}A_{\alpha}^{+}$	$\mathcal{S}_{-}$
CII	5	2	${}_{\alpha}U_{\beta,\beta}^{-\beta},\ {}_{\alpha}A_{\beta,\beta}^{+}$	$\mathcal{S}_{--}$
C	6	2	${}_{+}U_{-\alpha}^{\alpha},\ {}_{-}A_{\alpha}^{+}$	$\mathcal{S}_{-}$
CI	7	2	${}_{\alpha}U_{\beta,\beta}^{-\alpha\beta},\ {}_{\alpha}A_{\beta,\beta}^{-\alpha}$	$\mathcal{S}_{--}$
AI	0	3	${}_{-}U_{\alpha}^{\alpha},\ {}_{-}A_{\alpha}^{+}$	$\mathcal{CS}_{+}$
BDI	1	3	${}_{\alpha}U_{-\beta,\beta}^{\alpha\beta},\ {}_{\alpha}A_{-\beta,\beta}^{-\alpha}$	$\mathcal{S}_{-+}$
D	2	3	${}_{-}U_{-\alpha}^{\alpha},\ {}_{+}A_{\alpha}^{-}$	$\mathcal{CS}_{-}$
DIII	3	3	${}_{\alpha}U_{\beta,-\beta}^{\beta},\ {}_{\alpha}A_{\beta,-\beta}^{-}$	$\mathcal{S}_{+-}$
AII	4	3	${}_{-}U_{\alpha}^{\alpha},\ {}_{-}A_{\alpha}^{-}$	$\mathcal{CS}_{+}$
CII	5	3	${}_{\alpha}U_{-\beta,\beta}^{\alpha\beta},\ {}_{\alpha}A_{-\beta,\beta}^{\alpha}$	$\mathcal{S}_{-+}$
C	6	3	${}_{-}U_{-\alpha}^{\alpha},\ {}_{+}A_{\alpha}^{+}$	$\mathcal{CS}_{-}$
CI	7	3	${}_{\alpha}U_{\beta,-\beta}^{\beta},\ {}_{\alpha}A_{\beta,-\beta}^{+}$	$\mathcal{S}_{+-}$

TABLE 2.4. Shiozaki-Sato equivalence classes of symmetry and antisymmetry operations for the eight real Altland-Zirnbauer classes. The symbols ${}_{\sigma}U_{\eta_{\mathcal{T}},\eta_{\mathcal{P}}}^{\pm}$ and ${}_{\sigma}A_{\eta_{\mathcal{T}},\eta_{\mathcal{P}}}^{\pm}$ are used to denote unitary symmetry (U, $\sigma=+$), unitary antisymmetry (U, $\sigma=-$), antiunitary symmetry (A, $\sigma=+$), and antiunitary antisymmetry (A, $\sigma=-$) operations that square to ±1 and commute ($\eta_{\mathcal{T},\mathcal{P}}=+$) or anticommute ($\eta_{\mathcal{T},\mathcal{P}}=-$) with time-reversal and particle-hole conjugation, if applicable. The last column lists a unitary crystalline symmetry $\mathcal{S}_{\eta_{\mathcal{T}},\eta_{\mathcal{P}}}$ or the product of a unitary crystalline symmetry and the chiral operation $\mathcal{C}$ as a representative of the equivalence class.

in Appendix B.1.4). For the complex Altland-Zirnbauer classes with unitary (anti)symmetry these isomorphisms are (with $d_\parallel < d$)

$$\begin{aligned} K^{\mathbb{C}}(s,t|d_\parallel,d) &= K^{\mathbb{C}}(s,t+1|d_\parallel+1,d) \\ &= K^{\mathbb{C}}(s-1,t|d_\parallel,d-1), \end{aligned} \tag{2.6}$$

with the integers s and t taken mod 2. For the complex Altland-Zirnbauer classes with antiunitary

class	s	t	$d=2$ $\mathcal{M}$	$d=2$ $\mathcal{R}$	$d=3$ $\mathcal{M}$	$d=3$ $\mathcal{R}$	$d=3$ $\mathcal{I}$
$\mathrm{A}^{\mathcal{S}}$	0	0	0	$\mathbb{Z}^2\,(\mathbb{Z})$	$\mathbb{Z}$	0	$\mathbb{Z}$
$\mathrm{AIII}^{\mathcal{S}_+}$	1	0	$\mathbb{Z}$	0	0	$\mathbb{Z}^2\,(\mathbb{Z})$	0
$\mathrm{A}^{\mathcal{CS}}$	0	1	$\mathbb{Z}^2\,(\mathbb{Z})$	0	0	$\mathbb{Z}$	0
$\mathrm{AIII}^{\mathcal{S}_-}$	1	1	0	$\mathbb{Z}$	$\mathbb{Z}^2\,(\mathbb{Z})$	0	$\mathbb{Z}^2\,(\mathbb{Z})$

TABLE 2.5. Classification of topological crystalline phases with an order-two crystalline symmetry or antisymmetry for the complex Altland-Zirnbauer classes, based on Ref. 19. The symbols $\mathcal{M}$, $\mathcal{R}$, and $\mathcal{I}$ refer to mirror reflection ($d_\parallel=1$), twofold rotation ($d_\parallel=2$), and inversion ($d_\parallel=d=3$), respectively. The entries in brackets give the purely crystalline component $K'^{\mathbb{C}}(s,t|d_\parallel,d)$ if different from the full group $K^{\mathbb{C}}(s,t|d_\parallel,d)$.

(anti)symmetry the isomorphisms read

$$\begin{aligned} K^{\mathbb{C}}(s|d_\parallel,d) &= K^{\mathbb{C}}(s-2|d_\parallel+1,d) \\ &= K^{\mathbb{C}}(s-1|d_\parallel,d-1), \end{aligned} \tag{2.7}$$

where the label s is taken mod 8. Finally, the isomorphisms for the real Altland-Zirnbauer classes are

$$\begin{aligned} K^{\mathbb{R}}(s,t|d_\parallel,d) &= K^{\mathbb{R}}(s,t+1|d_\parallel+1,d) \\ &= K^{\mathbb{R}}(s-1,t|d_\parallel,d-1), \end{aligned} \tag{2.8}$$

where the integers s and t are taken mod 8 and mod 4, respectively. When applied repeatedly, these isomorphisms can be used to relate the classification problem of d-dimensional Hamiltonians with an order-two crystalline symmetry to a zero-dimensional classification problem, which can be solved with elementary methods. The Shiozaki-Sato classification for two and three dimensional crystals with a mirror reflection $\mathcal{M}$, twofold rotation $\mathcal{R}$, or inversion symmetry $\mathcal{I}$ is summarized in tables 2.5-2.7. The corresponding classifying groups for complex and real Altland-Zirnbauer classes without crystalline symmetries are denoted $K^{\mathbb{C}}(s,d)$ and $K^{\mathbb{R}}(s,d)$, respectively. Since they are well known[15–17, 42–45] we do not list them here explicitly; if needed, they can be inferred from Table 2.1, which lists $K(s,d-1)$ for $d=2$ and $d=3$.

Some of the topological crystalline phases remain topologically nontrivial if the crystalline symmetry is broken. These are strong topological insulators or superconductors, which have gapless states at all boundaries, not only at boundaries that are invariant under the symmetry operation. The remaining "purely crystalline" topological phases, which become trivial if the crystalline symmetry is broken, are classified by a subgroup of the classifying groups $K^{\mathbb{C}}(s,t|d_\parallel,d)$, $K^{\mathbb{C}}(s|d_\parallel,d)$, and $K^{\mathbb{R}}(s,t|d_\parallel,d)$, which we denote $K'^{\mathbb{C}}(s,t|d_\parallel,d)$, $K'^{\mathbb{C}}(s|d_\parallel,d)$, and $K'^{\mathbb{R}}(s,t|d_\parallel,d)$, respectively. The quotient groups $K(s,t|d_\parallel,d)/K'(s,t|d_\parallel,d)$, which are subgroups of the classifying groups $K(s,d)$ without crystalline symmetries, classify the strong topological phases that are compatible with the crystalline symmetry. Tables 2.5–2.7 also list the groups $K'^{\mathbb{C}}$ and $K'^{\mathbb{R}}$ between

class	s	$d=2$ $\mathcal{M}$	$d=2$ $\mathcal{R}$	$d=3$ $\mathcal{M}$	$d=3$ $\mathcal{R}$	$d=3$ $\mathcal{I}$
$\mathrm{A}^{\mathcal{T}^+\mathcal{S}}$	0	$\mathbb{Z}\,(0)$	$\mathbb{Z}_2$	0	$\mathbb{Z}_2$	0
$\mathrm{AIII}^{\mathcal{T}^+\mathcal{S}_+}$	1	$\mathbb{Z}_2$	0	$\mathbb{Z}\,(0)$	$\mathbb{Z}_2$	$2\mathbb{Z}\,(0)$
$\mathrm{A}^{\mathcal{P}^+\mathcal{S}}$	2	$\mathbb{Z}_2$	$2\mathbb{Z}\,(0)$	$\mathbb{Z}_2$	0	0
$\mathrm{AIII}^{\mathcal{T}^-\mathcal{S}_-}$	3	0	0	$\mathbb{Z}_2$	$2\mathbb{Z}\,(0)$	0
$\mathrm{A}^{\mathcal{T}^-\mathcal{S}}$	4	$2\mathbb{Z}\,(0)$	0	0	0	0
$\mathrm{AIII}^{\mathcal{T}^-\mathcal{S}_+}$	5	0	0	$2\mathbb{Z}\,(0)$	0	$\mathbb{Z}\,(0)$
$\mathrm{A}^{\mathcal{P}^-\mathcal{S}}$	6	0	$\mathbb{Z}\,(0)$	0	0	$\mathbb{Z}_2$
$\mathrm{AIII}^{\mathcal{T}^+\mathcal{S}_-}$	7	0	$\mathbb{Z}_2$	0	$\mathbb{Z}\,(0)$	$\mathbb{Z}_2$

TABLE 2.6. Classification of topological crystalline phases with an order-two antiunitary crystalline symmetry or antisymmetry for the complex Altland-Zirnbauer classes, based on Ref. 19. The symbols $\mathcal{M}$, $\mathcal{R}$, and $\mathcal{I}$ refer to mirror reflection ($d_\parallel = 1$), twofold rotation ($d_\parallel = 2$), and inversion ($d_\parallel = d = 3$), respectively. The entries in brackets give the purely crystalline component $K'^{\mathbb{C}}(s|d_\parallel, d)$ if different from the full group $K^{\mathbb{C}}(s|d_\parallel, d)$.

brackets if they are different from the full classifying groups $K^{\mathbb{C}}$ and $K^{\mathbb{R}}$. The "purely crystalline" subgroups are evaluated in Sec. 2.4 2 and App. A.3.

The Shiozaki-Sato classification of topological crystalline insulators and superconductors with an order-two crystalline symmetry,[19] as well as the preceding complete classifications of mirror-symmetric topological insulators and superconductors,[20, 21] is a "strong" classification, in the sense that it addresses topological features that are robust to a resizing of the unit cell, allowing the addition of perturbations that break the translation symmetry of the original (smaller) unit cell, while preserving the crystalline symmetries. Reference 19 argues that for such a strong classification it is sufficient to classify Hamiltonians $H_d(\mathbf{k})$ with argument $\mathbf{k}$ defined on a sphere, rather than on a Brillouin zone of a shape determined by the underlying Bravais lattice. The construction and classification of second-order topological insulators and superconductors that we pursue here also follows the paradigm of a strong classification scheme. Since boundaries play an essential role when considering second-order topological phases, we will not deform the Brillouin zone into a sphere, as in Ref. 19, but instead use the freedom offered by the possibility to resize the unit cell to restrict ourselves to rectangular Bravais lattice with mirror plane and rotation axes aligned with the coordinate axes. This is consistent with the mathematical form of the symmetry operations given in Eqs. (2.2)–(2.5) above.

2.3. DIMENSIONAL REDUCTION

The dimension-raising and lowering isomorphisms devised by Shiozaki and Sato apply to Hamiltonians with argument $\mathbf{k}$ defined on a sphere, [19] rather than on a

class	s	t	$d=2$ $\mathcal{M}$	$d=2$ $\mathcal{R}$	$d=3$ $\mathcal{M}$	$d=3$ $\mathcal{R}$	$d=3$ $\mathcal{I}$
$\mathrm{AI}^{\mathcal{S}_+}$	0	0	0	$2\mathbb{Z}$	0	0	$2\mathbb{Z}$
$\mathrm{BDI}^{\mathcal{S}_{++}}$	1	0	$\mathbb{Z}$	0	0	$2\mathbb{Z}$	0
$\mathrm{D}^{\mathcal{S}_+}$	2	0	$\mathbb{Z}_2$	$\mathbb{Z}\,(0)$	$\mathbb{Z}$	0	0
$\mathrm{DIII}^{\mathcal{S}_{++}}$	3	0	$\mathbb{Z}_2$	0	$\mathbb{Z}_2$	$\mathbb{Z}\,(0)$	0
$\mathrm{AII}^{\mathcal{S}_+}$	4	0	0	$2\mathbb{Z}\,(4\mathbb{Z})$	$\mathbb{Z}_2$	0	$\mathbb{Z}\,(2\mathbb{Z})$
$\mathrm{CII}^{\mathcal{S}_{++}}$	5	0	$2\mathbb{Z}$	0	0	$2\mathbb{Z}\,(4\mathbb{Z})$	$\mathbb{Z}_2\,(0)$
$\mathrm{C}^{\mathcal{S}_+}$	6	0	0	$\mathbb{Z}\,(0)$	$2\mathbb{Z}$	0	$\mathbb{Z}_2$
$\mathrm{CI}^{\mathcal{S}_{++}}$	7	0	0	0	0	$\mathbb{Z}\,(0)$	0
$\mathrm{AI}^{\mathcal{CS}_-}$	0	1	0	0	0	0	0
$\mathrm{BDI}^{\mathcal{S}_{+-}}$	1	1	0	$\mathbb{Z}$	0	0	$2\mathbb{Z}$
$\mathrm{D}^{\mathcal{CS}_+}$	2	1	$\mathbb{Z}^2\,(\mathbb{Z})$	$\mathbb{Z}_2$	0	$\mathbb{Z}$	0
$\mathrm{DIII}^{\mathcal{S}_{-+}}$	3	1	$\mathbb{Z}_2^2\,(\mathbb{Z}_2)$	$\mathbb{Z}_2$	$\mathbb{Z}^2\,(\mathbb{Z})$	$\mathbb{Z}_2$	$\mathbb{Z}\,(0)$
$\mathrm{AII}^{\mathcal{CS}_-}$	4	1	$\mathbb{Z}_2^2\,(\mathbb{Z}_2)$	0	$\mathbb{Z}_2^2\,(\mathbb{Z}_2)$	$\mathbb{Z}_2$	0
$\mathrm{CII}^{\mathcal{S}_{+-}}$	5	1	0	$2\mathbb{Z}$	$\mathbb{Z}_2^2\,(\mathbb{Z}_2)$	0	$2\mathbb{Z}\,(4\mathbb{Z})$
$\mathrm{C}^{\mathcal{CS}_+}$	6	1	$2\mathbb{Z}^2\,(2\mathbb{Z})$	0	0	$2\mathbb{Z}$	0
$\mathrm{CI}^{\mathcal{S}_{-+}}$	7	1	0	0	$2\mathbb{Z}^2\,(2\mathbb{Z})$	0	$\mathbb{Z}\,(0)$
$\mathrm{AI}^{\mathcal{S}_-}$	0	2	0	0	$2\mathbb{Z}$	0	0
$\mathrm{BDI}^{\mathcal{S}_{--}}$	1	2	0	0	0	0	0
$\mathrm{D}^{\mathcal{S}_-}$	2	2	0	$\mathbb{Z}^2\,(\mathbb{Z})$	0	0	$\mathbb{Z}$
$\mathrm{DIII}^{\mathcal{S}_{--}}$	3	2	$\mathbb{Z}\,(2\mathbb{Z})$	$\mathbb{Z}_2^2\,(\mathbb{Z}_2)$	0	$\mathbb{Z}^2\,(\mathbb{Z})$	$\mathbb{Z}_2$
$\mathrm{AII}^{\mathcal{S}_-}$	4	2	$\mathbb{Z}_2\,(0)$	$\mathbb{Z}_2^2\,(\mathbb{Z}_2)$	$\mathbb{Z}\,(2\mathbb{Z})$	$\mathbb{Z}_2^2\,(\mathbb{Z}_2)$	$\mathbb{Z}_2$
$\mathrm{CII}^{\mathcal{S}_{--}}$	5	2	$\mathbb{Z}_2$	0	$\mathbb{Z}_2\,(0)$	$\mathbb{Z}_2^2\,(\mathbb{Z}_2)$	0
$\mathrm{C}^{\mathcal{S}_-}$	6	2	0	$2\mathbb{Z}^2\,(2\mathbb{Z})$	$\mathbb{Z}_2$	0	$2\mathbb{Z}$
$\mathrm{CI}^{\mathcal{S}_{--}}$	7	2	$2\mathbb{Z}$	0	0	$2\mathbb{Z}^2\,(2\mathbb{Z})$	0
$\mathrm{AI}^{\mathcal{CS}_+}$	0	3	$2\mathbb{Z}$	0	0	$2\mathbb{Z}$	0
$\mathrm{BDI}^{\mathcal{S}_{-+}}$	1	3	0	0	$2\mathbb{Z}$	0	0
$\mathrm{D}^{\mathcal{CS}_-}$	2	3	$\mathbb{Z}\,(0)$	0	0	0	0
$\mathrm{DIII}^{\mathcal{S}_{+-}}$	3	3	0	$\mathbb{Z}\,(2\mathbb{Z})$	$\mathbb{Z}\,(0)$	0	$\mathbb{Z}^2\,(\mathbb{Z})$
$\mathrm{AII}^{\mathcal{CS}_+}$	4	3	$2\mathbb{Z}\,(4\mathbb{Z})$	$\mathbb{Z}_2\,(0)$	0	$\mathbb{Z}\,(2\mathbb{Z})$	$\mathbb{Z}_2^2\,(\mathbb{Z}_2)$
$\mathrm{CII}^{\mathcal{S}_{-+}}$	5	3	0	$\mathbb{Z}_2$	$2\mathbb{Z}\,(4\mathbb{Z})$	$\mathbb{Z}_2\,(0)$	$\mathbb{Z}_2^2\,(\mathbb{Z}_2)$
$\mathrm{C}^{\mathcal{CS}_-}$	6	3	$\mathbb{Z}\,(0)$	0	0	$\mathbb{Z}_2$	0
$\mathrm{CI}^{\mathcal{S}_{+-}}$	7	3	0	$2\mathbb{Z}$	$\mathbb{Z}\,(0)$	0	$2\mathbb{Z}^2\,(2\mathbb{Z})$

TABLE 2.7. Classification of topological crystalline phases with an order-two crystalline symmetry or antisymmetry for the real Altland-Zirnbauer classes, based on Ref. 19. The symbols $\mathcal{M}$, $\mathcal{R}$, and $\mathcal{I}$ refer to mirror reflection ($d_\parallel = 1$), twofold rotation ($d_\parallel = 2$), and inversion ($d_\parallel = d = 3$), respectively. The entries in brackets give the purely crystalline component $K'^{\mathbb{R}}(s, t|d_\parallel, d)$ if different from the full group $K^{\mathbb{R}}(s, t|d_\parallel, d)$.

torus, which complicates a direct application to crystals with boundaries and corners. For that reason, we here make use of an alternative dimension-lowering map, which maps a Shiozaki-Sato class with index s in d dimensions to a Shiozaki-Sato class with index $s-1$ in $d-1$ dimensions, while preserving the second Shiozaki-Sato index t and the number of inverted dimensions $d_\parallel$. Our dimension-lowering map is a generalization of a map first proposed by Fulga *et al.* for the standard Altland-Zirnbauer classes,[46] and recently extended to mirror-reflection-symmetric models by two of us.[22] Though not as powerful as the isomorphisms of Ref. 19, which also relate symmetry classes with different $d_\parallel$, this map is sufficient for the purpose of determining the conditions under which a nontrivial bulk crystalline phase implies the exis-

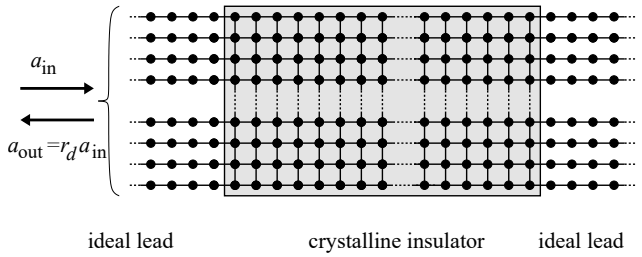

FIG. 2.3. Schematic picture of a lattice model for a crystalline insulator in a two-terminal scattering geometry. The reflection matrix r_d relates the amplitudes a_{in} and a_{out} of incident and reflected waves as shown in the figure. The ideal leads are modeled as a grid of parallel one-dimensional chains, which endows the reflection matrix r_d with a real-space structure.

tence of zero-energy corner states (for a two-dimensional crystal) or gapless hinge modes (for a three-dimensional crystal).

The dimension-lowering procedure starts from the calculation of the reflection matrix r_d for a d-dimensional Hamiltonian H_d embedded in a two-terminal scattering geometry. Following Ref. 46 the reflection matrix is reinterpreted as a Hamiltonian H_{d-1} in $d-1$ dimensions, but with a symmetry class that is different from that of the original Hamiltonian H_d. This reinterpretation is different for Hamiltonians H_d with and without chiral antisymmetry. If H_d has a chiral antisymmetry, one can choose a basis of scattering states such that r_d is a hermitian matrix, allowing the definition of a Hamiltonian H_{d-1} *without* chiral antisymmetry as

$$H_{d-1} = r_d. \tag{2.9}$$

On the other hand, if H_d has no chiral antisymmetry, Fulga *et al.* set

$$H_{d-1} = \begin{pmatrix} 0 & r_d \\ r_d^\dagger & 0 \end{pmatrix}, \tag{2.10}$$

which has a chiral antisymmetry with $U_{\mathcal{C}} = \text{diag}\,(1,-1)$. A more detailed review of the reflection-matrix based dimensional reduction scheme is given in App. A.1. In the appendix we also show that if H_d has a crystalline symmetry or antisymmetry of Shiozaki-Sato class (s,t) with $d_\parallel < d$ then H_{d-1} has a crystalline symmetry of class $(s-1,t)$ with the same value of $d_\parallel$. (This was shown in Ref. 22 for unitary mirror symmetries and antisymmetries with $d_\parallel = 1$.)

Although Refs. 22 and 46 apply the reflection-matrix-based reduction scheme to Hamiltonians with periodic boundary conditions, the mapping of Eqs. (2.9) and (2.10) can also be used in a real-space formulation, where it can be applied to crystals with boundaries. In particular, the mapping of Eqs. (2.9) and (2.10) maps d'-dimensional protected boundary modes of H_d to $d'-1$-dimensional boundary modes of H_{d-1} for all $1 \leq d' < d$, thus not only providing a link between regular first-order topological insulators and superconductors in different dimensions, but also between second-order topological insulators and superconductors.

To show how this works explicitly, we consider a d-dimensional crystalline insulator or superconductor, embedded in a two-terminal scattering geometry and of finite size in the transverse directions, as shown schematically in Fig. 2.3 for a two-dimensional lattice model. We then calculate the reflection matrix $r_d(\mathbf{r}_\perp, \mathbf{r}'_\perp)$ for an ideal lead consisting of a grid of one-dimensional chains at discrete coordinates $\mathbf{r}_\perp$ in the transverse direction, see Fig. 2.3, and construct a hermitian lattice Hamiltonian $H_{d-1}(\mathbf{r}_\perp, \mathbf{r}'_\perp)$ using the mapping of Eqs. (2.9) and (2.10). Since it is derived from a reflection matrix r_d for a lead with a finite $(d-1)$-dimensional cross section and open boundary conditions in the transverse direction, H_{d-1} also describes a $(d-1)$-dimensional system of finite size and open boundary conditions. For a crystalline insulator or superconductor of finite width, the existence of gapless modes along the sample boundary implies the existence of perfectly transmitted modes along sample boundaries (in case of a first-order topological insulator or superconductor) or hinges (for a second-order topological insulator or superconductor). Since the total scattering matrix, describing reflection *and* transmission, is unitary, any such perfectly transmitted modes correspond to a zero singular value of the reflection matrix $r_d(\mathbf{r}_\perp, \mathbf{r}'_\perp)$ and, hence, to a zero-energy eigenstate of H_{d-1}. Since these gapless modes derive from transmitted modes proceeding along the sample boundary, their eigenvectors have support near the lead's boundaries (if H_d is a first-order topological insulator) or the intersection of two of the lead's boundaries (if H_d is a second-order topological insulator), so that they represent true boundary/corner/hinge modes of H_{d-1}.

As an example, we consider a Chern insulator in two dimensions and a second-order Chern insulator in three dimensions, shown schematically in Fig. 2.4. In both cases, the corresponding Altland-Zirnbauer class is Cartan class A. The two-dimensional Chern insulator has chiral modes propagating along the sample's edges, see Fig. 2.4 (left). When the Chern insulator is embedded in a two-terminal scattering geometry, the presence of the edge modes leads to perfectly transmitted modes or, equivalently, to zero singular values of the reflection matrix r_d. The left and right eigenvectors corresponding to this zero mode, which build the corresponding eigenvectors of the Hamiltonian H_{d-1} calculated via Eq. (2.10), are localized near the lead edges. Similarly, a three-dimensional second-order Chern insulator has chiral hinge modes, as shown schematically in Fig. 2.4 (right). Again, when embedded in a scattering geometry, the presence of the hinge modes leads to perfectly transmitted modes and, hence, zero singular values of the reflection matrix r_d. The support of the corresponding left and right eigenvectors is near the lead hinges that are connected to the sample hinges carrying the chiral modes. Correspondingly, the Hamiltonian H_{d-1} obtained from the dimensional reduction scheme

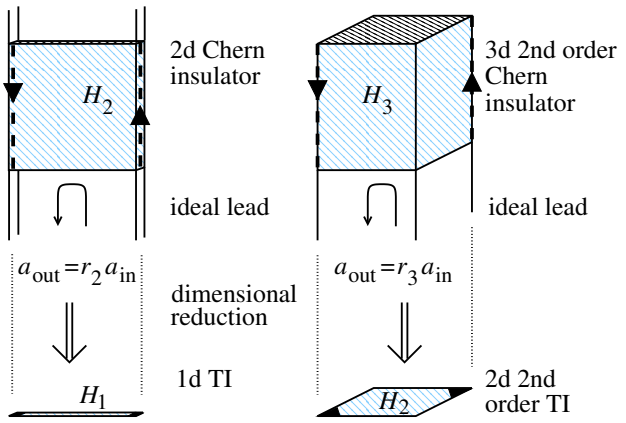

FIG. 2.4. Comparison of the reflection-matrix-based dimensional reduction scheme applied to a two-dimensional Chern insulator (left) and a three-dimensional second-order Chern insulator. In each case a lower-dimensional Hamiltonian can be constructed out of the reflection matrix r_d describing scattering from a half-infinite crystal coupled to an ideal lead. Upon constructing the lower-dimensional Hamiltonian H_{d-1}, the chiral edge states (left) and hinge states (right) map to protected zero-energy eigenstates localized near ends (left) or corners (right).

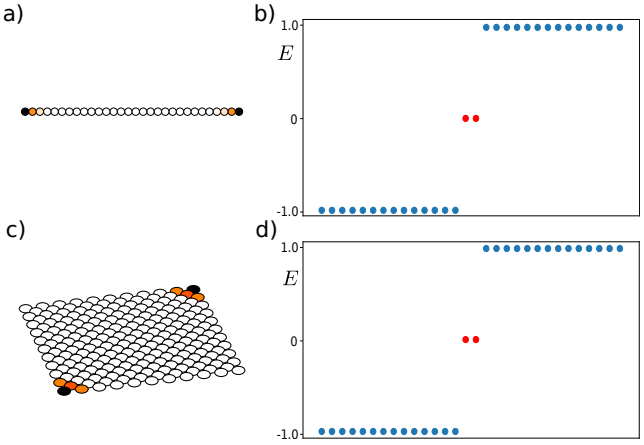

FIG. 2.5. Support of the zero-energy eigenstates (a) and 30 lowest energies of the spectrum (b) of the mapped Hamiltonian H_1 for a two-dimensional Chern insulator with Hamiltonian H_2 given in Eq. (2.11), following the reflection-matrix-based dimensional reduction scheme. Panels (c) and (d) show the same for the mapped Hamiltonian H_2 for the three-dimensional second-order Chern insulator with Hamiltonian H_3 of Eq. (2.12) with $b = 0.4$.

has zero-energy eigenstates at sample corners. Hence, H_{d-1} is a second-order topological insulator.

A numerical simulation of this scenario is shown in Fig. 2.5. The dimensional reduction scheme has been applied to a two-dimensional lattice model with Hamiltonian

$$H = (m + 2 - \cos k_1 - \cos k_2)\sigma_1 + \sin k_1 \sigma_2 + \sin k_2 \sigma_3, \tag{2.11}$$

which describes a two-dimensional Chern insulator for $-2 < m < 0$, and to a lattice model of a three-dimensional second-order Chern insulator,[4, 9] which has Hamiltonian

$$\begin{aligned} H_3 = (m + 3 - \cos k_1 - \cos k_2 - \cos k_3)\tau_1\sigma_1 \\ + \tau_1\sigma_3 \sin k_1 + \tau_2 \sin k_2 + \tau_3 \sin k_3 + b\tau_1 \end{aligned} \tag{2.12}$$

with $-2 < m < 0$ and b numerically small. In both models, the σ_j and τ_j are Pauli matrices acting on different spinor degrees of freedom. Figure 2.5 shows the spectra of the mapped Hamiltonians H_{d-1} (Fig. 2.5b and d), calculated using the Kwant software package,[47] as well as the support of the zero-energy eigenstates (c and d). Consistent with the scenario laid out above, the spectra are gapped up to two zero eigenvalues, which have support at the ends of the mapped one-dimensional chain (Fig. 2.5a) and at mirror-reflection-symmetric corners (Fig. 2.5c).

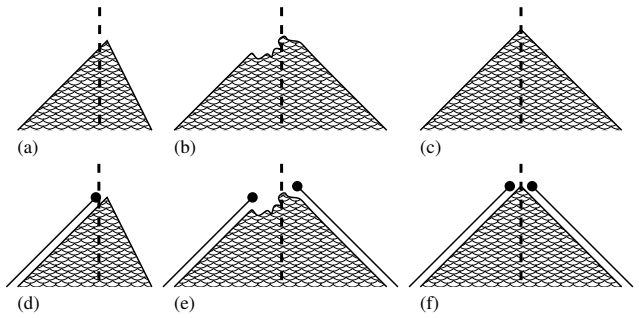

FIG. 2.6. Schematic picture of a generic corner (a), a mirror-symmetric corner with locally broken mirror symmetry (b), and a mirror-symmetric corner in a crystal with a bulk mirror symmetry. Panels (d)–(f) represent the possibility to add zero-energy corner states by changing the lattice termination. Effectively, this amounts to the addition of one-dimensional topological insulators or superconductors to the boundaries. At a generic corner, it is possible to change the termination of only one boundary, as shown in panel (d). In a symmetric corner, such a change in termination needs to be applied to both symmetry-related boundaries, shown schematically in panels (e) and (f) for a corner with and without a perturbation that locally breaks the mirror symmetry.

2.4. MIRROR REFLECTION-SYMMETRIC SECOND-ORDER TOPOLOGICAL INSULATORS AND SUPERCONDUCTORS

2.4.1. Classification of mirror-symmetric corners and hinges

We now proceed with the classification of zero-energy states at mirror-symmetric corners and gapless hinge modes at mirror-symmetric hinges of a mirror-symmetric

AZ class	s	t	$d=2$	$d=3$
$\mathrm{A}^{\mathcal{M}}$	0	0	-	$\mathbb{Z},\mathbb{Z}_2\,(\mathbb{Z}^2,\mathbb{Z})$
$\mathrm{AIII}^{\mathcal{M}_+}$	1	0	$\mathbb{Z},\mathbb{Z}_2\,(\mathbb{Z}^2,\mathbb{Z})$	-
$\mathrm{A}^{\mathcal{CM}}$	0	1	$\mathbb{Z},0\,(\mathbb{Z},0)$	-
$\mathrm{AIII}^{\mathcal{M}_-}$	1	1	-	$\mathbb{Z},0\,(\mathbb{Z},0)$

TABLE 2.8. Classification of mirror-symmetric corners ($d=2$) or hinges ($d=3$) of second-order topological insulators and superconductors in the complex Altland-Zirnbauer classes with unitary symmetries or antisymmetries. The first two entries in the fourth and fifth column give the intrinsic, termination-independent, classification without and with perturbations that locally break mirror symmetry at the corner or hinge. The entries between brackets give the corresponding extrinsic, termination-dependent classification. The ordering is $\mathcal{K}_{\mathrm{i}},\bar{\mathcal{K}}_{\mathrm{i}}(\mathcal{K}_{\mathrm{e}},\bar{\mathcal{K}}_{\mathrm{e}})$.

AZ class	s	$d=2$	$d=3$
$\mathrm{A}^{\mathcal{T}^+\mathcal{M}}$	0	-	-
$\mathrm{AIII}^{\mathcal{T}^+\mathcal{M}_+}$	1	$\mathbb{Z}_2,\mathbb{Z}_2\,(\mathbb{Z},\mathbb{Z})$	-
$\mathrm{A}^{\mathcal{P}^+\mathcal{M}}$	2	$\mathbb{Z}_2,0\,(\mathbb{Z}_2,0)$	$\mathbb{Z}_2,\mathbb{Z}_2\,(\mathbb{Z},\mathbb{Z})$
$\mathrm{AIII}^{\mathcal{T}^-\mathcal{M}_-}$	3	$0,0\,(\mathbb{Z}_2,0)$	$\mathbb{Z}_2,0\,(\mathbb{Z}_2,0)$
$\mathrm{A}^{\mathcal{T}^-\mathcal{M}}$	4	-	$0,0\,(\mathbb{Z}_2,0)$
$\mathrm{AIII}^{\mathcal{T}^-\mathcal{M}_+}$	5	$0,0\,(2\mathbb{Z},2\mathbb{Z})$	-
$\mathrm{A}^{\mathcal{P}^-\mathcal{M}}$	6	-	$0,0\,(2\mathbb{Z},2\mathbb{Z})$
$\mathrm{AIII}^{\mathcal{T}^+\mathcal{M}_-}$	7	-	-

TABLE 2.9. Classification of mirror-symmetric corners ($d=2$) or hinges ($d=3$) of second-order topological insulators and superconductors in the complex Altland-Zirnbauer classes with antiunitary symmetries or antisymmetries. The ordering is $\mathcal{K}_{\mathrm{i}},\bar{\mathcal{K}}_{\mathrm{i}}(\mathcal{K}_{\mathrm{e}},\bar{\mathcal{K}}_{\mathrm{e}})$.

crystalline insulator or superconductor. As explained in the introduction, such a classification depends on the possible presence of local mirror-symmetry-breaking perturbations at corners or hinges, and on whether it is an "intrinsic" (termination-independent) classification or an "extrinsic" (termination-dependent) one. We recall that we term a classification intrinsic if it is invariant under a change of lattice termination, as long as the mirror symmetry of the corner or hinge is preserved, and extrinsic if it depends on termination. The intrinsic classification describes properties of the bulk lattice, which is why it is closely related to the classification of bulk topological crystalline phases, as we discuss below. Although the extrinsic classification is termination dependent, it is important to point out that the extrinsic classification remains valid in the presence of perturbations that do not close the boundary gap, such as weak disorder. Figure 2.6 schematically shows the four classification rules that follow from the options discussed above for the case of a two-dimensional mirror-symmetric crystal, and contrasts these with the classification of a generic corner discussed in the Introduction.

We denote the classifying groups for corners according to the four possible classification rules that arise from

class	s	t	$d=2$	$d=3$
$\mathrm{AI}^{\mathcal{M}_+}$	0	0	-	-
$\mathrm{BDI}^{\mathcal{M}_{++}}$	1	0	$\mathbb{Z},\mathbb{Z}_2\,(\mathbb{Z}^2,\mathbb{Z})$	-
$\mathrm{D}^{\mathcal{M}_+}$	2	0	$\mathbb{Z}_2,\mathbb{Z}_2\,(\mathbb{Z}_2^2,\mathbb{Z}_2)$	$\mathbb{Z},\mathbb{Z}_2\,(\mathbb{Z}^2,\mathbb{Z})$
$\mathrm{DIII}^{\mathcal{M}_{++}}$	3	0	$\mathbb{Z}_2,\mathbb{Z}_2\,(\mathbb{Z}_2^2,\mathbb{Z}_2)$	$\mathbb{Z}_2,\mathbb{Z}_2\,(\mathbb{Z}_2^2,\mathbb{Z}_2)$
$\mathrm{AII}^{\mathcal{M}_+}$	4	0	-	$\mathbb{Z}_2,\mathbb{Z}_2\,(\mathbb{Z}_2^2,\mathbb{Z}_2)$
$\mathrm{CII}^{\mathcal{M}_{++}}$	5	0	$2\mathbb{Z},\mathbb{Z}_2\,(2\mathbb{Z}^2,2\mathbb{Z})$	-
$\mathrm{C}^{\mathcal{M}_+}$	6	0	-	$2\mathbb{Z},\mathbb{Z}_2\,(2\mathbb{Z}^2,2\mathbb{Z})$
$\mathrm{CI}^{\mathcal{M}_{++}}$	7	0	-	-
$\mathrm{AI}^{\mathcal{CM}_-}$	0	1	-	-
$\mathrm{BDI}^{\mathcal{M}_{+-}}$	1	1	-	-
$\mathrm{D}^{\mathcal{CM}_+}$	2	1	$\mathbb{Z},\mathbb{Z}_2\,(\mathbb{Z},\mathbb{Z}_2)$	-
$\mathrm{DIII}^{\mathcal{M}_{-+}}$	3	1	$\mathbb{Z}_2,\mathbb{Z}_2\,(\mathbb{Z}_2,\mathbb{Z}_2)$	$\mathbb{Z},\mathbb{Z}_2\,(\mathbb{Z},\mathbb{Z}_2)$
$\mathrm{AII}^{\mathcal{CM}_-}$	4	1	$\mathbb{Z}_2,0\,(\mathbb{Z}_2,0)$	$\mathbb{Z}_2,\mathbb{Z}_2\,(\mathbb{Z}_2,\mathbb{Z}_2)$
$\mathrm{CII}^{\mathcal{M}_{+-}}$	5	1	-	$\mathbb{Z}_2,0\,(\mathbb{Z}_2,0)$
$\mathrm{C}^{\mathcal{CM}_+}$	6	1	$2\mathbb{Z},0\,(2\mathbb{Z},0)$	-
$\mathrm{CI}^{\mathcal{M}_{-+}}$	7	1	-	$2\mathbb{Z},0\,(2\mathbb{Z},0)$
$\mathrm{AI}^{\mathcal{M}_-}$	0	2	-	$2\mathbb{Z},0\,(2\mathbb{Z},0)$
$\mathrm{BDI}^{\mathcal{M}_{--}}$	1	2	$0,0\,(2\mathbb{Z},2\mathbb{Z})$	-
$\mathrm{D}^{\mathcal{M}_-}$	2	2	-	$0,0\,(2\mathbb{Z},2\mathbb{Z})$
$\mathrm{DIII}^{\mathcal{M}_{--}}$	3	2	$2\mathbb{Z},\mathbb{Z}_2\,(2\mathbb{Z},\mathbb{Z}_2)$	-
$\mathrm{AII}^{\mathcal{M}_-}$	4	2	-	$2\mathbb{Z},\mathbb{Z}_2\,(2\mathbb{Z},\mathbb{Z}_2)$
$\mathrm{CII}^{\mathcal{M}_{--}}$	5	2	$\mathbb{Z}_2,\mathbb{Z}_2\,(2\mathbb{Z},2\mathbb{Z})$	-
$\mathrm{C}^{\mathcal{M}_-}$	6	2	-	$\mathbb{Z}_2,\mathbb{Z}_2\,(2\mathbb{Z},2\mathbb{Z})$
$\mathrm{CI}^{\mathcal{M}_{--}}$	7	2	$2\mathbb{Z},0\,(2\mathbb{Z},0)$	-
$\mathrm{AI}^{\mathcal{CM}_+}$	0	3	$\mathbb{Z},0\,(\mathbb{Z},0)$	-
$\mathrm{BDI}^{\mathcal{M}_{-+}}$	1	3	$0,0\,(\mathbb{Z}_2,0)$	$\mathbb{Z},0\,(\mathbb{Z},0)$
$\mathrm{D}^{\mathcal{CM}_-}$	2	3	$0,0\,(\mathbb{Z}_2,0)$	$0,0\,(\mathbb{Z}_2,0)$
$\mathrm{DIII}^{\mathcal{M}_{+-}}$	3	3	-	$0,0\,(\mathbb{Z}_2,0)$
$\mathrm{AII}^{\mathcal{CM}_+}$	4	3	$2\mathbb{Z},0\,(2\mathbb{Z},0)$	-
$\mathrm{CII}^{\mathcal{M}_{-+}}$	5	3	-	$2\mathbb{Z},0\,(2\mathbb{Z},0)$
$\mathrm{C}^{\mathcal{CM}_-}$	6	3	-	-
$\mathrm{CI}^{\mathcal{M}_{+-}}$	7	3	-	-

TABLE 2.10. Classification of mirror-symmetric corners ($d=2$) or hinges ($d=3$) of second-order topological insulators and superconductors in the real Altland-Zirnbauer classes. The ordering is $\mathcal{K}_{\mathrm{i}},\bar{\mathcal{K}}_{\mathrm{i}}(\mathcal{K}_{\mathrm{e}},\bar{\mathcal{K}}_{\mathrm{e}})$.

the above considerations as $\mathcal{K}_{\mathrm{i}}(s,t|d_\parallel,d)$, $\bar{\mathcal{K}}_{\mathrm{i}}(s,t|d_\parallel,d)$, $\mathcal{K}_{\mathrm{e}}(s,t|d_\parallel,d)$, and $\bar{\mathcal{K}}_{\mathrm{e}}(s,t|d_\parallel,d)$, where the subscripts i, e refer to intrinsic (termination-independent) and extrinsic (termination-dependent) classification and the bar refers to corners or hinges with locally broken mirror reflection symmetry. For mirror reflection $d_\parallel=1$ throughout. (The second argument is omitted for the complex Altland-Zirnbauer classes with antiunitary symmetries and antisymmetries.) Tables 2.8-2.10 contain the complete classification results, ordered as $\mathcal{K}_{\mathrm{i}}$, $\bar{\mathcal{K}}_{\mathrm{i}}$ ($\mathcal{K}_{\mathrm{e}}$, $\bar{\mathcal{K}}_{\mathrm{e}}$).

Although we will explain the derivation of each entry in the table in detail below and in the appendix, we first outline the general strategy that results in this classification. Our first observation is that the extrinsic, termination-dependent, classification of mirror symmetric corners/hinges is identical to the classification of end states of $(d-1)$-dimensional insulators and superconductors with a crystalline symmetry with $d_\parallel-1=0$ inverted coordinates, see Fig. 2.7 for $d=2$. By the bulk-boundary

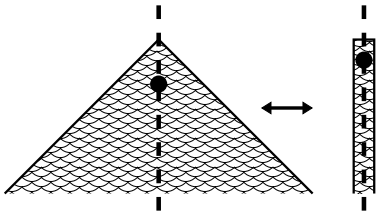

FIG. 2.7. The extrinsic classification of corner states in a mirror-symmetric corner of a two-dimensional crystal is the same as that of end states of a one-dimensional crystal with a transverse mirror symmetry with $d_\parallel = 0$. The vertical dashed line is the mirror axis.

correspondence, this latter classification is identical to the corresponding bulk crystalline classification, so that we have

$$\mathcal{K}_{\rm e}(s,t|d_\parallel = 1,d) = K(s,t|d_\parallel = 0,d-1). \qquad (2.13)$$

The classifying groups $K(s,t|d_\parallel = 0,d-1)$ are given in Ref. 19. They can also be obtained from Tables 2.5–2.7 using the isomorphisms (2.6)–(2.8). Similarly, upon locally breaking the mirror symmetry, we obtain the equality

$$\bar{\mathcal{K}}_{\rm e}(s,t|1,d) = K(s,t|0,d-1)/K'(s,t|0,d-1), \quad (2.14)$$

where $K'(s,t|d_\parallel = 0,d-1)$ is the "purely crystalline" subgroup of the classifying group $K(s,t|d_\parallel = 0,d-1)$, see the discussion at the end of Sec. 2.2.

The intrinsic, termination-independent, classification of mirror-symmetric corners or hinges can be obtained via the homomorphism

$$K(s,d-1) \xrightarrow{c_t} \mathcal{K}_{\rm e}(s,t|d_\parallel = 1,d), \qquad (2.15)$$

which embeds the equivalence class of the Hamiltonian $H(\mathbf{k})$ into corresponding Shiozaki-Sato class of Hamiltonian

$$c_t[H(\boldsymbol{k})] = \begin{pmatrix} H(\boldsymbol{k}) & 0 \\ 0 & \sigma_{\mathcal{S}} U_{\mathcal{S}} H(\boldsymbol{k}) U_{\mathcal{S}}^\dagger \end{pmatrix}, \qquad (2.16)$$

for $U_{\mathcal{S}}$ a unitary onsite symmetry ($\sigma_{\mathcal{S}} = 1$) or antisymmetry ($\sigma_{\mathcal{S}} = -1$) and

$$c_t[H(\boldsymbol{k})] = \begin{pmatrix} H(\boldsymbol{k}) & 0 \\ 0 & \sigma_{\mathcal{S}} U_{\mathcal{S}} H^*(-\boldsymbol{k}) U_{\mathcal{S}}^\dagger \end{pmatrix}, \qquad (2.17)$$

for $U_{\mathcal{S}}$ an antiunitary onsite symmetry or antisymmetry.

For the intrinsic classification corner states or hinge modes that differ by termination effects are identified. Such corner states or hinge modes are precisely those in the image $c_t[K(s,d-1)]$, so that we have

$$\mathcal{K}_{\rm i}(s,t|1,d) = \mathcal{K}_{\rm e}(s,t|1,d)/c_t[K(s,d-1)]. \qquad (2.18)$$

In other words, the elements of the group $\mathcal{K}_{\rm i}(s,t|1,d)$ can be viewed as topologically non-trivial $d-1$-dimensional crystalline insulators or superconductors with an onsite twofold symmetry that cannot be obtained by gluing two corresponding non-crystalline $d-1$-dimensional topological insulators or superconductors.

In the next Subsection we demonstrate, by explicit consideration of all symmetry classes, that the intrinsic (termination-independent) classification group $\mathcal{K}_{\rm i}(s,t|1,d)$ of corner or hinge states is identical to the "pure crystalline" group $K'(s,t|1,d)$ classifying topological crystalline bulk phases that are not at the same time strong topological phases,

$$\mathcal{K}_{\rm i}(s,t|1,d) = K'(s,t|1,d). \qquad (2.19)$$

Equation (2.19) says that a mirror-symmetric topological crystalline phase is either a strong topological phase, with gapless modes at all boundaries, or a topological crystalline phase which can be *uniquely* characterized using protected modes at mirror-symmetric corners (for a two-dimensional crystal) or hinges (for a three-dimensional crystal). For such "pure crystalline" topological crystalline phases Eq. (2.19) this extends the bulk-boundary correspondence to a "corner-to-bulk correspondence" or "hinge-to-bulk correspondence".

We now discuss the classification table for the complex Altland-Zirnbauer classes with unitary mirror symmetries and antisymmetries in detail. The classification of mirror-symmetric corners of two-dimensional crystals for the complex Altland-Zirnbauer classes with antiunitary mirror symmetries and antisymmetries and of the real classes is given in Appendix A.2. mirror-symmetric hinges for these classes can be obtained from the dimensional reduction scheme of Sec. 2.3 and is not discussed in detail.

Class $A^{\mathcal{M}}$, $(s,t) = (0,0)$, $d = 2$.— This class does not allow protected zero energy states at corners.

Class $AIII^{\mathcal{M}_+}$, $(s,t) = (1,0)$, $d = 2$.— At a mirror-symmetric corner zero-energy states can be counted according to their parity under mirror reflection $\mathcal{M}$ and the chiral operation $\mathcal{C}$, since $\mathcal{M}$ and $\mathcal{C}$ commute. (Recall that we use the convention that the mirror operation $\mathcal{M}$ squares to one.) We denote the number of corresponding modes with $N_{\sigma_{\mathcal{C}},\mathcal{M}}$. Since pairs of zero modes with opposite $\sigma_{\mathcal{C}}$ but equal $\sigma_{\mathcal{M}}$ can be gapped out by a mirror-symmetric mass term acting locally at the corner, only $N_{++} - N_{-+}$ and $N_{+-} - N_{--}$ are well defined. This gives the $\mathbb{Z}^2$ extrinsic classification listed in Table 2.8.

By changing the termination, *e.g.* by adding a suitably chosen chain of atoms on a crystal face, such that the global mirror symmetry is preserved, one can add a pair of zero modes with the same $\sigma_{\mathcal{C}}$, but opposite values of $\sigma_{\mathcal{M}}$, see Fig. 2.8. (Note that such a procedure involves closing the boundary gap.) As a result, the difference $N = N_{++} + N_{--} - N_{+-} - N_{-+}$ is the only remaining invariant, and one finds a $\mathbb{Z}$ intrinsic classification, which is the same classification as the one arising from the bulk classification of Refs. 19–22, and 39.

With a mirror-symmetry-breaking local perturbation at the corner, one may only distinguish corner states by

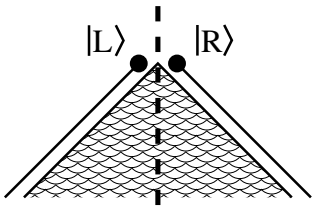

FIG. 2.8. Pairs of corner states may be created by "glueing" one-dimensional topologically nontrivial chain to the crystal edges. Mirror symmetry requires that the chains added to mirror-related edges are mirror images of each other.

their parity under $\mathcal{C}$. We use $N_{\sigma_\mathcal{C}}$ to denote the number of zero modes with parity $\sigma_\mathcal{C}$. Since pairs of zero modes with opposite $\sigma_\mathcal{C}$ can be gapped out by a mass term acting locally at the corner, only the difference $N_+ - N_-$ is well defined. This gives a $\mathbb{Z}$ extrinsic classification in the presence of a mirror-symmetry-breaking perturbation. Moreover, changes of the termination allow one to change N_+ or N_- by an even number, resulting in a $\mathbb{Z}_2$ intrinsic classification in that case.

Class $A^{\mathcal{CM}}$, $(s,t) = (0,1)$, $d = 2$.— This class allows corner modes only if the mirror antisymmetry is not broken locally at the crystal corner. In that case, corner modes can be counted according to their parity $\sigma_{\mathcal{CM}}$ under the mirror antisymmetry $\mathcal{CM}$. (Recall that we use the convention that $\mathcal{CM}^2 = 1$.) The mirror antisymmetry protects zero modes at the same value of $\sigma_{\mathcal{CM}}$, but allows pairs of zero modes at opposite mirror parity $\sigma_{\mathcal{CM}}$ to gap out. We conclude that the difference $N = N_+ - N_-$ is the corresponding topological invariant, giving the $\mathbb{Z}$ classification listed in Table 2.8. There is no difference between an "extrinsic" and an "intrinsic" classification because the Altland-Zirnbauer class A is trivial for $d = 1$, so that no protected zero modes can be added by changing the lattice termination. This phase is trivial if the mirror antisymmetry is broken locally at the corner.

Class $AIII^{\mathcal{M}-}$, $(s,t) = (1,1)$, $d = 2$.— The bulk crystalline phase in this class is trivial. However, since the Altland-Zirnbauer class AIII is nontrivial in one dimension, one should consider the possibility that corner states can arise by suitable decoration at the crystal edges, see Fig. 2.8. Hereto, consider the addition of two one-dimensional chains with zero-energy end states, labeled $|\mathrm{L}\rangle$ and $|\mathrm{R}\rangle$. The chains are placed symmetrically, so that $|\mathrm{L}\rangle = \mathcal{M}|\mathrm{R}\rangle$. Since $\mathcal{M}$ anticommutes with $\mathcal{C}$, the end states $|\mathrm{L}\rangle$ and $|\mathrm{R}\rangle$ have opposite parity under $\mathcal{C}$. Upon coupling the chains to each other, a term $|\mathrm{L}\rangle\langle\mathrm{R}| + |\mathrm{R}\rangle\langle\mathrm{L}|$ that gaps the two zero modes out is allowed under $\mathcal{C}$ antisymmetry and mirror reflection symmetry. Hence, we conclude that no stable corner states can be created by changing the lattice termination. (Alternatively, one may note that a mirror reflection operation that anticommutes with $\mathcal{C}$ can be viewed as a valid term in the Hamiltonian, which gaps out zero-energy states on the left and right of the corner.)

We point out that whereas in this symmetry class a mirror-symmetric corner does not allow for protected zero-energy states, a generic corner still does. The reason is that in a generic corner one may separately choose lattice terminations at both edges that meet at that corner, whereas in a mirror-symmetric corner the lattice terminations at the edges meeting in that corner are symmetry-related.

Class $A^{\mathcal{M}}$, $(s,t) = (0,0)$, $d = 3$.— We use y to denote the coordinate running along the hinge. Hinge modes can be characterized by their mirror parity $\sigma_\mathcal{M}$ and by their propagation direction in the y direction. Whereas counterpropagating modes with the same mirror parity can mutually gap out, counterpropagating hinge modes constructed with opposite $\sigma_\mathcal{M}$ are protected by mirror symmetry. Using $N_{\sigma_\mathcal{M}\pm}$ to denote the number of hinge modes of mirror parity $\sigma_\mathcal{M}$ propagating in the $\pm y$ direction, the differences $N_{++} - N_{+-}$ and $N_{-+} - N_{--}$ are two well-defined integer extrinsic topological invariants, consistent with the $\mathbb{Z}^2$ extrinsic classification of gapless hinge states.

By adding, *e.g.*, integer quantum Hall insulators on the mirror-related faces adjacent to the hinge, two copropagating hinge modes with opposite mirror parity can be created, leaving $N_{++} - N_{+-} - N_{-+} + N_{--}$ as the only remaining intrinsic integer topological invariant. If mirror symmetry is broken locally at the hinge, all counterpropagating modes can in principle be gapped out, giving rise to $\mathbb{Z}$ and $\mathbb{Z}_2$ extrinsic and intrinsic topological invariants, respectively.

Class $AIII^{\mathcal{M}+}$, $(s,t) = (1,0)$, $d = 3$.— This class does not allow for topologically protected hinge modes.

Class $A^{\mathcal{CM}}$, $(s,t) = (0,1)$, $d = 3$.— The mirror antisymmetry rules out the existence of protected hinge modes for this class — recall that for a mirror-symmetric hinge the mirror antisymmetry $\mathcal{CM}$ is effectively a *local* operation. Whereas a single dispersing hinge mode can not be an eigenmode of the antisymmetry $\mathcal{CM}$, two modes $|\mathrm{L}\rangle$ and $|\mathrm{R}\rangle = \mathcal{CM}|R\rangle$ can be gapped out by the mirror-antisymmetric perturbation $i(|\mathrm{L}\rangle\langle\mathrm{R}| - |\mathrm{R}\rangle\langle\mathrm{L}|)$. Note that for class $\mathrm{A}^{\mathcal{CM}}$ a generic hinge may still carry a protected hinge mode. (Compare with the discussion of class $\mathrm{AIII}^{\mathcal{M}-}$ for $d = 2$.)

Class $AIII^{\mathcal{M}-}$, $(s,t) = (1,1)$, $d = 3$.— The hinge modes can be chosen to have a well-defined mirror parity $\sigma_\mathcal{M}$. Since $\mathcal{M}$ anticommutes with $\mathcal{C}$, they occur as doublets with opposite $\sigma_\mathcal{M}$ and opposite propagation direction. For each doublet the "mixed parity" σ, the product of propagation direction and mirror parity $\sigma_\mathcal{M}$, is well-defined. The corresponding integer invariant N counts the difference of the number of such doublets with positive and negative σ. Since Altland-Zirnbauer class AIII is trivial in two dimensions, there is no difference between an extrinsic and intrinsic classifications for this class. Breaking the mirror symmetry locally at the hinge removes the protection of the hinge modes.

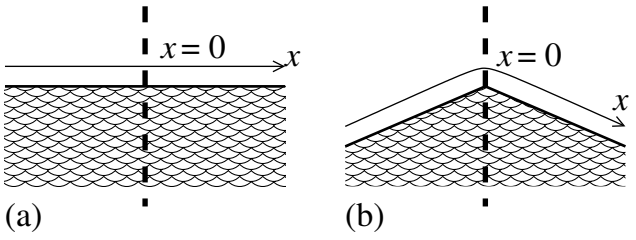

FIG. 2.9. A mirror-symmetric edge, with coordinate x running along the edge (a) can be deformed into a corner joining two mirror-related edges (b). The situation shown in (a) has mirror symmetry acting everywhere along the edge; in (b) mirror symmetry exists only for a mirror reflection axis going through the corner at $x = 0$.

2.4.2. From bulk crystalline phase to second-order phase

The above classification of tables 2.8–2.10 is based on a classification of zero-energy states localized at corners and gapless modes at hinges only. To make a connection with the bulk topology we use the bulk-boundary correspondence for mirror-symmetric topological crystalline insulators, which uniquely connects the bulk crystalline phase with the existence of gapless boundary modes at boundaries that are invariant under the mirror reflection operation.

In a two-dimensional crystal the edge is one dimensional and we can introduce a coordinate x running along the edge. If the boundary is tilted slightly away from the invariant direction, such that a corner connecting to mirror-related edges emerges at $x = 0$, as shown schematically in Fig. 2.9, generically a mass term is generated, which is *odd* under the mirror reflection operation $\mathcal{M}$. Such a mass term gaps out the edge states, but the fact that it is odd under mirror reflection implies the existence of a domain wall and an associated zero-energy state at the corner at $x = 0$. There is a one-to-one relationship between the number of topologically protected edge modes and the number of zero modes obtained in this way — with the caveats that such zero modes may be annihilated by local mirror-symmetry breaking perturbations at the corner and that additional zero modes may be generated by a modification of the lattice termination. In a three-dimensional crystal in principle the same arguments apply, with the only modification that in this case the invariant boundary is a surface.

Reference 9 has implemented this construction for all Shiozaki-Sato classes that have unitary mirror symmetries, and for which the mass term is unique. A unique mass term guarantees that a single corner or hinge mode cannot be gapped out by a perturbation that breaks the mirror symmetry locally at the corner. To complete the discussion of the complex Altland-Zirnbauer classes with a unitary mirror symmetry, we here discus how the presence of gapless states at a mirror-symmetric edge or surface gives rise to zero-energy corner states at mirror-symmetric corners or gapless hinge modes at mirror-symmetric hinges. Comparing to the analysis of the previous Subsection, we thus verify that we precisely recover the zero-energy corner state found by inspection of the corner alone. Appendix A.3 carries out the same program for the remaining Shiozaki-Sato classes.

Class AIII$^{\mathcal{M}_+}$, $(s,t) = (1,0)$, $d = 2$.— For concreteness, we use $U_{\mathcal{C}} = \sigma_3$ and $U_{\mathcal{M}} = \sigma_3\tau_3$ to represent the commuting operations $\mathcal{C}$ and $\mathcal{M}$. The bulk phase has a $\mathbb{Z}$ classification[19–21] with an integer topological invariant N, which counts the difference of counterpropagating pairs of edge modes with positive and negative mixed parity $\sigma_{\mathcal{MC}}$ at zero energy. (Although the product $\mathcal{MC}$ is an antisymmetry of the Hamiltonian, not a symmetry, edge modes can be chosen to be eigenmodes of $\mathcal{MC}$ at zero energy. Pairs of counterpropagating edge modes can not mutually gap out if they have the same eigenvalue $\sigma_{\mathcal{MC}}$.) After a suitable basis transformation and rescaling, the Hamiltonian of a "minimal" edge, in which all gapless modes have the same mixed parity $\sigma_{\mathcal{MC}}$, may be written as

$$H_{\text{edge}} = -iv\sigma_1\partial_x \mathbb{1}_N, \tag{2.20}$$

where x is the coordinate along the edge, see Fig. 2.9a, $\mathbb{1}_N$ the $N \times N$ unit matrix, and v a constant with the dimension of velocity. A corner between two mirror-related edges meeting at $x = 0$, as shown in Fig. 2.9b, is represented by a mass term $m(x)\sigma_2$ with $m(x) = -m(-x)$ a $N \times N$ hermitian matrix. The eigenvalues of $m(x)$ have "domain walls" at $x = 0$, allowing for N zero modes localized around $x = 0$. The bulk theory does not specify the sign of the limiting values of the eigenvalues of the mass term $m(x)$ at a large distance from the corner. The two choices for this sign give corner states with different parity eigenvalues $\sigma_{\mathcal{C}}$ and $\sigma_{\mathcal{M}}$, but the same value of $\sigma_{\mathcal{MC}} = \sigma_{\mathcal{C}}\sigma_{\mathcal{M}}$: A domain wall with $m(x) > 0$ for $x \gg 0$ gives a solution with $\sigma_{\mathcal{C}} = \sigma_{\mathcal{MC}}\sigma_{\mathcal{M}} = +$, whereas a domain wall with $m(x) < 0$ for $x \gg 0$ gives a solution with $\sigma_{\mathcal{C}} = \sigma_{\mathcal{MC}}\sigma_{\mathcal{M}} = -$. One verifies that if mirror symmetry is present locally around $x = 0$, neither perturbations coupling such zero-energy states with the same value of $\sigma_{\mathcal{MC}} = \sigma_{\mathcal{C}}\sigma_{\mathcal{M}}$, nor perturbations coupling zero-energy states with different values of $\sigma_{\mathcal{M}}$ are allowed.

The analysis of corner states of the previous Subsection counted their numbers $N_{\sigma_{\mathcal{C}},\sigma_{\mathcal{M}}}$ with parities $\sigma_{\mathcal{C}}$ and $\sigma_{\mathcal{M}}$ (at zero energy) and found that the differences $N_{++} - N_{-+}$ and $N_{+-} - N_{--}$ are the extrinsic topological invariants, whereas $N = N_{++} + N_{--} - N_{+-} - N_{-+}$ is the intrinsic topological invariant. The above analysis provides a confirmation of the differences $N_{++} - N_{-+}$ and $N_{+-} - N_{--}$ as extrinsic, termination-dependent invariants, and identifies the intrinsic invariant N describing the corner states with the bulk topological invariant N.

Class $A^{\mathcal{CM}}$, $(s,t) = (0,1)$, $d = 2$.— This phase has a $\mathbb{Z}^2$ bulk classification,[19, 22] with a purely crystalline classifying group $K' = \mathbb{Z}$. The first-order (strong) topological phase has chiral edge modes. For a second-order topological phase we restrict ourselves to purely crys-

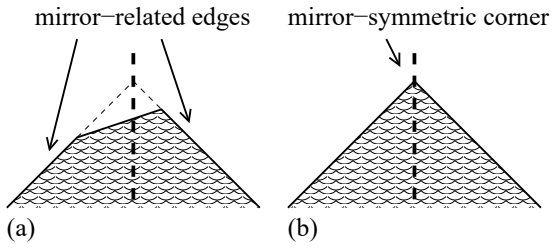

FIG. 2.10. (a) A two-dimensional crystal with a pair of mirror-related edges, but without a mirror-symmetric corner. (b) The crystal may be smoothly deformed into a crystal with a mirror-symmetric corner. The parity of the number of zero-energy states between the two mirror-related edges in (a) is the same as the parity of the number of zero-energy states at the mirror-symmetric corner in (b).

talline topological phases with equal numbers of counterpropagating modes. The corresponding integer index N counts the difference of the numbers of pairs of counterpropagating edge modes with positive and negative parity $\sigma_{\mathcal{CM}}$ at zero energy. (One verifies that a pair of counterpropagating modes can not mutually gap out if both modes have the same parity under $\mathcal{CM}$, *i.e.*, the same eigenvalue of $U_{\mathcal{CM}}$.) For a minimal edge, in which all edge modes have the same parity $\sigma_{\mathcal{CM}}$, we may represent the mirror antisymmetry with the unit matrix, $U_{\mathcal{CM}} = 1$. After a suitable rescaling and basis transformation, the edge Hamiltonian may then be written as

$$H_{\text{edge}} = -iv\sigma_3\partial_x \mathbb{1}_N, \tag{2.21}$$

where x is the coordinate along the crystal edge, $\mathbb{1}_N$ is the $N \times N$ unit matrix, and σ_3 a Pauli matrix acting on pairs of counterpropagating modes. Although mirror antisymmetry does not allow a uniform mass term, a mass term $m_1(x)\sigma_1 + m_2(x)\sigma_2$ in which $m_1(x)$ and $m_2(x)$ are hermitian $N \times N$ matrix-valued antisymmetric functions of x is allowed if the edge is deformed into two mirror-related edges meeting in a corner at $x = 0$. Such a mass term allows for N zero-energy states localized near $x = 0$. No further topology or symmetry related numbers can be associated with the zero-energy states, consistent with the integer classification obtained by inspection of corner states given in the previous Subsection.

Class $A^{\mathcal{M}}$, $(s,t) = (0,0)$, $d = 3$.— We use $U_{\mathcal{M}} = \sigma_2$ to represent mirror reflection. This class admits surface states with dispersion $-iv(\sigma_1\partial_x \pm \sigma_2\partial_y)$, where the sign $\pm$ defines the "mirror chirality" and x and y are coordinates along the surface, such that the mirror reflection sends $x \to -x$. The bulk crystalline phase has a $\mathbb{Z}$ topological classification,[19–22] with an integer topological invariant N equal to the difference of surface states with positive and negative mirror chirality.[48] For a minimal surface, all surface states have the same mirror chirality. With a suitable choice of basis and after rescaling the corresponding surface Hamiltonian reads

$$H_{\text{surface}} = -iv(\sigma_1\partial_x + \sigma_2\partial_y)\mathbb{1}_N, \tag{2.22}$$

with $\mathbb{1}_N$ the $N \times N$ identity matrix and x and y coordinates at the invariant surface. The unique mass term $m(x,y)\sigma_3$ with $m(x,y) = -m(-x,y)$ an $N \times N$ hermitian matrix gaps out the surface states. The fact that the mass term is odd under mirror reflection guarantees the existence of gapless hinge modes at mirror-symmetric hinges.

Considering the surface Hamiltonian (2.22) with a mass term $m(x)\sigma_3$ with $m(x) = -m(-x)$, the propagation direction of the hinge states and their mirror parity $\sigma_{\mathcal{M}}$ are determined by the signs of the eigenvalues of $m(x)$ for $x \gg 0$, such that a positive eigenvalue corresponds to a hinge state with positive $\sigma_{\mathcal{M}}$, moving in the positive y direction, whereas a negative eigenvalue corresponds to a hinge state with negative $\sigma_{\mathcal{M}}$, moving in the negative y direction. (The mirror parity $\sigma_{\mathcal{M}}$ and the propagation direction are opposite if we would have started from a surface Hamiltonian describing surface states with negative mirror chirality.) Counterpropagating hinge modes constructed this way have opposite $\sigma_{\mathcal{M}}$ and are, hence, protected by mirror symmetry. Since the sign of m depends on the details of the surface termination, changing the surface termination allows to simultaneously switch the propagation direction $\pm$ and the mirror parity $\sigma_{\mathcal{M}}$ of the hinge states, consistent with the intrinsic topological invariant $N_{++} - N_{+-} - N_{-+} + N_{--}$.

Class $AIII^{\mathcal{M}-}$, $(s,t) = (1,1)$, $d = 3$.— We choose $U_{\mathcal{C}} = \sigma_3$ and $U_{\mathcal{M}} = \sigma_2$ to represent $\mathcal{C}$ and $\mathcal{M}$, respectively. This class supports gapless surface states with dispersion $\propto -iv(\sigma_1\partial_x \pm \sigma_2\partial_y)$, which defines the chirality $\pm$. The crystalline bulk has a $\mathbb{Z}^2$ classification,[19–22] with purely crystalline classifying group $K' = \mathbb{Z}$, see Table 2.5. The strong integer index counts the number of such surface Dirac cones, weighted by chirality. For a second-order topological phase we are interested in the purely crystalline topological phases, in which the surface carries multiple pairs of Dirac cones of opposite chirality. Their dispersion is $-iv(\sigma_1\tau_3\partial_x \pm \sigma_2\tau_0\partial_y)$, where the sign $\pm$ defines the mirror chirality and the τ_j, $j = 0,1,2,3$, are Pauli matrices acting on a different spinor degree of freedom than the matrices σ_j, $j = 0,1,2,3$. The corresponding (second, purely crystalline) integer topological invariant N counts the number of such pairs of Dirac cones, weighted by mirror chirality. A minimal surface with $N \geq 0$ has surface Hamiltonian

$$H_{\text{surface}} = -iv(\sigma_1\tau_3\partial_x + \sigma_2\tau_0\partial_y)\mathbb{1}_N, \tag{2.23}$$

where $\mathbb{1}_N$ is the $N \times N$ unit matrix. The mass terms allowed by chiral symmetry and mirror reflection symmetry are $m_1(x,y)\sigma_1\tau_1 + m_2(x,y)\sigma_1\tau_2$ with $m_{1,2}(x,y) = -m_{1,2}(-x,y)$ $N \times N$ hermitian matrices. This ensures the presence of gapless hinge modes at mirror-symmetric hinges. One verifies that the surface Hamiltonian (2.23) gives N doublets for which the mixed parity, the product of mirror parity $\sigma_{\mathcal{M}}$ and the propagation direction,

is positive. Similarly, surface Dirac cones with negative mirror chirality give hinge doublets of negative mixed parity, thus allowing one to identify the topological invariants derived from counting gapless hinge states and the (purely crystalline) topological invariant N describing the bulk crystalline topology.

2.4.3. Mirror-symmetric crystals without mirror-symmetric corners

In principle, a mirror-symmetric crystal need not have mirror-symmetric corners. However, as long as the crystal has at least a pair of mirror-related edges (for a two-dimensional crystal) or a pair of mirror-related faces (for a three-dimensional crystal), the bulk topology determines the *parity* of the number of corner or hinge states *between* the two mirror-related edges or surfaces. An example of such a situation is shown in Fig. 2.10. Since such a crystal without mirror-symmetric corners or hinges (but with two mirror-related edges or surfaces) may be smoothly deformed into a crystal with a mirror-symmetric corner without closing the bulk gap, and since corner states and hinge modes can only be generated or annihilated pairwise in such a deformation, one immediately finds that the parity of corner states or hinge modes is the same as the parity of corner states or hinge modes at a mirror-symmetric corner. The corresponding entry in Tables 2.8–2.10 is the classifying group $\bar{\mathcal{K}}_{\rm i}$.

2.5. CLASSIFICATION OF SECOND-ORDER TOPOLOGICAL INSULATORS AND SUPERCONDUCTORS WITH TWOFOLD ROTATION AND INVERSION SYMMETRY

2.5.1. Twofold rotation symmetry for $d = 3$

The construction of Sec. 2.4 2, in which the existence of a protected corner state or hinge mode is derived from a nontrivial bulk crystalline topology, can be directly extended to the case of a three-dimensional insulator or superconductor with a twofold rotation symmetry, provided a (generic) hinge allows for the existence of a protected hinge mode, see Table 2.1. In that case, the argument starts from the existence of a gapless mode on a surface that is invariant under the twofold rotation operation. We first consider the case that the number of gapless modes is "minimal", *i.e.*, we consider a generator of the topological crystalline phase. Following the construction of Sec. 2.4 2, one then argues that a unique mass term is generated upon tilting this surface away from the invariant direction. The mass term m depends on the tilt angle θ and the azimuthal angle ϕ of the tilted surface, see Fig. 2.11(a), and is odd under the twofold rotation operation, $m(\theta, \phi) = -m(\theta, \phi + \pi)$, since the twofold rotation symmetry forbids a mass term for the rotation-invariant surface. As a consequence, a protected gapless hinge mode forms at the intersection of surfaces with masses of different sign, see Fig. 2.11(b). Since the

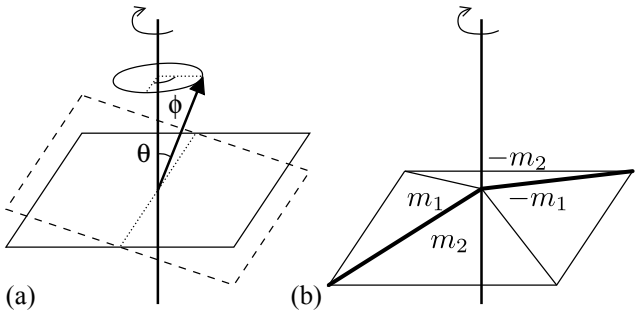

FIG. 2.11. (a) A surface perpendicular to the twofold rotation axis hosts a gapless mode in a nontrivial topological crystalline phase. The surface Hamiltonian acquires a mass term $m(\theta, \phi)$ upon tilting the surface away from the normal direction, which depends on the tilt angle θ and the azimuthal angle ϕ. The mass term is odd under the twofold rotation operation, $m(\theta, \phi) = -m(\theta, \phi + \pi)$ (b) A generic rotation symmetric surface. Surfaces related by twofold rotation have opposite mass terms. As a result, a protected gapless hinge mode (thick black line) forms at the intersection of surfaces with masses of different sign. The situation shown in the figure corresponds to $\mathrm{sign}(m_1) = -\mathrm{sign}(m_2)$.

number of sign changes of the mass term for $0 \leq \phi < 2\pi$ must be an odd multiple of two, the number of such hinge modes intersecting a generic cross section of the crystal is an odd multiple of two.

The above argument guarantees the existence of hinge modes globally, as long as the lattice termination is consistent with the twofold rotation symmetry, but it does not address the existence of a hinge mode at a given hinge. Indeed, generically, single hinges are not mapped to themselves under the twofold rotation operation; in this sense, *all* hinges are "generic" in a crystal with twofold rotation symmetry. This is a difference with the mirror-reflection symmetric case, for which a nontrivial mirror-symmetric topological crystalline phase can guarantee the existence of hinge modes at mirror-symmetric hinges.

All hinges being generic, hinges modes at a given hinge can also be induced by a suitable manipulation of the lattice termination. However, a change of lattice termination that is compatible with the twofold rotation symmetry always changes the total number of hinge modes passing a generic cross section of the crystal by a multiple of *four*. Since, as seen above, nontrivial bulk crystalline topology can also induce a number of hinge modes that is an odd multiple of two, we conclude that second-order topological phases protected by a twofold rotation symmetry have a $\mathbb{Z}_2$ invariant, which is nontrivial if the number of hinge modes is an odd multiple of two. Generators of the topological crystalline classes have a nontrivial $\mathbb{Z}_2$ index; if the bulk topological crystalline phase has an integer classification, only the odd topological numbers map to a nontrivial second-order phase.

It is interesting to point out that for a nontrivial bulk crystalline phase in a symmetry class that does not allow

class	s	t	$d=2$ $\mathcal{R}$	$d=3$ $\mathcal{R}$	$d=3$ $\mathcal{I}$
$\mathrm{A}^{\mathcal{S}}$	0	0	0	0	$\mathbb{Z}_2$
$\mathrm{AIII}^{\mathcal{S}_+}$	1	0	0	0	0
$\mathrm{A}^{\mathcal{CS}}$	0	1	0	$\mathbb{Z}_2$	0
$\mathrm{AIII}^{\mathcal{S}_-}$	1	1	$\mathbb{Z}_2$	0	0

TABLE 2.11. Classification of topological crystalline phases with an order-two rotation symmetry or an inversion symmetry for the complex Altland-Zirnbauer classes. The symbols $\mathcal{R}$ and $\mathcal{I}$ refer to twofold rotation ($d_\parallel = 2$) and inversion ($d_\parallel = d = 3$), respectively.

class	s	$d=2$ $\mathcal{R}$	$d=3$ $\mathcal{R}$	$d=3$ $\mathcal{I}$
$\mathrm{A}^{\mathcal{T}^+\mathcal{S}}$	0	0	$\mathbb{Z}_2$	0
$\mathrm{AIII}^{\mathcal{T}^+\mathcal{S}_+}$	1	0	0	0
$\mathrm{A}^{\mathcal{P}^+\mathcal{S}}$	2	0	0	0
$\mathrm{AIII}^{\mathcal{T}^-\mathcal{S}_-}$	3	0	0	0
$\mathrm{A}^{\mathcal{T}^-\mathcal{S}}$	4	0	0	0
$\mathrm{AIII}^{\mathcal{T}^-\mathcal{S}_+}$	5	0	0	0
$\mathrm{A}^{\mathcal{P}^-\mathcal{S}}$	6	0	0	$\mathbb{Z}_2$
$\mathrm{AIII}^{\mathcal{T}^+\mathcal{S}_-}$	7	$\mathbb{Z}_2$	0	0

TABLE 2.12. Same as table 2.11, but for antiunitary symmetries and antisymmetries.

for protected hinge modes, *i.e.*, for which the corresponding Altland-Zirnbauer class in $d = 2$ dimensions is trivial, the mass term obtained by tilting the surface away from the invariant direction is not unique. With two or more masses $m_1(\theta, \phi)$ and $m_2(\theta, \phi)$, the antisymmetry relation $m_{1,2}(\theta, \phi) = -m_{1,2}(\theta, \phi + \pi)$ no longer forces the mass to be zero for certain values of the azimuthal angle ϕ, so that no stable gapless modes exist at hinges. This is a key difference with the case of mirror reflection-symmetric crystalline insulators, where protected modes are guaranteed at mirror-symmetric corners or hinges even in the presence of multiple mass terms.

The resulting classification is shown in the Tables 2.11–2.13. The nontrivial entries in these tables are those Shiozaki-Sato symmetry classes, for which both the purely crystalline classification groups K' of Tables 2.5–2.7 and the corresponding entry Table 2.1 are both nonzero. Below we give detailed considerations making this construction explicit for the nontrivial complex Altland-Zirnbauer classes with unitary twofold rotation symmetry or antisymmetry. The complex Altland-Zirnbauer classes with antiunitary twofold rotation symmetry or antisymmetry and the real Altland-Zirnbauer classes are discussed in App. A.4.

Class AIII$^{\mathcal{R}_+}$, $(s,t) = (1,0)$.— The presence of the chiral antisymmetry with $U_{\mathcal{C}} = \sigma_3$ allows one to assign a chirality $\pm$ to surface modes with Dirac-like dispersion $\propto -i\sigma_1\partial_x \pm i\sigma_2\partial_y$, where x and y are the Cartesian coordinates parameterizing the surface and the twofold

class	s	t	$d=2$ $\mathcal{R}$	$d=3$ $\mathcal{R}$	$d=3$ $\mathcal{I}$
$\mathrm{AI}^{\mathcal{S}_+}$	0	0	0	0	0
$\mathrm{BDI}^{\mathcal{S}_{++}}$	1	0	0	0	0
$\mathrm{D}^{\mathcal{S}_+}$	2	0	0	0	0
$\mathrm{DIII}^{\mathcal{S}_{++}}$	3	0	0	0	0
$\mathrm{AII}^{\mathcal{S}_+}$	4	0	0	0	$\mathbb{Z}_2$
$\mathrm{CII}^{\mathcal{S}_{++}}$	5	0	0	0	0
$\mathrm{C}^{\mathcal{S}_+}$	6	0	0	0	$\mathbb{Z}_2$
$\mathrm{CI}^{\mathcal{S}_{++}}$	7	0	0	0	0
$\mathrm{AI}^{\mathcal{CS}_-}$	0	1	0	0	0
$\mathrm{BDI}^{\mathcal{S}_{+-}}$	1	1	$\mathbb{Z}_2$	0	0
$\mathrm{D}^{\mathcal{CS}_+}$	2	1	$\mathbb{Z}_2$	$\mathbb{Z}_2$	0
$\mathrm{DIII}^{\mathcal{S}_{-+}}$	3	1	$\mathbb{Z}_2$	$\mathbb{Z}_2$	0
$\mathrm{AII}^{\mathcal{CS}_-}$	4	1	0	$\mathbb{Z}_2$	0
$\mathrm{CII}^{\mathcal{S}_{+-}}$	5	1	$\mathbb{Z}_2$	0	0
$\mathrm{C}^{\mathcal{CS}_+}$	6	1	0	$\mathbb{Z}_2$	0
$\mathrm{CI}^{\mathcal{S}_{-+}}$	7	1	0	0	0
$\mathrm{AI}^{\mathcal{S}_-}$	0	2	0	0	0
$\mathrm{BDI}^{\mathcal{S}_{--}}$	1	2	0	0	0
$\mathrm{D}^{\mathcal{S}_-}$	2	2	$\mathbb{Z}_2$	0	$\mathbb{Z}_2$
$\mathrm{DIII}^{\mathcal{S}_{--}}$	3	2	$\mathbb{Z}_2$	$\mathbb{Z}_2$	$\mathbb{Z}_2$
$\mathrm{AII}^{\mathcal{S}_-}$	4	2	0	$\mathbb{Z}_2$	$\mathbb{Z}_2$
$\mathrm{CII}^{\mathcal{S}_{--}}$	5	2	0	0	0
$\mathrm{C}^{\mathcal{S}_-}$	6	2	0	0	$\mathbb{Z}_2$
$\mathrm{CI}^{\mathcal{S}_{--}}$	7	2	0	0	0
$\mathrm{AI}^{\mathcal{CS}_+}$	0	3	0	0	0
$\mathrm{BDI}^{\mathcal{S}_{-+}}$	1	3	0	0	0
$\mathrm{D}^{\mathcal{CS}_-}$	2	3	0	0	0
$\mathrm{DIII}^{\mathcal{S}_{+-}}$	3	3	$\mathbb{Z}_2$	0	$\mathbb{Z}_2$
$\mathrm{AII}^{\mathcal{CS}_+}$	4	3	0	$\mathbb{Z}_2$	$\mathbb{Z}_2$
$\mathrm{CII}^{\mathcal{S}_{-+}}$	5	3	$\mathbb{Z}_2$	0	0
$\mathrm{C}^{\mathcal{CS}_-}$	6	3	0	$\mathbb{Z}_2$	0
$\mathrm{CI}^{\mathcal{S}_{+-}}$	7	3	0	0	0

TABLE 2.13. Classification of topological crystalline phases with an order-two crystalline symmetry or antisymmetry for the real Altland-Zirnbauer classes. The symbols $\mathcal{R}$ and $\mathcal{I}$ refer to twofold rotation ($d_\parallel = 2$), and inversion ($d_\parallel = d = 3$), respectively.

rotation operation sends $x \to -x$ and $y \to -y$. The crystalline bulk has a $\mathbb{Z}^2$ classification,[19] with purely crystalline classifying group $K' = \mathbb{Z}$, see Table 2.5. For a second-order topological phase we restrict ourselves to the purely crystalline topological phases, which have equal numbers of Dirac cones of both chiralities. Such Dirac cones can not mutually gap out for a rotation-invariant surface if they have the same parity under $\mathcal{RC}$. At a minimal surface, in which all surface modes have the same parity under $\mathcal{RC}$, the twofold rotation symmetry may be represented by $U_{\mathcal{R}} = U_{\mathcal{C}} = \sigma_3$.

With a suitable choice of basis and after rescaling, the surface Hamiltonian of a minimal surface may be written as

$$H_{\text{surface}} = -iv(\sigma_1\tau_3\partial_x + \sigma_2\partial_y)\mathbb{1}_N, \tag{2.24}$$

where $\mathbb{1}_N$ is the $N \times N$ unit matrix. The mass terms allowed by chiral symmetry and rotation symme-

try are $m_1(x,y)\sigma_1\tau_1 + m_2(x,y)\sigma_1\tau_2$ with $m_{1,2}(x,y) = -m_{1,2}(-x,-y)$ $N \times N$ hermitian matrices. Although surfaces related by the twofold rotation operation have opposite masses, the existence of two mass terms allows the crystal faces to avoid domain walls and the associated protected hinge modes.

Class $A^{\mathcal{CR}}$, $(s,t) = (0,1)$.— The bulk has a $\mathbb{Z}$ topological classification, with an integer topological invariant N equal to the difference of surface states with positive and negative parity $\sigma_{\mathcal{CR}}$ at zero energy. For a minimal surface, all surface states have the same value of $\sigma_{\mathcal{CR}}$ and one may effectively represent $\mathcal{CR}$ using $U_{\mathcal{CR}} = 1$. With a suitable choice of basis and after rescaling the corresponding surface Hamiltonian reads

$$H_{\text{surface}} = -iv(\sigma_1\partial_x + \sigma_2\partial_y)\mathbb{1}_N, \qquad (2.25)$$

with $\mathbb{1}_N$ the $N \times N$ identity matrix and x and y are coordinates at the invariant surface. The unique mass term $m(x,y)\sigma_3$ with $m(x,y) = -m(-x,-y)$ an $N \times N$ hermitian matrix gaps out the surface states. If N is odd the existence of hinge modes at the intersection of surfaces with opposing signs of $\det m(x,y)$ is guaranteed by the rotation antisymmetry. If N is even one can still construct a mass term which is nonzero everywhere (except at the origin), corresponding to a state without hinge modes.

2.5.2. Twofold rotation symmetry for $d = 2$ and inversion symmetry

The above construction can not be applied to two-dimensional crystals with twofold rotation symmetry and to three-dimensional crystals with inversion symmetry, because these do not have symmetry-invariant boundaries. Instead, we argue for the existence of a second-order topological phase in this case using the reflection-matrix based dimensional reduction scheme outlined in Sec. 2.3. Starting from a second-order topological phase in $d+1$ dimensions in Shiozaki-Sato symmetry class $(s+1,t)$ (class $s+1$ for complex Hamiltonians with antiunitary symmetries) and $d_\parallel < d+1$ inverted coordinates, the dimensional reduction scheme allows one to construct a second-order topological insulator or superconductor in Shiozaki-Sato symmetry class (s,t) (class s for complex Hamiltonians with antiunitary symmetries) in d dimensions, with the same number $d_\parallel$ of inverted dimensions. The real-space version of the reflection-matrix based dimensional reduction scheme directly maps hinge states in a three-dimensional second-order topological insulator or superconductor with twofold rotation symmetry to corner states in a two-dimensional topological insulator or superconductor with twofold rotation symmetry, see Fig. 2.12. Similarly, it maps generalized hinge states of a four-dimensional second-order topological insulator or superconductor with an order-two inversion with $d_\parallel = 3$ to hinge states of a three-dimensional second-order topological insulator or superconductor with inversion symmetry. The resulting $\mathbb{Z}_2$ classification is given in Tables 2.11–2.13.

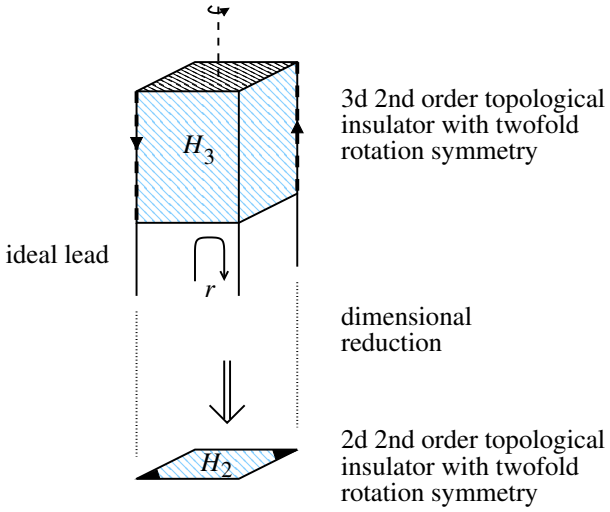

FIG. 2.12. Dimensional reduction scheme from a three-dimensional second-order topological insulator with twofold rotation symmetry to a two-dimensional second-order topological insulator with inversion symmetry. Upon dimensional reduction, the Altland-Zirnbauer class changes from s to $s-1$ (modulo 2 for the complex classes, modulo 8 for the real classes), see the discussion in the main text.

2.6. EXAMPLES

In this section we give various tight-binding model realizations of the second-order topological insulators. The models we consider all follow the same pattern. We first describe their general structure and then turn to a description of specific Shiozaki-Sato symmetry classes. The model Hamiltonian we consider is of the general form $H(\mathbf{k}) = H_0(\mathbf{k}) + H_1$, with

$$H_0(\mathbf{k}) = \sum_{j=0}^{d} d_j(\mathbf{k})\Gamma_j, \quad H_1 = \sum_{j=1}^{d} b_j B_j, \qquad (2.26)$$

where the Γ_j and the B_j, $j = 1,\dots,d$, are matrices that depend on the specific Shiozaki-Sato class and that satisfy $\Gamma_j^2 = B_j^2 = 1$, the b_j are real numbers typically chosen to be numerically small, and

$$\begin{aligned} d_0(\mathbf{k}) &= m + \sum_{j'=1}^{d}(1 - \cos k_{j'}), \\ d_j(\mathbf{k}) &= \sin k_j, \quad j = 1,\dots,d. \end{aligned} \qquad (2.27)$$

The matrices Γ_0 and Γ_j, $j = 1,\dots,d$, anticommute mutually, which ensures that for small numbers b_j, the Hamiltonian (2.26) is in a nontrivial topological crystalline phase for $-2 < m < 0$. We further choose the matrix B_1 such that it commutes with Γ_1 and Γ_0 and

anticommutes with Γ_j with $j \geq 1$. For the remaining matrices B_j with $j > 1$ we set

$$B_j = \Gamma_j \Gamma_1 B_1, \quad j = 2, \ldots, d, \tag{2.28}$$

which ensures that B_i commutes with Γ_i and Γ_0 and anticommutes with Γ_j for $j \neq i$. Mirror symmetry with $k_1 \to -k_1$ requires $b_2 = b_3 = 0$; twofold rotation symmetry with rotation around the x_3 axis requires $b_3 = 0$. The role of the perturbation H_1 is to reduce the symmetry of the Hamiltonian, while preserving the crystalline symmetry of interest. Further, as we will show below, each B_j term gaps the surface that is perpendicular to the x_j direction. When appropriate, we will simplify our notation by writing the matrices Γ_j and B_j and the numbers b_j as vectors, $\mathbf{\Gamma} = (\Gamma_1, \ldots, \Gamma_d)$, $\mathbf{B} = (B_1, \ldots, B_d)$, and $\mathbf{b} = (b_1, \ldots, b_d)$.

For all of the examples that we discuss below we verified the existence of Majorana corner modes or gapless hinge modes by numerical diagonalization of a finite cluster. (All numerical calculations in this Section were performed using the Kwant software package.[47]) Alternatively, for a Hamiltonian of the form (2.26), with the constraints as described above, the existence of zero-energy corner modes or gapless hinge modes can also be concluded from an explicit solution of the low-energy theory, modeling the crystal boundaries as interfaces between regions with negative and positive m, with negative m corresponding to the interior of the crystal. The low-energy limit of H_0 near a sample boundary has the form

$$H_0 = m(x_\perp)\Gamma_0 - i\hbar \mathbf{\Gamma} \cdot \partial_{\mathbf{r}}, \tag{2.29}$$

where $x_\perp = \mathbf{n} \cdot \mathbf{r}$ is the coordinate transverse to a boundary with outward-pointing normal $\mathbf{n}$. We require $m(x_\perp) > 0$ for $x_\perp > 0$ and $m(x_\perp) < 0$ for $x_\perp < 0$, so that the sample interior corresponds to negative $x_\perp$. The Hamiltonian (2.29) admits a zero-energy boundary mode with spinor wavefunction $\psi(x_\perp)$ satisfying

$$\partial_{x_\perp} \psi(x_\perp) = -\frac{i}{\hbar} m(x_\perp)(\mathbf{n} \cdot \mathbf{\Gamma})\Gamma_0 \psi(x_\perp). \tag{2.30}$$

For $2b$-dimensional spinors, this equation has b bounded solutions with an $x_\perp$-independent spinor structure. The projection operator to the b-dimensional space of allowed spinors is

$$P(\mathbf{n}) = \frac{1}{2}[i(\mathbf{n} \cdot \mathbf{\Gamma})\Gamma_0 + 1]. \tag{2.31}$$

The effective b-band surface Hamiltonian is obtained using the projection operator $P(\mathbf{n})$. To illustrate this procedure, we consider a family of surfaces with surface normal $\mathbf{n} = (\cos\phi, \sin\phi)$ for $d = 2$ or $\mathbf{n} = (\cos\phi, \sin\phi, 0)$ for $d = 3$. In this case we write the projection operator as

$$\begin{aligned} P(\phi) &= \frac{1}{2}(i\Gamma_1\Gamma_0 \cos\phi + i\Gamma_2\Gamma_0 \sin\phi + 1) \\ &= e^{\phi\Gamma_2\Gamma_1/2} P(0) e^{-\phi\Gamma_2\Gamma_1/2}. \end{aligned} \tag{2.32}$$

The projected Hamiltonian then reads,

$$\begin{aligned} P(\mathbf{n})HP(\mathbf{n}) = {} & e^{\phi\Gamma_2\Gamma_1/2} P(0) \\ & \times [-i\hbar(\Gamma_2 \partial_{x_\parallel} + \Gamma_3 \partial_{x_3}) + m(\phi) B_1] \\ & \times P(0) e^{-\phi\Gamma_2\Gamma_1/2}, \end{aligned} \tag{2.33}$$

where $m(\phi) = b_1 \cos\phi + b_2 \sin\phi$ and $\partial_{x_\parallel} = \cos\phi\, \partial_{x_2} - \sin\phi\, \partial_{x_1}$ is the derivative with respect to a coordinate along the surface. (For $d = 2$ the terms proportional to ∂_{x_3} should be omitted from Eq. (2.33) and from Eq. (2.34) below.) From Eq. (2.33) we derive the effective boundary Hamiltonian

$$H_{\text{boundary}} = -i\hbar(\Gamma_2' \partial_{x_\parallel} + \Gamma_3' \partial_{x_3}) + m(\phi) B_1', \tag{2.34}$$

where $\Gamma_2' = P(0)\Gamma_2 P(0)$, $\Gamma_3' = P(0)\Gamma_3 P(0)$, and $B_1' = P(0)B_1 P(0)$ are effectively $b \times b$ matrices because of the projection operator $P(0)$. (Note that Γ_2, Γ_3, and B_1 commute with $P(0)$.) The boundary Hamiltonian (2.34) supports boundary modes with a gap $|m(\phi)|$. For $d = 2$ zero-energy corner states appear between crystal edges with opposite sign of $m(\phi)$; for $d = 3$ gapless hinge modes appear between crystal faces with opposite sign of $m(\phi)$.

2.6.1. Examples in two dimensions

1. *Class D with $t = d_\parallel$*

This example applies to symmetry class $\mathrm{D}^{\mathcal{CM}_+}$, $(s,t) = (2,1)$ and to symmetry class $D^{\mathcal{R}-}$, $(s,t) = (2,2)$. We represent the symmetry operations using $U_{\mathcal{P}} = \sigma_1$, $U_{\mathcal{CM}} = \sigma_1$, and $U_{\mathcal{R}} = \sigma_3$. The mirror operation sends $k_1 \to -k_1$. For the matrices Γ_j and B_j in the tight-binding Hamiltonian (2.26) we choose

$$\Gamma_0 = \sigma_3, \quad \mathbf{\Gamma} = (\tau_3\sigma_1, \sigma_2), \quad \mathbf{B} = (\tau_2\sigma_3, -\tau_1). \tag{2.35}$$

For class $\mathrm{D}^{\mathcal{CM}_+}$, the mirror antisymmetry imposes that $b_2 = 0$; for class $D^{\mathcal{R}-}$ nonzero b_1 and b_2 are allowed. We note that for $b_1 = 0$ this example also possesses a mirror symmetry for mirror reflection $k_2 \to -k_2$, which is represented by $\sigma_2\tau_3$. The mirror-symmetric case hosts Majorana zero modes at corners that are bisected by the mirror axis. The rotation-symmetric case also hosts Majorana modes at corners, but these corners are determined by the orientation of the vector $\mathbf{b}$ (numerical data not shown).

2. *Class D with $t = d_\parallel + 3 \mod 4$*

This example applies to symmetry class $\mathrm{D}^{\mathcal{M}_+}$, $(s,t) = (2,0)$ and to symmetry class $D^{\mathcal{CR}_+}$, $(s,t) = (2,1)$. We represent the symmetry operations using $U_{\mathcal{P}} = 1$, $U_{\mathcal{M}} = \sigma_1$, and $U_{\mathcal{CR}} = \tau_3\sigma_1$. For the matrices Γ_j and B_j in the tight-binding Hamiltonian (2.26) we choose

$$\Gamma_0 = \tau_2, \quad \mathbf{\Gamma} = (\tau_1\sigma_3, \tau_3), \quad \mathbf{B} = (\tau_2\sigma_1, -\sigma_2). \tag{2.36}$$

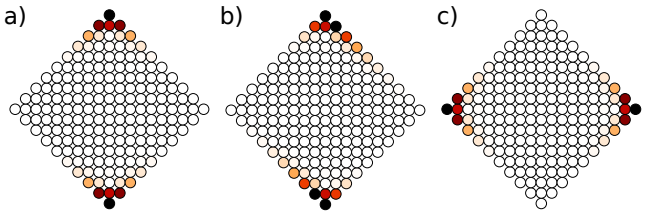

FIG. 2.13. Support of the zero-energy corner state obtained from exact diagonalization of the two-dimensional time-reversal invariant superconductor in class DIII with Hamiltonian (2.26) with $m = -1$ and $\mathbf{\Gamma}$ and $\mathbf{B}$ given by Eq. (2.37) with $\mathbf{b} = (0.3, 0)$ (a), $\mathbf{b} = (0.3, 0.1)$ (b), and $\mathbf{b} = (0, 0.3)$ (c).

Again the mirror symmetry imposes that $b_2 = 0$; for class $D^{\mathcal{CR}-}$ nonzero b_1 and b_2 are allowed. As in the previous example, the mirror-symmetric case hosts Majorana zero modes at corners that are bisected by the mirror axis.[9] The rotation-symmetric case also hosts Majorana zero modes at corners that are determined by the orientation of the vector $\mathbf{b}$ (numerical date not shown).

3. *Class DIII with* $t = d_\parallel - 1 \mod 4$

This example applies to symmetry classes $\mathrm{DIII}^{\mathcal{M}++}$ and $\mathrm{DIII}^{\mathcal{R}-+}$, which both have a $\mathbb{Z}_2$ classification. We consider an eight-band model, for which we represent the symmetry operations using $U_\mathcal{T} = \sigma_2$, $U_\mathcal{P} = \tau_1$, $U_\mathcal{M} = \rho_3$, and $U_\mathcal{R} = \sigma_3$, where the ρ_j, σ_j, and τ_j are Pauli matrices acting on different spinor degrees of freedom. For the matrices Γ_j and B_j in the tight-binding Hamiltonian (2.26) we choose

$$\begin{aligned} &\Gamma_0 = \tau_3, \quad \mathbf{\Gamma} = (\rho_1\tau_1\sigma_1, \rho_3\tau_1\sigma_1), \\ &\mathbf{B} = (\rho_3\tau_3, -\rho_1\tau_3). \end{aligned} \tag{2.37}$$

Mirror symmetry imposes that $b_2 = 0$. The perturbation $b_1 B_1$ preserves both mirror and rotation symmetries, but breaks a mirror symmetry with $x_2 \to -x_2$, represented by ρ_1. As shown in figure 2.13a, the mirror-symmetric model with nonzero b_1 hosts Majorana Kramers pairs at its symmetry-invariant corners. The corner states persist if the mirror-symmetry-breaking perturbation $b_2 B_2$ is switched on, see Fig. 2.13b. In this case, the ratio of b_1 and b_2 determines the corner at which the Majorana Kramers pairs reside, such that they move to the other corners if $b_1 = 0$, see Fig. 2.13c.

4. *Class AII with* $t = d_\parallel + 2 \mod 4$

This example applies to symmetry classes $\mathrm{AII}^{\mathcal{CM}+}$ and $\mathrm{AII}^{\mathcal{R}+}$. We represent the symmetry operations using $U_\mathcal{T} = \sigma_2$, $U_{\mathcal{CM}} = \tau_2\sigma_3$, and $U_\mathcal{R} = \tau_2\sigma_1$. This symmetry class allows a perturbation H_1 of the form

$$H_1 = \sum_{j=1}^{d} b_j B_j + \sum_{j=1}^{d} c_j C_j, \tag{2.38}$$

where the matrices C_j anticommute with the matrices B_j and otherwise satisfy the same properties, see Eq. (2.28) and the discussion preceding that equation. For the matrices Γ_j, B_j, and C_j we choose

$$\begin{aligned} &\Gamma_0 = \tau_2\sigma_1, \quad \mathbf{\Gamma} = (\sigma_3, \sigma_2), \\ &\mathbf{B} = (\mu_2\tau_3\sigma_3, \mu_2\tau_3\sigma_2), \quad \mathbf{C} = (\mu_2\tau_1\sigma_3, \mu_2\tau_1\sigma_2), \end{aligned} \tag{2.39}$$

where the μ_j, σ_j, and τ_j are Pauli matrices acting on different spinor degrees of freedom. As in the previous examples the mirror antisymmetry imposes that $b_2 = c_2 = 0$; for class $\mathrm{AII}^{\mathcal{R}+}$ nonzero $b_{1,2}$ and $c_{1,2}$ are allowed. The mirror antisymmetry can protect a zero-energy Kramers pair at mirror-symmetric corners. However, if the mirror antisymmetry is broken, the twofold rotation symmetry alone cannot protect a topologically protected zero-energy state if both $\mathbf{b}$ and $\mathbf{c}$ are nonzero and linearly independent. (If $\mathbf{b}$ and $\mathbf{c}$ are both nonzero and linearly dependent, the model specified by Eq. (2.39) obeys an accidental chiral antisymmetry, effectively placing it in the Shiozaki-Sato symmetry classes $\mathrm{CII}^{\mathcal{M}--}$ and $\mathrm{CII}^{\mathcal{R}+-}$, which stabilizes a zero-energy corner mode even if mirror symmetry is broken.)

Figure 2.14 shows the result of the exact diagonalization of this model on a finite-sized lattice. Panel (a) shows the support of the Kramers pairs for a system with $b_2 = c_1 = c_2 = 0$ as well as the spectrum near zero energy. Upon adding the mirror-antisymmetry-breaking perturbation $c_2 C_2$ locally near the top corner, the Kramers pair located there acquires a finite energy, see panel (b). Both Kramers pairs disappear if the mirror-symmetry-breaking perturbation is added to both top and bottom corners, see Fig. 2.14c.

2.6.2. Examples in three dimensions

1. *Class A with* $t = d_\parallel + 1 \mod 4$

Langbehn *et al.*[9] considered this class for the case of a mirror symmetry with $k_1 \to -k_1$ represented by $U_\mathcal{M} = \sigma_1$. Here we give an example that also has twofold rotation antisymmetry, represented by $U_{\mathcal{CR}} = \tau_2\sigma_1$, and inversion symmetry, represented by $U_\mathcal{I} = \tau_1\sigma_1$. For the matrices Γ_j and B_j in the tight-binding Hamiltonian (2.26) we choose

$$\Gamma_0 = \tau_1\sigma_1, \quad \mathbf{\Gamma} = (\tau_1\sigma_3, \tau_2, \tau_3), \quad \mathbf{B} = (\tau_1, \tau_2\sigma_3, \tau_3\sigma_3). \tag{2.40}$$

Mirror symmetry imposes that $b_2 = b_3 = 0$; twofold rotation antisymmetry imposes that $b_3 = 0$. The mirror-symmetric model with $b_2 = b_3 = 0$ was already considered in Sec. 2.3. Additionally, the system has a mirror symmetry sending $k_2 \to -k_2$ ($k_3 \to -k_3$) represented

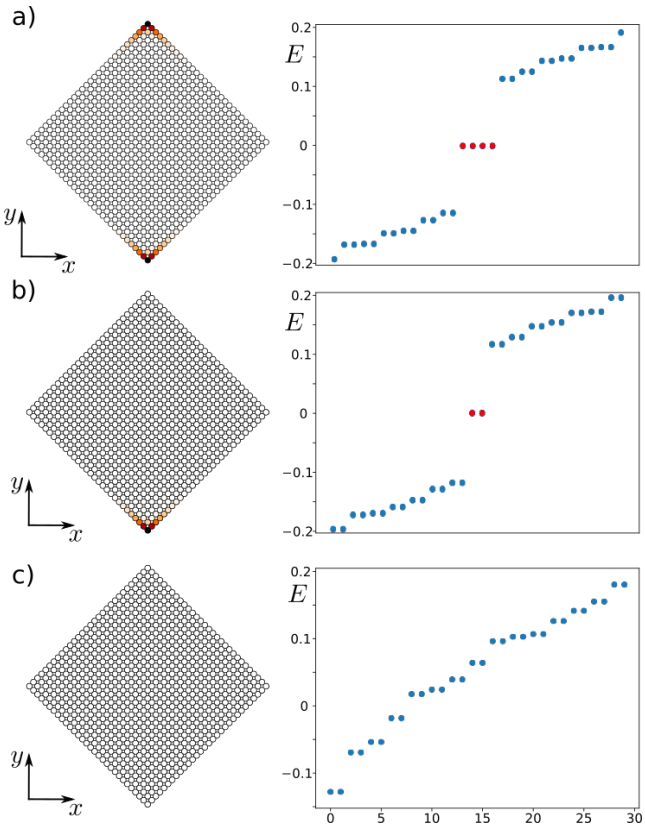

FIG. 2.14. Support of the zero-energy eigenstates (if present, left) and the lowest 30 eigenvalues (right a, b and c) of the model discussed in Sec. 2.6 1 4. Panel (a) is for the case that mirror antisymmetry is present, $\mathbf{b} = (0.4, 0)$ and $\mathbf{c} = (0, 0)$, which has a Kramers pair of zero-energy states localized at the mirror-symmetric top and bottom corners. Breaking the mirror antisymmetry locally at the top corner removes one zero-energy Kramers pair, as shown in panel (b). No zero-energy Kramers pairs remain after removing the mirror antisymmetry at both the top and the bottom corner, as shown in panel (c).

by $U_{\mathcal{M}} = \tau_3\sigma_2$ ($U_{\mathcal{M}} = \tau_2\sigma_2$) and a twofold rotation antisymmetry around x_1-axis (x_2-axis) represented by $U_{\mathcal{CR}} = \sigma_2$ ($U_{\mathcal{CR}} = \tau_3\sigma_1$). The mirror-symmetric case $\mathrm{A}^{\mathcal{M}}$ in which only the perturbation $b_1 B_1$ is present has a single chiral mode wrapping around the sample hinges. [9] These modes persist when all three perturbations $b_j B_j$ are switched on, where the orientation of the vector $\mathbf{b}$ determines which hinges support the chiral hinge modes. As an example, Figure 2.15 shows the support of the chiral hinge modes for two different choices of $\mathbf{b}$.

Upon performing the reflection-matrix dimensional reduction scheme of Sec. 2.3 the model defined by the choice (2.40) can be used to generate an eight-band two-dimensional Hamiltonian in classes $\mathrm{AIII}^{\mathcal{M}+}$ and $\mathrm{AIII}^{\mathcal{R}-}$ with $U_{\mathcal{C}} = \mu_3$, $U_{\mathcal{M}} = \sigma_1$, and $U_{\mathcal{R}} = \mu_1\tau_2\sigma_1$. Figure 2.5 shows the support of the zero-energy corner states of the two-dimensional Hamiltonian that is obtained this way. For comparison, we may consider a four-band model

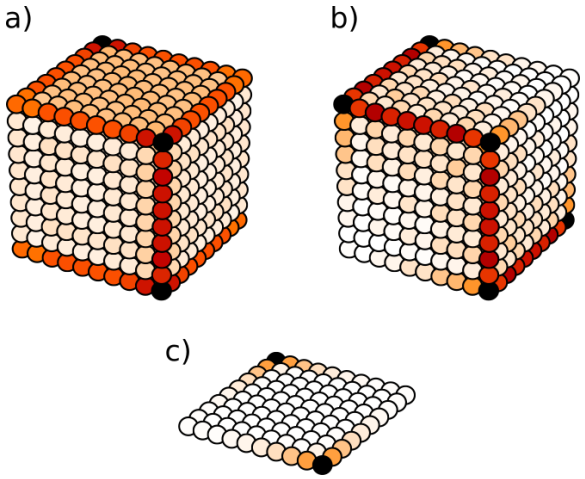

FIG. 2.15. Support of the zero-energy hinge modes for a three-dimensional crystal with tight-binding Hamiltonian specified by Eqs. (2.26) and (2.40) for $\mathbf{b} = (0.8, 0.8, 0.8)/\sqrt{3}$ (a) and $\mathbf{b} = (0.8, 0.8, 0)/\sqrt{2}$ (b). The example shown in panel (a) has mirror-reflection symmetry, twofold rotation symmetry, and inversion symmetry; the example in panel (b) has inversion symmetry only. Panel (c) shows the support of the zero-energy corner modes obtained for the two-dimensional tight-binding model specified by Eqs. (2.26) and (2.41) with $\mathbf{b} = (0.4, 0)$.

for a two-dimensional tight-binding Hamiltonian, with $U_{\mathcal{C}} = \tau_3$, $U_{\mathcal{M}} = \sigma_1$, and $U_{\mathcal{R}} = \tau_1\sigma_1$ and Hamiltonian specified by

$$\Gamma_0 = \tau_1\sigma_1, \quad \mathbf{\Gamma} = (\tau_1\sigma_3, \tau_2), \quad \mathbf{B} = (\tau_1, \tau_2\sigma_3). \tag{2.41}$$

The above model has a mirror symmetry for $b_2 = 0$ and a twofold rotation symmetry for arbitrary b_1, b_2. This model has zero-energy corner states. Figure 2.15c shows the support of these zero-energy corner states for the parameter choice $\mathbf{b} = (0.4, 0)$.

2. *Class AII with $s = 4$, $t = d_\parallel + 1 \mod 4$*

This example applies to the classes $\mathrm{AII}^{\mathcal{M}-}$, $\mathrm{AII}^{\mathcal{CR}+}$, and $\mathrm{AII}^{\mathcal{I}+}$, which all have a $\mathbb{Z}$ bulk crystalline classification, with purely crystalline component $K' = 2\mathbb{Z}$.[19–23, 49] We use $U_{\mathcal{T}} = \sigma_2$, represent the (spinful) mirror operation by $U_{\mathcal{M}} = \sigma_3\tau_3$, rotation antisymmetry by $U_{\mathcal{CR}} = \sigma_1\tau_2$, and inversion as $U_I = \tau_3$. The lattice Hamiltonian is specified by

$$\begin{aligned}\Gamma_0 &= \tau_3, \quad \mathbf{\Gamma} = (\sigma_3\tau_1, \sigma_2\tau_1, \sigma_1\tau_1),\\ \mathbf{B} &= (\sigma_3\tau_0\rho_2, \sigma_2\tau_0\rho_2, \sigma_1\tau_0\rho_2),\end{aligned} \tag{2.42}$$

where mirror symmetry forces $b_2 = b_3 = 0$ and rotation antisymmetry forces $b_3 = 0$. In addition to the spatial symmetries mentioned above, the model has a mirror symmetry with $k_2 \to -k_2$ if $b_1 = b_3 = 0$, represented by $\sigma_2\tau_3$, a mirror symmetry with $k_3 \to -k_3$ if

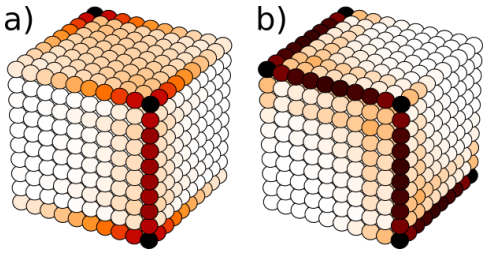

FIG. 2.16. Support of helical hinge modes of the tight-binding Hamiltonian (2.26) with $\mathbf{\Gamma}$ and $\mathbf{B}$ given by Eq. (2.42) and $\mathbf{b} = (0.4, 0.4, 0)$ (a) and $\mathbf{b} = (0.4, 0.4, 0.4)$ (b). For the example shown in panel (a) the top and bottom surfaces are invariant with respect to the twofold rotation symmetry, which explains the presence of gapless surface modes at the top and bottom surface. The twofold rotation symmetry is broken in panel (b), which has inversion symmetry only.

$b_1 = b_2 = 0$, represented by $\sigma_1\tau_3$, and rotation antisymmetries around the x_1 axis (if $b_1 = 0$) and x_2 axis (if $b_2 = 0$), represented by $\sigma_3\tau_2$ and $\sigma_2\tau_2$, respectively. The model with mirror symmetry has a single helical mode located at the mirror-symmetric sample hinges.[9] The helical modes persist upon turning on all perturbations $b_j B_j$, $j = 1, 2, 3$, leaving inversion as the only symmetry of the model. Figure 2.16 shows the helical hinge modes for two different choices of $\mathbf{b}$. The existence of hinge modes in the presence of inversion symmetry is consistent with Refs. 14 and 36, where the same symmetry class was considered. The case of a spinful mirror symmetry was analyzed previously in Refs. 4 and 9.

3. *Class AII with $s = 4$, $t = d_\parallel$*

This example applies to the classes $\mathrm{AII}^{\mathcal{CM}_-}$, $\mathrm{AII}^{\mathcal{R}_-}$, and $\mathrm{AII}^{\mathcal{CI}_+}$, which all have a $\mathbb{Z}_2^2$ bulk crystalline classification,[19–23, 49] with purely crystalline component $K' = \mathbb{Z}_2$. Here we again represent time-reversal as $U_\mathcal{T} = \sigma_2$, and use $U_{\mathcal{CM}} = \sigma_1\tau_3$, $U_\mathcal{R} = \sigma_3$, and $U_{\mathcal{CI}} = \tau_3$ to represent the mirror antisymmetry, spinful rotation symmetry, and inversion antisymmetry. We choose the matrices of the tight-binding Hamiltonian as

$$\begin{aligned} \Gamma_0 = \tau_1\rho_3, \quad \mathbf{\Gamma} = (\sigma_1\tau_3\rho_3, \sigma_2\tau_3, \sigma_3\tau_3), \\ \mathbf{B} = (\sigma_0\tau_2\rho_2, -\sigma_3\tau_2\rho_1, \sigma_2\tau_2\rho_1), \end{aligned} \tag{2.43}$$

where mirror antisymmetry forces $b_2 = b_3 = 0$ and rotation symmetry forces $b_3 = 0$. The model has additional mirror antisymmetries with $k_2 \to -k_2$ (if $b_1 = b_3 = 0$) and $k_3 \to -k_3$ (if $b_1 = b_2 = 0$), represented by $\sigma_2\tau_3$ and $\sigma_3\tau_3$, respectively, and rotation symmetries around the x_1 axis (if $b_1 = 0$) and x_2 axis (if $b_2 = 0$), represented by σ_1 and σ_2, respectively. A numerical diagonalization gives results that are indistinguishable from those of Fig. 2.16. The existence of hinge modes in the presence of spinful twofold rotation symmetry is consistent with Ref. 36, where the same symmetry class was considered.

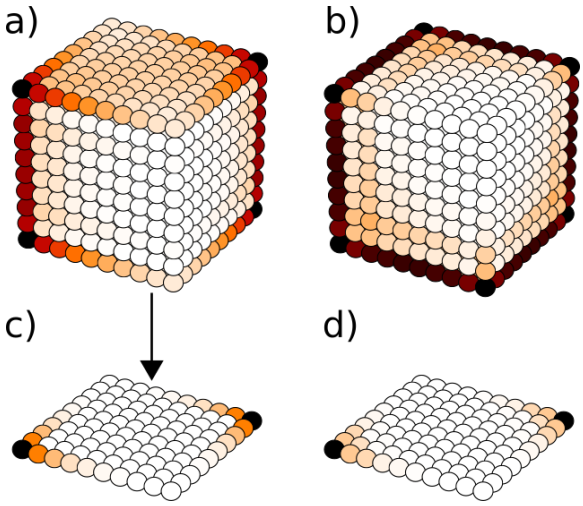

FIG. 2.17. Support of the zero-energy states of the tight-binding Hamiltonian (2.26) with $\mathbf{\Gamma}$ and $\mathbf{B}$ given by Eq. (2.44) and $\mathbf{b} = (0.4, -0.4, 0)$ (a) and $\mathbf{b} = (0.4, -0.4, 0.4)$ (b). For the example shown in panel (a) the top and bottom surfaces are invariant with respect to the twofold rotation symmetry, which explains the presence of gapless surface modes at the top and bottom surface. The twofold rotation symmetry is broken in panel (b), which only has inversion symmetry. Panel (c) shows the support of the zero-energy corner modes of the two-dimensional Hamiltonian in class $\mathrm{AIII}^{\mathcal{T}^+\mathcal{R}_-}$ obtained by dimensional reduction of the three-dimensional model, with parameter $\mathbf{b} = (0.4, -0.4, 0)$. For comparison, panel (d) shows the support of the zero-energy corner modes obtained for the two-dimensional tight-binding model specified by Eqs. (2.26) and (2.45) with $\mathbf{b} = (0.4, -0.4)$.

4. *Antiunitary symmetry: Class A with $s = 4 - 2d_\parallel \mod 8$*

This example applies to the classes $\mathrm{A}^{\mathcal{P}^+\mathcal{M}}$, $\mathrm{A}^{\mathcal{T}^+\mathcal{R}}$, and $\mathrm{A}^{\mathcal{P}^-\mathcal{I}}$. We represent the symmetry operations using $U_{\mathcal{PM}} = \tau_3$, $U_{\mathcal{TR}} = \sigma_1$, and $U_{\mathcal{PI}} = \sigma_2$ and consider a tight-binding Hamiltonian of the form (2.26) with

$$\begin{aligned} \Gamma_0 = \sigma_2\tau_0, \quad \mathbf{\Gamma} = (\sigma_1\tau_1, \sigma_1\tau_3, \sigma_3\tau_0), \\ \mathbf{B} = (\sigma_2\tau_3, -\sigma_2\tau_1, \sigma_0\tau_2), \end{aligned} \tag{2.44}$$

where the antiunitary mirror antisymmetry requires that $b_2 = b_3 = 0$ and the twofold antiunitary rotation symmetry requires that $b_3 = 0$. Figures 2.17a and b show the hinge states for two example lattice structures with $m = -1$ and $\mathbf{b} = (0.4, -0.4, 0)$ and $b = (0, 4, -0.4, 0.4)$, respectively.

Upon performing the reflection-matrix dimensional reduction scheme of Sec. 2.3 the model defined by the choice (2.44) can be used to generate a two-dimensional Hamiltonian in classes $\mathrm{AIII}^{\mathcal{T}^+\mathcal{M}_+}$ and $\mathrm{AIII}^{\mathcal{T}^+\mathcal{R}_-}$ with $U_\mathcal{C} = \rho_3$, $U_{\mathcal{TM}} = \sigma_0\tau_3$, and $U_{\mathcal{TR}} = \sigma_1\rho_1$. Figure 2.17d shows the support of the zero-energy corner states of the two-dimensional Hamiltonian that is obtained this way.

The model that is obtained using the dimensional reduction scheme is an eight-band model. This is not the

minimal number of bands for which a nontrivial second-order topological insulator in the classes AIII$^{\mathcal{T}^+\mathcal{M}_+}$ and AIII$^{\mathcal{T}^+\mathcal{R}_-}$ exists. An example of a minimal model is given by a two-dimensional tight-binding Hamiltonian of the form (2.26) with

$$\Gamma_0 = \sigma_2\tau_0, \quad \mathbf{\Gamma} = (\sigma_1\tau_1, \sigma_1\tau_3), \quad \mathbf{B} = (\sigma_2\tau_3, -\sigma_2\tau_1), \tag{2.45}$$

which has a chiral symmetry $U_{\mathcal{C}} = \sigma_3$, mirror symmetry $U_{\mathcal{TM}} = \sigma_3\tau_3$ for $b_2 = 0$ and a twofold rotation symmetry $U_{\mathcal{TR}} = \sigma_1$ for arbitrary b_1, b_2. This model has zero-energy corner states, as shown in Fig. 2.17d for the parameter choice $m = -1$, $\mathbf{b} = (0.4, -0.4)$.

2.7. CONCLUSION

In this work we extend the construction scheme introduced by Langbehn *et al.* [9] for second-order topological insulators and superconductors with mirror reflection symmetry to the larger class of topological insulators and superconductors stabilized by any order-two crystalline symmetry or antisymmetry, unitary or antiunitary. The order-two crystalline symmetries include mirror reflection, twofold rotation, and inversion.

For the mirror-symmetric topological crystalline insulator and superconductors we showed that a topologically nontrivial bulk implies that either all boundaries have gapless modes, in which case the topological crystalline insulator or superconductor is a strong topological insulator or superconductor which does not rely on the crystalline symmetry for its protection, or it is a second-order topological insulator, with zero-energy states at mirror-symmetric corners or gapless modes at mirror-symmetric hinges. Moreover, we showed that there is a "corner-to-bulk correspondence" or "hinge-to-bulk correspondence", according to which the classification of possible protected corner or hinge states modulo lattice termination effects is identical to the that of the bulk topology, after removal of the strong topological phases. On the other hand, no complete corner-to-bulk correspondence or hinge-to-bulk correspondence exists for topological crystalline phases protected by a twofold rotation symmetry or by inversion symmetry, since these symmetries do not allow for symmetry-invariant corners or hinges in two and three dimensions. Instead, there is a partial correspondence, which relates the parity of the number of corner states or hinge modes to the bulk topology.

For topological crystalline phases in which the number $d_\parallel$ of inverted spatial dimensions is smaller than the spatial dimension d, such as phases protected by mirror reflection for $d \geq 2$ or twofold rotation for $d \geq 3$, there is a bulk-to-boundary correspondence, which uniquely links the bulk topology with the boundary states on a symmetry-invariant boundary. The corner-to-bulk correspondence or hinge-to-bulk correspondence for those phases shows that they may have protected states at corners or hinges, too, but it does not provide information beyond what is already known from considering symmetry-invariant boundaries. This is different for topological crystalline phases with $d_\parallel = d$, such as twofold rotation symmetry for $d = 2$ or inversion symmetry for $d = 3$, for which there are no symmetry-invariant boundaries and, hence, no (first-order) bulk-to-boundary correspondence. In this case the $\mathbb{Z}_2$ sum rule for the number of corner states or hinge modes that we derive here provides a unique boundary signature of a nontrivial topological crystalline phase for a case in which no other boundary signatures are known to exist.[14, 36] Correspondingly, the demonstration that a nontrivial topological crystalline phase implies the existence of protected corner states or hinge modes cannot start from a theory of gapless boundary modes, as it does for $d_\parallel < d$,[9] but, instead, must start from the gapped bulk, as is done in Ref. 36 and Sec. 2.6 for specific examples, or, as a general construction, by dimensional reduction from a hypothetical higher-dimensional topological crystalline phase for which symmetry-invariant boundaries exist. This is the route we take in Sec. 2.5, using a real-space dimensional reduction scheme based on the scattering matrix.[22, 46]

It is important to stress that, although crystalline symmetries are key to our construction of second-order topological phases, second-order topological phases are immune to weak perturbations that break the crystalline symmetry, as long as the boundary gaps are preserved.[9] In our description, this stability is reflected in the use of two classification schemes: An *extrinsic* classification scheme, which classifies corner states or hinge modes with respect to continuous transformations of the Hamiltonian that preserve both bulk and boundary gaps, and an *intrinsic* classification, which allows transformations of the Hamiltonian in which the boundary gap is closed, as long as the bulk gap is preserved. The intrinsic classification depends on the bulk topology only, and is independent of the lattice termination. On the other hand, it is the extrinsic classification, with the possible inclusion of local symmetry-breaking perturbations, that captures the robustness of the phenomena associated with a second-order topological phase to weak symmetry-breaking perturbations.

Not all two-dimensional materials with corner states or all three-dimensional materials with gapless hinge modes are in a second-order topological phase — just like not all materials with a gapped bulk and gapless boundary states are topological. For a second-order topological phase it is necessary that the corner states or hinge modes have a topological protection. A classification of the type that we present here is a key prerequisite to determine whether a true topological protection can exist, or whether the existence of corner states or hinge modes in a given model is merely a matter of coincidence. For example, the existence of zero-energy corner modes always requires that the Hamiltonian satisfy an *antisymmetry*, ruling out a second-order phase in a two-dimensional lattice model with *symmetries* only — in contrast to recent claims in the literature.[50–52]

The phenomenology of a second-order topological phase — the existence of protected zero-energy corner states or gapless hinge modes on an otherwise gapped boundary — is not the only possible manifestation of a nontrivial bulk topology if the standard bulk-to-boundary correspondence does not apply. As pointed out in Refs. 6, 7, 50, 53, and 54, a nontrivial bulk crystalline topology may also manifest itself through a nontrivial quantized electric multipole moment or through the existence of fractional end or corner charges. (Note that a corner charge is different from a zero-energy corner state: A zero-energy corner state implies a degeneracy of the many-body ground state, whereas a corner charge implies the local accumulation of charge in an otherwise non-degenerate many-particle ground state.) If the Hamiltonian possesses an antisymmetry, as is the case for certain models considered in the literature,[6, 53] a nontrivial electric multipole moment and protected zero-energy corner states can exist simultaneously, but this need not always be case. A counterexample is the "breathing pyrochlore lattice" of Ref. 50, for which the nontrivial bulk topology manifests itself through a quantized bulk polarization, whereas the zero-energy corner states of Ref. 50 lack topological protection.

Only few materials have been proposed as realizations of second-order phases. Examples are strained SnTe[4] or odd-parity superconducting order in doped nodal-loop materials[55] both with mirror symmetry, and bismuth [56] with inversion symmetry. Simultaneously, the phenomenology of second-order phases has been reproduced experimentally in artificial "materials", such as electrical[57] or microwave[58] circuits, or coupled mechanical oscillators.[59] We hope that the complete classification presented here will help to identify new material candidates for the solid-state realizations of second-order topological insulators and superconductors.

[1] M. Z. Hasan and C. L. Kane, Rev. Mod. Phys. **82**, 3045 (2010).
[2] B. A. Bernevig and T. L. Hughes, *Topological Insulators and Topological Superconductors* (Princeton University Press, 2013).
[3] X.-L. Qi and S.-C. Zhang, Rev. Mod. Phys. **83**, 1057 (2011).
[4] F. Schindler, A. M. Cook, M. G. Vergniory, Z. Wang, S. S. P. Parkin, B. A. Bernevig, and T. Neupert, Science Advances **4** (2018), 10.1126/sciadv.aat0346.
[5] W. A. Benalcazar, J. C. Y. Teo, and T. L. Hughes, Phys. Rev. B **89**, 224503 (2014).
[6] W. A. Benalcazar, B. A. Bernevig, and T. L. Hughes, Science **357**, 61 (2017).
[7] W. A. Benalcazar, B. A. Bernevig, and T. L. Hughes, Phys. Rev. B **96**, 245115 (2017).
[8] Y. Peng, Y. Bao, and F. von Oppen, Phys. Rev. B **95**, 235143 (2017).
[9] J. Langbehn, Y. Peng, L. Trifunovic, F. von Oppen, and P. W. Brouwer, Phys. Rev. Lett. **119**, 246401 (2017).
[10] M. Sitte, A. Rosch, E. Altman, and L. Fritz, Phys. Rev. Lett. **108**, 126807 (2012).
[11] F. Zhang, C. L. Kane, and E. J. Mele, Phys. Rev. Lett. **110**, 046404 (2013).
[12] G. E. Volovik, JETP Letters **91**, 201 (2010).
[13] Z. Song, Z. Fang, and C. Fang, Phys. Rev. Lett. **119**, 246402 (2017).
[14] C. Fang and L. Fu, Science Advances **5** (2019), 10.1126/sciadv.aat2374.
[15] A. P. Schnyder, S. Ryu, A. Furusaki, and A. W. W. Ludwig, Phys. Rev. B **78**, 195125 (2008).
[16] A. P. Schnyder, S. Ryu, A. Furusaki, and A. W. W. Ludwig, AIP Conference Proceedings **1134**, 10 (2009).
[17] A. Kitaev, AIP Conference Proceedings **1134**, 22 (2009).
[18] A. Altland and M. R. Zirnbauer, Phys. Rev. B **55**, 1142 (1997).
[19] K. Shiozaki and M. Sato, Phys. Rev. B **90**, 165114 (2014).
[20] C.-K. Chiu, H. Yao, and S. Ryu, Phys. Rev. B **88**, 075142 (2013).
[21] T. Morimoto and A. Furusaki, Phys. Rev. B **88**, 125129 (2013).
[22] L. Trifunovic and P. W. Brouwer, Phys. Rev. B **96**, 195109 (2017).
[23] Y.-M. Lu and D.-H. Lee, arXiv:1403.5558v1 (2014).
[24] K. Shiozaki, M. Sato, and K. Gomi, Phys. Rev. B **93**, 195413 (2016).
[25] C. Fang, M. J. Gilbert, and B. A. Bernevig, Phys. Rev. B **86**, 115112 (2012).
[26] C. Fang, M. J. Gilbert, and B. A. Bernevig, Phys. Rev. B **87**, 035119 (2013).
[27] R.-J. Slager, A. Mesaros, V. Juricic, and J. Zaanen, Nature Phys. **9**, 98 (2013).
[28] P. Jadaun, D. Xiao, Q. Niu, and S. K. Banerjee, Phys. Rev. B **88**, 085110 (2013).
[29] X.-J. Liu, J. J. He, and K. T. Law, Phys. Rev. B **90**, 235141 (2014).
[30] A. Alexandradinata, C. Fang, M. J. Gilbert, and B. A. Bernevig, Phys. Rev. Lett. **113**, 116403 (2014).
[31] X.-Y. Dong and C.-X. Liu, Phys. Rev. B **93**, 045429 (2016).
[32] J. Kruthoff, J. de Boer, J. van Wezel, C. L. Kane, and R.-J. Slager, Phys. Rev. X **7**, 041069 (2017).
[33] H. C. Po, A. Vishwanath, and H. Watanabe, Nature Comm. **8**, 50 (2017).
[34] B. Bradlyn, L. Elcoro, J. Cano, M. G. Vergniory, Z. Wang, C. Felser, M. I. Aroyo, and B. A. Bernevig, Nature **547**, 298 (2017).
[35] K. Shiozaki, M. Sato, and K. Gomi, Phys. Rev. B **95**, 235425 (2017).
[36] E. Khalaf, H. C. Po, A. Vishwanath, and H. Watanabe, Phys. Rev. X **8**, 031070 (2018).
[37] J. C. Y. Teo and C. L. Kane, Phys. Rev. B **82**, 115120 (2010).
[38] Although $\mathcal{P}$ and and $\mathcal{C}$ are commonly referred to as "particle-hole symmetry" and "chiral symmetry", we will refer to these as antisymmetries, because they connect H to $-H$, see Eq. (2.1).
[39] C.-K. Chiu, J. C. Y. Teo, A. P. Schnyder, and S. Ryu, Rev. Mod. Phys. **88**, 035005 (2016).
[40] For spin 1/2 electrons often spatial symmetries squaring

to -1 are used. Multiplication by i then gives a symmetry operation squaring to 1. Note, however, that multiplication with i turns a symmetry that commutes with $\mathcal{T}$ or $\mathcal{P}$ into a symmetry that anticommutes with $\mathcal{T}$ or $\mathcal{P}$ and vice versa.

[41] The algebraic relations of the symmetry operations define the factor system as introduced in Section 1.1 of Chapter 1.

[42] M. Stone, C.-K. Chiu, and A. Roy, J. Math. Phys. A: Math. Theor. **44**, 045001 (2011).

[43] X.-G. Wen, Phys. Rev. B **85**, 085103 (2012).

[44] G. Abramovici and P. Kalugin, Int. J. Geom. Methods Mod. Phys. **9**, 125003 (2012).

[45] R. Kennedy and M. R. Zirnbauer, Commun. Math. Phys. **342**, 909 (2016).

[46] I. C. Fulga, F. Hassler, and A. R. Akhmerov, Phys. Rev. B **85**, 165409 (2012).

[47] C. W. Groth, M. Wimmer, A. R. Akhmerov, and X. Waintal, New J. Phys. **16**, 063065 (2014).

[48] J. C. Y. Teo, L. Fu, and C. L. Kane, Phys. Rev. B **78**, 045426 (2008).

[49] A. M. Turner, Y. Zhang, R. S. K. Mong, and A. Vishwanath, Phys. Rev. B **85**, 165120 (2012).

[50] M. Ezawa, Phys. Rev. Lett. **120**, 026801 (2018).

[51] M. Ezawa, Phys. Rev. B **98**, 045125 (2018).

[52] Y. Xu, R. Xue, and S. Wan, arXiv:1711.09202 (2017).

[53] A. Lau, J. van den Brink, and C. Ortix, Phys. Rev. B **94**, 165164 (2016).

[54] G. van Miert, C. Ortix, and C. Morais Smith, 2D Materials **4**, 015023 (2017).

[55] H. Shapourian, Y. Wang, and S. Ryu, Phys. Rev. B **97**, 094508 (2018).

[56] F. Schindler, Z. Wang, M. G. Vergniory, A. M. Cook, A. Murani, S. Sengupta, A. Y. Kasumov, R. Deblock, S. Jeon, I. Drozdov, H. Bouchiat, S. Guéron, A. Yazdani, B. A. Bernevig, and T. Neupert, Nature Physics **14**, 918 (2018).

[57] S. Imhof, C. Berger, F. Bayer, J. Brehm, L. W. Molenkamp, T. Kiessling, F. Schindler, C. H. Lee, M. Greiter, T. Neupert, and R. Thomale, Nature Physics **14**, 925 (2018).

[58] C. W. Peterson, W. A. Benalcazar, T. L. Hughes, and G. Bahl, Nature **555**, 346 (2018).

[59] M. Serra-Garcia, V. Peri, R. Süsstrunk, O. R. Bilal, T. Larsen, L. G. Villanueva, and S. D. Huber, Nature (2018).

3. Bulk-boundary-defect correspondence at disclinations in crystalline topological insulators and superconductors

3.1. INTRODUCTION

Topological crystalline insulators and superconductors have an excitation gap in the bulk and feature protected gapless or zero-energy modes on their boundaries [1–3]. These boundary modes are anomalous in the sense that they can only be realized in the presence of a topological bulk. Crystalline symmetries, such as rotation or inversion symmetry, may protect higher-order topological phases for which anomalous states are located at corners or hinges of the crystal [4–27] (see also Chapter 2). In particular, a d-dimensional topological crystalline phase of order n hosts $(d-n-1)$-dimensional anomalous states at hinges or corners of the corresponding dimension. This correspondence between bulk topology and boundary anomaly is a fundamental aspect of topological insulators and superconductors [12, 25, 28–33].

Topological lattice defects violate a crystalline symmetry locally while the rest of the lattice remains locally indistinguishable from a defect-free lattice. They can be constructed by cutting and gluing symmetry-related sections of the lattice by means of a Volterra process [19, 34–36]. Topological lattice defects are characterized by their holonomy, which is defined as the action on a local coordinate system transported around the defect. Common examples are dislocations and disclinations. The latter violate rotation symmetry locally and carry a rotation holonomy. The association to a holonomy is the property that distinguishes topological lattice defects from other lattice defects. For example, atomic defects such as vacancies, substitutions, or atoms at interstitial positions are not associated to a holonomy, and therefore are not considered topological. For grain boundaries separating regions of different lattice orientations, it has been suggested that they can be described as arrays of dislocations [37–39] or disclinations [40–45].

Previous works have shown that dislocations carry anomalous states in weak topological phases [31, 46–52]. The label weak indicates that the topological phase is protected by translation symmetry. The existence of anomalous states at disclinations in the absence of weak topological phases has been shown in Refs. 14, 19, 36, 53–55. Moreover, crystalline topological phases generally have a topological response associated with topological lattice defects [36]. A possible link between second-order topology and anomalous states at disclinations has been put forward in Refs. 14 and 19. Furthermore, a correspondence between a fractional corner charge in two-dimensional topological crystalline insulators [5, 6, 18, and 56] and a fractional disclination charge has been shown in Refs. 16 and 20. A correspondence between a topological phase realized on a lattice with dislocations and a topological phase realized on a defect-free lattice on a manifold with a larger genus has been suggested in Refs. 57–59.

In this chapter, we establish a precise relation between second-order topological phases protected by rotation symmetry and anomalous states at disclinations. By using both heuristic arguments and the framework of topological crystals [22], we work out for all Cartan classes of spinful fermionic systems the exact conditions under which this *bulk-boundary-defect correspondence* holds. In the cases where it breaks down, the anomaly at the disclination depends on the microscopic properties of the system. Under certain conditions, this obstruction manifests as a domain wall that is connected to the disclination.

The analysis in this chapter covers both topological phases defined in the long-wavelength limit where the lattice may be neglected, and topological phases enabled by the presence of the discrete translation symmetry of a lattice. The former shows that the bulk-boundary-defect correspondence does not require an underlying lattice. The latter identifies weak topological phases associated with the anomaly at the disclination.

This chapter is organized as follows. Section 3.2 reviews the construction and the holonomy classification of disclinations in lattice models of fermionic systems. In Sec. 3.3, we begin by giving a brief overview of second-order topological phases and their bulk-boundary correspondence. We determine the existence of anomalous states at disclinations for models defined in the long-wavelength limit. In the following Sec. 3.4, we construct real-space representations of second-order and weak topological phases in the presence of discrete translation symmetry to deduce the existence of anomalous disclination states. This section may be skipped at first reading. In Sec. 3.5, we cumulate our results to show that each topological property of a disclination, i.e., its translation and rotation holonomies as well as the presence of quantized vortices, is linked to a unique bulk topological invariant determining the existence of anomalous states at the defect. For all symmetry classes we detail whether the bulk-disclination correspondence holds and whether there exist weak and strong first- and second-order topological phases that may contribute $d-2$ dimensional anomalous states bound to a disclination. In Sec. 3.6, we apply our construction to concrete examples before summarizing our results in Sec. 3.7.

3.2. TOPOLOGICAL LATTICE DEFECTS

3.2.1. Volterra process

A lattice is abstractly defined by its space group G that contains all crystalline symmetry elements, e.g., translations, rotations, and inversion symmetry. A topological

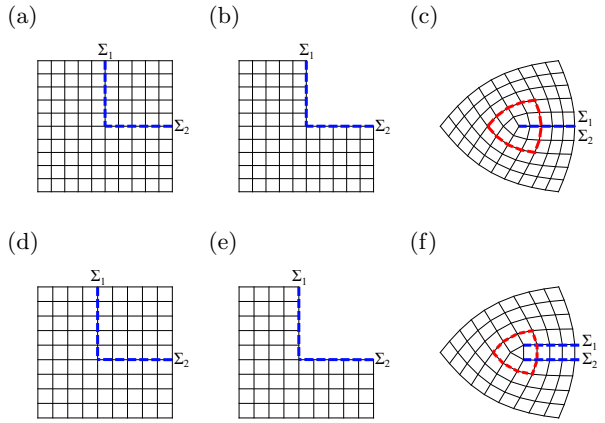

Figure 3.1. Volterra processes to construct two different $\pi/2$ disclinations in a C_4-symmetric lattice: (a)-(c) type-0 disclination centered at a 3-vertex ; (d)-(f) type-1 disclination centered at a triangular cell. The red dashed lines in (c) and (f) indicate paths encircling the respective disclination.

lattice defect breaks an element of G locally such that the lattice remains indistinguishable from a defect-free arrangement everywhere else. These defects are topological in the sense that local rearrangements of the lattice can only move, but not remove the lattice defect. This implies that there exists a topological quantity, defined on a closed loop or surface enclosing the defect, that quantifies the lattice defect. This topological quantity can be expressed in terms of the holonomy associated with the defect. For lattice defects with co-dimension 2, the holonomy is defined as the action on a local coordinate system upon parallel transport along a closed loop around the defect [54]. Common examples of topological lattice defects are dislocations and disclinations, which locally violate translation symmetry and rotation symmetry, respectively. In the following, we show how topological lattice defects are constructed using a Volterra process [34 and 35] for the example of a square lattice with C_4 symmetry.

We first cut the crystal along two lines, Σ_1 and Σ_2, intersecting in a point p and related by a rotation about an angle $\Omega = \pi/2$ consistent with the lattice symmetry [see Figs. 3.1(a), and (d)]. We then remove the enclosed segment [see Figs. 3.1(b), and (e)], deform the crystal such that the lines Σ_1 and Σ_2 come together, and finally glue the lattice back together along the cut [see Figs. 3.1(c) and (f)]. This procedure may be used to construct distinct types of $\pi/2$ disclinations depending on the number of additional lattice translations along the direction of the cut: in Fig. 3.1(c), no extra translation is applied, thereby forming a disclination centered at a vertex with three connections. In Fig. 3.1(f), one additional translation leads to a disclination centered at a triangular cell. The presence of the disclination strains the lattice close to the defect.

We point out that instead of cutting and removing a segment, one can also cut the crystal along a single line and insert a segment with boundaries related by a Ω rotation. This process constructs a disclination with a negative Franck angle $-\Omega$ (see below).

3.2.2. Holonomy of disclinations

Disclinations are classified by their holonomy, which is defined as the amount of excess translation and rotation accumulated by parallel transporting a coordinate system on a closed path around the disclination [54]. Holonomic quantities are path-independent as long as the starting point is fixed and the path encircles the disclination only once. By considering equivalence classes of holonomies that can be reached by a change of starting point, the holonomic quantities become also independent of the starting point. The rotation holonomy Ω is called the *Franck angle* and is, by construction, identical to the angle Ω in the Volterra process defined above. The equivalence classes $\mathrm{Hol}(\Omega)$ of Ω disclinations in $2\pi/\Omega$-fold rotation symmetric lattices are [50 and 54]

$$\begin{aligned} \mathrm{Hol}(\pi) &= \mathbb{Z}_2 \oplus \mathbb{Z}_2, \\ \mathrm{Hol}(2\pi/3) &= \mathbb{Z}_3, \\ \mathrm{Hol}(\pi/2) &= \mathbb{Z}_2, \\ \mathrm{Hol}(\pi/3) &= 0. \end{aligned} \tag{3.1}$$

For twofold symmetric lattices, there are four types of π disclinations. They are distinguished by the parity of the number of translations along the x and y direction of the crystal (see Fig. 3.2). Threefold rotation-symmetric lattices may host three distinct types of $2\pi/3$ disclinations distinguished by their rotation holonomy modulo three, which is illustrated in Fig. 3.2. For fourfold symmetric lattices, there are two types of $\pi/2$ disclinations corresponding to whether an even (type 0) or odd (type 1) number of translations by primitive Bravais lattice vectors is required to move around the disclination This is illustrated in Figs. 3.1(c) and (f), respectively. Finally, sixfold symmetric lattices allow for only a single type of $\frac{\pi}{3}$ disclination (see Fig. 3.2).

Notice that a local rearrangement of the lattice allows to split a topological lattice defect into its elemental components, and vice versa. For example, a $\pi/2$ disclination of type 1 can be split into a $\pi/2$ disclination of type 0 and a dislocation with odd translation holonomy.

3.2.3. Screw disclinations in three dimensions

In three dimensions, a disclination can also carry a translation holonomy T_z in the direction of the rotation axis. These disclinations can be constructed through a Volterra process by translating one of the cut surfaces, Σ_1 or Σ_2, along the z direction before they are reconnected. A disclination that carries such a translation holonomy is called a screw disclination.

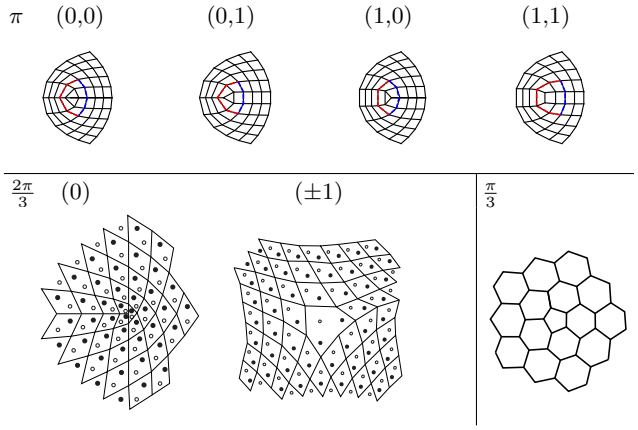

Figure 3.2. Disclinations in twofold-, threefold-, and sixfold-symmetric lattices: π disclinations in twofold-symmetric lattices come in four types ($T_x \bmod 2, T_y \bmod 2$) distinguished by the parity of their translation holonomy T_i ($i = x, y$). The translation holonomy is indicated by the dashed lines, where red (blue) lines are translations in the x (y) direction of the local coordinate system. The unit cells of three- and sixfold-symmetric lattice are parallelograms composed of two equilateral triangles (see Fig. 3.5). For a threefold-symmetric lattice, there are three types of $2\pi/3$-disclinations. Different threefold rotation centers within the unit cell are denoted by filled and hollow dots. The two types (± 1) of $2\pi/3$-disclinations differ by exchanging the filled-dot rotation centers with the hollow-dot rotation centers. Finally, in sixfold-symmetric lattices there is only a single type of $\frac{\pi}{3}$ disclinations, which is centered at a five-sided cell.

3.2.4. Decorating a lattice with disclination

A physical system is constructed by decorating the abstract lattice, defined by its symmetry group G, with local orbitals in space while respecting the symmetries. The physical properties of the local degrees of freedom on the lattice are then described by the Hamiltonian H. Below, we discuss how to construct a Hamiltonian H on a lattice with disclination from a defect-free Hamiltonian, such that H is locally indistinguishable from the defect-free system everywhere except at the disclination.

For our construction, we consider the lattice containing the disclination as the result of a Volterra process [see again Fig. 3.1(b) and (c)] with the real space positions $\vec{r}$ and $\mathcal{R}_\Omega \vec{r}$ along the cut lines identified, where $\mathcal{R}_\Omega$ denotes a rotation by the angle Ω. In this picture, both the coordinate system and the local degrees of freedom of two adjacent unit cells across the cut lines are rotated with respect to each other by the Franck angle Ω. A particle hopping across this branch cut has to respect this local change of basis. Hence, its wavefunction $|\psi(\vec{r}-\delta\vec{r})\rangle$ has to transform to $U(\mathcal{R}_\Omega)|\psi(\mathcal{R}_\Omega\vec{r}+\delta\vec{r})\rangle$ when moving from $\vec{r}-\delta\vec{r}$ to $\mathcal{R}_\Omega\vec{r}+\delta\vec{r}$ across the branch cut. Here, $U(\mathcal{R}_\Omega)$ is the representation of rotation symmetry acting on the local degrees of freedom within a unit cell and $\delta\vec{r}$ is a finite but small integer mulitple of the lattice vectors. As mentioned above, the points $\vec{r}$ and $\mathcal{R}_\Omega\vec{r}$ are identified. This implies that all hopping terms crossing the branch cut have to incorporate the basis transformation. Requiring that the hopping across the branch cut be indistinguishable from the corresponding hopping in the bulk, the hopping terms $H^{\text{cut}}_{\vec{r},\vec{r}+\vec{a}_n}$, in mathematically positive direction with respect to the Franck angle Ω of the disclination, can be expressed as

$$H^{\text{cut}}_{\vec{r},\vec{r}+\vec{a}_n} = U(\mathcal{R}_\Omega) H_{\vec{r}_i,\vec{r}_i+\vec{a}_n} \tag{3.2}$$

where $H_{\vec{r}_i,\vec{r}_i+\vec{a}_n}$ is a corresponding hopping element between unit cells at $\vec{r}_i$ and $\vec{r}_i+\vec{a}_n$ in the bulk.

The hopping terms across the branch cut in Eq. (3.2) have to respect all *internal symmetries* $g \in G_{\text{int}}$ of the crystal, where g denotes the symmetry element and G_{int} is the group of internal symmetries. Internal symmetries are global onsite symmetries that act trivially on the real space coordinates. Examples are time-reversal symmetry $\mathcal{T}$, particle-hole antisymmetry $\mathcal{P}$, chiral antisymmetry $\mathcal{C} = \mathcal{P}\mathcal{T}$, and $SU(2)$ spin rotation symmetry $\mathcal{S}$. The onsite action of each (crystalline or internal) symmetry element $g \in G \times G_{\text{int}}$ on the Hamiltonian H is expressed by its representation $U(g)$. For general hopping elements $H_{\vec{r}_i,\vec{r}_i+\vec{a}_n}$, the internal unitary symmetries/antisymmetries $\mathcal{U} = \mathcal{S}, \mathcal{C}$ require

$$U(\mathcal{U}) H^{\text{cut}}_{\vec{r}_i,\vec{r}_i+\vec{a}_n} U(\mathcal{U})^\dagger = \pm H^{\text{cut}}_{\vec{r}_i,\vec{r}_i+\vec{a}_n}. \tag{3.3}$$

This condition can only be fulfilled if the representation of the unitary rotation symmetry commutes with all internal symmetries/antisymmetries of the crystal. If rotation and internal symmetries do not commute, any finite hopping across the branch cut that respects the internal symmetries/antisymmetries necessarily breaks rotation symmetry locally along the branch cut. In this case, the algebraic relations between the symmetry operators obstruct the choice of a hopping across the branch cut that is locally indistinguishable from the bulk hopping. As such, the branch cut can be regarded as a physical domain wall separating regions that are distinguishable by a local order parameter that relates to the local arrangement of the orbitals in the unit cell (see Appendix B.1.1 for an in-depth discussion).

We point out that this domain wall may become locally unobservable if the sample as a whole breaks at least one of the internal symmetries, or if the translation holonomy of the disclination involves a translation holonomy by a fractional lattice vector, see Appendix B.1.1. Throughout this chapter we aim to make general statements for the topological properties in each symmetry class, and omit model specific details. Therefore, we assume throughout the chapter that (i) the sample as a whole obeys all internal symmetries and (ii) that the translation holonomy of the disclination is restricted to integer multiples of the lattice vectors. The latter condition is fulfilled by the topological lattice defects as constructed in this section, because this construction provides a global definition of the unit cell even in the presence of a disclination.

The internal antiunitary symmetries/antisymmetries $\mathcal{A} = \mathcal{T}, \mathcal{P}$ give the constraint

$$U(\mathcal{A}) \left(H^{\text{cut}}_{\vec{r}_i,\vec{r}_i+\vec{a}_n}\right)^* U(\mathcal{A})^\dagger = \pm H^{\text{cut}}_{\vec{r}_i,\vec{r}_i+\vec{a}_n}. \tag{3.4}$$

Note that there is generally a $U(1)$ phase ambiguity in choosing the representation of rotation symmetry: the Hamiltonian is symmetric under $e^{i\phi}U(\mathcal{R}_\Omega)$ for all phases ϕ. The value of ϕ enters in the commutation relations of $e^{i\phi}U(\mathcal{R}_\Omega)$ with antiunitary time-reversal symmetry $\mathcal{T}$ and particle-hole antisymmetry $\mathcal{P}$ as $U(\mathcal{R}_\Omega)U(\mathcal{A}) = e^{-2i\phi}U(\mathcal{A})U(\mathcal{R}_\Omega)^*$. The condition in Eq. (3.4) therefore fixes the phase factor $e^{i\phi}$ up to a sign, but does not otherwise obstruct the formation of disclinations which are indistinguishable away from their core.

If a system is symmetric under the combined action of rotation and time-reversal symmetry $\mathcal{RT}$, but neither under the action of rotation nor time-reversal symmetry separately, the system is said to have *magnetic* rotation symmetry. When constructing a $2\pi/n$ disclination in a lattice with an n-fold magnetic rotation axis using a Volterra process, we have to connect two parts of the lattice that are mapped onto each other under magnetic rotation symmetry. Since the disclination cannot involve the time-reversal operation, any finite hopping across the branch cut necessarily breaks magnetic rotation symmetry. Thus, the branch cut forms a domain wall separating regions distinguishable by a local order parameter that is odd under time reversal symmetry, see Appendix B.1.3 for an explicit example.

In summary, a necessary condition for the application of a *bulk-equivalent* hopping across the branch cut [see Eq. (3.2)] is a unitary rotation symmetry that commutes with all unitary internal symmetries and antisymmetries of the system. In the absence of additional crystalline symmetries, this condition is also sufficient. If this condition is violated, the Volterra process leads to a domain wall emanating from the disclination.

3.2.5. Rotation holonomy for spinful fermions

Rotating a particle with half-integer spin by 2π shifts the phase of its wavefunction by π. As a consequence, it seems as if the rotation holonomy of disclinations for particles with half-integer spin should be defined modulo 4π [54]. However, when transporting a half-integer spinful particle around a 2π disclination [1], there are two effects contributing a π phase to its wavefunction: (i) the rotation of the real space coordinate system and (ii) the basis rotation of the local degrees of freedom. The total phase acquired is thus $\pi + \pi = 2\pi$.

The geometric phase shift α obtained upon parallel transport of a particle along a closed loop can be quantized to multiples of π by two different mechanisms: a quantized magnetic flux or a fluxoid quantization in superconductors [60]. In the presence of time-reversal symmetry, the magnetic flux enclosed by a closed loop is quantized to multiples of the magnetic flux quantum $\phi_0 = hc/2e$. Parallel transporting a charged particle around a magnetic flux quantum leads to a π phase shift of its wavefunction. Throughout the chapter we say a defect carries a π-flux if the geometric phase shift α is equal to $\pi \mod 2\pi$.

As by the above argument parallel transporting a half-integer spin particle around a 2π disclination does not cause a π phase shift, we distinguish between disclinations on the one hand and point defects binding magnetic flux quanta on the other hand. Throughout the chapter, we therefore assume that a disclination does not bind a magnetic flux quantum unless otherwise stated.

[1] A 2π disclination may also be formed through a Volterra process, for example by inserting a segment.

3.3. SECOND-ORDER TOPOLOGY AND DISCLINATIONS

In this section we identify the minimal set of assumptions required to show that a strong, rotation symmetry-protected second-order topological phase hosts anomalous disclination states. We first describe general properties of rotation-symmetry protected topological phases and then derive the existence of anomalous states at disclinations from those properties.

3.3.1. Strong rotation-symmetry protected second-order topological phases

A *strong* topological phase remains unaffected when translation symmetries are broken. This allows to coarse-grain the lattice and perform any deformation that breaks the translation symmetries while preserving internal and rotation symmetries. For strong topological phases, we only need to require that the topological properties are realized when the system size is much larger than any microscopic length scale associated with the Hamiltonian. Consequently, during a Volterra process of a topological crystalline phase we can assume that also the cut-out part is in the same topological phase.

A second-order topological phase protected by rotation symmetry has $(d-2)$ dimensional anomalous boundary states, for example isolated Majorana bound states at the corners of a two-dimensional crystal or chiral/helical modes at the hinges of a three-dimensional crystal (see also Chapter 2 for an in-depth discussion). This is illustrated in Figs. 3.3(a) and (b). We require that the anomalous boundary excitations are *intrinsic* [11, 12, and 25], i.e., we allow any changes of the crystal termination consistent with the rotation symmetry, for instance a decoration of the boundary with lower-dimensional topological phases. This property ensures that the anomalous boundary excitations are truly attributed to the topology of the d-dimensional bulk. Furthermore, throughout this chapter we focus on tenfold-way anomalous bound-

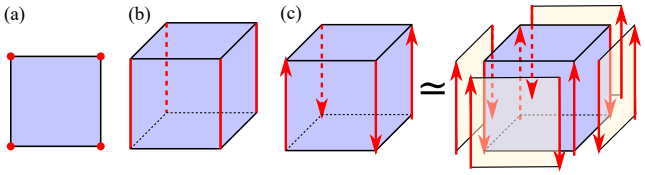

Figure 3.3. Examples of strong topological phases protected by a fourfold rotation symmetry: (a) with Majorana corner states in two dimensions, and (b) with helical hinge modes in three dimensions. In (c), a three-dimensional insulator with chiral hinge modes consistent with a magnetic rotation symmetry $C_4\mathcal{T}$ is depicted. A symmetry-allowed decoration as indicated changes the propagation direction of the chiral modes after hybridization.

ary states appearing in systems described by quadratic fermionic Hamiltonians.

3.3.2. Topological charge

The topological charge associated with an anomalous boundary state quantifies the anomaly. For topological insulators, helical hinge modes are characterized by a $\mathbb{Z}_2$ topological charge $Q \in \{0, 1\}$ measuring their existence. Chiral hinge modes are quantified by a $\mathbb{Z}$ topological charge $Q = n_+ - n_-$ defined as the difference of the number of forward-propagating (n_+) and backward-propagating (n_-) chiral modes. The Abelian groups $\mathbb{Z}_2$ and $\mathbb{Z}$ determine how the anomalous boundary states hybridize (fusion rules). For topological superconductors, Majorana corner modes and helical Majorana hinge modes have a $\mathbb{Z}_2$ topological charge, while chiral Majorana modes have a $\mathbb{Z}$ topological charge. Zero-energy eigenstates in Cartan classes AIII, BDI and CII are simultaneous eigenstates of the unitary chiral antisymmetry $\mathcal{C} = \mathcal{PT}$ with eigenvalue $c = \pm 1$. This symmetry prohibits to hybridize and gap out zero-modes with the same eigenvalue c. Therefore, a $\mathbb{Z}$ topological charge is obtained by counting the number of zero-energy eigenstates weighted with their eigenvalue c.

Anomalous states always appear in pairs with canceling anomaly at the boundary or at defects of a topological bulk [31]. Consequently, in a closed system, isolated Majorana bound states, or Kramers pairs thereof, always come in pairs. The zero-dimensional anomalous states with $\mathbb{Z}$ topological charge occur in pairs with opposite eigenvalue under chiral antisymmetry. One-dimensional anomalous states form closed loops at the boundary or along defect lines of a topological bulk. For a three-dimensional system with anomalous hinge states, the number of inward and outward propagating modes intersecting any closed (or infinite open) surface needs to be equal and the associated topological charge needs to cancel.

In summary, for anomalous states with $\mathbb{Z}_2$ topological charge Q_i the total topological charge Q_{tot} needs to be even

$$Q_{\text{tot}} = \sum_i Q_i \mod 2 = 0, \tag{3.5}$$

where for zero-dimensional anomalous states we sum over all anomalous states in the system, and for one-dimensional anomalous states we sum over all states intersecting an arbitrary closed (or infinite open) surface. Similarly, for zero- and one-dimensional anomalous states with $\mathbb{Z}$ topological charge Q_i, the total topological charge Q_{tot} must vanish

$$Q_{\text{tot}} = \sum_i Q_i = 0. \tag{3.6}$$

3.3.3. Boundary-signature constraints from rotation symmetry

A rotation-symmetric sample can be divided into asymmetric sections. An asymmetric section is the maximal volume such that no two points in the volume are related by rotation symmetry. The rotation symmetry then relates the topological charge in symmetry-related sections. Because anomalous states always come in pairs ($Q_{\text{tot}} = 0$), asymmetric sections with non-zero topological charge can only exist in systems with even order of rotation symmetry, i.e., C_2, C_4 and C_6. The anomalous boundary signatures in rotation symmetric topological phases have also been discussed in Refs. 4–6, 8, 9, 11–27, and 55 and in chapter 2.

For asymmetric sections exhibiting a non-zero $\mathbb{Z}$ topological charge, the internal action of rotation must invert the topological charge of the anomalous states to satisfy the anomaly cancellation criterion in Eq. (3.6). In particular, a rotation-symmetry protected second-order topological phase hosting anomalous zero-energy corner states in Cartan classes AIII, BDI and CII can exist only if the representation of rotation symmetry anticommutes with chiral antisymmetry. In this case, the chiral eigenvalue $c = \pm 1$ of states related by rotation symmetry alternates. Similarly, a second-order topological phase with chiral (Majorana) hinge modes may exist only in the presence of magnetic rotation symmetry. The reason is that the time-reversal operation is required to invert the propagation direction of modes related by symmetry.

For second-order anomalous states with $\mathbb{Z}$ topological charge protected by rotation symmetry, only a $\mathbb{Z}_2$ factor can be attributed to the bulk topology as an intrinsic boundary signature [4, 11, 12, and 25] (see also Section 2.5 of Chapter 2). This factor merely measures the existence of anomalous states but not their number. To illustrate this, consider a cubic crystal with chiral hinge modes, as depicted in Fig. 3.3(c), as an example of a second-order topological phase protected by magnetic fourfold rotation symmetry $C_4\mathcal{T}$. A symmetry-allowed decoration with Chern insulators reverses the propagation direction of the chiral hinge modes, thereby changing their $\mathbb{Z}$ topological charge by an even number.

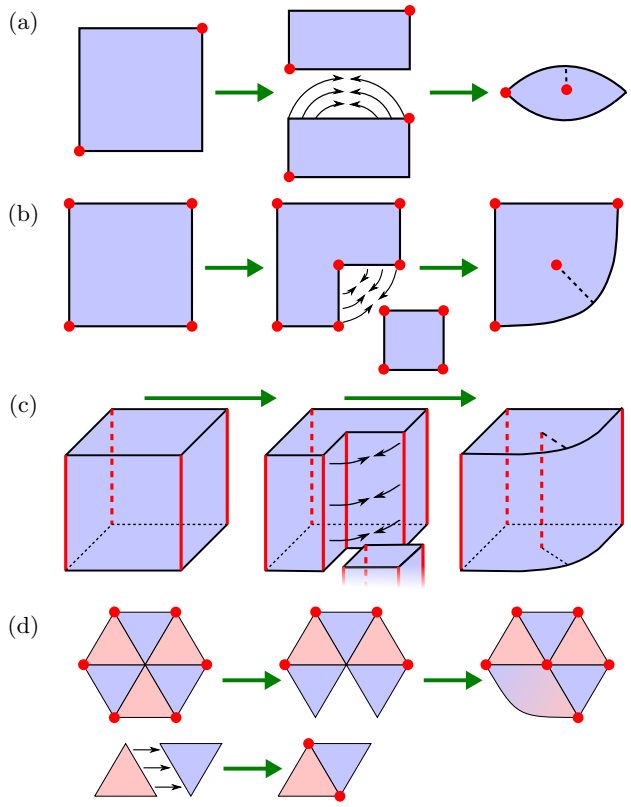

Figure 3.4. Volterra processes to construct disclinations in systems with second-order topology and different rotation symmetries: (a) twofold symmetry in two dimensions, (b) four-fold symmetry in two dimensions, (c) four-fold symmetry in three dimensions, (d) sixfold symmetry in two dimensions. Red dots and red lines indicate anomalous corner and hinge modes, respectively. In (d), adjacent triangles in red and purple are related by a sixfold rotation.

3.3.4. Volterra process with a second-order topological bulk

In the following, we establish the existence of anomalous disclination states in a given second-order topological phase by performing a Volterra process. Recall that we consider strong topological phases that do not rely on the presence of translation symmetries. Therefore, we allow to coarse-grain the lattice or break the translation symmetries. In this case, disclinations are characterized only by their Franck angle Ω. We lay out our arguments for two-dimensional systems in particular. Nevertheless, they are generalized straightforwardly to $d > 2$ dimensions by considering a symmetric-pillar geometry. In this case, we apply the anomaly cancellation criterion to the $(d-2)$-dimensional hinge modes with respect to a plane perpendicular to the rotation axis.

A unique correspondence between bulk topology and disclination anomaly exists only if the system can be made locally indistinguishable from the bulk everywhere away from the disclination as a result of the Volterra process. This requires us to connect the lines/surfaces at the branch cut using the appropriate hybridization terms given by the conditions imposed by Eq. (3.2). Below, we establish the correspondence for symmetry classes in which these conditions can be fulfilled.

In some symmetry classes, however, these conditions can not be satisfied. For instance, we showed above that second-order topological phases with zero-energy states of $\mathbb{Z}$ topological charge exist only if rotation symmetry anticommutes with chiral antisymmetry. However, a chiral antisymmetry anticommuting with rotation symmetry forbids to construct bulk-equivalent hopping terms across the branch cut in the Volterra process (see Sec. 3.2 4). Similarly, second-order topological phases hosting one-dimensional chiral hinge states require magnetic rotation symmetry, for which bulk-equivalent hopping terms across the branch cut are also not allowed. These arguments can be generalized to second-order topological phases protected by rotation symmetry with $\mathbb{Z}$ anomalous boundary states in any dimension $d \geq 2$ (see Appendix B.1.4).

A detailed discussion on other symmetry classes where the branch-cut hopping condition in Eq. (3.2) cannot be satisified is provided in Appendix B.1.

Twofold rotation symmetry

Twofold rotation-symmetry protected second-order topological phases host anomalous states on symmetry-related points of their boundary. The Volterra process to construct a π disclination is illustrated in Fig. 3.4(a). The first step is to cut the sample into two symmetric halves. We require that the cutting process preserve the bulk and surface Hamiltonians except for the breaking of bonds along the cut. Therefore, the two symmetric halves host anomalous boundary states at corners with the same orientation as the original sample. Note that this requires the energy gap to close and reopen along the cut. Upon deforming the sample and hybridizing the bonds across the cut to complete the Volterra process, the two upper corners connect to form a smooth boundary. In the resulting sample, the bulk and all boundaries are gapped by construction. Consequently, the anomalous state formerly located at one of the upper corners moves to the disclination in the process. An equivalent way to see this is to note that, upon gluing the surface, the boundary gap closes and reopens in the same way as when cutting the sample.

Fourfold rotation symmetry

In Fig. 3.4(b), we show the Volterra process for a fourfold rotation-symmetric system in two dimensions along with its boundary signatures. The removed segment in this process is itself fourfold symmetric and has, by the anomaly cancellation criterion, second-order boundary

signatures at its corners. After deforming and gluing the other part, the resulting lattice has four singular points that may host zero-dimensional anomalous states: the three corners and the disclination. As the three corners remain unaffected during the deformation, the disclination has to host an anomalous state to satisfy the anomaly cancellation criterion. Fig. 3.4(c) shows the same process for a three dimensional system.

Sixfold rotation symmetry

We consider a sixfold symmetric sample in the shape of a hexagon. It can be divided into six equilateral triangles as demonstrated in Fig. 3.4(d). A two-dimensional second-order topological phase protected by sixfold rotation symmetry hosts anomalous boundary states on symmetry-related corners of a hexagonal sample. Since each triangle has only threefold rotation symmetry, there are two types of triangles related by a sixfold rotation. The anomaly cancellation criterion together with threefold rotation symmetry requires that the topological charge at each corner of the triangle must cancel, i.e., the topological charge at each corner, if present, must be even. In order for the hexagonal sample to exhibit its anomalous corner states, hybridizing two triangles along a shared boundary needs to close and reopen the excitation gap to create a pair of anomalous states [see Fig. 3.4(d)]. Conversely, breaking the bonds between two triangles closes and reopens the gap along the shared boundary, thereby removing the anomalous corner states. Putting all triangles together results in six anomalous states at the center of the hexagon, which gap out upon hybridization.

In the first step of the Volterra process, we remove a triangle from the hexagon. This requires to break the bonds between adjacent triangles of opposite orientation. By the arguments above, the excitation gap closes and reopens along both of the cut lines, thereby removing the anomalous corner states. In the second step, we deform one triangle adjacent to the cut to glue the sample back together. This process rotates the part of the deformed triangle close to the cut by $\pi/3$. As the type of triangle is determined by the orientation of the triangle in space, the deformation smoothly interpolates between the two types as defined above. Thus, hybridizing the deformed sample across the cut creates a pair of anomalous boundary states, one at the disclination and one at the corner. The disclination state appears because the gap closes and reopens an odd number of times during the Volterra process: once along each of the two cut lines when removing a triangle, and once when gluing the edges back together.

3.4. TOPOLOGICAL CRYSTALS

Our considerations thus far were independent of translation symmetries. In this section, we extend our arguments to lattice models with discrete translation symmetries. As discussed in Sec. 3.2, disclinations in lattices are classified into topological equivalence classes according to their rotation *and* translation holonomy. Real-space representations of topological crystalline phases naturally including translation symmetries can be constructed using the framework of *topological crystals* [22]. Below, we briefly review and discuss the essential steps of the topological-crystal construction applied to lattices with rotation symmetries. Moreover, we extend the recipe developed in Ref. 22 by showing how to relate the constructed real-space representation to weak and higher-order topological phases obtained from other classification schemes [12, 25, and 61]. Finally, we apply the topological-crystal construction to determine the existence of anomalous states at disclinations of all types.

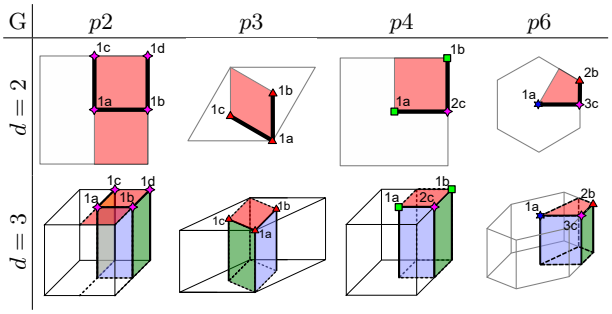

Figure 3.5. Cell decompositions of unit cells in space group G in dimensions $d = 2, 3$: Pink stars, red triangles, green squares and blue stars denote inequivalent twofold, threefold, fourfold and sixfold rotation axes, respectively. Colored areas and bold lines denote inequivalent 2-cells and 1-cells, respectively. In two dimensions, the 2-cell is the asymmetric unit. The 0-cells coincide with the rotation axis. In three dimensions, the asymmetric unit is a 3-cell whose hinges are denoted by dotted lines. The 0-cells lie at the end of the rotation axes. We use the standard labels for Wyckoff positions.

3.4.1. Cell decomposition

Consider a d-dimensional space $\mathbb{R}^d$ subject to the symmetry group $G \times G_{int}$. As only topological crystalline phases protected by translation and/or rotation symmetry can contribute to the anomaly at a disclination (see Sec. 3.5 2 below), we focus on the (magnetic) space groups $G = pn$ ($G = pn'$) generated by n-fold (magnetic) rotation symmetry and translations. Further note that only ($n \in \{2, 3, 4, 6\}$)-fold rotations are compatible with translation symmetry. First, one defines an *asymmetric unit* (AU) as the interior of the largest region in $\mathbb{R}^d$ such that no two distinct points in this region are related by a crystalline symmetry $g \in G$. A cell complex structure is generated by copying the AU throughout $\mathbb{R}^d$ using all elements of the space group G. Next, one places cells of dimension $(d-1)$ on faces where adjacent AUs meet. Throughout the following, cells of spatial dimension d_b are denoted as d_b-cells. These cells are chosen as large

as possible, such that no two distinct points in the same cell are related by a crystalline symmetry. Furthermore, cells are not allowed to extend over corners or hinges of the AUs. In the same way, one continues iteratively by placing $(d-n-1)$-cells on faces where $(d-n)$-cells coincide. We present the resulting cell complex structures for $p2$, $p3$, $p4$ and $p6$ in two and three dimensions in Fig. 3.5 (see Appendix B.2.1 for more details).

3.4.2. Decoration with topological phases

The considered space is filled with matter by decorating the d_b-cells with d_b-dimensional topological phases. The topological phases have to satisfy all internal symmetries of the cell. Furthermore, a cell located on a mirror plane or on a rotation axis can only be decorated with topological phases satisfying the crystalline symmetries that leave the cell invariant. As one aims to construct only phases with an excitation gap in the bulk, one also requires that gapless modes on adjacent faces or edges of the decorated cells gap out mutually.

The tenfold-way topological phases have an Abelian group structure where the group operation is the direct sum "$\oplus$" of two Hamiltonians [1, 3, and 31]. Topological crystals constructed as decorations with tenfold-way topological phases inherit this Abelian group structure. This allows to choose a set of generators from which all topological crystals can be constructed using the direct sum and symmetry-allowed deformations of the generating topological crystals.

The labels *weak* and *strong* for topological crystalline phases refer to the behavior of the topological crystalline phase under breaking of translation symmetry. A topological crystalline phase is called weak if its topological invariant can be changed by a redefinition of the unit cell, thereby breaking the translation symmetry of the original crystal. If this is not possible, the topological crystalline phase is termed strong. For a topological crystal, we determine whether it is weak or strong using the following procedure: we first double the unit cell by combining two adjacent unit cells of the original crystal. After this redefinition we allow for symmetric deformations to express the result in terms of generating topological crystals. A topological crystal that remains invariant during this procedure corresponds to a strong topological crystalline phase.

Furthermore, we identify the order of the topological crystal from its boundary signature. A topological crystal corresponding to a decoration of d_b cells has a (d_b-1)-dimensional boundary signature. This is because its anomalous boundary states are inherited from the decoration. Hence, it represents a topological phase of order $(d-d_b-1)$.

3.4.3. Decorations of lattices with rotation symmetry

Without specifying the set of internal symmetries, we first work out for each space group the set of generating topological crystal decorations. For these generators, we then check whether they describe a weak or a strong topological phase, and finally determine the order of this phase. The group of internal symmetries together with the space group and the algebraic relations of their representations finally decides whether the decoration is valid. In other words, we determine whether the d-dimensional topological phases required to decorate the d-cells of the system exist for a given set of internal symmetries, and whether the anomalous states at the cell interfaces can be gapped out. In particular, to decide whether the asymmetric unit can be decorated with a topological phase, we have to ensure that all boundaries, corners, and hinges are gapped at the rotation axis.

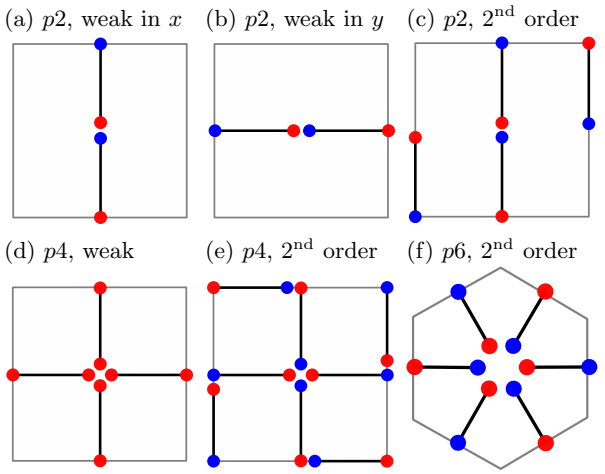

Figure 3.6. Generating sets of valid 1-cell decorations (cross sections of 2-cell decorations parallel to the rotation axis) of two (three) dimensional lattices with twofold, fourfold, and sixfold rotation axes. Black lines denote one (two) dimensional topological phases with anomalous boundary states depicted as dots: for $\mathbb{Z}$ topological phases, the red and blue dots distinguish between topological charges $q = +1$ and $q = -1$, respectively. For $\mathbb{Z}_2$ topological phases with topological charges $q \mod 2$, the two colors are equivalent.

For three-dimensional systems we omit decorations of 1-cells parallel to the rotation axis as they cannot give rise to anomalous states with the same dimension as the disclination line. Moreover, the plane perpendicular to the rotation axis corresponds to a two-dimensional rotation-symmetric system. The decorations in this plane acquire the label weak because their topological invariant can be changed by a redefinition of the unit cell in the z direction.

We defer the detailed derivation of the generating 1-cell (2-cell) decorations for rotation-symmetric lattices in two (three) dimensions to Appendix B.2.2. Below, we present the generating sets together with their properties for decorations with $\mathbb{Z}$ topological phases. The results for decorations with $\mathbb{Z}_2$ phases are straightforwardly obtained by taking the topological charge of the decorations modulo two.

Twofold rotation symmetry. With twofold rotation symmetry, there exist two distinct weak topological phases and one strong second-order topological phase, which we depict in Figs. 3.6(a)-(c).

Threefold rotation symmetry. For threefold symmetry, there is no valid 1-cell decoration (2-cell decoration parallel to the rotation axis). The reason is that each 1-cell (2-cell) ends at a threefold rotation axis at which the anomaly cancellation criteria (3.5) and (3.6) cannot be satisfied locally. Thus, there are neither weak nor second-order topological phases with threefold rotation symmetry.

Fourfold rotation symmetry. In a two (three) dimensional lattice with fourfold rotation symmetry, all 1-cell decorations (2-cell decorations parallel to the rotation axis) are generated from one weak and one strong second-order topological phase, which we show in Figs. 3.6(d) and (e). The weak phase exists only for 1-cell (2-cell) decorations with $\mathbb{Z}_2$ topological phases.

Sixfold rotation symmetry. With sixfold rotation symmetry, the only valid 1-cell decoration (2-cell decoration parallel to the rotation axis), which we depict in Fig. 3.6(f), corresponds to a strong second-order topological phase.

Furthermore, in a symmetry class in which the $(d-2)$-dimensional anomalous states have $\mathbb{Z}$ topological charge, one can show that the direct sum of a strong second order topological phase with itself can be adiabatically deformed such that no $(d-2)$-dimensional anomalous states remain in the system (see Appendix B.2.2). This holds for all $(n = 2, 4, 6)$-fold symmetric systems. It confirms our statement from Sec. 3.3 that only a $\mathbb{Z}_2$ factor of the topological charge of anomalous boundary states in these systems is an intrinsic property of the topological bulk.

3.4.4. Disclinations with weak and second-order topological phases

In the following, we determine for each generator of weak and second-order topological phases (see Fig. 3.6) whether it hosts topological disclination states. We realize this by decorating a lattice with disclination, as constructed through a Volterra process, with its topological-crystal limit. The disclination breaks rotation symmetry locally, thus only internal symmetries constrain the hybridization of disclination states.

We require that the system is locally indistinguishable from the bulk along the branch cut. As we have shown in Sec. 3.3 4, this is not possible in symmetry classes that host rotation-symmetry protected second-order topological phases with $\mathbb{Z}$ topological charge. In fact, in these symmetry classes a decoration with weak or second-order topological phases represents an obstruction to forming a lattice with an isolated disclination (see Appendix B.2.3). We therefore restrict our discussion to symmetry classes whose $d-2$ dimensional anomalous states have $\mathbb{Z}_2$ topological charge.

We show the corresponding decorations for twofold, fourfold, and sixfold symmetric lattices in Figs. 3.7, 3.8, and 3.9. The decoration pattern is unique up to an arbitrary decoration at the disclination itself, which cannot change the total topological disclination charge due to the anomaly cancellation criterion of Sec. 3.3 2. Therefore, the unique bulk decoration pattern determines the existence of anomalous states at the topological lattice defect.

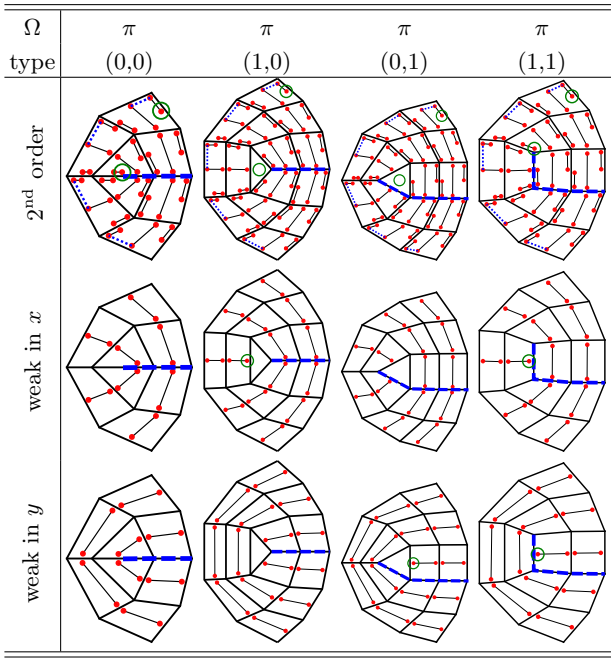

Figure 3.7. Decorations of twofold rotation-symmetric lattices with π disclinations of all types as defined in Fig. 3.2: decorations with second-order topological phases protected by twofold rotation symmetry and decorations with weak topological phases as stacks in the x and y directions. Red dots represent $d-2$ dimensional anomalous states with $\mathbb{Z}_2$ topological charge. Dashed blue lines indicate the branch cut in the Volterra process across which anomalous states hybridize. Green circles denote locations where unpaired anomalous states remain.

In three dimensions, also screw disclinations with a translation holonomy T_z along the rotation axis may occur. However, by a local rearrangement of the lattice a screw disclination can be separated into a disclination with trivial translation holonomy $T_z = 0$ and a screw dislocation carrying the translation holonomy T_z. The topological charge bound to the topological lattice defects depends only on its holonomies defined on a loop enclosing the defects. These defects can be pulled apart arbitrarily. Hence, the topological charge at a defect with multiple non-trivial holonomies can be determined from the sum of the topological charge at the individual defects with a single non-trivial holonomy.

The arguments of Ref. 46 show that the weak topological phases obtained by stacking 2D first-order phases along the rotation axis contribute $(d-2)$-dimensional

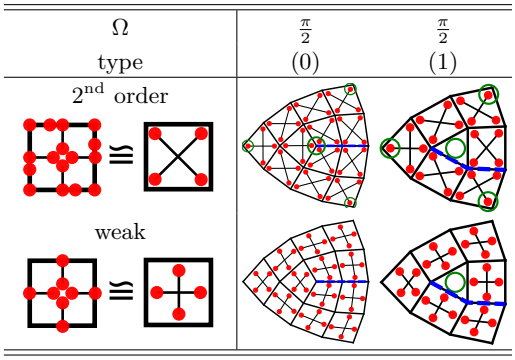

Figure 3.8. Decorations of fourfold-symmetric lattices with $\pi/2$ disclinations of both types: decorations with second-order topological phases and decorations with weak topological phases. The left column depicts the corresponding topological crystals. For simplicity, anomalous bound states hybridizing within a unit cell are not shown. We use the same symbols and colors as in Fig. 3.7.

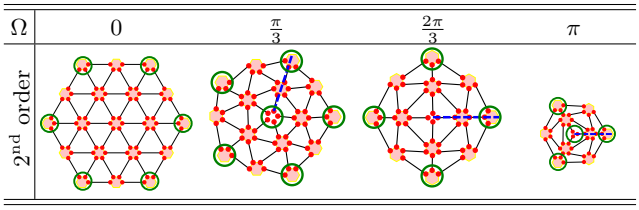

Figure 3.9. Unique decoration patterns of a sixfold rotation symmetric lattice without disclination ($\Omega = 0$) and with disclination of Franck angle $\Omega \neq 0$: decorations with second-order topological phases of $\mathbb{Z}_2$ topological charge. Symbols and colors are as in Fig. 3.7.

anomalous states to screw dislocations with odd translation holonomy T_z. While Ref. 46 considered explicitly weak topological insulators in class AII, their arguments generalize straightforwardly to other symmetry classes as well [2] [47].

In summary, we deduce that the contributions of weak and second-order topological phases with topological invariants $\vec{G}_\nu = (\nu_x, \nu_y, \nu_z)^T$ and $\nu_{2\pi/n}$, respectively, to the number of $(d-2)$-dimensional anomalous states θ_n^{disc} at a disclination with rotation holonomy Ω and translation holonomy $\vec{T}$ are

$$\theta_2^{\text{disc}} = \frac{\Omega}{2\pi}\nu_\pi + \vec{T}\cdot\vec{G}_\nu \mod 2 \tag{3.7}$$

$$\theta_3^{\text{disc}} = T_z\nu_z \tag{3.8}$$

$$\theta_4^{\text{disc}} = \frac{\Omega}{2\pi}\nu_{\pi/2} + \vec{T}\cdot\vec{G}_\nu \mod 2 \tag{3.9}$$

$$\theta_6^{\text{disc}} = \frac{\Omega}{2\pi}\nu_{\pi/3} + T_z\nu_z \mod 2. \tag{3.10}$$

In two dimensions, the dimension spanned by the z direction is absent such that T_z and ν_z are absent.

3.5. BULK-BOUNDARY-DEFECT CORRESPONDENCE

The bulk-boundary correspondence and the bulk-defect correspondence link the bulk topological invariant of a sample to the existence of anomalous states at its boundaries and its defects, respectively. Cumulating our results from previous sections, we now determine the precise relationship between the topological charge at point defects and bulk topological invariants in rotation-symmetric systems.

3.5.1. Topological charge at disclinations

In Sec. 3.2, we argued that the rotation and translation holonomies of disclinations on the one hand and bound magnetic flux quanta on the other hand are distinct topological properties of point defects. In the previous Sec. 3.4, we worked out the contributions of weak and second-order topological phases to the topological charge at a disclination. Conversely, to determine the bulk topological invariants from the topological charge at the lattice defect, we first need to investigate under which conditions a *first-order* topological phase hosts anomalous states at a point defect.

As a result, we find that tenfold-way (first-order) topological phases, which are independent of crystalline or internal unitary symmetries for their protection, host anomalous states at disclinations only if bound to a geometric π-flux quantum (see Appendix B.3 for the proof). Our general result is in agreement with case studies in the literature indicating that these phases may bind $(d-2)$-dimensional anomalous states to point and line defects with geometric π-flux quanta [31, 47, 48, 62–65] if allowed in the respective symmetry class. Furthermore, we find that this statement can be generalized to all dimensions $d \geq 2$ (see Appendix B.3.2). As a consequence, a tenfold-way topological phase in a symmetry class that allows for $(d-2)$-dimensional anomalous defect states hosts an anomalous state at a disclination if and only if the disclination also binds a geometric π-flux quantum.

Hence, we can express the total number of $(d-2)$-dimensional anomalous state θ_n at a disclination in an n-fold rotation-symmetric system, in the presence of a unitary rotation symmetry whose representation commutes

[2] In particular, Ref. 46 considers a finite sample with screw dislocation. The screw dislocation is the termination of two step edges on the two opposite surfaces perpendicular to the screw dislocation. In a corresponding weak topological phase, these step edges host one-dimensional anomalous states. As the one-dimensional anomalous state cannot terminate at the screw dislocation, it must continue along the screw disclination and connect to the opposite surface. This argument holds for all symmetry classes hosting one-dimensional anomalous states.

with all internal unitary symmetries and antisymmetries (see Sec. 3.2 4), as

$$\theta_n \mod 2 = \theta_n^{\text{disc}} + \frac{\alpha}{\pi}\nu_1, \tag{3.11}$$

where θ_n^{disc} is defined as in Eqs. (3.7)–(3.10), $\alpha = l\pi$, $l \in \mathbb{Z}$, is the geometric phase obtained by parallel transporting a particle around the defect, and ν_1 is the tenfold-way strong first-order topological invariant of the system's bulk Hamiltonian. In the presence of time-reversal symmetry, the geometric phase $\alpha = \frac{\phi}{\phi_0}$ is given by the quantized magnetic flux $\phi = l\phi_0$ bound to the defect, where $\phi_0 = \frac{hc}{2e}$ is the magnetic flux quantum.

One can determine the second-order topological invariant $\nu_{2\pi/n}$ and the weak topological invariants $\vec{G}_\nu = (\nu_x, \nu_y, \nu_z)$ by probing disclinations with different translation holonomies. The parity of the first-order topological invariant is determined from the existence of an anomalous state at a π-flux point defect. For phases of matter that obey rotation symmetry but no translation symmetry, Eqs. (3.7)–(3.11) apply with trivial translation holonomy $\vec{T} = \vec{0}$, in agreement with our arguments in Sec. 3.3. Equations (3.7)–(3.11) are the central result of this chapter.

If the representation of the unitary rotation symmetry does not commute with all internal unitary symmetries and antisymmetries, or if the symmetry group does not contain a unitary rotation symmetry, the cut in the Volterra process remains *distinguishable* from the bulk (see Sec 3.2 4). In these cases, the disclination must be the end point of a domain wall between regions distinguishable by their local arrangements of orbitals in the unit cell (see Appendix B.1.1 for details). Moreover, the hopping across the domain wall is not restricted to a unique pattern. Thus, we cannot determine the topological charge at the disclination from the bulk and the lattice topology alone. We can only make a statement about the parity of the topological charge along the domain wall, for which we refer the interested reader to Appendix B.1.2. A few remarks and implications related to our central results are in order.

Eqs. (3.7) to (3.11) are derived for symmetry classes whose $(d-2)$-dimensional anomalous states have $\mathbb{Z}_2$ topological charge. Nevertheless, also for symmetry classes with $\mathbb{Z}$ topological charges we can make a couple of statements. For this purpose, we note that these symmetry classes can be divided into two subsets (which are contained in Tables 3.1 and 3.2 below): (i) in symmetry classes that, at the same time, allow for strong, rotation-symmetry protected second-order topological phases, our arguments from Sec. 3.3 show that the anomaly at the disclination depends on the microscopic properties of the system. This situation gives again rise to the appearance of a domain wall, as discussed in detail in Appendix B.1. (ii) In the remaining subset of symmetry classes where strong, rotation-symmetry protected second-order topological phases are forbidden, the anomaly at the disclination may still be determined from the bulk topology alone. In particular, in three-dimensions these symmetry classes may allow for two-dimensional first-order topological phases stacked along the rotation axis. Their contribution to the number of one-dimensional anomalous states at a disclination or dislocation is $\theta = \nu_z T_z$. This is in fact the only contribution, as both first-order topological phases as well as weak topological phases obtained by stacking two-dimensional first-order topological phases in the x- or y-direction are forbidden in these symmetry classes. The former statement follows from the structure of the tenfold-way classification. The latter is a consequence of the topological crystal construction (see App. B.2). Tables 3.1 and 3.2 below contain a list of the corresponding symmetry classes in two and three dimensions, respectively.

In three dimensions, a disclination may also host a one-dimensional stack of zero-dimensional anomalous states whose pairwise annihilation is prohibited by translation symmetry along the lattice defect. These states exist in the presence of weak topological phases obtained by stacking two-dimensional topological phases along the defect direction. The contributions of stacks of two-dimensional first-order, second-order and weak topological phases are determined by similar equations as Eqs. (3.7) to (3.11), where the topological invariants $\{\nu_1, \nu_{2\pi/n}, \nu_x, \nu_y, \nu_z\}$ must be replaced by $\{\nu_z, \nu_{2\pi/n,z}, \nu_{x,z}, \nu_{y,z}, 0\}$ measuring the presence of weak topological phases obtained by a stack of two-dimensional strong first-order (ν_z), second-order ($\nu_{2\pi/n,z}$) and two-dimensional weak topological phases ($\nu_{x,z}, \nu_{y,z}$) along the defect direction. There are no contributions proportional to the translation holonomy T_z. Therefore, ν_z can be replaced by 0.

Putting our results into perspective, for lattices with rotation symmetry we have shown: (i) as any anomaly at a disclination has to be canceled somewhere else in the system, any crystalline topological phase with an anomalous state at a disclination also hosts anomalous boundary states. This provides a sufficient condition for the existence of anomalous boundary states based on the topological properties of the lattice defect alone. (ii) Each crystalline-symmetry protected topological phase contributes anomalous states only to defects that carry a holonomy of the protecting crystalline symmetry. As summarized in Eqs. (3.7) to (3.10), the rotation holonomy only contributes to disclination states in the presence of a nontrivial second-order topological invariant, whereas the translation holonomy only contributes if there are nonzero weak topological invariants. This establishes a bridge between two distinct phenomenologies of topological crystalline phases: their higher-order bulk-boundary correspondence on the one hand and their topological response with respect to topological lattice defects [36] on the other hand.

3.5.2. Presence of additional symmetries

Disclinations may exist in all space groups with rotation symmetry. For space groups with additional symmetry elements other than translations and rotations, our findings apply as follows: a strong crystalline topological phase hosts anomalous disclination states if it realizes a strong second-order topological phase after lifting all symmetry constraints except for rotation symmetries. This statement holds because we have shown the existence of anomalous disclination states for all Hamiltonians realizing second-order topological phases, which may also satisfy additional symmetries. This allows us to identify the anomaly at disclinations by considering only topological crystalline phases with translation, rotation and internal symmetries. Note, however, that we also have to respect any additional crystalline symmetries when we construct the hopping terms across the branch cut of the Volterra process, as defined in Eq. (3.2).

Furthermore, the presence of additional internal unitary symmetries $\mathcal{U}$ may protect anomalous states at points with $\mathcal{U}$-symmetry flux in first-order topological phases (see Appendix B.3.3).

3.5.3. Application to all Cartan classes

To complete our discussion, we summarize our results in Tables 3.1 and 3.2. We present a classification of first-order, second-order, and weak topological crystalline phases with real-space limits as in Fig. 3.6 for all Cartan classes describing spinful fermions with magnetic and non-magnetic rotation symmetry in two and three dimensions. Those cover all topological phases that give rise to $d-2$ dimensional anomalous states at disclinations in rotation-symmetric lattices. For each symmetry class we determine whether the disclinations have to be connected to a domain wall as discussed in section 3.2 4. This criterion determines whether the bulk-boundary-defect correspondence holds (the disclination is not associated to a domain wall), or whether it does not hold (domain wall necessarily exists).

A few remarks are in order. For spinful fermions, rotation symmetry satisfies $U(\mathcal{R}_{2\pi/n})^n = -1$ and commutes with time-reversal symmetry $U(\mathcal{R}_{2\pi/n})U(\mathcal{T})K = U(\mathcal{T})U(\mathcal{R}_{2\pi/n})^*K$, where K denotes complex conjugation. Spin-rotation symmetry, if present, can be combined with rotation symmetry such that the representation of rotation symmetry within a spin subspace satisfies $U(R_{2\pi/n})^n = 1$. For superconductors, our discussion covers all possible pairing symmetries for which $u(R_{2\pi/n})\Delta(R_{2\pi/n}\vec{k})u^\dagger(R_{2\pi/n}) = e^{i\phi}\Delta(\vec{k})$, where $u(R_{2\pi/n})$ is the representation of n-fold rotation symmetry acting on the normal-state Hamiltonian (see Appendix B.5.1 for details). We interpret Cartan class AIII as a time-reversal symmetric superconductor with $U(1)$ spin-rotation symmetry. Cartan classes BDI and CII can be realized in superconductors of spinful fermions only with an emergent time-reversal symmetry which we assume to commute with the crystalline symmetry. We present the detailed results for each symmetry class of our classification in Appendix B.5.

Cartan class	Q	G	ϕ	Weak in x / y	2^{nd} order	1^{st} order	BBDC
D	$\mathbb{Z}_2$	$p2$	0	$\mathbb{Z}_2^2$	$\mathbb{Z}_2$	$\mathbb{Z}$	✓
			π	-	-	$2\mathbb{Z}$	✓
		$p4$	$0, \pi$	$\mathbb{Z}_2$	$\mathbb{Z}_2$	$\mathbb{Z}$	✓
			$\frac{\pi}{2}, \frac{3\pi}{2}$	-	-	$2\mathbb{Z}$	✓
		$p6$	$0, \frac{2\pi}{3}, \frac{4\pi}{3}$	-	$\mathbb{Z}_2$	$\mathbb{Z}$	✓
			$\pi, \frac{\pi}{3}, \frac{5\pi}{3}$	-	-	$2\mathbb{Z}$	✓
		$p2'$		$\mathbb{Z}_2^2$	$\mathbb{Z}_2$	-	-
		$p4'$		$\mathbb{Z}_2$	$\mathbb{Z}_2$	-	-
		$p6'$		-	$\mathbb{Z}_2$	-	-
DIII	$\mathbb{Z}_2$	$p2$	0	$\mathbb{Z}_2^2$	$\mathbb{Z}_2$	$\mathbb{Z}_2$	✓
			π	$\mathbb{Z}_2^2$	$\mathbb{Z}_2$	-	-
		$p4$	0	$\mathbb{Z}_2$	$\mathbb{Z}_2$	$\mathbb{Z}_2$	✓
			π	$\mathbb{Z}_2$	$\mathbb{Z}_2$	-	-
		$p6$	0	-	$\mathbb{Z}_2$	$\mathbb{Z}_2$	✓
			π	-	$\mathbb{Z}_2$	-	-
AIII, BDI, CII	$\mathbb{Z}$	$p2$	0	-	-	-	✓
			π	$\mathbb{Z}^2$	$\mathbb{Z}_2$	-	-
		$p4$	0	-	-	-	✓
			π	-	$\mathbb{Z}_2$	-	-
		$p6$	0	-	-	-	✓
			π	-	$\mathbb{Z}_2$	-	-

Table 3.1. Classification of two-dimenional n-fold rotation-symmetric weak, second-order, and first-order topological superconductors that give rise to anomalous boundary states. Q indicates the topological charge of zero-dimensional anomalous states in the given Cartan class. G denotes the space group pn (pn') with n-fold unitary (magnetic) rotation symmetry. ϕ is the $U(1)$ phase determining the superconducting pairing symmetry. The three central columns show the structure of the topological invariants. For systems with first-order invariant $2\mathbb{Z}$, the rotation symmetry constrains the Chern number to be even. The last column indicates whether the bulk-boundary-defect correspondence (BBDC) holds at a disclination (✓). The remaining (non-superconducting) Cartan classes do not allow for zero-dimensional anomalous states, i.e., they have $Q = 0$.

Finally, we point out that our results for anomalies at disclinations respect the Abelian group structure of topological crystalline phases with respect to their direct sum. In particular, in symmetry classes for which the bulk-boundary-defect correspondence holds, the direct sum of a first-order topological phase with itself cannot lead to a second-order topological phase. In symmetry classes in which a disclination is connected to a domain wall, meaning that the bulk-boundary-defect classification does not hold, the direct sum of a first-order topological phase with itself may result in a second-order topological phase. The latter scenario is absent for all cases discussed here. Our classification results are consistent with corresponding results from Refs. 12, 61, and 66.

Cartan class	Q	G	ϕ	Weak in x / y	Weak in z	2nd order	1st order	BBDC
A	$\mathbb{Z}$	$p2$		-	$\mathbb{Z}$	-	-	✓
		$p4$		-	$\mathbb{Z}$	-	-	✓
		$p6$		-	$\mathbb{Z}$	-	-	✓
		$p2'$		$\mathbb{Z}^2$	-	$\mathbb{Z}_2$	-	-
		$p4'$		-	-	$\mathbb{Z}_2$	-	-
		$p6'$		-	-	$\mathbb{Z}_2$	-	-
D	$\mathbb{Z}$	$p2$	0	-	$\mathbb{Z}$	-	-	✓
			π	-	$2\mathbb{Z}$	-	-	✓
		$p4$	$0, \pi$	-	$\mathbb{Z}$	-	-	✓
			$\frac{\pi}{2}, \frac{3\pi}{2}$	-	$2\mathbb{Z}$	-	-	✓
		$p6$	$0, \frac{2\pi}{3}, \frac{4\pi}{3}$	-	$\mathbb{Z}$	-	-	✓
			$\pi, \frac{\pi}{3}, \frac{5\pi}{3}$	-	$2\mathbb{Z}$	-	-	✓
		$p2'$		$\mathbb{Z}^2$	-	$\mathbb{Z}_2$	-	-
		$p4'$		-	-	$\mathbb{Z}_2$	-	-
		$p6'$		-	-	$\mathbb{Z}_2$	-	-
DIII	$\mathbb{Z}_2$	$p2$	0	$\mathbb{Z}_2^2$	$\mathbb{Z}_2$	$\mathbb{Z}_2$	$\mathbb{Z}$	✓
			π	$\mathbb{Z}_2^2$	-	$\mathbb{Z}_2$	-	-
		$p4$	0	$\mathbb{Z}_2$	$\mathbb{Z}_2$	$\mathbb{Z}_2$	$\mathbb{Z}$	✓
			π	$\mathbb{Z}_2$	-	$\mathbb{Z}_2$	-	-
		$p6$	0	-	$\mathbb{Z}_2$	$\mathbb{Z}_2$	$\mathbb{Z}$	✓
			π	-	-	$\mathbb{Z}_2$	-	-
AII	$\mathbb{Z}_2$	$p2$	$\mathbb{Z}_2$	$\mathbb{Z}_2^2$	$\mathbb{Z}_2$	$\mathbb{Z}_2$	$\mathbb{Z}_2$	✓
		$p4$	$\mathbb{Z}_2$	$\mathbb{Z}_2$	$\mathbb{Z}_2$	$\mathbb{Z}_2$	$\mathbb{Z}_2$	✓
		$p6$	$\mathbb{Z}_2$	-	$\mathbb{Z}_2$	$\mathbb{Z}_2$	$\mathbb{Z}_2$	✓
C	$\mathbb{Z}$	$p2$	0	-	$2\mathbb{Z}$	-	-	✓
			π	-	$2\mathbb{Z}$	-	-	✓
		$p4$	$0, \pi$	-	$2\mathbb{Z}$	-	-	✓
			$\frac{\pi}{2}, \frac{3\pi}{2}$	-	$2\mathbb{Z}$	-	-	✓
		$p6$	$0, \frac{2\pi}{3}, \frac{4\pi}{3}$	-	$2\mathbb{Z}$	-	-	✓
			$\pi, \frac{\pi}{3}, \frac{5\pi}{3}$	-	$2\mathbb{Z}$	-	-	✓
		$p2'$	-	$\mathbb{Z}^2$	-	$\mathbb{Z}_2$	-	-
		$p4'$		-	-	$\mathbb{Z}_2$	-	-
		$p6'$		-	-	$\mathbb{Z}_2$	-	-

Table 3.2. Classification of three-dimenional n-fold rotation-symmetric weak, second-order, and first-order topological insulators and superconductors that give rise to one-dimensional anomalous defect states. We use the same notations as in Table 3.1. Here, Q denotes the topological charge of the one-dimensional anomalous states in the given symmetry class. Since non-magnetic rotation symmetry preserves the propagation direction of chiral modes, there are neither weak nor higher-order phases in Cartan classes A, D, and C with non-magnetic rotation symmetry.

3.6. EXAMPLES

Having laid out the general theory, we now turn to demonstrating our statements for specific models of second-order topological phases. In particular, we illustrate how to carry out the Volterra process explicitly and how anomalous disclination states arise in these phases. Throughout this section, we use $\tau_i, \rho_i, \eta_i, \sigma_i$, $i \in \{0, 1, 2, 3\}$, to denote Pauli matrices acting in different subspaces.

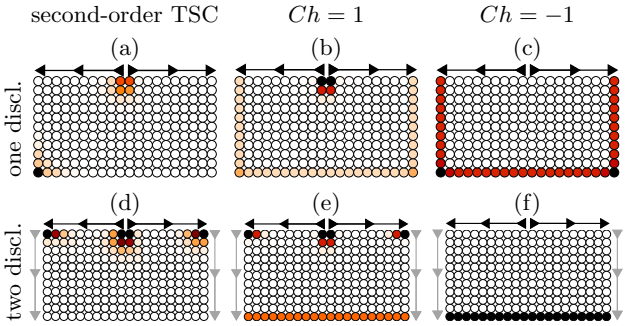

Figure 3.10. Model of a 2D second-order topological phase in class D protected by twofold rotation symmetry, as defined in Eq. (3.12), on a lattice with one and two disclinations: real-space weights for the wavefunctions of the two lowest eigenstates with $E \geq 0$. Darker colors denote larger weights. The boundary conditions forming the disclinations are indicated by black and gray arrows: sites along corresponding lines of arrows are connected respecting the arrow orientation. The model is based on a two-layer stack of Chern superconductors with opposite Chern numbers $Ch = \pm 1$. The model parameters are $m = -1$ and $b_1 = b_2 = 0.4$. The first column shows the full model with both layers coupled. The second and third columns correspond to the individual, decoupled layers when we set $b_1 = b_2 = 0$. In (e), we plot four instead of two lowest eigenstates to also indicate the presence of the chiral edge modes.

3.6.1. Class D in two dimensions

Cartan class D allows for topological phases in one and two dimensions. In one dimension, this phase corresponds to a Kitaev chain with zero-energy Majorana end states. In two dimensions, it is a superconductor with nontrivial Chern number and chiral Majorana edge states. We consider superconductors whose superconducting order parameter is even under rotation ($\phi = 0$ as in Table 3.1). In this case the representation of n-fold rotation symmetry satisfies $U(\mathcal{R}_{2\pi/n})^n = -1$ and commutes with particle-hole antisymmetry.

Using symmetry-based indicators, we derive in Appendix B.4 an explicit expression for the number of Majorana bound states at a disclination in terms of the Chern number and rotation invariants. This specific result for class D is in agreement with previous literature [54]. Moreover, our method is applicable to other symmetry classes as well.

1. *Twofold rotation symmetry*

A model for a second-order topological superconductor protected by twofold rotation symmetry is

$$H_{\mathrm{D},2}(\vec{k}) = \tau_2\rho_3(m + 2 - \cos k_x - \cos k_y) \qquad (3.12)$$
$$+\tau_3\rho_3 \sin k_x + \tau_1\rho_3 \sin k_y + b_1\tau_1\rho_2 + b_2\tau_3\rho_2$$

with particle-hole symmetry $\mathcal{P} = K$ in the Majorana basis and rotation symmetry $U(\mathcal{R}_\pi) = i\tau_2\rho_3$. The 4×4 matrices $\tau_i\rho_j$ are Kronecker products of Pauli matrices acting on the four sublattice degrees of freedom. For $-2 < m < 0$ and $b_1 = b_2 = 0$, this model corresponds to a stack of two Chern superconductors in the τ subspace with opposite Chern numbers hosting counterpropagating chiral edge modes. The terms proportional to b_1 and b_2 hybridize the two layers. The hybridization gaps the counterpropagating chiral edge modes such that a pair of Majorana bound states appears on corners related by twofold rotation.

Exact diagonalization of the Hamiltonian on a lattice with disclination shows that the model hosts one Majorana bound state at the disclination [see Fig. 3.10(a)]. This is in agreement with our general results from Eqs. (3.7) and (3.11) where, in this case, only the nontrivial second-order invariant contributes to the topological charge at the disclination. We observe that the Majorana bound state persists upon decoupling the layers by setting $b_1 = b_2 = 0$. As there is only a single Majorana at the disclination, our general results suggest that one of the two decoupled Chern superconductors must therefore bind a π-flux to the disclination. This is indeed the case as we confirm by investigating the hybridization across the branch cut in the two layers. According to Eq. (3.2), the nearest-neighbor hopping along the surface normal $\vec{n}$ is constructed from the bulk hopping $H_{\vec{r},\vec{r}+\vec{n}}$ in the direction of $\vec{n}$ as $H^{\mathrm{cut}}_{\vec{r},\vec{r}+\vec{n}} = U(\mathcal{R}_\pi)H_{\vec{r},\vec{r}+\vec{n}}$. As the representation of twofold rotation differs by a π phase between the subspaces of the two layers, the disclination binds a π-flux in only one of the layers. We confirm this picture by exactly diagonalizing the two layers in the decoupled limit separately, as shown in Figs. 3.10(b) and (c).

We also construct a lattice with two π disclinations by connecting the surfaces as shown in Fig. 3.10(d). The exact diagonalization results confirm that the second-order topological phase hosts one anomalous state at each of the two disclinations. Moreover, recall that the total phase shift of a particle after transporting it around a 2π disclination is 2π (see Sec. 3.2). As a consequence, each of the two decoupled layers of Chern superconductors hosts an even number of Majorana bound states, zero or two in this case, distributed over the two disclinations [see Figs. 3.10(e) and (f)].

2. *Fourfold rotation symmetry*

To construct a model for a second-order topological superconductor protected by fourfold rotation symmetry

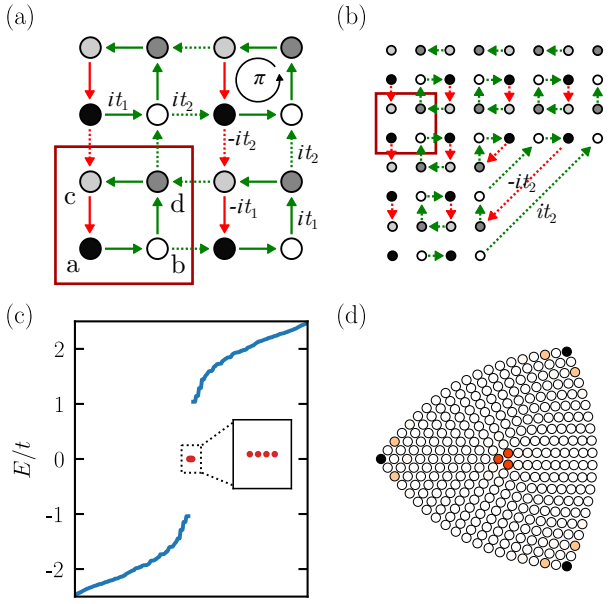

Figure 3.11. Model of a 2D second-order topological superconductor in class D protected by fourfold rotation symmetry as defined in Eq. (3.13): (a) depiction of the model Hamiltonian with $t_{1,2} = t \pm \delta t$. Majoranas hopping along red arrows pick up an additional π phase giving rise to a total magnetic flux of ϕ_0 per lattice plaquette. The red square denotes the unit cell of the model. (b) Illustration of how to connect sites across the cuts in the Volterra process for the fully dimerized limit ($t_1 = 0$), which leads to a $\pi/2$ disclination at the center of the lattice. Finally, on a lattice with $\pi/2$ disclination and model parameters $\delta t = -0.5t$ we show in (c) the spectrum close to $E = 0$ and in (d) the real-space weights of the zero modes. In (c), the four zero modes in the spectrum are highlighted in red.

[5 and 67], we consider a square lattice in the xy plane and place at each lattice site a Majorana mode $\gamma_i = \gamma_i^\dagger$. We add imaginary nearest-neighbor hopping between the Majorana modes, which we dimerize in the x and in the y direction. Finally, we thread a magnetic flux quantum through each lattice plaquette. The model is illustrated in Fig. 3.11(a). It can be viewed as an array of alternatingly coupled Kitaev chains in the presence of a gauge field. The Bloch Hamiltonian of the model reads

$$H_{\mathrm{D},4}(\mathbf{k}) = (t + \delta t)\,[\tau_3\rho_2 + \tau_2\rho_0]$$
$$-(t - \delta t)\,[\cos(k_x)\tau_3\rho_2 + \sin(k_x)\tau_3\rho_1]$$
$$-(t - \delta t)\,[\cos(k_y)\tau_2\rho_0 + \sin(k_y)\tau_1\rho_0] \qquad (3.13)$$

with the real hopping parameters t and δt. The model is written in the Majorana basis $\{\gamma_{a,\vec{k}}, \gamma_{b,\vec{k}}, \gamma_{c,\vec{k}}, \gamma_{d,\vec{k}}\}$, as indicated in Fig. 3.11(a). It satisfies particle-hole antisymmetry $H^*(-\vec{k}) = -H(\vec{k})$ and fourfold rotation symmetry $U_{\frac{\pi}{2}}H(k_y, -k_x)U^\dagger_{\frac{\pi}{2}} = H(\vec{k})$. The representation of fourfold rotation $U_{\frac{\pi}{2}}$ describes a couterclockwise rotation of the Majorana particles in the unit cell including a sign

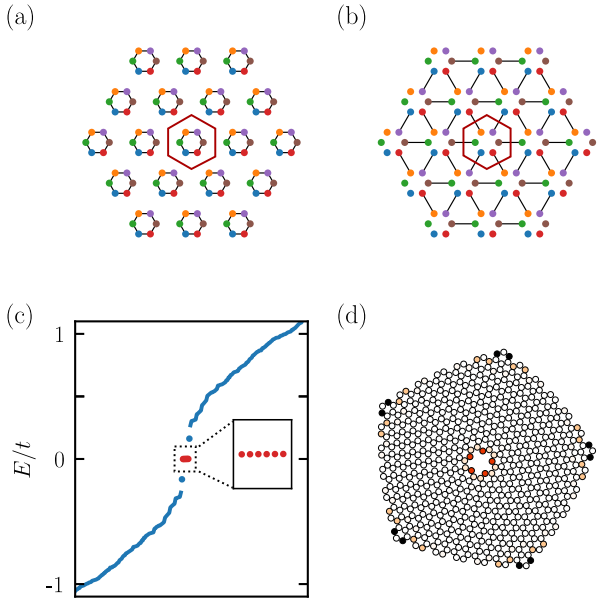

Figure 3.12. Model of a 2D second-order topological superconductor in class D protected by sixfold rotation symmetry: (a), (b) depiction of the model in the two fully dimerized limits, where (a) describes the trivial phase H_{triv} and (b) the second-order topological phase H_{topo}. The unit cell (red hexagon) consists of six Majorana fermions depicted by different colors. For a lattice with $\pi/3$ disclination and model parameters $t_1 = 1.5$ and $t_2 = 0.5$, we show in (c) the spectrum close to $E = 0$ and in (d) the real-space weights of the six zero modes. In our model, there is another pair of in-gap modes localized at the disclination. These modes are not anomalous and can be pushed into the bulk spectrum by a local deformation at the disclination.

change $\gamma_a \to -\gamma_c$.

For $\delta t < 0$, the model realizes a second-order topological superconductor with Majorana corner states. Figure 3.11(b) shows explicitly for the fully dimerized limit ($\delta t = -t$) how unit cells are connected across the cuts in the Volterra process to form a $\pi/2$ disclination. In this limit, it is apparent that unpaired Majorana bound states occur only at the three corners and at the disclination. Nevertheless, exact diagonalization of the model confirms that the Majorana bound states persist also away from the completely dimerized limit [see Fig. 3.11(c) and (d)]. This is in agreement with our general results from Eqs. (3.9) and (3.11) with only the second-order invariant contributing to the topological charge at the disclination.

3. Sixfold rotation symmetry

A model Hamiltonian for a second-order topological superconductor protected by sixfold rotation symmetry can similarly be constructed from a sixfold-symmetric arrangement of Majorana fermions in the unit cell [54]. Our model is composed of two hybridization patterns thereby interpolating between trivial and topological phase,

$$H_{\mathrm{D},6} = t_1 H_{\mathrm{triv}} + t_2 H_{\mathrm{topo}}. \tag{3.14}$$

H_{triv} describes the trivial phase [see Fig. 3.12(a)] as all Majorana fermions are recombined within the unit cell. H_{topo}, on the other hand, corresponds to a second-order topological phase [see Fig. 3.12(b)] where Majorana bound states hybridize across unit cells. A Bloch Hamiltonian for the topological phase is given in Ref. 54.

In the topological phase, the model features a Majorana zero mode bound to a $\pi/3$ disclination, as illustrated in Figs. 3.12(c) and (d), in accordance with the general result for the topological charge at a disclination presented in Eq. (3.10).

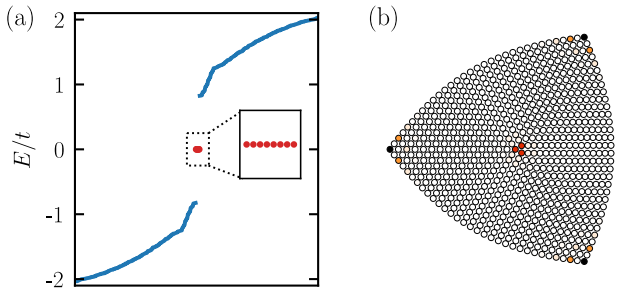

Figure 3.13. Model of a 2D second-order topological superconductor in class DIII on a square lattice with disclination as defined in Eq. (3.15): the model parameters are $\delta t = -0.5t$, $\lambda = 0.5t$. (a) Low-energy spectrum with four Kramers pairs of Majorana zero modes highlighted in red. (b) Real-space weights of the Majorana zero modes.

3.6.2. Class DIII in two dimensions

Cartan class DIII describes time-reversal symmetric superconductors in the absence of spin-rotation symmetry. As before, we assume a pairing symmetry of the form $U(\mathcal{R})\Delta(\mathcal{R}\vec{k})U^\dagger(\mathcal{R}) = \Delta(\vec{k})$. We can straight-forwardly construct a class-DIII second-order topological superconductor from a corresponding model $H_D(\mathbf{k})$ in class D by augmenting it with its time-reversed copy $H_D^*(-\mathbf{k})$. We do this explicitly for the fourfold-symmetric model defined in Eq. (3.13) Note that models for the other rotation symmetries can be constructed in the same way.

The resulting model $H_D(\mathbf{k}) \oplus H_D^*(-\mathbf{k})$ is time-reversal symmetric with the anitunitary operator $\mathcal{T} = i\tau_0\rho_0\sigma_2 K$ and $\mathbf{k} \to -\mathbf{k}$, where σ_i are Pauli matrices acting on the pseudo-spin degree of freedom. The model is particle-hole symmetric with the antiunitary operator $\mathcal{P} = K$, $\mathbf{k} \to -\mathbf{k}$. The representation of fourfold rotation symmetry is $\tilde{R}_{\frac{\pi}{2}} = U_{\frac{\pi}{2}}\sigma_0$, $(k_x, k_y) \to (k_y, -k_x)$, where $U_{\frac{\pi}{2}}$ is the same as for the class-D model. In our model we allow for symmetry-preserving nearest-neighbour coupling between the pseudo-spins. The Bloch Hamiltonian takes

the form,

$$H_{\mathrm{DIII},4}(\mathbf{k}) = \begin{pmatrix} H_{\mathrm{D},4}(k_x,k_y) & \lambda A(k_x,k_y) \\ \lambda A(k_x,k_y) & H^*_{\mathrm{D},4}(-k_x,-k_y) \end{pmatrix} \quad (3.15)$$

with the term

$$\begin{aligned} A(\mathbf{k}) = {} & [1-\cos(k_x)]\tau_3\rho_2 - \sin(k_x)\tau_3\rho_1 \\ & + [1-\cos(k_y)]\tau_2\rho_0 - \sin(k_y)\tau_1\rho_0, \end{aligned}$$

coupling the two pseudo-spin subblocks.

In the second-order topological phase, this system features one Majorana Kramers pair at each of the four corners of a square-shaped sample. After carrying out the Volterra process, the resulting $\pi/2$ disclination binds one Majorana Kramers pair, as illustrated in Fig. 3.13. This again confirms our general results from Eqs. (3.9) and (3.11).

3.6.3. Class DIII in three dimensions

In Cartan class DIII, second-order topological superconductors exist both in two and three dimensions. In three dimensions, those come in two different variants: First, a strong second-order topological phase is constructed from a corresponding two-dimensional model in class D by using the dimensional raising map [47, 68, and 69]. Alternatively, since class DIII already features second-order topological phases in 2D, these nontrivial class-DIII models can be stacked along the rotation axis to produce a weak second-order topological superconductor. In the following, we demonstrate these two cases explicitly for fourfold symmetric systems, but the same procedures are applicable also to models with other rotation symmetries.

1. *Strong second-order topological superconductor*

Applying the dimensional raising map to the Hamiltonian $H_{\mathrm{D},4}(\mathbf{k})$ from Eq. (3.13) (see Appendix B.5.3) results in the following Bloch Hamiltonian,

$$\begin{aligned} H^{\mathrm{st}}_{\mathrm{DIII}}(\mathbf{k}) = {} & H_{\mathrm{D},4}[k_x,k_y;\delta t \to \delta t\cos(k_z)]\sigma_3 \\ & + \sin(k_z)\tau_0\rho_0\sigma_1, \end{aligned} \quad (3.16)$$

where we replace δt in the definition of $H_{\mathrm{D},4}(\mathbf{k})$ by $\delta t\cos(k_z)$. The model is defined on a cubic lattice and has particle-hole, time-reversal, and fourfold rotation symmetry around an axis parallel to the z axis. The respective operators have the same structure as for the two-dimensional model in class DIII discussed at the end of the previous section: $\mathcal{P} = K$, $\mathcal{T} = i\tau_0\rho_0\sigma_2 K$, and $\tilde{R}_{\frac{\pi}{2}} = U_{\frac{\pi}{2}}\sigma_0$ with the C_4 operator $U_{\frac{\pi}{2}}$ of the underlying model in class D.

We consider this model in a pillar geometry, infinite along the z direction and having a finite, square-shaped cross section with open boundary conditions in the x and y directions. We carry out a Volterra process, as depicted in Fig. 3.4(c), resulting in an infinitely long $\pi/2$ line disclination parallel to the z axis. The bandstructure shows that the disclination binds one helical Majorana mode. We observe the same features at the three hinges of the lattice [see Fig. 3.14(a)]. This strong topological phase is robust against translation symmetry breaking.

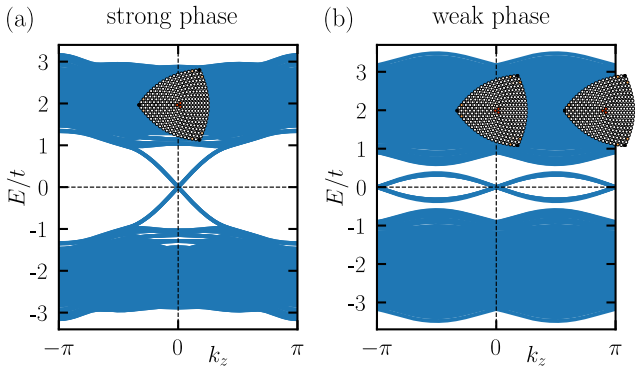

Figure 3.14. Bandstructures of 3D second-order topological superconductors in class DIII protected by fourfold symmetry: (a) strong topological phase and (b) weak topological phase, with model Hamiltonians as defined in Eqs. (3.16) and (3.17), respectively. The corresponding models are realized in a pillar geometry with a line disclination parallel to the z axis. The insets show the real-space weights of the zero-energy states at the respective momenta.

2. *Weak second-order topological superconductor*

A stack of the two-dimensional systems $H_{\mathrm{DIII}}(k_x,k_y)$ as defined in Eq. (3.15) is described by a Hamiltonian of the form

$$H^{\mathrm{w}}_{\mathrm{DIII}}(k_x,k_y,k_z) = H_{\mathrm{DIII}}(k_x,k_y) + t_z\sin(k_z)\tau_0\rho_0\sigma_z, \quad (3.17)$$

where we have included a symmetry-allowed hybridization between adjacent layers proportional to t_z. The symmetries of this system and their representations are identical to the two-dimensional class-DIII model.

We consider this model in the same pillar geometry as for the strong second-order phase above and apply the Volterra process accordingly. We show the bandstructure of the lattice with disclination in Fig. 3.14(b). For each of the three hinges and for the disclination line, there is a pair of particle-hole symmetric bands within the bulk energy gap. Most notably, these bands are detached from the bulk continuum but pinned to the momenta $k_z = 0$ and π at $E = 0$ by symmetry. The hinge and disclination spectra correspond to chains of Majorana Kramers pairs. This is a weak topological phase because it can be trivialized by breaking translation symmetry such that states at $k = 0$ and π hybridize.

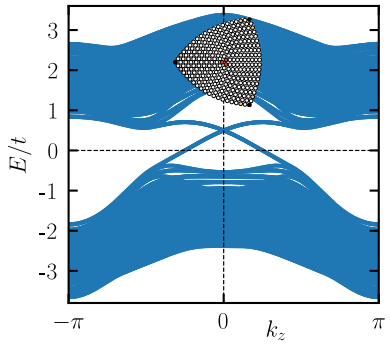

Figure 3.15. Bandstructure of a 3D second-order topological insulator in class AII protected by fourfold symmetry as defined in Eq. (3.18): the model is realized in a pillar geometry with a line disclination parallel to the z axis. The inset shows the real-space weight of the electronic in-gap states at $k_z = 0$.

3.6.4. Class AII in three dimensions.

A class-AII model can formally be constructed from a Hamiltonian $H^{\mathrm{st}}_{\mathrm{DIII}}$ in class DIII [see Eq. (3.16)] by breaking its particle-hole antisymmetry while preserving time-reversal and rotation symmetry. In addition, this requires that the corresponding single-particle Hamiltonian is defined in terms of electronic operators $d^\dagger_{\mathbf{k}a\sigma}$ instead of Majorana operators $\gamma_{\mathbf{k}a\sigma}$, where a and σ denote the sublattice and pseudo-spin degrees of freedom, respectively.

With the above transformation, a suitable model in class AII is given by

$$H_{\mathrm{AII}}(\mathbf{k}) = H^{\mathrm{st}}_{\mathrm{DIII}}(\mathbf{k}) + t_b \cos(k_z)\tau_0\rho_0\sigma_0 \qquad (3.18)$$

where the term proportional to t_b breaks particle-hole antisymmetry. The symmetry operators are $\mathcal{T} = i\tau_0\rho_0\sigma_2 K$ with $\mathcal{T}^2 = -1$, and $\tilde{R}_{\frac{\pi}{2}} = U_{\frac{\pi}{2}}\sigma_0$ with $(\tilde{U}_{\frac{\pi}{2}})^4 = -1$.

The spectrum for the same pillar geometry with disclination as above reveals the presence of helical electronic states running along the line disclination (see Fig. 3.15). The energy bands corresponding to the helical states traverse the bulk-energy gap. As opposed to the model in class DIII, the crossing point of the helical bands is no longer at zero energy due to the absence of particle-hole antisymmetry.

We point out that models for second-order topological insulators in class AII protected by twofold or sixfold rotation symmetries can be constructed in the same way.

3.7. CONCLUSION

We have shown that disclinations in second-order topological insulators may host anomalous states such as Majorana bound states or helical modes. More concretely, we have determined the precise relation between bulk topology and the number of anomalous disclination states. Our result, as summarized in Eqs. (3.7) to (3.11), shows that topological phases protected by a crystalline symmetry contribute anomalous states only at lattice defects that carry a holonomy of the protecting crystalline symmetry. In contrast, tenfold-way first order topological phases contribute anomalous states only at defects that bind a π-flux.

Furthermore, we have identified the set of symmetry classes in which the disclination as construced from the Volterra process is the edge of a domain wall. The domain wall is present in the absence of a unitary rotation symmetry that commutes with all internal unitary symmetries and antisymmetries of the system's Hamiltonian. In case the disclination is connected to a domain wall, the anomaly at the disclination depends on the microscopic properties of the domain wall. Therefore, in these symmetry classes the presence of the domain wall prohibits a unique determination of the disclination anomaly from the bulk topology. We note that the domain wall may become locally unobservable if the disclination breaks some internal symmetries otherwise present in the bulk, or if the disclination involves a translation holonomy by a fractional lattice vector.

Due to the large elastic stress associated with a disclination in ordered media, disclinations typically appear in pairs with canceling Franck angle or at the edges of grain boundaries [35]. More specifically, in the disclination model of grain boundaries, they come in bound pairs [40 and 44]. Therefore, anomalous disclination states along a grain boundary may gap out pairwise through hybridization. On the contrary, *isolated* disclinations may be realized at the center of nanowires.

Possible platforms for the study of anomalous disclination states are SnTe and antiperovskite materials. These materials classes have been put forward as candidates for second-order topological insulators protected by rotation symmetry [4 and 15]. Our findings suggest that disclinations in these materials may bind helical modes. Moreover, SnTe nanowires with a pentagonal crossection have been succesfully fabricated [70]. Their unusual shape hints at the presence of an isolated disclination at their core, rendering them a promising experimental platform for the study of anomalous disclination states.

On the other hand, second-order topological superconductors protected by rotation symmetry may be realized in the superconducting phases of certain topological crystalline insulators [26] or in iron-based superconductors [71]. In these materials, disclinations may bind helical Majorana modes.

Disclinations can also appear in mesomorphic phases [35, 72–74]. Our arguments of Sec. 3.3 show that the bulk-boundary-disclination correspondence also holds for these partially ordered phases. Furthermore, a bulk-disclination correspondence has been observed in photonic crystals [75].

Going beyond our results in this work, we conjecture that relations similar to Eqs. (3.7)–(3.10), relating the topological charge at a defect to the higher-order topology of the bulk also exist for crystalline symmetries other

than rotations. Topological lattice defects can be defined for all space-group symmetries and it has been shown that crystalline topological phases generally exhibit a topological response with respect to a corresponding topological lattice defect [36]. Hence, we expect that higher-order topological phases host anomalous states at topological lattice defects whose holonomy corresponds to an action of the protecting crystalline symmetry.

Our results have extended the higher-order bulk-boundary correspondence of topological crystalline phases to disclinations in rotation-symmetric systems. We have thereby established a link to the topological response theory for defects familiar from the study of interacting symmetry-protected topological phases [36 and 76].

All files and data used in this study are available in the repository at Ref. 77.

[1] A. Kitaev, AIP Conference Proceedings **1134**, 22 (2009).
[2] A. P. Schnyder, S. Ryu, A. Furusaki, and A. W. W. Ludwig, AIP Conference Proceedings **1134**, 10 (2009).
[3] S. Ryu, A. P. Schnyder, A. Furusaki, and A. W. W. Ludwig, New Journal of Physics **12**, 065010 (2010).
[4] F. Schindler, A. M. Cook, M. G. Vergniory, Z. Wang, S. S. P. Parkin, B. A. Bernevig, and T. Neupert, Science Advances **4** (2018), 10.1126/sciadv.aat0346.
[5] W. A. Benalcazar, B. A. Bernevig, and T. L. Hughes, Science **357**, 61 (2017).
[6] W. A. Benalcazar, B. A. Bernevig, and T. L. Hughes, Phys. Rev. B **96**, 245115 (2017).
[7] J. Langbehn, Y. Peng, L. Trifunovic, F. von Oppen, and P. W. Brouwer, Phys. Rev. Lett. **119**, 246401 (2017).
[8] Z. Song, Z. Fang, and C. Fang, Phys. Rev. Lett. **119**, 246402 (2017).
[9] H. Song, S.-J. Huang, L. Fu, and M. Hermele, Phys. Rev. X **7**, 011020 (2017).
[10] F. Schindler, Z. Wang, M. G. Vergniory, A. M. Cook, A. Murani, S. Sengupta, A. Y. Kasumov, R. Deblock, S. Jeon, I. Drozdov, H. Bouchiat, S. Guéron, A. Yazdani, B. A. Bernevig, and T. Neupert, Nature Physics **14**, 918 (2018).
[11] M. Geier, L. Trifunovic, M. Hoskam, and P. W. Brouwer, Phys. Rev. B **97**, 205135 (2018).
[12] L. Trifunovic and P. W. Brouwer, Phys. Rev. X **9**, 011012 (2019).
[13] E. Khalaf, H. C. Po, A. Vishwanath, and H. Watanabe, Phys. Rev. X **8**, 031070 (2018).
[14] Y. You, T. Devakul, F. J. Burnell, and T. Neupert, Phys. Rev. B **98**, 235102 (2018).
[15] C. Fang and L. Fu, Science Advances **5** (2019), 10.1126/sciadv.aat2374.
[16] W. A. Benalcazar, T. Li, and T. L. Hughes, Phys. Rev. B **99**, 245151 (2019).
[17] J. Ahn, S. Park, D. Kim, Y. Kim, and B.-J. Yang, Chinese Physics B **28**, 117101 (2019).
[18] J. Ahn, S. Park, and B.-J. Yang, Phys. Rev. X **9**, 021013 (2019).
[19] D. Varjas, A. Lau, K. Pöyhönen, A. R. Akhmerov, D. I. Pikulin, and I. C. Fulga, Phys. Rev. Lett. **123**, 196401 (2019).
[20] S. Liu, A. Vishwanath, and E. Khalaf, Phys. Rev. X **9**, 031003 (2019).
[21] N. Okuma, M. Sato, and K. Shiozaki, Phys. Rev. B **99**, 085127 (2019).
[22] Z. Song, S.-J. Huang, Y. Qi, C. Fang, and M. Hermele, Science Advances **5**, eaax2007 (2019).
[23] E. Roberts, J. Behrends, and B. Béri, Phys. Rev. B **101**, 155133 (2020).
[24] A. Rasmussen and Y.-M. Lu, Phys. Rev. B **101**, 085137 (2020).
[25] L. Trifunovic and P. W. Brouwer, (2020), arXiv:2003.01144.
[26] J. Ahn and B.-J. Yang, (2020), arXiv:2005.13507.
[27] J.-H. Zhang, Q.-R. Wang, S. Yang, Y. Qi, and Z.-C. Gu, Phys. Rev. B **101**, 100501 (2020).
[28] A. M. Essin and V. Gurarie, Phys. Rev. B **84**, 125132 (2011).
[29] L. Fidkowski, T. S. Jackson, and I. Klich, Phys. Rev. Lett. **107**, 036601 (2011).
[30] R.-J. Slager, L. Rademaker, J. Zaanen, and L. Balents, Phys. Rev. B **92**, 085126 (2015).
[31] C.-K. Chiu, J. C. Y. Teo, A. P. Schnyder, and S. Ryu, Rev. Mod. Phys. **88**, 035005 (2016).
[32] Y. Peng, Y. Bao, and F. von Oppen, Phys. Rev. B **95**, 235143 (2017).
[33] A. Alldridge, C. Max, and M. R. Zirnbauer, Communications in Mathematical Physics **377**, 1761 (2020).
[34] V. Volterra, Annales scientifiques de l'École Normale Supérieure **3e série, 24**, 401 (1907).
[35] M. Kleman and J. Friedel, Rev. Mod. Phys. **80**, 61 (2008).
[36] R. Thorngren and D. V. Else, Phys. Rev. X **8**, 011040 (2018).
[37] A. P. Sutton, R. W. Balluffi, and V. Vitek, Scripta Metallurgica **15**, 989 (1981).
[38] A. P. Sutton and V. Vitek, Phil. Trans. R. Soc. Lond. A **309**, 55 (1983).
[39] G. J. Wang, A. P. Sutton, and V. Vitek, Acta Metallurgica **32**, 1093 (1984).
[40] J. C. M. Li, Surface Science **31**, 12 (1972).
[41] K. K. Shih and J. C. M. Li, Surface Science **50**, 109 (1975).
[42] V. Y. Gertsman, A. A. Nazarov, A. E. Romanov, R. Z. Valiev, and V. I. Vladimirov, Philosophical Magazine A **59**, 1113 (1989).
[43] R. Z. Valiyev, A. N. V. I. Vladimirov, V. Yu. Gertsman, and A. Romanov, Physics of Metals and Metallography **69**, 30 (1990).
[44] A. A. Nazarov, O. A. Shenderov, and D. W. Brenner, Materials Science and Engineering: A **281**, 148 (2000).
[45] A. A. Nazarov, Advances in Natural Sciences: Nanoscience and Nanotechnology **4**, 033002 (2013).
[46] Y. Ran, Y. Zhang, and A. Vishwanath, Nature Physics **5**, 298 (2009).
[47] J. C. Y. Teo and C. L. Kane, Phys. Rev. B **82**, 115120 (2010).
[48] V. Juričić, A. Mesaros, R.-J. Slager, and J. Zaanen, Phys. Rev. Lett. **108**, 106403 (2012).
[49] R.-J. Slager, A. Mesaros, V. Juričić, and J. Zaanen,

Phys. Rev. B **90**, 241403 (2014).
[50] J. C. Teo and T. L. Hughes, Annual Review of Condensed Matter Physics **8**, 211 (2017).
[51] G. van Miert and C. Ortix, Phys. Rev. B **97**, 201111 (2018).
[52] R.-J. Slager, Journal of Physics and Chemistry of Solids **128**, 24 (2019).
[53] J. C. Y. Teo and T. L. Hughes, Phys. Rev. Lett. **111**, 047006 (2013).
[54] W. A. Benalcazar, J. C. Y. Teo, and T. L. Hughes, Phys. Rev. B **89**, 224503 (2014).
[55] Y. You, D. Litinski, and F. von Oppen, Phys. Rev. B **100**, 054513 (2019).
[56] F. Schindler, M. Brzezińska, W. A. Benalcazar, M. Iraola, A. Bouhon, S. S. Tsirkin, M. G. Vergniory, and T. Neupert, Phys. Rev. Research **1**, 033074 (2019).
[57] M. Barkeshli and X.-L. Qi, Phys. Rev. X **2**, 031013 (2012).
[58] M. Barkeshli, C.-M. Jian, and X.-L. Qi, Phys. Rev. B **87**, 045130 (2013).
[59] A. Mesaros, Y. B. Kim, and Y. Ran, Phys. Rev. B **88**, 035141 (2013).
[60] M. Tinkham, *Introduction to superconductivity*, 2nd ed. (Dover Publications Inc, 2004).
[61] K. Shiozaki, (2019), arXiv:1907.09354.
[62] N. Read and D. Green, Phys. Rev. B **61**, 10267 (2000).
[63] D. A. Ivanov, Phys. Rev. Lett. **86**, 268 (2001).
[64] B. A. Bernevig and T. L. Hughes, *Topological insulators and topological superconductors* (Princeton university press, 2013).
[65] S. S. Hong, Y. Zhang, J. J. Cha, X.-L. Qi, and Y. Cui, Nano Lett. **14**, 2815 (2014).
[66] E. Cornfeld and A. Chapman, Phys. Rev. B **99**, 075105 (2019).
[67] Y. Wang, M. Lin, and T. L. Hughes, Phys. Rev. B **98**, 165144 (2018).
[68] K. Shiozaki and M. Sato, Phys. Rev. B **90**, 165114 (2014).
[69] K. Shiozaki, M. Sato, and K. Gomi, Phys. Rev. B **95**, 235425 (2017).
[70] P. Dziawa (private communication).
[71] T. Kawakami and M. Sato, Phys. Rev. B **100**, 094520 (2019).
[72] R. B. Meyer, The Philosophical Magazine: A Journal of Theoretical Experimental and Applied Physics **27**, 405 (1973).
[73] M. Mackley, F. Pinaud, and G. Siekmann, Polymer **22**, 437 (1981).
[74] M. Murayama, J. M. Howe, H. Hidaka, and S. Takaki, Science **295**, 2433 (2002).
[75] Y. Liu, S. Leung, F.-F. Li, Z.-K. Lin, X. Tao, Y. Poo, and J.-H. Jiang, (2020), arXiv:2003.08140.
[76] M. Barkeshli, P. Bonderson, M. Cheng, and Z. Wang, Phys. Rev. B **100**, 115147 (2019).
[77] M. Geier, I. C. Fulga, and A. Lau, Zenodo (2020), 10.5281/zenodo.3950566.

4. Symmetry-based indicators for topological Bogoliubov-de Gennes Hamiltonians

4.1. INTRODUCTION

Although topological phases of matter have been known for four decades now, starting with the discovery of the quantized Hall effect, [1] the study of topological phases and phase transitions became central to quantum condensed matter physics only in the early 2000s, after the theoretical proposals for topological superconducting phases [2, 3] and the quantum spin Hall effect [4, 5] and the subsequent experimental observation of these phases of matter. [6, 7] These theoretical and experimental developments paved the way for the complete classification of all possible topological phases of single-particle systems, protected by either time-reversal, particle-hole or sublattice symmetries — the so-called "tenfold way classification"[8] —, which, reflecting its periodicity as a function of dimensionality and honoring its fundamental importance to the field, was coined "periodic table of topological phases". [9, 10]

In addition to the presence or absence of the fundamental non-spatial symmetries that define the tenfold-way classes, real materials have crystalline symmetries. The combination of topology and crystalline symmetries leads to an exceedingly rich set of "topological crystalline phases". [11] Unlike non-crystalline tenfold-way topological phases, for which a nontrivial topology of the bulk is always associated with a unique anomalous boundary signature, topological crystalline phases may come with a variety of possible boundary signatures. These include the protected existence of anomalous boundary states on all boundaries — a "first-order" topological phase, for which the crystalline symmetry is not essential for the protection of the nontrivial topology —, the appearance of higher-order boundary states on hinges or corners of a crystal (see also Chapter 2), [12–26] or even the complete absence of protected boundary states. The latter scenario applies to "atomic-limit phases", in which the electronic states can be continuously deformed to a collection of localized orbitals, while preserving all relevant symmetries as discussed by Po *et al.* [27] and Bradlyn *et al.* [28]. In such cases, the presence of the crystalline symmetry may form an "obstruction" that prevents from different arrangements of localized orbitals to be continuously connected to each other, [1] allowing for the existence of multiple topologically-distinct atomic-limit phases. [29–35]

Although the classification of topological crystalline phases can be considered largely under control [36–43] (for initial partial classifications results, see Refs. 44–56) the explicit computation of topological invariants for a given band structure is often computationally expensive. Explicit expressions for the invariants need not always be readily available, since a full classification does not always come with explicit expressions for topological invariants. A practical — but partial — solution to this problem is the use of a set of easy-to-compute "symmetry-based indicators", which, when nonzero, are a sufficient indicator of a nontrivial topology of the bulk band structure. [27] The Fu-Kane criterion, which links the existence of a strong [2] topological insulator phase in an inversion-symmetric crystal to the parity of the number of occupied bands with odd-inversion-parity at the high-symmetry momenta, is an example of such a symmetry-based indicator. [57] For normal-state insulating phases, symmetry-based indicators were constructed for the complete set of point group symmetries in two and three dimensions, [27, 28, 58, 59] taking into account the order of the boundary states. [24, 60] Like the classifying groups of topological phases, symmetry-based indicators of topological phases have a group structure, the group operation being the direct sum "$\oplus$" of representative Hamiltonians. [3]

The general strategy underlying the construction of symmetry-based indicators for a Hamiltonian $h(\mathbf{k})$ is to replace the topological classification of the matrix-valued function $h(\mathbf{k})$ by the simpler problem of the topological characterization of the hermitian matrices $h(\mathbf{k}_s)$ at a selected set of "high-symmetry" points $\{\mathbf{k}_s\}$ in the Brillouin zone. [27] The topological characterization of the hermitian matrices $h(\mathbf{k}_s)$ may be considered a set of "topological band labels", the calculation of which is considerably easier to obtain than the topological classification of the full functions $h(\mathbf{k})$. The group SI of symmetry-based indicators then follows by "dividing out" all com-

[1] Although atomic-limit phases have no protected boundary states, they may have protected fractional charges at ends or corners, see, *e.g.*, Refs. 29–31.

[2] In this work, the term "strong topological phase" is reserved for a phase that remains topologically non-trivial after the translational symmetry is broken. Topological crystalline phases that do not rely on the crystalline symmetry for their protection will be referred to as "first-order", corresponding to the dimension of their boundary signature.

[3] Although Refs. 27 and 28 have equivalent definitions of "atomic-limit phases", Bradlyn *et al.* [28] consider band labels that lack the full group structure — one can perform addition of the band labels, but not their subtraction. Subsequent careful comparison revealed that some phases without protected boundary states are topologically equivalent to a "difference" of atomic-limit phases, *i.e.*, they can only be deformed to an atomic-limit phase after addition of topologically trivial bands, see H. C. Po, H. Watanabe, and A. Vishwanath, Phys. Rev. Lett. **121**, 126402 (2018). Such phases were called "fragile topological insulators". They are trivial in the classifying scheme of Po *et al.* [27], while Bradlyn *et al.* [28] label them as non-trivial. The extension of the definition of atomic-limit insulators to superconductors discussed in the present work allows one to define "fragile topological superconductors" in analogous way, although this analogy is not being pursued here.

binations of topological band labels that correspond to atomic phases and imposing a set of compatibility constraints derived from the topological classification of the matrices $h(\mathbf{k})$ at lower-symmetry points in the Brillouin zone.[27, 28] This procedure ensures that only topological phases with a nontrivial boundary signature have nontrivial symmetry-based indicators.

Despite their enormous computational advantage,[28] symmetry-based indicators are not guaranteed to give complete classification information: There exist topologically nontrivial phases with protected anomalous boundary signatures, but trivial symmetry-based indicators. An example is the quantized Hall effect in the absence of any crystalline symmetries, for which no symmetry-based indicators exist (*i.e.*, the group SI is trivial), in spite of the existence of topological phases with nonzero Chern number.

In this chapter, we extend the construction of symmetry-based indicators to superconductors, which, on the mean-field level, are described by Hamiltonians $H(\mathbf{k})$ of Bogoliubov-de Gennes (BdG) type. [61, 62] We explicitly construct the topological band labels and the symmetry-based indicators for selected point groups using the complete topological classification of the BdG Hamiltonian $H(\mathbf{k}_\mathrm{s})$ at high-symmetry momenta $\mathbf{k}_\mathrm{s}$ and compare the symmetry-based indicators with a full classification of topological phases with nontrivial boundary signature. Such a comparison gives information to what extent the symmetry-based indicators can be used as a proxy for a complete classification. Depending on the crystalline symmetries considered, we find that certain aspects of the wealth of boundary signatures available to superconducting phases — Majorana modes at surfaces or hinges, zero-energy Majorana bound states at corners — are reflected in the symmetry-based indicators, but not all.

Recently, a number of articles appeared in the literature that also consider the construction of symmetry-based indicators for superconducting phases. Based on a general analysis of the principles underlying the construction of symmetry-based indicators, Ono and Watanabe [63] arrive at the conclusion that the sets of symmetry-based indicators that describe superconducting phases and the underlying normal-state phases are essentially the same. Our construction of symmetry-based indicators, which is based on the full classification of "zero-dimensional" Hamiltonians at high-symmetry momenta,[64] shows that this statement needs to be corrected to the extent that we successfully put to use a topological band label based on the Pfaffian of a BdG-type Hamiltonian $H(\mathbf{k}_\mathrm{s})$ at high-symmetry momenta $\mathbf{k}_\mathrm{s}$, which has no counterpart in the normal state. A different approach to the problem of symmetry-based indicators in superconductors was taken in a later article by these authors, together with Yanase, [65] as well as by Skurativska, Neupert, and Fischer, [66] who consider the "weak-pairing limit" (superconducting order parameter Δ much smaller than energy scales typical for the normal-state band structure) and derive a classification of superconducting phases that is based on the topological classification of the normal state and the symmetry of the superconducting order parameter. An approach that uses the normal-state Hamiltonian as its sole input has the practical advantage that the symmetry-based indicators can be calculated from the vast body of band-structure knowledge available for normal phases. Furthermore, we show that there exists a consistent definition of an "atomic-limit superconductor"as an "array" of zero-dimensional superconductors [39]. Our definition is consistent with the definition in the published version of Skurativska et al. [66]. In the weak-pairing limit, the symmetry-based indicators derived here can be expressed in terms of the normal part of the Hamiltonian only, so that in that limit our approach offers the same computational advantages as the approaches that rely on the weak-pairing limit at the outset. Very recently, an article by Ono, Po, and Watanabe appeared,[67] which bases its symmetry indicators on the full BdG Hamiltonian, be it without the Pfaffian band labels, and has a definition of an atomic limit that is consistent with ours. A recent article by Shiozaki also reports the construction of symmetry-based indicators for Hamiltonians of BdG-type and which has results very similar to ours. [68]

The remaining part of this chapter is organized as follows: In Sec. 4.2 we discuss the symmetry of the superconducting order parameter and the set of data that needs to be specified in order to define a "topological class" for a crystalline superconductor. In Sec. 4.3 we discuss the classification and topological invariants of zero-dimensional Hamiltonians. This discussion is the cornerstone for defining topological invariants at high-symmetry momenta in Brillouin zone. We present our main result, a method to construct and calculate symmetry-based indicators for superconductors, in Sec. 4.4. Sections 4.5–4.7 contain examples for various crystalline symmetries compatible with a square or cubic lattice structure, for which we present a detailed calculation of symmetry-based indicators and relate this to higher-order boundary phenomenology. We conclude in Sec. 4.8. The appendices contain additional examples as well as fully worked-out classifications of anomalous boundary states for crystalline symmetry groups not readily available in the literature.

4.2. SUPERCONDUCTORS WITH CRYSTALLINE SYMMETRIES

The mean-field theory of superconductors uses an effective non-interacting description with a Hamiltonian of the Bogoliubov-de Gennes (BdG) form [61, 62]

$$H(\mathbf{k}) = \begin{pmatrix} h(\mathbf{k}) & \Delta(\mathbf{k}) \\ \Delta^\dagger(\mathbf{k}) & -h^*(-\mathbf{k}) \end{pmatrix}, \tag{4.1}$$

where the normal-state Hamiltonian $h(\mathbf{k})$ is hermitian and the superconducting order parameter $\Delta(\mathbf{k}) =$

$-\Delta(-\mathbf{k})^{\mathrm{T}}$ is antisymmetric. The 2×2 block structure describes particle and hole degrees of freedom. The special choice of the blocks in Eq. (4.1) is equivalent to imposing that $H(\mathbf{k})$ is antisymmetric under particle-hole conjugation $\mathcal{P} = \tau_1 K$,

$$H(\mathbf{k}) = -\tau_1 H(-\mathbf{k})^* \tau_1, \tag{4.2}$$

where τ_1 is a Pauli matrix acting within particle-hole space and K is complex conjugation. (Note that $\mathbf{k} \to -\mathbf{k}$ under complex conjugation.) In addition to the BdG structure, we assume that the system obeys translation invariance — which is what allows us to use the Fourier language in Eqs. (4.1) and (4.2) in the first place — and that it has additional symmetries described by the point group G. We restrict ourselves to symmorphic symmetries, for which the unit cell can be chosen in such a way that it is left invariant under G. For the initial discussion we focus on systems without time-reversal symmetry or other antiunitary symmetries.

Requiring that the normal part $h(\mathbf{k})$ be symmetric under G implies that there exists a projective representation $u(g)$ for $g \in G$ such that

$$h(\mathbf{k}) = u(g) h(g\mathbf{k}) u^\dagger(g). \tag{4.3}$$

Note that the unitary matrix $u(g)$ does not depend on $\mathbf{k}$, as the symmetry group G acts within the unit cell. The representation $u(g)$ is projective, because the transformation rule (4.3) determines $u(g)$ up to a phase factor only. In general, a consistent choice of these phase factors is possible up to a sign only, the sign ambiguities being captured by the "factor system"

$$\{z_{g,h} = u(gh)^{-1} u(g) u(h) = \pm 1 \text{ for } g,\, h \in G\} \tag{4.4}$$

of the projective representation. Two realizations $u_1(g)$ and $u_2(g)$ that have the same factor system may still differ by a one-dimensional representation $\Theta(g)$ of G with trivial factor system. Although the mathematical structure of the theory allows many non-equivalent factor groups for the representation $u(g)$, for physical systems only two factor groups are relevant: The trivial one, which applies to spinless particles, and the nontrivial factor system associated with the spinful particles. The representation $\Theta(g)$, which describes the difference between two representations with the same factor system, always has the trivial factor group.

The canonical form for the representation $u(g)$ is

$$u(g) = \mathrm{diag}\,[r_1(g) \otimes \mathbb{1}_{N_1}, \ldots, r_n(g) \otimes \mathbb{1}_{N_n}], \tag{4.5}$$

where the $r_\alpha(g)$ are irreducible representations ("irreps") of G (with the appropriate factor system) and $\mathbb{1}_{N_\alpha}$ the $N_\alpha \times N_\alpha$ unit matrix. The dimension of $h(\mathbf{k})$, corresponding to the total number of orbitals in the unit cell, is $\sum_\alpha d_\alpha N_\alpha$, where d_α is the dimension of the irreducible presentation α. For notational simplicity, we choose to set $N_1 = N_2 = \ldots = N_n \equiv N$.

The general symmetry constraint for the full BdG Hamiltonian $H(\mathbf{k})$ is obtained by allowing different realizations $u_{1,2}(g)$ of the transformation matrices for the particle and hole degrees of freedom. Such a symmetry constraint is compatible with the group operation of G if $u_1(g)$ and $u_2(g)$ have the same factor system, *i.e.*, if there exists a one-dimensional representation $\Theta(g)$ of the symmetry group G with trivial factor system such that

$$u_1(g) \equiv u(g) = u_2(g)\Theta(g). \tag{4.6}$$

For the BdG Hamiltonian $H(\mathbf{k})$ one then finds the general symmetry constraint

$$H(\mathbf{k}) = U(g) H(g\mathbf{k}) U(g)^\dagger, \tag{4.7}$$

with

$$U(g) = \begin{pmatrix} u(g) & 0 \\ 0 & u(g)^* \Theta(g) \end{pmatrix}. \tag{4.8}$$

For the superconducting order parameter $\Delta(\mathbf{k})$, Eqs. (4.7) and (4.8) imply that

$$\Delta(\mathbf{k}) = u(g) \Delta(g\mathbf{k}) u(g)^{\mathrm{T}} \Theta(g)^*, \tag{4.9}$$

i.e., $\Delta(\mathbf{k})$ transforms under a one-dimensional representation of the group G.[69] Whereas the projective representation $u(g)$ is a property of the normal phase, the additional phase factor $\Theta(g)$ exists by virtue of the superconducting order only. Together, the representation u and the one-dimensional representation Θ fully determine the symmetry class of the Bogoliubov-de Gennes Hamiltonian (4.1).

Alternatively, Eqs. (4.7) and (4.8) may be recast in the form of an algebraic relation between the elements g of the symmetry group G and the particle-hole conjugation operation $\mathcal{P}$,

$$g\mathcal{P} = \Theta(g)\mathcal{P}g. \tag{4.10}$$

This is the formulation used in Refs. 36, 38, 39, 46, 48, and 70, which considered the full classification of BdG Hamiltonians in the presence of a single order-two spatial symmetry $\mathcal{S}$ and discriminated between the cases in which $\mathcal{S}$ commutes or anticommutes with the Fermi constraint $\mathcal{P}$.

The presence of time-reversal symmetry and/or spin-rotation symmetry does not change the above considerations, provided these commute with the crystalline symmetries. Time-reversal symmetry imposes the additional constraints[8]

$$h(\mathbf{k}) = \sigma_2 h(-\mathbf{k})^* \sigma_2, \quad \Delta(\mathbf{k}) = \sigma_2 \Delta(-\mathbf{k})^* \sigma_2, \tag{4.11}$$

where σ_2 is a Pauli matrix that acts in spin space. With time-reversal symmetry, the one-dimensional representation $\Theta(g)$ of G that characterizes the superconducting state must be real. In the presence of spin rotation symmetry, one arrives at an effective description in terms of a BdG-type Hamiltonian of the form (4.1), but with

	Γ	$\mathbf{1}$	$\mathcal{I}_\pi$
r_+	A_g	1	1
r_-	A_u	1	-1

TABLE 4.1. Irreducible representations of the point group C_i. The second column lists the standard crystallographic notation for the representations, the first column gives the notation used in the text.

a symmetric order parameter $\Delta(\mathbf{k}) = \Delta(-\mathbf{k})^{\mathrm{T}}$, so that $H(\mathbf{k})$ is antisymmetric under the antiunitary operation $\tau_2 K$, which plays the role of an effective particle-hole symmetry. If time-reversal symmetry is present additionally, $H(\mathbf{k})$ is symmetric under complex conjugation K, which plays the role of an effective time-reversal operation. Note that while $\mathcal{P}$ and $\mathcal{T}$ square to 1 and -1, respectively, in the spinful case, the effective particle-hole conjugation and time-reversal operations square to -1 and 1, respectively, if spin-rotation symmetry is present. Similarly, in the presence of spin-rotation symmetry, the effective representation of crystalline symmetry operations is changed into the corresponding "spinless" type.

The general framework described here is best illustrated using examples. As a first example, we consider a system with inversion symmetry. In this case the group $G = C_i = \{\mathbf{1}, \mathcal{I}\}$, where $\mathbf{1}$ is the identity and $\mathcal{I}$ is the inversion operation. Choosing a basis that has a well-defined parity under inversion, one finds that one may represent G by

$$u(g) = \mathrm{diag}\,[r_+(g), r_-(g)], \tag{4.12}$$

where $r_\pm(g)$ are the two irreducible representations of G, see Table 4.1, which are both one-dimensional. Specifically, Eq. (4.12) reads

$$u(\mathbf{1}) = \rho_0, \quad u(\mathcal{I}) = \rho_3, \tag{4.13}$$

where ρ_3 is a Pauli matrix that acts in the space of even/odd-parity states and ρ_0 is the 2×2 unit matrix. From the two one-dimensional representations of G we also find two possibilities for the representation $U(g)$ for the BdG Hamiltonian $H(\mathbf{k})$. Choosing the trivial one-dimensional representation $\Theta(g) = r_+(g)$ in Eq. (4.7) (the A_g representation, see Table 4.1), we find that the BdG Hamiltonian $H(\mathbf{k})$ obeys the symmetry constraint

$$H(\mathbf{k}) = (\rho_3\tau_0)H(-\mathbf{k})(\rho_3\tau_0), \tag{4.14}$$

where τ_0 is the identity matrix in particle-hole space and ρ_3 is a Pauli matrix that acts in the space of even/odd-parity states. For the blocks $h(\mathbf{k})$ and $\Delta(\mathbf{k})$ this implies

$$h(\mathbf{k}) = \rho_3 h(-\mathbf{k})\rho_3, \quad \Delta(\mathbf{k}) = \rho_3\Delta(-\mathbf{k})\rho_3, \tag{4.15}$$

i.e., the order parameter is even under inversion. Alternatively, choosing the nontrivial one-dimensional representation $\Theta(g) = u_-(g)$ in Eq. (4.7) (the A_u representation), we find that the BdG Hamiltonian $H(\mathbf{k})$ satisfies

	Γ	$\mathbf{1}$	$\mathcal{R}_{\pi/2}$	$\mathcal{R}^2_{\pi/2}$	$\mathcal{R}^3_{\pi/2}$
r_0	A	1	1	1	1
$r_{\pi/2}$	${}^2E$	1	i	-1	$-i$
r_π	B	1	-1	1	-1
$r_{3\pi/2}$	${}^1E$	1	$-i$	-1	i
$r_{\pi/4}$	${}^1\overline{E}_1$	1	$e^{i\pi/4}$	i	$e^{3\pi i/4}$
$r_{3\pi/4}$	${}^2\overline{E}_2$	1	$e^{3\pi i/4}$	$-i$	$e^{i\pi/4}$
$r_{5\pi/4}$	${}^1\overline{E}_2$	1	$e^{5\pi i/4}$	i	$e^{7\pi i/4}$
$r_{7\pi/4}$	${}^2\overline{E}_1$	1	$e^{7\pi i/4}$	$-i$	$e^{5\pi i/4}$

TABLE 4.2. Spinless representations (top four rows) and one-dimensional spinful representations (bottom four rows) of the point group C_4. The second column lists the standard crystallographic notation for the representations, the first column gives the notation used in the text.

$$H(\mathbf{k}) = (\rho_3\tau_3)H(-\mathbf{k})(\rho_3\tau_3). \tag{4.16}$$

In this case the blocks $h(\mathbf{k})$ and $\Delta(\mathbf{k})$ satisfy the constraint

$$h(\mathbf{k}) = \rho_3 h(-\mathbf{k})\rho_3, \quad \Delta(\mathbf{k}) = -\rho_3\Delta(-\mathbf{k})\rho_3, \tag{4.17}$$

so that the order parameter is odd under inversion. The two different transformation rules of the order parameter $\Delta(\mathbf{k})$ under inversion imply two different algebraic relations between the inversion operation $\mathcal{I}$ and the Fermi constraint $\mathcal{P}$: If $\Delta(\mathbf{k})$ is even under $\mathcal{I}$, $\mathcal{I}$ and $\mathcal{P}$ commute, whereas $\mathcal{I}$ and $\mathcal{P}$ anticommute if $\Delta(\mathbf{k})$ is odd under inversion.

As a second example, we consider a fourfold rotation around a fixed axis for a system of spinful particles. We write $G = C_4 = \{\mathbf{1}, \mathcal{R}_{\pi/2}, \mathcal{R}^2_{\pi/2}, \mathcal{R}^3_{\pi/2}\}$, where the generator $\mathcal{R}_{\pi/2} \equiv \mathcal{R}$ denotes a clockwise rotation by $\pi/2$. In this case one has $\mathcal{R}^4 = -\mathbf{1}$, which corresponds to the factor system

$$z_{\mathcal{R}^k,\mathcal{R}^l} = \begin{cases} 1 & \text{if } 0 \le k+l < 4, \\ -1 & \text{if } 4 \le k+l < 8. \end{cases} \tag{4.18}$$

Choosing basis states with well-defined angular momentum $j = \frac{1}{2}$, $\frac{3}{2}$, $\frac{5}{2}$, and $\frac{7}{2}$ (defined modulo 4), we find the spinful representation

$$u(g) = \mathrm{diag}\,[r_{\pi/4}(g), r_{3\pi/4}(g), r_{5\pi/4}(g), r_{7\pi/4}(g)], \tag{4.19}$$

see Table 4.2.

The transformation rule for the BdG Hamiltonian $H(\mathbf{k})$ requires the choice of a a one-dimensional spinless representation Θ of G. There are four of those, and we denote these as r_θ with $\theta = 0$, $\pi/2$, π, and $3\pi/2$, see Table 4.2. Proceeding as before, we find four possible transformation rules for the BdG Hamiltonian $H(\mathbf{k})$ under a $\pi/2$ rotation $\mathcal{R}$,

$$H(\mathbf{k}) = U_\theta(\mathcal{R})H(\mathcal{R}\mathbf{k})U_\theta(\mathcal{R})^\dagger, \tag{4.20}$$

with

$$U_\theta(\mathcal{R}) = \begin{pmatrix} u(\mathcal{R}) & 0 \\ 0 & u(\mathcal{R})^* e^{i\theta} \end{pmatrix}. \tag{4.21}$$

Alternatively, the transformation rules for the blocks $h(\mathbf{k})$ and $\Delta(\mathbf{k})$ are

$$\begin{aligned} h(\mathbf{k}) &= u(\mathcal{R}) h(\mathcal{R}\mathbf{k}) u(\mathcal{R})^\dagger, \\ \Delta(\mathbf{k}) &= e^{i\theta} u(\mathcal{R}) \Delta(\mathcal{R}\mathbf{k}) u(\mathcal{R})^{\mathrm{T}}, \end{aligned} \tag{4.22}$$

which corresponds to a superconducting order parameter with finite angular momentum.

The time-reversal symmetry operation is represented by $U(\mathcal{T})K$, where the definition of $U(\mathcal{T})$ in the angular momentum basis is

$$U(\mathcal{T}) = \begin{pmatrix} 0 & 0 & 0 & -i \\ 0 & 0 & -i & 0 \\ 0 & i & 0 & 0 \\ i & 0 & 0 & 0 \end{pmatrix}. \tag{4.23}$$

Time-reversal commutes with $\mathcal{P}$ and satisfies the property $\mathcal{T}^2 = -1$. Time-reversal symmetry imposes the additional conditions (4.11) on the blocks $h(\mathbf{k})$ and $\Delta(\mathbf{k})$. One easily verifies that these additional conditions allow for a nonzero superconducting order parameter $\Delta(\mathbf{k})$ for the real one-dimensional representations corresponding to $\theta = 0$ or $\theta = \pi$ only.

As a third example, we consider spinful fermions in a system with two perpendicular mirror symmetries, $G = C_{2v}$. We write the point group elements as $G = \{\mathbf{1}, \mathcal{M}_x, \mathcal{M}_y, \mathcal{R}_\pi\}$, where $\mathcal{M}_x$ and $\mathcal{M}_x$ are mirror reflections in planes perpendicular to the x and y axis, respectively, and $\mathcal{R}_\pi = \mathcal{M}_y\mathcal{M}_x$ is a rotation around the z axis by π. For spinful particles the factor system is nontrivial with $\mathcal{M}_x^2 = \mathcal{M}_y^2 = \mathcal{R}_\pi^2 = -1$. In that case there is only one (projective) representation u of G (up to unitary transformations), which is two dimensional, see Table 4.3. Superconducting phases are characterized by one-dimensional representations of G with a trivial factor system. There are four of these, denoted $r_{\sigma_x,\sigma_y}(g)$, with $\sigma_{x,y} = \pm 1$, see Table 4.3. Each of the one-dimensional representations of G corresponds to a distinct symmetry of the superconducting order parameter Δ. For example, for the one-dimensional representation r_{--}, the order parameter is odd under mirror reflections in the yz and xz planes and even under a twofold rotation around the z axis.

	Γ	$\mathbf{1}$	$\mathcal{R}_\pi$	$\mathcal{M}_x$	$\mathcal{M}_y$
r_{++}	A_1	1	1	1	1
r_{--}	A_2	1	1	-1	-1
r_{-+}	B_1	1	-1	1	-1
r_{+-}	B_2	1	-1	-1	1
u	E	σ_0	$i\sigma_3$	$i\sigma_1$	$i\sigma_2$

TABLE 4.3. Spinful representation (bottom row) and one-dimensional spinless representations (top four rows) of the point group C_{2v}. The representation u is unique up to unitary transformations. The second column lists the standard crystallographic notation for the representations, the first column gives the notation used in the text.

$\eta = (\eta_\mathcal{T}, \eta_\mathcal{P}, \eta_\mathcal{C})$	Cartan	$\mathfrak{K}[0]$	ν
$(0,0,0)$	A	$\mathbb{Z}$	$\mathfrak{N}$
$(0,0,1)$	AIII	0	-
$(1,0,0)$	AI	$\mathbb{Z}$	$\mathfrak{N}$
$(1,1,1)$	BDI	$\mathbb{Z}_2$	$\mathfrak{p}$
$(0,1,0)$	D	$\mathbb{Z}_2$	$\mathfrak{p}$
$(-1,1,1)$	DIII	0	-
$(-1,0,0)$	AII	$\mathbb{Z}$	$\mathfrak{N}$
$(-1,-1,1)$	CII	0	-
$(0,-1,0)$	C	0	-
$(1,-1,1)$	CI	0	-

TABLE 4.4. The tenfold-way symmetry classes are defined by the absence or presence time-reversal symmetry, particle-hole antisymmetry, or chiral antisymmetry. The triple $\eta = (\eta_\mathcal{T}, \eta_\mathcal{P}, \eta_\mathcal{C})$ (left column) indicates the presence or absence of these symmetries as well as the square of the symmetry operation if it is present. The second column gives the Cartan label for the symmetry class; the third column lists the corresponding classifying group $\mathfrak{K}_\eta[0]$ for zero-dimensional Hamiltonians. The rightmost column lists the topological invariant ν, where $\mathfrak{N}$ is the number of eigenstates (Kramers pairs in class AII) with negative energy and $\mathfrak{p}$ is the Pfaffian invariant as defined in Eq. (4.40).

4.3. CLASSIFICATION OF ZERO-DIMENSIONAL HAMILTONIANS

The cornerstone of the construction of symmetry-based indicators is the classification of zero-dimensional Hamiltonians with additional unitary symmetries. Concretely, the classification problem is that of a Hamiltonian H with or without time-reversal symmetry, particle-hole antisymmetry, or chiral antisymmetry, and with additional unitary symmetries specified by the group G. The presence or absence of time-reversal symmetry, particle-hole antisymmetry, and chiral antisymmetry determines the tenfold-way (Altland-Zirnbauer) class and is indicated by the triple[8]

$$\eta = (\eta_\mathcal{T}, \eta_\mathcal{P}, \eta_\mathcal{C}). \tag{4.24}$$

Here $\eta_\mathcal{T} = \mathcal{T}^2 = \pm 1$ if time-reversal symmetry is present and $\eta_\mathcal{T} = 0$ if time-reversal symmetry is absent. Similarly, $\eta_\mathcal{P} = \mathcal{P}^2 = \pm 1$ or 0 if particle-hole antisymmetry is present or absent and $\eta_\mathcal{C} = \mathcal{C}^2 = 1$ or 0 in the presence or absence of chiral antisymmetry, respectively. Table 4.4 summarizes the tenfold way classification and lists both the notation using the triple $(\eta_\mathcal{T}, \eta_\mathcal{P}, \eta_\mathcal{C})$ and the Cartan labeling. If the context allows, we will use the Cartan label instead of the triple $\eta = (\eta_\mathcal{T}, \eta_\mathcal{P}, \eta_\mathcal{C})$.

For physically relevant systems, the crystalline symmetry group G commutes with the time-reversal operation $\mathcal{T}$, which is what we assume throughout. The algebraic relation between G and the particle-hole conjugation op-

eration $\mathcal{P}$ or the chiral operation $\mathcal{C} = \mathcal{P}\mathcal{T}$ is characterized by a one-dimensional representation $\Theta(g)$ of G, as discussed in Sec. 4.2.

With a suitable choice of basis, the (projective) representation $U(g)$ for a Bogoliubov-de Gennes Hamiltonian H can be brought into a canonical form analogous to Eq. (4.5),

$$U(g) = \mathrm{diag}\,[r_1(g) \otimes \mathbb{1}_{2N_1}, \ldots, r_n(g) \otimes \mathbb{1}_{2N_n}], \quad (4.25)$$

where the $r_\alpha(g)$ are irreducible representations of G. To keep the notation simple, we make the choice $N_1 = N_2 = \ldots = N_n = N$. The Bogoliubov-de Gennes Hamiltonian H is then brought into a block-diagonal form,

$$H = \mathrm{diag}\,(\mathbb{1}_{d_1} \otimes H_1, \ldots, \mathbb{1}_{d_n} \otimes H_n), \quad (4.26)$$

where d_α is the dimension of the irreducible representation r_α. The diagonal blocks H_α have dimension $2N$ and are no longer subject to additional unitary symmetries. However, because of the basis change involved in representing U in the canonical form (4.25), the action of the fundamental symmetry operations $\mathcal{T}$, $\mathcal{P}$, and/or $\mathcal{C}$ on these blocks need not be the same as their action on the original Hamiltonian H and different blocks may be related to each other by $\mathcal{T}$, $\mathcal{P}$ and/or $\mathcal{C}$. Hence, additional considerations are needed to determine which blocks are independent and to what tenfold-way class they belong, which we now discuss.

Time-reversal operation $\mathcal{T}$.— If the irreducible representations r_α and r_α^* are the same (up to a unitary transformation), the time-reversal operation $\mathcal{T}$ acts within the diagonal block corresponding to r_α and takes the form of an effective time-reversal operation for H_α, but with a square $W_\mathcal{T}(\alpha)$ that may differ from $\eta_\mathcal{T}$. If the irreducible representations r_α and r_α^* are different, $\mathcal{T}$ interchanges the diagonal blocks corresponding to r_α and r_α^*. In most examples, which of these cases applies can easily be found by inspection, although one may also obtain the answer from the "Wigner test" by calculating the quantity[27, 64, 71]

$$W_\mathcal{T}(\alpha) = \eta_\mathcal{T} \left\langle z_{g,g} \chi_\alpha(g^2) \right\rangle_G, \quad (4.27)$$

where $\langle \ldots \rangle_G$ denotes an average over all $g \in G$, $z_{g,g}$ is an element of the factor system, see Eq. (4.4), and $\chi_\alpha(g) = \mathrm{tr}\, r_\alpha(g)$ is the character of the irreducible representation. The quantity $W_\mathcal{T}(\alpha)$ can take the values $W_\mathcal{T}(\alpha) = \pm 1$ or 0, corresponding to the two cases discussed above.

Particle-hole conjugation $\mathcal{P}$.— Similarly, if the irreducible representations r_α and Θr_α^* are the same, $\mathcal{P}$ acts as an effective particle-hole conjugation operator for H_α with square $W_\mathcal{P}(\alpha) = \pm 1$, whereas if r_α and Θr_α^* are different irreducible representations of G, $\mathcal{P}$ interchanges the corresponding diagonal blocks. Again, one may find out which of the three cases applies by calculating

$$W_\mathcal{P}(\alpha) = \eta_\mathcal{P} \left\langle \Theta(g)^* z_{g,g} \chi_\alpha(g^2) \right\rangle_G, \quad (4.28)$$

which takes the values ± 1 or 0, respectively, for the two cases described above.

Chiral operation $\mathcal{C}$.— Finally, for the chiral operation $\mathcal{C} = \mathcal{P}\mathcal{T}$ one only needs to distinguish two cases: If r_α and Θr_α are the same irreducible representation of G, $\mathcal{C}$ acts as an effective antisymmetry of H_α, whereas $\mathcal{C}$ interchanges the diagonal blocks corresponding to r_α and Θr_α if they are different. This defines the quantity $W_\mathcal{C}(\alpha)$, which takes the values 0 or 1.

We denote the full classifying group for zero-dimensional Hamiltonians with the additional symmetry group G as $\mathfrak{K}_\eta[G, \Theta]$, where the multiindex η indicates the tenfold-way class, see Table 4.4, and Θ is the one-dimensional representation of G that characterizes the superconducting order parameter. The classifying group also depends on the factor system of G, but we do not write this dependence explicitly. The argument Θ is omitted for non-superconducting phases. The above considerations then lead to the result

$$\mathfrak{K}_\eta[G, \Theta] = \prod_{r_\alpha \text{ irrep of } G} \mathfrak{K}_{W(\alpha)}[0], \quad (4.29)$$

where the multiindex $W(\alpha) = (W_\mathcal{T}(\alpha), W_\mathcal{P}(\alpha), W_\mathcal{C}(\alpha))$ and the product is over the irreducible representations r_α of G, where only one representative appears in the product if multiple irreps are linked by the fundamental symmetries $\mathcal{T}$, $\mathcal{P}$, or $\mathcal{C}$. The classifying groups $\mathfrak{K}_\eta[0]$, which apply to tenfold-way classes without additional crystalline symmetries,[9, 72] can be found in Table 4.4. We remark that the classification approach described here also works for d-dimensional Hamiltonians $H(\mathbf{k})$, as long as G contains only onsite (*i.e.* non-spatial, $\mathbf{k}$-independent) crystalline symmetries.

Examples.— We illustrate this general procedure using the three examples already discussed in the previous Section. The classification results for these three examples as well as for other relevant point groups are summarized in Tables 4.5–4.8.

We first consider a zero-dimensional superconductor with inversion symmetry. The symmetry group $G = C_i = \{\mathbf{1}, \mathcal{I}\}$ and the two one-dimensional representations Θ of G that characterize the superconducting phase are the two irreducible representations $r_\pm$ of G, see Table 4.1. If the superconducting order is even under inversion, corresponding to $\Theta = r_+$ (the "A_g" representation), Eqs. (4.5) and (4.8) give

$$U(\mathbf{1}) = \rho_0 \tau_0, \quad U(\mathcal{I}) = \rho_3 \tau_0,$$

where ρ_3 is the Pauli matrix in parity space. Correspondingly, the BdG Hamiltonian $H = \mathrm{diag}\,(H_+, H_-)$ is the diagonal sum of blocks with even and odd parity under inversion. Since U is real and does not involve the particle-hole degree of freedom, the particle-hole conjugation operation $\mathcal{P}$ commutes with G, so that it acts within each parity subblock. Its square is $W_\mathcal{P} = \eta_\mathcal{P}$, *i.e.,* the same as for the full Hamiltonian H. We conclude that

$$\mathfrak{K}_\eta[C_i, A_g] = \mathfrak{K}_\eta[0]^2 \quad (4.30)$$

for all tenfold-way symmetry classes η. The groups $\mathfrak{K}_\eta[0]$ are listed in Table 4.4. This conclusion is consistent with

G	Θ		$(r_\alpha)_{W_\mathcal{P}(\alpha)}$	$\mathfrak{K}_\mathrm{D}[G,\Theta]$
C_1	A	1	$(A)_{\eta_\mathcal{P}}$	$\mathbb{Z}_2$
C_i	A_g	r_+	$(A_g)_{\eta_\mathcal{P}}, (A_u)_{\eta_\mathcal{P}}$	$\mathbb{Z}_2^2$
	A_u	r_-	$(A_g, A_u)_0$	$\mathbb{Z}$
C_s	A'	r_+	$({}^1\bar{E}, {}^2\bar{E})_0$	$\mathbb{Z}$
	A''	r_-	$({}^1\bar{E})_{\eta_\mathcal{P}}, ({}^2\bar{E})_{\eta_\mathcal{P}}$	$\mathbb{Z}_2^2$
C_2	A	r_+	$({}^1\bar{E}, {}^2\bar{E})_0$	$\mathbb{Z}$
	B	r_-	$({}^1\bar{E})_{\eta_\mathcal{P}}, ({}^2\bar{E})_{\eta_\mathcal{P}}$	$\mathbb{Z}_2^2$
C_3	A_1	r_0	$\bar{E}_{\eta_\mathcal{P}}, ({}^1\bar{E}, {}^2\bar{E})_0$	$\mathbb{Z}\times\mathbb{Z}_2$
	${}^2E$	$r_{2\pi/3}$	${}^2\bar{E}_{\eta_\mathcal{P}}, (\bar{E}, {}^1\bar{E})_0$	$\mathbb{Z}\times\mathbb{Z}_2$
	${}^1E$	$r_{4\pi/3}$	${}^1\bar{E}_{\eta_\mathcal{P}}, (\bar{E}, {}^2\bar{E})_0$	$\mathbb{Z}\times\mathbb{Z}_2$
C_4	A	r_0	$({}^1\bar{E}_1, {}^2\bar{E}_1)_0, ({}^1\bar{E}_2, {}^2\bar{E}_2)_0$	$\mathbb{Z}^2$
	B	r_π	$({}^1\bar{E}_1, {}^2\bar{E}_2)_0, ({}^1\bar{E}_2, {}^2\bar{E}_1)_0$	$\mathbb{Z}^2$
	${}^2E$	$r_{\pi/2}$	$({}^1\bar{E}_1)_{\eta_\mathcal{P}}, ({}^1\bar{E}_2)_{\eta_\mathcal{P}}, ({}^2\bar{E}_1, {}^2\bar{E}_2)_0$	$\mathbb{Z}\times\mathbb{Z}_2^2$
	${}^1E$	$r_{3\pi/2}$	$({}^2\bar{E}_1)_{\eta_\mathcal{P}}, ({}^2\bar{E}_2)_{\eta_\mathcal{P}}, ({}^1\bar{E}_1, {}^1\bar{E}_2)_0$	$\mathbb{Z}\times\mathbb{Z}_2^2$
C_6	A	r_0	$({}^1\bar{E}_1, {}^2\bar{E}_1)_0, ({}^1\bar{E}_2, {}^2\bar{E}_2)_0, ({}^1\bar{E}_3, {}^2\bar{E}_3)_0$	$\mathbb{Z}^3$
	B	r_π	$({}^1\bar{E}_1)_{\eta_\mathcal{P}}, ({}^2\bar{E}_1)_{\eta_\mathcal{P}}, ({}^1\bar{E}_3, {}^2\bar{E}_2)_0, ({}^2\bar{E}_3, {}^1\bar{E}_2)_0$	$\mathbb{Z}^2\times\mathbb{Z}_2^2$
	${}^2E_1$	$r_{4\pi/3}$	$({}^1\bar{E}_1, {}^2\bar{E}_3)_0, ({}^2\bar{E}_1, {}^1\bar{E}_2)_0, ({}^2\bar{E}_2, {}^1\bar{E}_3)_0$	$\mathbb{Z}^3$
	${}^2E_2$	$r_{\pi/3}$	$({}^1\bar{E}_3)_{\eta_\mathcal{P}}, ({}^2\bar{E}_2)_{\eta_\mathcal{P}}, ({}^2\bar{E}_1, {}^2\bar{E}_3)_0, ({}^1\bar{E}_1, {}^1\bar{E}_2)_0$	$\mathbb{Z}^2\times\mathbb{Z}_2^2$
	${}^1E_1$	$r_{2\pi/3}$	$({}^1\bar{E}_1, {}^2\bar{E}_2)_0, ({}^2\bar{E}_1, {}^1\bar{E}_3)_0, ({}^2\bar{E}_3, {}^1\bar{E}_2)_0$	$\mathbb{Z}^3$
	${}^1E_2$	$r_{-\pi/3}$	$({}^1\bar{E}_2)_{\eta_\mathcal{P}}, ({}^2\bar{E}_3)_{\eta_\mathcal{P}}, ({}^1\bar{E}_1, {}^1\bar{E}_3)_0, ({}^2\bar{E}_1, {}^2\bar{E}_2)_0$	$\mathbb{Z}^2\times\mathbb{Z}_2^2$
C_{2v}	A_1	r_{++}	$(E)_{-\eta_\mathcal{P}}$	0
	A_2	r_{--}	$(\bar{E})_{\eta_\mathcal{P}}$	$\mathbb{Z}_2$
	B_1	r_{-+}	$(\bar{E})_{\eta_\mathcal{P}}$	$\mathbb{Z}_2$
	B_2	r_{+-}	$(\bar{E})_{\eta_\mathcal{P}}$	$\mathbb{Z}_2$
C_{3v}	A_1		$({}^1\bar{E}, {}^2\bar{E})_0, (\bar{E}_1)_{-\eta_\mathcal{P}}$	$\mathbb{Z}$
	A_2		$({}^1\bar{E})_{\eta_\mathcal{P}}, ({}^2\bar{E})_{\eta_\mathcal{P}}, (\bar{E}_1)_{\eta_\mathcal{P}}$	$\mathbb{Z}_2^3$
C_{4v}	A_1		$(\bar{E}_1)_{-\eta_\mathcal{P}}, (\bar{E}_2)_{-\eta_\mathcal{P}}$	0
	A_2		$(\bar{E}_1)_{\eta_\mathcal{P}}, (\bar{E}_2)_{\eta_\mathcal{P}}$	$\mathbb{Z}_2^2$
	B_1		$(\bar{E}_1, \bar{E}_2)_0$	$\mathbb{Z}$
	B_2		$(\bar{E}_1, \bar{E}_2)_0$	$\mathbb{Z}$
C_{6v}	A_1		$(\bar{E}_1)_{-\eta_\mathcal{P}}, (\bar{E}_2)_{-\eta_\mathcal{P}}, (\bar{E}_3)_{-\eta_\mathcal{P}}$	0
	A_2		$(\bar{E}_1)_{\eta_\mathcal{P}}, (\bar{E}_2)_{\eta_\mathcal{P}}, (\bar{E}_3)_{\eta_\mathcal{P}}$	$\mathbb{Z}_2^3$
	B_1		$(\bar{E}_3)_1, (\bar{E}_1, \bar{E}_2)_0$	$\mathbb{Z}\times\mathbb{Z}_2$
	B_2		$(\bar{E}_3)_1, (\bar{E}_1, \bar{E}_2)_0$	$\mathbb{Z}\times\mathbb{Z}_2$

TABLE 4.5. Classification of zero-dimensional BdG Hamiltonians with point group G and one-dimensional representation Θ describing the symmetry of the superconducting order parameter in the absence of time-reversal symmetry and spin-rotation symmetry, corresponding to tenfold-way class D, $\eta_\mathcal{P} = 1$. The second and third columns list the one-dimensional representation Θ using the standard crystallographic notation and the notation used in the examples in the main text, respectively. The fourth column lists the set $(r_\alpha)_{W_\mathcal{P}(\alpha)}$ of irreps r_α together with the result of the Wigner test $W_\mathcal{P}(\alpha)$. In case irreps r_α and Θr_α^* are paired by particle-hole antisymmetry ($W_\mathcal{P}(\alpha) = 0$), the paired representations are appear in brackets. From this information one can read off the classification, invariants, generators and representations using Table 4.10. For convenience we list the result for the classifying group $\mathfrak{K}_\mathrm{D}[G,\Theta]$ in the last column.

the Wigner test, which gives $W_\mathcal{P}(r_\pm) = 1$. If, on the other hand, Δ is odd under inversion, which corresponds to the one-dimensional representation $\Theta = r_-$ for the superconducting phase (the "A_u representation, see Table 4.1), the representation of G for the full BdG Hamiltonian is

$$U(\mathbf{1}) = \rho_0\tau_0, \quad U(\mathcal{I}) = \rho_3\tau_3,$$

see Eq. (4.14). The block-diagonal structure of H now involves one block with even-parity particle-like states and odd-parity hole-like states and one block with odd-parity particle-like states and even-parity hole-like states. The two blocks are interchanged by particle-hole conjugation. One arrives at the same conclusion by observing that r_+ and $\Theta r_+ = r_-$ are different irreducible representations of G. For the classifying group $\mathfrak{K}_\eta[G, A_u]$ we thus find

$$\mathfrak{K}_{(\eta_\mathcal{T},\eta_\mathcal{P},\eta_\mathcal{C})}[C_i, A_u] = \mathfrak{K}_{(\eta_\mathcal{T},0,0)}[0]. \tag{4.31}$$

Again, this conclusion is compatible with the Wigner test, which gives $W_\mathcal{P}(r_\pm) = 0$.

The second example deals with a spinful system with a fourfold rotation symmetry, $G = C_4$. The one-dimensional representation $\Theta \equiv r_\theta$ of G that characterizes the superconducting phase is labeled by an angle θ which can take the values 0, $\pi/2$, π, or $3\pi/2$, see Table 4.2. The representation (4.21) of the rotation generator $\mathcal{R}_{\pi/2}$ implies that H has a block-diagonal structure in which particle-like states with angular momentum $j = \frac{1}{2}$,

G	Θ		$(r_\alpha)_{W_\mathcal{P}(\alpha)}$	$\mathfrak{K}_\mathrm{C}[G,\Theta]$
C_1	A	1	$(A)_{\eta_\mathcal{P}}$	0
C_i	A_g	r_+	$(A_g)_{\eta_\mathcal{P}}, (A_u)_{\eta_\mathcal{P}}$	0
	A_u	r_-	$(A_g, A_u)_0$	$\mathbb{Z}$
C_s	A'	r_+	$(A')_{\eta_\mathcal{P}}, (A'')_{\eta_\mathcal{P}}$	0
	A''	r_-	$(A', A'')_0$	$\mathbb{Z}$
C_2	A	r_+	$(A)_{\eta_\mathcal{P}}, (B)_{\eta_\mathcal{P}}$	0
	B	r_-	$(A, B)_0$	$\mathbb{Z}$
C_3	A_1	r_0	$(A_1)_{\eta_\mathcal{P}}, ({}^1E, {}^2E)_0$	$\mathbb{Z}$
	${}^2E$	$r_{2\pi/3}$	$({}^1E)_{\eta_\mathcal{P}}, (A_1, {}^1E)_0$	$\mathbb{Z}$
	${}^1E$	$r_{4\pi/3}$	$({}^2E)_{\eta_\mathcal{P}}, (A_1, {}^2E)_0$	$\mathbb{Z}$
C_4	A	r_0	$A_{\eta_\mathcal{P}}, B_{\eta_\mathcal{P}}, ({}^1E, {}^2E)_0$	$\mathbb{Z}$
	B	r_π	$({}^1E)_{\eta_\mathcal{P}}, ({}^2E)_{\eta_\mathcal{P}}, (A, B)_0$	$\mathbb{Z}$
	${}^2E$	$r_{\pi/2}$	$(A, {}^2E)_0, (B, {}^1E)_0$	$\mathbb{Z}^2$
	${}^1E$	$r_{3\pi/2}$	$(A, {}^1E)_0, (B, {}^2E)_0$	$\mathbb{Z}^2$
C_6	A	r_0	$A_{\eta_\mathcal{P}}, B_{\eta_\mathcal{P}}, ({}^1E_1, {}^2E_1)_0, ({}^1E_2, {}^2E_2)_0$	$\mathbb{Z}^2$
	B	r_π	$(A, B)_0, ({}^1E_1, {}^2E_2)_0, ({}^1E_2, {}^2E_1)_0$	$\mathbb{Z}^3$
	${}^2E_1$	$r_{4\pi/3}$	$({}^1E_1)_{\eta_\mathcal{P}}, ({}^1E_2)_{\eta_\mathcal{P}}, (A, {}^2E_1)_0, (B, {}^2E_2)_0$	$\mathbb{Z}^2$
	${}^2E_2$	$r_{\pi/3}$	$(A, {}^2E_2)_0, (B, {}^2E_1)_0, ({}^1E_1, {}^1E_2)_0$	$\mathbb{Z}^3$
	${}^1E_1$	$r_{2\pi/3}$	$({}^2E_1)_{\eta_\mathcal{P}}, ({}^2E_2)_{\eta_\mathcal{P}}, (A, {}^1E_1)_0, (B, {}^1E_2)_0$	$\mathbb{Z}^2$
	${}^1E_2$	$r_{-\pi/3}$	$(A, {}^1E_2)_0, (B, {}^1E_1)_0, ({}^2E_1, {}^2E_2)_0$	$\mathbb{Z}^3$
C_{2v}	A_1	r_{++}	$(A_1)_{\eta_\mathcal{P}}, (A_2)_{\eta_\mathcal{P}}, (B_1)_{\eta_\mathcal{P}}, (A_2)_{\eta_\mathcal{P}}$	0
	A_2	r_{--}	$(A_1, A_2)_0, (B_1, B_2)_0$	$\mathbb{Z}^2$
	B_1	r_{-+}	$(A_1, B_1)_0, (A_2, B_2)_0$	$\mathbb{Z}^2$
	B_2	r_{+-}	$(A_1, B_2)_0, (B_1, A_2)_0$	$\mathbb{Z}^2$
C_{3v}	A_1		$(A_1)_{\eta_\mathcal{P}}, (A_2)_{\eta_\mathcal{P}}, (E)_{\eta_\mathcal{P}}$	$\mathbb{Z}_2^3$
	A_2		$(A_1, A_2)_0, (E)_{-\eta_\mathcal{P}}$	$\mathbb{Z}$
C_{4v}	A_1		$(A_1)_{\eta_\mathcal{P}}, (A_2)_{\eta_\mathcal{P}}, (B_1)_{\eta_\mathcal{P}}, (B_2)_{\eta_\mathcal{P}}, E_{\eta_\mathcal{P}}$	0
	A_2		$(A_1, A_2)_0, (B_1, B_2)_0, E_{-\eta_\mathcal{P}}$	$\mathbb{Z}^2 \times \mathbb{Z}_2$
	B_1		$(A_1, B_1)_0, (A_2, B_1)_0, E_{\eta_\mathcal{P}}$	$\mathbb{Z}^2$
	B_2		$(A_1, B_2)_0, (B_1, A_2)_0, E_{\eta_\mathcal{P}}$	$\mathbb{Z}^2$
C_{6v}	A_1		$(A_1)_{\eta_\mathcal{P}}, (A_2)_{\eta_\mathcal{P}}, (B_1)_{\eta_\mathcal{P}}, (B_2)_{\eta_\mathcal{P}}, (E_1)_{\eta_\mathcal{P}}, (E_2)_{\eta_\mathcal{P}}$	0
	A_2		$(A_1, A_2)_0, (B_1, B_2)_0, (E_1)_{-\eta_\mathcal{P}}, (E_2)_{-\eta_\mathcal{P}}$	$\mathbb{Z}^2 \times \mathbb{Z}_2^2$
	B_1		$(A_1, B_1)_0, (A_2, B_1)_0, (E_1, E_2)_0$	$\mathbb{Z}^3$
	B_2		$(A_1, B_1)_0, (A_2, B_1)_0, (E_1, E_2)_0$	$\mathbb{Z}^3$

TABLE 4.6. Same as Table 4.5, but in the presence of spin-rotation symmetry, *i.e.* for spinless representations of the crystalline symmetry group. BdG Hamiltonians with spin-rotation symmetry and without time-reversal symmetry correspond to tenfold-way class C, $\eta_\mathcal{P} = -1$.

$\frac{3}{2}$, $\frac{5}{2}$, or $\frac{7}{2}$ are combined with hole-like states of angular momentum $-j + 2\theta/\pi \mod 4$. In the following discussion, we use the angular momentum j of the particle-like states to label the blocks. If $\theta = 0$ (the "A" representation), particle-hole conjugation $\mathcal{P}$ interchanges the blocks with $j = \frac{1}{2}$ and $\frac{7}{2}$, as well as the blocks with $j = \frac{3}{2}$ and $\frac{5}{2}$. If $\theta = \pi/2$ (the "${}^2E$" representation), $\mathcal{P}$ interchanges the blocks with $j = \frac{3}{2}$ and $\frac{7}{2}$, but acts within the blocks with $j = \frac{1}{2}$ or $\frac{5}{2}$, squaring to one. If $\theta = \pi$ (the "A" representation), $\mathcal{P}$ interchanges the blocks with $j = \frac{1}{2}$ and $\frac{3}{2}$, as well as the blocks with $j = \frac{5}{2}$ and $j = \frac{7}{2}$. Finally, if $\theta = 3\pi/2$ (the "${}^1E$" representation), $\mathcal{P}$ interchanges the blocks with $j = \frac{1}{2}$ and $\frac{5}{2}$, but acts within the blocks with $j = \frac{3}{2}$ and $\frac{7}{2}$, again squaring to one. We conclude that

$$\begin{aligned}\mathfrak{K}_\mathrm{D}[C_4, A] &= \mathfrak{K}_\mathrm{D}[C_4, B] \\ &= \mathfrak{K}_\mathrm{A}[0]^2, \\ &= \mathbb{Z}^2 \end{aligned} \tag{4.32}$$

and

$$\begin{aligned}\mathfrak{K}_\mathrm{D}[C_4, {}^{1,2}E] &= \mathfrak{K}_\mathrm{A}[0] \times \mathfrak{K}_\mathrm{D}[0]^2 \\ &= \mathbb{Z} \times \mathbb{Z}_2^2. \end{aligned} \tag{4.33}$$

The same conclusions can be obtained by performing the Wigner test.

In the presence of time-reversal symmetry only the real one-dimensional representations A and B are relevant (corresponding to $\theta = 0$, π, respectively). In both cases the time-reversal operation $\mathcal{T}$ interchanges the blocks with angular momentum j and angular momentum $-j \mod 4$. For the A representation, $\mathcal{P}$ and $\mathcal{T}$ give the same pairing of diagonal blocks of H and the combined operation $\mathcal{C} = \mathcal{P}\mathcal{T}$ leaves the diagonal blocks invariant. It follows that

$$\begin{aligned}\mathfrak{K}_\mathrm{DIII}[C_4, A] &= \mathfrak{K}_\mathrm{A}[0]^2 \\ &= 0. \end{aligned} \tag{4.34}$$

G	Θ		$(r_\alpha)_{W_\mathcal{P}}(\alpha)$	$\mathfrak{K}_{\mathrm{DIII}}[G,\Theta]$	$\mathfrak{K}_{\mathrm{BDI}}[G,\Theta]$
C_1	A	1	$(A)_{(\eta_\mathcal{T},\eta_\mathcal{P},1)}$	0	$\mathbb{Z}_2$
C_i	A_g	r_+	$(A_g)_{(\eta_\mathcal{T},\eta_\mathcal{P},1)}, (A_u)_{(\eta_\mathcal{T},\eta_\mathcal{P},1)}$	0	$\mathbb{Z}_2^2$
	A_u	r_-	$(A_g, A_u)_{(\eta_\mathcal{T},0,0)}$	$\mathbb{Z}$	$\mathbb{Z}$
C_s	A'	r_+	$({}^1\bar{E}, {}^2\bar{E})_{(0,0,1)}$	0	0
	A''	r_-	$({}^1\bar{E}, {}^2\bar{E})_{(0,\eta_\mathcal{P},0)}$	$\mathbb{Z}_2$	$\mathbb{Z}_2$
C_2	A	r_+	$({}^1\bar{E}, {}^2\bar{E})_{(0,0,1)}$	0	0
	B	r_-	$({}^1\bar{E}, {}^2\bar{E})_{(0,\eta_\mathcal{P},0)}$	$\mathbb{Z}_2$	$\mathbb{Z}_2$
C_3	A_1	r_0	$\bar{E}_{(\eta_\mathcal{T},\eta_\mathcal{P},1)}, ({}^1\bar{E}, {}^2\bar{E})_{(0,0,1)}$	0	$\mathbb{Z}_2$
C_4	A	r_0	$({}^1\bar{E}_1, {}^2\bar{E}_1)_{(0,0,1)}, ({}^1\bar{E}_2, {}^2\bar{E}_2)_{(0,0,1)}$	0	0
	B	r_π	$({}^1\bar{E}_1, {}^2\bar{E}_1, {}^2\bar{E}_2, {}^1\bar{E}_2)_{(0,0,0)}$	$\mathbb{Z}$	$\mathbb{Z}$
C_6	A	r_0	$({}^1\bar{E}_1, {}^2\bar{E}_1)_{(0,0,1)}, ({}^1\bar{E}_2, {}^2\bar{E}_2)_{(0,0,1)}, ({}^1\bar{E}_3, {}^2\bar{E}_3)_{(0,0,1)}$	0	0
	B	r_π	$({}^1\bar{E}_1, {}^2\bar{E}_1)_{(0,\eta_\mathcal{P},0)}, ({}^1\bar{E}_2, {}^2\bar{E}_2, {}^2\bar{E}_3, {}^1\bar{E}_3)_{(0,0,0)}$	$\mathbb{Z}\times\mathbb{Z}_2$	$\mathbb{Z}\times\mathbb{Z}_2$
C_{2v}	A_1	r_{++}	$(\bar{E})_{(-\eta_\mathcal{T},-\eta_\mathcal{P},1)}$	0	0
	A_2	r_{--}	$(\bar{E})_{(-\eta_\mathcal{T},\eta_\mathcal{P},1)}$	$\mathbb{Z}_2$	0
	B_1	r_{-+}	$(\bar{E})_{(-\eta_\mathcal{T},\eta_\mathcal{P},1)}$	$\mathbb{Z}_2$	0
	B_2	r_{+-}	$(\bar{E})_{(-\eta_\mathcal{T},\eta_\mathcal{P},1)}$	$\mathbb{Z}_2$	0
C_{3v}	A_1		$({}^1\bar{E}, {}^2\bar{E})_{(0,0,1)}, (\bar{E}_1)_{(-\eta_\mathcal{T},-\eta_\mathcal{P},1)}$	0	0
	A_2		$({}^1\bar{E}, {}^2\bar{E})_{(0,\eta_\mathcal{P},0)}, (\bar{E}_1)_{(-\eta_\mathcal{T},\eta_\mathcal{P},1)}$	$\mathbb{Z}_2^2$	$\mathbb{Z}_2$
C_{4v}	A_1		$(\bar{E}_1)_{(-\eta_\mathcal{T},-\eta_\mathcal{P},1)}, (\bar{E}_2)_{(-\eta_\mathcal{T},-\eta_\mathcal{P},1)}$	0	0
	A_2		$(\bar{E}_1)_{(-\eta_\mathcal{T},\eta_\mathcal{P},1)}, (\bar{E}_2)_{(-\eta_\mathcal{T},\eta_\mathcal{P},1)}$	$\mathbb{Z}_2^2$	0
	B_1		$(\bar{E}_1, \bar{E}_2)_{(-\eta_\mathcal{T},0,0)}$	$\mathbb{Z}$	$\mathbb{Z}$
	B_2		$(\bar{E}_1, \bar{E}_2)_{(-\eta_\mathcal{T},0,0)}$	$\mathbb{Z}$	$\mathbb{Z}$
C_{6v}	A_1		$(E_1)_{(-\eta_\mathcal{T},-\eta_\mathcal{P},1)}, (E_2)_{(-\eta_\mathcal{T},-\eta_\mathcal{P},1)}, (E_3)_{(-\eta_\mathcal{T},-\eta_\mathcal{P},1)}$	0	0
	A_2		$(\bar{E}_1)_{(-\eta_\mathcal{T},\eta_\mathcal{P},1)}, (\bar{E}_2)_{(-\eta_\mathcal{T},\eta_\mathcal{P},1)}, (\bar{E}_3)_{(-\eta_\mathcal{T},\eta_\mathcal{P},1)}$	$\mathbb{Z}_2^3$	0
	B_1		$(\bar{E}_3)_{(-\eta_\mathcal{T},\eta_\mathcal{P},1)}, (\bar{E}_1, \bar{E}_2)_{(-\eta_\mathcal{T},0,0)}$	$\mathbb{Z}\times\mathbb{Z}_2$	$\mathbb{Z}$
	B_2		$(\bar{E}_3)_{(-\eta_\mathcal{T},\eta_\mathcal{P},1)}, (\bar{E}_1, \bar{E}_2)_{(-\eta_\mathcal{T},0,0)}$	$\mathbb{Z}\times\mathbb{Z}_2$	$\mathbb{Z}$

TABLE 4.7. Classification of zero-dimensional BdG Hamiltonians with point group G and one-dimensional representation Θ describing the symmetry of the superconducting order parameter with time-reversal symmetry without spin-rotation symmetry, corresponding to tenfold-way classes DIII, $\eta = (-1, 1, 1)$. We also include systems with emergent time-reversal symmetry, corresponding to class BDI, $\eta = (1, 1, 1)$. The second and third columns list the one-dimensional representation using the standard crystallographic notation and in the notation used in the examples in the main text, respectively. The fourth column lists the set $(r_\alpha)_{W_\mathcal{P}(\alpha)}$ of irreps r_α, together with the result of the Wigner tests $W(\alpha)$. Irreps that are connected by application of the fundamental symmetry operations $\mathcal{T}$, $\mathcal{P}$, or $\mathcal{C}$ are shown together, using brackets. If two of the three Wigner tests $W_\mathcal{T}(\alpha)$, $W_\mathcal{C}(\alpha)$, and $W_\mathcal{C}(\alpha)$ are zero, the irreps form a pair and the single symmetry operation that leave the irrep invariant is the one with the nonzero Wigner label $W(\alpha)$. If all three Wigner tests are zero, $W_\mathcal{T}(\alpha) = W_\mathcal{P}(\alpha) = W_\mathcal{C}(\alpha) = 0$, the irreps form a quartet. In that case the order of the four irreps between brackets is such, that the first two and last two irreps are interchanged by $\mathcal{T}$ and the first and third, and second and fourth irreps are interchanged by $\mathcal{P}$. From this information one can read off the classification, invariants, generators and representations using Table 4.9. For convenience we list the result for the classifying group $\mathfrak{K}_\eta[G,\Theta]$ in the last two columns.

On the other hand, for the B representation, $\mathcal{P}$, $\mathcal{T}$, and their product $\mathcal{C} = \mathcal{P}\mathcal{T}$ map all four diagonal blocks of H to each other and one has

$$\begin{aligned}\mathfrak{K}_{\mathrm{DIII}}[C_4, B] &= \mathfrak{K}_{\mathrm{A}}[0] \\ &= \mathbb{Z}. \end{aligned} \tag{4.35}$$

The third example is that of spinful particles with symmetry group $G = C_{2v}$. We refer to Table 4.3 for the irreducible representations with nontrivial and trivial factor system. Since there is only one (two-dimensional) irreducible representation u — the "$\overline{E}$" representation, see Table 4.3 —, it follows automatically that u^* and $r_{\sigma_x\sigma_y}u^*$ are the same representations of G. Indeed, one easily verifies that u^* and $r_{\sigma_x,\sigma_y}u^*$ are equal to u up to a unitary transformation. To find the square of the effective time-reversal and particle-hole conjugation operations, we consider the case of the one-dimensional irreducible representation $\Theta = r_{++}$ (the A_1 representation) in detail and summarize results for the remaining three one-dimensional representations r_{+-}, r_{-+}, and r_{--} (the B_2, B_1, and A_2 representations, respectively).

For $\Theta = r_{++}$ ("A_1" representation, see Table 4.3), and choosing the representation of Table 4.3 for the representation of the generators $\mathcal{M}_x$ and $\mathcal{M}_y$ for the normal-state block h, we find that their representation for the full BdG Hamiltonian H are $U(\mathcal{M}_x) = i\sigma_1\tau_3$ and $U(\mathcal{M}_y) = i\sigma_2\tau_0$. To bring the representation matrices to the canonical form (4.25) we have to perform the basis transformation

$$H \to \begin{pmatrix} 1 & 0 \\ 0 & i\sigma_2 \end{pmatrix} H \begin{pmatrix} 1 & 0 \\ 0 & -i\sigma_2 \end{pmatrix}.$$

After this basis transformation, $\mathcal{M}_x$ and $\mathcal{M}_y$ are represented as $i\sigma_1\tau_0$ and $i\sigma_2\tau_0$, respectively, consistent with Eq. (4.25). The particle-hole conjugation operation $\mathcal{P}$,

G	Θ		$(r_\alpha)_{W_{\mathcal{P}(\alpha)}}$	$\mathfrak{K}_{\mathrm{CI}}[G,\Theta]$	$\mathfrak{K}_{\mathrm{CII}}[G,\Theta]$
C_1	A	1	$(A)_{(\eta_\mathcal{T},\eta_\mathcal{P},1)}$	0	0
C_i	A_g	r_+	$(A_g)_{(\eta_\mathcal{T},\eta_\mathcal{P},1)}, (A_u)_{(\eta_\mathcal{T},\eta_\mathcal{P},1)}$	0	0
	A_u	r_-	$(A_g, A_u)_{(\eta_\mathcal{T},0,0)}$	$\mathbb{Z}$	$\mathbb{Z}$
C_s	A'	r_+	$(A')_{(\eta_\mathcal{T},\eta_\mathcal{P},1)}, (A'')_{(\eta_\mathcal{T},\eta_\mathcal{P},1)}$	0	0
	A''	r_-	$(A', A'')_{(\eta_\mathcal{T},0,0)}$	$\mathbb{Z}$	$\mathbb{Z}$
C_2	A	r_+	$(A)_{(\eta_\mathcal{T},\eta_\mathcal{P},1)}, (B)_{(\eta_\mathcal{T},\eta_\mathcal{P},1)}$	0	0
	B	r_-	$(A, B)_{(\eta_\mathcal{T},0,0)}$	$\mathbb{Z}$	$\mathbb{Z}$
C_3	A_1	r_0	$(A_1)_{(\eta_\mathcal{T},\eta_\mathcal{P},1)}, ({}^1E,{}^2E)_{(0,0,1)}$	0	0
C_4	A	r_0	$A_{(\eta_\mathcal{T},\eta_\mathcal{P},1)}, B_{(\eta_\mathcal{T},\eta_\mathcal{P},1)}, ({}^1E,{}^2E)_{(0,0,1)}$	0	0
	B	r_π	$({}^1E,{}^2E)_{(0,\eta_\mathcal{P},0)}, (A, B)_{(\eta_\mathcal{T},0,0)}$	$\mathbb{Z}$	$\mathbb{Z}$
C_6	A	r_0	$A_{(\eta_\mathcal{T},\eta_\mathcal{P},1)}, B_{(\eta_\mathcal{T},\eta_\mathcal{P},1)}, ({}^1E_1,{}^2E_1)_{(0,0,1)}, ({}^1E_2,{}^2E_2)_{(0,0,1)}$	0	0
	B	r_π	$(A, B)_{(\eta_\mathcal{T},0,0)}, ({}^1E_1,{}^2E_1,{}^2E_2,{}^1E_2)_{(0,0,0)}$	$\mathbb{Z}^2$	$\mathbb{Z}^2$
C_{2v}	A_1	r_{++}	$(A_1)_{(\eta_\mathcal{T},\eta_\mathcal{P},1)}, (A_2)_{(\eta_\mathcal{T},\eta_\mathcal{P},1)}, (B_1)_{(\eta_\mathcal{T},\eta_\mathcal{P},1)}, (A_2)_{(\eta_\mathcal{T},\eta_\mathcal{P},1)}$	0	0
	A_2	r_{--}	$(A_1, A_2)_{(\eta_\mathcal{T},0,0)}, (B_1, B_2)_{(\eta_\mathcal{T},0,0)}$	$\mathbb{Z}^2$	$\mathbb{Z}^2$
	B_1	r_{-+}	$(A_1, B_1)_{(\eta_\mathcal{T},0,0)}, (A_2, B_2)_{(\eta_\mathcal{T},0,0)}$	$\mathbb{Z}^2$	$\mathbb{Z}^2$
	B_2	r_{+-}	$(A_1, B_2)_{(\eta_\mathcal{T},0,0)}, (B_1, A_2)_{(\eta_\mathcal{T},0,0)}$	$\mathbb{Z}^2$	$\mathbb{Z}^2$
C_{3v}	A_1		$(A_1)_{(\eta_\mathcal{T},\eta_\mathcal{P},1)}, (A_2)_{(\eta_\mathcal{T},\eta_\mathcal{P},1)}, (E)_{(\eta_\mathcal{T},\eta_\mathcal{P},1)}$	0	0
	A_2		$(A_1, A_2)_{(\eta_\mathcal{T},0,0)}, (E)_{(\eta_\mathcal{T},-\eta_\mathcal{P},1)}$	$\mathbb{Z}\times\mathbb{Z}_2$	$\mathbb{Z}$
C_{4v}	A_1		$(A_1)_{(\eta_\mathcal{T},\eta_\mathcal{P},1)}, (A_2)_{(\eta_\mathcal{T},\eta_\mathcal{P},1)}, (B_1)_{(\eta_\mathcal{T},\eta_\mathcal{P},1)}, (A_2)_{(\eta_\mathcal{T},\eta_\mathcal{P},1)}, E_{(\eta_\mathcal{T},\eta_\mathcal{P},1)}$	0	0
	A_2		$(A_1, A_2)_{(\eta_\mathcal{T},0,0)}, (B_1, B_2)_{(\eta_\mathcal{T},0,0)}, E_{(\eta_\mathcal{T},-\eta_\mathcal{P},1)}$	$\mathbb{Z}^2\times\mathbb{Z}_2$	$\mathbb{Z}^2$
	B_1		$(A_1, B_1)_{(\eta_\mathcal{T},0,0)}, (A_2, B_1)_{(\eta_\mathcal{T},0,0)}, E_{(\eta_\mathcal{T},\eta_\mathcal{P},1)}$	$\mathbb{Z}^2$	$\mathbb{Z}^2$
	B_2		$(A_1, B_2)_{(\eta_\mathcal{T},0,0)}, (B_1, A_2)_{(\eta_\mathcal{T},0,0)}, E_{(\eta_\mathcal{T},\eta_\mathcal{P},1)}$	$\mathbb{Z}^2$	$\mathbb{Z}^2$
C_{6v}	A_1		$(A_1)_{(\eta_\mathcal{T},\eta_\mathcal{P},1)}, (A_2)_{(\eta_\mathcal{T},\eta_\mathcal{P},1)}, (B_1)_{(\eta_\mathcal{T},\eta_\mathcal{P},1)}, (A_2)_{(\eta_\mathcal{T},\eta_\mathcal{P},1)}, (E_1)_{(\eta_\mathcal{T},\eta_\mathcal{P},1)}, (E_2)_{(\eta_\mathcal{T},\eta_\mathcal{P},1)}$	0	0
	A_2		$(A_1, A_2)_{(\eta_\mathcal{T},0,0)}, (B_1, B_2)_{(\eta_\mathcal{T},0,0)}, (E_1)_{(\eta_\mathcal{T},-\eta_\mathcal{P},1)}, (E_2)_{(\eta_\mathcal{T},-\eta_\mathcal{P},1)}$	$\mathbb{Z}^2\times\mathbb{Z}_2^2$	$\mathbb{Z}^2$
	B_1		$(A_1, B_1)_{(\eta_\mathcal{T},0,0)}, (A_2, B_1)_{(\eta_\mathcal{T},0,0)}, (E_1, E_2)_{(\eta_\mathcal{T},0,0)}$	$\mathbb{Z}^3$	$\mathbb{Z}^3$
	B_2		$(A_1, B_1)_{(\eta_\mathcal{T},0,0)}, (A_2, B_1)_{(\eta_\mathcal{T},0,0)}, (E_1, E_2)_{(\eta_\mathcal{T},0,0)}$	$\mathbb{Z}^3$	$\mathbb{Z}^3$

TABLE 4.8. Same as Table 4.7, but in the presence of spin-rotation symmetry, *i.e.* for spinless representations of the crystalline symmetry group. Time-reversal symmetric BdG Hamiltonians with spin-rotation symmetry correspond to tenfold-way class CI, $\eta = (1,-1,1)$. We also include systems with emergent time-reversal symmetry, corresponding to class CII, $\eta = (-1,-1,1)$.

$W_\mathcal{P}(\alpha)$	Cartan	$\mathfrak{K}_{(0,W_\mathcal{P}(\alpha),0)}[0]$	ν	H_{gen}	H_{ref}	$\mathcal{P}$	U
1	D	$\mathbb{Z}_2$	$\mathfrak{p}_\alpha$	$-\tau_3\otimes 1_d$	$\tau_3\otimes 1_d$	$\tau_1 K$	$r_\alpha\otimes\tau_0$
-1	C	0	$-$	-	$\tau_3\otimes 1_d$	$\tau_2 K$	$r_\alpha\otimes\tau_0$
0	A	$\mathbb{Z}$	$\begin{cases}\mathfrak{N}_\alpha\\ -\mathfrak{N}_{\Theta\alpha^*}\end{cases}$	$-\tau_3\otimes 1_d$	$\tau_3\otimes 1_d$	$\tau_{1,2}K$	$\begin{pmatrix} r_\alpha & 0\\ 0 & \Theta r_\alpha^*\end{pmatrix}_\tau$

TABLE 4.9. Classifying groups $\mathfrak{K}_{W_\mathcal{P}(\alpha)}[0]$ and topological invariants ν for the tenfold-way classes D and C, $\eta = (0,\pm 1,0)$ (third and fourth columns). These depend on the irrep r_α through the outcome of the Wigner test $W_\mathcal{P}(\alpha)$ only, which is listed in the first column. The second column lists the effective tenfold-way class corresponding to $W_\mathcal{P}(\alpha)$. The fifth and sixth columns list a generating Hamiltonian H_{gen} and a reference Hamiltonian H_{ref}, respectively. The seventh and eighth columns give the representations of particle-hole conjugation $\mathcal{P}$ and the representation U of the elements of the crystalline symmetry group G. The dimension of the irreducible representation r_α is denoted d_α.

which was represented by $\sigma_0\tau_1 K$ before the basis change, now reads $\sigma_2\tau_2 K$. Since the C_{2v} symmetry enforces that H is of the form $\sigma_0 H_{\overline{E}}$, compare with Eq. (4.26), the factor σ_2 must be dropped from the representation of $\mathcal{P}$, since it does not affect $H_{\overline{E}}$, and one arrives at the effective particle-hole conjugation operator $\tau_2 K$: The effective particle-hole conjugation operator squares to minus one. The time-reversal operation $\mathcal{T}$, which was given by $\sigma_2\tau_0 K$ in the original basis, is unchanged by the basis transformation. Again omitting the factor σ_2, one finds that the effective time-reversal operation is $\tau_0 K$. It follows that

$$\mathfrak{K}_{(\eta_\mathcal{T},1,\eta_\mathcal{C})}[C_{2v}, A_1] = \mathfrak{K}_{(-\eta_\mathcal{T},-1,\eta_\mathcal{C})}[0]. \tag{4.36}$$

The same result is found if one performs the Wigner test, see Eqs. (4.27) and (4.28).

For $\Theta = r_{+-}$ (the "B_2" representation) one finds that the representation u of Table 4.3 for the normal-state block h gives the representations $U(\mathcal{M}_x) = i\sigma_1\tau_0$ and $U(\mathcal{M}_y) = i\sigma_2\tau_0$ for the full BdG Hamiltonian H, which is already in the canonical form (4.25). It then immediately follows that the effective particle-hole conjugation operation is $\tau_1 K$ and the effective time-reversal operation is $\tau_0 K$. For the remaining two cases r_{-+}, and r_{--} (the "B_1" and "A_2" representations), one may proceed as described above for the A_1 representation, by performing a suitable basis transformation, or use an alter-

native normal-state representation with $u(\mathcal{M}_x) = i\sigma_2$, $u(\mathcal{M}_y) = i\sigma_3$ for B_1 and $u(\mathcal{M}_x) = i\sigma_3$, $u(\mathcal{M}_y) = i\sigma_1$ for A_2, to which the canonical form (4.25) applies without the need for a basis transformation. Either way, we find that both the effective time-reversal operation and the effective particle-hole conjugation operation square to unity, $W_\mathcal{T} = -\eta_\mathcal{T} = 1$ and $W_\mathcal{P} = \eta_\mathcal{P} = 1$. As a result, we have

$$\begin{aligned}\mathfrak{K}_{(\eta_\mathcal{T},1,\eta_\mathcal{C})}[C_{2v}, B_{1,2}] &= \mathfrak{K}_{(\eta_\mathcal{T},1,\eta_\mathcal{C})}[C_{2v}, A_2] \\ &= \mathfrak{K}_{(-\eta_\mathcal{T},1,\eta_\mathcal{C})}[0]. \end{aligned} \tag{4.37}$$

A remark on classifying groups.— We close this section by making a few remarks regarding the group structure of topological classification within K-theory. Formally, the group structure within K-theory is given by the Grothendieck construction,[32, 73] where the group elements are represented by ordered pairs (H_1, H_2) of hermitian matrix-valued functions $H_{1,2}(\mathbf{k})$ of equal dimension. The two pairs (H_1, H_2) and (H_1', H_2') are topologically equivalent if $H_1 \oplus H_2'$ is continuously deformable to $H_1' \oplus H_2$. Loosely speaking the ordered pair (H_1, H_2) represents the "difference" of the two Hamiltonians H_1 and H_2.

For gapped phases with dimension $d > 0$, a meaningful concept of "topologically nontrivial" Hamiltonians can be obtained by defining a reference atomic-limit Hamitonian $H_{\mathrm{ref}}(\mathbf{k})$ as a "topologically trivial phase". (A precise definition of "atomic-limit Hamiltonians" will be given in the next Section.) Such a strategy results in a unique and well-defined topological classification that is independent of the choice of the precise reference Hamiltonian $H_{\mathrm{ref}}(\mathbf{k})$ if one considers Hamiltonians that differ by an atomic-limit Hamiltonian to be in the same topological class. It is this classification principle that underlies the classifying groups $\mathcal{K}_\eta[G, \Theta]$ used throughout the remainder of this chapter for Hamiltonians of dimension $d \geq 1$. On other hand, for zero-dimensional Hamiltonians, there is no natural choice for the trivial phase and it is important to adhere to the notion that a topological classification classifies pairs of Hamiltonians only. It is this stricter notion of topological classification that is used for the definition of the classifying groups $\mathfrak{K}_\eta[G, \Theta]$ of zero-dimensional Hamiltonians, which play a key role in the construction of symmetry-based indicators in the next Section.

Generators and invariants for the classifying groups $\mathfrak{K}_\eta[G, \Theta]$.— The classifying groups $\mathfrak{K}_\eta[G, \Theta]$ of zero-dimensional Hamiltonians with additional point group G and with one-dimensional representation Θ governing the pairing term Θ are determined by the effective Cartan class of diagonal blocks corresponding to the irreducible representation α or by pairs or quadruples of such blocks, as discussed above. We tabulate the classification $\mathfrak{K}_\eta[0]$, the invariants ν, generators H and representations $U(g)$ of all symmetry elements g, $\mathcal{T}$ and $\mathcal{P}$ for all cases in Tables 4.9, 4.10. The zero-dimensional invariants can be given as the number $\mathfrak{N}_\alpha$ of negative energy eigenstates (Kramers pairs in case the block H_α is invariant under an antiunitary symmetry UK with $(UK)^2 = -1$, *i. e.* in Cartan class AII) with representation α or the Pfaffian invariant $\mathfrak{p}_\alpha$ of the block H_α belonging to the irreducible representation r_α. In case there are multiple blocks related by $\mathcal{T}$ or $\mathcal{P}$ we present all equivalent invariants.

For the calculation the zero-dimensional invariants $\nu_\alpha = \mathfrak{N}_\alpha$ or $\nu_\alpha = \mathfrak{p}_\alpha$ it may be helpful to use the projector [74] onto a subspace spanned by irreducible representation α

$$P_\alpha = d_\alpha \langle \chi_\alpha^*(g) U(g) \rangle_G, \tag{4.38}$$

where $\langle \ldots \rangle_G$ denotes the average over all elements $g \in G$ and $\chi_\alpha(g)$ is the character. Choosing a basis in which the projector P_α is block diagonal — which can be done for all irreps r_α simultaneously, although this is not necessary for the calculation to succeed —, the projected Hamiltonian $P_\alpha H P_\alpha$ takes the form $\mathrm{diag}(H_\alpha, 0_{N-N_\alpha})$, and the topological invariant can be computed as

$$\nu_\alpha(H) \equiv \nu(H_\alpha). \tag{4.39}$$

The Pfaffian invariant $\mathfrak{p}_\alpha$ of a subblock H_α invariant under an (effective) antiunitary antisymmetry with representation U with $(UK)^2 = 1$ is defined as

$$(-1)^{\mathfrak{p}_\alpha} = \mathrm{sign}\,\mathrm{Pf}\,(H_\alpha U). \tag{4.40}$$

4.4. SYMMETRY-BASED INDICATORS OF BAND TOPOLOGY

Whereas a full topological classification of a gapped Hamiltonians in d dimensions — as described by the classifying group $\mathcal{K}_\eta[G, \Theta]$ — requires the analysis of matrix-valued *functions* $H(\mathbf{k})$ with the momentum $\mathbf{k}$ taken on the full Brillouin zone, partial information on the topological phase can be already obtained by inspection of the topological class of matrices $H(\mathbf{k}_\mathrm{s})$ at a discrete set of high-symmetry momenta $\mathbf{k}_\mathrm{s}$. Such an approach has been developed by Po *et al.* for non-superconducting insulators[27] (see also Refs. 28 and 59.) We here present this approach in such a way that it can immediately be generalized to Hamiltonians of Bogoliubov-de Gennes type.

We consider a band structure defined by the Hamiltonian $H(\mathbf{k})$, with $\mathbf{k}$ an element of the Brillouin zone of a d-dimensional crystal with (discrete) translation invariance and with symmorphic crystalline symmetry described by the point group G. In addition, there may be nonspatial symmetries such as time-reversal symmetry, particle-hole antisymmetry, or chiral antisymmetry, which determine the tenfold-way symmetry class. These nonspatial symmetries are characterized by the triple $\eta = (\eta_\mathcal{T}, \eta_\mathcal{P}, \eta_\mathcal{C})$, as explained in the previous Section. For superconductors, *i.e.* for Hamiltonians of BdG type, one further needs to specify a one-dimensional representation Θ of G, which characterizes the superconducting phase, see the discussion in Sec. 4.2.

$W(\alpha)$	Cartan	$\mathfrak{K}_{W(\alpha)}[0]$	ν	H_{gen}	H_{ref}	$\mathcal{T}$	$\mathcal{P}$	U
(0,0,0)	A	$\mathbb{Z}$	$\begin{cases}\mathfrak{N}_\alpha\\ \mathfrak{N}_{\alpha^*}\\ -\mathfrak{N}_{\Theta\alpha^*}\\ -\mathfrak{N}_{\Theta\alpha}\end{cases}$	$-\sigma_0\tau_3\otimes 1_{d_\alpha}$	$\sigma_0\tau_3\otimes 1_{d_\alpha}$	$\sigma_{1,2}K$	$\tau_{1,2}K$	$\begin{pmatrix}\begin{pmatrix} r & 0\\ 0 & r_\alpha^*\end{pmatrix}_\sigma & 0\\ 0 & \Theta\begin{pmatrix} r_\alpha & 0\\ 0 & r_\alpha^*\end{pmatrix}^*_\sigma\end{pmatrix}_\tau$
(0,0,1)	AIII	0	-	-	$\sigma_0\tau_3\otimes 1_{d_\alpha}$	$\sigma_{1,2}K$	$\sigma_{1,2}\tau_1 K$	$\begin{pmatrix} r_\alpha & 0\\ 0 & r_\alpha^*\end{pmatrix}_\sigma\otimes\tau_0$
(1,0,0)	AI	$\mathbb{Z}$	$\begin{cases}\mathfrak{N}_\alpha\\ -\mathfrak{N}_{\Theta\alpha^*}\end{cases}$	$-\tau_3\otimes 1_{d_\alpha}$	$\tau_3\otimes 1_{d_\alpha}$	K	$\tau_{1,2}K$	$\begin{pmatrix} r_\alpha & 0\\ 0 & \Theta r_\alpha^*\end{pmatrix}_\tau$
(1,1,1)	BDI	$\mathbb{Z}_2$	$\mathfrak{p}_\alpha$	$-\tau_3\otimes 1_{d_\alpha}$	$\tau_3\otimes 1_{d_\alpha}$	K	$\tau_1 K$	$r_\alpha\otimes\tau_0$
(0,1,0)	D	$\mathbb{Z}_2$	$\begin{cases}\mathfrak{p}_\alpha\\ \mathfrak{p}_{\alpha^*}\end{cases}$	$-\sigma_0\tau_3\otimes 1_{d_\alpha}$	$\sigma_0\tau_3\otimes 1_{d_\alpha}$	$\sigma_{1,2}K$	$\tau_1 K$	$\begin{pmatrix} r_\alpha & 0\\ 0 & r_\alpha^*\end{pmatrix}_\sigma\otimes\tau_0$
(-1,1,1)	DIII	0	-	-	$\sigma_0\tau_3\otimes 1_{d_\alpha}$	$\sigma_2 K$	$\tau_1 K$	$r_\alpha\otimes\sigma_0\tau_0$
(-1,0,0)	AII	$\mathbb{Z}$	$\begin{cases}\mathfrak{N}_\alpha\\ -\mathfrak{N}_{\Theta\alpha^*}\end{cases}$	$-\sigma_0\tau_3\otimes 1_{d_\alpha}$	$\sigma_0\tau_3\otimes 1_{d_\alpha}$	$\sigma_2 K$	$\tau_{1,2}K$	$\begin{pmatrix} r_\alpha & 0\\ 0 & \Theta r_\alpha^*\end{pmatrix}_\tau\otimes\sigma_0$
(-1,-1,1)	CII	0	-	-	$\sigma_0\tau_3\otimes 1_{d_\alpha}$	$\sigma_2 K$	$\tau_2 K$	$r_\alpha\otimes\sigma_0\tau_0$
(0,-1,0)	C	0	-	-	$\sigma_0\tau_3\otimes 1_{d_\alpha}$	$\sigma_{1,2}K$	$\tau_2 K$	$\begin{pmatrix} r_\alpha & 0\\ 0 & r_\alpha^*\end{pmatrix}_\sigma\otimes\tau_0$
(1,-1,1)	CI	0	-	-	$\tau_3\otimes 1_{d_\alpha}$	K	$\tau_2 K$	$r_\alpha\otimes\tau_0$

TABLE 4.10. Classifying groups $\mathfrak{K}_{W_\mathcal{P}(\alpha)}[0]$ and topological invariants ν for the tenfold-way classes with time-reversal symmetry (third and fourth columns). These depend on the irrep r_α through the outcome of the Wigner test $W_\mathcal{P}(\alpha)$ only, which is listed in the first column. The second column lists the effective tenfold-way class corresponding to $W_\mathcal{P}(\alpha)$. The fifth and sixth columns list a generating Hamiltonian H_{gen} and a reference Hamiltonian H_{ref}, respectively. The seventh, eighth, and ninth columns give the representations of time-reversal $\mathcal{T}$, particle-hole conjugation $\mathcal{P}$, and the representation U of the elements of the crystalline symmetry group G. The dimension of the irreducible representation r_α is denoted d_α.

4.4.1. Construction of a reference set of high-symmetry momenta

To define a representative set of high-symmetry momenta, we consider the group $\tilde{G}$ of automorphisms of the Brillouin zone that are induced by elements of G and by the operations $\mathcal{T}$ and $\mathcal{P}$, if present. (The element $g\in G$ induces an automorphism of the Brillouin zone by sending $\mathbf{k}\to g\mathbf{k}$, whereas $\mathcal{T}$ and $\mathcal{P}$ send $\mathbf{k}$ to $-\mathbf{k}$, in both cases identifying wavevectors that differ by a reciprocal lattice vector.) For each momentum $\mathbf{k}$ we define the "little group" $\tilde{G}_\mathbf{k}$ as the subgroup of elements $\tilde{g}\in\tilde{G}$ such that $\tilde{g}\mathbf{k}=\mathbf{k}$. Two momenta $\mathbf{k}_1$ and $\mathbf{k}_2$ are considered equivalent for classification purposes if there exists an element $\tilde{g}\in\tilde{G}$ and a continuous path between $\mathbf{k}_1$ and $\tilde{g}\mathbf{k}_2$ along which the little group $\tilde{G}_\mathbf{k}$ does not change. (In particular, this implies that $\mathbf{k}_1$ and $\mathbf{k}_2$ are equivalent if $\mathbf{k}_1=\tilde{g}\mathbf{k}_2$ and that equivalent momenta have the same little group.) A set of equivalent momenta is called of "high-symmetry" if it does not border to another set of equivalent momenta with a strictly larger little group. The representative set $\{\mathbf{k}_\text{s}\}$ of high-symmetry momenta is then constructed by arbitrarily selecting one momentum from each set of equivalent high-symmetry momenta.

4.4.2. Definition of the groups "BS" and "SI"

To each high-symmetry momentum $\mathbf{k}_\text{s}$ we may associate a subgroup $G_{\mathbf{k}_\text{s}}\subset G$ of crystalline symmetry operations that leave $\mathbf{k}_\text{s}$ invariant and a triple $\eta_{\mathbf{k}_\text{s}}=(\eta_{\mathcal{T},\mathbf{k}_\text{s}},\eta_{\mathcal{P},\mathbf{k}_\text{s}},\eta_\mathcal{C})$ that indicate whether $\mathbf{k}_\text{s}$ is invariant under the operations $\mathcal{T}$ and $\mathcal{P}$, if present. The group $G_{\mathbf{k}_\text{s}}$, the symmetry indices $\eta_{\mathbf{k}_\text{s}}$, and the one-dimensional representation Θ of G (suitably restricted to $G_{\mathbf{k}_\text{s}}$) determine the symmetry of the Hamiltonian $H(\mathbf{k}_\text{s})$ at the high-symmetry momentum $\mathbf{k}_\text{s}$. The group of "band labels" BL is defined as the combined set of topological invariants that can be obtained from the topological information at these high-symmetry momenta alone, [64]

$$\text{BL}_\eta[G,\Theta]=\prod_{\mathbf{k}_\text{s}}\mathfrak{K}_{\eta_{\mathbf{k}_\text{s}}}[G_{\mathbf{k}_\text{s}},\Theta]. \tag{4.41}$$

The classifying group $\mathfrak{K}_{\eta_\mathbf{k}}[G_\mathbf{k},\Theta]$ describes zero-dimensional topological phases protected by the on-site symmetry group $G_\mathbf{k}$ and can be calculated from Eq. (4.29).

Although this procedure associates a well-defined topological invariant with each Hamiltonian $H(\mathbf{k})$, there are three reasons why $\text{BL}_\eta[G,\Theta]$ is different from the classifying group $\mathcal{K}_\eta[G,\Theta]$ of topological phases with tenfold-way symmetries η, point group G, and a superconducting phase with symmetry described by Θ: (i) Not every element in BL represents the band labels of a gapped Hamiltonian $H(\mathbf{k})$, (ii) there may exist d-dimensional Hamiltonians $H(\mathbf{k})$ without topologically protected anomalous boundary states for which the band labels are nontrivial nevertheless, and (iii) there may be Hamiltonians $H(\mathbf{k})$ with topologically protected anomalous boundary states

for which the band labels are trivial.

Problem (i) is addressed by the introduction of "compatibility relations", constraints on the band labels, which follow from the fact that $H(\mathbf{k})$ is not only gapped at the high-symmetry momenta $\mathbf{k}_\mathrm{s}$ — which is what allows the band labels to be defined in the first place —, but also in the remainder of the Brillouin zone.[27, 28, 56] These constraints appear, in the first place, because for a gapped Hamiltonian $H(\mathbf{k})$ any band labels that can be defined for lower-symmetry momenta $\mathbf{k} \notin \{\mathbf{k}_\mathrm{s}\}$ remain well-defined and continuous if $\mathbf{k}$ approaches a high-symmetry momentum $\mathbf{k}_\mathrm{s}$. Since band labels are essentially zero-dimensional topological invariants, see the discussion above, we call these compatibility relations of "zero-dimensional" ("0d") type. Po *et al.* use these "0d compatibility relations" to define the subgroup BS $\subset$ BL of "topological band labels",

$$\mathrm{BS} = \mathrm{BL}|_{0d \text{ compatibility relations}}. \tag{4.42}$$

We use $B[H(\mathbf{k})]$ to denote the element of BS associated with the gapped Hamiltonian $H(\mathbf{k})$.

Whereas the group BL of band labels in principle depends on the choice of the set of high-symmetry momenta $\{\mathbf{k}_\mathrm{s}\}$, the group BS is independent of this choice, as long as sufficiently many momenta included. To see this, we note that the inclusion of additional momenta beyond those appearing in the set $\{\mathbf{k}_\mathrm{s}\}$ of high-symmetry momenta of Sec. 4.4 1 adds band labels to BL, but not to BS, as band labels at lower-symmetry-momenta are fully determined by the $0d$ compatibility relations.

Additional constraints on topological band labels of gapped Hamiltonians — compatibility relations of "one-dimensional" ("1d") or "two-dimensional" ("2d") type — may also appear because of the existence of topological invariants on families of higher-dimensional subspaces of the Brillouin zone,[32, 58] as we discuss below in more detail. Elements in BL or BS that violate the compatibility constraints describe "representation-enforced" gapless phases. [27, 58, 63] Depending on the dimension of the lower-symmetry region in reciprocal space and the type of constraint imposed on it, these representation-enforced gapless phases may have nodal points, nodal lines, or nodal planes.

Problem (ii) can be remedied by passing to the quotient group[27]

$$\mathrm{SI} = \mathrm{BS}/\mathrm{AI}, \tag{4.43}$$

the group of "symmetry-based indicators". Here AI $\subset$ BS is the subgroup generated by the image under B of all Hamiltonians $H(\mathbf{k})$ without boundary signature. A generating set of Hamiltonians without boundary states consists of the "atomic-limit" Hamiltonians, d-dimensional Hamiltonians that correspond to the arrangement of zero-dimensional Hamiltonians on a suitably defined lattice. After dividing out AI, a gapped Hamiltonian $H(\mathbf{k})$ is associated with a nontrivial element of SI only if it has topologically protected anomalous boundary states. Po *et al.* use the notation X_BS to refer to the group of symmetry-based indicators.

There is no general solution to address problem (iii), however. This is why the group SI is said to contain "indicators" of the topology, not a full classification. [27]

Although the topological invariants of zero-dimensional Hamiltonians are only defined for pairs of Hamiltonians, the symmetry-based indicators are expressed in terms of the band labels of a general Hamiltonian $H(\mathbf{k})$ with $\mathbf{k}$-independent symmetry representation, without comparing to a reference Hamiltonian.

4.4.3. Construction of the subgroup AI $\subset$ BS

Following Po *et al.* [27] and Bradlyn *et al.* [28], the construction of the subgroup AI proceeds in three steps: (1) One first selects a representative collection W of high-symmetry Wyckoff positions in the unit cell. Hereto, one defines the site symmetry group $G_\mathbf{x}$ for a position $\mathbf{x}$ in the unit cell as the subgroup of G that leaves $\mathbf{x}$ invariant, possibly up to lattice translations, and arranges lattice positions with the same site symmetry group which are related by a continuous path and/or by an element of G into equivalence classes ("Wyckoff positions"). A representative collection of positions W in the unit cell is then obtained by choosing a position from each equivalence class that does not border on an equivalence class with a larger site symmetry group. (2) For each position $\mathbf{x} \in W$ the "orbit" of $\mathbf{x}$ is defined as the set $\{g\mathbf{x} + \boldsymbol{t} | \, g \in G\}$ for $\boldsymbol{t}$ in Bravais lattice. The orbit defines a G-symmetric Bravais lattice. We label the lattice sites within the unit cell by $O_\mathbf{x} = \{\mathbf{x}_\sigma\}_{\sigma=1,2,\ldots}$, with the convention $\mathbf{x}_1 \equiv \mathbf{x}$. (3) For each Wyckoff position $\mathbf{x}$ and each pair (α, Θ) of an irreducible representation of the site symmetry group $G_\mathbf{x}$ and the associated one-dimensional representation Θ describing the symmetry of the superconducting order parameter, we construct a *pair* of atomic-limit Hamiltonians $H^{(\alpha,\Theta)}_{\mathbf{x},\mathrm{ref}}$ and $H^{(\alpha,\Theta)}_{\mathbf{x},\mathrm{gen}}$ by placing the zero-dimensional reference and generating Hamiltonians H_ref and H_gen of $\mathfrak{K}_\eta[G_\mathbf{x}, \Theta]$ on the positions $\mathbf{x}_\sigma$ of the orbit of $\mathbf{x}$. One verifies that invariance of the zero-dimensional Hamiltonians $H^{(\alpha,\Theta)}_{\mathbf{x},\mathrm{ref}}$ and $H^{(\alpha,\Theta)}_{\mathbf{x},\mathrm{gen}}$ under the site symmetry group $G_\mathbf{x}$ ensures that such a procedure yields well-defined G-symmetric, translationally invariant, Hamiltonians $H^{(\alpha,\Theta)}_{\mathbf{x},\mathrm{ref}}(\mathbf{k})$ and $H^{(\alpha,\Theta)}_{\mathbf{x},\mathrm{gen}}(\mathbf{k})$ on a d-dimensional lattice. The subgroup AI $\subset$ BS is generated by the *differences* $B[H^{(\alpha,\Theta)}_{\mathbf{x},\mathrm{gen}}(\mathbf{k})] - B[H^{(\alpha,\Theta)}_{\mathbf{x},\mathrm{ref}}(\mathbf{k})]$ of the images of the Hamiltonians obtained in this manner.

The procedure of taking differences of images under B is necessary for the construction of AI, because, although the reference Hamiltonians H_ref in Tables 4.9 and 4.10 have been chosen such that they map to the trivial element under B, the band labels need not be trivial for atomic-limit Hamiltonian obtained by placing copies of H_ref on nontrivial Wyckoff positions. The nontrivial band labels for the reference Hamiltonian have their origin in the $\mathbf{k}$-dependence of the representation of the

point group G, which is unavoidable if minimal $0d$ superconductors are placed at nontrivial Wyckoff positions. Such a $\mathbf{k}$ dependence of the representation is not compatible with our construction of the topological band labels $B[H(\mathbf{k})]$, which assume a $\mathbf{k}$-independent representation of G. (The simplest example where this is the case is a one-dimensional superconductor with inversion symmetry and odd-parity superconducting order, see Sec. 4.5 2).

One can resolve this issue either by adding multiple copies of the "trivial" $0d$ Hamiltonian H_{ref} at the same Wyckoff position, which eventually allows one to construct a $\mathbf{k}$-independent representation of G. We here prefer to take an equivalent, but computationally more efficiently approach, in which we remedy this situation by comparing atomic-limit Hamiltonians with the same number of orbitals (per representation pair (α, Θ)) at each Wyckoff position only. We construct a "trivial" reference atomic-limit Hamiltonian for this case, and define the band labels of each other atomic-limit Hamiltonian as the difference of the band labels with the reference atomic-limit Hamiltonian. The trivial reference atomic-limit Hamiltonian is chosen such that all Wyckoff positions and all representation pairs (α, Θ) are represented: It is the direct sum of $0d$ reference Hamiltonians H_{ref} from Tables 4.9 and 4.10 for all pairs (α, Θ), placed at all Wyckoff positions. Generator atomic-limit Hamiltonians $H^{(\alpha,\Theta)}_{\mathbf{x},\mathrm{gen}}(\mathbf{k})$ are obtained by replacing a $0d$ reference Hamiltonian in this direct sum by a generator from Tables 4.9 and 4.10 for the orbit $O_{\mathbf{x}}$ and representation pair (α, Θ) only. Since the map B is additive under the taking of direct sums, taking the difference of the band labels of this generator Hamiltonian and the reference atomic-limit Hamiltonian is the same as taking the difference $B[H^{(\alpha,\Theta)}_{\mathbf{x},\mathrm{gen}}(\mathbf{k})] - B[H^{(\alpha,\Theta)}_{\mathbf{x},\mathrm{ref}}(\mathbf{k})]$ for atomic-limit Hamiltonians involving a single Wyckoff position $\mathbf{x}$ and representation pair (α, Θ) only, which justifies the procedure outlined step (iii) above.

Each reference Hamiltonian or generator Hamiltonian is compactly expressed as[27, 28, 71]

$$H^{(\alpha,\Theta)}_{\mathbf{x}}(\mathbf{k}) = \mathbb{1}_{|O_{\mathbf{x}}|\times|O_{\mathbf{x}}|} \otimes H^{(\alpha,\Theta)}_{\mathbf{x}}, \tag{4.44}$$

where $|O_{\mathbf{x}}|$ is the number of sites in the orbit of $\mathbf{x}$. The representation of $g \in G$ is

$$[U^{\mathbf{x},\alpha}(g,\mathbf{k})]_{\sigma' j,\sigma i} = \delta'_{\mathbf{x}_{\sigma'},g\mathbf{x}_\sigma} e^{-i\mathbf{k}\cdot(g\mathbf{x}_\sigma - \mathbf{x}_{\sigma'})} \times \frac{z_{g,g_\sigma}}{z_{g_{\sigma'},g^{-1}_{\sigma'}gg_\sigma}} [u^\alpha_{\mathbf{x}}(g^{-1}_{\sigma'} t_{\mathbf{x}_{\sigma'}-\mathbf{x}_\sigma} g g_\sigma)]_{ji}, \tag{4.45}$$

where the indices σ and σ' label the positions $\mathbf{x}_\sigma$ in the orbit of $\mathbf{x}$ and the indices i and j the degree of freedom of $H^{(\alpha,\Theta)}_{\mathbf{x}}$. Further, a choice $\{g_\sigma\}_{\sigma=1,\ldots,|O_{\mathbf{x}}|}$ from G was made in such a way that $g_{\sigma=1}$ is the identity and $g_\sigma \mathbf{x} = \mathbf{x}_\sigma$ for $\sigma = 2, \ldots, |O_{\mathbf{x}}|$. Each group element is decomposed as $g = t_{\mathbf{R}} g_\sigma h$ with $h \in G_{\mathbf{x}}$, $t_{\mathbf{R}} \in T$ and $\mathbf{R} = g\mathbf{x}_\sigma - \mathbf{x}_{\sigma'}$. The Kronecker symbol $\delta'_{\mathbf{x}_1,\mathbf{x}_2}$ is nonzero and equal to one only when $\mathbf{x}_1 = \mathbf{x}_2 + \mathbf{R}$ for some $\mathbf{R}$ in Bravais lattice. The representation u_α is given in Tables 4.9 and 4.10.

In this construction it is important that time-reversal $\mathcal{T}$ and particle-hole conjugation $\mathcal{P}$ are *local* operations. If $\mathcal{P}$ is not a local operation, an arrangement of disconnected onsite Hamiltonians can acquire a spurious nonlocality, in spite of the absence of inter-site matrix elements.

4.4.4. Compatibility relations

In the examples that we consider in the next Sections, we find that it is sufficient to use compatibility relations for gapped hermitian matrices $H(\mathbf{k})$ based on local-in-$\mathbf{k}$ symmetries only. These compatibility relations may be applied to the entire matrix $H(\mathbf{k})$ or to a diagonal block, if $H(\mathbf{k})$ has a block structure that is preserved throughout a part of the Brillouin zone. The compatibility relations involve topological invariants of $H(\mathbf{k})$ defined using information about $H(\mathbf{k})$ away from the high-symmetry points $\mathbf{k}_{\mathrm{s}}$. Depending on the dimensionality of the subspace required to define these topological invariants, we distinguish between compatibility relations of $0d$ type (which are used to define the group BS of topological band labels) and of $1d$ or $2d$ type.[64] We now discuss the construction of $0d$, $1d$, and $2d$ compatibility relations in detail.

0a.— The number of negative eigenvalues of a hermitian matrix $H(\mathbf{k})$ with a gapped spectrum does not change if $\mathbf{k}$ is changed continuously. This gives a compatibility constraint if $\mathbf{k}$ can be changed continuously between high-symmetry points $\mathbf{k}_{\mathrm{s},1}$ and $\mathbf{k}_{\mathrm{s},2}$, while preserving Hermiticity of (a subblock of) the Hamiltonian, and if the number of negative eigenvalues can be related to the band labels at $\mathbf{k}_{\mathrm{s},1}$ and $\mathbf{k}_{\mathrm{s},2}$.

0b.— The sign of the Pfaffian of a gapped, antisymmetric matrix $UH(\mathbf{k})$, with U an appropriately chosen unitary operator, does not change if $\mathbf{k}$ is changed continuously. This results in a compatibility constraint for topological band labels if $\mathbf{k}$ can be changed continuously between high-symmetry points $\mathbf{k}_{\mathrm{s},1}$ and $\mathbf{k}_{\mathrm{s},2}$, while preserving the antisymmetry of (a subblock of) the matrix $UH(\mathbf{k})$, and if the sign of the Pfaffian can be related to the band labels at $\mathbf{k}_{\mathrm{s},1}$ and $\mathbf{k}_{\mathrm{s},2}$.

1.— The topological invariant of a one-dimensional Hamiltonian $H(k)$, obtained by restricting $H(\mathbf{k})$ to a one-dimensional closed contour in reciprocal space, does not change if this contour is continuously deformed. Such a topological invariant can be a winding number, if $H(k)$ has a chiral antisymmetry, but it may also be a $\mathbb{Z}_2$ invariant (the first Stiefel-Whitney number [75, 76]), if $H(k)$ or a diagonal block of it satisfy local-in-$\mathbf{k}$ symmetries that place it effectively in tenfold-way classes AI or BDI. This gives an additional compatibility relation if the topological invariant can be related to the topological band labels of $H(\mathbf{k}_{\mathrm{s}})$ at high-symmetry points $\mathbf{k}_{\mathrm{s}}$ on the contour and if the contour can be deformed so that it can be made to pass through different sets of high-symmetry momenta, while preserving local-in-$\mathbf{k}$ symmetries of $H(\mathbf{k})$. An example of such a $1d$ compatibility relation is given in the

example discussed in Sec. 4.7 4 (tenfold-way class CI with inversion symmetry).

2.— The topological invariant of a gapped hermitian matrix $H(k_1, k_2)$, which is defined on a two-dimensional plane cutting through the Brillouin zone, does not change if the position of the plane is shifted continuously. The topological invariant is a Chern number if the local-in-$\mathbf{k}$ crystalline symmetries are such that $H(k_1, k_2)$ or a diagonal block of it are effectively in tenfold-way classes A, D, or C, or it may be a $\mathbb{Z}_2$ invariant (the second Stiefel-Whitney number [75, 76]), if $H(k_1, k_2)$ is effectively in tenfold-way classes CI or AI. This yields an additional compatibility relation if the topological invariant can be related to the band labels of $H(\mathbf{k}_\mathrm{s})$ at high-symmetry points $\mathbf{k}_\mathrm{s}$ on the plane and if the plane can be shifted continuously, such that it can be made to pass through different sets of high-symmetry momenta while preserving the hermiticity of (the relevant subblock of) $H(\mathbf{k})$. This "$2d$ compatibility relation" is used in Ref. 27 to identify representation-enforced nodal semimetals (see also Ref. 32 and 58). It also appears, *e.g.*, in the example discussed in Sec. 4.7 1 (tenfold-way class D with inversion symmetry).

Unlike the construction of the groups BS and AI, we are not aware of a method that allows one to implement the compatibility relations based on higher-dimensional topological invariants in an algorithmic way. The "bottleneck" is the relation between the n-dimensional topological invariant used to construct the compatibility relation and the topological band labels of $H(\mathbf{k})$ at high-symmetry momenta $\mathbf{k}_\mathrm{s}$, which requires knowledge of the full classification of n-dimensional crystalline phases. This is not a problem if the symmetry-based indicators are used to determine the topological phase of a given BdG Hamiltonian with a gapped spectrum, but it does affect the use of SI as a proxy for the full boundary classification group $\mathcal{K}$.

Generalizing the definition of BS, see Eq. (4.42), we may define the subgroup series

$$\mathrm{BS}^{(2)} \subset \mathrm{BS}^{(1)} \subset \mathrm{BS}^{(0)} \equiv \mathrm{BS}, \tag{4.46}$$

where $\mathrm{BS}^{(n)}$ is the subgroup of BL obtained by imposing all compatibility constraints involving topological invariants of dimension $\leq n$. Correspondingly, we may define the group $\mathrm{SI}^{(n)} \subset \mathrm{SI}$ of symmetry-based indicators as

$$\mathrm{SI}^{(2)} \subset \mathrm{SI}^{(1)} \subset \mathrm{SI}^{(0)} \equiv \mathrm{SI}, \tag{4.47}$$

with

$$\mathrm{SI}^{(n)} = \mathrm{BS}^{(n)}/\mathrm{AI} \tag{4.48}$$

and $\mathrm{SI}^{(0)} = \mathrm{SI}$. For the examples we consider, we find that $\mathrm{SI}^{(d-1)}$ contains no gapless phases, implying that the compatibility relations based on local-in-$\mathbf{k}$ symmetries are sufficient for these cases.

4.4.5. Weak-pairing limit

In the weak-pairing limit — superconducting order parameter Δ much smaller than energy scales typical for the normal-state band structure — the band labels $\mathfrak{N}_\alpha^{\mathbf{k}_\mathrm{s}}$ and $\mathfrak{p}_\alpha^{\mathbf{k}_\mathrm{s}}$ of the BdG Hamiltonian $H(\mathbf{k}_\mathrm{s})$ at the high-symmetry momentum $\mathbf{k}_\mathrm{s}$ can be expressed in terms of zero-dimensional topological invariants of the normal-state Hamiltonians $h(\mathbf{k}_\mathrm{s})$ and $h(-\mathbf{k}_\mathrm{s})$. For $\mathfrak{N}_\alpha^{\mathbf{k}_\mathrm{s}}$ one has [65, 67, 68]

$$\begin{aligned}\mathfrak{N}_\alpha^{\mathbf{k}_\mathrm{s}} &= n_\alpha^{\mathbf{k}_\mathrm{s}}|_\mathrm{occ} + n_{\Theta\alpha^*}^{-\mathbf{k}_\mathrm{s}}|_\mathrm{unocc} \\ &= n_\alpha^{\mathbf{k}_\mathrm{s}}|_\mathrm{occ} - n_{\Theta\alpha^*}^{-\mathbf{k}_\mathrm{s}}|_\mathrm{occ} + n_{\Theta\alpha^*}^{-\mathbf{k}_\mathrm{s}}\end{aligned} \tag{4.49}$$

where $n_\alpha^{\mathbf{k}_\mathrm{s}}$, $n_\alpha^{\mathbf{k}_\mathrm{s}}|_\mathrm{occ}$ and $n_\alpha^{\mathbf{k}_\mathrm{s}}|_\mathrm{unocc}$ are the total number, the number of occupied, and the number of unoccupied bands of the subblock $h_\alpha(\mathbf{k}_\mathrm{s})$ of the normal-state Hamiltonian, respectively. Similarly, the Pfaffian invariant $\mathfrak{p}_\alpha^{\mathbf{k}_\mathrm{s}}$ can be expressed as [68]

$$\mathfrak{p}_\alpha^{\mathbf{k}_\mathrm{s}} = n_\alpha^{\mathbf{k}_\mathrm{s}}|_\mathrm{occ} \mod 2. \tag{4.50}$$

4.5. EXAMPLES: ONE DIMENSION

We now discuss symmetry-based indicators for Bogoliubov-de Gennes-type Hamiltonians for a selected set of point groups G and tenfold-way classes.

4.5.1. Trivial point group $G = C_1$, class D

Without crystalline symmetries, the Hamiltonian $H(k)$ is particle-hole antisymmetric at both high-symmetry momenta $k = 0$ and $k = \pi$. In the absence of time-reversal symmetry and spin-rotation symmetry (class D), this gives a $\mathbb{Z}_2$-classification for $H(0)$ and $H(\pi)$, so that $\mathrm{BL} = \mathbb{Z}_2^2$. There are no compatibility relations, hence

$$\mathrm{BS} = \mathbb{Z}_2^2. \tag{4.51}$$

The corresponding topological invariants are $(-1)^{\mathfrak{p}^{(0)}} = \operatorname{sign}\mathrm{Pf}\,[H(0)\tau_1]$ and $(-1)^{\mathfrak{p}^{(\pi)}} = \operatorname{sign}\mathrm{Pf}\,[H(\pi)\tau_1]$, giving

$$B[H(k)] = \{\mathfrak{p}^{(0)}, \mathfrak{p}^{(\pi)}\}. \tag{4.52}$$

Without crystalline symmetries there is only one Wyckoff position in a one-dimensional crystal. Placing zero-dimensional Hamiltonians on the generic Wyckoff position, one obtains two topologically different classes of atomic-limit Hamiltonians,

$$\mathrm{AI} = \mathbb{Z}_2.$$

As a subgroup of BS, AI corresponds to the pairs $(\mathfrak{p}^{(0)}, \mathfrak{p}^{(\pi)})$ with $\mathfrak{p}^{(0)} = \mathfrak{p}^{(\pi)}$. The group $\mathrm{SI} = \mathrm{BS}/\mathrm{AI} = \mathbb{Z}_2$ is identical to the full classification group

$$\mathrm{SI}_\mathrm{D}[C_1] = \mathcal{K}_\mathrm{D}[C_1] = \mathbb{Z}_2, \tag{4.53}$$

the nontrivial element of which describes one-dimensional topological superconductors (the "Kitaev chain"). The

symmetry-based indicator for the topological superconductor phase is

$$z_1 = \sum_{k_s} \mathfrak{p}^{(k_s)} \mod 2. \tag{4.54}$$

In the weak pairing limit, the indicator (4.54) gives the parity of the number of Fermi level crossings between $k = 0$ and $k = \pi$. [77, 78] The same expression for the full BdG Hamiltonian was obtained in Ref. 68.

4.5.2. Inversion symmetry C_i, class D

Representation $\Theta = A_g$.— For a superconducting order parameter that transforms according to the representation A_g, inversion may be represented as $\rho_3\tau_0$, the Pauli matrices ρ_3 and τ_0 acting in parity and particle-hole space, respectively, see Sec. 4.2. At the high symmetry momenta $k_s = (0), (\pi)$, the Hamiltonian $H(k_s) = \mathrm{diag}\,(H_+(k_s), H_-(k_s))$ is the diagonal sum of blocks acting within the even and odd parity subspaces, where the blocks correspond to the irreducible representations A_g and A_u of C_i. The preceding discussion of a one-dimensional Hamiltonian $H(k)$ without crystalline symmetries applies to the two blocks separately. In particular, it follows that $\mathrm{BL} = \mathbb{Z}_2^4$.

To find the compatibility constraints for gapped Hamiltonians, we note that the combination of inversion and particle-hole conjugation gives an antiunitary antisymmetry local in momentum space,

$$H(k) = -\rho_3\tau_1 H(k)^* \rho_3\tau_1.$$

As a result, $H(k)\rho_3\tau_1$ is antisymmetric for all k, so that $\mathrm{sign}\,\mathrm{Pf}\,[H(k)\rho_3\tau_1]$ is well-defined and k-independent if $H(k)$ is gapped. Considering that at the high-symmetry momenta $k = 0$ and $k = \pi$ one has $\mathrm{sign}\,\mathrm{Pf}\,[H(k)\rho_3\tau_1] = (-1)^{\mathfrak{p}_+^{(k)}+\mathfrak{p}_-^{(k)}}$, one finds the compatibility constraint

$$\mathfrak{p}_+^{(0)} + \mathfrak{p}_-^{(0)} = \mathfrak{p}_+^{(\pi)} + \mathfrak{p}_-^{(\pi)} \mod 2 \tag{4.55}$$

for gapped Hamiltonians, where we use the subscripts $+$ and $-$ for the representations A_g and A_u, respectively. Using the compatibility relation (4.55) to eliminate $\mathfrak{p}_-^{(\pi)}$ as an independent band label, we find

$$\mathrm{BS} = \mathbb{Z}_2^3, \quad B[H(k)] = \{\mathfrak{p}_+^{(0)}, \mathfrak{p}_+^{(\pi)}, \mathfrak{p}_-^{(0)}\}, \tag{4.56}$$

With inversion symmetry there are two inequivalent Wyckoff positions, labeled $x = 0$ and $x = \frac{1}{2}$. A generating set of atomic-limit Hamiltonians is obtained by placing zero-dimensional inversion-symmetric Hamiltonians at each of the Wyckoff positions. Placing a generator of $\mathfrak{K}_D[0]$ with topological invariant $\mathfrak{p} = 1$ and irreducible representation A_g or A_u at position $x = 0$ we obtain a k-independent Hamiltonian for which inversion is represented as by τ_0 or $-\tau_0$, respectively, and particle-hole conjugation by $\tau_1 K$. Under the map B, these Hamiltonians are mapped to $\{1, 0, 1\}$ and $\{0, 1, 0\}$ for the A_g and

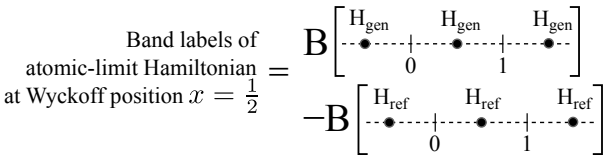

FIG. 4.1. Topological band labels associated with an atomic-limit superconductor are calculated as the difference of band labels of arrays with the $0d$ generator Hamiltonian H_{gen} and with the $0d$ reference Hamiltonian H_{ref} at Wyckoff position x. The figure shows this schematically for the Wyckoff position $x = \frac{1}{2}$.

A_u representations, respectively. Placing a generator of $\mathfrak{K}_D[0]$ with topological invariant $\mathfrak{p} = 1$ and irreducible representation A_g or A_u at the Wyckoff position $x = \frac{1}{2}$, one obtains a k-independent Hamiltonian for which inversion is represented by $\tau_0 e^{ik}$ or $-\tau_0 e^{ik}$ for A_g and A_u, respectively. At $k = \pi$ the irreducible representations are interchanged, so that under B such a Hamiltonian is mapped to $\{1, 0, 0\}$ and $\{0, 1, 1\}$ for the irreducible representations A_g and A_u, respectively. The images of these four generating atomic-limit Hamiltonians under B span the whole group $\mathrm{AI} = \mathrm{BS}$. The quotient group

$$\mathrm{SI_D}[C_i, A_g] = 0. \tag{4.57}$$

The conclusion that SI contains no nontrivial gapped phases is consistent with the triviality of the classifying group

$$\mathcal{K}_\mathrm{D}[C_i, A_g] = 0 \tag{4.58}$$

for this symmetry class. [39]

Representation A_u.— For the representation A_u the inversion operation for the BdG Hamiltonian is represented as $\rho_3\tau_3$, see Sec. 4.2. The Hamiltonian $H(k) = \mathrm{diag}\,(H_+(k), H_-(k))$ is block diagonal with respect to the eigenvalues $\pm$ of $\rho_3\tau_3$, corresponding to the fundamental representations $A_{g,u}$ of C_i. At $k = 0$ and $k = \pi$ the two blocks are minus the particle-hole conjugate of each other. The topological invariants of $H(0)$ and $H(\pi)$ are $\mathfrak{N}_+^{(0)}$ and $\mathfrak{N}_+^{(\pi)}$, where $\mathfrak{N}_\pm^{(k)}$ is the number of positive eigenvalues of $H_\pm(k)$. (Note that the topological invariants involve the numbers $\mathfrak{N}_+^{(k)}$ for $k = 0, \pi$ only; Particle-hole antisymmetry implies that $\mathfrak{N}_+^{(k)} = -\mathfrak{N}_-^{(k)}$ at $k = 0, \pi$.) Accordingly, $\mathrm{BL} = \mathbb{Z}^2$.

The combination of inversion and particle-hole conjugation gives an antiunitary antisymmetry of $H(k)$ that is local in momentum space and squares to -1, thus $H(k)$ belongs to class C with trivial classification in zero-dimension. We conclude that there are no compatibility constraints for $\mathfrak{N}_+^{(0)}$ and $\mathfrak{N}_+^{(\pi)}$, so that

$$\mathrm{BS} = \mathbb{Z}^2, \quad B[H(k)] = \{\mathfrak{N}_+^{(0)}, \mathfrak{N}_+^{(\pi)}\}. \tag{4.59}$$

To construct the subgroup $\mathrm{AI} \subset \mathrm{BS}$ we place zero-dimensional generator Hamiltonians at the Wyckoff positions $x = 0$ or $x = \frac{1}{2}$, which gives the k-independent

Hamiltonian $H = \mathrm{diag}\,(-1, 1) = -\tau_3$, with representation $\tau_1 K$ for particle-hole conjugation. For the Wyckoff position $x = 0$ inversion is represented by τ_3, so that the corresponding atomic-limit Hamiltonian maps to the element $\{1, 1\}$ of BS. For the Wyckoff position $x = \frac{1}{2}$ inversion is represented by $\tau_3 e^{ik}$. The A_g and A_u blocks are interchanged at $k = \pi$ and the corresponding atomic-limit Hamiltonian maps to $\{1, -1\}$, where the -1 originates from the difference with an atomic-limit superconductor obtained by placing the reference Hamiltonian at the same Wyckoff position, see Fig. 4.1 for a schematic picture. The subgroup $\mathrm{AI} = \mathbb{Z} \times 2\mathbb{Z}$ thus consists of all elements $\{\mathfrak{N}_+^{(0)}, \mathfrak{N}_+^{(\pi)}\}$ for which $\mathfrak{N}_+^{(0)} - \mathfrak{N}_+^{(\pi)}$ is even. The quotient $\mathrm{SI} = \mathrm{BS}/\mathrm{AI} = \mathbb{Z}_2$ contains the symmetry-based indicator

$$z_1 = \sum_{k_\mathrm{s}} \mathfrak{N}_+^{k_\mathrm{s}} \mod 2. \tag{4.60}$$

The conclusion that

$$\mathrm{SI}_\mathrm{D}[C_i, A_u] = \mathbb{Z}_2 \tag{4.61}$$

is consistent with the classifying group

$$\mathcal{K}_\mathrm{D}[C_i, A_u] = \mathbb{Z}_2 \tag{4.62}$$

for this symmetry class, [39] which describes a topological superconductor phase with a single zero-energy Majorana bound state at each end. An example of a nontrivial Hamiltonian in this symmetry class is

$$H(k) = \mathrm{diag}\,\left(\tau_3(1 - m - \cos k) + \tau_1 \sin k, \tau_3\right)$$

with $0 < m < 2$.

The weak-pairing limit (4.49) of the symmetry-based indicator z_1 agrees Refs. 66–68. The symmetry-based indicator z_1 for the full BdG Hamiltonian agrees with the forms defined in Refs. 67 and 68.

4.6. EXAMPLES: TWO DIMENSIONS

4.6.1. Two mirror symmetries C_{2v}, class D

The four high-symmetry momenta are $\mathbf{k}_\mathrm{s} = (0, 0)$, $(0, \pi)$, $(\pi, 0)$, and (π, π). Each of these four momenta is invariant under the full group C_{2v} and under particle-hole conjugation, so that the Hamiltonian $H(\mathbf{k})$ has the symmetries corresponding to a zero-dimensional Hamiltonian of tenfold-way class D and with symmetry group C_{2v}. As discussed in Sec. 4.3, such Hamiltonians are topologically trivial if the superconducting phase transforms according to the A_1 representation of C_{2v}, whereas there is a $\mathbb{Z}_2$ invariant $\mathfrak{p}$ for the representations A_2, B_1, and B_2. Hence, we find that

$$\mathrm{BL} = \begin{cases} 0 & \text{for } \Theta = A_1, \\ \mathbb{Z}_2^4 & \text{for } \Theta = A_2,\ B_1, \text{ or } B_2. \end{cases}$$

Representation $\Theta = A_1$.— For the case $\Theta = A_1$ the group of symmetry-based indicators is

$$\mathrm{SI}_\mathrm{D}[C_{2v}, A_1] = 0, \tag{4.63}$$

consistent with the triviality

$$\mathcal{K}_\mathrm{D}[C_{2v}, A_1] = 0 \tag{4.64}$$

of the full classifying group, see App. C.2.4.

Representation $\Theta = B_2$.— For this representation we have $\mathcal{M}_x\mathcal{P} = -\mathcal{P}\mathcal{M}_x$, $\mathcal{M}_y\mathcal{P} = \mathcal{P}\mathcal{M}_y$ and $\mathcal{M}_x^2 = \mathcal{M}_y^2 = -1$. For $k_y = 0$ one has the effective "particle-hole antisymmetry" $\mathcal{P}\mathcal{M}_x$ with $(\mathcal{P}\mathcal{M}_x)^2 = 1$, which is local in momentum space. The mirror operation $i\mathcal{M}_y$ is also local in momentum space if $k_y = 0$, squares to one, and commutes with the effective particle-hole symmetry, $(\mathcal{P}\mathcal{M}_x)(i\mathcal{M}_y) = (i\mathcal{M}_y)(\mathcal{P}\mathcal{M}_x)$. We conclude that for each $0 < k_x < \pi$ the Hamiltonian $H(k_x, 0)$ satisfies an onsite "inversion symmetry" with $\Theta = A_g$, so that it has a nontrivial topological classification given by the classifying group $\mathfrak{K}_\mathrm{D}(C_i, A_g) = \mathbb{Z}_2^2$. Upon taking the limits $k_x \to 0, \pi$, the classification of $H(k_x, 0)$ for generic k_x can be related to the classification at the high-symmetry momenta $k_x = 0, \pi$, which is given by the topological band labels $\mathfrak{p}^{(0,0)}$ and $\mathfrak{p}^{(\pi,0)}$. Explicit calculation gives that only the diagonal elements $(\mathfrak{p}, \mathfrak{p})$ of $\mathfrak{K}_\mathrm{D}(C_i, A_g) = \mathbb{Z}_2^2$ are allowed, with $\mathfrak{p} = \mathfrak{p}^{(0,0)} = \mathfrak{p}^{(\pi,0)}$. It follows that one has the compatibility constraint

$$\mathfrak{p}^{(0,0)} = \mathfrak{p}^{(\pi,0)}. \tag{4.65}$$

In the same way one finds

$$\mathfrak{p}^{(0,\pi)} = \mathfrak{p}^{(\pi,\pi)}. \tag{4.66}$$

One may obtain the same compatibility relations using the explicit representations $\mathcal{P} = \rho_0\tau_1 K$, $U(\mathcal{M}_x) = i\rho_1\tau_0$, $U(\mathcal{M}_y) = i\rho_2\tau_0$ used in Sec. 4.3, so that $H(\mathbf{k})$ satisfies

$$\begin{aligned} H(k_x, k_y) &= \rho_1\tau_0 H(-k_x, k_y)\rho_1\tau_0 \\ &= \rho_2\tau_0 H(k_x, -k_y)\rho_2\tau_0 \\ &= -\rho_0\tau_1 H(-k_x, -k_y)^*\rho_0\tau_1. \end{aligned}$$

For $k_y = 0$ these constraints imply that $H(k_x, 0) = -\rho_1\tau_1 H(k_x, 0)^*\rho_1\tau_1 = \rho_2\tau_0 H(k_x, 0)\rho_2\tau_0$, so that we may write $H(k_x, 0) = \rho_0 h_0 + \rho_2 h_2$ with $h_0\tau_1$ and $h_2\tau_1$ antisymmetric. Further, $h_0 \pm h_2$ is gapped for all $0 \le k_x \le \pi$, so that the Pfaffian of $\tau_1(h_0 \pm h_2)$ is nonzero and cannot change sign for $0 \le k_x \le \pi$. Since $h_2 = 0$ for $k_x = 0, \pi$, the compatibility relations (4.65) and (4.66) follow immediately. It follows that

$$\mathrm{BS} = \mathbb{Z}_2^2, \quad B[H(\mathbf{k})] = \{\mathfrak{p}(\pi, 0), \mathfrak{p}(\pi, \pi)\}. \tag{4.67}$$

To construct AI, we place generators at one of the four Wyckoff positions. The Wyckoff positions are $(x, y) =$

$(0,0)$, $(0,\frac{1}{2})$, $(\frac{1}{2},0)$, and $(\frac{1}{2},\frac{1}{2})$. From the onsite representations $U(\mathcal{M}_x) = i\rho_1\tau_0$, $U(\mathcal{M}_y) = i\rho_2\tau_0$ we derive the $\mathbf{k}$-dependent representations

$$U^{\mathbf{x}}(\mathcal{M}_x,\mathbf{k}) = i\rho_1\tau_0 e^{2ik_x x},$$
$$U^{\mathbf{x}}(\mathcal{M}_y,\mathbf{k}) = i\rho_2\tau_0 e^{2ik_y y}$$

for a zero-dimensional Hamiltonian placed at Wyckoff position $\mathbf{x} = (x,y)$. The $\mathbf{k}$-dependent factors appear, because for the Wyckoff positions other than $(0,0)$ the operations $\mathcal{M}_x$ and/or $\mathcal{M}_y$ correspond to an onsite operation followed by a translation by a lattice vector. As these induced representations differ from the onsite representations by a sign for half of the elements of the symmetry group, which is a change that can be accommodated by a basis transformation, the induced representation is the same at all high-symmetry momenta. After verifying that placing the trivial reference Hamiltonian H_{ref} at the same Wyckoff positions produces the trivial element in BS, we conclude that the subgroup AI $\subset$ BS consists of the elements with $\mathfrak{p}^{(0,0)} = \mathfrak{p}^{(0,\pi)}$. We conclude that

$$\text{SI}_{\text{D}}[C_{2v},B_2] = \mathbb{Z}_2, \tag{4.68}$$

corresponding to the symmetry-based indicator

$$z_{1;x} = \sum_{\mathbf{k}_{\text{s}}|k_{\text{s},x}=\pi} \mathfrak{p}^{\mathbf{k}_{\text{s}}} \mod 2. \tag{4.69}$$

This symmetry-based indicator describes a weak phase of one-dimensional C_{2v}-symmetric topological superconductors in the y direction, stacked in the x direction,

$$\mathcal{K}_{\text{D}}[C_{2v},B_2] = \mathbb{Z}_2, \tag{4.70}$$

see App. C.2.4. An example of a generator Hamiltonian is

$$H_{(1;x)} = \rho_0\tau_3(1-m-\cos k_y) + \rho_1\tau_2 \sin k_y,$$

with $0 < m < 2$.

Representation $\Theta = B_1$.— The discussion for the B_1 representation is similar to the discussion above. One finds

$$\text{SI}_{\text{D}}[C_{2v},B_1] = \mathbb{Z}_2, \tag{4.71}$$
$$\mathcal{K}_{\text{D}}[C_{2v},B_1] = \mathbb{Z}_2. \tag{4.72}$$

The only topologically nontrivial gapped phase is a weak phase of one-dimensional C_{2v}-symmetric topological superconductors in the x direction, stacked in the y direction, for which $z_{1;y} = \mathfrak{p}^{(0,0)} + \mathfrak{p}^{(\pi,0)} \mod 2$ is the associated symmetry-based indicator.

Representation $\Theta = A_2$.— The discussion of this representation is easiest if we choose the representation $U(\mathcal{M}_x) = i\rho_3\tau_0$, $U(\mathcal{M}_y) = i\rho_1\tau_0$, see the discussion in Sec. 4.3. With this choice of representation, one finds that $H(k_x,k_y) = h_0\rho_0$ at the high-symmetry momenta $(k_x,k_y) = (0,0)$, $(0,\pi)$, $(\pi,0)$, and (π,π). The matrix $\tau_1 h_0$ is antisymmetric and the sign $(-1)^{\mathfrak{p}}$ of its Pfaffian is used as the topological invariant of $H(k_x,k_y)$. In contrast to the B_1 and B_2 representations, there are no compatibility constraints for the A_2 representation, hence

$$\text{BS} = \mathbb{Z}_2^4,$$
$$B[H(\mathbf{k})] = \{\mathfrak{p}(0,0),\mathfrak{p}(\pi,0),\mathfrak{p}(0,\pi),\mathfrak{p}(\pi,\pi)\}. \tag{4.73}$$

The subgroup AI for the A_2 representation consists of the elements with $\mathfrak{p}^{(0,0)} = \mathfrak{p}^{(0,\pi)} = \mathfrak{p}^{(\pi,0)} = \mathfrak{p}^{(\pi,\pi)}$, so that

$$\text{SI}_{\text{D}}[C_{2v},A_2] = \mathbb{Z}_2^3. \tag{4.74}$$

The classifying group $\mathcal{K}$ for the A_2 representation is

$$\mathcal{K}_{\text{D}}[C_{2v},A_2] = \mathbb{Z}_2^4, \tag{4.75}$$

see App. C.2.4. Two factors $\mathbb{Z}_2$ correspond to weak phases stacked in the x and y directions, with labels "$1;x$" and "$1;y$", symmetry-based indicators

$$z_{1;j} = \sum_{\mathbf{k}_{\text{s}}|k_{\text{s},j}=\pi} \mathfrak{p}^{\mathbf{k}_{\text{s}}} \mod 2, \quad j = x,y, \tag{4.76}$$

The corresponding generating Hamiltonians are

$$H_{(1;x)} = \rho_0\tau_3(1-m-\cos k_y) + \rho_3\tau_1 \sin k_y,$$

and

$$H_{(1;y)} = \rho_0\tau_3(1-m-\cos k_x) + \rho_1\tau_1 \sin k_x,$$

with $0 < m < 2$, respectively. The remaining two factors $\mathbb{Z}_2$ in the classifying group $\mathcal{K}$ and the single remaining factor $\mathbb{Z}_2$ in SI correspond to strong second-order phases. These have generator Hamiltonians

$$H'_{(2,\pm)} = \rho_0\tau_3(2-m-\cos k_x-\cos k_y) \pm \rho_1\tau_1 \sin k_x + \rho_3\tau_1 \sin k_y,$$

with $0 < m < 2$, but only a single associated symmetry-based indicator

$$z_2 = \sum_{\mathbf{k}_{\text{s}}} \mathfrak{p}^{\mathbf{k}_{\text{s}}} \mod 2. \tag{4.77}$$

As discussed in App. C.2.4, the generator Hamiltonians $H_{(2;\pm)}$ describe a second-order phase with a single Majorana corner state at each mirror-symmetric corner, whereas the direct sum $H_{(2;+)} \oplus H_{(2;-)}$, which is mapped to the trivial element in SI, has pairs of even and odd parity Majorana corner states at the corners bisected by one mirror axis, but no corner states at the corners bisected by the other mirror axis.

The results are summarized in Table 4.11. Following the notation of Ref. 39, we list a full boundary-signature-resolved subgroup series for each singly-generated group $\mathcal{K}_i$ contributing to the full classification group $\mathcal{K} = \prod_i \mathcal{K}_i$ that admits topological phases with a higher-order boundary signature. The subgroup $\mathcal{K}'_i \subset \mathcal{K}_i$ is the subset of all topological phases with boundary signature of

$\mathcal{K}_i' \subseteq \mathcal{K}_i$	Phase	BS $\mathfrak{p}^{(0,0)}$	BS $\mathfrak{p}^{(\pi,0)}$	BS $\mathfrak{p}^{(0,\pi)}$	BS $\mathfrak{p}^{(\pi,\pi)}$	SI $\mathbb{Z}_2^3$
	$\mathbf{x}=(0,0)$	1	1	1	1	0
	$\mathbf{x}=(\frac{1}{2},0)$	1	1	1	1	0
	$\mathbf{x}=(0,\frac{1}{2})$	1	1	1	1	0
	$\mathbf{x}=(\frac{1}{2},\frac{1}{2})$	1	1	1	1	0
$\mathbb{Z}_2$	$(1;x)$	1	1	0	0	$\mathrm{e}_{1;x}^{(2)}$
$\mathbb{Z}_2$	$(1;y)$	1	0	1	0	$\mathrm{e}_{1;y}^{(2)}$
$\mathbb{Z}_2 \subseteq \mathbb{Z}_2$	$(2;+)'$	1	0	0	0	$\mathrm{e}_{2}^{(2)}$
$\mathbb{Z}_2 \subseteq \mathbb{Z}_2$	$(2;-)'$	1	0	0	0	$\mathrm{e}_{2}^{(2)}$

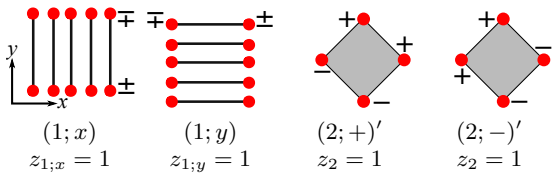

TABLE 4.11. Band labels and symmetry-based indicators for atomic-limit Hamiltonians obtained by placing 0d generators at Wyckoff position $\mathbf{x}$ (upper four rows) and for the generators $H_{(1;x)}$, $H_{(1;y)}$, $H'_{(2,+)}$, $H'_{(2,-)}$ of the weak and second-order phases for the symmetry group C_{2v} and representation $\Theta = A_2$ in two dimensions, class D. The weak phases $(1;x)$ and $(1;y)$ can be constructed from one dimensional topological superconductors with Majorana bound states, as schematically indicated below (red dots with indicated mirror parity $\pm$), stacked in the x or y direction, respectively. A possible boundary signature of the generators of second-order phases consists of Majorana bound states at mirror symmetric corners with indicated mirror parity. The first column contains the boundary-signature-resolved subgroup sequence for each of the factor groups contributing to the full classification group $\mathcal{K} = \prod_i \mathcal{K}_i$.

order larger than one. Weak topological phases in two dimensions, which are essentially stacks of one-dimensional phases, do not have a higher-order boundary signature, so that we do not give a subgroup sequence for factors $\mathcal{K}_i$ representing a weak phase.

Table 4.11 also lists the topological band labels for the four Hamiltonians generating the classifying group $\mathcal{K}$, as well as their image in the quotient group SI. Here we use the symbol $\mathrm{e}_j^{(n)}$ to denote the jth generator of SI. The superscript n indicates its order, *i.e.*, $n\mathrm{e}_j^{(n)} = 0$.

4.6.2. Fourfold rotation symmetry C_4, class D

General considerations.— There are three non-equivalent high-symmetry momenta, $\{\mathbf{k}_\mathrm{s}\} = \{(0,0),(0,\pi),(\pi,\pi)\}$. All three non-equivalent high symmetry momenta are invariant under particle-hole conjugation. In addition, the momenta $(0,0)$ and (π,π) are invariant under fourfold rotation, while $(0,\pi)$ is invariant under twofold rotation only.

On a square lattice we can choose the set W of representative Wyckoff positions as $W = \{(0,0),(\frac{1}{2},\frac{1}{2}),(\frac{1}{2},0)\}$. The two Wyckoff positions $\mathbf{x} = (0,0)$ and $\mathbf{x} = (\frac{1}{2},\frac{1}{2})$ are invariant under fourfold rotations; the Wyckoff position $\mathbf{x} = (\frac{1}{2},0)$ is invariant under twofold rotations only. This Wyckoff position has a nontrivial orbit consisting of the positions $(\frac{1}{2},0)$ and $(0,\frac{1}{2})$, generated by fourfold rotation. The induced representations $U^{\mathbf{x},\alpha}(g,\mathbf{k})$ of orbitals located at $\mathbf{x}$ can be written in terms of the onsite (*i.e.*, zero-dimensional) representations $U^\alpha(g)$ using

$$\begin{aligned} U^{(0,0),\alpha}(\mathcal{R}_{\pi/2},\mathbf{k}) &= U^\alpha(\mathcal{R}_{\pi/2}),\\ U^{(\frac{1}{2},\frac{1}{2}),\alpha}(\mathcal{R}_{\pi/2},\mathbf{k}) &= U^\alpha(\mathcal{R}_{\pi/2})e^{ik_x},\\ U^{(\frac{1}{2},0),\alpha}(\mathcal{R}_{\pi/2},\mathbf{k}) &= U^\alpha(\mathcal{R}_{\pi/2}) \otimes \begin{pmatrix} 0 & 1 \\ e^{ik_y} & 0 \end{pmatrix}, \end{aligned} \tag{4.78}$$

where $\mathcal{R}_{\pi/2}$ is a rotation by $\pi/2$ and the matrices for the Wyckoff position $(\frac{1}{2},0)$ act in the space of orbitals contained in its orbit. As in Sec. 4.2 we use the half-integer angular momentum j to denote the irreps α of the rotation symmetry. The angular momentum j is defined modulo 4 for fourfold rotation and modulo 2 for twofold rotation.

The computation of the band labels can be performed with the help of the projector $P_j(\mathbf{k}_\mathrm{s})$ of Eq. (4.38), which projects the Hamiltonian $H(\mathbf{k}_\mathrm{s})$ at the high-symmetry momentum $\mathbf{k}_\mathrm{s}$ onto its diagonal block with irreducible representation $\alpha = j$. In addition to using Eq. (4.38) to project on the angular momentum j subspace, a unitary basis transformation V_j must be implemented to ensure that $V_j P_j(\mathbf{k}_\mathrm{s}) V_j^\dagger$ is block diagonal. (The unitary matrix V_j depends on $\mathbf{k}_\mathrm{s}$, but we suppress this dependence to keep the notation simple.) In the present case, all irreps are one-dimensional and the characters χ_j of Eq. (4.38) are given by

$$\chi_j(\mathcal{R}_{\pi/2}^n) = r_j^n(\mathcal{R}_{\pi/2}) = e^{inj\pi/2}.$$

We may then choose the unitary matrix $V \equiv V_j$ independent of j by requiring that $VU(g,\mathbf{k}_\mathrm{s})V^\dagger$ be diagonal as in Eq. (4.19), with $U(g) = \mathrm{diag}_\alpha[U^\alpha(g,\mathbf{k}_\mathrm{s})]$ and $U^\alpha(g,\mathbf{k}_\mathrm{s})$ given in Eq. (4.78). Indeed, one verifies that with this choice $VP_j(\mathbf{k}_\mathrm{s})V^\dagger$ is a diagonal matrix with unit entries for each band n with $(VU(\mathcal{R}_{\pi/2})V^\dagger)_{nn} = r_j(\mathcal{R}_{\pi/2})$ and zeroes otherwise. The transformed Hamiltonian $VH(\mathbf{k}_\mathrm{s})V^\dagger$ is block diagonal and all zero-dimensional invariants can be computed from the block $VP_j(\mathbf{k}_\mathrm{s})H(\mathbf{k}_\mathrm{s})P_j(\mathbf{k}_\mathrm{s})V^\dagger$. In case the block is characterized by a Pfaffian invariant $\mathfrak{p}_j(\mathbf{k}_\mathrm{s})$, the transformed representation of the corresponding antiunitary antisymmetry $VU(\mathcal{P})V^T$ acts within the block such that $(-1)^{\mathfrak{p}}_j(\mathbf{k}_\mathrm{s}) = \mathrm{sign}\,\mathrm{Pf}(VP_j(\mathbf{k}_\mathrm{s})H(\mathbf{k}_\mathrm{s})U(\mathcal{P})V^TVP_j(\mathbf{k}_\mathrm{s})V^\dagger)$ is well defined.

Representations $\Theta = A$ and $\Theta = B$.— These two representations have the same algebraic structure, so that it is sufficient to discuss the case $\Theta = A$ only. (To see this, one considers $i\mathcal{R}_{\pi/2}$ as the generator of C_4 for the B representation and verifies that $i\mathcal{R}_{\pi/2}$ commutes with particle-hole conjugation $\mathcal{P}$.)

The Hamiltonian has fourfold rotation symmetry at the high-symmetry momenta $(0,0)$ and (π,π). As discussed in Sec. 4.3, for zero-dimensional BdG Hamiltonians with additional symmetry group C_4 and representation $\Theta = A$, particle-hole conjugation pairs the eigensectors corresponding to the irreducible representations $j = \frac{1}{2}$ and $j = \frac{7}{2}$ (mod 4), as well as $j = \frac{3}{2}$ and $j = \frac{5}{2}$ (mod 4). The classifying group $\mathcal{K}_{\mathrm{D}}[C_4, A] = \mathbb{Z}^2$ and the topological invariants are $\mathfrak{N}_{\frac{1}{2}}$ and $\mathfrak{N}_{\frac{5}{2}}$. At the high-symmetry momentum $(0,\pi)$ there is twofold rotation symmetry only. In this case, particle-hole conjugation pairs the angular momenta $j = \frac{1}{2}$ and $j = \frac{3}{2}$ (mod 2) and one has the classification group $\mathcal{K}_{\mathrm{D}}[C_2, A] = \mathbb{Z}$ and topological invariant $\mathfrak{N}_{\frac{1}{2}}$. A general momentum $\mathbf{k}$ is invariant under $\mathcal{R}_\pi\mathcal{P}$ with $(\mathcal{R}_\pi\mathcal{P})^2 = -1$ such that the corresponding zero-dimensional Hamiltonians are in class C with trivial classification. Hence, there are no compatibility relations in this symmetry class. We conclude that

$$\begin{aligned} &\mathrm{BS} = \mathbb{Z}^5, \qquad (4.79)\\ &B[H(\mathbf{k})] = \{\mathfrak{N}^{(0,0)}_{\frac{1}{2}}, \mathfrak{N}^{(0,0)}_{\frac{5}{2}}, \mathfrak{N}^{(\pi,0)}_{\frac{1}{2}}, \mathfrak{N}^{(\pi,\pi)}_{\frac{1}{2}}, \mathfrak{N}^{(\pi,\pi)}_{\frac{5}{2}}\}. \end{aligned}$$

The reference and generating Hamiltonians for all Wyckoff positions and (paired) irreducible representations labeled by the angular momentum j, as well as the onsite representations of the symmetry group, can be taken directly from Table 4.9. In particular, we note that

$$U^{j,4-j}(\mathcal{R}_{\pi/2}) = \mathrm{diag}\,(e^{ij\pi/2}, e^{i(4-j)\pi/2})_\tau, \qquad (4.80)$$

for $j = \frac{1}{2}$ and $\frac{5}{2}$, where we recall that particle-hole conjugation pairs $j = \frac{1}{2}$ with $j = \frac{7}{2}$ and $j = \frac{3}{2}$ with $j = \frac{5}{2}$. From the induced representation (4.78) one can then directly compute the band labels of the reference Hamiltonian as well as all generators, see Table C.1 in Appendix C.4 for the result. Upon computing the quotient BS/AI, one finds that the group of symmetry indicators is

$$\mathrm{SI}_{\mathrm{D}}[C_4, A] = \mathrm{SI}_{\mathrm{D}}[C_4, B] = \mathbb{Z}_2 \times \mathbb{Z}_8. \qquad (4.81)$$

To interpret the symmetry-based indicators for this representation, we note that this symmetry class has a classifying group [49, 50]

$$\mathcal{K}_{\mathrm{D}}[C_4, A] = \mathcal{K}_{\mathrm{D}}[C_4, B] = \mathbb{Z} \times \mathbb{Z}_2^2. \qquad (4.82)$$

The factor $\mathbb{Z}$ in the above group corresponds to a Chern superconductor phase, for which the generating Hamiltonian is

$$H_{(2)}(\mathbf{k}) = \tau_3(2 - m - \cos k_x - \cos k_y) + \tau_1 \sin k_x + \tau_2 \sin k_y$$

with $0 < m < 2$ and with (standard) representations $U(\mathcal{P}) = \tau_1$, $U(\mathcal{R}_{\pi/2}) = e^{-i\pi\tau_3/4}$. Chern superconductors with even Chern numbers Ch can be deformed such that they have a BdG Hamiltonian with zero pairing-potential Δ and normal part h corresponding to a Chern insulator with Chern number Ch/2.

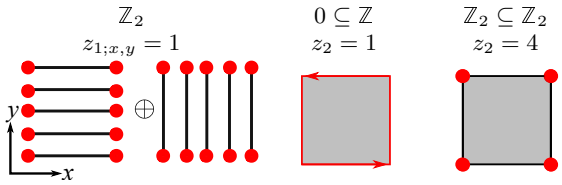

FIG. 4.2. Topological phases of a two-dimensional superconductor in tenfold-way class D and with additional C_4 symmetry with one-dimensional representation $\Theta = A, B$. For each boundary signature, the boundary subgroup sequence (top row) and the nonzero symmetry-based indicators for a generator of that phase are given (middle row).

Next, one of the factors $\mathbb{Z}_2$ of the group (4.82) correspond to a weak phase, consisting of two "layers" of C_2-symmetric Kitaev chains related by a fourfold rotation. (Note that $\mathcal{K}_{\mathrm{D}}[C_2, A] = \mathbb{Z}_2$ in one dimension, see Refs. 36 and 39.) The generator Hamiltonian is

$$\begin{aligned} H_{(1;x,y)}(\mathbf{k}) = &[\tau_3(1 - m - \cos k_x) + \tau_1 \sin k_x] \\ &\oplus_\mu [\tau_3(1 - m - \cos k_y) - \tau_2 \sin k_y] \qquad (4.83) \end{aligned}$$

with $0 < m < 2$, where $\oplus_\mu$ denotes that the direct sum acts in "layer space" with Pauli matrices μ_α. The representations are $U(\mathcal{P}) = \mu_0\tau_1$, $U(\mathcal{R}_{\pi/2}) = \mu_1 e^{i\pi\tau_3/4}$. The second factor $\mathbb{Z}_2$ corresponds to a second-order phase with four Majorana corner states. The generating Hamiltonian is the direct sum of a twofold symmetric second-order topological superconductor [70] and a copy related by a fourfold rotation,

$$\begin{aligned} H'_{(2)}(\mathbf{k}) = &[\rho_0\tau_3(2 - m - \cos k_x - \cos k_y) \\ &+ \rho_3\tau_1 \sin k_x + \rho_0\tau_2 \sin k_y] \\ &\oplus_\mu [\rho_0\tau_3(2 - m - \cos k_x - \cos k_y) \\ &+ \rho_0\tau_1 \sin k_x + \rho_3\tau_2 \sin k_y] \qquad (4.84) \end{aligned}$$

with $0 < m < 2$, and representations $U(\mathcal{P}) = \mu_0\rho_0\tau_1$, $U(\mathcal{R}_{\pi/2}) = \mu_1\rho_0 e^{i\pi\tau_3/4}$.

One verifies that the weak phase generates the factor $\mathbb{Z}_2$ of SI and has the symmetry-based indicator

$$z_{1;x,y} = \mathfrak{N}^{(\pi,0)}_{\frac{1}{2}} + \mathfrak{N}^{(\pi,\pi)}_{\frac{1}{2}} + \mathfrak{N}^{(\pi,\pi)}_{\frac{5}{2}} \mod 2. \qquad (4.85)$$

The factor $\mathbb{Z}_8$, with the symmetry-based indicator

$$\begin{aligned} z_2 = &-\mathfrak{N}^{(0,0)}_{\frac{1}{2}} + 3\mathfrak{N}^{(0,0)}_{\frac{5}{2}} - 2\mathfrak{N}^{(\pi,0)}_{\frac{1}{2}} \\ &+ 3\mathfrak{N}^{(\pi,\pi)}_{\frac{1}{2}} - \mathfrak{N}^{(\pi,\pi)}_{\frac{5}{2}} \mod 8, \qquad (4.86) \end{aligned}$$

is generated by the band labels of the Chern superconductor. The element "$z_2 = 4$" of the factor $\mathbb{Z}_8$ of SI is ambiguous, as it corresponds to the second-order phase or the Chern superconductor with four Majorana modes, see Fig. 4.2. These classification results and symmetry-based indicators agree with the results from Refs. 49 and 50.

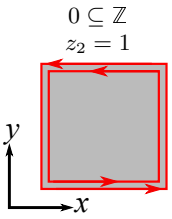

FIG. 4.3. The only topological phase with nontrivial boundary signature for a two-dimensional superconductor in tenfold-way class D and with additional C_4 symmetry with one-dimensional representation $\Theta = \Theta = {}^{1,2}E$ is a Chern superconductor with an even number of chiral Majorana boundary modes. The boundary subgroup sequence for this phase is given in the top row; the symmetry-based indicator for a generator of the phase is given in the middle row.

Representations $\Theta = {}^1E$ and $\Theta = {}^2E$.— Here we consider the case $\Theta = {}^1E$ only and note that the case $\Theta = {}^2E$ is analogous. In Sec. 4.3 we found that the particle-hole conjugation $\mathcal{P}$ with $\Theta = {}^1E$ relates the eigensectors with angular momentum $j = \frac{3}{2}$ and $j = \frac{7}{2}$, while $\mathcal{P}$ acts within the $j = \frac{1}{2}$ and $j = \frac{5}{2}$ eigensectors. The eigensectors $j = \frac{1}{2}$ and $j = \frac{3}{2}$ of twofold rotation symmetry are left invariant by particle-hole conjugation. From Table 4.5 we conclude that at each of the high-symmetry momenta $(0,0)$ and (π,π) with fourfold rotation symmetry we obtain a $\mathfrak{K}_{\mathrm{D}}[C_4, {}^1E] = \mathbb{Z} \times \mathbb{Z}_2^2$ classification of the band labels, with invariants $\mathfrak{N}_{\frac{3}{2}}$, $\mathfrak{p}_{\frac{1}{2}}$, and $\mathfrak{p}_{\frac{5}{2}}$, whereas for the momentum $(0,\pi)$ with twofold rotation symmetry the classifying group is $\mathfrak{K}_{\mathrm{D}}[C_2, B] = \mathbb{Z}_2^2$, with invariants $\mathfrak{p}_{\frac{1}{2}}$ and $\mathfrak{p}_{\frac{3}{2}}$. It follows that $\mathrm{BL} = \mathbb{Z}^2 \times \mathbb{Z}_2^6$.

The combination of twofold rotation and particle-hole conjugation provides an antiunitary antisymmetry operation that is local in momentum space and squares to one. For gapped Hamiltonians, the quantity $(-1)^{\mathfrak{p}(\mathcal{R}_\pi\mathcal{P})} = \mathrm{sign}\,\mathrm{Pf}[H(\mathbf{k})U(\mathcal{R}_\pi\mathcal{P})]$ is well-defined and constant throughout the Brillouin zone, from which one derives the $(0d)$ compatibility constraints

$$\begin{aligned} &\mathfrak{p}_{\frac{1}{2}}^{(0,\pi)} + \mathfrak{p}_{\frac{3}{2}}^{(0,\pi)} \\ &= \mathfrak{p}_{\frac{1}{2}}^{(0,0)} + \mathfrak{p}_{\frac{5}{2}}^{(0,0)} + \mathfrak{N}_{\frac{3}{2}}^{(0,0)} \\ &= \mathfrak{p}_{\frac{1}{2}}^{(\pi,\pi)} + \mathfrak{p}_{\frac{5}{2}}^{(\pi,\pi)} + \mathfrak{N}_{\frac{3}{2}}^{(\pi,\pi)} \mod 2. \end{aligned} \tag{4.87}$$

We therefore conclude that

$$\begin{aligned} &\mathrm{BS} = \mathbb{Z}^2 \times \mathbb{Z}_2^4, \\ &B[H(\mathbf{k})] = \{\mathfrak{p}_{\frac{1}{2}}^{(0,0)}, \mathfrak{p}_{\frac{5}{2}}^{(0,0)}, \mathfrak{N}_{\frac{3}{2}}^{(0,0)}, \mathfrak{p}_{\frac{3}{2}}^{(\pi,0)}, \mathfrak{p}_{\frac{5}{2}}^{(\pi,\pi)}, \mathfrak{N}_{\frac{3}{2}}^{(\pi,\pi)}\}. \end{aligned} \tag{4.88}$$

As before, we take the onsite reference Hamiltonian and generating Hamiltonians as well as the onsite representations from Table 4.9. For the angular momenta $j = \frac{3}{2}$ and $j = \frac{7}{2}$, which are paired by particle-hole conjugation, one has the representation

$$U^{\frac{3}{2},\frac{7}{2}}(\mathcal{R}_{\pi/2}) = \mathrm{diag}\,(e^{3\pi i/4}, e^{7\pi i/4})_\tau. \tag{4.89}$$

With the help of the induced representation Eq. (4.78) the band labels of the atomic-limit Hamiltonians then easily follow, see Table C.2 in Appendix C.4 for the result. By taking the quotient group, one arrives at

$$\mathrm{SI}_{\mathrm{D}}[C_4, {}^1E] = \mathrm{SI}_{\mathrm{D}}[C_4, {}^2E] = \mathbb{Z}_4. \tag{4.90}$$

The group is generated by a Chern superconductor with Chern number 2,

$$\begin{aligned} H_{(2)}(\mathbf{k}) = {}& \rho_0\tau_3(2 - m - \cos k_x - \cos k_y) \\ &+ \rho_1\tau_2 \sin k_x + \rho_1\tau_1 \sin k_y, \end{aligned} \tag{4.91}$$

with $0 < m < 2$, and representations

$$U(\mathcal{P}) = \rho_0\tau_1, \quad U(\mathcal{R}_{\pi/2}) = \tau_3 e^{-i\pi/4} \oplus_\rho \tau_0 e^{i\pi/4}.$$

The symmetry-based indicator is

$$\begin{aligned} z_2 = {}& -\mathfrak{N}_{\frac{3}{2}}^{(0,0)} - \mathfrak{N}_{\frac{3}{2}}^{(\pi,\pi)} + 2\mathfrak{p}_{\frac{5}{2}}^{(0,0)} \\ &+ 2\mathfrak{p}_{\frac{3}{2}}^{(\pi,0)} + 2\mathfrak{p}_{\frac{5}{2}}^{(\pi,\pi)} \mod 4. \end{aligned} \tag{4.92}$$

A Hamiltonian with Chern number 1 is not compatible with the constrains given by the algebraic relations between the representations in this symmetry class.

For comparison, we note that the classifying group is

$$\mathcal{K}_{\mathrm{D}}[C_4, {}^1E] = \mathcal{K}_{\mathrm{D}}[C_4, {}^2E] = \mathbb{Z}, \tag{4.93}$$

which is generated by the even-Chern-number superconductors, see Fig. 4.3. There are no weak or second-order phases in this symmetry class. This observation is compatible with the absence of weak or second-order phases for a twofold rotation symmetry with B pairing symmetry. [36, 39, 70] We note that the Chern superconductor with even Chern number Ch is topologically equivalent to a BdG Hamiltonian (4.1) with zero pairing-potential, corresponding to a non-superconducting Chern insulator with the Chern number Ch/2.

4.7. EXAMPLES: THREE DIMENSIONS

4.7.1. Inversion symmetry, class D

There are eight high-symmetry momenta $\mathbf{k}_{\mathrm{s}}$ with $k_{\mathrm{s},x}$, $k_{\mathrm{s},y}$, $k_{\mathrm{s},z} \in \{0,\pi\}$. With the classifying group $\mathfrak{K}_\eta[C_i, A_g] = \mathfrak{K}_\eta[0]^2 = \mathbb{Z}_2^2$ and $\mathfrak{K}_\eta[C_i, A_u] = \mathfrak{K}_{(0,0,0)}[0] = \mathbb{Z}$ the group of the band labels is

$$\mathrm{BL} = \begin{cases} \mathbb{Z}_2^{16} & \text{for } \Theta = A_g, \\ \mathbb{Z}^8 & \text{for } \Theta = A_u. \end{cases} \tag{4.94}$$

The band labels are given by the sets of topological invariants $\{\mathfrak{p}_\pm(\mathbf{k}_{\mathrm{s}})\}$ or $\{\mathfrak{N}_+(\mathbf{k}_{\mathrm{s}})\}$ for all high-symmetry momenta $\mathbf{k}_{\mathrm{s}}$ for $\Theta = A_g$ and $\Theta = A_u$, respectively.

In an inversion-symmetric cubic lattice the set of representative Wyckoff positions W consists of elements

(x, y, z) with $x, y, z \in \{0, \frac{1}{2}\}$. The induced representation $U^{\mathbf{x},\alpha}(\mathcal{I}, \mathbf{k})$ can be written in terms of the onsite representations $U^{\alpha}(\mathcal{I})$ as

$$U^{\mathbf{x},\alpha}(\mathcal{I}, \mathbf{k}) = U^{\alpha}(\mathcal{I}) e^{2i\mathbf{k}\cdot\mathbf{x}}. \tag{4.95}$$

Representation $\Theta = A_g$.— The Hamiltonian $H(\mathbf{k})$ satisfies the antiunitary antisymmetry $\mathcal{IP}$ with $(\mathcal{IP})^2 = 1$, which is local in momentum space. As a result, the quantity $(-1)^{\mathfrak{p}(\mathcal{IP})} = \operatorname{sign} \operatorname{Pf}[H(\mathbf{k})U(\mathcal{IP})]$ is well-defined and constant throughout the Brillouin zone, which gives the compatibility relations

$$\mathfrak{p}_+^{\mathbf{k}_\mathrm{s}} + \mathfrak{p}_-^{\mathbf{k}_\mathrm{s}} = \mathfrak{p}_+^{\mathbf{0}} + \mathfrak{p}_-^{\mathbf{0}} \mod 2 \tag{4.96}$$

for the high-symmetry momenta $\mathbf{k}_\mathrm{s}$. It follows that

$$\begin{aligned} \mathrm{BS} &= \mathbb{Z}_2^9 \qquad (4.97)\\ B[H(\mathbf{k})] &= \Big\{ \mathfrak{p}_+^{(0,0,0)}, \mathfrak{p}_-^{(0,0,0)}, \mathfrak{p}_+^{(\pi,0,0)}, \mathfrak{p}_+^{(0,\pi,0)}, \mathfrak{p}_+^{(\pi,\pi,0)}, \\ &\qquad \mathfrak{p}_+^{(0,0,\pi)}, \mathfrak{p}_+^{(\pi,0,\pi)}, \mathfrak{p}_+^{(0,\pi,\pi)}, \mathfrak{p}_+^{(\pi,\pi,\pi)} \Big\}. \end{aligned}$$

Further, for a gapped Hamiltonian $H(\mathbf{k})$ a Chern number Ch_i can be defined on planes with fixed k_i with $i = x$, y, or z. For the representation $\Theta = A_g$ the combination of particle-hole and inversion symmetry allows for even Chern numbers Ch_i only. At high-symmetry planes with $k_i = 0$ or π, the Chern number Ch_i is related to the band labels as

$$\begin{aligned} \mathrm{Ch}_i &= 2 \left(\sum_{\mathbf{k}_\mathrm{s} | k_{\mathrm{s},i} = 0} \mathfrak{p}_+^{\mathbf{k}_\mathrm{s}} \right) \mod 4 \\ &= 2 \left(\sum_{\mathbf{k}_\mathrm{s} | k_{\mathrm{s},i} = \pi} \mathfrak{p}_+^{\mathbf{k}_\mathrm{s}} \right) \mod 4, \end{aligned} \tag{4.98}$$

where we used Eq. (4.96) to arbitrarily select the invariant $\mathfrak{p}_+^{\mathbf{k}_\mathrm{s}}$ in the even inversion parity subspace. Imposing this $2d$ compatibility relation further reduces the group of band labels to $\mathrm{BS}^{(2)} = \mathbb{Z}_2^8$, the independent band labels (4.97) with the exception of $\mathfrak{p}_+^{(\pi,\pi,\pi)}$.

The band labels of atomic insulators, which span the subgroup $\mathrm{AI} \subset \mathrm{BS}$, can be directly computed using the induced representation (4.95), see table C.4 in Appendix C.4 for the result. Computing the quotient, we find that

$$\mathrm{SI}_\mathrm{D}[C_i, A_g] = \mathbb{Z}_2^4, \quad \mathrm{SI}_\mathrm{D}^{(2)}[C_i, A_g] = \mathbb{Z}_2^3, \tag{4.99}$$

where the four generators of SI are related to the symmetry-based indicators

$$\begin{aligned} z_{2;i} &= \sum_{\mathbf{k}_\mathrm{s} | k_{\mathrm{s},i} = \pi} \mathfrak{p}_+^{\mathbf{k}_\mathrm{s}} \mod 2, \quad i = x, y, z, \\ z_3 &= \sum_{\mathbf{k}_\mathrm{s}} \mathfrak{p}_+^{\mathbf{k}_\mathrm{s}} \mod 2. \end{aligned} \tag{4.100}$$

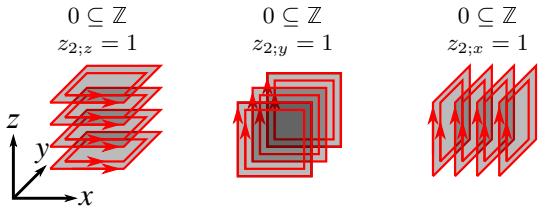

FIG. 4.4. Topological phases of a three-dimensional superconductor in tenfold-way class D and with additional C_i symmetry with one-dimensional representation $\Theta = A_g$. For each boundary signature, the boundary subgroup sequence (top row) and the nonzero symmetry-based indicators for a generator of that phase are given (middle row).

(The three generators of $\mathrm{SI}^{(2)}$ have symmetry-based indicators $z_{2;i}$, $i = x, y, z$.) The $\mathbb{Z}_2$ indicator z_3 corresponds to a representation-enforced nodal superconductor with different Chern numbers at parallel planes in the Brillouin zone, see Eq. (4.98), and a nodal point at a generic position in the Brillouin zone. The three $\mathbb{Z}_2$ indicators $z_{2;i}$, $i = x, y, z$, correspond to weak Chern superconductors with even Chern number in stacking planes, see Fig. 4.4. Generator Hamiltonians are

$$\begin{aligned} H_{(2;l)}(\mathbf{k}) = \rho_0\tau_3(2 - m - \cos k_i - \cos k_j) \\ + \rho_1\tau_1 \sin k_i + \rho_1\tau_2 \sin k_j, \end{aligned} \tag{4.101}$$

with $(k_i, k_j) = (k_y, k_z)$, (k_z, k_x), or (k_x, k_y) for $l = x$, y, or z, respectively. For all three cases, the representations are

$$U(\mathcal{P}) = \rho_0\tau_1, \quad U(\mathcal{I}) = \rho_3\tau_0. \tag{4.102}$$

For comparison, we note that this symmetry class has a classifying group

$$\mathcal{K}_\mathrm{D}[C_i, A_g] = \mathbb{Z}^3, \tag{4.103}$$

which contains the weak phases with even Chern numbers in the three stacking planes. Generators for these weak phases are shown schematically in Fig. 4.4. Since each factor $\mathbb{Z}$ in $\mathcal{K}$ describes a weak topological phase, which is obtained by stacking two-dimensional superconductors, only second-order boundary signatures are allowed in principle, which is why the subgroup sequences listed in Fig. 4.4 contains one subgroup only. The three weak Chern superconductors with even Chern numbers Ch per layer can be continuously deformed to normal-state weak Chern insulators with vanishing superconducting correlations and Chern number Ch/2 per layer.

For comparison, we note that Ref. 67 found no symmetry-based indicators due to the absence of Pfaffian band labels in their construction.

Representation $\Theta = A_u$.— For the case of the A_u representation, there are no compatibility relations of $0d$ type, so that

$$\mathrm{BS}_\mathrm{D}[C_i, A_u] = \mathrm{BL}_\mathrm{D}[C_i, A_u] = \mathbb{Z}^8. \tag{4.104}$$

There is a compatibility relation of $2d$ type, however, which follows from the existence of Chern numbers Ch_i along planes at constant k_i, $i = x, y, z$, [32]

$$\begin{aligned}\mathrm{Ch}_i &= \sum_{\mathbf{k}_\mathrm{s}|k_{\mathrm{s},i}=0} \mathfrak{N}_+^{\mathbf{k}_\mathrm{s}} \\ &= \sum_{\mathbf{k}_\mathrm{s}|k_{\mathrm{s},i}=\pi} \mathfrak{N}_+^{\mathbf{k}_\mathrm{s}} \mod 2, \end{aligned} \tag{4.105}$$

with $i = x, y, z$. Computing the quotient $\mathrm{SI} = \mathrm{BS}/\mathrm{AI}$, we find that the group of symmetry-based indicators is

$$\mathrm{SI}_\mathrm{D}[C_i, A_u] = \mathbb{Z}_2^3 \times \mathbb{Z}_4^3 \times \mathbb{Z}_8. \tag{4.106}$$

Here the three factors $\mathbb{Z}_2$ with symmetry-based indicators

$$z_{1;i,j} = \sum_{\mathbf{k}_\mathrm{s}|k_{\mathrm{s},i}=k_{\mathrm{s},j}=\pi} \mathfrak{N}_+^{\mathbf{k}_\mathrm{s}} \mod 2, \tag{4.107}$$

for $(i, j) = (x, y)$, (z, x), and (y, z) correspond to weak phases consisting of stacks of one-dimensional topological superconductors, see Fig. 4.5. Generator Hamiltonians are

$$H_{(1;x,y)}(\mathbf{k}) = \tau_3(1-m-\cos k_z)+\tau_1 \sin k_z, \text{ cycl.}, \tag{4.108}$$

with the representations

$$U(\mathcal{P}) = \tau_1, \quad U(\mathcal{I}) = \tau_3. \tag{4.109}$$

The three factors $\mathbb{Z}_4$, which have indicators

$$z_{2;l} = -\sum_{\mathbf{k}_\mathrm{s}|k_{\mathrm{s},l}=\pi} \mathfrak{N}_+^{\mathbf{k}_\mathrm{s}} (-1)^{(k_{\mathrm{s},x}+k_{\mathrm{s},y}+k_{\mathrm{s},z})/\pi} \mod 4, \tag{4.110}$$

for $l = x, y, z$, correspond to weak Chern superconductors, see Fig. 4.5. Generator Hamiltonians are

$$\begin{aligned}H_{(2,x)}(\mathbf{k}) =& \tau_3(2 - m - \cos k_y - \cos k_z) \\ &+ \tau_1 \sin k_y + \tau_2 \sin k_z, \text{ cycl.}\end{aligned} \tag{4.111}$$

with $0 < m < 2$, and the same representations as above. Similar to previous examples, we find that the weak even-Chern-number superconductors are continuously deformable to weak normal-state Chern insulators. The symmetry-based indicators $z_{2,l} = 2$ are ambiguous as they may also correspond to a weak second-order topological superconductor,

$$\begin{aligned}H'_{(2,x)}(\mathbf{k}) =& \rho_0\tau_3(2 - m - \cos k_y - \cos k_z) \\ &+ \rho_3\tau_1 \sin k_y + \rho_0\tau_2 \sin k_z, \text{ cycl.}\end{aligned} \tag{4.112}$$

with $0 < m < 2$, and the representations

$$U(\mathcal{P}) = \rho_0\tau_1, \quad U(\mathcal{I}) = \rho_0\tau_3. \tag{4.113}$$

Finally, the factor $\mathbb{Z}_8$ with indicator

$$z_3 = \sum_{\mathbf{k}_\mathrm{s}} \mathfrak{N}_+^{\mathbf{k}_\mathrm{s}} (-1)^{(k_{\mathrm{s},x}+k_{\mathrm{s},y}+k_{\mathrm{s},z})/\pi} \mod 8 \tag{4.114}$$

is generated by a representation-enforced nodal superconductor with different Chern number at parallel planes. The direct sum of two representation enforced-nodal superconductors may produce a strong second-order topological superconductor with chiral Majorana hinge states and generator Hamiltonian

$$\begin{aligned}H'_{(3)}(\mathbf{k}) =& \rho_3\tau_3(3 - m - \cos k_x - \cos k_y - \cos k_z) \\ &+ \rho_0\tau_1 \sin k_x + \rho_0\tau_2 \sin k_y + \rho_2\tau_3 \sin k_z\end{aligned} \tag{4.115}$$

with $0 < m < 2$, and with representations

$$U(\mathcal{P}) = \rho_0\tau_1, \quad U(\mathcal{I}) = \rho_3\tau_3. \tag{4.116}$$

The direct sum of two strong second-order topological superconductors in this symmetry class, corresponding to $z_3 = 4$, generates a third-order topological superconductor. [25, 39] This identifies $z_3 = 2$ and $z_3 = 6$ as indicators of strong second-order phases, whereas $z_3 = 4$ indicates a third-order phase, see Fig. 4.5.

For comparison, we note that the classifying group for this case is

$$\mathcal{K}_\mathrm{D}[C_i, A_u] = \mathbb{Z}_2^6 \times \mathbb{Z}_4 \times \mathbb{Z}^3, \tag{4.117}$$

where three factors $\mathbb{Z}_2$ correspond to weak phases consisting of stacks of one-dimensional topological superconductors, the other three factors $\mathbb{Z}_2$ correspond to stacks of second-order two-dimensional topological superconductors, the three factors $\mathbb{Z}$ correspond to weak phases consisting of stacks of two-dimensional Chern superconductors, whereas the factor $\mathbb{Z}_4$ consists of (strong) second- and third-order topological superconductors, as described above. Following the notation of Ref. 39, Fig 4.5 lists the appropriate boundary-resolved subgroup sequence $\mathcal{K}_i'' \subset \mathcal{K}_i' \subset \mathcal{K}$ for each of the factors $\mathcal{K}_i$ contained in the full classification group $\mathcal{K} = \prod_i \mathcal{K}_i$, where $\mathcal{K}_i'$ and $\mathcal{K}_i''$ are the subgroups of $\mathcal{K}$ containing topological phases with boundary signature of order larger than one or two, respectively. Weak phases have a shorter subgroup sequence, because they do not admit boundary states of order larger than one or two for stacks of one-dimensional topological phases or two-dimensional topological phases, respectively.

Symmetry-based indicators corresponding to the class considered in this example were previously considered in Refs. 65–67. The explicit expression for z_3 in Ref. 66 in the weak pairing limit differs from our Eqs. (4.110) and (4.114) by the absence of the sign factors in these references. (Reference 67 contains no explicit expression for the symmetry-based indicators; Reference 65 defines a $\mathbb{Z}_2$ invariant only, for which the sign factors are not important.) This difference affects the assignment of a strong (higher-order) topological index z_3 to weak phases, such as those described by the Hamiltonian $H_{(2,x)}(\mathbf{k})$ of Eq. (4.111). The assignment of a strong index to these weak phases is ambiguous, as the presence of gapless surfaces in the weak phases makes it impossible to uniquely associate a boundary signature with a nonzero value of the

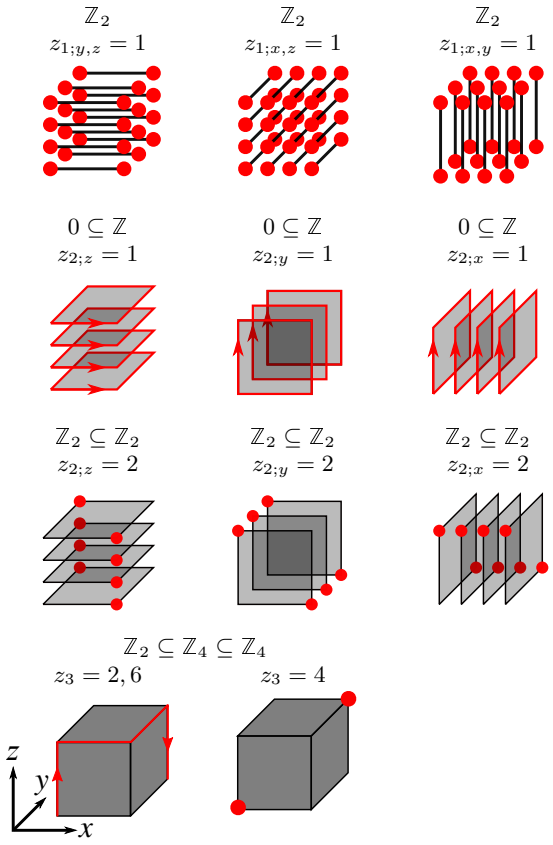

FIG. 4.5. Topological phases of a three-dimensional superconductor in tenfold-way class D, with additional C_i symmetry and one-dimensional representation $\Theta = A_u$. For each boundary signature, the subgroup sequence and the symmetry-based indicators of the generators of that phase are given. The third-order topological superconductor with $z_3 = 4$ can be constructed as the direct sum of two second-order topological superconductors with $z_3 = 2$.

strong indicator in a weak phase. We here follow the convention of Refs. 32 and 79, according to which weak phases are constructed as stack of layers containing the unit cell center, *i.e.* with momentum independent representations.

4.7.2. Inversion symmetry, class DIII

Representation $\Theta = A_g$. — Bogoliubov-de Gennes-type Hamiltonians in tenfold-way class DIII with inversion symmetry and with a superconducting order parameter transforming according to the A_g representation have a trivial classifying group $\mathfrak{K}_{\mathrm{DIII}}[C_i, A_g] = \mathfrak{K}_{\mathrm{DIII}}[0]^2 = 0$ at the high-symmetry momenta, so that no topological band labels can be defined. Also, the boundary classifying group of topological phases $\mathcal{K} = 0$ is trivial in this symmetry class in three dimensions. [39]

Representation $\Theta = A_u$. — For the A_u representation we have the classifying group of inversion symmetric momenta and Wyckoff positions $\mathfrak{K}_{\mathrm{DIII}}[C_i, A_u] = \mathfrak{K}_{\mathrm{AII}}[0] = \mathbb{Z}$. The results for class DIII can be constructed from the class D results by taking the direct sum

$$H_{\mathrm{DIII}}(\mathbf{k}) = H(\mathbf{k}) \oplus_\sigma H(-\mathbf{k})^*, \tag{4.118}$$

where $H(\mathbf{k})$ is a class-D Hamiltonian satisfying particle-hole antisymmetry and inversion symmetry with representation $\Theta = A_u$. Time-reversal is represented as $\mathcal{T} = \sigma_2 K$; Particle-hole conjugation and inversion are diagonal with respect to the σ degree of freedom, where it is important that the representation for inversion be real. With the relation (4.118) the construction of symmetry-based indicators is the same as in class D, with the exception of the 2d compabitility relation (4.105), which does not apply to class DIII since no Chern numbers can be defined at two-dimensional planes in the Brillouin zone.

The boundary classifying group for class DIII is

$$\mathcal{K}_{\mathrm{DIII}}[C_i, A_u] = \mathbb{Z}_2^3 \times \mathbb{Z}_4^4 \times \mathbb{Z}. \tag{4.119}$$

With the exception of the one factor $\mathbb{Z}$, the interpretation of these factors and their relation to the topological band labels is the same as for class D. In particular, the construction (4.118) takes an inversion-symmetric Kitaev chain to its time-reversed couterpart and each Chern superconductor with odd Chern number to a two-dimensional topological superconductor with helical Majorana edge states. Both the even-Chern number superconductor and the two-dimensional second-order topological superconductor in class D map to the two-dimensional second-order topological superconductor in class DIII. Upon adding weak odd-parity superconducting correlation to an inversion-symmetric quantum spin Hall insulator or three-dimensional strong topological insulator in class AII, the edge states gap and create a second-order topological superconductor with a Kramers pair of Majorana corner states or helical Majorana hinge states, respectively. Correspondingly, the inversion-symmetry-protected second-order topological insulator in class AII turns into an odd-parity third-order topological superconductor. For the remaining factor $\mathbb{Z}$, we observe that the construction (4.118) maps the representation-induced nodal superconductor in class D, which has difference in Chern numbers for parallel planes cutting through the Brillouin zone, to the generator of the three-dimensional (gapped) time-reversal symmetric topological superconductors, which has indicator $z_3 = 1$. The classification results together with the subgroup sequences are illustrated in Figure 4.6.

The generator of the first-order time-reversal symmetric topological superconductor is

$$\begin{aligned} H^{\mathrm{DIII}}_{(3)}(\mathbf{k}) = {} & \sigma_2\tau_2(3 - m - \cos k_x - \cos k_y - \cos k_z) \\ & + \sigma_1\tau_0 \sin k_x + \sigma_2\tau_3 \sin k_y \\ & + \sigma_3\tau_0 \sin k_z, \end{aligned}$$

with $0 < m < 2$ where we used the representations

$$U(\mathcal{P}) = \sigma_0\tau_1,\ U(\mathcal{I}) = \sigma_2\tau_2,\ U(\mathcal{T}) = \sigma_2\tau_0.$$

Direct summation of this phase generates the free ($\mathbb{Z}$) group of first-order topological superconducting phases. Direct summation of the two generators as $H^{\mathrm{DIII}}_{(3)} \otimes \mu_3$, with inversion represented as $U(\mathcal{I}) \otimes \mu_3$, constructs the generator of the factor $\mathbb{Z}_4$ in Eq. (4.119), a second-order TSC that becomes a third-order topological superconductor upon taking the direct sum with itself. Consequently, all "even" symmetry-based indicators belonging to the factor $\mathbb{Z}_8$ are ambiguous: The elements $z_3 = 2$ or 6 and $z_3 = 4$ may correspond to two or four copies of the strong three dimensional first-order TSC or to the strong second or third-order topological superconductor, respectively.

The group of symmetry indicators $\mathrm{SI} = \mathbb{Z}_2^3 \times \mathbb{Z}_4^3 \times \mathbb{Z}_8$ that we obtain agrees with results from Refs. 67 and 68. Reference 65 finds a subgroup $\mathbb{Z}_2^3 \otimes \mathbb{Z}_4 \subseteq \mathrm{SI}$ consisting of the "even" elements only. The explicit expressions for the symmetry-based indicators differ from those in Refs. 65–67 by the presence of the sign factors, see the discussion at the end of Sec. 4.7 1.[4] The expression for the symmetry-based indicator for strong phases z_3 in Eq. (4.114) agrees with the corresponding expression in Ref. 68. However, in Ref. 68 the symmetry-based indicators for the weak phases are defined on planes or lines with $k_l = k_m = 0$, while our symmetry-based indicators $z_{1;l,m}$ and $z_{2;l}$ are defined on planes or lines with $k_l = k_m = \pi$. This definition ensures that no spurious weak indices are assigned to other weak phases or to strong phases. In the weak-pairing limit, the criterion $z_3 = 1 \mod 2$ for the three-dimensional first-order topological superconductor agrees with the well-known condition that there must be an odd number of Fermi level crossings between high-symmetry momenta, see Refs. 77 and 78.

Very recently, the possibility of hybrid higher-order topology was discussed in the literature. [80] We note that for such "hybrid" of first- and second-order topology, it is sufficient to consider inversion symmetric superconductor as the current example shows: A "hybrid" phase can be identified as a direct sum of a first-order phase (last row, first column in Fig. 4.6) and one of the weak phases from the third row of Fig. 4.6.

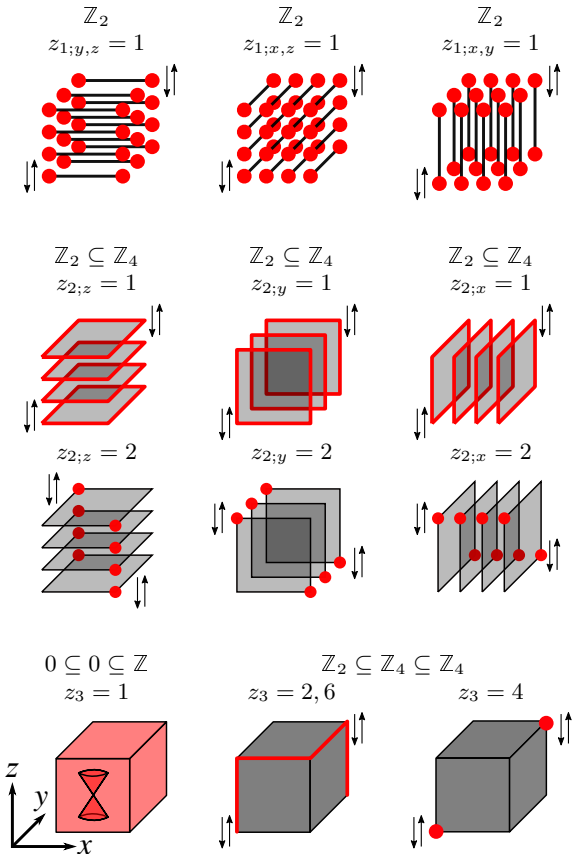

FIG. 4.6. Topological phases of a three-dimensional superconductor in tenfold-way class DIII, with additional C_i symmetry and one-dimensional representation $\Theta = A_u$. For each boundary signature, the subgroup sequence and the symmetry-based indicators of the generators of that phase are given. The two-dimensional second-order topological superconductor with $z_{2;l} = 2$ can be constructed as the direct sum of two two-dimensional first-order topological superconductors with $z_{2;l} = 1$, $l = x, y, z$. Similarly, the three dimensional third-order topological superconductor with $z_3 = 4$ can be constructed as the direct sum of two three dimensional second-order topological superconductors with $z_3 = 2$.

4.7.3. Inversion symmetry, class C

General considerations. With spin-rotation symmetry, the Hamiltonian is of the form $H(\mathbf{k}) = H_C(\mathbf{k}) \otimes \sigma_0$ where $H_C(\mathbf{k})$ satisfies an effective particle-hole antisymmetry $\mathcal{P} = \tau_2 K$ squaring to -1. This is the tenfold-way class C.

Representation $\Theta = A_g$. — With the A_g representation for the transformation behavior of the superconducting order parameter, the classifying group of the Hamiltonian at each of the high-symmetry momenta is trivial, $\mathfrak{K}_{\mathrm{C}}[C_i, A_g] = \mathfrak{K}_{\mathrm{C}}[0]^2 = 0$, so that no topological band labels can be defined. The classifying group is

$$\mathcal{K}_{\mathrm{C}}[C_i, A_g] = \mathbb{Z}^3 \times \mathbb{Z}_2, \tag{4.120}$$

see Ref. 39. It contains a factor $\mathbb{Z}^3$ corresponding to weak Chern superconductors in all three stacking directions and a factor $\mathbb{Z}_2$ corresponding to a strong second-order TSC with chiral hinge states. None of those phases can be detected by symmetry-based indicators. The boundary signatures of all topological phases in this class are

[4] For symmetry class DIII, the gapless surface states of the weak phases can be removed by breaking translation symmetry. If inversion symmetry is maintained, a strong higher-order phase can result, which has helical Majorana modes along hinges. Such breaking of translation symmetry requires a doubling of the unit cell. Our convention that Hamiltonians such as Eq. (4.111) have no strong index requires that the inversion center is shifted by half a unit cell upon doubling the unit cell, see, *e.g.*, the discussion in Ref. 79.

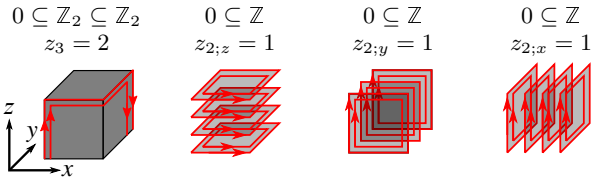

FIG. 4.7. Topological phases of a three-dimensional superconductor in tenfold-way class C, with additional C_i symmetry and one-dimensional representation $\Theta = A_u$. For each boundary signature, the subgroup sequence and the symmetry-based indicators of the generators of that phase are given.

pairs of chiral Majorana modes. In the limit of vanishing superconducting correlations, they can be adiabatically deformed to corresponding normal-state topological insulators with chiral fermionic modes on their boundaries. Our results for the $\Theta = A_g$ representation are consistent with the results of Ref. 67.

Representation $\Theta = A_u$. — The discussion in class C with the one-dimensional representation $\Theta = A_u$ of inversion symmetry is analogous to the discussion in class D. Each of the high-symmetry momenta and each of the Wyckoff positions comes with the classification group $\mathfrak{K}_{\mathrm{C}}[C_i, A_u] = \mathfrak{K}_{\mathrm{A}}[0] = \mathbb{Z}$. Compatibility relations of $0d$ type follow from the observation that the product $\mathcal{IP}$ acts as an effective particle-hole symmetry that is local in reciprocal space and squares to one. As a result, one may define a Pfaffian invariant $\mathfrak{p}(\mathcal{IP})$ for $H(\mathbf{k})$ at generic $\mathbf{k}$. Relating $\mathfrak{p}(\mathcal{IP})$ to the integer invariants $\mathfrak{N}_+^{\mathbf{k}_\mathrm{s}}$ at the eight high-symmetry momenta $\mathbf{k}_\mathrm{s}$, we obtain the seven compatibility relations

$$\mathfrak{N}_+^{\mathbf{k}_\mathrm{s}} = \mathfrak{N}_+^{(\pi,\pi,\pi)} \mod 2 \tag{4.121}$$

for $\mathbf{k}_\mathrm{s} \neq (\pi,\pi,\pi)$. Defining the integer band labels

$$\mathfrak{n}_+^{\mathbf{k}_\mathrm{s}} = (\mathfrak{N}_+^{\mathbf{k}_\mathrm{s}} - \mathfrak{N}_+^{(\pi,\pi,\pi)})/2, \tag{4.122}$$

we arrive at

$$\begin{aligned} &\mathrm{BS} = \mathbb{Z}^8, \qquad (4.123)\\ &B[H(\mathbf{k})] = \Big\{\mathfrak{n}_+^{(0,0,0)}, \mathfrak{n}_+^{(\pi,0,0)}, \mathfrak{n}_+^{(0,\pi,0)}, \mathfrak{n}_+^{(\pi,\pi,0)},\\ &\qquad \mathfrak{n}_+^{(0,0,\pi)}, \mathfrak{n}_+^{(\pi,0,\pi)}, \mathfrak{n}_+^{(0,\pi,\pi)}, \mathfrak{N}_+^{(\pi,\pi,\pi)}\Big\}. \end{aligned}$$

The group SI of symmetry-based indicators is

$$\mathrm{SI}_{\mathrm{C}}[C_i, A_u] = \mathbb{Z}_2^3 \times \mathbb{Z}_4. \tag{4.124}$$

An additional compatibility relation of $2d$ type follows by noting that for a gapped Hamiltonian a Chern number can be defined on planes with fixed k_l with $l = x$, y, or z and that this Chern number is always even. At high-symmetry planes with $k_l = 0$ or π the Chern number Ch_l is related to the topological band labels as

$$\begin{aligned} \frac{1}{2}\mathrm{Ch}_l &= \sum_{\mathbf{k}_\mathrm{s}|_{k_{\mathrm{s},l}=0}} \mathfrak{n}_+^{\mathbf{k}_\mathrm{s}} \mod 2\\ &= \sum_{\mathbf{k}_\mathrm{s}\neq(\pi,\pi,\pi)|_{k_{\mathrm{s},l}=\pi}} \mathfrak{n}_+^{\mathbf{k}_\mathrm{s}} \mod 2. \end{aligned} \tag{4.125}$$

One verifies that the generator of the factor $\mathbb{Z}_4$ in Eq. (4.124), which has symmetry-based indicator

$$z_3 = \sum_{\mathbf{k}_\mathrm{s}\neq(\pi,\pi,\pi)} \mathfrak{n}_+^{\mathbf{k}_\mathrm{s}} (-1)^{(k_{\mathrm{s},x}+k_{\mathrm{s},y}+k_{\mathrm{s},z})/\pi} \mod 4, \tag{4.126}$$

is a representation-enforced nodal superconductor, which violates the compatibility relation (4.125). The three factors $\mathbb{Z}_2$ with indicators

$$z_{2;i} = \sum_{\mathbf{k}_\mathrm{s}\neq(\pi,\pi,\pi)|k_{\mathrm{s},i}=\pi} \mathfrak{n}_+^{\mathbf{k}_\mathrm{s}} \mod 2, \quad i = x, y, z, \tag{4.127}$$

correspond to weak Chern superconductor phases, see Fig. 4.7.

For comparison, we note that the boundary classification group is [39]

$$\mathcal{K}_{\mathrm{C}}[C_i, A_u] = \mathbb{Z}^3 \times \mathbb{Z}_2. \tag{4.128}$$

Here the three factors $\mathbb{Z}$ correspond to weak Chern superconductors with generator Hamiltonians

$$\begin{aligned} H^{\mathrm{C}}_{(2,x)}(\mathbf{k}) &= \mu_0\tau_3(2 - m - \cos k_y - \cos k_z)\\ &\quad + \mu_1\tau_1 \sin k_y + \mu_1\tau_2 \sin k_z, \quad \text{cycl.} \end{aligned}$$

with $0 < m < 2$. The corresponding representations are

$$U(\mathcal{P}) = \mu_3\tau_2, \quad U(\mathcal{I}) = \mu_0\tau_3.$$

The Hamiltonians $H^{\mathrm{C}}_{(2,l)}$ have Chern number $\mathrm{Ch}_l = 2$ and generate the elements "1" in the three factors $\mathbb{Z}_2$ of SI, see Eq. (4.124). The remaining factor $\mathbb{Z}_2$ of SI is generated by a second-order topological superconductor with chiral hinge states

$$\begin{aligned} H'^{\mathrm{C}}_{(3)}(\mathbf{k}) &= \mu_0\rho_3\tau_3(3 - m - \cos k_x - \cos k_y - \cos k_z)\\ &\quad + \mu_1\rho_0\tau_1 \sin k_x + \mu_1\rho_0\tau_2 \sin k_y + \mu_1\rho_1\tau_3 \sin k_z \end{aligned} \tag{4.129}$$

with $0 < m < 2$, where we used the representations

$$U(\mathcal{P}) = \mu_3\rho_0\tau_2, \quad U(\mathcal{I}) = \mu_0\rho_3\tau_3.$$

The above phase has symmetry-based indicator $z_3 = 2$, see Fig. 4.7. As for the A_g representation, the boundary signatures of all topological phases in this class are pairs of chiral Majorana modes. They can be adiabatically deformed to corresponding normal-state topological insulators with chiral fermionic boundary modes.

Our result (4.124) for the group of symmetry-based indicators is more constrained than the corresponding result from Ref. 67, which finds $\mathrm{SI} = \mathbb{Z}_2^3 \times \mathbb{Z}_4^3 \times \mathbb{Z}_8$. The origin of the difference is that we include the $0d$ compatibility constraint arising from the conservation of the Pfaffian invariant.

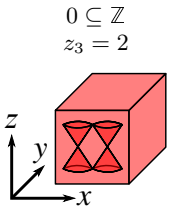

FIG. 4.8. In tenfold-way class CI with additional C_i symmetry and one-dimensional representation $\Theta = A_u$, there is a single topological phase with first order boundary signature consisting of pairs of Majorana Dirac cones. The subgroup sequence and the symmetry-based indicator of the generator of this phase is given.

4.7.4. Inversion symmetry, class CI

Representation $\Theta = A_g$. — Here the discussion is the same as for class C. Both the group SI of symmetry-based indicators and the classifying group $\mathcal{K} = 0$ are trivial. [39]

Representation $\Theta = A_u$. — In the presence of spin-rotation symmetry, time-reversal symmetry can be represented as $\mathcal{T} = K$. Class CI has the same topological band labels as class C, and the generators of atomic limits in classes C and CI have the same band labels, too. The 0d compatibility relations (4.121) continue to be valid. Thus, it follows that the group SI of symmetry-based indicators is again given by Eq. (4.124).

The higher-dimensional compatibility relations differ from those in class C. On the one hand, there is no Chern number for two-dimensional cuts of the Brillouin zone. On the other hand, $H(\mathbf{k})$ is subject to the chiral antisymmetry $\mathcal{PT}$ and a local-in-$\mathbf{k}$ antiunitary symmetry $\mathcal{IT}$ for generic $\mathbf{k}$, which effectively places it in tenfold-way class BDI. For a one-parameter family of gapped Hamiltonian that are (effectively) in class BDI for each $\mathbf{k}$, there exists a $\mathbb{Z}_2$ topological invariant, the first Stiefel-Whitney number [75, 76]. [81] Considering this $\mathbb{Z}_2$ invariant along one-dimensional cuts through the Brillouin zone and using its relation to the band labels at high-symmetry momenta, one finds four compatibility relations of $1d$ type (see App. C.3),

$$\mathfrak{n}_+^{\mathbf{k}_\mathrm{s}} - \mathfrak{n}_+^{\mathbf{k}_\mathrm{s}+\pi\mathbf{e}_l} = \mathfrak{n}_+^{(\pi,\pi,\pi)-\pi\mathbf{e}_l} \mod 2, \tag{4.130}$$

for $k_{\mathrm{s},l} = 0$, $\mathbf{k}_\mathrm{s} + \pi\mathbf{e}_l \neq (\pi,\pi,\pi)$ where $\mathbf{e}_l$ is the unit vector in the l-direction, $l = x, y, z$. These 1d compatibility relations impose the conditions $z_{2;l} = 0$ and $z_3 = 0$ mod 2 for gapped phases. Phases violating these conditions, corresponding to the elements "1" in the three factors $\mathbb{Z}_2$ and the elements "1" and "3" in the factor $\mathbb{Z}_4$ are representation-enforced nodal-line superconductors. The group of symmetry-based indicators for phases satifying all compatibility relations is, hence,

$$\mathrm{SI}_{\mathrm{CI}}^{(2)}[C_i, A_u] = \mathbb{Z}_2. \tag{4.131}$$

For comparison, we note that the boundary classification group is

$$\mathcal{K}_{\mathrm{CI}}[C_i, A_u] = \mathbb{Z}. \tag{4.132}$$

It is generated by a strong first-order phase in three dimension whose boundary signature is illustrated in Fig. 4.8. Its generator Hamiltonian can be written as

$$\begin{aligned} H_{(3)}^{\mathrm{CI}}(\mathbf{k}) =& \mu_0\rho_0\tau_3(3 - m - \cos k_x - \cos k_y - \cos k_z) \\ &+ \mu_2\rho_1\tau_1 \sin k_x + \mu_0\rho_2\tau_1 \sin k_y + \mu_2\rho_3\tau_1 \sin k_z \end{aligned} \tag{4.133}$$

with $0 < m < 2$. Here we used the representations

$$U(\mathcal{P}) = \mu_0\rho_0\tau_2,\ U(\mathcal{I}) = \mu_0\rho_0\tau_3,\ U(\mathcal{T}) = \mu_0\rho_0\tau_0.$$

It has band labels $\mathfrak{n}_+^{\mathbf{0}} = 2$, $\mathfrak{N}_+^{(\pi,\pi,\pi)} = 0$, and $\mathfrak{n}_+^{\mathbf{k}_\mathrm{s}} = 0$ for $\mathbf{k}_\mathrm{s} \neq (0,0,0)$, (π,π,π). Its band labels generate the element "2" in the factor $\mathbb{Z}_4$ of SI and the element "1" in the factor $\mathbb{Z}_2$ of $\mathrm{SI}^{(2)}$, see Eq. (4.131).

Similar to the previous section, our group (4.124) of symmetry-based indicators is more constrained than the corresponding result from Ref. 67, as we include the compatibility relation due to the conservation of the Pfaffian invariant. As discussed above, one finds an even smaller group of symmetry-based indicators if $1d$ compatibility relations based on the Stiefel-Whitney number are included as well.

4.8. CONCLUSION

Symmetry-based indicators have proven to be a pragmatic substitute for a full classification of topological insulator phases using a complete set of topological invariants. [27, 28, 56, 58, 59] Their main advantage is that symmetry-based indicators are easier to calculate than other types of topological invariants, since they require local information in reciprocal space only. On the other hand, a nonzero value of a symmetry-based indicators is sufficient to establish that a phase has nontrivial topology and may, in addition, contain information of the type of anomalous boundary states. [24, 60]

In this work, we extend the concept of symmetry-based indicators to Hamiltonians of Bogoliubov-de Gennes (BdG) type, which appear in the mean-field theory superconducting phases. Hamiltonians of BdG type are antisymmetric with respect to particle-hole conjugation. Additionally, for Hamiltonians of BdG type, a crystalline symmetry class is defined by the presence or absence of time-reversal and spin-rotation symmetry, by the point group G, and by a one-dimensional representation Θ of G that describes how the superconducting order parameter Δ transforms under the crystalline symmetry. [69]

Like the symmetry-based indicators for non-superconducting insulating phases, [27, 28, 58, 59] the symmetry-based indicators for BdG Hamiltonians can be constructed in a fully algorithmic manner. Input for our construction are "band labels", which are the complete set of "zero-dimensional" topological invariants of the BdG Hamiltonian $H(\mathbf{k}_\mathrm{s})$ evaluated at high-symmetry points $\mathbf{k}_\mathrm{s}$ in Brillouin zone. Such band

labels were first considered by Shiozaki, Sato, and Gomi in Ref. 64. Unlike previous works on the symmetry-based indicators for topological superconductors, [63, 65–67] the set of zero-dimensional topological invariants considered by us (and by Ref. 64) is provably complete — it is not possible to resolve more boundary signatures through the prism of zero-dimensional bulk topological invariants. In particular, the set of topological invariants considered in this work includes not only integer topological invariants of the type used in the construction of symmetry-based indicators for non-superconducting Hamiltonians — counting the number of occupied bands corresponding to a certain symmetry representation of the crystalline symmetry —, but also $\mathbb{Z}_2$ topological invariants constructed using Pfaffians, which do not appear in Refs. 63, 65–67. Pfaffians play a role not only as useful topological band labels, but they also give rise to additional compatibility relations,[64] even in cases in which there are symmetry-based indicators of integer type only. The latter point is well illustrated by the example of tenfold-way classes C and CI with inversion symmetry and $\Theta = A_u$, discussed in Secs. 4.7 3 and 4.7 4.

In the weak-pairing limit (superconducting gap Δ small in comparison to characteristic energy scales of the normal-state band structure), the band labels of the BdG Hamiltonian can be expressed in terms of conventional integer band labels of the normal-state Hamiltonian, provided the symmetry of the superconducting order parameter is known.[67, 68] This applies both to the integer invariant and to the $\mathbb{Z}_2$ Pfaffian invariant. This means that in the weak-pairing the symmetry-based indicators constructed here can be calculated using the vast amount of known band structure data in the normal state.

The main difference between zero-dimensional band labels and symmetry-based indicators [27] is that the latter are designed to "see" only the topological phases with non-trivial boundary signatures. Topologically non-trivial superconductors without gapless boundary states are deformable to atomic-limit phases. In this work we combine the complete set of zero-dimensional band labels [64] and the definition of atomic-limit superconductors as an "array" of zero-dimensional superconductors, [39] to arrive at an extension of symmetry-based indicators [27] to Hamiltonians of Bogoliubov-de Gennes type. Our definition of atomic-limit superconductors agrees with the definitions of Refs. 67 and 68. Since Pfaffian invariants do not appear in Refs. 65–67, the symmetry-based indicators we obtain may be expected to be consistent with these references once all topological band labels and all compatibility relations associated with Pfaffian invariants are omitted from our construction. (For inversion-symmetric superconductors, however, our concrete expressions for the symmetry-based indicators differ from those of Refs. 65–67. This is discussed in detail in Sec. 4.7.) Reference 68 contains results closely related to and consistent with ours.

If the symmetry-based indicators are used as a substitute for a full classification, ideally, one wants symmetry-based indicators to detect gapped phases only. The algorithmic construction defined in this work partially meets this goal: It only guarantees that no indicator corresponds to gapless topological superconductor phases with its gapless points on high-symmetry lines in Brillouin zone that connect the high-symmetry points. Nev-

d	G	Cartan	Θ	SI	$\mathrm{SI}^{(d-1)}$	$\mathcal{K}$
1	C_1	D	A	$\mathbb{Z}_2$	$\mathbb{Z}_2$	$\mathbb{Z}_2$
		DIII	A	0	0	$\mathbb{Z}_2$
		C	A	0	0	0
		CI	A	0	0	0
1	C_i	D	A_g	0	0	0
			A_u	$\mathbb{Z}_2$	$\mathbb{Z}_2$	$\mathbb{Z}_2$
2	C_1	D	A	$\mathbb{Z}_2^3$	$\mathbb{Z}_2^3$	$\mathbb{Z}_2^2 \times \mathbb{Z}$
		DIII	A	0	0	$\mathbb{Z}_2^3$
		C	A	0	0	$\mathbb{Z}$
		CI	A	0	0	0
2	C_i	D	A_g	$\mathbb{Z}_2$	$\mathbb{Z}_2$	$\mathbb{Z}$
			A_u	$\mathbb{Z}_2^2 \times \mathbb{Z}_4$	$\mathbb{Z}_2^2 \times \mathbb{Z}_4$	$\mathbb{Z}_2^3 \times \mathbb{Z}$
2	C_s	D	A'	$\mathbb{Z}_2$	$\mathbb{Z}_2$	$\mathbb{Z}_2$
			A''	$\mathbb{Z}_2^3$	$\mathbb{Z}_2^3$	$\mathbb{Z}_2^3$
2	C_2	D	A	$\mathbb{Z}_2^2 \times \mathbb{Z}_4$	$\mathbb{Z}_2^2 \times \mathbb{Z}_4$	$\mathbb{Z}_2^3 \times \mathbb{Z}$
			B	$\mathbb{Z}_2$	$\mathbb{Z}_2$	$\mathbb{Z}$
2	C_{2v}	D	A_1	0	0	0
			A_2	$\mathbb{Z}_2^3$	$\mathbb{Z}_2^3$	$\mathbb{Z}_2^4$
			B_1	$\mathbb{Z}_2$	$\mathbb{Z}_2$	$\mathbb{Z}_2$
			B_2	$\mathbb{Z}_2$	$\mathbb{Z}_2$	$\mathbb{Z}_2$
2	C_4	D	A, B	$\mathbb{Z}_2 \times \mathbb{Z}_8$	$\mathbb{Z}_2 \times \mathbb{Z}_8$	$\mathbb{Z}_2^2 \times \mathbb{Z}$
			${}^{1,2}E$	$\mathbb{Z}_4$	$\mathbb{Z}_4$	$\mathbb{Z}$
3	C_1	D	A	$\mathbb{Z}_2^7$	$\mathbb{Z}_2^6$	$\mathbb{Z}_2^3 \times \mathbb{Z}^3$
		DIII	A	0	0	$\mathbb{Z}_2^6 \times \mathbb{Z}$
		C	A	0	0	$\mathbb{Z}^3$
		CI	A	0	0	$\mathbb{Z}$
3	C_i	D	A_g	$\mathbb{Z}_2^4$	$\mathbb{Z}_2^3$	$\mathbb{Z}^3$
			A_u	$\mathbb{Z}_2^3 \times \mathbb{Z}_4^3 \times \mathbb{Z}_8$	$\mathbb{Z}_2^3 \times \mathbb{Z}_4^4$	$\mathbb{Z}_2^6 \times \mathbb{Z}_4 \times \mathbb{Z}^3$
		DIII	A_g	0	0	0
			A_u	$\mathbb{Z}_2^3 \times \mathbb{Z}_4^3 \times \mathbb{Z}_8$	$\mathbb{Z}_2^3 \times \mathbb{Z}_4^3 \times \mathbb{Z}_8$	$\mathbb{Z}_2^3 \times \mathbb{Z}_4^4 \times \mathbb{Z}$
		C	A_g	0	0	$\mathbb{Z}^3 \times \mathbb{Z}_2$
			A_u	$\mathbb{Z}_2^3 \times \mathbb{Z}_4$	$\mathbb{Z}_2^4$	$\mathbb{Z}^3 \times \mathbb{Z}_2$
		CI	A_g	0	0	0
			A_u	$\mathbb{Z}_2^3 \times \mathbb{Z}_4$	$\mathbb{Z}_2$	$\mathbb{Z}$
3	C_s	D	A'	$\mathbb{Z}_2$	$\mathbb{Z}_2$	$\mathbb{Z}_2 \times \mathbb{Z}$
			A''	$\mathbb{Z}_2^9$	$\mathbb{Z}_2^9$	$\mathbb{Z}_2^7 \times \mathbb{Z}^2$
3	C_2	D	A	$\mathbb{Z}_2^2 \times \mathbb{Z}_4$	$\mathbb{Z}_2^2 \times \mathbb{Z}_4$	$\mathbb{Z}_2^3 \times \mathbb{Z}$
			B	$\mathbb{Z}_2^6$	$\mathbb{Z}_2^5$	$\mathbb{Z}_2^4 \times \mathbb{Z}$
3	C_{2v}	D	A_1	0	0	0
			A_2	$\mathbb{Z}_2^7$	$\mathbb{Z}_2^7$	$\mathbb{Z}_2^5 \times \mathbb{Z}^4$
			B_1	$\mathbb{Z}_2^3$	$\mathbb{Z}_2^3$	$\mathbb{Z}_2^3 \times \mathbb{Z}^2$
			B_2	$\mathbb{Z}_2^3$	$\mathbb{Z}_2^3$	$\mathbb{Z}_2^3 \times \mathbb{Z}^2$
3	C_4	D	A, B	$\mathbb{Z}_2 \times \mathbb{Z}_8$	$\mathbb{Z}_2 \times \mathbb{Z}_8$	$\mathbb{Z}_2^2 \times \mathbb{Z}$
			${}^{1,2}E$	$\mathbb{Z}_2^4 \times \mathbb{Z}_4$	$\mathbb{Z}_2^3 \times \mathbb{Z}_4$	$\mathbb{Z}_2^3 \times \mathbb{Z}$

TABLE 4.12. The group of symmetry-based indicators SI obtained by including compatiblity relations of $0d$ type only, the group $\mathrm{SI}^{(d-1)}$ obtained by including compatibility relations of n-dimensional type, with $n < d$, and the full boundary classification group $\mathcal{K}$ for the combinations of tenfold-way classes, dimension d, and point group G considered in this work.

ertheless, for the examples considered in this work, we were able to explicitly relate *all* gapless phases, including gapless phases with gapless points occurring on high-symmetry planes and in the bulk of the Brillouin zone, to symmetry-based indicators by invoking additional compatibility relations that involve winding numbers, Chern numbers, as well as first and second Stiefel-Whitney numbers. These compatibility relations are defined on one-dimensional and two-dimensional cuts through the Brillouin zone, respectively, involve local-in-$\mathbf{k}$ properties of $H(\mathbf{k})$ only, and generalize the compatibility relations that make use of the continuity of zero-dimensional invariants in the Brillouin zone. [27, 28, 56] Formally, the inclusion of higher (up to n)-dimensional compatibility relations allows one to define a smaller group $\mathrm{SI}^{(n)} \subset \mathrm{SI}$ of symmetry-based indicators. The relevant (smallest) groups $\mathrm{SI}^{(d-1)}$ are listed in Table 4.12 for the examples considered. For the examples we considered, we find that all phases indexed by $\mathrm{SI}^{(d-1)}$ are gapped. It would be interesting to find out, whether this feature holds in general, *i.e.*, whether the inclusion of these two "higher dimensional" compatibility relations involving local-in-$\mathbf{k}$ symmetries of $H(\mathbf{k})$ only is sufficient to identify all symmetry-based indicators that correspond to enforced gapless phases.

To see to what extent symmetry-based indicators offer a faithful representation of all (crystalline) topological phases we compared the symmetry-based indicators with the complete classification information for selected examples. To this end, we used the classifying group $\mathcal{K}$, which classifies all topological phases with protected boundary states. (This excludes atomic-limit phases with nontrivial topology from the topological classification, which is consistent with the fact that symmetry-based indicators of atomic-limit phases are *defined* to be zero.[27, 28]) A summary of this comparison is shown in Table 4.12. Only for a small number of the examples we consider — such as tenfold-way class D in three dimensions with symmetry groups C_s or C_{2v} and representations $\Theta = A'$ and $\Theta = B_2$, respectively —, entire classes of topological phases are missed by the symmetry-based indicators, whereas for some crystalline symmetry classes the full classifying group $\mathcal{K}$ and the group SI of symmetry-based indicators are identical. In most cases, all generators of topological phases are detectable by symmetry-based indicators, although there may be ambiguities preventing a unique identification of the precise nature of the topological phase. Although these examples clearly show that symmetry-based indicators are not equivalent to a complete classification, it remains an interesting observation that zero-dimensional invariants alone perform so well at this task.

[1] K. v. Klitzing, G. Dorda, and M. Pepper, Phys. Rev. Lett. **45**, 494 (1980).
[2] A. Y. Kitaev, Phys. Usp. **44**, 131 (2001).
[3] D. A. Ivanov, Phys. Rev. Lett. **86**, 268 (2001).
[4] C. L. Kane and E. J. Mele, Phys. Rev. Lett. **95**, 146802 (2005).
[5] C. L. Kane and E. J. Mele, Phys. Rev. Lett. **95**, 226801 (2005).
[6] V. Mourik, K. Zuo, S. M. Frolov, S. R. Plissard, E. P. A. M. Bakkers, and L. P. Kouwenhoven, Science **336**, 1003 (2012).
[7] C. Brüne, C. X. Liu, E. G. Novik, E. M. Hankiewicz, H. Buhmann, Y. L. Chen, X. L. Qi, Z. X. Shen, S. C. Zhang, and L. W. Molenkamp, Phys. Rev. Lett. **106**, 126803 (2011).
[8] A. Altland and M. R. Zirnbauer, Phys. Rev. B **55**, 1142 (1997).
[9] A. Kitaev, AIP Conference Proceedings **1134**, 22 (2009).
[10] A. P. Schnyder, S. Ryu, A. Furusaki, and A. W. W. Ludwig, AIP Conference Proceedings **1134**, 10 (2009).
[11] L. Fu, Phys. Rev. Lett. **106**, 106802 (2011).
[12] S. A. Parameswaran and Y. Wan, Physics **10**, 132 (2017).
[13] F. Schindler, A. M. Cook, M. G. Vergniory, Z. Wang, S. S. P. Parkin, B. A. Bernevig, and T. Neupert, Science Advances **4** (2018), 10.1126/sciadv.aat0346.
[14] Y. Peng, Y. Bao, and F. von Oppen, Phys. Rev. B **95**, 235143 (2017).
[15] J. Langbehn, Y. Peng, L. Trifunovic, F. von Oppen, and P. W. Brouwer, Phys. Rev. Lett. **119**, 246401 (2017).
[16] Z. Song, Z. Fang, and C. Fang, Phys. Rev. Lett. **119**, 246402 (2017).
[17] C. Fang and L. Fu, Science Advances **5** (2019), 10.1126/sciadv.aat2374.
[18] M. Ezawa, Phys. Rev. Lett. **120**, 026801 (2018).
[19] H. Shapourian, Y. Wang, and S. Ryu, Phys. Rev. B **97**, 094508 (2018).
[20] X. Zhu, Phys. Rev. B **97**, 205134 (2018).
[21] Z. Yan, F. Song, and Z. Wang, Phys. Rev. Lett. **121**, 096803 (2018).
[22] Y. Wang, M. Lin, and T. L. Hughes, Phys. Rev. B **98**, 165144 (2018).
[23] Q. Wang, C.-C. Liu, Y.-M. Lu, and F. Zhang, Phys. Rev. Lett. **121**, 186801 (2018).
[24] E. Khalaf, H. C. Po, A. Vishwanath, and H. Watanabe, Phys. Rev. X **8**, 031070 (2018).
[25] E. Khalaf, Phys. Rev. B **97**, 205136 (2018).
[26] N. Okuma, M. Sato, and K. Shiozaki, Phys. Rev. B **99**, 085127 (2019).
[27] H. C. Po, A. Vishwanath, and H. Watanabe, Nature Comm. **8**, 50 (2017).
[28] B. Bradlyn, L. Elcoro, J. Cano, M. G. Vergniory, Z. Wang, C. Felser, M. I. Aroyo, and B. A. Bernevig, Nature **547**, 298 (2017).
[29] A. Lau, J. van den Brink, and C. Ortix, Phys. Rev. B **94**, 165164 (2016).
[30] W. A. Benalcazar, B. A. Bernevig, and T. L. Hughes, Science **357**, 61 (2017).
[31] W. A. Benalcazar, B. A. Bernevig, and T. L. Hughes, Phys. Rev. B **96**, 245115 (2017).
[32] A. M. Turner, Y. Zhang, R. S. K. Mong, and A. Vish-

wanath, Phys. Rev. B **85**, 165120 (2012).
[33] A. Lau, C. Ortix, and J. van den Brink, Phys. Rev. B **91**, 085106 (2015).
[34] G. van Miert and C. Ortix, Phys. Rev. B **96**, 235130 (2017).
[35] J.-W. Rhim, J. Behrends, and J. H. Bardarson, Phys. Rev. B **95**, 035421 (2017).
[36] K. Shiozaki and M. Sato, Phys. Rev. B **90**, 165114 (2014).
[37] K. Shiozaki, M. Sato, and K. Gomi, Phys. Rev. B **93**, 195413 (2016).
[38] C.-K. Chiu, J. C. Y. Teo, A. P. Schnyder, and S. Ryu, Rev. Mod. Phys. **88**, 035005 (2016).
[39] L. Trifunovic and P. W. Brouwer, Phys. Rev. X **9**, 011012 (2019).
[40] E. Cornfeld and A. Chapman, Phys. Rev. B **99**, 075105 (2019).
[41] K. Shiozaki, (2019), arXiv:1907.09354.
[42] S.-J. Huang, H. Song, Y.-P. Huang, and M. Hermele, Phys. Rev. B **96**, 205106 (2017).
[43] R. Thorngren and D. V. Else, Phys. Rev. X **8**, 011040 (2018).
[44] C. Fang, M. J. Gilbert, and B. A. Bernevig, Phys. Rev. B **86**, 115112 (2012).
[45] C. Fang, M. J. Gilbert, and B. A. Bernevig, Phys. Rev. B **87**, 035119 (2013).
[46] C.-K. Chiu, H. Yao, and S. Ryu, Phys. Rev. B **88**, 075142 (2013).
[47] P. Jadaun, D. Xiao, Q. Niu, and S. K. Banerjee, Phys. Rev. B **88**, 085110 (2013).
[48] T. Morimoto and A. Furusaki, Phys. Rev. B **88**, 125129 (2013).
[49] J. C. Y. Teo and T. L. Hughes, Phys. Rev. Lett. **111**, 047006 (2013).
[50] W. A. Benalcazar, J. C. Y. Teo, and T. L. Hughes, Phys. Rev. B **89**, 224503 (2014).
[51] X.-J. Liu, J. J. He, and K. T. Law, Phys. Rev. B **90**, 235141 (2014).
[52] A. Alexandradinata, C. Fang, M. J. Gilbert, and B. A. Bernevig, Phys. Rev. Lett. **113**, 116403 (2014).
[53] F. Zhang, C. L. Kane, and E. J. Mele, Phys. Rev. Lett. **111**, 056403 (2013).
[54] R.-J. Slager, A. Mesaros, V. Juricic, and J. Zaanen, Nature Phys. **9**, 98 (2013).
[55] X.-Y. Dong and C.-X. Liu, Phys. Rev. B **93**, 045429 (2016).
[56] J. Kruthoff, J. de Boer, J. van Wezel, C. L. Kane, and R.-J. Slager, Phys. Rev. X **7**, 041069 (2017).
[57] L. Fu and C. L. Kane, Phys. Rev. B **76**, 045302 (2007).
[58] Z. Song, T. Zhang, and C. Fang, Phys. Rev. X **8**, 031069 (2018).
[59] Z. Song, T. Zhang, and C. Fang, Nat. Comm. **9**, 3530 (2018).
[60] T. Zhang, Y. Jiang, Z. Song, H. Huang, Y. He, Z. Fang, H. Weng, and C. Fang, Nature **566**, 475 (2019).
[61] L. P. Gorkov, Soviet Physics JETP **7**, 505 (1958).
[62] P. G. de Gennes, *Superconductivity of Metals and Alloys* (Benjamin (NewYork), 1966).
[63] S. Ono and H. Watanabe, Phys. Rev. B **98**, 115150 (2018).
[64] K. Shiozaki, M. Sato, and K. Gomi, (2018), arXiv:1802.06694.
[65] S. Ono, Y. Yanase, and H. Watanabe, Phys. Rev. Research **1**, 013012 (2019).
[66] A. Skurativska, T. Neupert, and M. H. Fischer, Phys. Rev. Research **2**, 013064 (2020).
[67] S. Ono, H. C. Po, and H. Watanabe, Science Advances **6** (2020), 10.1126/sciadv.aaz8367.
[68] K. Shiozaki, (2019), arXiv:1907.13632.
[69] M. Sigrist and K. Ueda, Rev. Mod. Phys. **63**, 239 (1991).
[70] M. Geier, L. Trifunovic, M. Hoskam, and P. W. Brouwer, Phys. Rev. B **97**, 205135 (2018).
[71] C. J. Bradley, *The mathematical theory of symmetry in solids; representation theory for point groups and space groups* (Clarendon Press, Oxford, 1972).
[72] S. Ryu, A. P. Schnyder, A. Furusaki, and A. W. W. Ludwig, New Journal of Physics **12**, 065010 (2010).
[73] M. Nakahara, *Geometry, Topology and Physics, Second Edition*, Graduate student series in physics (Taylor & Francis, 2003).
[74] M. S. Dresselhaus, G. Dresselhaus, and A. Jorio, *Group theory: application to the physics of condensed matter* (Springer Science & Business Media, 2007).
[75] C. Fang, Y. Chen, H.-Y. Kee, and L. Fu, Phys. Rev. B **92**, 081201 (2015).
[76] J. Ahn, D. Kim, Y. Kim, and B.-J. Yang, Phys. Rev. Lett. **121**, 106403 (2018).
[77] M. Sato, Phys. Rev. B **81**, 220504 (2010).
[78] L. Fu and E. Berg, Phys. Rev. Lett. **105**, 097001 (2010).
[79] L. Trifunovic and P. W. Brouwer, Phys. Rev. B **96**, 195109 (2017).
[80] N. Bultinck, B. A. Bernevig, and M. P. Zaletel, Phys. Rev. B **99**, 125149 (2019).
[81] J. C. Y. Teo and C. L. Kane, Phys. Rev. B **82**, 115120 (2010).

5. CONCLUSION AND OUTLOOK

In Chapters 2 and 3 we have established a link between the bulk topology and the appearance of gapless or ingap anomalous states at boundaries and defects in crystalline topological insulators and superconductors. In particular, in Chapter 2, we have shown that crystalline topological phases may exhibit a *higher-order* bulk boundary correspondence, i.e. they may harbor anomalous states on lower-dimensional manifolds of the boundary such as corners or hinges. An important step in this work was the identification of which configuration of gapless, anomalous boundary states (called the boundary signature) can be related to the bulk topology. We showed that one can distinguish *intrinsic* anomalous boundary signatures that necessitate the presence of a topological bulk, and *extrinsic* anomalous boundary signatures that may result from the presence on lower-dimensional topological phases on the surface of the crystal. The latter have later been discussed also under the name of *boundary-obstructed* topological phases [1]. The work of Chapter 2 has been extended in follow-up projects to general higher-order boundary signatures [2] and general point groups [3].

In Chapter 3 we have discussed in detail the relation between bulk topology and the appearance of anomalous states at disclinations. We have linked which type of topological phase hosts anomalous states at which type of defect, in the following sense: (i) Second-order topological phases protected by rotation symmetry may contribute anomalous states at disclinations. (ii) Weak topological phases protected by rotation symmetry may contribute anomalous states at dislocations or disclinations with a nontrivial translation holonomy. (iii) Tenfold-way topological phases may contribute anomalous states of codimension 2 at defects binding a π-flux, which is the quantized geometric phase acquired by parallel transport of an eigenstate around the defect. (iv) First-order topological phases protected by an unitary internal symmetry $\mathcal{U}$ may contribute anomalous states of codimension 2 at defects binding a $\mathcal{U}$-symmetry flux, which is present if an eigenstate parallel transported around the defect acquires an action of the internal symmetry $\mathcal{U}$. Furthermore, we have found that in some symmetry classes, a prediction of the the anomaly at the disclination solely in terms of the bulk topology is impossible.

This obstruction manifested in terms of a domain wall connected to the disclination, whose microscopic properties may influence the disclination anomaly. In conclusion, this work establishes a link between the characterization of topological phases in terms of their boundary signatures familiar from the K-theoretic classification of topological phases in quadratic fermionic Hamiltonians [4], and the characterization of topological phases in terms of their bulk excitations and response to defects [5, 6].

In Chapter 4 we have shown how to construct symmetry-based indicators for topological Bogoliubov-de Gennes Hamiltonians. The construction consists out of the five steps:

- (i) *Topological band labels BL.* Define the topological band labels in terms of the full classifying group $\mathfrak{K}(\mathbf{k}_\mathrm{s})$ of the matrix-valued Bogoliubov-de Gennes Hamiltonian $H(\mathbf{k}_\mathrm{s})$ at the high symmetry momenta $\mathbf{k}_\mathrm{s}$. The classifying group is defined using a full stable homotopy equivalence classification of the matrices $H(\mathbf{k}_\mathrm{s})$. By using the full classifying group, we ensure to extract the maximal information on the topology of the matrix valued function $H(\mathbf{k})$ that can be extract from evaluation at a set of high symmetry momenta $\mathbf{k}_\mathrm{s}$.

- (ii) *Compatibility relations $\mathcal{C}$.* By identifying the full classifying group $K(\mathbf{k}, d)$ of all general points, lines and planes in the Brillouin zone connecting distinct (sets of) high symmetry momenta, we identify the subgroup of topological band labels that corresponds to gapped Hamiltonians. By omitting the "higher-dimensional" compatibility relations derived from lines and planes, one can derive symmetry-based indicators for topological semimetals and nodal superconductors.

- (iii) *Atomic limits AI.* We construct all atomic limits by using the full classifying group of all high symmetry positions in the unit cell and identify the subgroup of the topological band labels that is spanned by the atomic limits. An atomic limit for superconductors is defined using the Grothendieck construction of pairs of Hamiltonians.

- (iv) *Symmetry-based indicators $SI = BL \cap \mathcal{C}/AI$.* By taking the quotient of the topological band labels consistent with the compatibility relations with the atomic limits, one identifies the band labels that correspond to gapped topological phases that do not correspond to any atomic limit. These topological phases host anomalous boundary states (see Sec. 1.3 of Chapter 1).

- (v) *Identification.* By comparing to a complete classification of topological phases with anomalous boundary states in the given symmetry class, the elements of SI can be identified and topological invariants for the individual topological phases can be formulated.

Steps (i) to (iv) are expected to be implementable in an algorithm as they are an extension of the algorithmic solution in Refs. 7, 8. Step (v) would require an algorithmic classification of topological crystalline phases that at the same time characterizes the corresponding anomalous boundary states in terms of their codimension and protecting crystalline symmetries. Such an algorithm does not yet exist to the knowledge of the author. However, partial algorithmic solutions have been suggested:

Ref. 9 contains an algorithmic construction of time-reversal symmetric topological crystalline insulators in Cartan class AII. Within a reasonable assumption on the entanglement properties of the crystalline topological phase, this construction is expected to be complete. In Chapter 3 we utilized this construction, and suggested how to identify a set of generating phases, the order of the boundary states and the whether the crystalline topological phase is protected by translation symmetry. However, it is not yet clear whether an algorithmic extension of this approach to all Cartan classes is possible, because the solution of Ref. 9 utilized some simplifications that are unique to Cartan class AII. In particular, the existence of zero-dimensional anomalous states in Cartan classes AIII, BDI, D, DIII and CII poses a significant challenge for an algorithmic construction.

Furthermore, Ref. 10 contains an extensive classification of strong topological crystalline insulators and superconductors in general magnetic point groups. This approach is an extension of the methods discussed in the introduction of this thesis. The extension discussed in Ref. 10 is capable of identifying the subgroup of atomic limits as well as the first-order topological phases in the classifying group. However, this approach does not yet incorporate topological phases protected by translational symmetries, but the author of Ref. 10 suggests how this could be approached. Furthermore, it remains to distinguish topological phases with second- and third-order anomalous states on the surface.

Symmetry-based indicators offer a significant reduction in complexity for diagnosing topological phases of matter. The expressions of the resulting criteria in the weak-pairing limit allow to formulate easily accessible criteria for topological superconductivity. The simplest example is the one-dimensional topological superconductor in Cartan class D. In Section V.A. of Chapter 4 we derived that the topological invariant for the $\mathbb{Z}_2$ topological phase can be expressed as the sum of

the Pfaffian invariant at $k = 0$ and $k = \pi$ modulu 2, in agreement with Ref. 11. In the weak pairing limit, see Sec. IV.E of Chapter 4, this invariant is expressed as the difference of the number of occupied bands of the normal-state Hamiltonian at $k = 0$ and $k = \pi$ modulu 2. Therefore, if a normal-state Hamiltonian with an odd number of band crossings between $k = 0$ and $k = \pi$ opens a gap by introducing superconductivity, it turns into a one-dimensional topological superconductor. This criterion reproduces the familiar result for topological superconductivity in multichannel nanowires [12]. Similar lines of argumentation can be employed to reproduce the criteria for topological superconductivity in inversion and time reversal symmetric metals [13, 14, 15].

Outlook

In the following we list open research questions that relate to the results presented in this thesis.

Non-symmorphic symmetries. A symmetry-group is said to be non-symmorphic if it contains point group operations (such as mirror or rotation) only in combination with a translations, but not individually [1] [16]. Open reasearch questions for non-symmorphic space groups that related to the work presented in this thesis are (i) how to obtain a complete classification for all Cartan classes, (ii) how to identify the boundary signatures of non-symmorphic symmetry protected topological phases, (iii) how to extend symmetry-based indicators for Bogoliubov-de Gennes Hamiltonians with non-symmorphic symmetries. A general answer to these questions has been approached for insulators in two and three dimensions, for which a selection of relevant literature is summarized below. To the knowledge of the author of this thesis, a general solution of these problems for superconductors has not been approached.

An extensive K-theoretic classification exists only for crystalline insulators in Cartan class A [17] which contains also a list of topological invariants. For time-reversal symmetric insulators in Cartan class AII, the crystalline topological phases have been constructed using the topological crystal approach in Ref. 9 from which the order of the boundary signatures can be inferred, see Section IV of Chapter 3. The anomalous boundary signatures of non-symmorphic crystalline symmetry protected topological phases have further been discussed in Refs. 18, 19, 20, 21, 22, 23, 24, 25, 26. Symmetry-based indicators have been formulated for insulators

[1] For example, a non-symmorphic rotation symmetry is composed out of a rotation and a translation along the rotation axis. In contrast, in a symmorphic space group, all symmetry operations except translations have a common fixed point.

for all space groups in Refs. 7, 8 and their corresponding anomalous boundary states have been identified [27, 28].

Topological semimetals and nodal superconductors. Topological invariants defined on closed, lower-dimensional manifolds of the Brillouin zone torus may protect nodal points, lines and surfaces in single-particle Hamiltonian [29]. These nodal points and lines may come with associated Fermi arc surface states. The prime example is the Weyl semimetal [30, 31, 32, 33]. Also crystalline symmetries may allow a topological invariant to be defined on a submanifold of the Brillouin zone which may protect nodal points and lines (see our discussion on compatibility relations in Chapter 4). Recently, it has been suggested that these crystalline topological semimetals and nodal superconductors may host higher-order Fermi arcs at hinges of the crystal [34, 35], but an exhaustive discussion of the anomalous surface theories in general Cartan classes has not been done yet. Furthermore, an exhaustive classification of nodal semimetals does not exist yet for general space groups. Ref. 36 contains a discussion on nodal points protected by general wallpaper group symmetries. We note that, our symmetry-based indicators can also be formulated to indicate topological semimetals and nodal superconductors.

Topological phases in the presence of electron-electron interactions. The classification of topological insulators and superconductors in terms of K-theory [4] assumes that the system is described by a free fermionic theory where all electron-electron interactions are captured by an appropriate mean-field theory. An important question in how this classification changes once interactions beyond mean-field theory are taken into account [37, 38]. In many case studies, it was shown that the classification of free fermionic theory with $\mathbb{Z}$ distinct topological phases collapses to a finite abelian group $\mathbb{Z}_n$ [37, 39, 40, 41, 42, 43, 44, 45, 38, 46]. This phenomenon has also been called *symmetric mass generation* [47, 48, 49]. Furthermore, the presence of interactions may allow new topological phases that do not occur in the absence of strong interactions [39, 42, 38, 50], where the most famous example is the fractional quantum Hall effect [51]. General approaches to classifying interacting symmetry-protected topological phases have been developed [6, 52, 5]. Identifying the phenomenology of these strongly interaction phases of matter and finding ways to diagnose them in a given system remains a challenge in current research. Furthermore, even for topological phases that do not require strong interactions, it remains a challenge to find topological invariants that can be efficiently evaluated for a strongly interacting system.

Identification and verification of new topological insulators and superconductors. The final frontier of each theory in the natural sciences is its experimental verification. The tools and concepts that this thesis has refined have been utilized

in many instances to suggest new material realizations of topological insulators which have been subsequently experimentally verified. The search for new topological insulators and topological superconductors is an ongoing quest in current research.

The experimentally verified topological insulators include HgTe/CdTe quantum well structures realizing a quantum spin Hall insulator [53], three dimensional, time reversal symmetric topological insulators in $B_{1-x}Se_x$ [54], B_2Se_3 [55], B_2Te_3 [56], higher-order topological insulating states in SnTe [57] and Bismuth [58] as well as antiferromagnetic topological insulators in $MnBi_2Te_4$ [59].

The identification of topological superconductors poses additional challenges. On the theoretical side, one needs to understand the nature of the superconducting pairing mechanism. For superconductors that admit a description within the Bogoliubov-de Gennes framework, the topology of the Bogoliubov-de Gennes Hamiltonian depends on the superconducting pairing. Furthermore, it is challenging to identify unambiguous signatures of topological superconductors [60]. Signatures consistent with topological superconductivity have been observed in InSb [61, 62, 63] and InAs [64] nanowires proximitized to a s-wave superconductor, a chain of ferromagnetic adatoms on a s-wave superconductor [65], in the doped topological insulators $Cu_xBi_2Se_3$ [66, 14, 67] and $Sn_{1-x}In_xTe$ [68, 67], in the spin-triplet superconductor Sr_2RuO_4 [69] and on the surface of Fe-based superconductors [70].

Bibliography

[1] E. Khalaf, W. A. Benalcazar, T. L. Hughes, and R. Queiroz, (2019), arXiv:1908.00011 .

[2] L. Trifunovic and P. W. Brouwer, Phys. Rev. X **9**, 011012 (2019).

[3] L. Trifunovic and P. W. Brouwer, (2020), arXiv:2003.01144 .

[4] A. Kitaev, AIP Conference Proceedings **1134**, 22 (2009).

[5] R. Thorngren and D. V. Else, Phys. Rev. X **8**, 011040 (2018).

[6] M. Barkeshli, P. Bonderson, M. Cheng, and Z. Wang, Phys. Rev. B **100**, 115147 (2019).

[7] H. C. Po, A. Vishwanath, and H. Watanabe, Nature Communications **8**, 50 (2017).

[8] B. Bradlyn, L. Elcoro, J. Cano, M. G. Vergniory, Z. Wang, C. Felser, M. I. Aroyo, and B. A. Bernevig, Nature **547**, 298 (2017).

[9] Z. Song, S.-J. Huang, Y. Qi, C. Fang, and M. Hermele, Science Advances **5**, eaax2007 (2019).

[10] K. Shiozaki, (2019), arXiv:1907.09354 .
[11] A. Y. Kitaev, Physics-Uspekhi **44**, 131 (2001).
[12] A. C. Potter and P. A. Lee, Phys. Rev. Lett. **105**, 227003 (2010).
[13] M. Sato, Phys. Rev. B **81**, 220504 (2010).
[14] L. Fu and E. Berg, Phys. Rev. Lett. **105**, 097001 (2010).
[15] X.-L. Qi, T. L. Hughes, and S.-C. Zhang, Phys. Rev. B **81**, 134508 (2010).
[16] M. S. Dresselhaus, G. Dresselhaus, and A. Jorio, *Group Theory: Application to the Physics of Condensed Matter*, 1st ed. (Springer-Verlag Berlin Heidelberg, 2008).
[17] K. Shiozaki, M. Sato, and K. Gomi, (2018), arXiv:1802.06694 .
[18] C.-X. Liu, R.-X. Zhang, and B. K. VanLeeuwen, Phys. Rev. B **90**, 085304 (2014).
[19] K. Shiozaki, M. Sato, and K. Gomi, Phys. Rev. B **91**, 155120 (2015).
[20] C. Fang and L. Fu, Phys. Rev. B **91**, 161105 (2015).
[21] D. Varjas, F. de Juan, and Y.-M. Lu, Phys. Rev. B **92**, 195116 (2015).
[22] Q.-Z. Wang and C.-X. Liu, Phys. Rev. B **93**, 020505 (2016).
[23] Z. Wang, A. Alexandradinata, R. J. Cava, and B. A. Bernevig, Nature **532**, 189 (2016).
[24] K. Shiozaki, M. Sato, and K. Gomi, Phys. Rev. B **93**, 195413 (2016).
[25] P.-Y. Chang, O. Erten, and P. Coleman, Nature Physics **13**, 794 (2017).
[26] Y. Liu, Y. Wang, N. C. Hu, J. Y. Lin, C. H. Lee, and X. Zhang, Phys. Rev. B **102**, 035142 (2020).
[27] Z. Song, T. Zhang, Z. Fang, and C. Fang, Nature Communications **9**, 3530 (2018).
[28] E. Khalaf, H. C. Po, A. Vishwanath, and H. Watanabe, Phys. Rev. X **8**, 031070 (2018).
[29] C.-K. Chiu, J. C. Y. Teo, A. P. Schnyder, and S. Ryu, Rev. Mod. Phys. **88**, 035005 (2016).
[30] S. Murakami, New Journal of Physics **9**, 356 (2007).
[31] A. A. Burkov and L. Balents, Phys. Rev. Lett. **107**, 127205 (2011).
[32] A. A. Burkov, M. D. Hook, and L. Balents, Phys. Rev. B **84**, 235126 (2011).
[33] X. Wan, A. M. Turner, A. Vishwanath, and S. Y. Savrasov, Phys. Rev. B **83**, 205101 (2011).
[34] B. J. Wieder, Z. Wang, J. Cano, X. Dai, L. M. Schoop, B. Bradlyn, and B. A. Bernevig, Nature Communications **11**, 627 (2020).
[35] R.-X. Zhang, Y.-T. Hsu, and S. Das Sarma, (2019), arXiv:1909.07980 .
[36] K. Shiozaki, M. Sato, and K. Gomi, Phys. Rev. B **95**, 235425 (2017).
[37] L. Fidkowski and A. Kitaev, Phys. Rev. B **81**, 134509 (2010).
[38] T. Senthil, Annu. Rev. Condens. Matter Phys. **6**, 299 (2015).
[39] Y.-M. Lu and A. Vishwanath, Phys. Rev. B **86**, 125119 (2012).

[40] H. Yao and S. Ryu, Phys. Rev. B **88**, 064507 (2013).
[41] Z.-C. Gu and M. Levin, Phys. Rev. B **89**, 201113 (2014).
[42] C. Wang and T. Senthil, Phys. Rev. B **89**, 195124 (2014).
[43] Y.-Z. You and C. Xu, Phys. Rev. B **90**, 245120 (2014).
[44] T. Yoshida and A. Furusaki, Phys. Rev. B **92**, 085114 (2015).
[45] S. Ryu, Physica Scripta **T164**, 014009 (2015).
[46] X.-Y. Song and A. P. Schnyder, Phys. Rev. B **95**, 195108 (2017).
[47] Y.-Z. You, Y.-C. He, C. Xu, and A. Vishwanath, Phys. Rev. X **8**, 011026 (2018).
[48] P. Boyle Smith and D. Tong, (2020), arXiv:2006.07369 .
[49] D. Tong and C. Turner, SciPost Phys. Lect. Notes , 14 (2020).
[50] M. F. Lapa, J. C. Y. Teo, and T. L. Hughes, Phys. Rev. B **93**, 115131 (2016).
[51] X. G. Wen and Q. Niu, Phys. Rev. B **41**, 9377 (1990).
[52] Q.-R. Wang and Z.-C. Gu, Phys. Rev. X **8**, 011055 (2018).
[53] M. König, S. Wiedmann, C. Brüne, A. Roth, H. Buhmann, L. W. Molenkamp, X.-L. Qi, and S.-C. Zhang, Science **318**, 766 (2007).
[54] D. Hsieh, D. Qian, L. Wray, Y. Xia, Y. S. Hor, R. J. Cava, and M. Z. Hasan, Nature **452**, 970 (2008).
[55] D. Hsieh, Y. Xia, D. Qian, L. Wray, J. H. Dil, F. Meier, J. Osterwalder, L. Patthey, J. G. Checkelsky, N. P. Ong, A. V. Fedorov, H. Lin, A. Bansil, D. Grauer, Y. S. Hor, R. J. Cava, and M. Z. Hasan, Nature **460**, 1101 (2009).
[56] Y. L. Chen, J. G. Analytis, J.-H. Chu, Z. K. Liu, S.-K. Mo, X. L. Qi, H. J. Zhang, D. H. Lu, X. Dai, Z. Fang, S. C. Zhang, I. R. Fischer, Z. Hussain, and Z.-X. Shen, Science **325**, 178 (2009).
[57] F. Schindler, A. M. Cook, M. G. Vergniory, Z. Wang, S. S. P. Parkin, B. A. Bernevig, and T. Neupert, Sci Adv **4**, eaat0346 (2018).
[58] F. Schindler, Z. Wang, M. G. Vergniory, A. M. Cook, A. Murani, S. Sengupta, A. Y. Kasumov, R. Deblock, S. Jeon, I. Drozdov, H. Bouchiat, S. Guéron, A. Yazdani, B. A. Bernevig, and T. Neupert, Nature Physics **14**, 918 (2018).
[59] M. M. Otrokov, I. I. Klimovskikh, H. Bentmann, D. Estyunin, A. Zeugner, Z. S. Aliev, S. Gaß, A. U. B. Wolter, A. V. Koroleva, A. M. Shikin, M. Blanco-Rey, M. Hoffmann, I. P. Rusinov, A. Y. Vyazovskaya, S. V. Eremeev, Y. M. Koroteev, V. M. Kuznetsov, F. Freyse, J. Sánchez-Barriga, I. R. Amiraslanov, M. B. Babanly, N. T. Mamedov, N. A. Abdullayev, V. N. Zverev, A. Alfonsov, V. Kataev, B. Büchner, E. F. Schwier, S. Kumar, A. Kimura, L. Petaccia, G. Di Santo, R. C. Vidal, S. Schatz, K. Kißner, M. Ünzelmann, C. H. Min, S. Moser, T. R. F. Peixoto, F. Reinert, A. Ernst, P. M. Echenique, A. Isaeva, and E. V. Chulkov, Nature **576**, 416 (2019).
[60] R. M. Lutchyn, E. P. A. M. Bakkers, L. P. Kouwenhoven, P. Krogstrup, C. M. Marcus, and Y. Oreg, Nature Reviews Materials **3**, 52 (2018).

[61] V. Mourik, K. Zuo, S. M. Frolov, S. R. Plissard, E. P. A. M. Bakkers, and L. P. Kouwenhoven, Science **336**, 1003 (2012).
[62] M. T. Deng, C. L. Yu, G. Y. Huang, M. Larsson, P. Caroff, and H. Q. Xu, Nano Lett. **12**, 6414 (2012).
[63] L. P. Rokhinson, X. Liu, and J. K. Furdyna, Nature Physics **8**, 795 (2012).
[64] A. Das, Y. Ronen, Y. Most, Y. Oreg, M. Heiblum, and H. Shtrikman, Nature Physics **8**, 887 (2012).
[65] S. Nadj-Perge, I. K. Drozdov, J. Li, H. Chen, S. Jeon, J. Seo, A. H. MacDonald, B. A. Bernevig, and A. Yazdani, Science **346**, 602 (2014).
[66] Y. S. Hor, A. J. Williams, J. G. Checkelsky, P. Roushan, J. Seo, Q. Xu, H. W. Zandbergen, A. Yazdani, N. P. Ong, and R. J. Cava, Phys. Rev. Lett. **104**, 057001 (2010).
[67] M. Sato and Y. Ando, Reports on Progress in Physics **80**, 076501 (2017).
[68] S. Sasaki, Z. Ren, A. A. Taskin, K. Segawa, L. Fu, and Y. Ando, Phys. Rev. Lett. **109**, 217004 (2012).
[69] Y. Maeno, S. Kittaka, T. Nomura, S. Yonezawa, and K. Ishida, J. Phys. Soc. Jpn. **81**, 011009 (2012).
[70] P. Zhang, K. Yaji, T. Hashimoto, Y. Ota, T. Kondo, K. Okazaki, Z. Wang, J. Wen, G. D. Gu, H. Ding, and S. Shin, Science **360**, 182 (2018).

Acknowledgements

I am thankful to Piet Brouwer for an excellent supervision, support and advice during the thesis, for his enthusiasm, and for encouraging me to come forward with my own ideas and collaborate with different groups. A special thanks goes to Luka Trifunovic for many enlightening discussions and for his support and supervision in our collaborative projects. I thank Stefan Ludwig, Jaan Freudenfeld, Ion Cosma Fulga and Alexander Lau for collaborating with me and many illuminating discussions. To all of them I wish to express my gratitude for their trust in me.

Furthermore, I thank the Dahlem Center for Complex Quantum Systems within the Freie Universität Berlin for providing an excellent study and work environment. I wish to thank all the participants of the Dice seminar for our countless discussions. Special thanks goes to Sergio, Björn, "The Obstoffice Markus, Andi and Alex", Laetitia, Christian, Laura, Juani, Max H., Max T., Maxim, Ulrike, Zheng, Tommy, Elina, Flore, Thomas, Kevin, Jonas, David, Jakob, Peter, Larissa, Daniel, Johannes, Felix, Katharina, Ryan and Marek for a good time in and out of the office. Further special thanks go to Felix, Johannes, Jens and Katharina for their scientific advice. I enjoyed working with my bachelor students Max Hoskam, Steve Bartz, Hendrik Timme and Sophia Simon.

I thank the CRC 183 for funding my PhD position and providing an excellent environment for young academic researchers. The CRC 183 opened up the possibility for me to organize a summer school together with Kyrylo Snizkho, Laura Baez and Christopher Max. Special thanks go to Alexander Altland, Martin Zirnbauer, Karsten Flensberg, Mark Rudner, Michele Burrello, Charles Marcus, Raquel Queiroz, Ady Stern, Haim Beidenkopf and Yuval Oreg who left a deep impression on me during many discussions and conferences. I wish to mention in particular Alexander Altland who is the second referee to my thesis and encouraged me at the start of my PhD, and Karsten Flensberg, who opens up an exciting path for me to continue after my PhD.

Furthermore, I wish to thank Andrei Bernevig, Titus Neupert, Shinsei Ryu, Stuart Parkin, Liliana Arrachea and Jörg Schmalian for valuable discussions that left an impression on me. I also wish to thank Tommy Li, Harley Scammell, Julian Ingham, Matthias Hecker and Maxim Breitkreiz for many recent discussions and working with me.

Finally, I thank my family and especially Flavie for their endless support and always being there for me.

A. Appendix to "Second-order topological insulators and superconductors with an order-two crystalline symmetry

A.1. REFLECTION-MATRIX-BASED DIMENSIONAL REDUCTION SCHEME

In this appendix we describe details of the reflection-matrix based dimensional reduction scheme. We first review how this method works in the absence of crystalline symmetry, following the original article by Fulga *et al.*,[1] and then show how to include order-two crystalline symmetries with $d_\parallel < d$, generalizing the analysis of Ref. 2. The reflection-matrix based dimensional reduction scheme leaves $d_\parallel$ unchanged, so that the minimal dimension it can achieve is $d = d_\parallel$. The main text discusses how the reflection-matrix based dimensional reduction scheme can also be applied to second-order topological insulators and superconductors.

A.1.1. Altland-Zirnbauer classes without crystalline symmetries

The key step in the method of Ref. 1 is the construction of a $(d-1)$-dimensional gapped Hamiltonian H_{d-1} for each d dimensional gapped Hamiltonian H_d. The Hamiltonians H_d and H_{d-1} have different symmetries, but the same (strong) topological invariants. Fulga *et al.* show how the Hamiltonian H_{d-1} can be constructed from the reflection matrix r_d if a gapped system with Hamiltonian H_d is attached to an ideal lead with a $(d-1)$-dimensional cross section.

To be specific, following Ref. 1 we consider a d-dimensional gapped insulator with Hamiltonian $H_d(\mathbf{k}) = H_d(\mathbf{k}_\perp, k_d)$, occupying the half space $x_d > 0$ and periodic boundary conditions in the transverse directions, see Fig. A.1. The half space $x_d < 0$ consists of an ideal lead with transverse modes labeled by the $d-1$ dimensional wavevector $\mathbf{k}_\perp$. The amplitudes $a_{\rm out}(\mathbf{k}_\perp)$ and $a_{\rm in}(\mathbf{k}_\perp)$ of outgoing and incoming modes are related by the reflection matrix $r_d(\mathbf{k}_\perp)$,

$$a_{\rm out}(\mathbf{k}_\perp) = r_d(\mathbf{k}_\perp) a_{\rm in}(\mathbf{k}_\perp). \tag{A.1}$$

Since H_d is gapped, $r_d(\mathbf{k}_\perp)$ is unitary. Time-reversal symmetry, particle-hole antisymmetry, or chiral antisymmetry pose additional constraints on $r_d(\mathbf{k}_\perp)$. These follow from the action of these symmetries on the amplitudes $a_{\rm in}$ and $a_{\rm out}$,

$$\begin{aligned} \mathcal{T} a_{\rm in}(\mathbf{k}_\perp) &= Q_\mathcal{T}\, a^*_{\rm out}(-\mathbf{k}_\perp), \\ \mathcal{T} a_{\rm out}(\mathbf{k}_\perp) &= V_\mathcal{T} a^*_{\rm in}(-\mathbf{k}_\perp), \end{aligned} \tag{A.2}$$

$$\begin{aligned} \mathcal{P} a_{\rm in}(\mathbf{k}_\perp) &= V_\mathcal{P}\, a^*_{\rm in}(-\mathbf{k}_\perp), \\ \mathcal{P} a_{\rm out}(\mathbf{k}_\perp) &= Q_\mathcal{P}\, a^*_{\rm out}(-\mathbf{k}_\perp), \end{aligned} \tag{A.3}$$

$$\begin{aligned} \mathcal{C} a_{\rm in}(\mathbf{k}_\perp) &= Q_\mathcal{C}\, a_{\rm out}(\mathbf{k}_\perp), \\ \mathcal{C} a_{\rm out}(\mathbf{k}_\perp) &= V_\mathcal{C}\, a_{\rm in}(\mathbf{k}_\perp), \end{aligned} \tag{A.4}$$

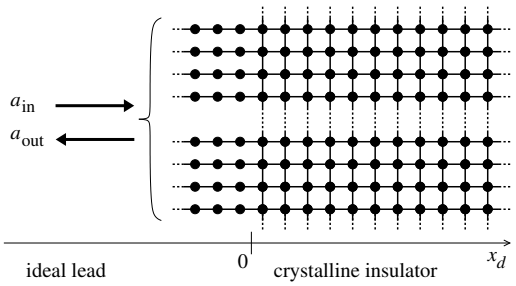

FIG. A.1. Schematic picture of a d-dimensional gapped crystalline insulator occupying the half space $x_d > 0$, with periodic boundary conditions applied along the remaining $(d-1)$-dimension, coupled to an ideal lead with a $(d-1)$-dimensional cross section. The reflection matrix $r_d(\mathbf{k}_\perp)$ relates the amplitudes $a_{\rm out}(\mathbf{k}_\perp)$ and $a_{\rm in}(\mathbf{k}_\perp)$ of outgoing and incoming modes in the lead.

where $V_\mathcal{T}$, $Q_\mathcal{T}$, $V_\mathcal{P}$, $Q_\mathcal{P}$, $V_\mathcal{C}$, and $Q_\mathcal{C}$ are $\mathbf{k}_\perp$-independent unitary matrices that satisfy $V_\mathcal{T} Q^*_\mathcal{T} = Q_\mathcal{T} V^*_\mathcal{T} = \mathcal{T}^2$, $V_\mathcal{P} V^*_\mathcal{P} = Q_\mathcal{P} Q^*_\mathcal{P} = \mathcal{P}^2$, and $Q_\mathcal{C} V_\mathcal{C} = \mathcal{C}^2 = 1$. Systems with both time-reversal symmetry and particle-hole antisymmetry also have a chiral antisymmetry, with $Q_\mathcal{C} = V_\mathcal{P} Q^*_\mathcal{T} = \mathcal{T}^2\mathcal{P}^2 Q_\mathcal{T} Q^*_\mathcal{P}$ and $V_\mathcal{C} = Q_\mathcal{P} V^*_\mathcal{T} = \mathcal{T}^2\mathcal{P}^2 V_\mathcal{T} V^*_\mathcal{P}$. For the reflection matrix $r_d(\mathbf{k}_\perp)$ the presence of time-reversal symmetry, particle-hole antisymmetry, and/or chiral antisymmetry leads to the constraints

$$r_d(\mathbf{k}_\perp) = Q^{\rm T}_\mathcal{T} r_d(-\mathbf{k}_\perp)^{\rm T} V^*_\mathcal{T}, \tag{A.5}$$

$$r_d(\mathbf{k}_\perp) = Q^{\rm T}_\mathcal{P} r_d(-\mathbf{k}_\perp)^{*} V^*_\mathcal{P}, \tag{A.6}$$

$$r_d(\mathbf{k}_\perp) = Q^\dagger_\mathcal{C} r_d(\mathbf{k}_\perp)^\dagger V_\mathcal{C}. \tag{A.7}$$

The effective Hamiltonian H_{d-1} is constructed out of $r_d(\mathbf{k}_\perp)$ in different ways, depending on the presence or absence of chiral symmetry. With chiral symmetry one sets

$$H_{d-1}(\mathbf{k}) \equiv Q_\mathcal{C} r_d(\mathbf{k}), \tag{A.8}$$

using Eq. (A.7) to verify that H_{d-1} is indeed hermitian. (Recall that $V_\mathcal{C} = Q^\dagger_\mathcal{C}$ since $Q_\mathcal{C} V_\mathcal{C} = \mathcal{C}^2 = 1$.) Equation (A.8) simplifies to Eq. (2.9) of the main text if the basis of scattering states is chosen such that $Q_\mathcal{C} = V_\mathcal{C} = 1$. Without chiral symmetry one defines H_{d-1} as

$$H_{d-1}(\mathbf{k}) = \begin{pmatrix} 0 & r_d(\mathbf{k}) \\ r^\dagger_d(\mathbf{k}) & 0 \end{pmatrix}, \tag{A.9}$$

which is manifestly hermitian and satisfies a chiral symmetry with $U_\mathcal{C} = \sigma_3 = \mathrm{diag}\,(1,-1)$. Hence, for the complex classes the dimensional reduction procedure $H_d \to H_{d-1}$ maps a Hamiltonian with chiral symmetry to one without, and vice versa, corresponding to the period-two

sequence

$$\mathrm{A} \xrightarrow{d-1} \mathrm{AIII} \xrightarrow{d-1} \mathrm{A}.$$

Bulk-boundary correspondence implies that the bulk, which is described by the Hamiltonian $H_d(\mathbf{k})$, and the boundary, which determines the reflection matrix $r_d(\mathbf{k}_\perp)$, have the same topological classification. Since $r_d(\mathbf{k}_\perp)$ is in one-to-one correspondence with the Hamiltonian $H_{d-1}(\mathbf{k}_\perp)$, this implies that H_d and H_{d-1} have the same topological classification.

Central point in the construction of Ref. 1 is that if the Hamiltonian H_d possesses an additional antiunitary symmetry and/or antisymmetry, placing it in one of the real Altland-Zirnbauer classes labeled $s = 0, 1, \ldots, 7$, then H_{d-1} possesses an antiunitary symmetry and/or antisymmetry, too, such that it is in Altland Zirnbauer class $s-1$.[1, 2] Hence, for the real Altland-Zirnbauer classes, the reflection-matrix based dimensional reduction scheme generates the period-eight sequence

$$\begin{aligned}\mathrm{CI} \xrightarrow{d-1} \mathrm{C} \xrightarrow{d-1} \mathrm{CII} \xrightarrow{d-1} \mathrm{AII} \xrightarrow{d-1} \mathrm{DIII} \\ \xrightarrow{d-1} \mathrm{D} \xrightarrow{d-1} \mathrm{BDI} \xrightarrow{d-1} \mathrm{AI} \xrightarrow{d-1} \mathrm{CI},\end{aligned} \tag{A.10}$$

which is the well-known period-eight Bott periodicity known from the classification of topological insulators and superconductors.[3–8]

A.1.2. With order-two crystalline symmetries

Bulk-boundary correspondence continues to exist in the presence of an order-two crystalline symmetry with $d_\parallel < d$, if the sample surface is left invariant under the symmetry operation. (For $d_\parallel = d$ there are no such invariant surfaces.) Correspondingly, the reflection-matrix based dimensional reduction scheme may be used in the presence of such crystalline symmetries, too, as was shown for the case of reflection symmetry by two of us in Ref. 2.

Labeling the coordinates as in Sec. 2.2 the coordinate x_d is left invariant by the crystalline symmetry operation $\mathcal{S}$ if $d_\parallel < d$. Hence, taking the same geometry as above, the lead and the lead-crystal interface are mapped to themselves under $\mathcal{S}$. We now discuss the four cases of unitary symmetry, unitary antisymmetry, antiunitary symmetry, and antiunitary antisymmetry separately.

Unitary symmetry.— As with the non-spatial symmetries, the action of a unitary symmetry operation $\mathcal{S}$ on the amplitudes a_{in} and a_{out} of incoming and outgoing states in the leads involves multiplication with $\mathbf{k}_\perp$-independent unitary matrices,

$$\begin{aligned}\mathcal{S}a_{\mathrm{in}}(\mathbf{k}_\perp) &= V_{\mathcal{S}}\, a_{\mathrm{in}}(S\mathbf{k}_\perp), \\ \mathcal{S}a_{\mathrm{out}}(\mathbf{k}_\perp) &= Q_{\mathcal{S}} a_{\mathrm{out}}(S\mathbf{k}_\perp),\end{aligned} \tag{A.11}$$

where $S\mathbf{k}_\perp = (-k_1, \ldots, -k_{d_\parallel}, k_{d_\parallel+1}, \ldots, k_{d-1})$ denotes the action of the symmetry operation on the mode vector $\mathbf{k}$ and the matrices $V_{\mathcal{S}}$ and $Q_{\mathcal{S}}$ satisfy $V_{\mathcal{S}}^2 = Q_{\mathcal{S}}^2 = \mathcal{S}^2 = 1$. The presence of the order-two crystalline symmetry leads to a constraint on the reflection matrix,

$$r_d(\mathbf{k}_\perp) = Q_{\mathcal{S}}^\dagger r_d(S\mathbf{k}_\perp) V_{\mathcal{S}}. \tag{A.12}$$

The algebraic relations involving the matrices $Q_{\mathcal{S}}$, $V_{\mathcal{S}}$ depend on whether the symmetry operation $\mathcal{S}$ commutes or anticommutes with the non-spatial symmetry operations $\mathcal{T}$, $\mathcal{P}$, and $\mathcal{C}$, $Q_{\mathcal{T}} Q_{\mathcal{S}}^* = \eta_{\mathcal{T}} V_{\mathcal{S}} Q_{\mathcal{T}}$, $V_{\mathcal{T}} V_{\mathcal{S}}^* = \eta_{\mathcal{T}} Q_{\mathcal{S}} V_{\mathcal{T}}$, $V_{\mathcal{P}} V_{\mathcal{S}}^* = \eta_{\mathcal{P}} V_{\mathcal{S}} V_{\mathcal{P}}$, $Q_{\mathcal{P}} Q_{\mathcal{S}}^* = \eta_{\mathcal{P}} Q_{\mathcal{S}} Q_{\mathcal{P}}$, $Q_{\mathcal{C}} Q_{\mathcal{S}} = \eta_{\mathcal{C}} V_{\mathcal{S}} Q_{\mathcal{C}}$, and $V_{\mathcal{C}} V_{\mathcal{S}} = \eta_{\mathcal{C}} Q_{\mathcal{S}} V_{\mathcal{C}}$.

Unitary antisymmetry.— An order-two unitary antisymmetry $\mathcal{CS}$ also exchanges incoming and outgoing modes, such that one has

$$\begin{aligned}\mathcal{CS}a_{\mathrm{in}}(\mathbf{k}_\perp) &= Q_{\mathcal{CS}}\, a_{\mathrm{out}}(S\mathbf{k}_\perp), \\ \mathcal{CS}a_{\mathrm{out}}(\mathbf{k}_\perp) &= V_{\mathcal{CS}} a_{\mathrm{in}}(S\mathbf{k}_\perp),\end{aligned} \tag{A.13}$$

with $S\mathbf{k}_\perp$ defined a above. For an antisymmetry operation $\mathcal{CS}$ the matrices $V_{\mathcal{CS}}$ and $Q_{\mathcal{CS}}$ satisfy $V_{\mathcal{CS}} Q_{\mathcal{CS}} = Q_{\mathcal{SC}} V_{\mathcal{CS}} = (\mathcal{CS})^2 = 1$. The presence of the crystalline unitary antisymmetry $\mathcal{CS}$ implies that the reflection matrix satisfies

$$r_d(\mathbf{k}_\perp) = Q_{\mathcal{CS}}^\dagger r_d(S\mathbf{k}_\perp)^\dagger V_{\mathcal{CS}}, \tag{A.14}$$

and the matrices $Q_{\mathcal{CS}}$ and $V_{\mathcal{CS}}$ satisfy the algebraic relations $Q_{\mathcal{T}} V_{\mathcal{CS}}^* = \eta_{\mathcal{T}} Q_{\mathcal{CS}} V_{\mathcal{T}}$, $V_{\mathcal{T}} Q_{\mathcal{CS}}^* = \eta_{\mathcal{T}} V_{\mathcal{CS}} Q_{\mathcal{T}}$, $V_{\mathcal{P}} Q_{\mathcal{CS}}^* = \eta_{\mathcal{P}} Q_{\mathcal{CS}} Q_{\mathcal{P}}$, $Q_{\mathcal{P}} V_{\mathcal{CS}}^* = \eta_{\mathcal{P}} V_{\mathcal{CS}} V_{\mathcal{P}}$, $Q_{\mathcal{CS}} V_{\mathcal{C}} = \eta_{\mathcal{C}} Q_{\mathcal{C}} V_{\mathcal{CS}}$, $V_{\mathcal{CS}} Q_{\mathcal{C}} = \eta_{\mathcal{C}} V_{\mathcal{C}} Q_{\mathcal{CS}}$.

Antiunitary symmetry.— The action of an order-two antiunitary symmetry $\mathcal{T}^\pm\mathcal{S}$ on the scattering amplitudes is represented by unitary matrices $V_{\mathcal{TS}}$ and $Q_{\mathcal{TS}}$,

$$\begin{aligned}\mathcal{TS}a_{\mathrm{in}}(\mathbf{k}_\perp) &= Q_{\mathcal{TS}}\, a_{\mathrm{out}}^*(-S\mathbf{k}_\perp), \\ \mathcal{TS}a_{\mathrm{out}}(\mathbf{k}_\perp) &= V_{\mathcal{TS}} a_{\mathrm{in}}^*(-S\mathbf{k}_\perp),\end{aligned} \tag{A.15}$$

with $V_{\mathcal{TS}} Q_{\mathcal{TS}}^* = Q_{\mathcal{TS}} V_{\mathcal{TS}}^* = (\mathcal{TS})^2 = \pm 1$. The presence of the order-two crystalline antiunitary symmetry leads to a constraint on the reflection matrix,

$$r_d(\mathbf{k}_\perp) = Q_{\mathcal{TS}}^{\mathrm{T}} r_d(-S\mathbf{k}_\perp)^{\mathrm{T}} V_{\mathcal{TS}}^*, \tag{A.16}$$

and the matrices $Q_{\mathcal{TS}}$ and $V_{\mathcal{TS}}$ satisfy the algebraic relations $Q_{\mathcal{T}} V_{\mathcal{TS}}^* = \eta_{\mathcal{T}} Q_{\mathcal{TS}} V_{\mathcal{T}}^*$, $V_{\mathcal{T}} Q_{\mathcal{TS}}^* = \eta_{\mathcal{T}} V_{\mathcal{TS}} Q_{\mathcal{T}}^*$, $V_{\mathcal{P}} Q_{\mathcal{TS}}^* = \eta_{\mathcal{P}} Q_{\mathcal{TS}} Q_{\mathcal{P}}^*$, $Q_{\mathcal{P}} V_{\mathcal{TS}}^* = \eta_{\mathcal{P}} V_{\mathcal{TS}} V_{\mathcal{P}}^*$, $Q_{\mathcal{TS}} V_{\mathcal{C}}^* = \eta_{\mathcal{C}} Q_{\mathcal{C}} V_{\mathcal{TS}}$, $V_{\mathcal{TS}} Q_{\mathcal{C}}^* = \eta_{\mathcal{C}} V_{\mathcal{C}} Q_{\mathcal{TS}}$.

Antiunitary antisymmetry.— Finally, for an antiunitary antisymmetry $\mathcal{P}^\pm\mathcal{S}$ one has

$$\begin{aligned}\mathcal{PS}a_{\mathrm{in}}(\mathbf{k}_\perp) &= V_{\mathcal{PS}}\, a_{\mathrm{in}}^*(-S\mathbf{k}_\perp), \\ \mathcal{PS}a_{\mathrm{out}}(\mathbf{k}_\perp) &= Q_{\mathcal{PS}} a_{\mathrm{out}}^*(-S\mathbf{k}_\perp),\end{aligned} \tag{A.17}$$

with $V_{\mathcal{PS}} V_{\mathcal{PS}}^* = Q_{\mathcal{PS}} Q_{\mathcal{PS}}^* = (\mathcal{PS})^2 = \pm 1$. The reflection matrix satisfies

$$r_d(\mathbf{k}_\perp) = Q_{\mathcal{PS}}^{\mathrm{T}} r_d(-S\mathbf{k}_\perp)^* V_{\mathcal{PS}}^* \tag{A.18}$$

and the algebraic relations involving the matrices $Q_{\mathcal{PS}}$ and $V_{\mathcal{PS}}$ are $Q_{\mathcal{T}} Q_{\mathcal{PS}}^* = \eta_{\mathcal{T}} V_{\mathcal{PS}} Q_{\mathcal{T}}^*$, $V_{\mathcal{T}} V_{\mathcal{PS}}^* = \eta_{\mathcal{T}} Q_{\mathcal{PS}} V_{\mathcal{T}}^*$,

$V_{\mathcal{P}}V^*_{\mathcal{PS}} = \eta_{\mathcal{P}}V_{\mathcal{PS}}V^*_{\mathcal{P}}$, $Q_{\mathcal{P}}Q^*_{\mathcal{PS}} = \eta_{\mathcal{P}}Q_{\mathcal{PS}}Q^*_{\mathcal{P}}$, $Q_{\mathcal{C}}Q_{\mathcal{PS}} = \eta_{\mathcal{C}}V_{\mathcal{PS}}Q^*_{\mathcal{C}}$, and $V_{\mathcal{C}}V_{\mathcal{PS}} = \eta_{\mathcal{C}}Q_{\mathcal{PS}}V^*_{\mathcal{C}}$.

To see how the presence of an order-two crystalline symmetry or antisymmetry affects the dimensional reduction scheme we first consider the complex classes A and AIII. We start from a Hamiltonian in Shiozaki-Sato symmetry class $\mathrm{A}^{\mathcal{S}}$, $(s,t) = (0,0)$, which is represented by a Hamiltonian H_d in symmetry class A with a unitary symmetry $\mathcal{S}$. Constructing a Hamiltonian H_{d-1} in class AIII as described above, we find that the unitary symmetry $\mathcal{S}$ imposes the additional constraint

$$H_{d-1}(\mathbf{k}_\perp) = U^\dagger_{\mathcal{S}}H_{d-1}(S\mathbf{k}_\perp)U_{\mathcal{S}}, \tag{A.19}$$

on H_{d-1}, with

$$U_{\mathcal{S}} = \begin{pmatrix} Q_{\mathcal{S}} & 0 \\ 0 & V_{\mathcal{S}} \end{pmatrix}. \tag{A.20}$$

Since $U_{\mathcal{S}}$ commutes with σ_3 and $U^2_{\mathcal{S}} = 1$, we conclude that dimensional reduction maps the class $\mathrm{A}^{\mathcal{S}}$ to class $\mathrm{AIII}^{\mathcal{S}_+}$. In the classification of Shiozaki and Sato this class is labeled $(s,t) = (1,0)$. Similarly, if H_d is a Hamiltonian in Shiozaki class $(s,t) = (0,1)$, which is represented by a unitary antisymmetry $\mathcal{CS}$, the mapped Hamiltonian H_{d-1} satisfies the additional symmetry

$$U^\dagger_{\mathcal{CS}}H_{d-1}(S\mathbf{k}_\perp)U_{\mathcal{CS}} \tag{A.21}$$

with

$$U_{\mathcal{CS}} = \begin{pmatrix} 0 & V_{\mathcal{CS}} \\ Q_{\mathcal{CS}} & 0 \end{pmatrix}. \tag{A.22}$$

This is a unitary symmetry operation that anticommutes with the chiral operation σ_3, so that the mapped Hamiltonian is in Shiozaki-Sato class $\mathrm{AIII}^{\mathcal{S}_-}$, $(s,t) = (1,1)$. Finally, starting with a Hamiltonian with symmetry of type $(s,t) = (1,t)$, represented by a class AIII Hamiltonian with an order-two crystalline symmetry $\mathcal{S}$ commuting ($\eta_{\mathcal{C}} = 1$) or anticommuting ($\eta_{\mathcal{C}} = -1$) with $\mathcal{C}$ for $t = 0$, 1, respectively, the mapped Hamiltonian satisfies the constraint

$$H_{d-1}(\mathbf{k}_\perp) = \eta_{\mathcal{C}}V^\dagger_{\mathcal{S}}H_{d-1}(S\mathbf{k}_\perp)V_{\mathcal{S}}, \tag{A.23}$$

which is a symmetry of Shiozaki-Sato type $(s,t) = (0,t)$, $t = 0, 1$. (It is a unitary symmetry for $\eta_{\mathcal{C}} = 1$ and an antisymmetry for $\eta_{\mathcal{C}} = -1$.)

A similar procedure can be applied to the remaining complex Shiozaki-Sato classes, which are labeled by a single integer $s = 0, 1, \ldots, 7$. Starting with a Hamiltonian of Shiozaki classes $s = 0$ and $s = 4$ (classes $\mathrm{A}^{\mathcal{T}^+\mathcal{S}}$ and $\mathrm{A}^{\mathcal{T}^-\mathcal{S}}$, antiunitary symmetry $\mathcal{TS}$ squaring to 1 and -1, respectively), we find that the mapped Hamiltonian H_{d-1} satisfies the constraint

$$H_{d-1}(\mathbf{k}_\perp) = U^\dagger_{\mathcal{TS}}H_{d-1}(-S\mathbf{k}_\perp)^*U_{\mathcal{TS}} \tag{A.24}$$

with

$$U_{\mathcal{TS}} = \begin{pmatrix} 0 & V^*_{\mathcal{TS}} \\ Q^*_{\mathcal{TS}} & 0 \end{pmatrix}. \tag{A.25}$$

Hence, H_{d-1} satisfies an antiunitary symmetry that anticommutes with the chiral operation $\mathcal{C}$ and squares to 1 or -1, so that the mapped Hamiltonian is in Shiozaki classes $s = 7$ and $s = 3$, respectively. Similarly, for symmetry classes $s = 2$ and $s = 6$, corresponding to an antiunitary antisymmetry squaring to 1 or -1, respectively, we find that H_{d-1} satisfies the constraint

$$H_{d-1}(\mathbf{k}_\perp) = U^\dagger_{\mathcal{PS}}H_{d-1}(-S\mathbf{k}_\perp)^*U_{\mathcal{PS}} \tag{A.26}$$

with

$$U_{\mathcal{PS}} = \begin{pmatrix} Q^*_{\mathcal{PS}} & 0 \\ 0 & V^*_{\mathcal{PS}} \end{pmatrix}. \tag{A.27}$$

This is an antiunitary symmetry that commutes with the chiral operation and squares to 1 or -1, corresponding to symmetry classes $s = 1$ and $s = 5$, respectively. Finally, for the remaining symmetry classes we may start from an antiunitary symmetry squaring to ± 1 and find that the mapped Hamiltonian satisfies

$$H_{d-1}(\mathbf{k}_\perp) = \eta_{\mathcal{C}}(Q_{\mathcal{C}}V_{\mathcal{TS}})^\dagger H_{d-1}(-S\mathbf{k}_\perp)^*(Q_{\mathcal{C}}V_{\mathcal{TS}}), \tag{A.28}$$

which is an antiunitary symmetry (for $\eta_{\mathcal{C}} = 1$) or antisymmetry (for $\eta_{\mathcal{C}} = -1$) that squares to $\pm\eta_{\mathcal{C}}$, so that under dimensional reduction the class $s = 1$, 3, 5, 7 is mapped to $s = 0$, 2, 4, and 6, respectively.

For the real classes we may proceed in the same way. One finds that under dimensional reduction the Shiozaki-Sato symmetry class (s,t) is mapped to $(s-1,t)$, with s modulo 8. The derivation is identical to that given in Ref. 2 for the case of mirror reflection symmetry.

A.2. CLASSIFICATION OF MIRROR-SYMMETRIC CORNERS OF TWO-DIMENSIONAL CRYSTALS

In this Appendix we explain the origin of the entries in Tables 2.8 – 2.10. Throughout we will use the convention that the chiral operation $\mathcal{C}$ squares to one.

A.2.1. Complex classes with antiunitary symmetries and antisymmetries

Class $A^{\mathcal{T}^+\mathcal{M}}$, $s = 0$.— The topological crystalline phases coincide with the strong topological phases of Altland-Zirnbauer class A. No protected zero-energy corner states can persist in the trivial strong phase.

Class $AIII^{\mathcal{T}^+\mathcal{M}_+}$, $s = 1$.— Since the antiunitary mirror reflection operation $\mathcal{TM}$ commutes with the chiral operation $\mathcal{C}$, corner state have a well-defined parity $\sigma_{\mathcal{C}}$ under $\mathcal{C}$ and can be chosen to be mapped to themselves under the antiunitary mirror reflection operation $\mathcal{TM}$. Two corner states with opposite $\sigma_{\mathcal{C}}$ can be gapped out by a reflection-symmetric mass term, so that we may use the (extrinsic) integer topological index $N = N_+ - N_-$ to characterize the zero-energy states at a corner.

A decoration of the edges by a topologically nontrivial one-dimensional chain leads to the addition of two zero-energy states $|\mathrm{L}\rangle$ and $|\mathrm{R}\rangle = \mathcal{TM}|\mathrm{L}\rangle$ placed symmetrically around the corner as in Fig. 2.8. Since $\mathcal{TM}$ commutes with $\mathcal{C}$, these corner states have the same value of $\sigma_{\mathcal{C}}$. Moreover, the linear combinations $|\mathrm{L}\rangle + |\mathrm{R}\rangle$ and $i(|\mathrm{L}\rangle - |\mathrm{R}\rangle)$ map to themselves under $\mathcal{TM}$, so that they meet the classification criteria for corner states formulated above. Hence, by changing the lattice termination we may change N_+ or N_- and, hence, N, by two. The parity of N remains unchanged under such a change of termination, which corresponds to an intrinsic $\mathbb{Z}_2$ topological index.

If the antiunitary mirror reflection symmetry is broken locally near the corner these conclusions do not change. We may still define $N = N_+ - N_-$ as a topological invariant, which can not change without closing a boundary gap or the bulk gap, and by changing the lattice termination one may still change add pairs of zero modes to the corner, so that $N \mod 2$ is the appropriate invariant if topological equivalence is defined with respect to transformations that possibly close boundary gaps.

Class $A^{\mathcal{P}^+\mathcal{M}}$, $s = 2$.— In this symmetry class the antiunitary reflection antisymmetry $\mathcal{PM}$ may protect a single zero-energy state at a mirror-symmetric corner. A pair of zero-energy states can, however, be gapped out by a mirror-antisymmetric perturbation. To see this, consider two zero modes $|1\rangle$ and $|2\rangle$, for which we may assume that they are both invariant under $\mathcal{PM}$. Then $i(|1\rangle\langle 2| - |2\rangle\langle 1|)$ is a local perturbation that obeys the mirror reflection antisymmetry and gaps out the states $|1\rangle$ and $|2\rangle$. We conclude that a mirror-symmetric corner is described by a $\mathbb{Z}_2$ index.

Class $AIII^{\mathcal{T}^-\mathcal{M}_-}$, $s = 3$.— The bulk phase is always topologically trivial.[9] However, a single pair of corner states can be obtained by symmetrically decorating mirror-related edges with topologically nontrivial one-dimensional chains, as in Fig. 2.8. To see this, denote states $|\mathrm{L}\rangle$ and $|\mathrm{R}\rangle = \mathcal{TM}|\mathrm{L}\rangle$, as in Fig. 2.8. Since $(\mathcal{TM})^2 = -1$ the states $|\mathrm{L}\rangle$ and $|\mathrm{R}\rangle$ form a Kramers pair under the antiunitary mirror reflection operation, $|\mathrm{L}\rangle = -\mathcal{TM}|\mathrm{R}\rangle$. A single such pair of zero-energy states can not be gapped out by a perturbation that respects the antiunitary mirror reflection symmetry.

Class $A^{\mathcal{T}^-\mathcal{M}}$, $s = 4$.— The nontrivial topological crystalline insulator phases in this symmetry class are also strong topological phases, *i.e.,* they have protected edge modes on all edges, not only on mirror-symmetric edges. A second-order topological insulator phase with gapped edges and protected corner states does not exist for this symmetry class.

Class $AIII^{\mathcal{T}^-\mathcal{M}_+}$, $s = 5$.— The bulk phase is topologically trivial.[9] However, (multiple) pairs of corner states can be obtained by symmetrically decorating mirror-related edges with topologically nontrivial one-dimensional chains, as in Fig. 2.8. To see this, denote states $|\mathrm{L}\rangle$ and $|\mathrm{R}\rangle = \mathcal{TM}|\mathrm{L}\rangle$, as in Fig. 2.8. The states $|\mathrm{L}\rangle$ and $|\mathrm{R}\rangle$ have the same parity under the chiral operation $\mathcal{C}$, since the antiunitary mirror reflection operation $\mathcal{TM}$ commutes with $\mathcal{C}$. Antisymmetry of the Hamiltonian under $\mathcal{C}$ protects corner states of equal parity, corresponding to a $2\mathbb{Z}$ topological index.

Class $A^{\mathcal{P}^-\mathcal{M}}$, $s = 6$.— In this symmetry class the bulk phase is topologically trivial. Alternatively, one can see that no protected zero-energy corner states can be consistent with the existence of an antiunitary mirror reflection antisymmetry $\mathcal{PM}$ with $(\mathcal{PM})^2 = -1$: Such corner states would have to appear in pairs $|0\rangle$, $\mathcal{PM}|0\rangle$, which can be gapped out by the mass term $|0\rangle\langle 0|\mathcal{PM} + \mathcal{PM}|0\rangle\langle 0|$, which obeys the required antisymmetry under $\mathcal{PM}$.

Class $AIII^{\mathcal{T}^+\mathcal{M}_-}$, $s = 7$.— This symmetry class is topologically trivial as a bulk phase and no corner states can be obtained by symmetrically decorating mirror-related edges with topologically nontrivial one-dimensional chains. To see, we again denote these end states $|\mathrm{L}\rangle$ and $|\mathrm{R}\rangle = \mathcal{TM}|\mathrm{L}\rangle$, as in Fig. 2.8. The states $|\mathrm{L}\rangle$ and $|\mathrm{R}\rangle$ have opposite parity under the chiral operation $\mathcal{C}$, since the antiunitary mirror reflection operation $\mathcal{TM}$ anticommutes with $\mathcal{C}$. The Hamiltonian $|\mathrm{R}\rangle\langle\mathrm{L}| + |\mathrm{L}\rangle\langle\mathrm{R}|$ anticommutes with $\mathcal{C}$, commutes with $\mathcal{TM}$, and gaps out the zero modes $|\mathrm{L}\rangle$ and $|\mathrm{R}\rangle$.

A.2.2. Real classes

We represent the Shiozaki-Sato classes using unitary mirror reflection symmetries $\mathcal{M}$ or antisymmetries $\mathcal{CM}$ squaring to one.

Class $AI^{\mathcal{M}_+}$, $(s,t) = (0,0)$.— This class has a topologically trivial bulk phase and does not allow for protected corner modes.

Class $BDI^{\mathcal{M}_{++}}$, $(s,t) = (1,0)$.— In a mirror-symmetric corner, corner states can be chosen to have well-defined parities $\sigma_{\mathcal{C}}$ and $\sigma_{\mathcal{M}}$ with respect to the chiral operation $\mathcal{C}$ and mirror reflection $\mathcal{M}$. We use $N_{\sigma_{\mathcal{C}}\sigma_{\mathcal{M}}}$ to denote the number of corner states with the corresponding parities. No mass terms can be added that gap out states with the same parity $\sigma_{\mathcal{C}}$. Local mass terms may gap out pairs of corner states with different $\sigma_{\mathcal{C}}$, but only if they have the same value of $\sigma_{\mathcal{M}}$; corner states with different $\sigma_{\mathcal{C}}$ *and* different $\sigma_{\mathcal{M}}$ are protected. As a result, $N_{++} - N_{-+}$ and $N_{+-} - N_{--}$ are two independent topological invariants describing a mirror-symmetric corner. This gives rise to an extrinsic $\mathbb{Z}^2$ topological index.

Upon changing the lattice termination while preserving the global mirror reflection symmetry, *e.g.*, by "glueing" a topologically nontrivial one-dimensional chain to the crystal edges as in Fig. 2.8, a pair of corner states with the same parity $\sigma_{\mathcal{C}}$ and opposite parities $\sigma_{\mathcal{M}}$ can be added to a corner. Such changes of the lattice termination change the invariants $N_{++} - N_{-+}$ and $N_{+-} - N_{--}$, but leaves their difference $N_{++} - N_{-+} - N_{+-} + N_{--}$ unaffected. Hence, if crystals that differ only by lattice termination are considered equivalent, the relevant topological invariant is $N_{++} - N_{-+} - N_{+-} + N_{--}$, corresponding to an intrinsic $\mathbb{Z}$ topological index.

If mirror reflection symmetry is broken locally at the corner, corner states can be characterized by their parity $\sigma_{\mathcal{C}}$ only. Using $N_{\sigma_{\mathcal{C}}}$ to denote the number of corner states with parity $\sigma_{\mathcal{C}}$, $N_+ - N_-$ is a topological invariant — corresponding to an extrinsic $\mathbb{Z}$ classification —, which is defined modulo 2 only if crystals that differ only lattice termination are considered equivalent.

Class $D^{\mathcal{M}+}$, $(s,t) = (2,0)$.— In this class zero-energy corner states can be chosen to be particle-hole symmetric (*i.e.*, they are Majorana states) and with well-defined parity $\sigma_{\mathcal{M}}$ under mirror reflection $\mathcal{M}$. We use $N_{\sigma_{\mathcal{M}}}$ to denote the number of corner states at parity $\sigma_{\mathcal{M}}$. The numbers N_+ and N_- are defined modulo two only, since two zero modes of the same parity can be gapped out by a mirror-symmetric mass term. This gives an extrinsic $\mathbb{Z}_2^2$ topological classification of mirror-symmetric corners.

A change of lattice termination, *e.g.*, by the addition of topologically nontrivial one-dimensional superconductors on mirror-related edges, adds two zero modes of opposite mirror parity to the corner. This reduces the extrinsic $\mathbb{Z}_2^2$ classification to an intrinsic $\mathbb{Z}_2$ classification in case that crystals differ only by their lattice termination are considered equivalent. Without local mirror reflection symmetry at the corner, any pair of Majorana zero modes can gap out, corresponding to a $\mathbb{Z}_2$ classification.

Class $DIII^{\mathcal{M}++}$, $(s,t) = (3,0)$.— Since particle-hole conjugation $\mathcal{P}$ and time-reversal $\mathcal{T}$ anticommute with the chiral operation $\mathcal{C}$ — recall that we require that $\mathcal{C}^2 = 1$ — zero-energy corner states always appear in Kramers pairs $|0\rangle$ and $\mathcal{T}|0\rangle$, which have opposite parities under $\mathcal{C}$. Since both states of such a Kramers pair have the same mirror parity $\sigma_{\mathcal{M}}$, we may characterize the corner states with the help of the number $N_{\sigma_{\mathcal{M}}}$ of Kramers pairs of corner states of mirror parity $\sigma_{\mathcal{M}}$. Mirror reflection symmetry forbids the gapping out of Kramers pairs at opposite mirror parity $\sigma_{\mathcal{M}}$, but allows two Kramers pairs at same $\sigma_{\mathcal{M}}$ to annihilate. As a result, both N_+ and N_- are defined modulo two only, giving rise to a $\mathbb{Z}_2^2$ topological classification.

A change of lattice termination, *e.g.*, by the addition of topologically nontrivial one-dimensional superconductors on mirror-related edges, adds two Kramers pairs of zero-energy states of opposite mirror parity to the corner, thus reducing the extrinsic $\mathbb{Z}_2^2$ classification to an intrinsic $\mathbb{Z}_2$ classification. Without local mirror reflection symmetry at the corner, any two Kramers pairs of Majorana zero modes can gap out, corresponding to a $\mathbb{Z}_2$ classification.

Class $AII^{\mathcal{M}+}$, $(s,t) = (4,0)$.— This class has a topologically trivial bulk phase and does not allow for protected corner modes.

Class $CII^{\mathcal{M}++}$, $(s,t) = (5,0)$.— For Altland-Zirnbauer class CII the chiral operation $\mathcal{C}$ commutes with particle-conjugation $\mathcal{P}$ and time reversal $\mathcal{T}$, so that a corner hosts Kramers pairs of zero modes at the same parity $\sigma_{\mathcal{C}}$ under the chiral operation $\mathcal{C}$. Both states in such a Kramers pair have the same mirror parity $\sigma_{\mathcal{M}}$, which allows us to count the number $N_{\sigma_{\mathcal{C}},\sigma_{\mathcal{M}}}$ of Kramers pairs with the corresponding parities $\sigma_{\mathcal{C}}$ and $\sigma_{\mathcal{M}}$. Two Kramers pairs with opposite $\sigma_{\mathcal{C}}$ but the same $\sigma_{\mathcal{M}}$ may be gapped by a local mirror reflection-symmetric perturbation to the Hamiltonian, giving rise to integer topological invariants $N_{++} - N_{-+}$ and $N_{+-} - N_{--}$. This corresponds to a $2\mathbb{Z}^2$ extrinsic topological classification.

A change of lattice termination, *e.g.*, by the addition of topologically nontrivial one-dimensional chains on mirror-related edges, adds two Kramers pairs of zero modes of opposite parity $\sigma_{\mathcal{M}}$ to the corner. This leaves $N_{++} - N_{-+} - N_{+-} + N_{--}$ as the only integer invariant, corresponding to a $2\mathbb{Z}$ classification.

Without local mirror reflection symmetry at the corner, Kramers pairs corner states are characterized by their parity $\sigma_{\mathcal{C}}$ only. The difference $N_+ - N_-$ of the number of zero-energy Kramers doublets with the corresponding parities $\sigma_{\mathcal{C}}$ is an integer topological invariant. If crystals that differ only lattice termination are considered equivalent, this difference is defined modulo two only, leading to a $\mathbb{Z}_2$ topological invariant.

Classes $C^{\mathcal{M}+}$, $(s,t) = (6,0)$, *and* $CI^{\mathcal{M}++}$, $(s,t) = (7,0)$.— These classes have a topologically trivial bulk phase and do not allow for protected corner modes.

Class $AI^{\mathcal{CM}-}$, $(s,t) = (0,1)$.— This class has a topologically trivial bulk phase and does not allow for protected corner modes. This conclusion holds despite the presence of a mirror reflection antisymmetry $\mathcal{CM}$. Since $\mathcal{CM}$ anticommutes with the time-reversal operation, corner modes can not be simultaneously eigenstates of $\mathcal{CM}$ and of the time-reversal operation $\mathcal{T}$. Hence, corner modes appear as pairs, which can be chosen such that the two states $|\pm\rangle$ in the pair are invariant under $\mathcal{T}$ and $\mathcal{CM}|\pm\rangle = \pm i|\mp\rangle$. Then the local perturbation $|+\rangle\langle -|+|-\rangle\langle +|$ satisfies time-reversal symmetry and mirror reflection antisymmetry and gaps out these two corner states.

Class $BDI^{\mathcal{M}+-}$, $(s,t) = (1,1)$.— This class has a topologically trivial bulk phase. To see whether stable corner states may be induced by a suitably chosen lattice termination, we consider adding two topologically nontrivial one-dimensional chains in a symmetric fashion to two symmetry-related crystal edges, as in Fig. 2.8. The chains have zero energy end states $|\mathrm{L}\rangle$ and $|\mathrm{R}\rangle = \mathcal{M}|\mathrm{L}\rangle$, which may be chosen to be invariant under time reversal. Since the mirror reflection operation $\mathcal{M}$ anticommutes with $\mathcal{C}$, the states $|\mathrm{L}\rangle$ and $|\mathrm{R}\rangle$ have opposite parity under $\mathcal{C}$. The Hamiltonian $|\mathrm{L}\rangle\langle\mathrm{R}| + |\mathrm{R}\rangle\langle\mathrm{L}|$ is mirror reflection symmetric, satisfies the symmetry constraints of class BDI and gaps out the states $|\mathrm{L}\rangle$ and $|\mathrm{R}\rangle$. We conclude that no stable corner states may be induced on top of an otherwise trivial bulk by suitably adapting the lattice termination.

Class $D^{\mathcal{CM}+}$, $(s,t) = (2,1)$.— Particle-hole symmetric (*i.e.*, Majorana) corner states can be counted according to their parity $\sigma_{\mathcal{CM}}$ under the mirror reflection antisymmetry. Since a pair of corner states $|\pm\rangle$ with opposite parity $\sigma_{\mathcal{CM}}$ can be gapped by the local perturbation $i(|+\rangle\langle -| - |-\rangle\langle +|)$, whereas corner states with equal parity $\sigma_{\mathcal{CM}}$ are protected by the mirror reflection anti-

symmetry, the difference $N_+ - N_-$ of the numbers $N_{\sigma_\mathcal{C}}$ of corner states with parity $\sigma_\mathcal{C}$ is a well-defined topological invariant. This number remains unchanged if one-dimensional topological superconductors are "glued" to mirror-related edges, since this procedure adds a pair of zero-energy states with opposite $\sigma_{\mathcal{CM}}$. We conclude that there is a $\mathbb{Z}$ topological classification.

If the mirror reflection symmetry is broken locally at the corner, any pair of Majorana states can be gapped out by a local perturbation, and one arrives at a $\mathbb{Z}_2$ topological classification.

Class DIII$^{\mathcal{M}-+}$, $(s,t) = (3,1)$.— Since time-reversal $\mathcal{T}$ anticommutes with $\mathcal{C}$, zero-energy corner states appear as Kramers pairs with opposite parity with respect to the chiral operation $\mathcal{C}$. We denote such a Kramers pair as $|+\rangle$ and $|-\rangle = \mathcal{T}|+\rangle$, where the sign $\pm$ refers to the $\mathcal{C}$-eigenvalue. Since mirror reflection $\mathcal{M}$ anticommutes with $\mathcal{C}$, these states can not be chosen to simultaneously be $\mathcal{M}$-eigenstates. However, multiple Kramers pairs of zero modes can always be organized in such a way that $\mathcal{M}$ acts within a single Kramers pair. Since $\mathcal{M}$ anticommutes with $\mathcal{C}$ and $\mathcal{M}^2 = 1$, one has $\mathcal{M}|\pm\rangle = e^{\pm i\phi}|\mp\rangle$, where we may fix the phases of the basis kets $|\pm\rangle$ such that $\phi = 0$. Whereas a single such Kramers pair is topologically protected, two Kramers pairs $|\pm,1\rangle$ and $|\pm,2\rangle$ can be gapped out by the local perturbation $i(|+,1\rangle\langle-,2| - |-,2\rangle\langle+,1| - |+,2\rangle\langle-,1| + |-,1\rangle\langle+,2|)$, which obeys all relevant symmetries. We conclude that the only invariant is the parity of the number of zero-energy Kramers pairs, which gives a $\mathbb{Z}_2$ topological classification.

Class AII$^{\mathcal{CM}-}$, $(s,t) = (4,1)$.— A corner may host Kramers pairs of zero modes, which may also be chosen to have a well-defined parity under the mirror reflection antisymmetry $\mathcal{CM}$. Since $\mathcal{CM}$ anticommutes with time-reversal $\mathcal{T}$, the two states in the Kramers pair have opposite $\mathcal{CM}$-parity. Denoting the two members of a Kramers pair by $|\pm\rangle$, time-reversal symmetry forbids perturbations that have a nonzero matrix element between the states $|+\rangle$ and $|-\rangle$, whereas mirror reflection antisymmetry forbids perturbations that have nonzero matrix elements between $|+\rangle$ and $|+\rangle$ and between $|-\rangle$ and $|-\rangle$. We conclude that a single such Kramers pair is protected by the combination of time-reversal symmetry and mirror reflection antisymmetry. A pair of such Kramers pairs can, however, be gapped out: Denoting the states in the two Kramers pairs by $|\pm,1\rangle$ and $|\pm,2\rangle$, such a pair of Kramers pairs is gapped out by the local perturbation $i(|+,1\rangle\langle-,2| - |-,2\rangle\langle+,1| - |+,2\rangle\langle-,1| + |-,1\rangle\langle+,2|)$. As a result, we find that this class has a $\mathbb{Z}_2$ topological index. If mirror reflection (anti)symmetry is locally broken at the crystal corner, a Kramers pair can obtain a finite energy and no protected zero-energy corner states exist.

Class CII$^{\mathcal{M}+-}$, $(s,t) = (5,1)$.— This class has a topologically trivial bulk phase and does not admit corner states. To see this, note that a mirror reflection operator with $\mathcal{M}^2 = 1$ represents a hermitian operator which satisfies all symmetry requirements for this class: It commutes with time-reversal $\mathcal{T}$ and itself, and anticommutes with particle-hole conjugation $\mathcal{P}$. Hence $\mathcal{M}$ is a valid term in the Hamiltonian, which gaps out any mirror-symmetric configuration of corner states.

Class C$^{\mathcal{CM}+}$, $(s,t) = (6,1)$.— Corner states appear as pairs related by particle-hole conjugation $\mathcal{P}$. Since the mirror reflection antisymmetry $\mathcal{CM}$ commutes with $\mathcal{P}$, the two states in the Kramers pair have the same mirror eigenvalue $\sigma_{\mathcal{CM}}$. Multiple Kramers pairs with the same $\sigma_{\mathcal{CM}}$ can not be gapped out by a mirror reflection-antisymmetric Hamiltonian, but Kramers pairs of opposite parity $\sigma_{\mathcal{CM}}$ may be mutually gapped out by a local mirror reflection-antisymmetric Hamiltonian. (For example, in a representation in which $\mathcal{P} = \sigma_2 K$ and $\mathcal{CM} = \tau_3$, τ_2 gaps out two pairs of Kramers pairs at opposite $\mathcal{CM}$-parity.) We conclude that the difference $N = N_+ - N_-$ between the numbers of Kramers pairs with $\mathcal{CM}$-parity $\sigma_{\mathcal{CM}}$ is a well-defined topological invariant, giving a $\mathbb{Z}$ topological classification. Since Altland-Zirnbauer class C does not allow one-dimensional chains with protected zero-energy end states, this conclusion does not depend on whether freedom of lattice termination plays a role in the topological classification. No corner states can be stabilized in the absence of mirror reflection antisymmetry.

Classes CI$^{\mathcal{M}-+}$, $(s,t) = (7,1)$, and AI$^{\mathcal{M}-}$, $(s,t) = (0,2)$.— These classes have a topologically trivial bulk phase and do not allow for protected corner modes.

Class BDI$^{\mathcal{M}--}$, $(s,t) = (1,2)$.— This class has a topologically trivial bulk phase. To see whether stable corner states may be induced by a suitably chosen lattice termination, we consider adding two topologically nontrivial one-dimensional chains in a symmetric fashion to two symmetry-related crystal edges, as in Fig. 2.8. The chains have zero energy end states $|\mathrm{L}\rangle$ and $|\mathrm{R}\rangle = \mathcal{M}|\mathrm{L}\rangle$, which may be chosen to be invariant under time reversal and particle-hole conjugation. Since the mirror reflection operation $\mathcal{M}$ commutes with $\mathcal{C}$, the states $|\mathrm{L}\rangle$ and $|\mathrm{R}\rangle$ have equal parity $\sigma_\mathcal{C}$ under $\mathcal{C}$. Taking symmetric and antisymmetric linear combinations of the states $|\mathrm{L}\rangle$ and $|\mathrm{R}\rangle$, one obtains a corner state doublet with opposite parity under $\mathcal{M}$, but equal $\sigma_\mathcal{C}$. Multiple doublets of this type with the same $\sigma_\mathcal{C}$ cannot be gapped out by a local perturbation, whereas two corner state doublets with opposite $\sigma_\mathcal{C}$ can. Hence, $N_+ - N_-$ is a valid integer topological invariant, where $N_{\sigma_\mathcal{C}}$ is the number of zero-energy doublets of $\mathcal{C}$-parity $\sigma_\mathcal{C}$.

Class D$^{\mathcal{M}-}$, $(s,t) = (2,2)$.— This class has a topologically trivial bulk phase. No zero-energy corner states can be induced by a suitably chosen lattice termination. To see this, we consider a mirror reflection symmetry $\mathcal{M}$ that squares to one, so that $\mathcal{M}$ is represented by a hermitian operator. Since $\mathcal{M}$ anticommutes with particle-hole conjugation $\mathcal{P}$, $\mathcal{M}$ is itself a valid perturbation to the Hamiltonian which gaps out any set of corner states.

Class DIII$^{\mathcal{M}--}$, $(s,t) = (3,2)$.— Since $\mathcal{T}^2 = -1$ and $\mathcal{T}$ anticommutes with $\mathcal{C}$, corner modes consist of Kramers

Majorana pairs of opposite parity under the chiral operation $\mathcal{C}$. Since the product $\mathcal{MC}$ commutes with the time-reversal operation $\mathcal{T}$ and with the chiral operation $\mathcal{C}$, both states in a Kramers pair have the same "mixed parity" $\sigma_{\mathcal{MC}}$ under $\mathcal{MC}$. Two Kramers pairs of equal mixed parity $\sigma_{\mathcal{MC}}$ can not be gapped out by a mirror-symmetric perturbation, since $\mathcal{MC}$ anticommutes with the Hamiltonian. Two Kramers pairs of opposite mixed parity $\sigma_{\mathcal{MC}}$ can be gapped out by a local perturbation satisfying $\mathcal{T}$ and $\mathcal{M}$ symmetries and $\mathcal{C}$ antisymmetry. (For example, the two Kramers pairs $|\sigma_{\mathcal{MC}}, \sigma_{\mathcal{C}}\rangle$ with $\sigma_{\mathcal{MC}}$ and $\sigma_{\mathcal{C}} = \pm$ and $|\sigma_{\mathcal{MC}}, -\rangle = \mathcal{T}|\sigma_{\mathcal{MC}}, +\rangle$, are gapped out by the perturbation $|+,+\rangle\langle -,-| + |-,-\rangle\langle +,+| - |+,-\rangle\langle -,+| - |-,+\rangle|+,-\rangle$.) Denoting the number of zero-energy Kramers pairs with mixed parity $\sigma_{\mathcal{MC}}$ by $N_{\sigma_{\mathcal{MC}}}$, we thus find that $N_+ - N_-$ is a valid integer topological invariant. This invariant can not be changed by changing the lattice termination, since addition of two one-dimensional topological superconductors on mirror-related crystal edges as in Fig. 2.8 leads to the addition of two Kramers doublets with opposite mixed parities $\sigma_{\mathcal{MC}}$. If the mirror symmetry is broken locally at the corner, any pair of Majorana Kramers doublets can gap out, and the $\mathbb{Z}$ topological classification is reduced to a $\mathbb{Z}_2$ classification.

Class $AII^{\mathcal{M}--}$, $(s,t) = (4,2)$.— The bulk crystalline phase is a strong topological phase, and no stable zero-energy states can be induced by a suitably chosen lattice termination in the trivial bulk phase.

Class $CII^{\mathcal{M}--}$, $(s,t) = (5,2)$.— Corners allow Kramers doublets with equal $\mathcal{C}$ parity $\sigma_{\mathcal{C}}$ but opposite $\mathcal{M}$ parity $\sigma_{\mathcal{M}}$. Two doublets at the same $\mathcal{C}$-parity $\sigma_{\mathcal{C}}$ can not be gapped out, but two doublets with opposite $\mathcal{C}$ can. (For example, the two Kramers doublets $|\sigma_{\mathcal{C}}, \sigma_{\mathcal{M}}\rangle$ with $\sigma_{\mathcal{C}}$ and $\sigma_{\mathcal{M}} = \pm$ and $|\sigma_{\mathcal{C}}, -\rangle = \mathcal{T}|\sigma_{\mathcal{C},+}\rangle$, are gapped out by the perturbation $|+,+\rangle\langle -,+| + |-,+\rangle\langle +,+| + |-,-\rangle\langle +,-| + |+,-\rangle|-,-\rangle$.) Denoting the number of Kramers pairs with $\mathcal{C}$-parity $\sigma_{\mathcal{C}}$ by $N_{\sigma_{\mathcal{C}}}$, we thus find that $N_+ - N_-$ is a well-defined integer topological invariant.

A change of lattice termination, *e.g.*, by the addition of topologically nontrivial one-dimensional chains on mirror-related edges, adds two Kramers pairs of zero modes of the same parity $\sigma_{\mathcal{C}}$ to the corner. Taking symmetric and antisymmetric linear combinations these can be reorganized into two Kramers pairs $|\sigma_{\mathcal{C}}, \pm\rangle$ of the type discussed above. Since changing the lattice termination allows one to change $N_+ - N_-$ by an even number, it is only the modulo two part if this invariant which is determined by the bulk band structure. The above analysis does not change if the mirror reflection symmetry is broken locally at the corner.

Class $C^{\mathcal{M}-}$, $(s,t) = (6,2)$.— This class has a topologically trivial bulk phase and does not allow for protected corner modes.

Class $CI^{\mathcal{M}--}$, $(s,t) = (7,2)$.— Corner states appear in doublets related by particle-hole conjugation $\mathcal{P}$. Such doublets have opposite parity under the chiral operation, since $\mathcal{P}$ and the chiral operation $\mathcal{C}$ anticommute for this class. The product $\mathcal{MC}$ commutes with $\mathcal{P}$ and $\mathcal{C}$, so that both states in a doublet have the same mixed parity $\sigma_{\mathcal{MC}}$ under $\mathcal{MC}$. Two doublets of equal mixed parity $\sigma_{\mathcal{MC}}$ can not be gapped out by a mirror-symmetric perturbation, since $\mathcal{MC}$ anticommutes with the Hamiltonian. Two doublets of opposite mixed parity $\sigma_{\mathcal{MC}}$ can be gapped out by a local perturbation satisfying $\mathcal{M}$ symmetry and $\mathcal{P}$ and $\mathcal{C}$ antisymmetries. (For example, the two doublets $|\sigma_{\mathcal{MC}}, \sigma_{\mathcal{C}}\rangle$ with $\sigma_{\mathcal{MC}}$ and $\sigma_{\mathcal{C}} = \pm$ and $|\sigma_{\mathcal{MC}}, -\rangle = \mathcal{P}|\sigma_{\mathcal{MC}}, +\rangle$, are gapped out by the perturbation $|+,+\rangle\langle -,-| + |-,-\rangle\langle +,+| + |+,-\rangle\langle -,+| + |-,+\rangle|+,-\rangle$.) Denoting the number of zero-energy Kramers pairs with mixed parity $\sigma_{\mathcal{MC}}$ by $N_{\sigma_{\mathcal{MC}}}$, we thus find that $N_+ - N_-$ is a valid integer topological invariant. This invariant can not by changed by changing the lattice termination, since the Altland-Zirnbauer class CI does not allow a nontrivial one-dimensional phase with protected end states.

Class $AI^{\mathcal{CM}+}$, $(s,t) = (0,3)$.— The mirror reflection antisymmetry $\mathcal{CM}$ allows for the protection of corner states at a mirror-symmetric corner. Corner states can be chosen to be real and with well-defined parity $\sigma_{\mathcal{CM}}$ under mirror reflection. Corner states of equal parity can not be gapped out because of the mirror reflection antisymmetry; corner states with opposite parity can be gapped out. Hence $N = N_+ - N_-$ is an appropriate topological invariant, with $N_{\sigma_{\mathcal{CM}}}$ the number of corner states with $\mathcal{CM}$-parity $\sigma_{\mathcal{CM}}$.

Class $BDI^{\mathcal{M}-+}$, $(s,t) = (1,3)$.— This class has a trivial bulk phase. To see whether stable corner states may be induced by a suitably chosen lattice termination, we consider adding two topologically nontrivial one-dimensional chains in a symmetric fashion to two symmetry-related crystal edges, as in Fig. 2.8. The chains have zero energy end states $|\mathrm{L}\rangle$ and $|\mathrm{R}\rangle = \mathcal{M}|\mathrm{L}\rangle$, which may be chosen to be invariant under particle-hole conjugation since the mirror reflection operation $\mathcal{M}$ commutes with particle-hole conjugation $\mathcal{P}$. A pair of zero-energy states $|\mathrm{L},\mathrm{R}\rangle$ is protected by the combination of $\mathcal{P}$ antisymmetry and $\mathcal{M}$ symmetry. Two such doublets $|\mathrm{L},\mathrm{R},1\rangle$ and $|\mathrm{L},\mathrm{R},2\rangle$, however, can be gapped out by the local perturbation $i(|\mathrm{L},1\rangle\langle\mathrm{R},2| - |\mathrm{R},2\rangle\langle\mathrm{L},1| - |\mathrm{L},2\rangle\langle\mathrm{R},1| + |\mathrm{R},1\rangle\langle\mathrm{L},2|)$, which obeys $\mathcal{P}$ and $\mathcal{C}$ antisymmetries and $\mathcal{M}$ symmetry. We conclude that the only invariant is the parity of the number of such zero-energy doublets, which gives a $\mathbb{Z}_2$ topological classification. If mirror reflection symmetry is broken locally at the corner, the $\mathcal{M}$-induced protection of a single doublet disappears, and even a single doublet of zero-energy corner states can be gapped out.

Class $D^{\mathcal{CM}-}$, $(s,t) = (2,3)$.— This class is a strong topological phase, which has doublets of chiral Majorana modes at edges. A single chiral Majorana mode is not compatible with the symmetries, since such mode would have to be invariant under $\mathcal{P}$ and $\mathcal{CM}$, which is not possible since $\mathcal{P}$ and $\mathcal{CM}$ anticommute. Nevertheless, by a suitable choice of lattice termination, a protected pair of Majorana zero modes can be localized at a mirror-

symmetric corner in the topologically trivial bulk phase. To see this we consider adding two one-dimensional superconductors with Majorana end states $|\mathrm{L}\rangle$ and $|\mathrm{R}\rangle$ to mirror-related crystal edges of an otherwise topologically trivial bulk crystal, as in Fig. 2.8. The end states $|\mathrm{L},\mathrm{R}\rangle$ are chosen invariant under particle-hole conjugation $\mathcal{P}$. Since $\mathcal{CM}$ anticommutes with $\mathcal{P}$ we have $|\mathrm{R}\rangle = i\mathcal{CM}|\mathrm{L}\rangle$. A zero-energy doublet $|\mathrm{L},\mathrm{R}\rangle$ is then protected by the combination of $\mathcal{CM}$ and $\mathcal{P}$ antisymmetries. Two such doublets, however, can be gapped out by a local perturbation, which results in a $\mathbb{Z}_2$ topological classification.

Class DIII$^{\mathcal{M}_{+-}}$, $(s,t) = (3,3)$.— This class has a trivial bulk phase and cannot host protected corner states. (In a representation in which $\mathcal{M}^2 = 1$ the mirror reflection operation $\mathcal{M}$ is represented by a hermitian operator, which satisfies $\mathcal{P}$ antisymmetry and $\mathcal{T}$ symmetry and gaps out any set of zero-energy states localized at the corner.)

Class AII$^{\mathcal{CM}_{+}}$, $(s,t) = (4,3)$.— This class allows mirror-protected zero-energy Kramers pairs at corners. Since the mirror reflection antisymmetry $\mathcal{CM}$ commutes with the time-reversal operator $\mathcal{T}$, such Kramers pairs have the same parity $\sigma_{\mathcal{CM}}$ under mirror reflection. Reflection antisymmetry protects zero-energy Kramers pairs with equal parity $\sigma_{\mathcal{CM}}$, but allows the mutual gapping out of Kramers pairs with opposite $\sigma_{\mathcal{CM}}$. Hence, $N = N_+ - N_-$ is a valid integer topological index for this class, with $N_{\sigma_{\mathcal{CM}}}$ the number of zero-energy corner states with $\mathcal{CM}$ parity $\sigma_{\mathcal{CM}}$.

Class CII$^{\mathcal{M}_{-+}}$, $(s,t) = (5,3)$.— This class has a topologically trivial bulk phase, and does not allow protected zero-energy states at corners. To see this, we consider the addition of two topologically nontrivial one-dimensional chains in a symmetric fashion to two symmetry-related crystal edges, as in Fig. 2.8. We denote the doublets at the two chains by $|\mathrm{L}\rangle$, $|\mathrm{L}'\rangle = \mathcal{P}|\mathrm{L}\rangle$, $|\mathrm{R}\rangle = \mathcal{M}|\mathrm{L}\rangle$ and $|\mathrm{R}'\rangle = \mathcal{P}|\mathrm{R}\rangle = \mathcal{PM}|\mathrm{L}\rangle$. Since $\mathcal{M}$ anticommutes with $\mathcal{C}$, doublets at the ends of the left and right chains have opposite parity under the chiral operation $\mathcal{C}$. These four states can be gapped out by the perturbation $i(|\mathrm{L}\rangle\langle\mathrm{R}'| - |\mathrm{R}'\rangle\langle\mathrm{L}| + |\mathrm{R}\rangle\langle\mathrm{L}'| - |\mathrm{L}'\rangle\langle\mathrm{R}|)$.

Class C$^{\mathcal{CM}_{-}}$, $(s,t) = (6,3)$.— This class is a strong topological phase, which has chiral modes at edges. No corner modes can be constructed in the trivial bulk phase, because the Altland-Zirnbauer class C is topologically trivial in one dimension.

Class CI$^{\mathcal{M}_{+-}}$, $(s,t) = (7,3)$.— This class is topologically trivial and does not allow for protected zero-energy corner states.

A.3. EDGE-TO-CORNER CORRESPONDENCE FOR TWO-DIMENSIONAL MIRROR-SYMMETRIC CRYSTALS

A nontrivial mirror-symmetric topological crystalline bulk phase implies the existence of protected gapless states on mirror-symmetric edges. If the topological crystalline insulator or superconductor is not in a strong topological phase, these edge states can be gapped out for edges that are not invariant under the mirror operation. In that case protected zero-energy states remain at mirror-symmetric corners. The main text discusses this scenario in detail for the complex Altland-Zirnbauer classes with unitary mirror symmetries and antisymmetries. In this appendix we give details for the complex classes with antiunitary mirror symmetries and antisymmetries and for the real Altland-Zirnbauer classes. For completeness, we repeat the discussion of those mirror-symmetric topological phases that were already contained in Ref. 10.

Throughout this appendix we will use x as a coordinate along a mirror-symmetric edge, see Fig. 2.9a, or along an edge that is symmetrically deformed from a mirror-symmetric edge, with a mirror-symmetric corner located at $x = 0$, see Fig. 2.9b, Further, v is a constant with the dimension of velocity, and we use σ_j, τ_j, $j = 0,1,2,3$ to refer to Pauli matrices acting on different spinor degrees of freedom, and $\mathbb{1}_N$ to denote the $N \times N$ unit matrix. Edge Hamiltonians are always given in the simplest possible form, after a suitable basis transformation and after rescaling of energies and coordinates.

A.3.1. Complex Altland-Zirnbauer classes with antiunitary symmetries and antisymmetries

Class A$^{\mathcal{T}^+\mathcal{M}}$, $s = 0$.— Representing $\mathcal{TM}$ by complex conjugation K, this phase allows chiral edge modes with Hamiltonian $H_{\mathrm{edge}} = -iv\mathbb{1}_N\partial_x$. This is a strong topological phase, which does not allow localized zero-energy states at corners.

Class AIII$^{\mathcal{T}^+\mathcal{M}_{+}}$, $s = 1$.— We represent the chiral operation $\mathcal{C}$ using $U_{\mathcal{C}} = \sigma_3$ and the antiunitary mirror reflection operation using $U_{\mathcal{TM}} = 1$, so that the bulk Hamiltonian $H(k_x,k_y)$ satisfies the constraints $H(k_x,k_y) = -\sigma_3 H(k_x,k_y)\sigma_3 = H^*(k_x,k_y)$. A nontrivial mirror-symmetric edge is described by the edge Hamiltonian

$$H_{\mathrm{edge}} = -iv\sigma_1\partial_x. \tag{A.29}$$

This edge allows a unique mass term $m\sigma_2$, which is odd under $\mathcal{TM}$. The intersection of two mirror-related edges represents a domain wall with respect to such a mass term and hosts a protected zero-energy mode. The chiral parity $\sigma_{\mathcal{C}}$ of such a corner state depends on the sign of m far away from the corner, such that $\sigma_{\mathcal{C}}$ is negative if $m(x)$ is positive for $x \to \infty$. The $\mathbb{Z}$ (extrinsic) classification of corner states follows from the observation that corner states at equal parity $\sigma_{\mathcal{C}}$ can not mutually gap out.

Class A$^{\mathcal{P}^+\mathcal{M}}$, $s = 2$.— We represent the antiunitary mirror antisymmetry $\mathcal{PM}$ by complex conjugation K, so that $H(k_x,k_y) = -H^*(k_x,-k_y)$. The edge Hamiltonian at a mirror-symmetric edge is

$$H_{\mathrm{edge}} = -iv\sigma_2\partial_x. \tag{A.30}$$

Upon deforming the edge away symmetrically around a corner at $x = 0$, two mass terms $m_1(x)\sigma_1 + m_2(x)\sigma_3$ are allowed, with $m_{1,2}(x) = -m_{1,2}(-x)$. Such a Hamiltonian hosts a zero mode symmetrically located around the corner at $x = 0$. A mirror-symmetry-breaking perturbation near $x = 0$ can however push this state away from zero energy.

Class $A^{\mathcal{T}^-\mathcal{M}}$, $s = 2$.— We represent $\mathcal{TM}$ by $\sigma_2 K$, where K is complex conjugation. A mirror-symmetric edge can host multiple Kramers pairs of chiral modes, described by the edge Hamiltonian $H_{\text{edge}} = -iv\sigma_0 \mathbb{1}_N \partial_x$. This is a strong topological phase which does not allow for localized states at corners.

A.3.2. Real classes

Class $BDI^{\mathcal{M}_{++}}$, $(s,t) = (1,0)$.— We use $U_{\mathcal{T}} = 1$, $U_{\mathcal{P}} = \sigma_3$, $U_{\mathcal{C}} = \sigma_3$, and $U_{\mathcal{M}} = \sigma_3\tau_3$ to represent time-reversal, particle-hole conjugation, chiral operation, and mirror reflection. The integer topological invariant N for class $\text{BDI}^{\mathcal{M}_{++}}$ counts the difference of the number of helical edge states with positive and negative mixed parity $\sigma_{\mathcal{MC}}$ at zero energy. For a minimal mirror-invariant edge with $N \geq 0$, all edge states have the same (positive) mixed parity, so that effectively we may set $U_{\mathcal{M}} = \sigma_3$. With a suitable choice of basis and after rescaling the edge Hamiltonian takes the form

$$H_{\text{edge}} = -iv\sigma_2 \mathbb{1}_N \partial_x. \tag{A.31}$$

The unique mass term $m\sigma_1$, with m a $N \times N$ hermitian matrix, is odd under reflection. The intersection of two mirror-related edges represents a domain wall with respect to such a mass term and hosts N protected zero-energy modes. The parity $\sigma_{\mathcal{C}}$ of these modes depends on the sign of the eigenvalues of the matrix $m(x)$ away from the corner at $x = 0$, such that a positive eigenvalue for $x \to \infty$ corresponds to a corner state with positive $\sigma_{\mathcal{C}}$. This reproduces the $\mathbb{Z}^2$ (extrinsic) classification of corner states derived in App. A.2.

Class $D^{\mathcal{M}_+}$, $(s,t) = (2,0)$.— We choose the unitary matrices $U_{\mathcal{P}} = 1$ and $U_{\mathcal{M}} = \sigma_1$ to represent particle-hole conjugation and mirror reflection. The bulk topological crystalline phase has a $\mathbb{Z}_2$ classification, for which the nontrivial phase has counterpropagating edge modes at a mirror-symmetric edge described by the edge Hamiltonian $H_{\text{edge}} = -iv\sigma_3\partial_x$. This edge Hamiltonian has a unique mass term $m\sigma_2$. The intersection between two mirror-related edges represents a domain wall and hosts a localized zero-energy state. The mirror parity $\sigma_{\mathcal{M}}$ depends on the sign of m far away from the corner at $x = 0$, such that a positive value of m for $x \to \infty$ corresponds to a positive mirror parity $\sigma_{\mathcal{M}}$. Since no matrix elements may exist between two corner state with opposite mirror parity $\sigma_{\mathcal{M}}$, this reproduces the $\mathbb{Z}_2^2$ (extrinsic) classification of corner states derived in App. A.2.

Class $DIII^{\mathcal{M}_{++}}$, $(s,t) = (3,0)$.— We set $U_{\mathcal{T}} = \sigma_2$, $U_{\mathcal{P}} = 1$, and $U_{\mathcal{M}} = \sigma_2\tau_2$. With a suitable choice of basis, a mirror-invariant edge in the nontrivial topological crystalline phase has a pair of counter-propagating Majorana modes with Hamiltonian

$$H_{\text{edge}} = -iv\sigma_3\tau_0\partial_x. \tag{A.32}$$

The unique mass term $m\sigma_1\tau_2$ is odd under $\mathcal{M}$. As a result, intersection between two mirror-related edges represents a domain wall and hosts a Kramers pair localized zero-energy states. The mirror parity $\sigma_{\mathcal{M}}$ depends on the sign of m far away from the corner at $x = 0$. The $\mathbb{Z}_2^2$ (extrinsic) classification of corner states derived in App. A.2 follows upon noting that no matrix elements may exist between two corner state with opposite mirror parity $\sigma_{\mathcal{M}}$.

Class $CII^{\mathcal{M}_{++}}$, $(s,t) = (5,0)$.— We set $U_{\mathcal{T}} = \sigma_2$, $\mathcal{U}_{\text{P}} = \sigma_2\tau_3$, so that $U_{\mathcal{C}} = \tau_3$. The $2\mathbb{Z}$ bulk classification of this symmetry class counts the difference N of "edge quartets" with positive and negative "mixed parity" $\sigma_{\mathcal{CM}}$. For a minimal edge all edge modes have the same mixed parity, so that effectively $\mathcal{M}$ may be represented by $U_{\mathcal{M}} = \tau_3$. A minimal edge has Hamiltonian

$$H_{\text{edge}} = -iv\partial_x\sigma_0\tau_2\mathbb{1}_N. \tag{A.33}$$

The unique mass term gapping out such edge modes is $m\tau_1$, with m a real symmetric $N \times N$ matrix. This mass term is odd under mirror reflection, ensuring the existence of N Kramers pairs of corner states at the intersection between two mirror-related edges. Both states in such a Kramers pair have the same parity $\sigma_{\mathcal{C}}$, which is determined by the sign of the eigenvalues of m far away from the corner at $x = 0$. This corresponds to the $2\mathbb{Z}^2$ (extrinsic) classification of corner states derived in Sec. A.2.

Class $D^{\mathcal{CM}_+}$, $(s,t) = (2,1)$.— We represent particle-hole conjugation $\mathcal{P}$ by complex conjugation and the mirror antisymmetry $\mathcal{CM}$ by $U_{\mathcal{CM}} = \sigma_3$. We use $N_{\text{L}\sigma_{\mathcal{CM}}}$ and $N_{\text{R}\sigma_{\mathcal{CM}}}$ to denote the numbers of left-moving and right-moving edge modes with mirror parity $\sigma_{\mathcal{M}}$ at zero energy, respectively. Since edge modes moving in opposite directions and with opposite mirror parity can mutually gap out, the differences $N_{\text{R}+} - N_{\text{L}-}$ and $N_{\text{R}-} - N_{\text{L}+}$ are topological invariants, giving a $\mathbb{Z}^2$ classification of edge states. The sum $N_{\text{R}+} - N_{\text{L}-} + N_{\text{R}-} - N_{\text{L}+}$ is a strong topological invariant. For a second-order topological superconductor phase, we are interested in the case $N_{\text{R}+} - N_{\text{L}-} + N_{\text{R}-} - N_{\text{R}+} = 0$, a minimal realization of which has $N_{\text{L}-} = N_{\text{R}-} = 0$ and $N = N_{\text{R}+} = N_{\text{L}+}$. With a suitable choice of basis and after rescaling, the corresponding edge Hamiltonian reads

$$H_{\text{edge}} = -iv\tau_3\mathbb{1}_N\partial_x, \tag{A.34}$$

where τ_3 is a Pauli matrix in the left mover–right mover basis. The unique mass term $m\tau_2$ is odd under the mirror antisymmetry, so that the intersection between two mirror-related edges hosts N Majorana corner states. All N corner states have the same mirror parity, so that no

further classification is possible. This is consistent with the $\mathbb{Z}$ (extrinsic) classification derived in App. A.2.

Class DIII$^{\mathcal{M}-+}$, $(s,t)=(3,1)$.— Here we choose the representations $U_{\mathcal{T}}=\sigma_2$ and $U_{\mathcal{P}}=\sigma_1$, so that $U_{\mathcal{C}}=\sigma_3$. Although in the most general case the representation of $\mathcal{M}$ requires the introduction of additional spinor degrees of freedom, the generators for the nontrivial topological phases can be constructed using the simpler representation $U_{\mathcal{M}}=\sigma_1$. The two generators of the $\mathbb{Z}_2^2$ topological crystalline classification have edge Hamiltonians $H_{\text{edge},1}=-iv\sigma_2\partial_x$ and $H_{\text{edge},2}=-iv\sigma_2\tau_3\partial_x$. The former edge Hamiltonian represents a strong topological phase and is not compatible with a second-order topological phase. The latter edge Hamiltonian has a unique mass term $m\sigma_2\tau_2$, which is odd under mirror reflection. As a result, the intersection of two mirror-related edges hosts a Kramers pair of Majorana zero modes.

Class AII$^{\mathcal{CM}-}$, $(s,t)=(4,1)$.— We represent $\mathcal{T}$ by σ_2K and $\mathcal{CM}$ by σ_3. The two generators of the $\mathbb{Z}_2^2$ topological crystalline classification have edge Hamiltonians $H_{\text{edge},1}=-iv\sigma_3\partial_x$ and $H_{\text{edge},2}=-iv\tau_2\sigma_0\partial_x$, where x is the coordinate along the mirror-symmetric edge and the Pauli matrix τ_2 acts on a separate spinor degree of freedom. The former edge Hamiltonian $H_{\text{edge},1}$ describes a strong phase in which the edge state is protected by time-reversal symmetry alone and can not be gapped out. The latter Hamiltonian $H_{\text{edge},2}$ has two mass terms $m_1\tau_1\sigma_0+m_2\tau_3\sigma_0$, which are both odd under mirror reflection. Such a Hamiltonian hosts a zero mode symmetrically located around a mirror-symmetric corner at $x=0$. A local perturbation near the corner at $x=0$ that breaks the mirror symmetry can move this state away from zero energy.

Class C$^{\mathcal{CM}+}$, $(s,t)=(6,1)$.— We set $U_{\mathcal{P}}=\sigma_2$. This phase allows a strong topological phase with doublets of particle-hole conjugated co-propagating chiral edge modes. Pairs of counterpropagating doublets are prevented from mutually gapping out if they have the same parity under $\mathcal{CM}$. Hence, within the relevant subspace we may represent $\mathcal{CM}$ by the identity, $U_{\mathcal{CM}}=1$. The edge Hamiltonian for N such pairs of counterpropagating doublets reads

$$H_{\text{edge}}=-iv\sigma_1\tau_2\partial_x\mathbb{1}_N, \tag{A.35}$$

where τ_2 is a Pauli matrix acting on a different spinor degree of freedom than the σ matrices. Upon deforming the edge away symmetrically around a corner at $x=0$, four mass terms $m_1(x)\rho_0\sigma_2+m_2(x)\rho_0\sigma_3+m_3(x)\sigma_1\rho_1+m_4(x)\sigma_1\rho_3$ are allowed under a global reflection symmetry, with $m_j(x)=-m_j(-x)$, $j=1,2,3,4$. Such a Hamiltonian hosts N doublets of zero modes symmetrically located around the corner at $x=0$.

Class DIII$^{\mathcal{M}--}$, $(s,t)=(3,2)$.— We choose the representations $U_{\mathcal{T}}=\sigma_2$ and $U_{\mathcal{P}}=\sigma_1$, so that $U_{\mathcal{C}}=\sigma_3$. The $\mathbb{Z}$ bulk topological invariant N is the difference of the numbers of helical edge doublets with positive and negative "mixed parity" $\sigma_{\mathcal{MC}}$. For a "minimal" edge with $N\geq 0$ all modes have the same (positive) mixed parity and we may represent $U_{\mathcal{M}}=\sigma_3$. Only topological crystalline phases with an even number N of pairs of helical modes can be used for the construction of a second-order topological insulator, since a single helical Majorana mode corresponds to a strong topological phase. With a suitable rescaling and basis choice, an edge with N pairs of helical modes is described by the edge Hamiltonian

$$H_{\text{edge}}=-iv\sigma_1\tau_3\mathbb{1}_{N/2}\partial_x. \tag{A.36}$$

This edge Hamiltonian has the unique mass term $m\tau_2\sigma_1$, where m is a real symmetric $N/2\times N/2$ matrix. The mass term is odd under mirror reflection, ensuring the existence of $N/2$ Majorana Kramers pairs at a mirror-symmetric corner.

Class AII$^{\mathcal{M}-}$, $(s,t)=(4,2)$.— We represent time-reversal and mirror symmetry using $U_{\mathcal{T}}=\sigma_2$ and $U_{\mathcal{M}}=\sigma_3$, respectively. The bulk has a $\mathbb{Z}_2$ topological crystalline classification, the generator of which has edge Hamiltonian $H_{\text{edge}}=-iv\sigma_3\partial_x$, with x a coordinate along a mirror symmetric edge. This is a strong topological phase.

Class CII$^{\mathcal{M}--}$, $(s,t)=(5,2)$.— We choose $U_{\mathcal{T}}=\sigma_2$, $\mathcal{U}_{\text{P}}=\sigma_2\tau_3$, and $U_{\mathcal{M}}=\sigma_3$. With a suitable choice of basis, the nontrivial topological crystalline phase has edge Hamiltonian

$$H_{\text{edge}}=-iv\sigma_1\tau_1\partial_x. \tag{A.37}$$

The unique mass term $m\sigma_1\tau_2$ for this Hamiltonian is odd under mirror reflection, ensuring the existence of a Kramers pair of zero-energy states at a mirror-symmetric corner. A pair of corner states has a well defined parity $\sigma_{\mathcal{C}}$ with respect to the chiral operation $\mathcal{C}$, which depends on the asymptotic sign of the mass m far away from the corner. Multiple corner doublets with the same $\sigma_{\mathcal{C}}$ cannot gap out, consistent with the $2\mathbb{Z}$ (extrinsic) classification of corner states derived in App. A.2.

Class CI$^{\mathcal{M}--}$, $(s,t)=(7,2)$.— We represent $\mathcal{T}$ by σ_1K, $\mathcal{P}$ by σ_2K, so that $U_{\mathcal{C}}=\sigma_3$. An edge allows multiple pairs of counterpropagating states with support on orbitals with the same parity under the product $\mathcal{MC}$, so one may represent $\mathcal{M}$ by $U_{\mathcal{M}}=\sigma_3$ on a minimal edge. With a suitable basis transformation and after rescaling, an edge with N such pairs of counterpropagating modes is described by the edge Hamiltonian

$$H_{\text{edge}}=-iv\sigma_1\tau_2\partial_x\mathbb{1}_N, \tag{A.38}$$

where τ_2 is a Pauli matrix acting on an additional spinor degree of freedom. Upon deforming the edge away symmetrically around a corner at $x=0$, three mass terms $m_1(x)\sigma_1\tau_1+m_2(x)\sigma_2+m_3(x)\sigma_1\tau_3$ are allowed under a global reflection symmetry, with m_i real symmetric matrices satisfying $m_i(x)=-m_i(-x)$, $i=1,2,3$. Such a Hamiltonian hosts $2N$ zero-energy Majorana states symmetrically located around the corner at $x=0$.

Class AI$^{\mathcal{CM}+}$, $(s,t)=(0,3)$.— We represent $\mathcal{T}$ by complex conjugation K. An edge allows multiple pairs of counterpropagating states with support on orbitals with

the same mirror parity, so that we may represent the mirror antisymmetry $\mathcal{CM}$ using $U_{\mathcal{CM}} = 1$ for a minimal edge. The corresponding edge Hamiltonian reads

$$H_{\text{edge}} = -iv\tau_2\partial_x \mathbb{1}_N, \tag{A.39}$$

where τ_2 is a Pauli matrix acting on an additional spinor degree of freedom. Upon deforming the edge away symmetrically around a corner at $x = 0$, two mass terms $m_1(x)\tau_1 + m_2(x)\tau_3$ are allowed under a global reflection symmetry, with m_1 and m_2 real symmetric matrices satisfying $m_1(x) = -m_1(-x)$ and $m_2(x) = -m_2(-x)$. Such a Hamiltonian hosts N zero modes symmetrically located around the corner at $x = 0$.

Class $D^{\mathcal{CM}_-}$, $(s,t) = (2,3)$.— We choose $U_{\mathcal{P}} = 1$ and $U_{\mathcal{CM}} = \sigma_2$. These symmetries allow a chiral edge Hamiltonian $H_{\text{edge}} = -iv\sigma_0\mathbb{1}_N\partial_x$, with x a coordinate along the edge and $\mathbb{1}_N$ the $N \times N$ identity matrix. Such an edge represents a strong topological phase.

Class $AII^{\mathcal{CM}_+}$, $(s,t) = (4,3)$.— We represent $\mathcal{T}$ by $\sigma_2 K$. An edge allows multiple pairs of helical modes with support on orbitals with the same $\mathcal{CM}$ parity, so that we may represent $\mathcal{CM}$ using $U_{\mathcal{CM}} = 1$ for a minimal model. An insulator with an odd number of such helical edge modes is a strong topological insulator. With a suitable choice of basis, a "minimal" edge with an even number N of helical modes is described by the edge Hamiltonian

$$H_{\text{edge}} = -iv\sigma_1\tau_0\partial_x \mathbb{1}_N/2, \tag{A.40}$$

where τ_0 the 2×2 identity matrix acting an additional spinor degrees of freedom. Upon deforming the edge away symmetrically around a corner at $x = 0$, two mass terms $m_1(x)\tau_2\sigma_2 + m_2(x)\tau_2\sigma_3$ are allowed under a global reflection symmetry, with m_1 and m_2 real symmetric $N/2 \times N/2$ matrices satisfying $m_1(x) = -m_1(-x)$ and $m_2(x) = -m_2(-x)$. Such a Hamiltonian hosts $N/2$ Kramers pairs of zero modes symmetrically located around the corner at $x = 0$.

Class $C^{\mathcal{CM}_-}$, $(s,t) = (6,3)$.— We set $U_{\mathcal{P}} = \sigma_2$ and $U_{\mathcal{CM}} = \sigma_3$. An edge allows multiple pairs of chiral modes, described by the edge Hamiltonian $H_{\text{edge}} = -iv\sigma_1\mathbb{1}_N\partial_x$, where x is a coordinate along the edge and $\mathbb{1}_N$ the $N \times N$ identity matrix. This is a strong topological phase.

A.4. SURFACE-TO-HINGE CORRESPONDENCE WITH TWOFOLD ROTATION SYMMETRY

In this appendix we give details for the surface-to-hinge correspondence for topological crystalline insulators and superconductors with twofold rotation symmetry or antisymmetry and with mirror symmetry or antisymmetry, starting from a symmetry characterization of the gapless surface states on symmetry-invariant surfaces. The general idea underlying the surface-to-hinge correspondence is the same as for edge-to-corner correspondence with mirror-symmetric edges and corners, see Sec. 2.4.2 and App. A.3. The low-energy theory of the surface states is given in terms of one or multiple Dirac cones that are compatible with the non-spatial and spatial symmetries of the corresponding Shiozaki-Sato class.[9] Tilting the surface away from the invariant direction, as in Fig. 2.11, allows for mass terms which must be odd under twofold rotation or mirror reflection — because otherwise they would be allowed for the symmetry-invariant surface orientation. If the mass term is unique, the intersection of surfaces with opposite sign of the mass constitutes a domain wall, hosting a gapless hinge state. If the mass term is not unique, a mirror-symmetric hinge will still host a gapless mode, but there is no protection for gapless hinge modes in the rotation-symmetric case.

Throughout this appendix, x and y are coordinates on a (eventually tilted) rotation-invariant or mirror-symmetric surface, where the mirror reflections sends $x \to -x$, $\mathbb{1}_N$ is the $N \times N$ unit matrix, and σ_i, τ_i, ρ_i, and μ_i, $i = 0,1,2,3$, are Pauli matrices acting on different spinor degrees of freedom. We will restrict our discussion to symmetry classes with a nontrivial bulk topological crystalline phase, see Ref. 9 and Tables 2.6 and 2.7.

A.4.1. Complex classes with antiunitary symmetries and antisymmetries

Classes $A^{\mathcal{T}^+\mathcal{R}}$, $s = 0$, *and* $A^{\mathcal{P}^+\mathcal{M}}$, $s = 2$.— We choose $U_{\mathcal{TR}} = \sigma_1$ and $U_{\mathcal{PM}} = \sigma_3$ to represent the magnetic point group symmetry $\mathcal{TR}$ and mirror antisymmetry $\mathcal{PM}$, respectively. These symmetries can protect a single gapless surface state with a Dirac-like dispersion $H_{\text{surface}} = -iv(\sigma_1\partial_x + \sigma_2\partial_y)$ (with a suitable choice of basis). The unique mass term $m\sigma_3$ is odd under $\mathcal{TR}$ and $\mathcal{PM}$. A hinge at the intersection of crystal surfaces with opposite signs of m host a gapless hinge mode.

Classes $AIII^{\mathcal{T}^+\mathcal{R}_+}$, $s = 1$, *and* $AIII^{\mathcal{T}^-\mathcal{M}_-}$, $s = 3$.— We choose $U_{\mathcal{C}} = \sigma_3$, $U_{\mathcal{TR}} = 1$, $U_{\mathcal{TM}} = \sigma_2\tau_3$. The nontrivial phase hosts a pair of Dirac cones with dispersion $H_{\text{surface}} = -iv\sigma_1(\tau_1\partial_x + \tau_3\partial_y)$ (with a suitable choice of basis). There are two mass terms that may gap the Dirac cones if the surface is tilted away from the invariant direction, $m_1\sigma_2\tau_0 + m_2\sigma_1\tau_2$, where both m_1 and m_2 must change sign upon shifting to the rotated/mirror-reflected tilt direction. With two mass terms, there is a protected hinge mode at a mirror-symmetric hinge, but not generically in the presence of the twofold rotation symmetry $\mathcal{TR}$.

Classes $AIII^{\mathcal{T}^-\mathcal{R}_-}$, $s = 3$ *and* $AIII^{\mathcal{T}^-\mathcal{M}_+}$, $s = 5$.— We use $U_{\mathcal{C}} = \sigma_3$, $U_{\mathcal{TR}} = \sigma_2$, $U_{\mathcal{TM}} = \sigma_3\tau_2$ to represent the operations $\mathcal{C}$, $\mathcal{TR}$, and $\mathcal{TM}$, respectively. The twofold rotation symmetry is compatible with pairs of Dirac cones with dispersion $\propto -iv\tau_2(\sigma_1\partial_x \pm \sigma_2\partial_y)$, which defines the chirality $\pm$. The $2\mathbb{Z}$ bulk topological crystalline index for this symmetry class counts the difference $N = N_+ - N_-$ of such Dirac cones with positive and negative chirality. For a "minimal" surface all surface Dirac cones have the same chirality, so that after rescal-

ing and with suitable choice of basis the surface Hamiltonian reads $H_{\text{surface}} = -iv\tau_2(\sigma_1\partial_x + \sigma_2\partial_y)\mathbb{1}_N$. Since such surface states are protected by chiral antisymmetry alone, this represents a strong topological phase.

Classes AIII$^{\mathcal{T}^+\mathcal{R}_-}$, $s = 7$, and AIII$^{\mathcal{T}^+\mathcal{M}_+}$, $s = 1$.— Like the previous case, this is a strong phase, with gapless surface states on all surfaces. We choose $U_{\mathcal{C}} = \sigma_3$, $U_{\mathcal{TR}} = \sigma_1$ and $U_{\mathcal{M}} = 1$. The integer bulk topological crystalline index counts the difference $N = N_+ - N_-$ of surface Dirac cones with dispersion $\propto -iv(\partial_x\sigma_1 \pm \partial_y\sigma_2)$. For a "minimal" surface all surface Dirac cones have the same chirality, so that after rescaling and with suitable choice of basis the surface Hamiltonian reads $H_{\text{surface}} = -iv(\partial_x\sigma_1 + \partial_y\sigma_2)\mathbb{1}_N$. Such surface states are protected by chiral antisymmetry alone.

A.4.2. Real classes

Classes BDI$^{\mathcal{R}_{++}}$, $(s,t) = (1,0)$, and BDI$^{\mathcal{M}_{-+}}$, $(s,t) = (1,3)$.— We represent time-reversal and particle-hole conjugation using $U_{\mathcal{T}} = \sigma_0$, $U_{\mathcal{P}} = \sigma_3$, $U_{\mathcal{C}} = \sigma_3$, $U_{\mathcal{R}} = \sigma_3\rho_3$, and $U_{\mathcal{M}} = \sigma_2$. A symmetry-invariant surface may host multiple pairs of Dirac cones with dispersion $\propto -iv(\sigma_1\tau_2\partial_x \pm \sigma_2\tau_0\partial_y)$, which defines the "mirror chirality" $\pm$ for class BDI$^{\mathcal{M}_{-+}}$. The integer invariant N counts the number of such pairs of Dirac cones, weighted by the parity under $\mathcal{RC}$ (for class BDI$^{\mathcal{R}_{++}}$) or by mirror chirality (for class BDI$^{\mathcal{M}_{-+}}$). A minimal surface with $N \geq 0$ has pairs of Dirac cones of the same mirror chirality or the same $\mathcal{RC}$-parity, so that effectively we may use $U_{\mathcal{R}} = \sigma_3$ to represent $\mathcal{R}$. The corresponding surface Hamiltonian is

$$H_{\text{surface}} = -iv(\sigma_1\tau_2\partial_x + \sigma_2\tau_0\partial_y)\mathbb{1}_N. \tag{A.41}$$

Two mass terms $m_1\sigma_1\tau_1 + m_2\sigma_1\tau_3$, with m_1 and m_2 $N \times N$ real symmetric matrices, are allowed upon tilting the surface away from the symmetry-invariant orientation. These mass terms are odd under $\mathcal{R}$ and $\mathcal{M}$. Since there are two such mass terms, there are no protected hinge modes for the rotation-symmetric case. However, there are protected hinge modes at mirror-symmetric hinges in the mirror-symmetric case.

Classes DIII$^{\mathcal{R}_{++}}$, $(s,t) = (3,0)$, and DIII$^{\mathcal{M}_{+-}}$, $(s,t) = (3,3)$.— We set $U_{\mathcal{T}} = \sigma_2$, $U_{\mathcal{P}} = \sigma_1$, $U_{\mathcal{M}} = \sigma_1\tau_2$, and $U_{\mathcal{R}} = \tau_3$. Without rotation or mirror symmetry, there are protected surface states with dispersion $-iv(\sigma_1\partial_x \pm \sigma_2\partial_y)$, which defines the chirality $\pm$. The integer topological invariant N counts the number of such surface Dirac cones, weighted by the chirality. One such Dirac cone is not compatible with $\mathcal{R}$ or $\mathcal{M}$ symmetry on a symmetry-invariant surface, but two Dirac cones with the same chirality are, the dispersion for a pair of Dirac cones being $-iv\tau_1(\sigma_1\partial_x \pm \sigma_2\partial_y)$. Since they have the same chirality, such a pair of Dirac cones is protected by $\mathcal{T}$ and $\mathcal{P}$ alone. A phase with multiple such pairs of Dirac cones is a strong topological phase with gapless surface states for surfaces of arbitrary orientation.

Classes CII$^{\mathcal{R}_{++}}$, $(s,t) = (5,0)$, and CII$^{\mathcal{M}_{-+}}$, $(s,t) = (5,3)$.— We let time-reversal be represented by $U_{\mathcal{T}} = i\sigma_2$ and particle-hole by $U_{\mathcal{P}} = i\sigma_2\tau_3$, so that $U_{\mathcal{C}} = \tau_3$. We further set $U_{\mathcal{M}} = \tau_3$ and $U_{\mathcal{R}} = \tau_3\rho_3$. A symmetry-invariant surface admits pairs of gapless surface states with Dirac-like dispersion $\propto -i(\sigma_0\tau_2\partial_x \pm \sigma_1\tau_1\partial_y)$, which defines the mirror chirality $\pm$ for class CII$^{\mathcal{M}_{-+}}$. The integer invariant N counts the number of such pairs of Dirac cones, weighted by the parity under $\mathcal{RC}$ (for class CII$^{\mathcal{R}_{++}}$) or by mirror chirality (for class CII$^{\mathcal{M}_{-+}}$). A minimal surface with $N \geq 0$ has pairs of Dirac cones of the same mirror chirality or the same $\mathcal{RC}$-parity, so that effectively we may use $U_{\mathcal{R}} = \tau_3$ to represent $\mathcal{R}$. A single pair of Dirac cones is protected by $\mathcal{T}$ and $\mathcal{P}$ symmetry alone, corresponding to a strong topological phase with gapless surface states on all surfaces. A purely crystalline phase requires an even number N of pairs of surface Dirac cones, so that the corresponding surface Hamiltonian is

$$H_{\text{surface}} = -iv(\tau_1\sigma_1\partial_x + \tau_2\sigma_0\partial_y)\mu_0\mathbb{1}_{N/2}. \tag{A.42}$$

Such a Hamiltonian admits two mass terms $m_1\tau_1\sigma_2\mu_2 + m_2\tau_1\sigma_3\mu_2$, where m_1 and m_2 are $N/2 \times N/2$ real symmetric matrices, which change sign under mirror reflection and twofold rotation. Since there are two mass terms, the rotation-symmetric class CII$^{\mathcal{R}_{++}}$ does not have protected hinge modes, whereas the mirror-symmetric class CII$^{\mathcal{M}_{-+}}$ has protected gapless modes at mirror-symmetric hinges.

Classes CI$^{\mathcal{R}_{++}}$, $(s,t) = (7,0)$, and CI$^{\mathcal{M}_{+-}}$, $(s,t) = (7,3)$.— We set $U_{\mathcal{T}} = \sigma_1$ and $U_{\mathcal{P}} = \sigma_2$, so that $U_{\mathcal{C}} = \sigma_3$. We further set $U_{\mathcal{R}} = \tau_3$ and $U_{\mathcal{M}} = \sigma_1\tau_3$. A symmetry-invariant surface admits surface states with dispersion $-i\tau_2(\sigma_1\partial_x \pm \sigma_2\partial_y)$, where $\pm$ defines the chirality. The integer invariant counts the number of such pairs of surface Dirac cones, weighted by chirality. Since such pairs of surface Dirac cones do not rely on crystalline symmetries for their protection this is a strong phase, which has gapless surface states on surfaces of arbitrary orientation.

Classes D$^{\mathcal{CR}_+}$, $(s,t) = (2,2)$, and D$^{\mathcal{M}_+}$, $(s,t) = (2,1)$.— We set $U_{\mathcal{P}} = 1$, $U_{\mathcal{CR}} = \tau_3$, and $U_{\mathcal{M}} = \sigma_3$. A symmetry-invariant surface admits surface states with dispersion $\propto -i(\sigma_1\partial_x \pm \sigma_3\partial_y)$, which defines the mirror chirality $\pm$ (for class D$^{\mathcal{M}_+}$). This class has an integer topological invariant N, which counts the differences of the number of Dirac cones with positive and negative $\mathcal{CR}$-parity at zero energy or mirror chirality, as appropriate. On a minimal surface with $N \geq 0$ all surface Dirac cones have the same mirror chirality or $\mathcal{CR}$-parity, so that we may effectively represent $\mathcal{CR}$ by $U_{\mathcal{CR}} = 1$. The corresponding surface Hamiltonian reads

$$H_{\text{surface}} = -iv(\sigma_1\partial_x + \sigma_3\partial_y)\mathbb{1}_N. \tag{A.43}$$

Such a surface admits a unique mass term $\sigma_2 m$, with m an $N \times N$ real symmetric matrix, which changes sign under mirror reflection or under the rotation antisymmetry. Correspondingly, a mirror-symmetric hinge admits gapless modes. With twofold rotation antisymmetry, gapless hinge modes are guaranteed to exist if N is odd.

Classes DIII$^{\mathcal{R}-+}$, $(s,t) = (3,1)$, and DIII$^{\mathcal{M}++}$, $(s,t) = (3,0)$.— We set $U_{\mathcal{T}} = \sigma_2$ and $U_{\mathcal{P}} = \sigma_1$, so that $U_{\mathcal{C}} = \sigma_3$, $U_{\mathcal{R}} = \sigma_1\tau_3$, $U_{\mathcal{M}} = \tau_3$. The crystalline bulk phase has a $\mathbb{Z}_2$ topological classification, for which the nontrivial phase has a surface state with Hamiltonian

$$H_{\text{surface}} = -iv(\sigma_1\tau_1\partial_x + \sigma_2\tau_0\partial_y) \tag{A.44}$$

at a symmetry-invariant surface. There is a unique mass term $m\sigma_1\tau_2$, which is odd under twofold rotation and under mirror reflection. We conclude that the conditions for the existence of gapless hinge modes are met.

Classes AII$^{\mathcal{CR}-}$, $(s,t) = (4,1)$ and AII$^{\mathcal{M}+}$, $(s,t) = (4,0)$.— For a minimal model we choose $U_{\mathcal{T}} = \sigma_2$, $U_{\mathcal{CR}} = \sigma_1$, and $U_{\mathcal{M}} = \tau_3$. The crystalline bulk phase has a $\mathbb{Z}_2$ topological classification, for which the nontrivial phase has a surface state with Hamiltonian

$$H_{\text{surface}} = -iv\sigma_1(\tau_1\partial_x + \tau_3\partial_y) \tag{A.45}$$

The model admits a unique mass term $m\sigma_1\tau_2$, which changes sign under the twofold rotation antisymmetry operation and under mirror reflection. Correspondingly, this model admits a helical gapless hinge mode.

Classes C$^{\mathcal{CR}+}$, $(s,t) = (6,1)$ and C$^{\mathcal{M}+}$, $(s,t) = (6,0)$.— We set $U_{\mathcal{P}} = \sigma_2$, $U_{\mathcal{CR}} = \rho_3$, and $U_{\mathcal{M}} = \tau_2\sigma_3$. The surface admits pairs of surface states with a dispersion $-iv\tau_2(\sigma_1\partial_x \pm \sigma_3\partial_y)$, which defines the mirror chirality (for class C$^{\mathcal{M}+}$). The integer topological invariant N for class C$^{\mathcal{CR}+}$ counts the difference of the number of surface Dirac cones with $\mathcal{CR}$-eigenvalue 1 and -1 on a symmetry-invariant surface, and we may use $U_{\mathcal{CR}} = 1$ to represent $\mathcal{CR}$ on a minimal surface with $N \geq 0$. With mirror symmetry, N counts the number of pairs of surface Dirac cones weighted by mirror chirality. In both cases a minimal surface with $N \geq 0$ has Hamiltonian

$$H_{\text{surface}} = -iv\tau_2(\sigma_1\partial_x + \sigma_3\partial_y)\mathbb{1}_N. \tag{A.46}$$

Such a surface has a unique mass term $m\tau_2\sigma_2$, with m a real symmetric $N \times N$ matrix which is odd under $\mathcal{CR}$ and $\mathcal{M}$. Correspondingly, this mirror-symmetric model admits helical gapless hinge modes at a mirror-symmetric hinge for all N, whereas the rotation-antisymmetric model has gapless hinge modes if N is odd.

Classes DIII$^{\mathcal{R}--}$, $(s,t) = (3,2)$ and DIII$^{\mathcal{M}-+}$, $(s,t) = (3,1)$.— We set $U_{\mathcal{T}} = \sigma_2$, $U_{\mathcal{P}} = \sigma_1$, $U_{\mathcal{C}} = \sigma_3$, $U_{\mathcal{R}} = \sigma_3\tau_3$, and $U_{\mathcal{M}} = \sigma_1$. These classes admit surface states with Dirac dispersion $-iv(\sigma_2\partial_x \pm \sigma_1\partial_y)$, which defines the chirality $\pm$. Such a surface state is compatible with $\mathcal{R}$ and $\mathcal{M}$ symmetries, but protected by chiral antisymmetry $\mathcal{C}$ alone. The corresponding strong integer index counts their number, weighted by chirality. A pair of surface states of opposite chirality, with dispersion $-iv(\sigma_2\rho_3\partial_x \pm \sigma_1\rho_0\partial_y)$, where the sign $\pm$ defines the mirror chirality for class DIII$^{\mathcal{M}-+}$, is protected by rotation or mirror symmetry. The associated integer topological index N counts the number of such pairs of surface Dirac cones, weighted by $\mathcal{RC}$-parity (for class DIII$^{\mathcal{R}--}$) or by mirror chirality (for class DIII$^{\mathcal{M}-+}$). This allows one to effectively set $U_{\mathcal{R}} = \sigma_3$ for a minimal surface with $N \geq 0$. The corresponding surface Hamiltonian reads

$$H_{\text{surface}} = -iv(\sigma_2\rho_3\partial_x + \sigma_1\rho_0\partial_y)\mathbb{1}_N. \tag{A.47}$$

The surface Hamiltonian admits a unique mass term $m\sigma_2\rho_2$, with m a real symmetric $N \times N$ matrix which changes sign under the twofold rotation antisymmetry operation and under mirror reflection. Correspondingly, this mirror-symmetric model admits helical gapless hinge modes at a mirror-symmetric hinge for all N, whereas the rotation-antisymmetric model has gapless hinge modes if N is odd.

Classes AII$^{\mathcal{R}-}$, $(s,t) = (4,2)$, and AII$^{\mathcal{CM}-}$, $(s,t) = (4,1)$ We set $U_{\mathcal{T}} = \sigma_2$, $U_{\mathcal{R}} = \sigma_3$, and $U_{\mathcal{CM}} = \sigma_1$. These classes have a $\mathbb{Z}_2^2$ classification, with purely crystalline part $\mathbb{Z}_2$. A generator for the strong phase has a surface state with Dirac dispersion $-iv(\sigma_1\partial_x + \sigma_2\partial_y)$, which is protected by time-reversal symmetry alone. The generator for the purely crystalline topological phase has a pair of surface Dirac cones with surface Hamiltonian

$$H_{\text{surface}} = -iv(\sigma_1\tau_0\partial_x + \sigma_2\tau_3\partial_y). \tag{A.48}$$

This surface Hamiltonian has a unique mass term $m\sigma_2\tau_2$, which is odd under $\mathcal{R}$ or $\mathcal{M}$. We conclude that these classes admits a protected hinge mode.

Classes CII$^{\mathcal{R}--}$, $(s,t) = (5,2)$ and CII$^{\mathcal{M}+-}$, $(s,t) = (5,1)$.— We set $U_{\mathcal{T}} = \sigma_2$, $U_{\mathcal{P}} = \sigma_2\tau_3$, $U_{\mathcal{C}} = \tau_3$, $U_{\mathcal{R}} = \sigma_3$ and $U_{\mathcal{M}} = \sigma_2\tau_2$. These classes have a $\mathbb{Z}_2^2$ classification, with purely crystalline part $\mathbb{Z}_2$. On a symmetry-invariant surface, the generator for the strong phase has a pair of surface Dirac cones with dispersion $-iv\tau_1(\sigma_2\partial_x + \sigma_1\partial_y)$, which is compatible with $\mathcal{R}$ and $\mathcal{M}$ symmetries, but does not rely on those symmetry for its protection. The nontrivial purely crystalline phase has two pairs of surface Dirac cones with Hamiltonian

$$H_{\text{surface}} = -iv\tau_1(\sigma_1\rho_0\partial_x + \sigma_2\rho_3\partial_y). \tag{A.49}$$

This surface Hamiltonian admits two mass terms $m_1\sigma_2\tau_1\rho_2 + m_2\sigma_1\tau_2\rho_1$, which is odd under $\mathcal{R}$ or $\mathcal{M}$. We conclude that class CII$^{\mathcal{M}+-}$ admits a protected hinge mode along mirror-symmetric hinges, whereas class CII$^{\mathcal{R}--}$ does not allow protected hinge modes.

Classes CI$^{\mathcal{R}--}$, $(s,t) = (7,2)$, and CI$^{\mathcal{M}-+}$, $(s,t) = (7,1)$.— We choose $U_{\mathcal{T}} = \sigma_1$, $U_{\mathcal{P}} = \sigma_2$, $U_{\mathcal{C}} = \sigma_3$, $U_{\mathcal{R}} = \sigma_3\rho_3$, $U_{\mathcal{M}} = \sigma_2\tau_2$. These classes admit pairs of surface states with dispersion $-iv\tau_2(\sigma_1\partial_x \pm \sigma_2\partial_y)$, which defines the chirality $\pm$. Such a surface state is compatible with $\mathcal{R}$ and $\mathcal{M}$ symmetries, but protected by chiral antisymmetry $\mathcal{C}$ alone. The corresponding strong integer index counts their number, weighted by chirality. Two pairs of surface states of opposite chirality, with dispersion $-iv\tau_2(\sigma_1\mu_3\partial_x \pm \sigma_2\mu_0\partial_y)$, where the sign $\pm$ defines the mirror chirality for class CI$^{\mathcal{M}-+}$, are protected by rotation or mirror symmetry. The associated integer topological index N counts the number of such pairs of surface Dirac cones, weighted by $\mathcal{RC}$-parity (for class CI$^{\mathcal{R}--}$) or

by mirror chirality (for class CI$^{\mathcal{M}-+}$). This allows one to effectively set $U_{\mathcal{R}} = \sigma_3$ for a minimal surface with $N \geq 0$. The corresponding surface Hamiltonian reads

$$H_{\text{surface}} = -iv\tau_2(\sigma_1\mu_3\partial_x + \sigma_2\mu_0\partial_y)\mathbb{1}_N. \tag{A.50}$$

The surface Hamiltonian admits four mass terms $m_1\sigma_1\tau_2\mu_2 + m_2\sigma_2\tau_1\mu_1 + m_3\sigma_2\tau_3\mu_1 + m_4\sigma_1\tau_0\mu_1$, with m_1, m_2, m_3, and m_4 real symmetric $N \times N$ matrices which change sign under the twofold rotation antisymmetry operation and under mirror reflection. Correspondingly, this mirror-symmetric model admits helical gapless hinge modes at a mirror-symmetric hinge for all N, but the rotation-symmetric model has no protected hinge states.

Classes AI$^{\mathcal{CR}+}$, $(s,t) = (0,3)$, and AI$^{\mathcal{M}-}$, $(s,t) = (0,2)$.— We choose $U_{\mathcal{T}} = 1$, $U_{\mathcal{CR}} = \rho_3$, and $U_{\mathcal{M}} = \sigma_2\tau_3$ to represent time reversal, twofold rotation antisymmetry, and mirror reflection symmetry, respectively. A symmetry-invariant surface admits pairs of surface states with a dispersion $-iv\sigma_2(\tau_1\partial_x \pm \tau_3\partial_y)$, which defines the mirror chirality (for class AI$^{\mathcal{M}-}$). The integer topological invariant N counts the number of such pairs of surface Dirac cones, weighted by $\mathcal{CR}$-parity or by mirror chirality, as appropriate. On a minimal surface with $N \geq 0$ we may use $U_{\mathcal{CR}} = 1$ to represent $\mathcal{CR}$. The corresponding surface Hamiltonian reads

$$H_{\text{surface}} = -iv\sigma_2(\tau_1\partial_x + \tau_3\partial_y)\mathbb{1}_N. \tag{A.51}$$

Such a surface has three mass terms $m_1\sigma_1\tau_1 + m_2\sigma_2\tau_2 + m_3\sigma_3\tau_0$, with m_1, m_2, and m_3 real symmetric $N \times N$ matrices. Correspondingly, this mirror-symmetric model admits helical gapless hinge modes at a mirror-symmetric hinge for all N, but the rotation-antisymmetric model has no protected hinge states.

Classes AII$^{\mathcal{CR}+}$, $(s,t) = (4,3)$ and AII$^{\mathcal{M}-}$, $(s,t) = (4,2)$.— We set $U_{\mathcal{T}} = \sigma_2$, $U_{\mathcal{CR}} = \tau_3$, and $U_{\mathcal{M}} = \sigma_2$. This phase allows surface Dirac cones on symmetry-invariant surfaces with dispersion $-iv(\sigma_1\partial_x \pm \sigma_2\partial_y)$, which defines the mirror chirality for class AII$^{\mathcal{M}-}$. The integer invariant N counts the number of such surface Dirac cones, weighted by $\mathcal{CR}$-parity or mirror chirality, as appropriate. Odd values of N correspond to strong phases, which have gapless surface states irrespective of the surface orientation. For even N one has a purely crystalline phase. For a minimal model with $N \geq 0$ one may effectively use $U_{\mathcal{R}} = 1$ to represent twofold rotation. The corresponding surface Hamiltonian is

$$H_{\text{surface}} = -iv\rho_0(\sigma_1\partial_x + \sigma_2\partial_y)\mathbb{1}_{N/2}. \tag{A.52}$$

There is a unique mass term $m\sigma_3\rho_2$, with m an $N/2 \times N/2$ matrix, which is odd under $\mathcal{CR}$ or $\mathcal{M}$. Correspondingly, a mirror-symmetric hinge has $N/2$ protected helical modes, whereas there are protected hinge modes in the presence of twofold rotation antisymmetry if $N/2$ is odd.

Classes CII$^{\mathcal{R}-+}$, $(s,t) = (5,3)$, and CII$^{\mathcal{M}--}$, $(s,t) = (5,2)$.— We set $U_{\mathcal{T}} = \sigma_2$, $U_{\mathcal{P}} = \sigma_2\tau_3$, $U_{\mathcal{C}} = \tau_3$, $U_{\mathcal{R}} = \sigma_3\tau_1$, and $U_{\mathcal{M}} = \sigma_1$. These classes have a $\mathbb{Z}_2$ classification, for which the nontrivial phase has a pair of Dirac cones with dispersion $-i\tau_1(\sigma_1\partial_x + \sigma_2\partial_y)$ on a symmetry-invariant surface. Such a pair of Dirac cones is protected by time-reversal symmetry and particle-hole antisymmetry alone, so that this is a strong topological phase, which has gapless modes on all surfaces.

Classes C$^{\mathcal{CR}-}$, $(s,t) = (6,3)$, and C$^{\mathcal{M}-}$, $(s,t) = (6,2)$.— We choose $U_{\mathcal{P}} = \tau_2$, $U_{\mathcal{CR}} = \tau_3$, and $U_{\mathcal{M}} = \tau_3\sigma_3$. These classes have a $\mathbb{Z}_2$ classification, for which the nontrivial phase has a pair of Dirac cones with dispersion $-i\tau_0(\sigma_1\partial_x + \sigma_3\partial_y)$ on a symmetry-invariant surface. Such a surface admits a unique mass term $m\sigma_2\tau_0$, which is odd under $\mathcal{CR}$ and $\mathcal{M}$. We conclude that the conditions for gapless hinge modes on a mirror-symmetric hinge or with rotation-symmetric crystal termination at surfaces are met.

[1] I. C. Fulga, F. Hassler, and A. R. Akhmerov, Phys. Rev. B **85**, 165409 (2012).
[2] L. Trifunovic and P. W. Brouwer, Phys. Rev. B **96**, 195109 (2017).
[3] A. P. Schnyder, S. Ryu, A. Furusaki, and A. W. W. Ludwig, Phys. Rev. B **78**, 195125 (2008).
[4] A. Kitaev, AIP Conference Proceedings **1134**, 22 (2009).
[5] M. Stone, C.-K. Chiu, and A. Roy, J. Math. Phys. A: Math. Theor. **44**, 045001 (2011).
[6] X.-G. Wen, Phys. Rev. B **85**, 085103 (2012).
[7] G. Abramovici and P. Kalugin, Int. J. Geom. Methods Mod. Phys. **9**, 125003 (2012).
[8] R. Kennedy and M. R. Zirnbauer, Commun. Math. Phys. **342**, 909 (2016).
[9] K. Shiozaki and M. Sato, Phys. Rev. B **90**, 165114 (2014).
[10] J. Langbehn, Y. Peng, L. Trifunovic, F. von Oppen, and P. W. Brouwer, Phys. Rev. Lett. **119**, 246401 (2017).

B. Appendix to: "Bulk-boundary-defect correspondence at disclinations in crystalline topological insulators and superconductors"

The Appendix is organized as follows. Appendix B.1 contains a detailed discussion on the occurrence of domain walls bound to disclinations in certain certain symmetry classes. In Appendix B.2, we provide supplementary information on the derivation of the topological crystal construction and on the presence of the domain wall as an obstruction to a symmetric decoration in the topological crystal construction. In Appendix B.3, we present an argument that the contribution of first-order topological phases to the number of anomalous states at disclinations is independent of their rotation holonomy, but only depends on the presence of π-fluxes for tenfold-way topological phases. Appendix B.4 contains an example on how to apply symmetry-based indicators to determine the presence of anomalous states at a disclination. Finally, Appendix B.5 presents the details on how to derive the classification of anomalous disclination states in all symmetry classes in two and three dimensions as summarized in Tables 3.1 and 3.2 of the main text.

B.1. SYMMETRY CLASSES HOSTING DISCLINATIONS BINDING DOMAIN WALLS

We argued in Sec. 3.2.4 of the main text that in certain symmetry classes it is impossible to apply the bulk hopping across the cut during the Volterra process without breaking some internal symmetries. In Sec. B.1 1 below, we illustrate that for these symmetry classes the Volterra process leads to a domain wall bound to the disclination. The domain wall separates regions that are distinguishable by the local arrangement of orbitals in the unit cell. In particular, the presence of a domain wall implies that there is no unique hybridization pattern across the cut line. As a consequence, the topological charge at the disclination is not uniquely determined from rotation and translation holonomies and bulk topological invariants alone. However, we show in Sec. B.1 2 that the parity of the topological charge along the cut line can be related to the bulk topology. These facts are illustrated with an example of a magnetic topological insulator in Sec. B.1 3. Furthermore, we argue in Sec. B.1 4 that for all symmetry classes with $d-2$ dimensional anomalous states with $\mathbb{Z}$ topological charge and $(n \in 2, 3, 4, 6)$-fold rotation symmetry the following holds: either (i) no strong second-order or weak topological phase with topological crystal limit as shown in Fig. 3.6 of the main text exists, or (ii) their symmetry group does not contain a unitary rotation symmetry, i.e., it contains only an antiunitary rotation symmetry or a rotation antisymmetry. This provides a *no-go theorem* for a unique correspondence between strong bulk topology and $(d-2)$ dimensional disclination anomaly in these symmetry classes.

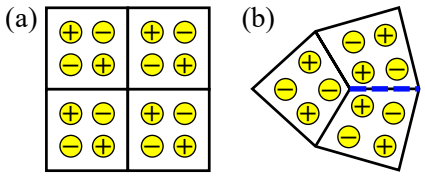

Figure B.1. An internal unitary symmetry or antisymmetry $\mathcal{U}$ with $\mathcal{U}^2 = 1$ allows to label the physical degrees of freedom in the unit cell, indicated by the signs $\pm$ on the orbitals depicted by yellow circles. In (a), we show a fourfold rotation symmetric lattice in which the representation of fourfold rotation symmetry has to anticommute with the internal unitary symmetry or antisymmetry because the rotation permutes the labels. In (b), we show a disclination that is connected to a domain wall (blue dashed line) between two regions related by a permutation of the labels.

B.1.1. Domain wall interpretation

In Sec. 3.2.4 of the main text, we showed that in certain symmetry classes the disclination necessarily connects to a line along which some symmetries are broken. These are precisely those symmetry classes that either do not contain a unitary rotation symmetry (for instance in magnetic space groups) or whose unitary rotation symmetry anticommutes with some internal unitary symmetries or antisymmetries. Here, we show that in these cases one can define labels or an order parameter that allow to distinguish the two regions bordered by the line. This shows that the line is in fact a domain wall.

Internal unitary symmetries or antisymmetries provide labels for the physical degrees of freedom on the lattice. These labels are defined in the diagonal basis of the internal unitary symmetry/antisymmetry. The representation of unitary rotation symmetry describes the action on the physical degrees of freedom that needs to be performed such that the system is invariant under the rotation. In case the representation of unitary rotation symmetry anticommutes with an internal unitary symmetry or antisymmetry, the rotation symmetry permutes the labelled degrees of freedom, as illustrated for a fourfold rotation symmetric sample in Fig. B.1(a). Thus, two patches that are rotated with respected to each other without applying the representation of internal symmetry are distinguishable by their configuration of labels. In this case, a disclination is therefore the end of a *domain wall* bordering two regions with permuted labelling, see Fig. B.1(b).

For magnetic space groups, where only the product of rotation and time reversal is preserved but not individually, one can define a vectorial order parameter, such

as a local magnetization, that is odd under time reversal. A disclination with Franck angle corresponding to the magnetic rotation symmetry is thus the end point of a domain wall separating regions that are related by time-reversal symmetry. This is further illustrated with an example in Sec. B.1 3 below.

In the presence of translation symmetry, the local order parameter can be expressed in terms of the labels under the unitary internal symmetry or antisymmetry $\mathcal{U}^2 = \pm 1$ (or the local magnetization for magnetic rotation symmetry) in the asymmetric unit within the unit cell, see Fig. 3.5 in the main text. The unit cell then consists of asymmetric sections with labels related by rotation symmetry. In case rotation symmetry anticommutes with the unitary internal symmetry or antisymmetry (in case of magnetic rotation symmetry), the labels (local magnetization) in symmetry related asymmetric sections are opposite. Here, despite rotations, a translation by half a lattice vector may interchange the labels. Therefore, the domain wall may become locally unobservable if the disclination contains a translation holonomy by a fraction of a lattice vector. Notice that in this case, the sample does not allow for a global and consistent definition of the unit cell. Throughout the paper, we restrict ourselves to lattice defects with a translation holonomy that is an integer multiple of the lattice vectors. These lattice defects can be constructed and analyzed with the methods from Sec. B.2 in the main text. By construction, the lattice with the defect contains a consistent definition of the unit cell. The interplay of topological phases and screw dislocations with fractional translation holonomy has been investigated in Ref. 1.

Furthermore, we point out that if the sample with disclination as a whole does not respect all internal symmetries of the bulk system, then the domain wall may become unobservable. In particular, this may be the case when constructing nearest-neighbor lattice models with an artificial 'sublattice' antisymmetry $\Gamma^2 = 1$ which indicates the absence of hopping terms between different sublattices and the equality of the chemical potential on both sublattices. In case n-fold rotation symmetry anticommutes with the sublattice antisymmetry, the sublattices are interchanged at adjacent unit cells across the branch cut attached to a disclination with Franck angle Ω equal to an odd integer multiple of $2\pi/n$. If the sublattices are indistinguishable up to their label, then applying the same nearest-neighbor hopping across the branch cut yields a branch cut indistinguishable from the bulk lattice. This breaks the sublattice antisymmetry along the branch cut as sites with same sublattice label are connected by a hopping term. As a consequence, also the disclination breaks the sublattice antisymmetry and a potentially bound state may acquire a finite energy and is not anomalous. For consistency, we assume throughout the paper that the sample with disclination as a whole respects the internal symmetries of the bulk system.

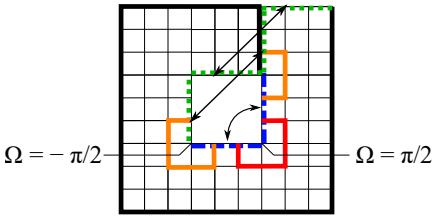

Figure B.2. A disclination dipole consisting of two disclinations with opposite Franck angle $\Omega = \pm\pi/2$ can be constructed in a fourfold rotation symmetric lattice by removing a square from the sample and connecting the boundaries as indicated by the blue dashed and green dotted lines. The blue dashed lines indicate boundary conditions that involve a rotation by $\pi/2$. The green dotted lines indicate boundary conditions that do not involve any rotation. A path around the disclination with Franck angle $\Omega = \pi/2$ ($\Omega = -\pi/2$) is indicated by the red (orange) bold line. For clarity, the sample boundary is highlighted by the black bold line.

B.1.2. Topological charge at the domain wall and a disclination dipole

In case the cut line forms a domain wall and connects to the boundary, the intersection of the line with the boundary forms another point defect. Then, the parity of the total topological charge along the domain wall is determined by identical expressions as in Eqs. (3.7) to (3.11) in the main text. This is because of the anomaly cancellation criterion: anomalous boundary states associated to the domain wall can only be created pairwise.

A disclination dipole consists of two disclinations with opposite Franck angle that are connected by a cut line, as depicted in Fig. B.2. In case none of the two disclinations involves a translation holonomy, the topological charge at the pair cancels. Thus, the topological charge at the disclinations cannot be predicted from the bulk topology if the cut line forms a domain wall.

B.1.3. Example: Magnetic topological insulator

A magnetic topological insulator breaks time-reversal symmetry, but preserves the product of time-reversal symmetry and a crystalline symmetry operation. In the following, we consider a three-dimensional magnetic topological insulator where the product of fourfold rotation and time-reversal symmetry is preserved. In this case, there is only a strong second-order phase. Weak phases corresponding to arrangements of Chern insulators parallel to the rotation axis are forbidden as the copropagating chiral modes at twofold rotation symmetric momenta in this decoration cannot gap out. Furthermore Chern insulators are not compatible with a perpendicular magnetic rotation axis.

A model for a second-order topological insulator with magnetic fourfold rotation symmetry can be constructed similar to the class D model in Eq. (3.13) of the main

text. The Hamiltonian of our model is given by

$$\begin{aligned} H_{\mathrm{A}}(\vec{k}) = & t(1-\cos k_z)\left[\tau_3\sigma_2 - \tau_2\sigma_0\right] \\ & -t(1+\cos k_z)\left[\cos(k_x)\tau_3\sigma_2 + \sin(k_x)\tau_3\sigma_1\right] \\ & +t(1+\cos k_z)\left[\cos(k_y)\tau_2\sigma_0 - \sin(k_y)\tau_1\sigma_0\right] \\ & +t_z \sin k_z \tau_3\sigma_3 \end{aligned} \tag{B.1}$$

As in the previous section, the hopping parameter t is real, $\tau_i\sigma_j$ are four-by-four matrices composed of Pauli matrices acting on the four degrees of freedom in the unit cell. Here, our basis consists of four fermionic operators $c_{\vec{k},a}, c_{\vec{k},b}, c_{\vec{k},c}, c_{\vec{k},d}$ arranged as depicted in Fig. B.3(a). Magnetic fourfold rotation exchanges the fermions in the unit cell counter-clockwise including a phase $c_{\vec{k},a} \to -c_{\vec{k},c}$ and a time-reversal operation implemented by complex conjugation. This model can be adiabatically deformed to the chiral higher-order topological insulator of Ref. 2.

To understand the topology of this model, consider an expansion in small k_z around $k_z = 0$ and $k_z = \pi$ separately. Both cases around $k_z = 0$ and $k_z = \pi$ correspond to a lattice of chiral modes whose chirality is determined by the term $t_z \sin k_z \tau_3\sigma_3$. Around $k_z = 0$ and for positive t_z the "a" and "d" ("b" and "c") lattice sites have positive (negative) chirality. The chiral modes are hybridized across unit cells such that there is a chiral mode remaining at each corner, as depicted by the dashed lines in Fig. B.3. Around the $k_z = \pi$ plane the chiralities are reversed and all chiral modes are hybridized within the unit cells such that no corner modes are remaining, as depicted by the full lines in Fig. B.3. The Hamiltonian interpolates between the two hybridizations and remains gapped for every k_z. As a consequence, the model realizes chiral hinge states in agreement with fourfold magnetic rotation symmetry.

In the Volterra process we need to determine the fate of the hybridizations of the chiral modes around $k_z = 0$ across the cut. As depicted in Fig. B.3 there are two choices realizing completely dimerized limits along the cut line. Both limits require a breaking of fourfold magnetic rotation symmetry along the cut line, in agreement with our results from Sec. 3.4 of the main text. The configuration in Fig. B.3(a) can be realized without closing the excitation gap along the cut line. It realizes a chiral disclination mode propagating into the plane and two chiral modes propagating out of the plane at the end of the cut line. In order to obtain the configuration in Fig. B.3(b) one needs to change the hybridization pattern along both cut lines which requires a closure of the excitation gap along these lines. This configuration has a disclination mode propagating out of the plane and gapped boundaries. Finally, Fig. B.3(c) depicts a hybridization pattern where the excitation gap needs to close only on one of the two cut lines. This pattern hosts no anomalous disclination state, but a single chiral mode at the end of the cut line.

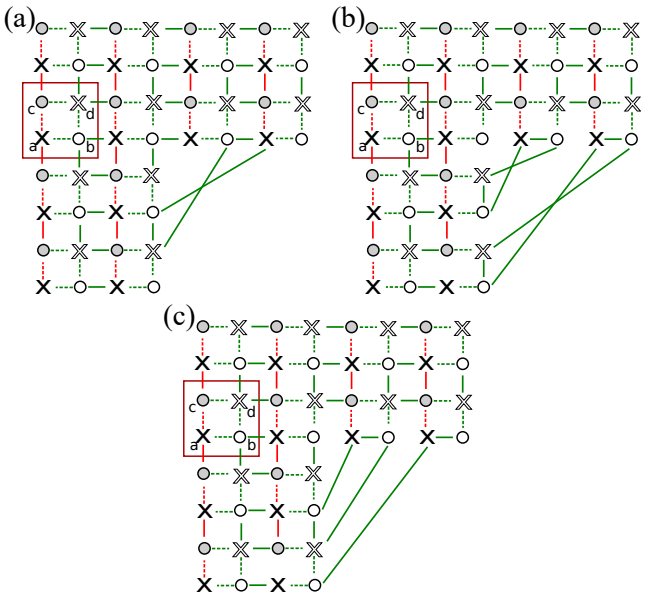

Figure B.3. Depiction of the model Hamiltonian for the magnetic second-order topological insulator defined in Eq. (B.2). Crosses and dots denote chiral modes with opposite chirality as defined from an expansion of the Hamiltonian around $k_z = 0$ and $k_z = \pi$. Full (dashed) lines denote the hybridization at $k_z = 0$ ($k_z = \pi$). Red lines include a π phase. The unit cell is highlighted by a red square. In (a)–(c), we show three different possibilities of connecting the hybridizations at $k_z = 0$ across the cut in the Volterra process to construct a $\frac{\pi}{2}$ disclination.

Domain wall interpretation

For an antiferromagnetic insulator with magnetic space group $p4'$, one can define a vectorial order parameter as the magnetization within a quarter of the unit cell. Thus, with a consistent definition of a unit cell as provided by the Volterra process in Sec. 3.2 of the main text, the order parameter distinguishes regions that are rotated by $\pi/2$ with respect to each other. A disclination with Franck angle $\Omega = \pi/2$ is thus the edge of a domain wall.

B.1.4. No-go theorem in symmetry classes whose $d-2$ dimensional anomalous states have $\mathbb{Z}$ topological charge

The purpose of this section is to show that for symmetry classes whose $d-2$ dimensional anomalous states have $\mathbb{Z}$ topological charge, either (i) no strong second-order topological phase exists, or (ii) the symmetry group does not contain a unitary rotation symmetry that commutes with all internal unitary symmetries or antisymmetries. We presented an argument that shows the correctness of this statement in two and three dimensions in Sec. 3.3.4 of the main text. Here, we show that the argument can be generalized to any dimension $d \geq 2$ using the dimensional raising map [3–5].

The dimensional raising map provides an isomorphism between the classifying groups of the strong topological phases in different symmetry classes and dimensions. It has been extended to be applied in the presence of crystalline symmetries [4 and 5]. Here, we apply the dimensional raising map such that rotation symmetry acts trivially in the added dimensions. Below we are going to review how the Hamiltonians and symmetry operators are mapped under the dimensional raising maps following Ref. 5. We refer to Ref. 5 for the derivation of the expressions and proof of the isomorphism property. The classification using the dimensional raising map has also been reviewed in Section 2.2 of Chapter 2.

First, we introduce the γ-matrices used in the expressions of the images of the Hamiltonian and representations under the dimensional raising map,

$$\gamma_{2n-1}^{(k)} = \left(\bigotimes^{n-1}\sigma_0\right)\otimes\sigma_2\otimes\left(\bigotimes^{k-n}\sigma_3\right) \tag{B.2}$$

$$\gamma_{2n}^{(k)} = \left(\bigotimes^{n-1}\sigma_0\right)\otimes-\sigma_1\otimes\left(\bigotimes^{k-n}\sigma_3\right) \tag{B.3}$$

for $1 \leq n \leq k$ and $\gamma_{2k+1}^{(k)} = \bigotimes^{k}\sigma_3, \gamma_1^{(0)} = 1$ where $\bigotimes^{n}\sigma_j = \sigma_j\otimes ...\otimes\sigma_j$ describes the n-fold Kronecker product of the Pauli matrix σ_j. The γ-matrices satisfy $\{\gamma_i^{(k)},\gamma_i^{(j)}\} = 2\delta_{i,j}$. We furthermore define

$$\begin{aligned}\mathbb{\Gamma}_j^{(+)} &= \mathbb{1}\otimes\gamma_{2j}^{(r)}\\ \mathbb{\Gamma}_j^{(-)} &= \mathbb{1}\otimes i\gamma_{2j-1}^{(r)}\end{aligned}. \tag{B.4}$$

1. *Dimensional raising from a symmetry class with chiral antisymmetry*

The dimensional raising map is expressed in terms of a map of a representative Hamiltonian $H(\vec{k})$ defined on the base space $\vec{k}\in X$ and representations $U(g)$ of the symmetry operators $g\in\mathcal{G}\times\mathcal{C}$. Here, $\mathcal{G}$ is the magnetic space group that includes all unitary or antiunitary symmetries of system, such as time-reversal and crystalline symmetry operations. The chiral antisymmetry $\mathcal{C}$ plays a special role in the construction of the dimensional raising map. In particular, one defines the subgroup $\mathcal{G}_\mathcal{C}\subset\mathcal{G}\times\mathcal{C}$ compatible with chiral antisymmetry $\mathcal{C}$ that consist of all elements $g\in\mathcal{G}\times\mathcal{C}$ that satisfy

$$\begin{aligned}U(g)H(g\vec{k})U^\dagger(g) &= c(g)H(\vec{k})\\ U(g)U(\mathcal{C})U^\dagger(g) &= c(g)U(\mathcal{C})\end{aligned} \tag{B.5}$$

for g unitary and

$$\begin{aligned}U(g)H^*(-g\vec{k})U^\dagger(g) &= c(g)H(\vec{k})\\ U(g)U^*(\mathcal{C})U^\dagger(g) &= c(g)U(\mathcal{C})\end{aligned} \tag{B.6}$$

for g antiunitary with the same value $c(g)\in\{-1,1\}$. For $c(g)=1$ ($c(g)=-1$) the element $g\in\mathcal{G}_\mathcal{C}$ is a symmetry (antisymmetry). Notice that $\mathcal{G}_\mathcal{C}$ is a normal subgroup of $\mathcal{G}\times\mathcal{C}$ and $\mathcal{G}_\mathcal{C}\times\mathcal{C} = \mathcal{G}\times\mathcal{C}$. The elements of $\mathcal{G}_\mathcal{C}$ are going to be used to construct the symmetry elements in the image of the dimensional raising map.

To define the dimensional raising map for a representative Hamiltonian $H_1(\vec{k})$ of a given (nontrivial) topological equivalence class, one considers a parameter family of Hamiltonians $H_{10}(\vec{k},m)$ with $m\in[m_0,m_1]$ such that $H(\vec{k},m_0) = H_0(\vec{k})$ is a representative Hamiltonian of a trivial topological equivalence class and $H(\vec{k},m_1) = H_1(\vec{k})$. As $H_0(\vec{k})$ and $H_1(\vec{k})$ are in distinct topological equivalence classes, the gap needs to close for some finite value of the parameter m.

For two-dimensional n-fold rotation symmetry protected second-order topological superconductors in a Cartan class with chiral antisymmetry, the symmetry group G is generated by rotations $\mathcal{R}_{2\pi/n}$ and, if present, time-reversal symmetry $\mathcal{T} = \mathcal{P}\mathcal{C}$. In the presence of spin-rotation symmetry (or other internal unitary symmetries), the Hamiltonian is block-diagonal such that the analysis can be restricted to separate blocks.

Raising by an odd number of dimensions – First, we show how to construct a Hamiltonian in dimension $d = 2+2r+1$ from a second-order topological phase in $d=2$. Without loss of generality, we assume that $H_{10}(\vec{k},m)$ interpolates between the second-order topological phase for $-2<m<0$ and a trivial phase for $m>0$. We denote the momentum directions of the two dimensional second-order topological phase by $\vec{k} = (k_x,k_y)^T$ and the newly added momentum directions by $\vec{k}_\perp$. The dimensional raising map is given by defining the $(d=2+2r+1)$-dimensional Hamiltonian $H(\vec{k},\vec{k}_\perp)$ inheriting its topological invariants from the family of two-dimensional Hamiltonians $H_{10}(\vec{k},m)$ as

$$\begin{aligned}H(\vec{k},\vec{k}_\perp) = {}& \mathbb{H}_{10}(\vec{k},m(\vec{k}_\perp))\\ &+\sum_{j=1}^{r}(i\mathbb{\Gamma}_j^{(-)}\sin k_{\perp,j}+\mathbb{\Gamma}_j^{(+)}\sin k_{\perp,r+j})\\ &+\mathbb{\Gamma}_\mathcal{C}\sin k_{\perp,2r+1}\end{aligned} \tag{B.7}$$

with $\mathbb{H}_{10}(\vec{k},m(\vec{k}_\perp)) = H_{10}(\vec{k},m(\vec{k}_\perp))\otimes\gamma_{2r+1}^{(r)}$, $\mathbb{\Gamma}_\mathcal{C} = U(\mathcal{C})\otimes\gamma_{2r+1}^{(r)}$ and $m(\vec{k}_\perp) = -1+\sum_j^{2r+1}(1-\cos k_{\perp,j})$. To express the corresponding representations of the symmetry elements $U(g,\vec{k},\vec{k}_\perp)$ we first introduce

$$\mathbb{U}(g,\vec{k}) = \begin{cases}U(g,\vec{k})\otimes\mathbb{1} & \text{for } c(g)=1\\ U(g,\vec{k})\otimes\gamma_{2r+1}^{(r)} & \text{for } c(g)=-1.\end{cases} \tag{B.8}$$

This allows us to express $U(g,\vec{k},\vec{k}_\perp)$ for $g\in\mathcal{G}_\mathcal{C}$ unitary as

$$U(g,\vec{k},\vec{k}_\perp) = \mathbb{U}(g,\vec{k}) \tag{B.9}$$

and for $g \in \mathcal{G}_\mathcal{C}$ antiunitary as

$$U(g,\vec{k},\vec{k}_\perp) = \left(\prod_{j=1}^{r} \Gamma_j^{(+)}\right) \Gamma_\mathcal{C} \mathbb{U}(g,\vec{k}). \tag{B.10}$$

The mapped Hamiltonian (B.7) satisfies for $g \in \mathcal{G}_\mathcal{C}$ unitary

$$U(g,\vec{k},\vec{k}_\perp) H(g\vec{k},\vec{k}_\perp) U^\dagger(g,\vec{k},\vec{k}_\perp) = c(g) H(\vec{k},\vec{k}_\perp) \tag{B.11}$$

and for $g \in \mathcal{G}_\mathcal{C}$ antiunitary

$$\begin{aligned} &U(g,\vec{k},\vec{k}_\perp) H^*(-g\vec{k},-\vec{k}_\perp) U^\dagger(g,\vec{k},\vec{k}_\perp) \\ &= (-1)^{r+1} c(g) H(\vec{k},\vec{k}_\perp). \end{aligned} \tag{B.12}$$

Raising by an even number of dimensions– Under the dimensional raising map a $d = 2+2r$ dimensional Hamiltonian inheriting its topological invariants from the family of two-dimensional Hamiltonians $H_{10}(\vec{k},m)$ is constructed as

$$\begin{aligned} H(\vec{k},\vec{k}_\perp) = {} & \mathbb{H}_{10}(\vec{k}, m(\vec{k}_\perp)) \\ & + \sum_{j=1}^{r-1} (i\Gamma_j^{(-)} \sin k_{\perp,j} + \Gamma_j^{(+)} \sin k_{\perp,r+j}) \\ & + \Gamma_r^{(-)} \sin k_{\perp,r} + \Gamma_\mathcal{C} \sin k_{\perp,2r} \end{aligned} \tag{B.13}$$

where the representations $U(g,\vec{k},\vec{k}_\perp)$ are given for $g \in \mathcal{G}_\mathcal{C}$ unitary as

$$U(g,\vec{k},\vec{k}_\perp) = \mathbb{U}(g,\vec{k}) \tag{B.14}$$

and for $g \in \mathcal{G}_\mathcal{C}$ antiunitary as

$$U(g,\vec{k},\vec{k}_\perp) = \left(\prod_{j=1}^{r-1} \Gamma_j^{(+)}\right) \Gamma_\mathcal{C} \mathbb{U}(g,\vec{k}). \tag{B.15}$$

In addition, the Hamiltonian (B.13) satisfies the unitary antisymmetry $U(\mathcal{C},\vec{k},\vec{k}_\perp) = \Gamma_r^{(+)}$,

$$\Gamma_r^{(+)} H(\vec{k},\vec{k}_\perp) \Gamma_r^{(+)} = -H(\vec{k},\vec{k}_\perp). \tag{B.16}$$

The mapped Hamiltonian (B.13) satisfies for $g \in \mathcal{G}_\mathcal{C}$ unitary

$$U(g,\vec{k},\vec{k}_\perp) H(g\vec{k},\vec{k}_\perp) U^\dagger(g,\vec{k},\vec{k}_\perp) = c(g) H(\vec{k},\vec{k}_\perp) \tag{B.17}$$

and for $g \in \mathcal{G}_\mathcal{C}$ antiunitary

$$\begin{aligned} &U(g,\vec{k},\vec{k}_\perp) H^*(-g\vec{k},-\vec{k}_\perp) U^\dagger(g,\vec{k},\vec{k}_\perp) \\ &= (-1)^r c(g) H(\vec{k},\vec{k}_\perp). \end{aligned} \tag{B.18}$$

The same commutation relations hold for the representations of the symmetry elements and the chiral antisymmetry $U(\mathcal{C},\vec{k},\vec{k}_\perp) = \Gamma_r^{(+)}$. In particular, they are for $g \in \mathcal{G}_\mathcal{C}$ unitary

$$U(g,\vec{k},\vec{k}_\perp) U(\mathcal{C},\vec{k},\vec{k}_\perp) U^\dagger(g,\vec{k},\vec{k}_\perp) = c(g) U(\mathcal{C},\vec{k},\vec{k}_\perp) \tag{B.19}$$

and for $g \in \mathcal{G}_\mathcal{C}$ antiunitary

$$\begin{aligned} &U(g,\vec{k},\vec{k}_\perp) U^*(\mathcal{C},\vec{k},\vec{k}_\perp) U^\dagger(g,\vec{k},\vec{k}_\perp) \\ &= (-1)^r c(g) U(\mathcal{C},\vec{k},\vec{k}_\perp). \end{aligned} \tag{B.20}$$

2. *No-go theorem*

Two-dimensional n-fold rotation symmetry protected second-order topological phases in Cartan classes AIII, BDI and CII (whose 0-dimensional anomalous states have $\mathbb{Z}$ topological charge) require that the representations of chiral antisymmetry $U(\mathcal{C})$ and n-fold rotation symmetry $U(\mathcal{R}_{2\pi/n})$ anticommute. In this case, the conditions (B.5), (B.6) imply that the group of symmetry elements compatible with chiral antisymmetry $\mathcal{G}_\mathcal{C}$ is generated by a rotation *antisymmetry* $\mathcal{R}_{2\pi/n}\mathcal{C}$ and, depending on the Cartan class, either time-reversal symmetry or particle-hole antisymmetry. Thus $\mathcal{G}_\mathcal{C}$ does not contain any unitary rotation symmetries.

Upon raising the dimension by an odd number, Eqs. (B.11) and (B.12) also show that the rotation elements in the image of the dimensional raising map cannot be both unitary and commute with the Hamiltonian. Upon raising the dimension by an even number, Eq. (B.19) shows that the anticommutation of the chiral antisymmetry with the representation of (unitary) rotation symmetry remains preserved. Antiunitary symmetry elements remain antiunitary under the dimensional raising map.

Finally, any $d > 2$ dimensional rotation symmetry protected second-order topological phase can be constructed from a $d = 2$ dimensional second-order topological phase where the corresponding model can be found by using the inverse dimensional reduction map of the isomorphism. The dimensional reduction map can be explicitly expressed in terms of a continuous deformation of the Hamiltonian [3] or in terms of the scattering matrix of a symmetric boundary [6 and 7] (see Section 2.3 of Chapter 2).

Therefore, the criterion from Sec. 3.2.4 of the main text for the application of the unique bulk hybridization as defined in Eq. (3.2) is violated for all symmetry classes and dimensions $d \geq 2$ that host n-fold rotation symmetry protected topological phases with $\mathbb{Z}$ anomalous boundary states. This proves the absence of a unique correspondence between $(d-2)$ dimensional disclination anomaly and strong bulk topology in these symmetry classes.

B.2. DETAILS ON THE TOPOLOGICAL CRYSTAL CONSTRUCTION

We present additional details on the topological crystal construction. Section B.2 1 shows in detail how to perform the cell decomposition with space group $p2$. Section B.2 2 contains details on how to determine the valid decorations as well as their properties in terms of weak

and strong topological phases as well as their Abelian group property. Finally, in Sec. B.2 3 we show that an obstruction exists to decorate the $d-1$ cells of lattices with disclination with $\mathbb{Z}$ topological phases.

B.2.1. Cell decomposition with space group $p2$

The cell decomposition of a cubic lattice with space group $p2$ in two and three dimensions is shown in Fig. 3.5 in the main text.

Two dimensions. In two dimensions, we choose the asymmetric unit to be bounded by the lines $(x,0)$ with $x\in[0,\frac{a}{2}]$, $(0,y)$ and $(\frac{a}{2},y)$ with $y\in[0,a]$. This choice is made such that a corner of the asymmetric unit lies at the unit cell center and its edges are parallel to the lattices vectors.

There are three symmetry inequivalent 1-cells which together cover the complete boundary of the 2-cell upon translating the them with the crystalline symmetries. They are given by the lines: i) $(x,0)$ with $x\in[0,\frac{a}{2}]$, ii) $(0,y)$ with $y\in[0,\frac{a}{2}]$, and iii) $(\frac{a}{2},y)$ with $y\in[0,\frac{a}{2}]$.

The symmetry-inequivalent 0-cells are the boundaries of the 1-cells. They coincide with maximal Wyckoff positions, which are labeled in standard notation as 1a at $\vec{x}=(0,0)$, 1b at $\vec{x}=(\frac{a}{2},0)$, 1c at $\vec{x}=(0,\frac{a}{2})$ and 1d at $\vec{x}=(\frac{a}{2},\frac{a}{2})$.

Three dimensions. In three dimensions, see Fig. 3.5 in the main text, the asymmetric unit is a cuboid where every x-y plane cut reproduces the two-dimensional asymmetric unit. Without loss of generality and for simplicity, we set the boundaries of the cube at the planes $z=\pm\frac{a}{2}$.

There are four symmetry-inequivalent 2-cells:

- (red) the x-y plane bounded between the lines $(x,0,\frac{a}{2})$ with $x\in[0,\frac{a}{2}]$, $(0,y,\frac{a}{2})$ and $(\frac{a}{2},y,\frac{a}{2})$ with $y\in[0,a]$,
- (blue) an x-z plane bounded between the lines $(x,0,\pm\frac{a}{2})$ with $x\in[0,\frac{a}{2}]$, $(0,0,z)$ (Wyckoff position 1a) and $(\frac{a}{2},0,z)$ (Wyckoff position 1b) with $z\in[-\frac{a}{2},\frac{a}{2}]$,
- (yellow) a y-z plane bounded by the lines $(0,y,\pm\frac{a}{2})$ with $y\in[0,\frac{a}{2}]$, $(0,0,z)$ (Wyckoff position 1a) and $(0,\frac{a}{2},z)$ (Wyckoff position 1c) with $z\in[-\frac{a}{2},\frac{a}{2}]$ and
- (green) another y-z plane bounded by the lines $(\frac{a}{2},y,\pm\frac{a}{2})$ with $y\in[0,\frac{a}{2}]$, $(\frac{a}{2},0,z)$ (Wyckoff position 1b) and $(\frac{a}{2},\frac{a}{2},z)$ (Wyckoff position 1d) with $z\in[-\frac{a}{2},\frac{a}{2}]$.

There are seven symmetry inequivalent 1-cells, three in the x-y-plane similar to the two dimensional cell decomposition, and four at the four maximal Wyckoff positions 1a at $\vec{x}=(0,0,z)$, 1b at $\vec{x}=(\frac{a}{2},0,z)$, 1c at $\vec{x}=(0,\frac{a}{2},z)$ and 1d at $\vec{x}=(\frac{a}{2},\frac{a}{2},z)$, $z\in[-\frac{a}{2},\frac{a}{2}]$.

Finally, there are four symmetry inequivalent 0-cells at $\vec{x}=(0,0,\frac{a}{2})$, $\vec{x}=(\frac{a}{2},0,\frac{a}{2})$, $\vec{x}=(0,\frac{a}{2},\frac{a}{2})$ and $\vec{x}=(\frac{a}{2},\frac{a}{2},\frac{a}{2})$.

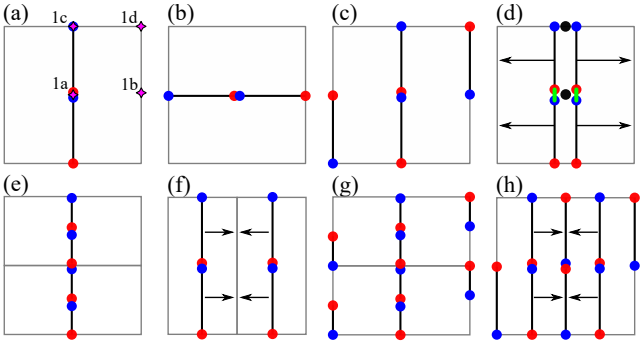

Figure B.4. Panels (a), (b) and (c) repeat for convenience the generating set of valid 1-cell decorations for two dimensional twofold rotation symmetric lattices with topological invariants as in Fig. 3.6 in the main text. In panel (a) we included the labels of the maximal Wyckoff positions at the twofold rotation axes denoted by the violet stars. The decorations (a), (b), (c) have the topological invariants $\vec{\nu}=(\nu_{1a|1b},\nu_{1a|1c},\nu_{1b|1d})=(0,1,0)$, $(1,0,0)$ and $(0,1,-1)$ as defined in the text, respectively. Figure (d) shows that a topological crystal $\vec{\nu}=(0,2,0)$ can be adiabatically and symmetrically deformed to a topological crystal $\vec{\nu}=(0,0,2)$ up to additional $d-2$ dimensional topological phases at and parallel to the rotation axis (black dots) by deforming the hybridization of the anomalous edge states (green bars) such that it allows a symmetric and adiabatic movement of the decoration. (e), (f) Doubling of the unit cell in y, x-direction with a decoration with the topological crystal shown in (a). The topological crystal shown in (a) is invariant under a doubling of the unit cell in y direction after hybridization of the anomalous edge states. A doubling of the unit cell in x direction takes the Hamiltonian H describing the topological crystal shown in (a) to $H\oplus H$ after a movement of the symmetry related pairs of 1-cells as shown in (f). In contrast, the topological crystal shown in (c) is invariant under a doubling of the unit cell in y, x direction shown in (g), (h) using hybridization and symmetry allowed deformations.

B.2.2. Decorations of topological crystals with rotation symmetry

In this section we present in detail the decoration of the 1-cells (2-cells parallel to the rotation axis) in two (three) dimensional rotation symmetric lattices with $\mathbb{Z}$ topological phases and the properties of the resulting decorations in terms of weak, strong and higher-order topological phases. The results for decorations with topological phases with $\mathbb{Z}_2$ anomalous edge states can be straightforwardly obtained by taking the fusion rules modulo two. Below we present the derivation for two dimensional lattices and comment on the straightforward extension to three dimensions. At the end of the section we show some criteria that simplify the determination of the existence of a decoration.

Twofold rotation symmetry in two dimensions. With twofold rotation symmetry, the unit cell and cell decomposition is shown in Fig. 3.5 in the main text.

The asymmetric unit is a 2-cell that can be decorated with a two dimensional topological phase. The decora-

tion describes a gapped topological phase if the anomalous state along its boundaries can be gapped by hybridization with anomalous boundary states of adjacent decorated 2-cells. Notice that the hybridization of edge states along the 1-cells may create anomalous states at the twofold rotation axis.

There are in total $\mathbb{Z}^3$ topological crystals that can be constructed from decorations of the three distinct 1-cells with $\mathbb{Z}$ topological phases. A given 1-cell decoration can be identified by the vector $\vec{\nu} = (\nu_{1a|1b}, \nu_{1a|1c}, \nu_{1b|1d})$ where $\nu_{i|j}$ is the topological invariant characterizing the topological phase occupying the 1-cell between Wyckoff positions i and j where $i, j \in \{1\text{a}, 1\text{b}, 1\text{c}, 1\text{d}\}$. As we show in Fig. B.4 (d) some topological crystals are topologically equivalent in the sense that they can be adiabatically deformed into each other: A topological crystal describing the element $(0, 2, 0)$ can be written as a direct sum $H_{(0,2,0)} = H_{(0,1,0)} \oplus_\mu H_{(0,1,0)}$ where $H_{\vec{\nu}}$ is a Hamiltonian describing the topological crystal with topological invariants $\vec{\nu}$ and the subscript μ indicates that Pauli matrices denoted by μ_j act in the space of the two systems. A simple check directly shows that if $H_{(0,1,0)}$ describes a gapped system whose anomalous edge states at the maximal Wyckoff positions hybridize and whose hybridization is given by h, then $h \otimes \mu_1$ is a possible hybridization of $H_{(0,2,0)}$. This hybridization is shown by the green bars in Figs B.4 (d) and allows to symmetrically move the decoration to the 1-cell pointing from 1b to 1d.

Notice that in order to adiabatically deform the hybridization $h \otimes \mu_0$ obtained from the direct sum $H_{(0,1,0)} \oplus_\mu H_{(0,1,0)}$ to the required $h \otimes \mu_1$ one may need to add extra gapped degrees of freedom at the rotation axis. In two dimensions, these additional degrees of freedom are a 0-cell describing a gapped orbital. In higher dimensions, the additional degrees of freedom can be a $d-2$-dimensional topological phase that decorates the $d-2$-cell that coincides with the rotation center. The additional degrees of freedom remain as $d-1$-cells are moved. As in this chapter we restrict the analysis to the properties of the topological crystals obtained from $d-2$-cells, we do not discuss under which conditions the addition of gapped degrees of freedoms is necessary, nor the properties of the resulting topological crystals.

This shows that the element $(0, 2, 0)$ is equivalent to the element $(0, 0, 2)$ up to an atomic limit or decorated $d-2$ cells parallel to the rotation axis. Notice that a similar deformation is not allowed for a decoration $(0, 1, 0)$ as this would require either a hybridization of non-overlapping anomalous edge states of the 1-cells or an absence of a hybridization of the anomalous edge states which corresponds to a bulk gap closure.

A complete set of 1-cell decorations from which all topological crystals can be constructed using the direct sum operation is given by $\vec{\nu} = (0, 1, 0)$, $(1, 0, 0)$ and $(0, 1, -1)$ shown in Fig. B.4 (a), (b) and (c), respectively. In order for the decorations to be valid, i.e., to describe a gapped topological phase, all anomalous edge states of the decorations need to gap out with overlapping anomalous states at the same location. Each 1-cell ends at a twofold rotation axis and thus has a partner under twofold rotation. A sufficient criterion for the validity of all decorations $\vec{\nu} = (0, 1, 0)$, $(1, 0, 0)$ and $(0, 1, -1)$ is that the anomalous states at the rotation axis gap out with their partner under twofold rotation. This requires that the topological charge at each rotation axis is balanced. For this space group, this criterion is also necessary as Wyckoff positions 1c and 1d border only to a twofold rotation symmetry related pairs of 1-cells.

The topological crystals shown in Fig. B.4 (a), (b) are real space limits of weak topological phases corresponding to stacks of twofold rotation symmetric one dimensional topological phases. Figure B.4 (f) shows that the topological crystal shown in Fig. B.4 (a) can be trivialized by a doubling of the unit cell in x direction. However, it is invariant under a doubling of the unit cell in y direction as shown in Figure B.4 (e). A similar argument holds for the topological crystal shown in Fig. B.4 (b). The topological crystal shown in Fig. B.4 (d) is the real space limit of a strong second-order topological superconductor. It is invariant under a redefinition of the unit cell in both x and y direction, as seen in Fig. B.4 (g) and (h), respectively. Due to the equivalence relation, the strong second-order topological phase has $\mathbb{Z}_2$ character, i.e. the topological crystal with topological invariants $(0, 2, -2)$ can be adiabatically deformed to the trivial crystal $(0, 0, 0)$ up to an atomic limit or decorated $d-2$ cells parallel to the rotation axis. In case decorated $d-2$ cells remain, the resulting topological crystal may be a strong third order topological phase, as expected from the K-theoretic results from Ref. 8.

Fourfold rotation symmetry, two dimensions. With fourfold rotation symmetry, the unit cell and cell decomposition is shown in Fig. 3.5 in the main text. The decoration of the 2-cell with a two dimensional topological phase is valid if all 1-cells and 0-cells of its boundaries gap out upon hybridizing the anomalous edge states of adjacent 2-cells.

There are two distinct 1-cell decorations shown in Fig. 3.6 (d) and (e) in the main text. Similar arguments as for twofold rotatation symmetry show that (a) is a weak topological phase and (b) is a strong topological second-order topological phase with $\mathbb{Z}_2$ character due to an equivalence relation invovling an adiabatic and symmetric deformation moving the 1-cell decorations between the two 1-cells. By construction, every fourfold rotation symmetric Wyckoff position is the edge of four 1-cell decorations and therefore hosts four zero-dimensional anomalous edge states of the 1-cells. As every fourfold rotation symmetric Wyckoff position also satisfies twofold rotation symmetry, gapping of twofold rotation symmetry related pairs of anomalous edge modes of 1-cells is a sufficient criterion for the existence of both 1-cell decorations. This criterion is also necessary for the weak topological phase shown in Fig. 3.6 (d) in the main text as the twofold rotation symmetric Wyckoff position 2c border only to a twofold rotation symmetry related pair

of 1-cells. However, this criterion is not necessary for the strong second-order topological phase shown in Fig. 3.6 (e) in the main text. In fact, the 1-cells of the weak topological crystal cannot be decorated with $\mathbb{Z}$ topological phases as the anomaly cancellation criterion cannot be satisfied both at twofold and fourfold rotation axis: In order to gap the anomalous states at fourfold rotation axis, fourfold rotation needs to invert the $\mathbb{Z}$ topological charge. As the action of twofold rotation is given by a double action of fourfold rotation, twofold rotation leaves the topological charge invariant. As in the weak phase, the twofold rotation axes are occupied only by two anomalous states related by twofold rotation, their topological charge needs to be equal. This prohibits anomalous states with $\mathbb{Z}$ topological charge to gap at the twofold rotation axis of the weak topological crystal. An example where the weak topological phase is forbidden while the strong second-order topological phase exists is a magnetic topological insulator as discussed in Sec. B.1 3.

Sixfold rotation symmetry, two dimensions. With sixfold rotation symmetry, the unit cell and cell decomposition is shown in Fig. 3.5. As before, the decoration of the 2-cell with a two dimensional topological phase is valid if all 1-cells and 0-cells of its boundaries gap out upon hybridizing the anomalous edge states of adjacent 2-cells. There is only a single decoration of 1-cells shown in Fig. 3.6 (f) that is consistent with the anomaly cancellation criterion at each rotation axis. A decoration of 1-cells ending at a threefold rotation symmetric momentum cannot be consistent with the anomaly cancellation criterion for tenfold-way topological insulators and superconductors. The valid 1-cell decoration is a strong second-order topological phase. As every sixfold rotation symmetric Wyckoff position also satisfies twofold rotation symmetry and Wyckoff position 3c borders only to a twofold rotation symmetry related pair of 1-cells, gapping of twofold rotation symmetry related pairs of anomalous edge modes of 1-cells is a sufficient and necessary criterion for the existence of both 1-cell decorations.

Extension to three dimensions. In three dimensions, the cell decompositions for space groups $p2$, $p4$ and $p6$ are shown in figures Fig. 3.5 in the main text. For the three dimensional asymmetric unit, all 2-cells and the 1-cells perpendicular to the rotation axis similar arguments as in two dimensions apply. Decorations of the 1-cells parallel to the rotation axis would give rise to a weak topological phase and a third order topological phase hosting an anomalous state at a rotation symmetric corner of the crystal. As in this chapter we focus on topological crytalline phases that may host second-order anomalous states at disclinations, we omit the construction of topological crystals corresponding to decorations of 1-cells parallel to the rotation axis.

A necessary criterion on a strong first order topological phase for fourfold and sixfold rotation symmetry. A first order topological phase in a given topological crystal exists if the decoration of the asymmetric unit with the first order topological phase is valid. As both the fourfold and sixfold rotation symmetric lattices contain a separate twofold rotation axis, the decoration with the first order topological phase in fourfold and sixfold rotation symmetric lattices is possible only if the corresponding decoration is possible in the twofold rotation symmetric lattice.

Connection to K-theoretic classification schemes. The existence of a mass term gapping anomalous states related by n-fold rotation symmetry can be determined from the existence of a strong second-order phase protected by n-fold rotation symmetry in the respective symmetry class and dimension as determined from K-theoretic methods (see Refs. 7–10). This follows as it has been shown in these articles that a strong second-order topological phase can be deformed into symmetry related $d-1$ dimensional building blocks decorated with $d-1$ dimensional first order topological phases. This limit is identical to the topological crystal limit locally around a rotation axis. This draws a one-to-one correspondence between the existence of mass terms hybridizing symmetry related $d-2$ dimensional anomalous states at a rotation axis and the existence of a second-order topological phase protected by the same rotation symmetry.

B.2.3. Obstruction to decorate a lattice with disclination with $\mathbb{Z}$ topological phases

We show that the topological crystal limit of second-order or weak topological phases in symmetry classes with $\mathbb{Z}$ anomalous boundary modes reveals an obstruction to realize these phases on a lattice with disclination such that the system is locally indistinguishable from the bulk everywhere except at the disclination.

Upon forming a $2\pi/n$ disclination by folding the lattice, the unit cells are rotated by $\frac{2\pi}{n}$ in real space without applying any interal action on the degrees of freedom within the unit cell. For $(d-1)$-cell decorations with edge states with $\mathbb{Z}$ topological charge, the onsite action is resposible for inverting the topological charge of symmetry related anomalous states within the unit cell. Due to the absence of the interal action in the rotation of the lattice during the Volterra process, unit cells whose configuration of anomalous states is rotated by $2\pi/n$ are brought next to each other. These unit cells form a continuous line connecting the disclination to the boundary or to another disclination. At each point along the line, the Hamiltonian is locally *distinguishable* from the bulk. Local rotations of unit cells can move, but not remove this line.

Fourfold rotation symmetry. For example, consider the fourfold rotation symmetric lattice with $\pi/2$ disclination depicted in the left column of Fig. B.5. The cut line over which the system was folded is visible as the decorations of adjacent unit cells are rotated with respect to each other. Along this line, the overlapping anomalous states are located in a way that is inconsistent with fourfold rotation symmetry as it is defined in the translation-invariant bulk. It is impossible to apply the same hy-

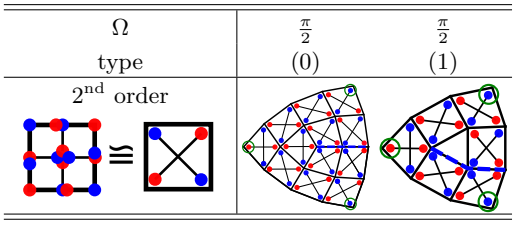

Figure B.5. Decoration of a fourfold symmetric lattice with $\pi/2$ disclinations of both types with strong second-order topological phases with $\mathbb{Z}$ anomalous boundary state. The first row shows the corresponding topological crystals. For simplicity, the anomalous bound states that hybridize within the unit cell are not shown.

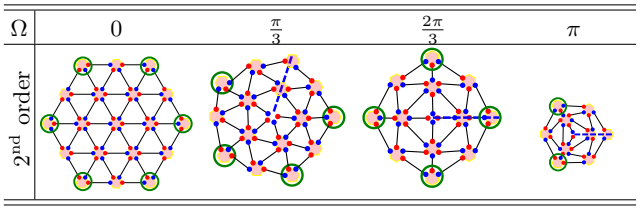

Figure B.6. Sixfold rotation symmetric lattice with disclination with Franck angle Ω decorated with a second-order topological phase whose $d-2$ dimensional anomalous states have $\mathbb{Z}$ topological charge. Notice for the lattice with $\pi/3$ or π disclination that it is impossible to choose a decoration along the cut line that preserve the sixfold rotation symmetry. In these cases we omit the decoration of the $(d-1)$-cells along the cut line. For the $2\pi/3$ disclination the unique decoration pattern of the second-order topological phase is shown.

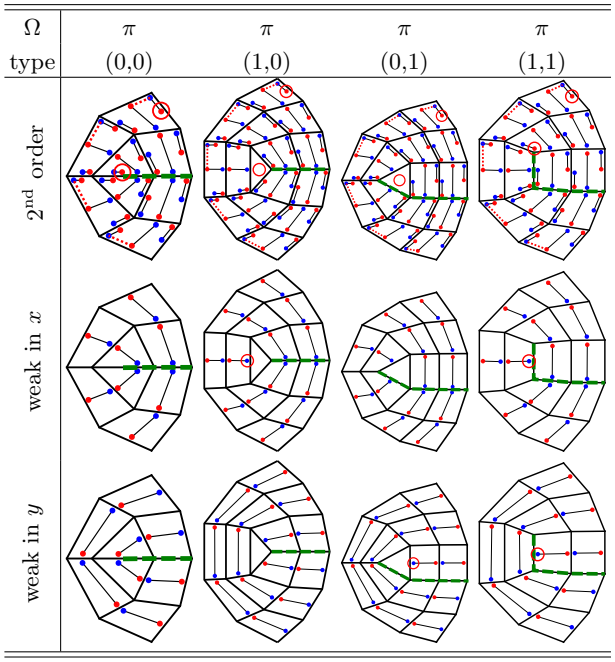

Figure B.7. Decorations of a twofold rotation symmetric lattice with π disclinations of all types with second-order topological phases protected by twofold rotation symmetry and weak phase as a stack in x, y direction. Red and blue dots denote $d-2$ dimensional anomalous states with $\mathbb{Z}$ topological charge ± 1. The red dashed lines denote a possible hybridization of the anomalous states on the surface. The green dashed line denotes the cut line.

bridization term as in the bulk.

Sixfold rotation symmetry. With sixfold rotation symmetry, the topological crystal construction of the second-order topological phase dictates that every line connecting nearest sixfold rotation centers is decorated with a topological phase. The corresponding decorations on a lattice with $\pi/3$, $2\pi/3$ or π disclination is shown in Fig. B.6. For a lattice with $\pi/3$ or π disclination, a decoration of the cut line with $\mathbb{Z}$ topological phases that respects the sixfold rotation symmetry all along the cut line is not possible. A symmetric decoration of a lattice with $2\pi/3$ disclination is possible. In this case the disclination does not host an anomalous state.

Twofold rotation symmetry. The generators of $d-2$ cell decorations of a twofold rotation symmetric lattice with π disclinations of all types are shown in Fig. B.7. As before, rotation symmetry is broken along the cut line. For weak topological phases, if the disclination is created by folding the gapless surface then there is an array of anomalous states with the same topological charge along the cut line which cannot be gapped. If the disclination is created by folding the gapped surfaces then the cut line in the folded lattice with π disclination is gapped. In this case the weak topological phase that corresponds to a stack of lower dimensional topological phases in the x, y direction hosts anomalous disclination states at disclination of type (1,0), (0,1), respectively. The anomalous states at the boundary switch their topological charge at the intersection of the cut line with the boundary.

1. *Relation to the no-go theorem from Sec. B.1 4*

In two dimensions, the local configuration of $\mathbb{Z}$ topological charges is expressed by the representation of chiral antisymmetry. In case the representations of chiral antisymmetry and rotation symmetry $\mathcal{R}_{2\pi/n}$ anticommute, a $2\pi/n$ rotation without applying the internal action of rotation symmetry exchanges the topological charges in the system. This implies that the pattern of $\mathbb{Z}$ topological charges in two unit cells adjacent over the cut line connected to a $2\pi/n$ disclination needs to be distinguishable from the pattern in the bulk, which is the obstruction found from the topological crystal decoration of lattices with disclination as shown in Figs. B.5, B.6, B.7.

The anticommutativity between the representations of chiral antisymmetry and rotation symmetry is necessary for the existence of the second-order and weak topological crystal as the anomaly cancellation criterion (3.6) needs to be satisfied at each rotation axis in the unit cell. This shows that the obstruction to decorating a lattice with disclination such that it is locally indistinguishable from

the bulk everywhere except at the disclination is related to the obstruction of applying the bulk hopping term due to the algebraic relations of the symmetry elements as discussed in Appendix B.1 4.

B.3. FIRST ORDER TOPOLOGY AND POINT OR LINE DEFECTS

Strong first order topological phases are classified in the tenfold way [11 and 12] and do not require any crystalline symmetries for their protection. They may be realized in systems without a lattice structure where the dimensionality is only enforced by the locality of the Hamiltonian. Crystalline symmetries however may prohibit the existence of first order topological phases. A typical example is that the presence of a mirror symmetry requires the Chern number in a plane perpendicular to the mirror plane to vanish.

In Sec. B.3 1 below we show that the independence on any type of underlying lattice of strong first order topological phases implies that there can be no term $\propto \Omega \cdot \nu_1$ linking the rotation holonomy Ω of disclinations with the first order topological invariant ν_1 contributing to the number of anomalous disclination states. However, tenfold-way first order topological phases respond to π-fluxes, which may be bound to point or line defects. In Sec. B.3 2 we list the cases in which they host anomalous states at point or line defects binding π-fluxes.

B.3.1. First order topology and disclinations

In two dimensional space without an underlying lattice one can define disclinations with arbitrary Franck angle Ω as point defects such that any coordinate system that is parallel transported in a closed loop enclosing the disclination (and no additional disclinations) is rotated by Ω. The rotation holonomy Ω_{tot} of a coordinate system parallel transported around several disclinations j is given by the sum of their Franck angles $\Omega_{\text{tot}} = \sum_j \Omega_j$. Now suppose that a disclination with Franck angle Ω_0 would host an anomalous disclination state in the strong first order topological phase. As the existence of disclination states in a topological phase has to be a property of the topological bulk, their existence may only depend on the rotation holonomy of a closed loop that may be deformed to be arbitrarily far away from the disclination (as long as the deformation of the loop does not cross any other disclinations). Thus a disclination with Franck angle $2\Omega_0$ can be constructed by moving two disclinations with Franck angle Ω_0 to the same point in space. As a consequence, the topological charge at a disclination with Franck angle $2\Omega_0$ is twice the topological charge of a disclination with Franck angle Ω_0. Furthermore, if a disclination with Franck angle Ω_0 hosts an anomalous state with topological charge $Q = 1$, the topological charge at a disclination with Franck angle $\Omega_0/2$ has to depend on microscopic details of the disclination and cannot be a property of the topological bulk as the topological charge is quantized to integers.

As first order topological phases do not require any rotation symmetry for their topological protection that would single out a specific Franck angle Ω_0, all disclinations independent on their Franck angle should have the same properties under topological deformations perseving the bulk gap of the first order topological phase. This is only possible if first order topological phases do not host anomalous states at disclinations.

These general arguments can be confirmed by combining the exact diagonalization results from Ref. 13 with the classification and corresponding topological invariants from Ref. 9 for twofold and fourfold rotation symmetric systems. In Ref. 13 models for topological superconductors with odd Chern number and trivial and nontrival weak invariants have been defined and systematically exactly diagonalized on lattices with disclinations. Applying the topological invariants from Ref. 9 to their corresponding models with twofold and fourfold rotation symmetry shows that these models are not simultaneously in a second-order topological phase. Thus the absence of Majorana bound states at disclinations of the odd Chern number model with trivial weak invariants confirms our general arguments from this section.

B.3.2. First-order topological phases and π-fluxes

In this section we show that first order topological phases in symmetry classes and dimension d that allow for $d-2$ dimensional anomalous states host anomalous states at $d-2$ dimensional defects with the property that the geometric phase α acquired by parallel transport around a closed a loop around the defect is π.

In two dimensions, this property corresponds to the familiar statement that p-wave superconductors with odd Chern number host Majorana bound states at vortex cores [14 and 15]. By augmenting such a Chern superconductor with its time reversed copy by applying the same procedure as in Section 3.6.2, one constructs a two dimensional topological superconductor in class DIII. This procedure defines a homomorphism $h_{\mathcal{T}} : \mathcal{K}_{\text{D}}(d=2) \to \mathcal{K}_{\text{DIII}}(d=2)$ from the classifying group $\mathcal{K}_{\text{D}}(d=2) \simeq \mathbb{Z}$ of two dimensional topological superconconducts in class D to the classifying group two dimensional topological superconductors in class DIII $\mathcal{K}_{\text{DIII}}(d=2) \simeq \mathbb{Z}_2$. Under this homomorphism, the Majorana bound state at a vortex is mapped to a Kramers pair of Majorana bound states at a vortex. This procedure shows that the two dimensional superconductor in class DIII hosts Kramers pairs of Majorana bound states at vortices, in agreement with Ref. 16.

By applying the dimensional raising maps from Refs. 3–5 to the two dimensional first order topological superconductors in class D and class DIII, one shows that $d-2$ dimensional defects binding a π-flux in all related symmetry classes and dimensions host $d-2$ dimensional

anomalous states. The dimensional raising maps starting from Cartan classes with a chiral antisymmetry were reviewed and applied in Appendix B.1 4. The dimensional raising map preserves the existence of $d-2$ dimensional states at point defects as long as all crystalline symmetries, if present, act trivially in the newly added dimensions. This was exemplified in Sec. 3.6.3 and was shown using a dimensional reduction scheme based on the scattering matrix in Section 2.3 of Chapter 2 [7] .

B.3.3. Presence of internal unitary symmetries

First-order topological phases protected by an internal unitary symmetry $\mathcal{U}$ may also host anomalous states at a $\mathcal{U}$-symmetry flux defect [17]. These defects are defined as the end of a branch cut upon which a crossing particle is acted upon by the symmetry $\mathcal{U}$. The presence of the symmetry flux thus is another property of point defects in addition to the $\mathbb{Z}_2$ geometric π-flux and the rotation and translation holonomies that needs to be specified when constructing a disclination. The construction of a lattice with $\mathcal{U}$-symmetry flux is similar as discussed in Sec. 3.2.4. Therefore, similar conditions hold for the algebraic relations on the symmetry elements in order to ensure the absence of a domain wall that allows a unique prediction of the existence of anomalous states at the $\mathcal{U}$-symmetry flux defect.

Furthermore, the classification of first-order topological phases in the presence of additional unitary symmetries follows by block diagonalizing the Hamiltonian under the irreducible representations of the unitary symmetries and identifying the Cartan class and relations between each block [18 and 19].

An example is a two-dimensional topological superconductor in Cartan class D with a $\mathbb{Z}_2$ unitary internal symmetry $\mathcal{U}$ with $\mathcal{U}^2=1$ that commutes with particle-hole conjugation. In this case the Hamiltonian can be block-diagonalized with respect to the two eigenvalues ±1 of $\mathcal{U}$ and the two blocks individually are in Cartan class D and can be characterized by a Chern number $\mathrm{Ch}_\pm$ where the subscript $\pm$ denotes the block. One can identify a generator of a $\mathbb{Z}_2$ symmetry enriched topological phase as a Hamiltonian with $\mathrm{Ch}_+=1$ and $\mathrm{Ch}_-=0$ and a generator of the $\mathbb{Z}_2$-symmetry protected topological phase as a Hamiltonian with $\mathrm{Ch}_-=-\mathrm{Ch}_+=1$.

In this example, one can distinguish a geometric π-flux from a $\mathcal{U}$-symmetry flux: the geometric π-flux is defined by introducing a branch cut through the system such that each particle crossing the branch cut acquires a π phase shift. In contrast, the $\mathcal{U}$-symmetry flux is defined by introducing a branch cut such that each particle crossing it is acted upon by $\mathcal{U}$. The geometric π-flux defect hosts a number of Majorana fermions that is given by the parity of the total Chern number $\theta^{\mathrm{flux}}=\mathrm{Ch}_++\mathrm{Ch}_-$ mod 2. The $\mathcal{U}$-symmetry flux hosts a number of Majorana fermions $\theta^{\mathcal{U}}=\mathrm{Ch}_-$ mod 2 given by the parity of the Chern number in the -1 block only. This can be seen as in the block-diagonal basis of $\mathcal{U}$, the $\mathcal{U}$-symmetry flux contributes a π phase shift only in the -1 subspace while it acts trivially in the $+1$ subspace.

As for our crystalline examples, each property of the defect is associated with exactly one generator of the topological phases that contributes anomalous states to the defect: only the generator of the symmetry-enriched topological phase with $\mathrm{Ch}_+=1$ and $\mathrm{Ch}_-=0$ contributes a Majorana bound state to the geometric π-flux defect, and only the generator of the $\mathbb{Z}_2$ internal-symmetry protected topological phase with $\mathrm{Ch}_-=-\mathrm{Ch}_+=1$ contributes a Majorana bound state to the $\mathcal{U}$-symmetry flux defect.

B.4. SYMMETRY-BASED INDICATORS FOR TWO DIMENSIONAL SUPERCONDUCTORS IN CLASS D

Symmetry-based indicators are easy-to-compute topological invariants for topological crystalline insulators and superconductors that are expressed using the matrix-valued single-particle Hamiltonian $H(\vec{k}_{\mathrm{s}})$ at a certain set of high-symmetry momenta $\vec{k}_{\mathrm{s}}$. The symmetry-based indicators for a Cartan class D superconductor with twofold and fourfold rotation symmetry have been derived in Section 4.6.2 of Chapter 4 and Appendix C.1.3 [9]. The symmetry-based indicators of Chapter 4 [9] are in one-to-one correspondence to the rotation invariants of Ref. 13. Here, we show how the symmetry-based indicators can be used to formulate a criterion on the existence of anomalous disclination states in terms of the bulk topological invariants.

Fourfold rotation symmetry. Anomalous states at point defects exist only for pairing symmetries $u(R_{\pi/2})\Delta(R_{\pi/2}\vec{k})u^\dagger(R_{\pi/2})=\pm\Delta(\vec{k})$. For the other pairing symmetries, there are no topological phases that can host zero-dimensional Majorana defect states (see Table 3.1 and Appendix B.5 2). Below we present the result for even pairing symmetry $u(R_{\pi/2})\Delta(R_{\pi/2}\vec{k})u^\dagger(R_{\pi/2})=\Delta(\vec{k})$. There are two symmetry-based indicators,

$$z_{1;x,y}=\mathfrak{N}^{(\pi,0)}_{\frac{1}{2}}+\mathfrak{N}^{(\pi,\pi)}_{\frac{1}{2}}+\mathfrak{N}^{(\pi,\pi)}_{\frac{5}{2}}\mod 2 \tag{B.21}$$

and

$$\begin{aligned} z_2=&-\mathfrak{N}^{(0,0)}_{\frac{1}{2}}+3\mathfrak{N}^{(0,0)}_{\frac{5}{2}}-2\mathfrak{N}^{(\pi,0)}_{\frac{1}{2}}\\ &+3\mathfrak{N}^{(\pi,\pi)}_{\frac{1}{2}}-\mathfrak{N}^{(\pi,\pi)}_{\frac{5}{2}}\mod 8. \end{aligned} \tag{B.22}$$

Here, $\mathfrak{N}^{\vec{k}_{\mathrm{s}}}_j$ is the number of eigenstates with negative eigenenergy and eigenvalues $e^{ij2\pi/n}$ under rotation symmetry of the Hamiltonian $H(\vec{k}_{\mathrm{s}})$ at the high symmetry momentum $\vec{k}_{\mathrm{s}}$ with n-fold rotation symmetry. The symmetry-based indicator $z_{1;x,y}$ detects the weak topological superconductor. The elements z_2 mod 8 correspond to a Chern superconductor. The element "4" $\in\mathbb{Z}_8$

is ambiguous and may either correspond to the second-order topological superconductor or to a Chern superconductor with Chern number $Ch = 4$.

Due to the ambiguity of the second-order topological superconductor with the Chern superconductor, it is impossible to define a necessary criterion on the existence of Majorana bound states at a disclination purely in terms of topological band labels. However, a criterion can be formulated assuming the Chern number Ch can be explicitly determined. The number of Majorana bound states at a disclination with Franck angle Ω and translation holonomy $\vec{T}$ is

$$\theta = \frac{\Omega}{2\pi}(z_2 - Ch) + \vec{T}\cdot\vec{G}_\nu \mod 2 \tag{B.23}$$

where $\vec{G}_\nu = (z_{1;x,y}, z_{1;x,y})^T$ is the weak invariant and $\vec{T}$ is the translation holonomy of the disclination.

Twofold rotation symmetry. Anomalous states at point defects exist only for even pairing symmetry $u(R_\pi)\Delta(R_\pi\vec{k})u^\dagger(R_\pi) = \Delta(\vec{k})$, see Table 3.1 and Appendix B.5 2. There are three symmetry-based indicators. The first two,

$$z_{1;x} = \mathfrak{N}^{(\pi,0)}_{\frac{1}{2}} + \mathfrak{N}^{(\pi,\pi)}_{\frac{1}{2}} \mod 2, \tag{B.24}$$

$$z_{1;y} = \mathfrak{N}^{(0,\pi)}_{\frac{1}{2}} + \mathfrak{N}^{(\pi,\pi)}_{\frac{1}{2}} \mod 2 \tag{B.25}$$

correspond to weak topological superconductors with topological crystal limits shown in Fig. 3.6 (a), (b) in the main text, respectively. Furthermore, there is a symmetry-based indicator

$$z_2 = \mathfrak{N}^{(0,0)}_{\frac{1}{2}} - \mathfrak{N}^{(0,\pi)}_{\frac{1}{2}} - \mathfrak{N}^{(\pi,0)}_{\frac{1}{2}} + \mathfrak{N}^{(\pi,\pi)}_{\frac{1}{2}} \mod 4 \tag{B.26}$$

whose odd elements detect the parity of the Chern number and the value $z_2 = 2$ is ambiguous between a Chern superconductor with even Chern number and a second-order topological superconductor. The number of Majorana bound states at a disclination with Franck angle Ω and translation holonomy $\vec{T}$ can be determined as

$$\theta = \frac{\Omega}{2\pi}(z_2 - Ch) + \vec{T}\cdot\vec{G}_\nu \mod 2 \tag{B.27}$$

where $\vec{G}_\nu = (z_{1;x}, z_{1;y})^T$ is the weak invariant.

B.5. DERIVATION OF TABLES 3.1 AND 3.2

This section shows how the classification of strong first order, strong rotation symmetry protected second-order, and weak topological phases summarized in tables 3.1 and 3.2 can be obtained using our results from B.2 2 and similar arguments as in the examples Sec. 3.6. In addition, we briefly review the symmetry classification of superconducting order parameters in Sec. B.5 1 as it determines the topological classification (see also Section 4.2 of Chapter 4 for a more detailed discussion). A complete discussion can be found in Ref. 9.

In Appendix B.2 2, we derived simple criteria for the existence of rotation symmetry protected second-order and weak topological phases. In particlar, we showed that a sufficient criterion for the existence of a second-order topological phase with fourfold and sixfold rotation symmetry is the existence of a second-order topological phase with twofold rotation symmetry with representation $U(R_\pi) = U(R_{\pi/2})^2$ and $U(R_\pi) = U(R_{\pi/3})^3$, respectively. For sixfold symmetric second-order topological phases on a lattice and for weak topological phases in fourfold symmetric lattices this criterion is also necessary. All entries have been verified by checking that i) the required hybridization terms to gap out the anomalous states in the topological crystal construction exist or ii) a tight binding model realizing the topological crystalline phase in question can be explicitly defined.

B.5.1. Symmetry of the superconducting order parameter

The classification of topological crystalline superconductors depends on the symmetry of superconducting order parameter, as the explicit examples in sections B.5 2 and B.5 3 below show. The following is a brief summary of the extensive discussion in Section 4.2 of Chapter 4 [9].

The BdG Hamiltonian describing superconducting systems is of the form

$$H_{BdG}(\vec{k}) = \begin{pmatrix} h(\vec{k}) & \Delta(\vec{k}) \\ \Delta(\vec{k})^\dagger & -h^*(-\vec{k}) \end{pmatrix} \tag{B.28}$$

where $\Delta(\vec{k}) = -\Delta^T(-\vec{k})$ is the superconducting order parameter and $h(\vec{k})$ is the normal state single particle Hamiltonian. The BdG Hamiltonian satisfies a particle-hole antisymmetry $H_{\mathrm{BdG}}(\vec{k}) = -\tau_1 H_{\mathrm{BdG}}(-\vec{k})^*\tau_1$ where τ are Pauli matrices in particle-hole space. The symmetry of the superconducting order parameter $\Delta(\vec{k})$ can be characterized by a one-dimensional representation Θ of the point group [9 and 20] as

$$\Delta(\vec{k}) = u(g)\Delta(g\vec{k})u^\dagger(g)\Theta^*(g) \tag{B.29}$$

where $u(g)$ is the representation of the point group element g on the normal-state Hamiltonian $h(\vec{k})$. The corresponding representation on the Bogoliubov-de Gennes Hamiltonian is

$$U(g) = \begin{pmatrix} u(g) & 0 \\ 0 & u^*(g)\Theta(g) \end{pmatrix}. \tag{B.30}$$

With this representation one finds directly the commutation relation between particle-hole antisymmetry and the point group elements

$$g\mathcal{P} = \Theta(g)\mathcal{P}g. \tag{B.31}$$

For point groups generated by a single n-fold rotation symmetry the one dimensional representation $\theta(g)$ is entirely specified by the phase ϕ of the generating element $e^{i\phi} = \theta(R_{2\pi/n})$.

B.5.2. Two dimensions

1. Class D

Twofold rotation. The existence of the mass term guaranteeing the existence of weak and second-order topological phases for both pairing symmetries characterized by the phase $\phi = 0$ and π follows from results of Refs. 7 and 8, as detailed in the last paragraph of Sec. B.2 2. For concreteness, for $\phi = 0$ we may choose the representations $U(\mathcal{R}_\pi) = i\tau_2$, $\mathcal{P} = K$ where the mass term that gaps a pair of symmetry related Majorana bound states is τ_2. For $\phi = \pi$ we may choose the representations $U(\mathcal{R}_\pi) = i\tau_2$, $\mathcal{P} = \tau_3 K$ where no mass term exists. Refs. 7 and 8 also show that a Chern superconductor with odd Chern number exists only for $\phi = 0$ while for $\phi = \pi$, the Chern number is constrained to be even.

Fourfold rotation. The topological classification of superconductors with pairing symmetry characterized by the phase $\phi = 0$ and π ($\phi = \pi/2$ and $3\pi/2$) are identical as they are related by a multiplication of the representation of rotation symmetry with a phase [9]. For $\phi = 0, \pi$, the weak and second-order phases exist as the Majorana bound states at the rotation axes gap out in twofold rotation symmetry related pairs. For $\phi = \pi/2, 3\pi/2$ Ref. 9 has shown that no strong second-order topological phase and no weak phase exists and the Chern number is constrained to be even.

Sixfold rotation. Similar as for fourfold rotation, the topological classification of superconductors with pairing symmetry characterized by the phase $\phi = 0, 2\pi/3$ and $4\pi/3$ ($\phi = \pi, \pi/3$ and $5\pi/3$) are identical. A second-order topological phase exists only for $\phi = 0, 2\pi/3$ and $4\pi/3$. For $\phi = 0$, a superconductor with Chern number $Ch = 1$ is given by the $p_x + ip_y$ superconductor [13],

$$H(\vec{k}) = \sum_{i=1}^{3} \sin(\vec{k}\cdot\vec{a}_1)\vec{a}_1\cdot\vec{\tau} + \cos(\vec{k}\cdot\vec{a}_1)\tau_3 \qquad \text{(B.32)}$$

with $\vec{\tau} = (\tau_x, \tau_y)^T$ and $a_1 = (1, 0)$, $a_2 = (-\frac{1}{2}, \frac{\sqrt{3}}{2})$ and $a_3 = (-\frac{1}{2}, -\frac{\sqrt{3}}{2})$ and representation of sixfold rotation symmetry $U(\mathcal{R}_{\pi/3}) = e^{i\pi\tau_3/6}$ and particle-hole antisymmetry $\mathcal{P} = \tau_1 K$. For $\phi = \pi$ a superconductor with odd Chern number does not exist. In this symmetry class, a model for a superconductor with Chern number $Ch = 2$ can be defined as

$$H(\vec{k}) = \sum_{i=1}^{3} \sin(\vec{k}\cdot\vec{a}_1)\vec{a}_1\cdot\vec{\tau}\rho_0 + \cos(\vec{k}\cdot\vec{a}_1)\tau_3\rho_0 \qquad \text{(B.33)}$$

with $\vec{\tau} = (\tau_x, \tau_y)^T$ and $a_1 = (1, 0)$, $a_2 = (-\frac{1}{2}, \frac{\sqrt{3}}{2})$ and $a_3 = (-\frac{1}{2}, -\frac{\sqrt{3}}{2})$ and representation of sixfold rotation symmetry $U(\mathcal{R}_{\pi/3}) = e^{i\pi\tau_3/6}\rho_3$ and particle-hole antisymmetry $\mathcal{P} = \tau_1\rho_1 K$.

Magnetic twofold rotation. A magnetic rotation symmetry consists of the combined action of rotation and time-reversal symmetry. For spinful fermions, these operators commute. Thus, for magnetic twofold rotation symmetry we have $(U(\mathcal{R}_\pi\mathcal{T})K)^2 = 1$. A pair of Majorana bound states related by $\mathcal{R}_\pi\mathcal{T}$ with $U(\mathcal{R}_\pi\mathcal{T}) = \tau_1$ gaps upon hybridization with the mass term τ_2. As a consequence, the second-order and weak topological phase exist. Twofold magnetic rotation symmetry requires the Chern number to vanish [].

Magnetic fourfold rotation. For magnetic fourfold rotation symmetry, the operator $\left(U(\mathcal{R}_{\pi/2}\mathcal{T})K\right)^2$ is a unitary twofold rotation operator that commutes with particle-hole antisymmetry. Furthermore, we have $\left(U(\mathcal{R}_{\pi/2}\mathcal{T})K\right)^4 = -1$ for spinful fermions. Here, Majorana bound states hybridize in twofold rotation symmetry related pairs. Thus a weak and second-order topological phase exists. Furthermore, magnetic fourfold rotation prohibits the existence of a Chern number.

Magnetix sixfold rotation. A system with magnetic sixfold rotation symmetry also satisfies magnetic twofold rotation symmetry. We have shown that for the latter, Majorana bound states hybridize in pairs and the Chern number needs to vanish. Thus only the second-order topological phase exists.

2. Class DIII

Pairing symmetry $\phi = 0$. Superconductors in class DIII with $\phi = 0$ can be constructed from the class D superconductors with $\phi = 0$ by taking two time reversed copies as shown in Sec. 3.6.2. This construction shows the existence of weak and strong first and second-order topological phases for twofold, fourfold and sixfold rotation symmetry.

Pairing symmetry $\phi = \pi$. For this pairing symmetry, Kramers pairs of Majorana bound states at rotation axes with representations $\mathcal{T} = i\sigma_2\tau_0 K$, $\mathcal{P} = \sigma_0\tau_3 K$ hybridize in partners related by twofold rotation $U(\mathcal{R}_\pi) = i\sigma_3\tau_1$ as the mass term $\sigma_1\tau_2$ exists. In systems with fourfold rotation symmetry with $\phi = \pi$, the representation of twofold rotation symmetry commutes with particle-hole symmetry. With the results from the previous paragraph on the pairing symmetry $\phi = 0$, also at fourfold rotation axes the Kramers pairs of Majorana bound states hybridize in partners related by twofold rotation symmetry. Thus, weak and second-order phases exist with twofold, fourfold and sixfold rotation symmetry. The first order topological phase is prohibited by n-fold rotation symmetry with pairing symmetry $\phi = \pi$.

Furthermore, with $\phi = \pi$ rotation symmetry anticommutes with particle-hole antisymmetry. As argued in Sec. 3.2.4, in this case it is impossible to construct a finite hopping across the cut that preserves all symmetries and is locally indistinguishable from the bulk. This implies

that there is in general no bulk-defect correspondence at disclinations for pairing symmetry $\phi = \pi$.

3. Classes AIII and BDI

In class AIII, the zero dimensional anomalous states have $\mathbb{Z}$ topological charge as zero-energy states with the same eigenvalue under chiral antisymmetry Γ do not gap out in pairs. Therefore, a set of symmetry related zero-energy states can only gap out if the rotation symmetry anticommutes with chiral antisymmetry such that the eigenvalue of chiral antisymmetry of symmetry related zero-energy states is opposite. In this case, twofold rotation symmetry related states gap out with a mass term τ_2 with representations $U(\mathcal{R}_\pi) = i\tau_2$ and $\Gamma = \tau_3$. As a consequence, second-order topological phases exist for twofold, fourfold and sixfold rotation symmetric lattices. Weak topological phases exist in twofold rotation symmetric lattices. There does not exist a first order topological phase in class AIII in two dimensions.

The same result holds for class BDI in two dimensions as the mass term also satisfies the antiunitary symmetry $\mathcal{T} = \tau_3 K$.

4. Class CII

Class CII has time-reversal symmetry $\mathcal{T}^2 = -1$ and particle-hole antisymmetry $\mathcal{P}^2 = -1$. Similar arguments as in class AIII hold here, except that the zero-energy states appear in Kramers pairs. Here, a mass term gapping twofold rotation symmetry related partners can be chosen as $\sigma_3\tau_2$ with representations $\mathcal{T} = i\sigma_2\tau_0 K$, $\mathcal{P} = \sigma_0\tau_2 K$ and $U(\mathcal{R}_\pi) = \sigma_3\tau_2$.

B.5.3. Three dimensions

In three dimensions, the $d-1$ dimensional anomalous states with $\mathbb{Z}$ topological charge are chiral states. Their topological charge (i.e. their propagation direction) is only inverted by magnetic rotation symmetry. As a consequence, there are no weak or second-order topological phases in classes A, D, C with non-magnetic rotation symmetry. Furthermore, these Cartan classes also do not host first order topological phases.

1. Classes A and D

In class A, chiral modes related by twofold magnetic rotation symmetry gap out in pairs, as the mass term τ_2 for two chiral modes related by twofold magnetic rotation symmetry $\mathcal{R}_\pi\mathcal{T} = \tau_1 K$ described by the low energy Hamiltonian $vk_z\tau_3$ exists. For fourfold magnetic rotation symmetry, it has been shown in Sec. B.1 3 that the mass term $\tau_3\sigma_2 - \tau_2\sigma_0$ describing a ring hybridization of rotation symmetry related chiral modes with low energy Hamiltonian $vk_z\tau_3\sigma_3$ creates a gap in the spectrum. As a consequence, second-order topological phases exist in lattices with twofold, fourfold and sixfold magnetic rotation symmetry. The weak topological phases as shown in Fig. 3.6 in the main text exist only in lattices with twofold rotation symmetry.

The mass terms and low energy Hamiltonians also satisfy particle-hole antisymmetry $\mathcal{P} = K$. Thus the results apply also to class D.

The weak phases corresponding to stacks of Chern insulators with stacking direction parallel to the rotation axis exist in class A with non-magnetic rotation symmetry as the Chern number is consistent with rotation symmetry. Magnetic rotation symmetry requires the Chern number to vanish. In class D, the results from section B.5 2 apply.

2. Class C

We regard physical systems in class C as superconductors in the presence of spin rotation symmetry. In this case, magnetic twofold rotation symmetry still satisfies $(\mathcal{R}_\pi\mathcal{T})^2 = 1$. With $\mathcal{R}_\pi\mathcal{T} = \tau_0\rho_1 K$ and $\mathcal{P} = \tau_2\rho_0 K$, the mass term $\tau_0\rho_2$ gaps out the low energy Hamiltonian $vk_z\tau_0\rho_3$ describing the minimal number of chiral modes related by magnetic twofold rotation symmetry. In class C, fourfold magnetic rotation symmetry satisfies $(\mathcal{R}_{\pi/2}\mathcal{T})^4 = 1$. Here a ring hybridization with real hopping elements gaps symmetry related chiral modes. This shows the existence of the weak and second-order topological phases as shown in Fig. 3.6 in the main text in lattices with twofold, fourfold and sixfold magnetic rotation symmetry in Cartan class C.

Two dimensional superconductors in class C allow for an even Chern number. The weak phases corresponding to stacks of Chern superconductors with even Chern number with stacking direction parallel to the rotation axis exist with non-magnetic rotation symmetry for any pairing symmetry.

3. Class DIII

Pairing symmetry $\phi = 0$. Three dimensional superconductors in class DIII with $\phi = 0$ can be constructed from two dimensional class D superconductors with $\phi = 0$ using the dimensional raising map as we also used in Appendix B.1 4. It has been shown using the reflection matrix dimension reduction scheme in Section 2.3 of Chapter 2 [7] that the dimensional raising map preserves anomalous states at defects.

Below we illustrate the usage of the dimensional raising map to define a model Hamiltonian for the second-order topological superconductor in class DIII in three dimensions.

In the model described by the Hamiltonian H_D in Eq. (3.13) the dimerization parameter (or mass) δt can

be used to tune between the trivial and the topological phase. In particular, the system undergoes a topological phase transition at $\delta t = 0$, where the bulk gap closes. The dimensional raising map requires to replace $\delta t \to \delta t \cos k_z$, such that the model interpolated between the trivial and the topological phase as a function of the additional momentum parameter k_z. In order to ensure that the system remains gapped for all k_z one adds another term $t_z \sin k_z \gamma_z$ to the Hamiltonian, requiring that γ_z anticommutes with the Hamiltonian at $k_z = 0, \pi$. Starting from a model without chiral antisymmetry one needs to introduce a new degree of freedom described by Pauli matrices σ by taking the original model $H_D \to H_D s_3$. Then we may choose $\gamma_z = \sigma_3$. Now the model satisfies an additional chiral antisymmetry $\Gamma = \sigma_2$ and, in combination with particle-hole antisymmetry, a time-reversal symmetry $\mathcal{T} = i\sigma_2 K$. Thus we may interpret the σ_3 degree of freedom as spin.

These arguments are collected in the dimensional raising map, which is expressed as

$$\begin{aligned} H_D(k_x, k_y; \delta t) \ \to \ & H_D(k_x, k_y; \delta t \cos[k_z])\sigma_3 \\ & + t_z \sin[k_z]\tau_0\rho_0\sigma_1. \end{aligned}$$

This lifts our two-dimensional model in class D to a three-dimensional model in class DIII realizing a strong second-order topological phase.

Pairing symmetry $\phi = \pi$. Similar to two dimensional class DIII superconductors with pairing symmetry $\phi = \pi$, helical Majorana modes $vk_z\sigma_3\tau_0$ related by twofold rotation $U(\mathcal{R}_\pi) = i\sigma_3\tau_1$ and representations $\mathcal{T} = i\sigma_2\tau_0 T$, $\mathcal{P} = \sigma_0\tau_3 K$ hybridize as the mass term $\sigma_1\tau_2$ exists. Weak and second-order phases exist with twofold, fourfold and sixfold rotation symmetry. The first order topological phase is prohibited by n-fold rotation symmetry with pairing symmetry $\phi = \pi$. These results are consistent with Ref. [19].

The existence of weak phases corresponding to stacks of two-dimensional first order topological superconductors with stacking direction parallel to the rotation axis follows from the results of section B.5 2.

4. Class AII

The classification of time reversal symmetric insulators in class AII is related to class DIII by lifting the particle-hole antisymmetry constraint of class DIII. This construction maps the first order topological phases in $d = 2, 3$ and corresponding anomalous states of class DIII to the corresponding first order topological phases and anomalous states in class AII [12]. Applying this construction to class DIII topological superconductors with pairing symmetry $\phi = 0$ shows the existence of first-order, second-order and weak topological phases in class AII.

Weak phases corresponding to stacks of two-dimensional first order topological insulators with stacking direction parallel to the rotation axis exist with twofold rotation symmetry.

[1] R. Queiroz, I. C. Fulga, N. Avraham, H. Beidenkopf, and J. Cano, Phys. Rev. Lett. **123**, 266802 (2019).
[2] F. Schindler, A. M. Cook, M. G. Vergniory, Z. Wang, S. S. P. Parkin, B. A. Bernevig, and T. Neupert, Science Advances **4** (2018), 10.1126/sciadv.aat0346.
[3] J. C. Y. Teo and C. L. Kane, Phys. Rev. B **82**, 115120 (2010).
[4] K. Shiozaki and M. Sato, Phys. Rev. B **90**, 165114 (2014).
[5] K. Shiozaki, M. Sato, and K. Gomi, Phys. Rev. B **95**, 235425 (2017).
[6] I. C. Fulga, F. Hassler, and A. R. Akhmerov, Phys. Rev. B **85**, 165409 (2012).
[7] M. Geier, L. Trifunovic, M. Hoskam, and P. W. Brouwer, Phys. Rev. B **97**, 205135 (2018).
[8] L. Trifunovic and P. W. Brouwer, Phys. Rev. X **9**, 011012 (2019).
[9] M. Geier, P. W. Brouwer, and L. Trifunovic, Phys. Rev. B **101**, 245128 (2020).
[10] L. Trifunovic and P. W. Brouwer, (2020), arXiv:2003.01144.
[11] A. Kitaev, AIP Conference Proceedings **1134**, 22 (2009).
[12] C.-K. Chiu, J. C. Y. Teo, A. P. Schnyder, and S. Ryu, Rev. Mod. Phys. **88**, 035005 (2016).
[13] W. A. Benalcazar, J. C. Y. Teo, and T. L. Hughes, Phys. Rev. B **89**, 224503 (2014).
[14] N. Read and D. Green, Phys. Rev. B **61**, 10267 (2000).
[15] D. A. Ivanov, Phys. Rev. Lett. **86**, 268 (2001).
[16] B. A. Bernevig and T. L. Hughes, *Topological insulators and topological superconductors* (Princeton university press, 2013).
[17] M. Barkeshli, P. Bonderson, M. Cheng, and Z. Wang, Phys. Rev. B **100**, 115147 (2019).
[18] E. Cornfeld and A. Chapman, Phys. Rev. B **99**, 075105 (2019).
[19] K. Shiozaki, (2019), arXiv:1907.09354.
[20] S. Ono, H. C. Po, and H. Watanabe, Science Advances **6**, eaaz8367 (2020).

C. Appendix to "Symmetry-based indicators for topological Bogoliubov-de Gennes Hamiltonians"

C.1. MORE EXAMPLES IN THREE DIMENSIONS

We discuss the classifying group $\mathcal{K}_\eta[G,\Theta]$, band labels, compatibility relations and symmetry-based indicators of the topological phases with nontrivial boundary signatures for a selection of point groups not covered in the main text.

C.1.1. The trivial point group C_1, classes D, DIII, C, CI

In the absence of crystalline symmetries (other than translation), for classes DIII, C and CI there are no topological band labels, as the classification of the inversion symmetric momenta $\mathfrak{K}_\eta[C_1,A]$ is trivial for those classes. The classifying groups are $\mathcal{K}_{\rm DIII}[C_1,A]=\mathbb{Z}_2^6\times\mathbb{Z}$, with three factors $\mathbb{Z}_2$ for weak phases corresponding to stacks of one-dimensional time-reversal symmetric topological superconductors, three factors $\mathbb{Z}_2$ for stacks of two-dimensional time-reversal symmetric topological superconductors, and one factor $\mathbb{Z}$ for a three-dimensional strong first-order superconductor phase , $\mathcal{K}_{\rm C}[C_1,A]=\mathbb{Z}^3$, the three factors $\mathbb{Z}$ describing weak phases corresponding to stacks of two-dimensional Chern superconductors with even Chern number, which can be adiabatically deformed to normal-state Chern insulators, and $\mathcal{K}_{\rm CI}[C_1,A]=\mathbb{Z}$, corresponding to a three-dimensional strong phase. None of these phases can be detected using symmetry-based indicators. The symmetry-based indicators for tenfold-way class D are nontrivial, as we discuss below.

Classifying group. The boundary classifying group for tenfold-way class D is

$$\mathcal{K}_{\rm D}[C_1,A]=\mathbb{Z}_2^3\times\mathbb{Z}^3.$$

The factor $\mathbb{Z}_2^3$ corresponds to Kitaev chains stacked in the y and z, x and z or x and y directions (labels $(1;y,z)$, $(1;x,z)$, and $(1;x,y)$) and the factor $\mathbb{Z}^3$ corresponds to Chern superconductors stacked in the z, y, or x direction (labels $(2;z)$, $(2;y)$, and $(2;x)$). The even-Chern-number superconductors can be deformed to Chern insulators with vanishing superconducting order parameter. The topological phases generate a $\mathbb{Z}_2^6$ subgroup of $\mathrm{SI}_{\rm D}[C_1,A]=\mathbb{Z}_2^7$. The boundary signatures of the topological phases together with their symmetry-based indicators are shown in Fig. C.1.

Band labels. There are $\mathrm{BL}\simeq\mathbb{Z}_2^8$ topological band labels given by the Pfaffian invariant $\mathfrak{p}^{\mathbf{k}_{\rm s}}$ at all high-symmetry momenta $\mathbf{k}_{\rm s}$.

Compatibility relations. There are no $0d$ compatibility relations. Hence $\mathrm{BL}\simeq\mathrm{BS}$ and

$$B[H(\mathbf{k})]=\{\mathfrak{p}^{\mathbf{k}_{\rm s}}\}.$$

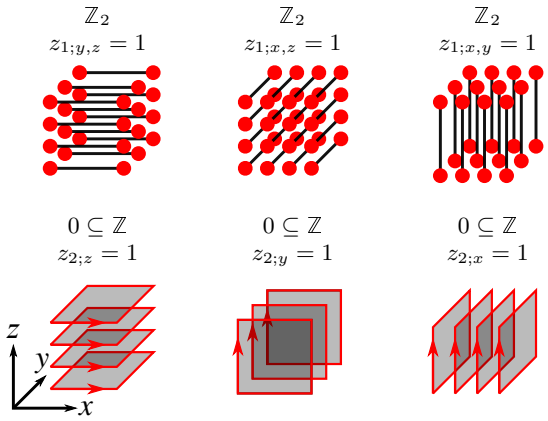

FIG. C.1. Topological phases of a three-dimensional superconductor in tenfold-way class D and with translation symmetry only (point group C_1). For each boundary signature, the boundary subgroup sequence (top row) and the nonzero symmetry-based indicators for a generator of that phase are given (middle row).

There is a $2d$ compability relation required by the conservation of the Chern number between parallel planes,

$$\sum_{\mathbf{k}_{\rm s}|k_{{\rm s},i}=0}\mathfrak{p}^{\mathbf{k}_{\rm s}}=\sum_{\mathbf{k}_{\rm s}|k_{{\rm s},i}=\pi}\mathfrak{p}^{\mathbf{k}_{\rm s}}\mod 2,\quad i=x,y,z.$$

The violation of this compatibility relation signals a gapless phase with nodal points.

Symmetry-based indicators. The group of symmetry-based indicators

$$\mathrm{SI}_{\rm D}[C_1,A]=\mathrm{BS/AI}\simeq\mathbb{Z}_2^7$$

contains a factor $\mathbb{Z}_2^6$ corresponding to stacks of one and two dimensional topological superconductors,

$$z_{1;i,j}=\sum_{\mathbf{k}_{\rm s}|k_{{\rm s},i}=k_{{\rm s},j}=\pi}\mathfrak{p}^{\mathbf{k}_{\rm s}}\mod 2,$$
$$z_{2;j}=\sum_{\mathbf{k}_{\rm s}|k_{{\rm s},j}=\pi}\mathfrak{p}^{\mathbf{k}_{\rm s}}\mod 2,$$

with $i\neq j=x,\,y,\,z$. The remaining factor $\mathbb{Z}_2$ corresponds to a nodal superconductor detected by the violation of the 2d compatibility relation with symmetry-based indicator

$$z_3=\sum_{\mathbf{k}_{\rm s}}\mathfrak{p}^{\mathbf{k}_{\rm s}}\mod 2.$$

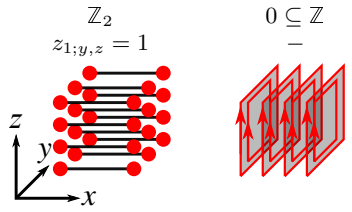

FIG. C.2. Topological phases of a three-dimensional superconductor in tenfold-way class D with point group C_s and representation $\Theta = A'$.

C.1.2. Point group C_s, class D

1. Representation $\Theta = A'$

Classifying group:

$$\mathcal{K}_{\mathrm{D}}[C_s, A'] = \mathbb{Z}_2 \times \mathbb{Z}.$$

The factor $\mathbb{Z}_2$ corresponds to a stack of mirror symmetric Kitaev chains in the y and z directions (label $(1; y, z)$) and the factor $\mathbb{Z}$ corresponds to a stack of two-dimensional Chern superconductors with even Chern number within the mirror plane (label $(2; x)$). The latter phase can not be detected by symmetry-based indicators. It can be adiabatically deformed to a Chern insulator that is robust to the introduction of odd-parity superconducting correlations. The boundary signatures of the topological phases together with their symmetry-based indicators are displayed in Fig. C.2.

Band labels. There are $\mathrm{BL} = \mathbb{Z}^8$ topological band labels given by the invariants $\mathfrak{N}_+^{\mathbf{k}_s}$ at all high-symmetry momenta $\mathbf{k}_s$.

Compatibility relations. Within a mirror plane $k_x = 0, \pi$ the invariant $\mathfrak{N}_+^{\mathbf{k}}$ is preserved for a gapped phase, which leads to the $0d$ compatibility relations

$$\begin{aligned}\mathfrak{N}_+^{(0,0,0)} &= \mathfrak{N}_+^{(0,\pi,0)} = \mathfrak{N}_+^{(0,0,\pi)} = \mathfrak{N}_+^{(0,\pi,\pi)},\\ \mathfrak{N}_+^{(\pi,0,0)} &= \mathfrak{N}_+^{(\pi,\pi,0)} = \mathfrak{N}_+^{(\pi,0,\pi)} = \mathfrak{N}_+^{(\pi,\pi,\pi)},\end{aligned}$$

which identifies a factor $\mathbb{Z}^6$ of the group of topological band labels BL as representation enforced gapless nodal-line superconductors such that we have $\mathrm{BS} \simeq \mathbb{Z}^2$ and

$$B[H(\mathbf{k})] = \{\mathfrak{N}_+^{(0,\pi,\pi)}, \mathfrak{N}_+^{(\pi,\pi,\pi)}\}.$$

Symmetry-based indicators. The group of symmetry-based indicators

$$\mathrm{SI}_{\mathrm{D}}[C_s, A'] \simeq \mathbb{Z}_2 \tag{C.1}$$

contains a single factor corresponding to the stack of Kitaev chains with indicator

$$z_{1;y,z} = \mathfrak{N}_+^{(\pi,\pi,\pi)} + \mathfrak{N}_+^{(0,\pi,\pi)} \mod 2.$$

Our result (C.1) for the group of symmetry-based indicators agrees with the corresponding result from 1.

2. Representation $\Theta = A''$

Classifying group:

$$\mathcal{K}_{\mathrm{D}}[C_s, A''] = \mathbb{Z}_2^7 \times \mathbb{Z}^2.$$

A factor $\mathbb{Z}_2^4$ corresponds to one-dimensional superconductors in the y or z directions, stacked in the x and z or x and y directions, respectively, and with $\mathcal{M}_x$ parities $\pm$ (labels $(1, \pm; x, z)$ and $(1, \pm; x, y)$). The factor $\mathbb{Z}^2$ corresponds to two-dimensional Chern superconductors in the yz plane with even or odd $\mathcal{M}_x$ parity, stacked in the x direction (labels $(2, \pm; x)$). Systems with an even Chern number in either mirror plane can be adiabatically deformed to Chern insulator with vanishing superconducting order parameter. A factor $\mathbb{Z}_2^2$ corresponds to two-dimensional second-order topological superconductors stacked in the z or y direction (labels $(2; z)$ and $(2; y)$). The remaining factor $\mathbb{Z}_2$ corresponds to a three dimensional second-order topological superconductor (label (3)). The boundary signatures of the topological phases together with their symmetry-based indicators are displayed in Fig. C.3.

Band labels. There are $\mathrm{BL} \simeq \mathbb{Z}_2^{16}$ topological band labels given by the Pfaffian invariants $\mathfrak{p}_\pm^{\mathbf{k}_s}$ in both even and odd mirror parity subspaces at all high-symmetry momenta $\mathbf{k}_s$.

Compatibility relations. From the fact that $\mathcal{PM}$ is a local antisymmetry along lines in reciprocal space one deduces the compatibility relations

$$\sum_{s=\pm} \mathfrak{p}_s^{(0,k_y',k_z')} = \sum_{s=\pm} \mathfrak{p}_s^{(\pi,k_y',k_z')}, \quad \text{for } k_y',\, k_z' = 0,\, \pi.$$

The compatibility relations identify a factor $\mathbb{Z}_2^4$ of BL as representation enforced gapless superconductors with nodal points on high-symmetry lines in the Brillouin zone such that we have $\mathrm{BS} \simeq \mathbb{Z}_2^{12}$ and

$$\begin{aligned}B[H(\mathbf{k})] = \{&\mathfrak{p}_-^{(0,0,0)}, \mathfrak{p}_-^{(0,0,\pi)}, \mathfrak{p}_-^{(0,\pi,0)}, \mathfrak{p}_-^{(0,\pi,\pi)}\\ &\mathfrak{p}_+^{(\pi,0,0)}, \mathfrak{p}_+^{(\pi,0,\pi)}, \mathfrak{p}_+^{(\pi,\pi,0)}, \mathfrak{p}_+^{(\pi,\pi,\pi)}\\ &\mathfrak{p}_-^{(\pi,0,0)}, \mathfrak{p}_-^{(\pi,0,\pi)}, \mathfrak{p}_-^{(\pi,\pi,0)}, \mathfrak{p}_-^{(\pi,\pi,\pi)}\}.\end{aligned}$$

Symmetry-based indicators. The group of symmetry-based indicators is

$$\mathrm{SI}_{\mathrm{D}}[C_s, A''] \simeq \mathbb{Z}_2^9, \tag{C.2}$$

where each factor corresponds to a different topological phase. For the stacks of Kitaev chains we have

$$\begin{aligned}z_{1,\pm;x,z} &= \mathfrak{p}_\pm^{(\pi,\pi,\pi)} + \mathfrak{p}_\pm^{(\pi,0,\pi)} \mod 2,\\ z_{1,\pm;x,y} &= \mathfrak{p}_\pm^{(\pi,\pi,\pi)} + \mathfrak{p}_\pm^{(\pi,\pi,0)} \mod 2,\end{aligned}$$

for the Chern superconductors within the mirror plane with even or odd mirror parity

$$z_{2,\pm;x} = \sum_{\mathbf{k}_s | k_{s,x} = \pi} \mathfrak{p}_\pm^{\mathbf{k}_s} \mod 2,$$

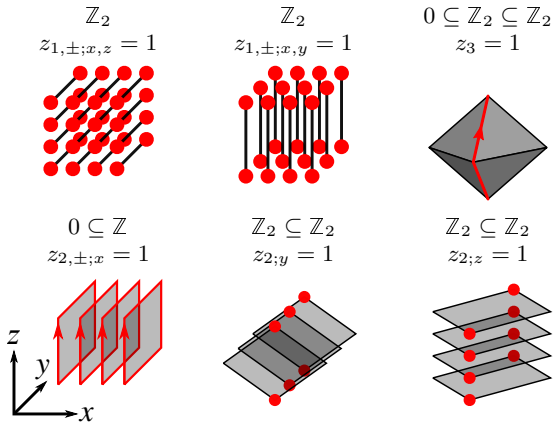

FIG. C.3. Topological phases of a three-dimensional superconductor in tenfold-way class D with point group C_s and representation $\Theta = A''$.

for two-dimensional second-order topological superconductors stacked in the $l = z$ or y direction,

$$z_{2;l} = \sum_{\mathbf{k}_s|_{k_{s,l}=\pi}} \mathfrak{p}_+^{\mathbf{k}_s} = \sum_{\mathbf{k}_s|_{k_{s,l}=\pi}} \mathfrak{p}_-^{\mathbf{k}_s} \mod 2,$$

where the equality follows from the compatibility constraint, and for the three dimensional second-order topological superconductor we have

$$z_3 = \sum_{\mathbf{k}_s} \mathfrak{p}_+^{\mathbf{k}_s} = \sum_{\mathbf{k}_s} \mathfrak{p}_-^{\mathbf{k}_s} \mod 2.$$

The group (C.2) of symmetry-based indicators differs from the result obtained in Ref. 1, where no symmetry-based indicators are found due to the absence of Pfaffian band labels.

C.1.3. Point group C_2, class D

1. *Representation* $\Theta = A$

Classifying group:

$$\mathcal{K}_{\mathrm{D}}[C_2, A] = \mathbb{Z}_2^3 \times \mathbb{Z}.$$

A factor $\mathbb{Z}_2^2$ corresponds to Kitaev chains perpendicular to the rotation axis (z) and stacked in the in the x and z or y and z directions (labels $(1; y, z)$ and $(1; x, z)$). The remaining factors $\mathbb{Z}_2$ and $\mathbb{Z}$ correspond to two-dimensional topological superconductors stacked perpendicular to the rotation axis (labels $(2, z)$' and $(2, z)$, respectively), where the factor $\mathbb{Z}_2$ describes a two-dimensional second-order phase and the factor $\mathbb{Z}$ a Chern superconductor. Even-Chern number superconductors can be adiabatically deformed to normal-state Chern insulators. The weak second-order phase and the stack of Chern superconductors with Chern number two have identical band labels. The boundary signatures of the

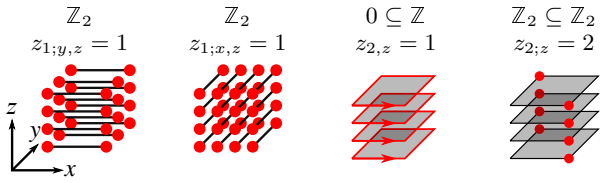

FIG. C.4. Topological phases of a three-dimensional superconductor in tenfold-way class D with point group C_2 and representation $\Theta = A$.

topological phases together with their symmetry-based indicators are displayed in Fig. C.4.

Band labels. There are BL $\simeq \mathbb{Z}^8$ topological band labels given by the invariants $\mathfrak{N}_+^{\mathbf{k}_s}$ at all high-symmetry momenta $\mathbf{k}_s$.

Compatibility relations. For gapped phases, the invariant $\mathfrak{N}_+(\mathbf{k})$ is preserved along high-symmetry lines in reciprocal space parallel to the rotation axis, which gives the compatibility relation

$$\mathfrak{N}_+^{(k_x',k_y',0)} = \mathfrak{N}_+^{(k_x',k_y',\pi)}, \quad \text{for } k_x',\, k_y' = 0,\, \pi.$$

This compatibility relation identifies a factor $\mathbb{Z}^4$ of BL as representation-enforced gapless superconductors with nodal points such that we have BS $\simeq \mathbb{Z}^4$ and

$$B[H(\mathbf{k})] = \{\mathfrak{N}_+^{(0,0,\pi)}, \mathfrak{N}_+^{(\pi,0,\pi)}, \mathfrak{N}_+^{(0,\pi,\pi)}, \mathfrak{N}_+^{(\pi,\pi,\pi)}\}.$$

Symmetry-based indicators. The group of symmetry-based indicators is

$$\mathrm{SI}_{\mathrm{D}}[C_2, A] \simeq \mathbb{Z}_2^2 \times \mathbb{Z}_4. \tag{C.3}$$

The factor $\mathbb{Z}_2^2$ correspond to stacks of Kitaev chains with indicators

$$z_{1;y,z} = \mathfrak{N}_+^{(0,\pi,\pi)} + \mathfrak{N}_+^{(\pi,\pi,\pi)} \mod 2,$$
$$z_{1;x,z} = \mathfrak{N}_+^{(\pi,0,\pi)} + \mathfrak{N}_+^{(\pi,\pi,\pi)} \mod 2$$

and the factor $\mathbb{Z}_4$ corresponds to stacks of two dimensional topological superconductors in the z direction with indicator

$$z_{2;z} = \sum_{\mathbf{k}_s|_{k_{s,z}=\pi}} \mathfrak{N}_+^{\mathbf{k}_s} (-1)^{(k_{s,x}+k_{s,y})/\pi} \mod 4.$$

The value $z_{2;z} = 2$ is ambiguous, since it may either correspond to a stack of first-order two-dimensional superconductors with Chern number two or to a stack of second-order two-dimensional superconductors, see Fig. C.4. Our result (C.3) for the group of symmetry-based indicators agrees with the corresponding result from 1.

2. *Representation* $\Theta = B$

Classifying group:

$$\mathcal{K}_{\mathrm{D}}[C_2, B] = \mathbb{Z}_2^4 \times \mathbb{Z}.$$

A factor $\mathbb{Z}_2^2$ corresponds to one-dimensional superconductors parallel to the rotation (z) axis, stacked in the x and y directions, and with rotation parities $\pm$ (labels $(1,\pm;x,y)$). A factor $\mathbb{Z}_2^2$ corresponds to two-dimensional second-order topological superconductors stacked in the x or y directions (labels $(2;x)$' and $(2;y)$'). The remaining factor $\mathbb{Z}$ describes a two-dimensional even-Chern-number superconductor stacked in the z direction with label $(2;z)$. They can be adiabatically deformed to normal-state Chern insulators. The boundary signatures of the topological phases together with their symmetry-based indicators are displayed in Fig. C.5.

Band labels. There are BL $\simeq \mathbb{Z}_2^{16}$ topological band labels given by the Pfaffian invariants $\mathfrak{p}_\pm^{\mathbf{k}_s}$ in both even and odd rotation parity subspaces at all high-symmetry momenta $\mathbf{k}_s$.

Compatibility relations. From the fact that $\mathcal{R}_\pi\mathcal{P}$ is a local symmetry in reciprocal space in high-symmetry planes, we derive the compatibility relation

$$\begin{aligned}\sum_{s=\pm}\mathfrak{p}_s^{(0,0,k_z)} &= \sum_{s=\pm}\mathfrak{p}_s^{(\pi,0,k_z)}\\ &= \sum_{s=\pm}\mathfrak{p}_s^{(0,\pi,k_z)}\\ &= \sum_{s=\pm}\mathfrak{p}_s^{(\pi,\pi,k_z)} \quad \text{for } k_z=0,\,\pi.\end{aligned}$$

The compatibility relations identify a factor $\mathbb{Z}_2^6$ of BL as representation-enforced gapless nodal-line superconductors such that BS $\simeq \mathbb{Z}_2^{10}$ and

$$\begin{aligned}B[H(\mathbf{k})] = \{&\mathfrak{p}_-^{(0,0,0)},\mathfrak{p}_-^{(\pi,0,0)},\mathfrak{p}_-^{(0,\pi,0)},\mathfrak{p}_+^{(\pi,\pi,0)},\mathfrak{p}_-^{(\pi,\pi,0)}\\ &\mathfrak{p}_-^{(0,0,\pi)},\mathfrak{p}_-^{(\pi,0,\pi)},\mathfrak{p}_-^{(0,\pi,\pi)},\mathfrak{p}_+^{(\pi,\pi,\pi)},\mathfrak{p}_-^{(\pi,\pi,\pi)}\}.\end{aligned}$$

A second compatibility relation for gapped phases, identical to Eq. (4.98) in the main text, follows by considering Chern numbers at two-dimensional cuts through the Brillouin zone.

Symmetry-based indicators. The group of symmetry-based indicators is

$$\mathrm{SI_D}[C_2,B] \simeq \mathbb{Z}_2^6, \tag{C.4}$$

out of which a factor $\mathbb{Z}_2^5$ corresponds to gapped topological phases. For phases corresponding to stacks of Kitaev chains we have

$$z_{1,\pm;x,y} = \mathfrak{p}_\pm^{(\pi,\pi,\pi)} + \mathfrak{p}_\pm^{(\pi,\pi,0)} \mod 2$$

and for phases corresponding to stacks of two dimensional superconductors in the $l=x,y,z$ direction we have

$$z_{(2;l)} = \sum_{\mathbf{k}_s|_{k_{s,l}=\pi}}\mathfrak{p}_+^{\mathbf{k}_s} = \sum_{\mathbf{k}_s|_{k_{s,l}=\pi}}\mathfrak{p}_-^{\mathbf{k}_s} \mod 2,$$

where the equality follows from the 0d compatibility relation. The remaining factor $\mathbb{Z}_2$ corresponds to a symmetry-based indicator for a nodal superconductor

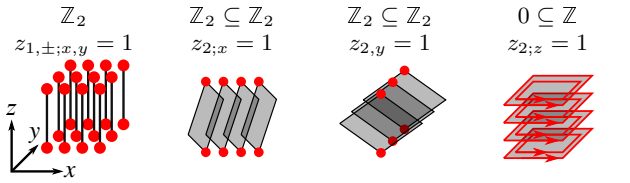

FIG. C.5. Topological phases of a three-dimensional superconductor in tenfold-way class D with point group C_2 and representation $\Theta = B$.

with different Chern number parity detected by the band labels,

$$z_3 = \sum_{\mathbf{k}_s}\mathfrak{p}_+^{\mathbf{k}_s} = \sum_{\mathbf{k}_s}\mathfrak{p}_-^{\mathbf{k}_s} \mod 2.$$

The group (C.4) of symmetry-based indicators differs from the result obtained in Ref. 1, where no symmetry-based indicators are found due to the absence of Pfaffian band labels.

C.1.4. Point group C_4, class D

1. *Representation $\Theta = A$ or $\Theta = B$*

Classifying group:

$$\mathcal{K}_\mathrm{D}[C_4,A] = \mathcal{K}_\mathrm{D}[C_4,B] = \mathbb{Z}_2^2\times\mathbb{Z}.$$

A factor $\mathbb{Z}_2$ corresponds to Kitaev chains aligned perpendicular to the rotation axis and to each other and stacked in all three spatial directions (label $(1;x,y,z)$). The remaining factor $\mathbb{Z}_2\times\mathbb{Z}$ corresponds to topological superconductors stacked perpendicular to the rotation axis (label $(2,z)$), where the factor $\mathbb{Z}_2$ describes a second-order phase and the factor $\mathbb{Z}$ a Chern superconductor. Even-Chern number superconductors can be adiabatically deformed to Chern insulators with vanishing superconducting correlations. The boundary signatures of the topological phases together with their symmetry-based indicators are displayed in Fig. C.6.

Band labels. There are BL $\simeq \mathbb{Z}^{10}$ topological band labels given by the invariants $\mathfrak{N}_j^{\mathbf{k}_s}$ with $j=\frac{1}{2},\frac{5}{2}$ at high-symmetry momenta $\mathbf{k}_s$ with fourfold rotation symmetry and $j=\frac{1}{2}$ at high-symmetry momenta $\mathbf{k}_s$ with twofold rotation symmetry.

Compatibility relations. For high-symmetry lines parallel to the rotation axis the invariant $\mathfrak{N}_j^{\mathbf{k}}$ is preserved for gapped phases, which gives the compatibility relation

$$\mathfrak{N}_j^{(k_x',k_y',0)} = \mathfrak{N}_j^{(k_x',k_y',\pi)}, \quad \text{for } k_x',\,k_y' = 0,\,\pi.$$

This identifies a factor $\mathbb{Z}^5$ of BL as representation-enforced gapless superconductors with nodal points on high-symmetry lines in the Brillouin zone. We find that BS $\simeq \mathbb{Z}^5$ and choose the independent band labels as

$$B[H(\mathbf{k})] = \{\mathfrak{N}_{\frac{1}{2}}^{(0,0,\pi)},\mathfrak{N}_{\frac{5}{2}}^{(0,0,\pi)},\mathfrak{N}_{\frac{1}{2}}^{(\pi,0,\pi)},\mathfrak{N}_{\frac{1}{2}}^{(\pi,\pi,\pi)},\mathfrak{N}_{\frac{5}{2}}^{(\pi,\pi,\pi)}\}.$$

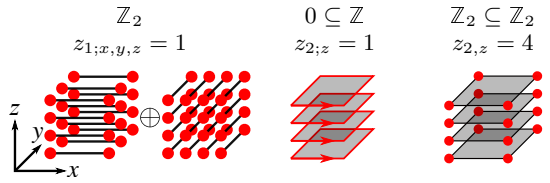

FIG. C.6. Topological phases of a three-dimensional superconductor in tenfold-way class D with point group C_4 and representation $\Theta = A$ or $\Theta = B$.

Symmetry-based indicators. The group of symmetry-based indicators is

$$\mathrm{SI}_{\mathrm{D}}[C_4, A] = \mathrm{SI}_{\mathrm{D}}[C_4, B] \simeq \mathbb{Z}_2 \times \mathbb{Z}_8, \tag{C.5}$$

isomorphic to the result of the two dimensional plane discussed in Sec. 4.6.2. The symmetry-based indicators for the stack of Kitaev chains $z_{1;x,y,z}$, two dimensional second-order and Chern superconductors $z_{2;z}$ are identical to the symmetry-based indicators of the two dimensional plane, Eqs. (4.85) and (4.86), respectively. As in the two-dimensional case, the weak second-order phase and the weak phase with Chern number 4 have identical band labels. In three dimensions, the symmetry-based indicators are expressed as

$$\begin{aligned} z_{1;x,y,z} &= \mathfrak{N}^{(0,0,\pi)}_{\frac{1}{2}} + \mathfrak{N}^{(0,0,\pi)}_{\frac{5}{2}} + \mathfrak{N}^{(\pi,0,\pi)}_{\frac{1}{2}} \mod 2, \\ z_{2;z} &= -\mathfrak{N}^{(0,0,\pi)}_{\frac{1}{2}} + 3\mathfrak{N}^{(0,0,\pi)}_{\frac{5}{2}} - 2\mathfrak{N}^{(\pi,0,\pi)}_{\frac{1}{2}} \\ &\quad + 3\mathfrak{N}^{(\pi,\pi,\pi)}_{\frac{1}{2}} - \mathfrak{N}^{(\pi,\pi,\pi)}_{\frac{5}{2}} \mod 8. \end{aligned}$$

The group of symmetry-based indicators (C.5) is identical with the result from 1.

2. *Representation* $\Theta = {}^1E$ *or* $\Theta = {}^2E$

Classifying group:

$$\mathcal{K}_{\mathrm{D}}[C_4, {}^2E] = \mathcal{K}_{\mathrm{D}}[C_4, {}^1E] = \mathbb{Z}_2^3 \times \mathbb{Z}.$$

A factor $\mathbb{Z}_2^2$ corresponds to one-dimensional topological superconductors parallel to the rotation axis (z) in the angular momentum subspaces $j = \frac{1}{2}, \frac{5}{2}$ (labels $(1, j; x, y)$). A factor $\mathbb{Z}$ corresponds to Chern superconductors with even Chern number stacked perpendicular to the rotation axis (label $(2, z)$). These phases can be adiabatically deformed to Chern insulators with vanishing superconducting correlations. The remaining factor $\mathbb{Z}_2$ corresponds to a pair of two-dimensional second-order topological superconductors parallel to the rotation axis, exchanged by fourfold rotation and stacked in both x and y directions (label $(2; x, y)$). The boundary signatures of the topological phases together with their symmetry-based indicators are displayed in Fig. C.7.

Band labels. There are BL $\simeq \mathbb{Z}_2^{12} \times \mathbb{Z}^4$ topological band labels given by the invariants $\mathfrak{N}^{\mathbf{k}_s}_{3/2}$, $\mathfrak{p}^{\mathbf{k}_s}_{1/2}$, $\mathfrak{p}^{\mathbf{k}_s}_{5/2}$ at fourfold rotation-symmetric high-symmetry momenta $\mathbf{k}_s = (0,0,0)$, $(0,0,\pi)$, $(\pi,\pi,0)$, and (π,π,π), and $\mathfrak{p}^{\mathbf{k}_s}_{1/2}$, $\mathfrak{p}^{\mathbf{k}_s}_{3/2}$ at twofold rotation symmetric high-symmetry momenta $\mathbf{k}_s = (0,\pi,0)$ and $(0,\pi,\pi)$.

Compatibility relations. From the fact that $\mathcal{R}_\pi\mathcal{P}$ is a local symmetry for high-symmetry planes in the Brillouin zone one derives the compatibility relation (4.87) of the main text. From the fact that $\mathfrak{N}_j$ is conserved along the fourfold symmetric lines in the Brillouin zone parallel to the rotation axis for $j = \frac{3}{2}, \frac{7}{2}$ one derives the further compatibility relations

$$\mathfrak{N}^{(k'_x,k'_y,0)}_{\frac{3}{2}} = \mathfrak{N}^{(k'_x,k'_y,\pi)}_{\frac{3}{2}},$$

for $(k'_x, k'_y) = (0,0)$, (π,π). The above compatibility relations associate factors $\mathbb{Z}_2^4$ and $\mathbb{Z}^2$ in BL with as representation-enforced gapless superconductors with nodal-line and nodal points, respectively. Hence we have BS $\simeq \mathbb{Z}_2^8 \times \mathbb{Z}^2$ with

$$\begin{aligned} B[H(\mathbf{k})] = \{&\mathfrak{p}^{(0,0,0)}_{\frac{1}{2}}, \mathfrak{p}^{(0,0,0)}_{\frac{5}{2}}, \mathfrak{p}^{(\pi,0,0)}_{\frac{3}{2}}, \mathfrak{p}^{(\pi,0,0)}_{\frac{5}{2}}, \mathfrak{p}^{(0,0,\pi)}_{\frac{1}{2}}, \\ &\mathfrak{p}^{(0,0,\pi)}_{\frac{5}{2}}, \mathfrak{N}^{(0,0,\pi)}_{\frac{3}{2}}, \mathfrak{p}^{(\pi,0,\pi)}_{\frac{3}{2}}, \mathfrak{p}^{(\pi,\pi,\pi)}_{\frac{5}{2}}, \mathfrak{N}^{(\pi,\pi,\pi)}_{\frac{3}{2}}\}. \end{aligned}$$

A third compatibility relation for gapped phases follows by considering Chern numbers at two-dimensional cuts through the Brillouin zone.

$$\begin{aligned} &-\mathfrak{N}^{(0,0,0)}_{\frac{3}{2}} - \mathfrak{N}^{(\pi,\pi,0)}_{\frac{3}{2}} \\ &+ 2\mathfrak{p}^{(0,0,0)}_{\frac{5}{2}} + 2\mathfrak{p}^{(\pi,0,0)}_{\frac{3}{2}} + 2\mathfrak{p}^{(\pi,\pi,0)}_{\frac{5}{2}} = \\ &-\mathfrak{N}^{(0,0,\pi)}_{\frac{3}{2}} - \mathfrak{N}^{(\pi,\pi,\pi)}_{\frac{3}{2}} \\ &+ 2\mathfrak{p}^{(0,0,\pi)}_{\frac{5}{2}} + 2\mathfrak{p}^{(\pi,0,\pi)}_{\frac{3}{2}} + 2\mathfrak{p}^{(\pi,\pi,\pi)}_{\frac{5}{2}} \mod 4. \end{aligned}$$

Symmetry-based indicators. The group of symmetry-based indicators is

$$\mathrm{SI}_{\mathrm{D}}[C_4, {}^1E] = \mathrm{SI}_{\mathrm{D}}[C_4, {}^2E] \simeq \mathbb{Z}_2^4 \times \mathbb{Z}_4, \tag{C.6}$$

out of which two factors $\mathbb{Z}_2$ correspond to stacks of Kitaev chains with indicator

$$z_{1,j;x,y} = \mathfrak{p}^{(\pi,\pi,0)}_j + \mathfrak{p}^{(\pi,\pi,\pi)}_j \mod 2$$

for $j = \frac{1}{2}, \frac{5}{2}$, the factor $\mathbb{Z}_4$ corresponds to a stack of Chern superconductors perpendicular to the rotation axis $z_{2;z}$ with indicator given by

$$\begin{aligned} z_{2;z} = &-\mathfrak{N}^{(0,0,\pi)}_{\frac{3}{2}} - \mathfrak{N}^{(\pi,\pi,\pi)}_{\frac{3}{2}} + 2\mathfrak{p}^{(0,0,\pi)}_{\frac{5}{2}} \\ &+ 2\mathfrak{p}^{(\pi,0,\pi)}_{\frac{3}{2}} + 2\mathfrak{p}^{(\pi,\pi,\pi)}_{\frac{5}{2}} \mod 4, \end{aligned}$$

and a factor $\mathbb{Z}_2$ corresponds to a stack of second-order Chern superconductors parallel to the rotation axis with symmetry-based indicator

$$z_{2;x,y} = \mathfrak{p}^{(\pi,0,0)}_{\frac{3}{2}} + \mathfrak{p}^{(\pi,0,\pi)}_{\frac{3}{2}} \mod 2.$$

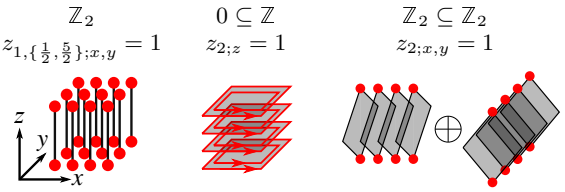

FIG. C.7. Topological phases of a three-dimensional superconductor in tenfold-way class D with point group C_4 and representation $\Theta = {}^1E$ or $\Theta = {}^2E$.

The remaining factor $\mathbb{Z}_2$ corresponds to a nodal superconductor the Chern number of which changes by $4n+2$ between parallel planes, with the difference detected by the band labels as

$$z_3 = \sum_{k_z=0,\pi} 2\mathfrak{p}^{(0,0,k_z)}_{\frac{5}{2}} + 2\mathfrak{p}^{(\pi,0,k_z)}_{\frac{3}{2}} + 2\mathfrak{p}^{(\pi,\pi,k_z)}_{\frac{5}{2}} \mod 4.$$

Note that a change of the Chern number by an odd number is prohibited by the zero dimensional compatibility constraint along rotation lines.

Reference 1 finds the group $\mathrm{SI} = \mathbb{Z}_2$. Upon omitting band labels corresponding to Pfaffians in our discussion, this single factor $\mathbb{Z}_2$ is identified as the parity of $z_{2;z}$, the Chern number of a stack of two dimensional topological superconductors in parallel to the rotation axis.

C.1.5. Point group C_{2v}, class D

The classification and symmetry labels are trivial for representation $\Theta = A_1$. The B_1 representation is analogous to the B_2 representation by exchanging the labels x, y.

For the A_1 representation, our results agree with those of Ref. 1. For the other representations A_2, B_1, B_2, the band labels are defined exclusively in terms of Pfaffians. Correspondingly, in Ref. 1, no symmetry-based indicators are found due to the absence of Pfaffian band labels in their construction.

1. *Representation* $\Theta = A_2$

Classifying group:

$$\mathcal{K}_{\mathrm{D}}[C_{2v}, A_2] = \mathbb{Z}_2^5 \times \mathbb{Z}^4,$$

see App. C.2 6 for a derivation and for the definition of the labels. The boundary signatures of the topological phases together with their symmetry-based indicators are displayed in Fig. C.8.

Band labels. There are $\mathrm{BL} \simeq \mathbb{Z}_2^8$ topological band labels given by the Pfaffian invariant $\mathfrak{p}^{\mathbf{k}_\mathrm{s}}$ at all high-symmetry momenta $\mathbf{k}_\mathrm{s}$.

Compatibility relations. There are no compatibility relations restricting the symmetry-based indicators for gapped phases. Thus $\mathrm{BS} = \mathrm{BL}$ and

$$B[H(\mathbf{k})] = \{\mathfrak{p}^{\mathbf{k}_\mathrm{s}}\}.$$

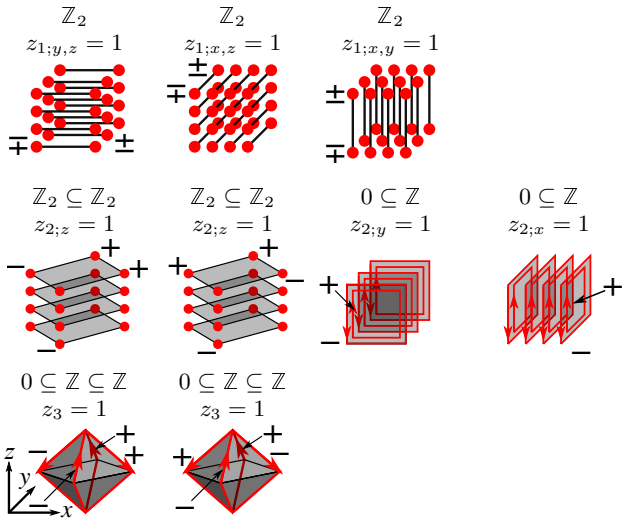

FIG. C.8. Topological phases of a three-dimensional superconductor in tenfold-way class D with point group C_{2v} and representation $\Theta = A_2$. The parity of the gapless states under corresponding mirror symmetry are denoted by $\pm$.

Symmetry-based indicators. The group of symmetry-based indicators is

$$\mathrm{SI}_{\mathrm{D}}[C_{2v}, A_2] \simeq \mathbb{Z}_2^7.$$

The symmetry-based indicators of the stacks of one dimensional topological superconductors with stacking directions $(i,j) = (y,z), (x,z), (x,y)$ are

$$z_{1;i,j} = \sum_{\mathbf{k}_\mathrm{s}|_{k_{\mathrm{s},i}=k_{\mathrm{s},j}=\pi}} \mathfrak{p}^{\mathbf{k}_\mathrm{s}} \mod 2,$$

and for the stacks of two dimensional topological superconductors with stacking directions $l = x, y, z$ they are

$$z_{2,l} = \sum_{\mathbf{k}_\mathrm{s}|_{k_{\mathrm{s},l}=\pi}} \mathfrak{p}^{\mathbf{k}_\mathrm{s}} \mod 2$$

and for the three dimensional second-order topological superconductors the symmetry-based indicator is

$$z_3 = \sum_{\mathbf{k}_\mathrm{s}} \mathfrak{p}^{\mathbf{k}_\mathrm{s}} \mod 2.$$

2. *Representation* $\Theta = B_2$

Classifying group:

$$\mathcal{K}_{\mathrm{D}}[C_{2v}, B_2] = \mathbb{Z}_2^3 \times \mathbb{Z}^2,$$

see App. C.2 6 for a derivation and for the definition of the labels. The boundary signatures of the topological phases together with their symmetry-based indicators are displayed in Fig. C.9.

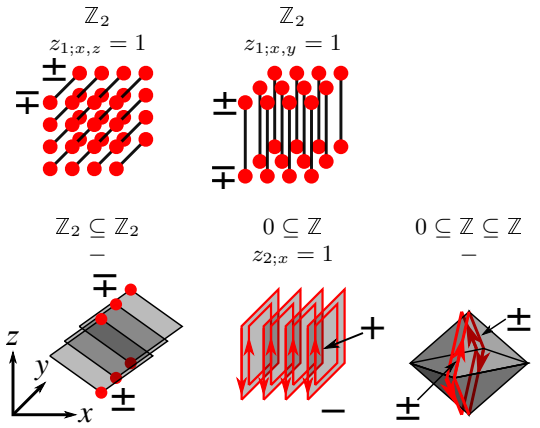

FIG. C.9. Topological phases of a three-dimensional superconductor in tenfold-way class D with point group C_{2v} and representation $\Theta = B_2$. The parity of the gapless states under corresponding mirror symmetry are denoted by $\pm$.

Band labels. There are BL $\simeq \mathbb{Z}_2^8$ topological band labels given by the Pfaffian invariant $\mathfrak{p}^{\mathbf{k}_s}$ at all high-symmetry momenta $\mathbf{k}_s$.

Compatibility relations. From the fact that $\mathcal{PM}_x$ acts locally on high-symmetry lines in reciprocal space we derive the compatibility relation

$$\mathfrak{p}^{(0,k_y',k_z')} = \mathfrak{p}^{(\pi,k_y',k_z')}, \quad \text{for } k_y',\, k_z' = 0,\, \pi.$$

The compatibility relations identify a factor $\mathbb{Z}_2^4$ of BL as representation-enforced gapless superconductors with nodal points such that BS $\simeq \mathbb{Z}_2^4$ and

$$B[H(\mathbf{k})] = \{\mathfrak{p}^{\mathbf{k}_s|_{k_x=\pi}}\}.$$

Symmetry-based indicators. The group of symmetry-based indicators is

$$\mathrm{SI_D}[C_{2v}, B_2] \simeq \mathbb{Z}_2^3.$$

The symmetry-based indicators of the stacks of one dimensional topological superconductors with stacking directions $(i,j) = (x,z), (x,y)$ are

$$z_{1;i,j} = \sum_{\mathbf{k}_s|_{k_{s,i}=k_{s,j}=\pi}} \mathfrak{p}^{\mathbf{k}_s} \mod 2,$$

and for the stacks of two dimensional topological superconductors with stacking direction x it is

$$z_{2,x} = \sum_{\mathbf{k}_s|_{k_{s,x}=\pi}} \mathfrak{p}^{\mathbf{k}_s} \mod 2.$$

The two dimensional second-order topological superconductor stacked in the y direction and the three dimensional second-order topological superconductor can not be detected from symmetry-based indicators.

C.2. BOUNDARY CLASSIFICATION GROUPS $\mathcal{K}$

For tenfold-way classes in d dimensions the classification groups $\mathcal{K}$ follow from the "periodic table of topological phases". [2, 3] They are the direct product of groups classifying strong phases and groups classifying weak phases obtained by stacking topological phases in dimension $d-n$, $n = 1, \ldots, d-1$.

In the presence of an additional order-two crystalline symmetry, such as inversion, mirror, or twofold rotation, the classifying group $\mathcal{K}$ can be obtained using the known classifications of strong phases given in Ref. 4 and 5 (see also Refs. 6–8), again accounting for weak phases by taking direct products of the appropriate classification groups in lower dimensions. [4] It is important to point out that the classification group $\mathcal{K}$ we consider in this chapter classifies topological phases with nontrivial boundary signature only — see the discussion at the end of Sec. 4.3. These "boundary classification groups" $\mathcal{K}$ are obtained from the groups K classifying the bulk band structure by dividing out the classifying group $K^{(d)}$ of atomic-limit phases.[5]

Classifications of strong tenfold-way phases with other additional crystalline symmetry groups can be found in the literature. [9, 10] We here give classification results for the examples discussed in the main text and in App. C.1. These classifications are derived from the enumeration of the possible anomalous boundary states compatible with the symmetries defining the topological class. Boundary states that can be removed by a change of lattice termination are removed from the classification, because they are not a consequence of the topology of the bulk band structure. (Such boundary states are called "extrinsic" in Refs. 5 and 11.)

Below we compute the classifying groups $\mathcal{K}_\eta[G|G_\mathcal{O}, \Theta, d]$ of d dimensional topological phases with point group G, where its normal subgroup $G_\mathcal{O}$ is assumed to act as onsite symmetry. For each factor of $\mathcal{K}_\eta[G|G_\mathcal{O}, \Theta, d]$ we present an interpretation in terms of higher order topological phases or stacks of lower dimensional topological (weak) phases and generators from which the band labels can be computed. We not only consider the dimensions d corresponding to the examples used in the main text, but also lower dimensions, since the classification results for lower dimensions d provides information on weak and higher-order phases.

C.2.1. One dimension, class D, $C_{2v}|C_s$

We consider a one dimensional system extended in the x direction, such that it lies within the mirror plane of $\mathcal{M}_y$. Hence $\mathcal{M}_y$ is an onsite symmetry, wheres $\mathcal{M}_x$ acts nonlocally. For spinful fermions there is a single irreducible representation $\alpha = \bar{E}$ with dimension $d_{\bar{E}} = 2$.

Representation $\Theta = A_1$. — For the representation $\Theta = A_1$, $\mathcal{M}_x$ and $\mathcal{M}_y$ commute with particle-hole conjugation $\mathcal{P}$. The parallel mirror plane $\mathcal{M}_y$ with $\mathcal{M}_y^2 = -1$ forbids a topological superconducting phase, as it effec-

tively turns the one-dimensional system into class $\mathrm{A}^{\mathcal{P}^-\mathcal{M}}$ with trivial classification, see the notation of Ref. 5. We conclude that

$$\mathcal{K}_{\mathrm{D}}[C_{2v}|C_s, A_1, d=1] = 0. \tag{C.7}$$

Representation $\Theta = A_2$.— In this case $\mathcal{M}_x$ and $\mathcal{M}_y$ anticommute with $\mathcal{P}$. The parallel mirror plane allows to block diagonalize the system into two blocks according to $\mathcal{M}_y$-parity $\pm$. Particle-hole conjugation acts within the blocks, whereas the perpendicular mirror plane $\mathcal{M}_x$ interchanges the two blocks. The system is thus completely specified by a single block in tenfold-way class D, which allows a Kitaev-chain topological phase. A generator of the nontrivial phase is

$$H_{(1)}(k_x) = \rho_0\tau_3(1 - m - \cos k_x) + \rho_1\tau_1 \sin k_x,$$

with $0 < m < 2$ and representations $\mathcal{P} = \rho_0\tau_1 K$, $U(\mathcal{R}_\pi) = i\rho_2\tau_0$, $U(\mathcal{M}_x) = i\rho_3\tau_0$, $U(\mathcal{M}_y) = i\rho_1\tau_0$.

Representation $\Theta = B_1$.— In this case $\mathcal{M}_x$ commutes with $\mathcal{P}$, whereas $\mathcal{M}_y$ anticommutes with $\mathcal{P}$. The discussion can be mapped to that of the case $\Theta = A_2$ by noting that $\mathcal{R}_\pi$ anticommutes with $\mathcal{P}$, so that the arguments put forward for $\Theta = A_1$ can be applied to the case $\Theta = B_2$ by exchanging the roles of $\mathcal{M}_x$ and $\mathcal{R}_\pi$. It follows that

$$\mathcal{K}_{\mathrm{D}}[C_{2v}|C_s, B_1, d=1] = \mathbb{Z}_2. \tag{C.8}$$

Representation $\Theta = B_2$.— The parallel mirror plane $\mathcal{M}_y$ with $\mathcal{M}_y^2 = -1$ forbids a topological superconducting phase, as it effectively turns the one-dimensional system into class $\mathrm{A}^{\mathcal{P}^+\mathcal{M}}$ with trivial classification, [5] so that

$$\mathcal{K}_{\mathrm{D}}[C_{2v}|C_s, B_2, d=1] = 0. \tag{C.9}$$

C.2.2. One dimension, class D, $C_{2v}|C_{2v}$

This case applies to a one-dimensional system along the z direction, such that it lies in the intersection of the mirror planes $\mathcal{M}_x$, $\mathcal{M}_y$ and the full crystalline symmetry group C_{2v} acts onsite. As shown in Table 4.5 and discussed in Sec. 4.3, for spinful fermions there is a single irreducible representation $\alpha = \bar{E}$ with dimension $d_{\bar{E}} = 2$, which effectively changes the tenfold-way symmetries from those of class D to those of class C for the case $\Theta = A_1$, but leaves them unchanged for $\Theta = A_2$, B_1, and B_2. It follows for $d = 1$ that

$$\mathcal{K}_{\mathrm{D}}[C_{2v}|C_{2v}, A_1, d=1] = 0 \tag{C.10}$$
$$\mathcal{K}_{\mathrm{D}}[C_{2v}|C_{2v}, \Theta, d=1] = \mathbb{Z}_2, \quad \Theta = A_2, B_1, B_2. \tag{C.11}$$

A generator for the nontrivial phases is

$$H_{(1)}(k_z) = \rho_0\tau_3(1 - m - \cos k_z) + \rho_1\tau_1 \sin k_z,$$

with $0 < m < 2$ and accordingly chosen representations.

C.2.3. Two dimensions, class D, $C_{2v}|C_s$

This case applies to a two-dimensional system in the xz plane, such that $\mathcal{M}_y$ acts as an onsite symmetry. A system with boundaries parallel to the coordinate axes has two $\mathcal{M}_x$-symmetric boundaries and two boundaries that are mapped to each other by $\mathcal{M}_x$.

Representation $\Theta = A_1$.— From an analysis of the reflection symmetric boundary, we find that there is no first-order topological superconducting phase. (The nontrivial first-order phase in class D has a chiral edge mode, which is not compatible with a mirror symmetry.) There are also no second-order or weak phases in this representation,

$$\mathcal{K}_{\mathrm{D}}[C_{2v}|C_s, A_1, d=2] = 0. \tag{C.12}$$

This follows from the triviality of the classifying groups $\mathcal{K}_{\mathrm{D}}[C_{2v}|C_s, A_1, d]$ and $\mathcal{K}_{\mathrm{D}}[C_{2v}|C_{2v}, A_1, d]$ for $d = 1$, into which an eventual higher-order phase can be deformed or which could be stacked to form a weak phase, see the discussions in Apps. C.2 1 and C.2 2.

Representation $\Theta = A_2$.— A $\mathcal{M}_x$-symmetric boundary allows counter-propagating chiral Majorana modes in opposite $\mathcal{M}_y$-parity subspaces. They are the first-order boundary signature of a pair of Chern superconductors related to each other by $\mathcal{M}_x$. Superconductors with even Chern number in a mirror plane can be adiabatically deformed to Chern insulators with vanishing superconducting correlations. From the nontriviality of the classifying groups $\mathcal{K}_{\mathrm{D}}[C_{2v}|C_s, A_2, d] = \mathcal{K}_{\mathrm{D}}[C_{2v}|C_{2v}, A_2, d] = \mathbb{Z}_2$ for $d = 1$ we conclude that two types of weak phases are possible, obtained by stacking one-dimensional superconductors in the x and z direction. There is no second-order phase, despite the fact that pairs of even and odd-$\mathcal{M}_y$-parity Majorana zero-energy bound states are allowed at corners. Such states are protected against local perturbations at corners, but they can be removed by a change of termination along the crystal edges. (Formally, this follows because the group $\mathcal{K}_{\mathrm{D}}[C_{2v}/C_{2v}, A_2]$ classifying $\mathcal{M}_x$-symmetric corner states is "separable" in the language of Ref. 5.) We thus conclude that

$$\mathcal{K}_{\mathrm{D}}[C_{2v}|C_s, A_2, d=2] = \mathbb{Z}_2^2 \times \mathbb{Z}. \tag{C.13}$$

The same result can be obtained by arguing that the onsite symmetry $\mathcal{M}_y$ commutes with $\mathcal{P}$, so that the Hamiltonian can be written as the diagonal sum of $\mathcal{M}_y$-even and $\mathcal{M}_y$-odd blocks that each satisfy particle-hole symmetry. The mirror symmetry $\mathcal{M}_x$ interchanges the two blocks. Hence, the topological classification is the same as of a two-dimensional Hamiltonian in tenfold-way class D without crystalline symmetries, which also gives Eq. (C.13).

Representation $\Theta = B_1$.— This case can be mapped to $\Theta = A_2$ by interchanging the roles of $\mathcal{M}_x$ and $\mathcal{R}_\pi$. One thus finds

$$\mathcal{K}_{\mathrm{D}}[C_{2v}|C_s, B_1, d=2] = \mathbb{Z}_2^2 \times \mathbb{Z}. \tag{C.14}$$

Representation $\Theta = B_2$.— In this case no first-order boundary signatures are allowed on a $\mathcal{M}_x$-symmetric boundary, because they are incompatible with the $\mathcal{M}_x$ symmetry. To check for the existence of second-order or weak phases, we note that one-dimensional superconductors in the z direction (*i.e.*, perpendicular to the mirror plane of $\mathcal{M}_x$) have classifying group $\mathcal{K}_{\mathrm{D}}[C_{2v}|C_s, B_2, d = 1]$, which is trivial, see App. C.2 1. Also, one-dimensional superconductors in the z direction, *i.e.*, in the intersection of both mirror planes, have classifying group $\mathcal{K}_{\mathrm{D}}[C_{2v}|C_{2v}, B_2, d = 1] = \mathbb{Z}_2$, as shown in App. C.2 2. This has two consequences: (i) A second-order boundary signature corresponding to a pair of Majorana bound states at the $\mathcal{M}_x$-symmetric corner is possible. The in-plane mirror symmetry $\mathcal{M}_y$ with $\mathcal{M}_y\mathcal{P} = \mathcal{P}\mathcal{M}_y$ forbids one-dimensional topological phases within the mirror $\mathcal{M}_y$ plane that do not satisfy $\mathcal{M}_x$ mirror symmetry. Hence the boundary signature can not be removed by a decoration of the crystal boundary and there is a second-order topological superconducting phase. A generator for this phase is

$$H_2'(\mathbf{k}) = \mu_0\rho_0\tau_3(\cos k_x + \cos k_z + m) + \mu_1\rho_0\tau_1 \sin k_x + \mu_2\rho_2\tau_1 \sin k_z,$$

with $0 < m < 2$ and representations $\mathcal{P} = \mu_0\rho_0\tau_1 K$, $U(\mathcal{R}_\pi) = i\mu_0\rho_3\tau_3$, $U(\mathcal{M}_x) = i\mu_3\rho_3\tau_0$, $U(\mathcal{M}_y) = i\mu_3\rho_0\tau_3$. Alternatively, the parallel mirror plane allows to block diagonalize the system into two blocks according to $\mathcal{M}_y$-parity $\pm$. Particle-hole conjugation interchanges the two blocks, and each block belongs to class $\mathrm{A}^{\mathcal{P}^+\mathcal{M}}$ with $0 \subseteq \mathbb{Z}_2 \subseteq \mathbb{Z}_2$ bulk subgroup sequence for $d = 2$. [5] (ii) There is a weak phase corresponding to one-dimensional topological superconductors in the z direction, which are stacked in the x direction. We thus conclude that

$$\mathcal{K}_{\mathrm{D}}[C_{2v}|C_s, B_2, d = 2] = \mathbb{Z}_2^2. \tag{C.15}$$

C.2.4. Two dimensions, class D, C_{2v}

We now derive the boundary classification for the example discussed in Sec. 4.6.1 of the main text. The two mirror symmetries forbid a phase with a nonzero Chern number. Hence, there are no first-order phases for all representations of the pairing term Θ.

Representation $\Theta = A_1$.— For this representation, both $\mathcal{M}_x$ and $\mathcal{M}_y$ with $\mathcal{M}_x^2 = \mathcal{M}_y^2 = -1$ commute with $\mathcal{P}$, ruling out the existence of zero-energy Majorana bound states at mirror-symmetric corners. There are no weak phases as the classifying group $\mathcal{K}_{\mathrm{D}}[C_{2v}|C_s, A_1, d = 1] = 0$ is trivial. We conclude that

$$\mathcal{K}_{\mathrm{D}}[C_{2v}, A_1, d = 2] = 0. \tag{C.16}$$

Representation $\Theta = A_2$.— In this case, both $\mathcal{M}_x$ and $\mathcal{M}_y$ anticommute with $\mathcal{P}$. We first investigate the possibility of second-order phases with non-degenerate zero-energy Majorana corner states at mirror-symmetric corners of a C_{2v}-symmetric crystal. Since the edges of such a crystal are gapped, it may be deformed into a "cross" shape

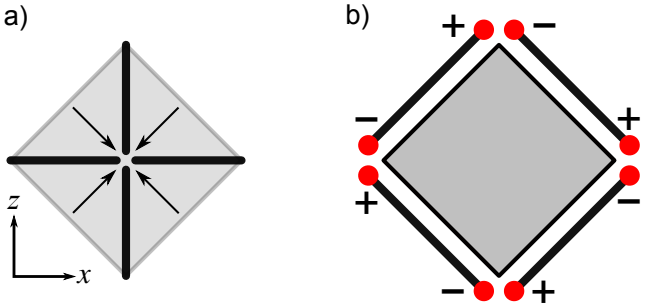

FIG. C.10. a) A C_{2v}-symmetric two-dimensional crystal with two perpendicular mirror symmetries with gapped edges may be deformed into a four one-dimensional chains in a cross-like arrangement. Corner states of the two-dimensional crystal are in one-to-one correspondence with end states of the one-dimensional structure. b) A C_{2v}-symmetric crystal may be decorated symmetrically with Kitaev chains, resulting in the appearance of extrinsic pairs of corner states at all four mirror-symmetric corners.

consisting of four one-dimensional chains, see Fig. C.10a. Each chain has a parallel mirror plane, which effectively acts as a local symmetry. Perpendicular mirror planes connect chains on opposite sides of the cross, but no longer act inside a chain. The parallel mirror planes allow the Hamiltonian to be block-diagonalized into blocks with odd and even mirror parity. Each of these blocks is in tenfold-way class D, thus in principle allowing for the existence of up to two zero-energy Majorana end states, which turn into corner states if the system is deformed back to a C_{2v}-symmetric two-dimensional crystal. The presence of the perpendicular mirror planes and the condition that the center of the cross be gapped restrict the possible configurations of corner states: Opposite corners must have Majorana states of opposite mirror parities, since the two mirror operations anticommute, and the total number of Majorana modes must be a multiple of four. This leaves a $\mathbb{Z}_2^3$ extrinsic classification of allowed Majorana corner modes. To obtain the classification of intrinsic second-order phases, we must divide out configurations of corner states that differ by a change of termination. Hereto we note that the four edges of a C_{2v}-symmetric crystal allow a "decoration" with Kitaev chains, which yield opposite-parity pairs of Majorana states at all four corners of the crystal, see Fig. C.10b, so that a $\mathbb{Z}_2^2$ classifying group of second-order phases remains. The generators of the two distinct $\mathbb{Z}_2$ second-order phases can be given as configurations with single zero-energy Majorana bound states at all corners of a C_{2v} symmetric sample with mirror parities as indicated in Table 4.11.

Furthermore there are two weak phases as the classifying group $\mathcal{K}_{\mathrm{D}}[C_{2v}|C_s, A_2, d = 1] = \mathbb{Z}_2$ (see App. C.2 1) allows stacking of one dimensional topological superconductors both in x and y directions. Combining every-

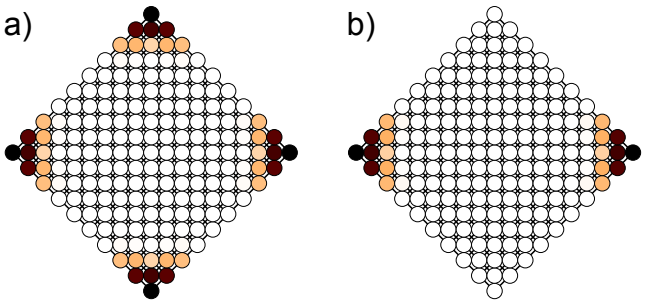

FIG. C.11. a) Support of Majorana bound states for the Hamiltonians $H'_{2,\pm}$ of Eq. (C.18). A symmetry-preserving next-nearest neighbor term $m_1\rho_2\tau_1 \sin k_x \sin k_y$ with $m_1 = 0.4$ is added to remove a spurious gapless edge mode. b) Support of Majorana bound states for $H'_{2,+} \oplus H'_{2,-}$, after adding an additional weak symmetry-preserving hybridization term $m_2\rho_0\tau_1\mu_2$ with strength $m_2 = 0.1$. The corner modes may appear at the other pair of corners if a different hybridization term is chosen.

thing, we have the classifying group

$$\mathcal{K}_{\mathrm{D}}[C_{2v}, A_2, d = 2] = \mathbb{Z}_2^4. \tag{C.17}$$

Generators of the second-order phases are

$$\begin{aligned} H'_{2,\pm}(\mathbf{k}) = \rho_0\tau_3(2 - m - \cos k_x - \cos k_y) \\ \pm \rho_1\tau_1 \sin k_x + \rho_3\tau_1 \sin k_y \end{aligned} \tag{C.18}$$

with $0 < m < 2$ and representations $\mathcal{P} = \tau_1 K$, $U(\mathcal{R}_\pi) = i\rho_2\tau_0$, $U(\mathcal{M}_x) = i\rho_3\tau_0$, $U(\mathcal{M}_y) = i\rho_1\tau_0$. To verify that these are indeed second-order phases with the desired properties, one may either count the number crystalline symmetry breaking mass terms,[5] or simply verify that these model Hamiltonians have the correct corner-state structure. Results of such a calculation, using the *kwant* software,[12] are shown in Fig. C.11a. As shown in Fig. C.11b, taking the direct sum of and hybridizing the two generating Hamiltonians $H'_{2,\pm}$ yields a pair of Majorana bound states with opposite mirror parity at a single pair corners within a single mirror plane only.

Representations $\Theta = B_{1,2}$.— The discussions for the cases $\Theta = B_1$ and $\Theta = B_2$ are analogous, as they are related by a $\pi/2$ rotation of the system. In the following we focus on the B_2 case, for which $\mathcal{M}_x$ anticommutes with $\mathcal{P}$ and $\mathcal{M}_y$ commutes with $\mathcal{P}$. As before, we first consider the possibility of second-order phases with zero-energy Majorana corner states. Only corners bisected by the mirror plane $\mathcal{M}_x$ can host Majorana bound states, as corners bisected by $\mathcal{M}_y$ are effectively in class A. Hence, the system can be deformed to a one dimensional system within the mirror plane $\mathcal{M}_x$. This one-dimensional system has classifying group is $\mathcal{K}_{\mathrm{D}}[C_{2v}|C_s, B_1, d = 1] = \mathbb{Z}_2$, as discussed in App. C.2 1. However, the corresponding configuration of boundary states, a pair of Majorana bound states in both mirror parity sectors at both corners bisected by the mirror $\mathcal{M}_x$ plane, can be removed by a decoration with Kitaev chains on each surface of a symmetric sample. We thus conclude that there are no intrinsic second-order phases for $\Theta = B_1$ or $\Theta = B_2$

Weak phases can be obtained by stacking one-dimensional chains in the y direction. Since $\mathcal{M}_x$ is an onsite symmetry for such chains, their classification is given by the one-dimensional classifying group $\mathcal{K}_{\mathrm{D}}[C_{2v}|C_s, B_1, d = 1] = \mathbb{Z}_2$, see App. C.2 1. (Note that for this stacking direction $\mathcal{M}_x$ and $\mathcal{M}_y$ are exchanged in comparison to the discussion in App. C.2 1.) Superconductors in the perpendicular stacking direction x are trivial since $\mathcal{K}_{\mathrm{D}}[C_{2v}|C_s, B_2, d = 1] = 0$, as shown in Sec. C.2 1. We conclude that

$$\mathcal{K}_{\mathrm{D}}[C_{2v}, B_{1,2}, d = 2] = \mathbb{Z}_2. \tag{C.19}$$

C.2.5. Two dimensions, class D, C_4

Representations $\Theta = A, B$. The representations $\Theta = A$ and $\Theta = B$ have the same algebraic structure, so that we may limit the discussion to the case $\Theta = A$. This case allows a strong first-order phase with a single chiral Majorana mode, corresponding to a $\mathbb{Z}$ topological classification. To check for higher-order phases with four Majorana bound states, we smoothly deform the two-dimensional system to four one-dimensional chains arranged in a C_4-symmetric cross-like shape, as in Fig. C.12. Each chain may harbor a zero-energy Majorana bound state at its end. The end states at the four chains are related to each other by C_4 symmetry. Since classification of zero-energy Majorana modes protected by C_4 is trivial for A and B superconducting pairing, see discussion in Sec. 4.3, the four Majorana states that would appear at the center of the cross can gap out, so that one obtains a true second-order phase with a $\mathbb{Z}_2$ classification. Finally, a weak phase may be obtained by stacking one-dimensional C_2-symmetric x lines (with representation $\Theta = A$) in the y direction and superimposing the same stack, rotated by $\pi/2$. The one-dimensional superconductors that are the building blocks of this phase have zero-energy Majorana states at their ends and a $\mathbb{Z}_2$ classification. We conclude that

$$\begin{aligned} \mathcal{K}_{\mathrm{D}}[C_4, A, d = 2] &= \mathcal{K}_{\mathrm{D}}[C_4, B, d = 2] \\ &= \mathbb{Z}_2^2 \times \mathbb{Z}. \end{aligned} \tag{C.20}$$

Representations $\Theta = {}^{1,2}E$.— The representations $\Theta = {}^1E$ and $\Theta = {}^2E$ allow a strong first-order phase with an even number of chiral Majorana modes. One verifies that a single Majorana mode is not allowed for this representation, since there is no one-dimensional representation of $\mathcal{R}_\pi$ and $\mathcal{P}$ meeting the conditions that (i) $i\mathcal{R}_\pi$ squares to one and (ii) $i\mathcal{R}_\pi$ anticommutes with $\mathcal{P}$. An even number of Majorana modes is allowed, since there are two-dimensional representations meeting these requirements. One also verifies that the constructions of a second-order phase and a weak phase used for the representations $\Theta = A, B$ discussed above do not work for the case $\Theta = {}^{1,2}E$. For the second-order phase, the reason is that at the center cross, where C_4 is a local

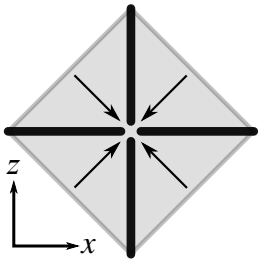

FIG. C.12. A C_4-symmetric two-dimensional crystal may be deformed into a four one-dimensional chains in a cross-like arrangement. Corner states of the two-dimensional crystal are in one-to-one correspondence with end states of the one-dimensional structure.

symmetry, one now ends up with states at all four allowed angular momenta $j = \frac{1}{2}, \frac{3}{2}, \frac{5}{2}$, and $\frac{7}{2}$, which can not gap out because particle-hole conjugation acts within two of the angular momentum sectors, see the discussion in Sec. 4.3. For the weak phases, this follows because the underlying C_2-symmetric one-dimensional building blocks have the representation $\Theta = B$, which does not allow for a topological phase. We thus conclude that

$$\mathcal{K}_{\mathrm{D}}[C_4, {}^{1,2}E, d = 2] = \mathbb{Z}. \tag{C.21}$$

C.2.6. Three dimensions, class D, C_{2v}

In class D, there are no three dimensional strong first-order topological phases without crystalline symmetries, so that no first-order phase is possible. To determine whether a strong phase is possible, with protected gapless Majorana modes along mirror-symmetric hinges, we deform the three-dimensional crystal into a "cross" of four two-dimensional planes, as shown schematically in Fig. C.13a and determine below for each representation Θ, whether a phase with chiral hinge states is possible and whether it is intrinsic or extrinsic (*i.e.*, whether it can be removed with a decoration of the surface). Intrinisic second-order boundary signatures are possible in representations $\Theta = A_2, B_1, B_2$ as we show below. To determine whether a third-order TSC is possible, we note that a protected corner state can exist only for a corner on the intersection of the two mirror planes. We find that pairs of corner states are allowed for the representations $\Theta = A_2$, B_1, and B_2, but not for $\Theta = A_1$. However, the corner state for $\Theta = A_2$, B_1, or B_2 is extrinsic, as they can be removed by the decoration of a pair of hinges in a mirror plane with one-dimensional topological superconductors.

Representation $\Theta = A_1$.— For the representation A_1 there are no intrinsic second-order boundary signatures: Although the edges of the planes in the deformed structure of Fig. C.13a not allow for pairs of co-propagating chiral Majorana modes, one for each mirror parity, such configurations of hinge modes can be removed by decorating the four symmetry-related crystal faces by two-dimensional quantum Hall phases, as shown schematically in Fig. C.13b. Further, all lower-dimensional building blocks that can be used for stacking are trivial, which rules out the existence of weak phases. We conclude that

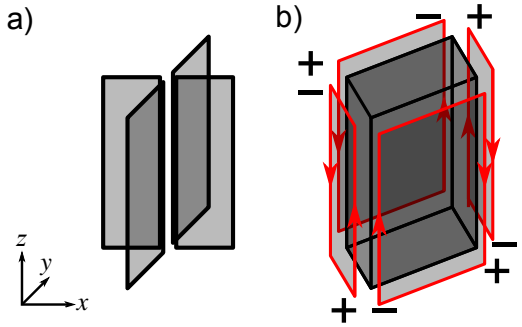

FIG. C.13. a) A C_{2v}-symmetric three-dimensional crystal with two perpendicular mirror symmetries may be deformed into a four two-dimensional planes in a cross-like arrangement. Hinge states of the two-dimensional crystal are in one-to-one correspondence with edge states of the two-dimensional structure. b) A C_{2v}-symmetric crystal may be decorated symmetrically with quantum Hall planes, resulting in the appearance of extrinsic configurations of chiral hinge modes at all four mirror-symmetric hinges.

$$\mathcal{K}_{\mathrm{D}}[C_{2v}, A_1, d = 3] = 0. \tag{C.22}$$

Representation $\Theta = A_2$.— We note that for each of the planes in the deformed structure of Fig. C.13a one of the mirror symmetries acts as an onsite symmetry, whereas the other mirror symmetry maps planes on opposite sides of the central "cross" onto each other. For representation A_2, each of the planes in the deformed structure of Fig. C.13a allows for chiral Majorana modes in both parity sectors of the onsite mirror symmetry. These Majorana modes turn into hinge modes upon deforming back to the full three-dimensional structure. The perpendicular mirror symmetry imposes the condition that opposite hinges have Majorana modes with the same propagation direction, but with opposite mirror parity. The condition that the center of the cross be gapped imposes the requirement that the net number of chiral modes, weighed with propagation direction, is zero. Hence, there is an extrinsic $\mathbb{Z}^3$ classification of C_{2v}-compatible hinge modes. To obtain the intrinsic second-order phases, configurations of hinge modes that differ by a change of surface termination must be divided out. Noting that the four surfaces of a C_{2v}-symmetric crystal admits a "decoration" with quantum Hall phases, which gives a pair of co-propagating opposite-parity hinge modes at each mirror-symmetric hinge, see Fig. C.13b, we find that a classifying group $\mathbb{Z}^2$ of intrinsic second-order phases remains. Generator Hamiltonians for these second-order

phases are

$$H'_{(3,\pm)} = \rho_0\tau_3(3 - m - \sum_{i=x,y,z} \cos k_i) \pm \rho_1\tau_1 \sin k_x + \rho_3\tau_1 \sin k_y + \rho_0\tau_2 \sin k_z$$

with $0 < m < 2$ and representations $U(\mathcal{M}_x) = i\rho_3\tau_0$, $U(\mathcal{M}_y) = i\rho_1\tau_0$, $\mathcal{P} = \rho_0\tau_1 K$.

The weak phases in this symmetry class can be constructed as stacks of one or two-dimensional topological phases. We find the following possibilities:

- Stack of two-dimensional C_{2v}-symmetric xy planes in the z direction with second-order topology. Such planes have a $\mathbb{Z}_2^2$ classification, see App. C.2 4. These phases are labeled "$(2; z)$" in Fig. C.8.
- Stack of two-dimensional "$C_{2v}|C_s$"-symmetric yz or xz planes in the x or y direction, respectively. These planes have a $\mathbb{Z}$ classification, corresponding to a first-order two-dimensional topological superconductor with counterpropagating Majorana modes in opposite in-plane mirror eigensectors, as shown in App. C.2 3. These phases are labeled "$(2; x)$" and "$(2; y)$" in Fig. C.8. Superconductors with even Chern number in a mirror plane can be adiabatically deformed to Chern insulators with vanishing superconducting correlations.
- Stacks of one-dimensional "$C_{2v}|C_{2v}$"-symmetric z lines in the x and y directions. These have a $\mathbb{Z}_2$ classification, corresponding to a one-dimensional topological superconductor with a pair of Majorana bound states at each end as shown in App. C.2 1. These phases are labeled "$(1; x; y)$" in Fig. C.8.
- Stacks of one-dimensional "$C_{2v}|C_s$"-symmetric y or x lines in the x and z and in the y and z directions, respectively. These, too, have a $\mathbb{Z}_2$ classification, corresponding to a one-dimensional topological superconductor with a pair of Majorana bound states at each end as shown in App. C.2 1. These phases are labeled "$(1; x; z)$" and "$(1; y; z)'$ in Fig. C.8.

The complete classifying group is hence

$$\mathcal{K}_{\mathrm{D}}[C_{2v}, A_2, d = 3] = \mathbb{Z}_2^5 \times \mathbb{Z}^4. \tag{C.23}$$

Representations $\Theta = B_{1,2}$.— The representations B_1 and B_2 are related by a rotation. For concreteness, we discuss the B_2 case in the following. In this phase, only one pair of mirror-symmetric hinges allows for intrinsic chiral Majorana modes, whereas any hinge modes appearing at the other pair of mirror-symmetric hinges can always be removed by adding a suitable decoration to the four mirror-related surfaces, as shown schematically in Fig. C.13b. As a result, for the discussion of second-order phases, the three-dimensional crystal may be deformed to a two-dimensional one with $C_{2v}|C_s$ symmetry. As shown in App. C.2 3, there exists a strong two-dimensional phase with counterpropagating Majorana edge modes with opposite mirror parity. This phase corresponds to a second-order phase of the three-dimensional crystal. One verifies that this second-order phase is intrinsic, since a surface decoration with quantum Hall planes is forbidden by the perpendicular mirror symmetry. A generator for the strong second-order phase is

$$H'_{(3)}(\mathbf{k}) = \mu_0\rho_0\tau_3(3 - m - \cos k_x - \cos k_y - \cos k_z) + \mu_3\rho_0\tau_1 \sin k_y + \mu_0\rho_0\tau_2 \sin k_z + \mu_2\rho_2\tau_1 \sin k_x$$

with $0 < m < 2$ and the representations $U(\mathcal{M}_x) = i\mu_3\rho_0\tau_0$, $U(\mathcal{M}_y) = i\mu_2\rho_0\tau_0$, $\mathcal{P} = \mu_0\rho_0\tau_1 K$. Second order topological superconductors with a pairs of counterpropagating Majorana modes within in a mirror plane can be adiabatically deformed to normal-state second-order topological insulators with chiral hinge mode.

The weak phases in this symmetry class can be constructed as stacks of one- or two-dimensional topological phases:

- A stack of two-dimensional xy planes with C_{2v} symmetry in the z direction is not possible, since there are no strong phases with C_{2v} symmetry and $\Theta = B_2$ in two dimensions, see App. C.2 4.
- A stack of two-dimensional xz planes with "$C_{2v}|C_s$" symmetry in the y direction. These planes have a $\mathbb{Z}_2$ classification, corresponding to a second-order topological superconducting phase with a pair of Majorana bound states at a corner bisected by the mirror $\mathcal{M}_x$ plane, as shown in App. C.2 3. These phases are labeled "$(2; y)$" in Fig. C.9.
- A stack of two-dimensional yz planes with "$C_{2v}|C_s$" symmetry in the x directions. These planes have a $\mathbb{Z}$ classification, corresponding to a first-order topological superconducting phase with counterpropagating Majorana modes in opposite in-plane mirror eigensectors, as shown in Sec. C.2 3. These phases are labeled "$(2; x)$" in Fig. C.9. Superconductors with even Chern number in a mirror plane can be adiabatically deformed to normal-state Chern insulators.
- A stack of one-dimensional z lines with "$C_{2v}|C_{2v}$" symmetry in the x and y directions. These lines have a $\mathbb{Z}_2$ classification, corresponding to a one-dimensional topological superconductor with a pair of Majorana bound states at each end, as shown in Sec. C.2 2. These phases are labeled "$(1; x, y)$" in Fig. C.9.
- A stack of one-dimensional x lines with "$C_{2v}|C_s$" symmetry in the y and z directions does not give a weak phase, since there are no appropriate strong phases in one dimension, see App. C.2 1.

- A stack of one-dimensional y lines with "$C_{2v}|C_s$" symmetry in the x and z directions. These lines have a $\mathbb{Z}_2$ classification, corresponding to a one dimensional topological superconducting phase with a pair of Majorana bound states at each end, as shown in App. C.2 1. These phases are labeled "$(1; x, z)$" in Fig. C.9.

The complete classifying group is hence

$$\mathcal{K}_{\mathrm{D}}[C_{2v}, B_{1,2}, d = 3] = \mathbb{Z}_2^3 \times \mathbb{Z}^2. \tag{C.24}$$

C.2.7. Three dimensions, class D, C_4

Three dimensional, fourfold rotation-symmetric topological superconductors can not have a first-order boundary signatures, as there are no first-order topological phases in three dimensions for class D. A strong second-order boundary signature is also forbidden as i) a rotation-symmetric chiral Majorana mode in a plane perpendicular to the rotation axis can be shrunk to a point and ii) planes parallel to the rotation axis satisfy a $(x, z) \to (-x, z)$ symmetry, which forbids a chiral mode.

In the following we determine whether a third-order boundary signature may exist at the rotation axis.

Representations $\Theta = A$ and $\Theta = B$.— For $\Theta = A$ or $\Theta = B$ the irreducible representations of fourfold rotation are exchanged under particle-hole conjugation as shown in Table 4.5. Each pair is effectively in class A, forbidding a one dimensional topological phase with boundary signature along rotation axis. Hence there are no third-order boundary signatures in these representations. Accounting for weak phases stacked in the z direction (parallel to the rotation axis), we thus find that

$$\begin{aligned}\mathcal{K}_{\mathrm{D}}[C_4, A, d = 3] &= \mathcal{K}_{\mathrm{D}}[C_4, B, d = 3] \\ &= \mathbb{Z}_2^2 \times \mathbb{Z},\end{aligned} \tag{C.25}$$

where we used the classification results for two-dimensional phases obtained in App. C.2 5.

Representations $\Theta = {}^1E$ and $\Theta = {}^2E$.— As in the main text, the discussion for the two representations $\Theta = {}^1E$ or $\Theta = {}^2E$ are analogous. We focus on the $\Theta = {}^1E$ representation in the following. As shown in Table 4.5, the $j = \frac{1}{2}$ and $j = \frac{5}{2}$ rotation eigenspaces are invariant under particle-hole conjugation while the $j = \frac{3}{2}, \frac{7}{2}$ eigenspaces are exchanged in this symmetry class. The $j = \frac{1}{2}$ and $j = \frac{5}{2}$ eigenspaces belong to class D allowing stable zero-dimensional gapless Majorana states. However, below we show that a three-dimensional superconductor with a single Majorana fermion on the fourfold rotation axis is an extrinsic (non-anomalous) third-order phase.

We consider two kinds of decorations, [5] see Fig. C.14. The first kind consists of four copies of one-dimensional Kitaev chains placed on the crystal surface and beginning and ending on the rotation axis. The four Kitaev chains are related to each other by a fourfold rotation,

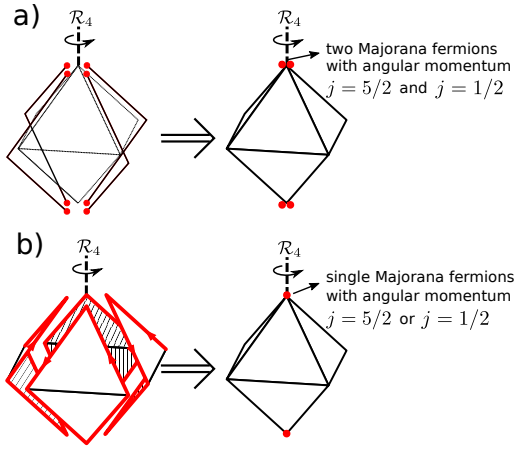

FIG. C.14. a) Decoration consisting of four copies of one-dimensional Kitaev chain. This decoration results in two Majorana fermions with angular momentum $j = \frac{1}{2}$ and $j = \frac{5}{2}$. b) Decoration consisting of four copies of two-dimensional p-wave superconductors, resulting in single Majorana fermion with angular momentum either $j = \frac{1}{2}$ or $j = \frac{5}{2}$.

which results in four Majorana end states, all with different angular momentum j. Majorana end states with $j = \frac{3}{2}$ and $j = \frac{7}{2}$ are not stable and can be gapped out, while Majorana stats with $j = \frac{1}{2}$ and $j = \frac{5}{2}$ remain. The second type of decoration consists of covering the crystal surface by four copies of a two-dimensional topological superconductor, such that the four two-dimensional superconductors are mapped onto each other by C_4 symmetry. Majorana modes running along the surface can be gapped out, Fig. C.14b. Since $\Theta = {}^1E$ or $\Theta = {}^2E$ representations correspond to an odd-parity superconductor, the resulting C_4-symmetric spinful superconductor needs to have a vortex at the rotation axis. [5] We therefore conclude that this type of decoration gives rise to a single Majorana bound state at the rotation axis, which needs to have angular momentum either $j = \frac{1}{2}$ or $j = \frac{5}{2}$. The combination of the two types of decorations described here can account for all configurations of Majorana corner states compatible with the C_4 rotation symmetry. We conclude that there are no intrinsic third-order anomalous boundary states in this class.

We conclude that the only possible topological phases in three dimensions are weak phases:

- A stack of xy planes with C_4 symmetry in the z direction allows for a Chern superconductor with even Chern number, see App. C.2 5. This phase is labeled "$(2; z)$" in Fig. C.7.

- A stack of xz and yz planes related by fourfold rotation symmetry stacked in both x and y direction. As the rotation axis lies in the intersection of the two planes, their classifying group is $\mathcal{K}_{(0,1,0)}[C_s, A'', d = 2] = \mathbb{Z}_2$ allowing a second-order topological superconductor. The configuration has

pairs of Majorana bound states at the rotation axis. This phase is labeled "$(2; x, y)$" in Fig. C.7.

- There is no stack of one dimensional superconductors pointing in the x and y direction, related by fourfold rotation symmetry, as the corresponding classifying group $\mathcal{K}_{(0,1,0)}[C_s, A'', d = 1] = 0$ is trivial.
- A stack of one dimensional z lines within the rotation axis in the x and y direction. These lines have a classifying group $\mathcal{K}_{(0,1,0)}[C_4, {}^1E, d = 1] = \mathbb{Z}_2^2$ corresponding to one dimensional TSC with Majorana bound states in the class D rotation subspaces $j = \frac{1}{2}, \frac{5}{2}$. The phases are labeled "$(1, j; x, y)$" in Fig. C.7.

The complete classifying group is hence

$$\mathcal{K}_{\mathrm{D}}[C_4, {}^{1,2}E, d = 3] = \mathbb{Z}_2^3 \times \mathbb{Z}. \tag{C.26}$$

C.3. $1d$ COMPATIBILITY RELATION FOR CLASS CI WITH INVERSION SYMMETRY

We here discuss how to obtain the compatibility relation (4.130) of Sec. 4.7.4. For definiteness, we choose the representations

$$\mathcal{T} = \rho_0\tau_0 K, \quad \mathcal{P} = \rho_0\tau_2 K, \quad \mathcal{I} = \rho_0\tau_3. \tag{C.27}$$

The following combinations of symmetries are local in $\mathbf{k}$:

$$\mathcal{I}\mathcal{T} = \rho_0\tau_3 K, \quad \mathcal{I}\mathcal{P} = \rho_0\tau_1 K, \tag{C.28}$$

as well as their product, which is a chiral antisymmetry. To construct the compatibility relation (4.130) we consider the one-parameter family of one-dimensinal Hamiltonians $H_t(k)$, defined by restricting $H(\mathbf{k})$ to the line $k_x = 0$, $k_y = t$, $k_z = k$. For $t = 0$ and $t = \pi$, the one-dimensional Hamiltonian $H_t(k)$ is a one-dimensional Hamiltonian in class CI with inversion symmetry and the A_u representation. The topological invariants at high-symmetry momenta for this one-dimensional Hamiltonian coincide with the corresponding band labels defined for the full three-dimensional Hamiltonian $H(\mathbf{k})$ and satisfy the same $0d$ compatibility relations, see Secs. 4.7.3 and 4.7.4. For generic $0 < t < \pi$, $H_t(k)$ is a one-dimensional Hamiltonian that has the local-in-k symmetries $\mathcal{I}\mathcal{T}$ and $\mathcal{I}\mathcal{P}$ only. Such a one-parameter family has a strong $\mathbb{Z}_2$ invariant, [13] which we call $\mathfrak{S}$. We can construct a compatibility relation by relating $\mathfrak{S}$ to the topological band labels of $H_t(k)$ at $t = 0$ and $t = \pi$. We find that this can be accomplished without knowledge of a general expression for the strong invariant $\mathfrak{S}$.

Before we can construct such a compatibility relation, it is necessary to obtain the full classification of the inversion-symmetric Hamiltonians $H_t(k)$ at $t = 0$ and $t = \pi$, including topologically nontrivial atomic-limit states. We recall that the topological band labels for this case are $\{\mathfrak{n}_+^{(0,t,0)}, \mathfrak{N}_+^{(0,t,\pi)}\}$, where

$$2\mathfrak{n}_+^{(0,t,0)} = \mathfrak{N}_+^{(0,t,0)} - \mathfrak{N}_+^{(0,t,\pi)} \quad t = 0, \pi, \tag{C.29}$$

see the discussion in Sec. 4.7.3. It follows that the group of topological band labels is $\mathbb{Z} \times 2\mathbb{Z}$, where we use $2\mathbb{Z}$ to indicate the integers spanned by the label $\mathfrak{n}_+^{(0,t,\pi)}$. Interpreting the topological band labels in terms of a topological classification, we note that the factor $\mathbb{Z}$ corresponds to weak phases, whereas the factor $2\mathbb{Z}$ describes strong one-dimensional atomic-limit phases. [5] We use $K_t|_{t=0,\pi} \simeq 2\mathbb{Z}$, to denote the strong phases of the model at $t = 0$ and $t = \pi$ and note that the topological band label $2\mathfrak{n}_+^{(0,t,0)}$ can be used as the corresponding topological invariant.

To obtain the compatibility relation, we have to determine, what values of $\mathfrak{n}_+^{(0,t,0)}$ are compatible with a given value of $\mathfrak{S}$. Such a problem requires understanding the homomorphism

$$K_t|_{t=0,\pi} \to K_t|_{0<t<\pi},$$

where $K_t|_{0<t<\pi} \simeq \mathbb{Z}_2$ is the group classifying strong phases of $H_t(k)$ for generic t. To construct this homomorphism, we notice that

$$H(k) = \rho_0\tau_3(1 - m - \cos k) + \rho_2\tau_1 \sin k \tag{C.30}$$

with $0 < m < 2$ is an example of a Hamiltonian that satisfies $\mathcal{T}$, $\mathcal{P}$, and $\mathcal{I}$ symmetries and that is nontrivial if only the local-in-k symmetries $\mathcal{I}\mathcal{T}$ and $\mathcal{I}\mathcal{P}$ are kept, *i.e.*, it has invariant $\mathfrak{S} = 1$. (Although no general expression for $\mathfrak{S}$ is available, $\mathfrak{S}$ can be calculated as the parity of a winding number if $H(k)$ is a 4×4 matrix.) It follows that the mapping $K_t|_{t=0,\pi} \to K_t|_{0<t<\pi}$ must be surjective. One verifies that the Hamiltonian (C.30) has topological band label $\mathfrak{n}_+^{(0)} = 1$. Since the trivial phase has $\mathfrak{n}_+^{(0)} = 0$ and since $\mathfrak{S}$ has a $\mathbb{Z}_2$ group structure, it directly follows that

$$\begin{aligned} \mathfrak{S} &= \mathfrak{n}_+^{(0,0,0)} \mod 2 \\ &= \mathfrak{n}_+^{(0,\pi,0)} \mod 2. \end{aligned} \tag{C.31}$$

This is one of the compatibility relations of Eq. (4.130). The other relations follow in analogous manner by considering other appropriately chosen families of one-dimensional Hamiltonians $H_t(k)$.

C.4. ADDITIONAL TABLES

		BL					SI
$\mathcal{K}_i' \subseteq \mathcal{K}_i$	Phase	$\mathfrak{N}_{\frac{1}{2}}^{(0,0)}$	$\mathfrak{N}_{\frac{5}{2}}^{(0,0)}$	$\mathfrak{N}_{\frac{1}{2}}^{(\pi,0)}$	$\mathfrak{N}_{\frac{1}{2}}^{(\pi,\pi)}$	$\mathfrak{N}_{\frac{5}{2}}^{(\pi,\pi)}$	$\mathbb{Z}_2 \otimes \mathbb{Z}_8$
-	$\mathbf{x} = (0,0),\ j = \frac{1}{2}$	1	0	1	1	0	0
-	$\mathbf{x} = (0,0),\ j = \frac{5}{2}$	0	1	1	0	1	0
-	$\mathbf{x} = (\frac{1}{2},\frac{1}{2}),\ j = \frac{1}{2}$	1	0	-1	0	1	0
-	$\mathbf{x} = (\frac{1}{2},\frac{1}{2}),\ j = \frac{5}{2}$	0	1	-1	1	0	0
-	$\mathbf{x} = (\frac{1}{2},0),\ j = \frac{1}{2}$	1	1	0	-1	-1	0
$\mathbb{Z}_2$	$(1;x,y)$	1	1	1	0	0	$\mathrm{e}_{1;x,y}^{(2)}$
$0 \subseteq \mathbb{Z}$	(2)	0	0	1	1	0	$\mathrm{e}_{2}^{(8)}$
$\mathbb{Z}_2 \subseteq \mathbb{Z}_2$	(2)'	2	2	0	0	0	$4\mathrm{e}_{2}^{(8)}$

TABLE C.1. Band labels and symmetry-based indicators for atomic-limit Hamiltonians obtained by placing 0d generators for representation j at Wyckoff position $\mathbf{x}$ for the symmetry group C_4 in two dimensions, class D with representation $\Theta = A$ or $\Theta = B$ (upper five rows) and band labels for the generators of the weak, Chern and second-order phases (lower three rows).

		BL								SI
$\mathcal{K}_i' \subseteq \mathcal{K}_i$	Phase	$\mathfrak{p}_{\frac{1}{2}}^{(0,0)}$	$\mathfrak{p}_{\frac{5}{2}}^{(0,0)}$	$\mathfrak{N}_{\frac{3}{2}}^{(0,0)}$	$\mathfrak{p}_{\frac{1}{2}}^{(\pi,0)}$	$\mathfrak{p}_{\frac{3}{2}}^{(\pi,0)}$	$\mathfrak{p}_{\frac{1}{2}}^{(\pi,\pi)}$	$\mathfrak{p}_{\frac{5}{2}}^{(\pi,\pi)}$	$\mathfrak{N}_{\frac{3}{2}}^{(\pi,\pi)}$	$\mathbb{Z}_4$
-	$\mathbf{x} = (0,0),\ j = \frac{1}{2}$	1	0	0	1	0	1	0	0	0
-	$\mathbf{x} = (0,0),\ j = \frac{5}{2}$	0	1	0	1	0	0	1	0	0
-	$\mathbf{x} = (0,0),\ j = \frac{3}{2}$	0	0	1	0	1	0	0	1	0
-	$\mathbf{x} = (\frac{1}{2},\frac{1}{2}),\ j = \frac{1}{2}$	1	0	0	0	1	0	1	0	0
-	$\mathbf{x} = (\frac{1}{2},\frac{1}{2}),\ j = \frac{5}{2}$	0	1	0	0	1	1	0	0	0
-	$\mathbf{x} = (\frac{1}{2},\frac{1}{2}),\ j = \frac{3}{2}$	0	0	1	1	0	0	0	-1	0
-	$\mathbf{x} = (\frac{1}{2},0),\ j = \frac{1}{2}$	1	1	0	1	1	0	0	0	0
-	$\mathbf{x} = (\frac{1}{2},0),\ j = \frac{3}{2}$	0	0	0	1	1	1	1	0	0
$0 \subseteq \mathbb{Z}$	(2)	0	0	0	1	1	1	0	1	$\mathrm{e}_{2}^{(4)}$

TABLE C.2. Band labels and symmetry-based indicators for atomic-limit Hamiltonians obtained by placing 0d generators for representation j at Wyckoff position $\mathbf{x}$ for the symmetry group C_4 in two dimensions, class D with representation $\Theta = {}^1E$ or $\Theta = {}^2E$ (upper eight rows) and band labels for the generator of the Chern phase (lowest row).

		BL								SI
$\mathcal{K}_i'' \subseteq \mathcal{K}_i' \subseteq \mathcal{K}_i$	Phase	$\mathfrak{p}^{(0,0,0)}$	$\mathfrak{p}^{(\pi,0,0)}$	$\mathfrak{p}^{(0,\pi,0)}$	$\mathfrak{p}^{(\pi,\pi,0)}$	$\mathfrak{p}^{(0,0,\pi)}$	$\mathfrak{p}^{(\pi,0,\pi)}$	$\mathfrak{p}^{(0,\pi,\pi)}$	$\mathfrak{p}^{(\pi,\pi,\pi)}$	$\mathbb{Z}_2^7$
-	$\mathbf{x} = (0,0,0)$	1	1	1	1	1	1	1	1	0
$\mathbb{Z}_2$	$(1;y,z)$	1	0	1	0	1	0	1	0	$\mathrm{e}_{1;y,z}^{(2)}$
$\mathbb{Z}_2$	$(1;x,z)$	1	1	0	0	1	1	0	0	$\mathrm{e}_{1;x,z}^{(2)}$
$\mathbb{Z}_2$	$(1;x,y)$	1	1	1	1	0	0	0	0	$\mathrm{e}_{1;x,y}^{(2)}$
$0 \subseteq \mathbb{Z}$	$(2;z)$	1	0	0	0	1	0	0	0	$\mathrm{e}_{2;z}^{(2)}$
$0 \subseteq \mathbb{Z}$	$(2;y)$	1	0	1	0	0	0	0	0	$\mathrm{e}_{2;y}^{(2)}$
$0 \subseteq \mathbb{Z}$	$(2;x)$	1	1	0	0	0	0	0	0	$\mathrm{e}_{2;x}^{(2)}$

TABLE C.3. Topological band labels of three-dimensional superconductors in tenfold-way class D with translation symmetry only (point group C_1).

$\mathcal{K}_i'' \subseteq \mathcal{K}_i' \subseteq \mathcal{K}_i$	Phase		BS $\mathfrak{p}_{(+,-)}^{(0,0,0)}$	$\mathfrak{p}_{(+,-)}^{(\pi,0,0)}$	$\mathfrak{p}_{(+,-)}^{(0,\pi,0)}$	$\mathfrak{p}_{(+,-)}^{(\pi,\pi,0)}$	$\mathfrak{p}_{(+,-)}^{(0,0,\pi)}$	$\mathfrak{p}_{(+,-)}^{(\pi,0,\pi)}$	$\mathfrak{p}_{(+,-)}^{(0,\pi,\pi)}$	$\mathfrak{p}_{(+,-)}^{(\pi,\pi,\pi)}$	SI $\mathbb{Z}_2^4$
-	$\mathbf{x}=(0,0,0),\ \alpha=$	$+$	$(1,0)$	$(1,0)$	$(1,0)$	$(1,0)$	$(1,0)$	$(1,0)$	$(1,0)$	$(1,0)$	0
		$-$	$(0,1)$	$(0,1)$	$(0,1)$	$(0,1)$	$(0,1)$	$(0,1)$	$(0,1)$	$(0,1)$	0
-	$\mathbf{x}=(\frac{1}{2},0,0),\ \alpha=$	$+$	$(1,0)$	$(0,1)$	$(1,0)$	$(0,1)$	$(1,0)$	$(0,1)$	$(1,0)$	$(0,1)$	0
		$-$	$(0,1)$	$(1,0)$	$(0,1)$	$(1,0)$	$(0,1)$	$(1,0)$	$(0,1)$	$(1,0)$	0
-	$\mathbf{x}=(0,\frac{1}{2},0),\ \alpha=$	$+$	$(1,0)$	$(1,0)$	$(0,1)$	$(0,1)$	$(1,0)$	$(1,0)$	$(0,1)$	$(0,1)$	0
		$-$	$(0,1)$	$(0,1)$	$(1,0)$	$(1,0)$	$(0,1)$	$(0,1)$	$(1,0)$	$(1,0)$	0
-	$\mathbf{x}=(\frac{1}{2},\frac{1}{2},0),\ \alpha=$	$+$	$(1,0)$	$(0,1)$	$(0,1)$	$(1,0)$	$(1,0)$	$(0,1)$	$(0,1)$	$(1,0)$	0
		$-$	$(0,1)$	$(1,0)$	$(1,0)$	$(0,1)$	$(0,1)$	$(1,0)$	$(1,0)$	$(0,1)$	0
-	$\mathbf{x}=(0,0,\frac{1}{2}),\ \alpha=$	$+$	$(1,0)$	$(1,0)$	$(1,0)$	$(1,0)$	$(0,1)$	$(0,1)$	$(0,1)$	$(0,1)$	0
		$-$	$(0,1)$	$(0,1)$	$(0,1)$	$(0,1)$	$(1,0)$	$(1,0)$	$(1,0)$	$(1,0)$	0
-	$\mathbf{x}=(\frac{1}{2},0,\frac{1}{2}),\ \alpha=$	$+$	$(1,0)$	$(0,1)$	$(1,0)$	$(0,1)$	$(0,1)$	$(1,0)$	$(0,1)$	$(1,0)$	0
		$-$	$(0,1)$	$(1,0)$	$(0,1)$	$(1,0)$	$(1,0)$	$(0,1)$	$(1,0)$	$(0,1)$	0
-	$\mathbf{x}=(0,\frac{1}{2},\frac{1}{2}),\ \alpha=$	$+$	$(1,0)$	$(1,0)$	$(0,1)$	$(0,1)$	$(0,1)$	$(0,1)$	$(1,0)$	$(1,0)$	0
		$-$	$(0,1)$	$(0,1)$	$(1,0)$	$(1,0)$	$(1,0)$	$(1,0)$	$(0,1)$	$(0,1)$	0
-	$\mathbf{x}=(\frac{1}{2},\frac{1}{2},\frac{1}{2}),\ \alpha=$	$+$	$(1,0)$	$(0,1)$	$(0,1)$	$(1,0)$	$(0,1)$	$(1,0)$	$(1,0)$	$(0,1)$	0
		$-$	$(0,1)$	$(1,0)$	$(1,0)$	$(0,1)$	$(1,0)$	$(0,1)$	$(0,1)$	$(1,0)$	0
$0\subseteq\mathbb{Z}$	$(2;z)$		$(1,1)$	$(0,0)$	$(0,0)$	$(0,0)$	$(1,1)$	$(0,0)$	$(0,0)$	$(0,0)$	$\mathrm{e}_{2;z}^{(2)}$
$0\subseteq\mathbb{Z}$	$(2;y)$		$(1,1)$	$(0,0)$	$(1,1)$	$(0,0)$	$(0,0)$	$(0,0)$	$(0,0)$	$(0,0)$	$\mathrm{e}_{2;y}^{(2)}$
$0\subseteq\mathbb{Z}$	$(2;x)$		$(1,1)$	$(1,1)$	$(0,0)$	$(0,0)$	$(0,0)$	$(0,0)$	$(0,0)$	$(0,0)$	$\mathrm{e}_{2;x}^{(2)}$

TABLE C.4. Topological band labels of three-dimensional superconductors in tenfold-way class D with point group C_i and representation $\Theta = A_g$.

$\mathcal{K}_i'' \subseteq \mathcal{K}_i' \subseteq \mathcal{K}_i$	Phase	BS $\mathfrak{N}_+^{(0,0,0)}$	$\mathfrak{N}_+^{(\pi,0,0)}$	$\mathfrak{N}_+^{(0,\pi,0)}$	$\mathfrak{N}_+^{(\pi,\pi,0)}$	$\mathfrak{N}_+^{(0,0,\pi)}$	$\mathfrak{N}_+^{(\pi,0,\pi)}$	$\mathfrak{N}_+^{(0,\pi,\pi)}$	$\mathfrak{N}_+^{(\pi,\pi,\pi)}$	SI $\mathbb{Z}_2^3\otimes\mathbb{Z}_4^3\otimes\mathbb{Z}_8$
-	$\mathbf{x}=(0,0,0)$	1	1	1	1	1	1	1	1	0
-	$\mathbf{x}=(\frac{1}{2},0,0)$	1	-1	1	-1	1	-1	1	-1	0
-	$\mathbf{x}=(0,\frac{1}{2},0)$	1	1	-1	-1	1	1	-1	-1	0
-	$\mathbf{x}=(\frac{1}{2},\frac{1}{2},0)$	1	-1	-1	1	1	-1	-1	1	0
-	$\mathbf{x}=(0,0,\frac{1}{2})$	1	1	1	1	-1	-1	-1	-1	0
-	$\mathbf{x}=(\frac{1}{2},0,\frac{1}{2})$	1	-1	1	-1	-1	1	-1	1	0
-	$\mathbf{x}=(0,\frac{1}{2},\frac{1}{2})$	1	1	-1	-1	-1	-1	1	1	0
-	$\mathbf{x}=(\frac{1}{2},\frac{1}{2},\frac{1}{2})$	1	-1	-1	1	-1	1	1	-1	0
$\mathbb{Z}_2$	$(1;y,z)$	1	0	1	0	1	0	1	0	$\mathrm{e}_{1;y,z}^{(2)}$
$\mathbb{Z}_2$	$(1;x,z)$	1	1	0	0	1	1	0	0	$\mathrm{e}_{1;x,z}^{(2)}$
$\mathbb{Z}_2$	$(1;x,y)$	1	1	1	1	0	0	0	0	$\mathrm{e}_{1;x,y}^{(2)}$
$0\subseteq\mathbb{Z}$	$(2;z)$	1	0	0	0	1	0	0	0	$\mathrm{e}_{2;z}^{(4)}$
$0\subseteq\mathbb{Z}$	$(2;y)$	1	0	1	0	0	0	0	0	$\mathrm{e}_{2;y}^{(4)}$
$0\subseteq\mathbb{Z}$	$(2;x)$	1	1	0	0	0	0	0	0	$\mathrm{e}_{2;x}^{(4)}$
$\mathbb{Z}_2\subseteq\mathbb{Z}_2$	$(2;z)'$	2	0	0	0	2	0	0	0	$2\mathrm{e}_{2;z}^{(4)}$
$\mathbb{Z}_2\subseteq\mathbb{Z}_2$	$(2;y)'$	2	0	2	0	0	0	0	0	$2\mathrm{e}_{2;y}^{(4)}$
$\mathbb{Z}_2\subseteq\mathbb{Z}_2$	$(2;x)'$	2	2	0	0	0	0	0	0	$2\mathrm{e}_{2;x}^{(4)}$
$\mathbb{Z}_2\subseteq\mathbb{Z}_4\subseteq\mathbb{Z}_4$	$(3)'$	2	0	0	0	0	0	0	0	$2\mathrm{e}_{3}^{(8)}$

TABLE C.5. Topological band labels of three-dimensional superconductors in tenfold-way class D with point group C_i and representation $\Theta = A_u$.

		BS								SI
$\mathcal{K}_i'' \subseteq \mathcal{K}_i' \subseteq \mathcal{K}_i$	Phase	$\mathfrak{N}_+^{(0,0,0)}$	$\mathfrak{N}_+^{(\pi,0,0)}$	$\mathfrak{N}_+^{(0,\pi,0)}$	$\mathfrak{N}_+^{(\pi,\pi,0)}$	$\mathfrak{N}_+^{(0,0,\pi)}$	$\mathfrak{N}_+^{(\pi,0,\pi)}$	$\mathfrak{N}_+^{(0,\pi,\pi)}$	$\mathfrak{N}_+^{(\pi,\pi,\pi)}$	$\mathbb{Z}_2^3 \otimes \mathbb{Z}_4^3 \otimes \mathbb{Z}_8$
-	$\mathbf{x} = (0,0,0)$	1	1	1	1	1	1	1	1	0
-	$\mathbf{x} = (\frac{1}{2},0,0)$	1	-1	1	-1	1	-1	1	-1	0
-	$\mathbf{x} = (0,\frac{1}{2},0)$	1	1	-1	-1	1	1	-1	-1	0
-	$\mathbf{x} = (\frac{1}{2},\frac{1}{2},0)$	1	-1	-1	1	1	-1	-1	1	0
-	$\mathbf{x} = (0,0,\frac{1}{2})$	1	1	1	1	-1	-1	-1	-1	0
-	$\mathbf{x} = (\frac{1}{2},0,\frac{1}{2})$	1	-1	1	-1	-1	1	-1	1	0
-	$\mathbf{x} = (0,\frac{1}{2},\frac{1}{2})$	1	1	-1	-1	-1	-1	1	1	0
-	$\mathbf{x} = (\frac{1}{2},\frac{1}{2},\frac{1}{2})$	1	-1	-1	1	-1	1	1	-1	0
$\mathbb{Z}_2$	$(1;y,z)$	1	0	1	0	1	0	1	0	$\mathrm{e}_{1;y,z}^{(2)}$
$\mathbb{Z}_2$	$(1;x,z)$	1	1	0	0	1	1	0	0	$\mathrm{e}_{1;x,z}^{(2)}$
$\mathbb{Z}_2$	$(1;x,y)$	1	1	1	1	0	0	0	0	$\mathrm{e}_{1;x,y}^{(2)}$
$\mathbb{Z}_2 \subseteq \mathbb{Z}_4$	$(2;z)$	1	0	0	0	1	0	0	0	$\mathrm{e}_{2;z}^{(4)}$
$\mathbb{Z}_2 \subseteq \mathbb{Z}_4$	$(2;y)$	1	0	1	0	0	0	0	0	$\mathrm{e}_{2;y}^{(4)}$
$\mathbb{Z}_2 \subseteq \mathbb{Z}_4$	$(2;x)$	1	1	0	0	0	0	0	0	$\mathrm{e}_{2;x}^{(4)}$
$0 \subseteq 0 \subseteq \mathbb{Z}$	(3)	1	0	0	0	0	0	0	0	$\mathrm{e}_3^{(8)}$
$\mathbb{Z}_2 \subseteq \mathbb{Z}_4 \subseteq \mathbb{Z}_4$	$(3)'$	2	0	0	0	0	0	0	0	$2\mathrm{e}_3^{(8)}$

TABLE C.6. Topological band labels of three-dimensional superconductors in tenfold-way class DIII with point group C_i and representation $\Theta = A_u$.

		BS								SI
$\mathcal{K}_i'' \subseteq \mathcal{K}_i' \subseteq \mathcal{K}_i$	Phase	$\mathfrak{N}_+^{(0,0,0)}$	$\mathfrak{N}_+^{(\pi,0,0)}$	$\mathfrak{N}_+^{(0,\pi,0)}$	$\mathfrak{N}_+^{(\pi,\pi,0)}$	$\mathfrak{N}_+^{(0,0,\pi)}$	$\mathfrak{N}_+^{(\pi,0,\pi)}$	$\mathfrak{N}_+^{(0,\pi,\pi)}$	$\mathfrak{N}_+^{(\pi,\pi,\pi)}$	$\mathbb{Z}_2^3 \otimes \mathbb{Z}_4$
-	$\mathbf{x} = (0,0,0)$	1	1	1	1	1	1	1	1	0
-	$\mathbf{x} = (\frac{1}{2},0,0)$	1	-1	1	-1	1	-1	1	-1	0
-	$\mathbf{x} = (0,\frac{1}{2},0)$	1	1	-1	-1	1	1	-1	-1	0
-	$\mathbf{x} = (\frac{1}{2},\frac{1}{2},0)$	1	-1	-1	1	1	-1	-1	1	0
-	$\mathbf{x} = (0,0,\frac{1}{2})$	1	1	1	1	-1	-1	-1	-1	0
-	$\mathbf{x} = (\frac{1}{2},0,\frac{1}{2})$	1	-1	1	-1	-1	1	-1	1	0
-	$\mathbf{x} = (0,\frac{1}{2},\frac{1}{2})$	1	1	-1	-1	-1	-1	1	1	0
-	$\mathbf{x} = (\frac{1}{2},\frac{1}{2},\frac{1}{2})$	1	-1	-1	1	-1	1	1	-1	0
$0 \subseteq \mathbb{Z}$	$(2;z)$	2	0	0	0	2	0	0	0	$\mathrm{e}_{2;z}^{(2)}$
$0 \subseteq \mathbb{Z}$	$(2;y)$	2	0	2	0	0	0	0	0	$\mathrm{e}_{2;y}^{(2)}$
$0 \subseteq \mathbb{Z}$	$(2;x)$	2	2	0	0	0	0	0	0	$\mathrm{e}_{2;x}^{(2)}$
$0 \subseteq \mathbb{Z}_2 \subseteq \mathbb{Z}_2$	$(3)'$	4	0	0	0	0	0	0	0	$2\mathrm{e}_3^{(4)}$

TABLE C.7. Topological band labels of three-dimensional superconductors in tenfold-way class C with point group C_i and representation $\Theta = A_u$.

		BS								SI
$\mathcal{K}_i'' \subseteq \mathcal{K}_i' \subseteq \mathcal{K}_i$	Phase	$\mathfrak{N}_+^{(0,0,0)}$	$\mathfrak{N}_+^{(\pi,0,0)}$	$\mathfrak{N}_+^{(0,\pi,0)}$	$\mathfrak{N}_+^{(\pi,\pi,0)}$	$\mathfrak{N}_+^{(0,0,\pi)}$	$\mathfrak{N}_+^{(\pi,0,\pi)}$	$\mathfrak{N}_+^{(0,\pi,\pi)}$	$\mathfrak{N}_+^{(\pi,\pi,\pi)}$	$\mathbb{Z}_2^3 \otimes \mathbb{Z}_4$
-	$\mathbf{x} = (0,0,0)$	1	1	1	1	1	1	1	1	0
-	$\mathbf{x} = (\frac{1}{2},0,0)$	1	-1	1	-1	1	-1	1	-1	0
-	$\mathbf{x} = (0,\frac{1}{2},0)$	1	1	-1	-1	1	1	-1	-1	0
-	$\mathbf{x} = (\frac{1}{2},\frac{1}{2},0)$	1	-1	-1	1	1	-1	-1	1	0
-	$\mathbf{x} = (0,0,\frac{1}{2})$	1	1	1	1	-1	-1	-1	-1	0
-	$\mathbf{x} = (\frac{1}{2},0,\frac{1}{2})$	1	-1	1	-1	-1	1	-1	1	0
-	$\mathbf{x} = (0,\frac{1}{2},\frac{1}{2})$	1	1	-1	-1	-1	-1	1	1	0
-	$\mathbf{x} = (\frac{1}{2},\frac{1}{2},\frac{1}{2})$	1	-1	-1	1	-1	1	1	-1	0
$0 \subseteq 0 \subseteq \mathbb{Z}$	(3)	4	0	0	0	0	0	0	0	$2\mathrm{e}_3^{(4)}$

TABLE C.8. Topological band labels of three-dimensional superconductors in tenfold-way class CI with point group C_i and representation $\Theta = A_u$.

$\mathcal{K}_i'' \subseteq \mathcal{K}_i' \subseteq \mathcal{K}_i$	Phase	BL $\mathfrak{N}_+^{(0,0,0)}$	$\mathfrak{N}_+^{(\pi,0,0)}$	$\mathfrak{N}_+^{(0,\pi,0)}$	$\mathfrak{N}_+^{(\pi,\pi,0)}$	$\mathfrak{N}_+^{(0,0,\pi)}$	$\mathfrak{N}_+^{(\pi,0,\pi)}$	$\mathfrak{N}_+^{(0,\pi,\pi)}$	$\mathfrak{N}_+^{(\pi,\pi,\pi)}$	SI $\mathbb{Z}_2$
-	$\mathbf{x}=(0,0,0)$	1	1	1	1	1	1	1	1	0
-	$\mathbf{x}=(\frac{1}{2},0,0)$	1	-1	1	-1	1	-1	1	-1	0
$\mathbb{Z}_2$	$(1;y,z)$	1	0	1	0	1	0	1	0	$\mathrm{e}^{(2)}_{1;y,z}$
$0\subseteq\mathbb{Z}$	$(2;x)$	0	0	0	0	0	0	0	0	0

TABLE C.9. Topological band labels of three-dimensional superconductors in tenfold-way class D with point group C_s and representation $\Theta = A'$.

$\mathcal{K}_i'' \subseteq \mathcal{K}_i' \subseteq \mathcal{K}_i$	Phase	BL $\mathfrak{p}_{(+,-)}^{(0,0,0)}$	$\mathfrak{p}_{(+,-)}^{(\pi,0,0)}$	$\mathfrak{p}_{(+,-)}^{(0,\pi,0)}$	$\mathfrak{p}_{(+,-)}^{(\pi,\pi,0)}$	$\mathfrak{p}_{(+,-)}^{(0,0,\pi)}$	$\mathfrak{p}_{(+,-)}^{(\pi,0,\pi)}$	$\mathfrak{p}_{(+,-)}^{(0,\pi,\pi)}$	$\mathfrak{p}_{(+,-)}^{(\pi,\pi,\pi)}$	SI $\mathbb{Z}_2^9$
-	$\mathbf{x}=(0,0,0),\ \alpha=+$	(1,0)	(1,0)	(1,0)	(1,0)	(1,0)	(1,0)	(1,0)	(1,0)	0
	$\alpha=-$	(0,1)	(0,1)	(0,1)	(0,1)	(0,1)	(0,1)	(0,1)	(0,1)	0
-	$\mathbf{x}=(\frac{1}{2},0,0),\ \alpha=+$	(1,0)	(0,1)	(1,0)	(0,1)	(1,0)	(0,1)	(1,0)	(0,1)	0
	$\alpha=-$	(0,1)	(1,0)	(0,1)	(1,0)	(0,1)	(1,0)	(0,1)	(1,0)	0
$\mathbb{Z}_2$	$(1,+;x,z)$	(1,0)	(1,0)	(0,0)	(0,0)	(1,0)	(1,0)	(0,0)	(0,0)	$\mathrm{e}^{(2)}_{1,+;x,z}$
$\mathbb{Z}_2$	$(1,-;x,z)$	(0,1)	(0,1)	(0,0)	(0,0)	(0,1)	(0,1)	(0,0)	(0,0)	$\mathrm{e}^{(2)}_{1,-;x,z}$
$\mathbb{Z}_2$	$(1,+;x,y)$	(1,0)	(1,0)	(1,0)	(1,0)	(0,0)	(0,0)	(0,0)	(0,0)	$\mathrm{e}^{(2)}_{1,+;x,y}$
$\mathbb{Z}_2$	$(1,-;x,y)$	(0,1)	(0,1)	(0,1)	(0,1)	(0,0)	(0,0)	(0,0)	(0,0)	$\mathrm{e}^{(2)}_{1,-;x,y}$
$0\subseteq\mathbb{Z}$	$(2,+;x)$	(1,0)	(1,0)	(0,0)	(0,0)	(0,0)	(0,0)	(0,0)	(0,0)	$\mathrm{e}^{(2)}_{2,+;x}$
$0\subseteq\mathbb{Z}$	$(2,-;x)$	(0,1)	(0,1)	(0,0)	(0,0)	(0,0)	(0,0)	(0,0)	(0,0)	$\mathrm{e}^{(2)}_{2,-;x}$
$\mathbb{Z}_2\subseteq\mathbb{Z}_2$	$(2;z)'$	(1,1)	(0,0)	(0,0)	(0,0)	(1,1)	(0,0)	(0,0)	(0,0)	$\mathrm{e}^{(2)}_{2;z}$
$\mathbb{Z}_2\subseteq\mathbb{Z}_2$	$(2;y)'$	(1,1)	(0,0)	(1,1)	(0,0)	(0,0)	(0,0)	(0,0)	(0,0)	$\mathrm{e}^{(2)}_{2;y}$
$0\subseteq\mathbb{Z}_2\subseteq\mathbb{Z}_2$	$(3)'$	(1,1)	(0,0)	(0,0)	(0,0)	(0,0)	(0,0)	(0,0)	(0,0)	$\mathrm{e}^{(2)}_{3}$

TABLE C.10. Topological band labels of three-dimensional superconductors in tenfold-way class D with point group C_s and representation $\Theta = A''$.

$\mathcal{K}_i'' \subseteq \mathcal{K}_i' \subseteq \mathcal{K}_i$	Phase	BL $\mathfrak{N}_+^{(0,0,0)}$	$\mathfrak{N}_+^{(\pi,0,0)}$	$\mathfrak{N}_+^{(0,\pi,0)}$	$\mathfrak{N}_+^{(\pi,\pi,0)}$	$\mathfrak{N}_+^{(0,0,\pi)}$	$\mathfrak{N}_+^{(\pi,0,\pi)}$	$\mathfrak{N}_+^{(0,\pi,\pi)}$	$\mathfrak{N}_+^{(\pi,\pi,\pi)}$	SI $\mathbb{Z}_2^2\times\mathbb{Z}_4$
-	$\mathbf{x}=(0,0,0)$	1	1	1	1	1	1	1	1	0
-	$\mathbf{x}=(\frac{1}{2},0,0)$	1	-1	1	-1	1	-1	1	-1	0
-	$\mathbf{x}=(0,\frac{1}{2},0)$	1	1	-1	-1	1	1	-1	-1	0
-	$\mathbf{x}=(\frac{1}{2},\frac{1}{2},0)$	1	-1	-1	1	1	-1	-1	1	0
$\mathbb{Z}_2$	$(1;y,z)$	1	0	1	0	1	0	1	0	$\mathrm{e}^{(2)}_{1;y,z}$
$\mathbb{Z}_2$	$(1;x,z)$	1	1	0	0	1	1	0	0	$\mathrm{e}^{(2)}_{1;x,z}$
$\mathbb{Z}_2\subseteq\mathbb{Z}_2$	$(2;z)$'	2	0	0	0	2	0	0	0	$2\mathrm{e}^{(4)}_{2;z}$
$0\subseteq\mathbb{Z}$	$(2;z)$	1	0	0	0	1	0	0	0	$\mathrm{e}^{(4)}_{2;z}$

TABLE C.11. Topological band labels of three-dimensional superconductors in tenfold-way class D with point group C_2 and representation $\Theta = A$.

$\mathcal{K}_i'' \subseteq \mathcal{K}_i' \subseteq \mathcal{K}_i$	Phase	BL $\mathfrak{p}_{(+,-)}^{(0,0,0)}$	BL $\mathfrak{p}_{(+,-)}^{(\pi,0,0)}$	BL $\mathfrak{p}_{(+,-)}^{(0,\pi,0)}$	BL $\mathfrak{p}_{(+,-)}^{(\pi,\pi,0)}$	BL $\mathfrak{p}_{(+,-)}^{(0,0,\pi)}$	BL $\mathfrak{p}_{(+,-)}^{(\pi,0,\pi)}$	BL $\mathfrak{p}_{(+,-)}^{(0,\pi,\pi)}$	BL $\mathfrak{p}_{(+,-)}^{(\pi,\pi,\pi)}$	SI $\mathbb{Z}_2^6$
-	$\mathbf{x}=(0,0,0),\ \alpha=+$	(1,0)	(1,0)	(1,0)	(1,0)	(1,0)	(1,0)	(1,0)	(1,0)	0
	$\alpha=-$	(0,1)	(0,1)	(0,1)	(0,1)	(0,1)	(0,1)	(0,1)	(0,1)	0
-	$\mathbf{x}=(\frac{1}{2},0,0),\ \alpha=+$	(1,0)	(0,1)	(1,0)	(0,1)	(1,0)	(0,1)	(1,0)	(0,1)	0
	$\alpha=-$	(0,1)	(1,0)	(0,1)	(1,0)	(0,1)	(1,0)	(0,1)	(1,0)	0
-	$\mathbf{x}=(0,\frac{1}{2},0),\ \alpha=+$	(1,0)	(1,0)	(0,1)	(0,1)	(1,0)	(1,0)	(0,1)	(0,1)	0
	$\alpha=-$	(0,1)	(0,1)	(1,0)	(1,0)	(0,1)	(0,1)	(1,0)	(1,0)	0
-	$\mathbf{x}=(\frac{1}{2},\frac{1}{2},0),\ \alpha=+$	(1,0)	(0,1)	(0,1)	(1,0)	(1,0)	(0,1)	(0,1)	(1,0)	0
	$\alpha=-$	(0,1)	(1,0)	(1,0)	(0,1)	(0,1)	(1,0)	(1,0)	(0,1)	0
$\mathbb{Z}_2$	$(1,+;x,y)$	(1,0)	(1,0)	(1,0)	(1,0)	(0,0)	(0,0)	(0,0)	(0,0)	$\mathrm{e}^{(2)}_{1,+;x,y}$
$\mathbb{Z}_2$	$(1,-;x,y)$	(0,1)	(0,1)	(0,1)	(0,1)	(0,0)	(0,0)	(0,0)	(0,0)	$\mathrm{e}^{(2)}_{1,-;x,y}$
$\mathbb{Z}_2 \subseteq \mathbb{Z}_2$	$(2;x)$'	(1,1)	(1,1)	(0,0)	(0,0)	(0,0)	(0,0)	(0,0)	(0,0)	$\mathrm{e}^{(2)}_{2;x}$
$\mathbb{Z}_2 \subseteq \mathbb{Z}_2$	$(2;y)$'	(1,1)	(0,0)	(1,1)	(0,0)	(0,0)	(0,0)	(0,0)	(0,0)	$\mathrm{e}^{(2)}_{2;y}$
$0 \subseteq \mathbb{Z}$	$(2;z)$	(1,1)	(0,0)	(0,0)	(0,0)	(1,1)	(0,0)	(0,0)	(0,0)	$\mathrm{e}^{(2)}_{2;z}$

TABLE C.12. Topological band labels of three-dimensional superconductors in tenfold-way class D with point group C_2 and representation $\Theta = B$.

$\mathcal{K}_i'' \subseteq \mathcal{K}_i' \subseteq \mathcal{K}_i$	Phase	BL $(0,0,0)$ $\mathfrak{N}_{\frac{1}{2}}$	BL $(0,0,0)$ $\mathfrak{N}_{\frac{5}{2}}$	BL $(\pi,0,0)$ $\mathfrak{N}_{\frac{1}{2}}$	BL $(\pi,\pi,0)$ $\mathfrak{N}_{\frac{1}{2}}$	BL $(\pi,\pi,0)$ $\mathfrak{N}_{\frac{5}{2}}$	BL $(0,0,\pi)$ $\mathfrak{N}_{\frac{1}{2}}$	BL $(0,0,\pi)$ $\mathfrak{N}_{\frac{5}{2}}$	BL $(\pi,0,\pi)$ $\mathfrak{N}_{\frac{1}{2}}$	BL (π,π,π) $\mathfrak{N}_{\frac{1}{2}}$	BL (π,π,π) $\mathfrak{N}_{\frac{5}{2}}$	SI $\mathbb{Z}_2\times\mathbb{Z}_8$
-	$\mathbf{x}=(0,0),\ j=\frac{1}{2}$	1	0	1	1	0	1	0	1	1	0	0
-	$\mathbf{x}=(0,0),\ j=\frac{5}{2}$	0	1	1	0	1	0	1	1	0	1	0
-	$\mathbf{x}=(\frac{1}{2},\frac{1}{2}),\ j=\frac{1}{2}$	1	0	-1	0	1	1	0	-1	0	1	0
-	$\mathbf{x}=(\frac{1}{2},\frac{1}{2}),\ j=\frac{5}{2}$	0	1	-1	1	0	0	1	-1	1	0	0
-	$\mathbf{x}=(\frac{1}{2},0),\ j=\frac{1}{2}$	1	1	0	-1	-1	1	1	0	-1	-1	0
$\mathbb{Z}_2$	$(1;x,y,z)$	1	1	1	0	0	1	1	1	0	0	$\mathrm{e}^{(2)}_{1;x,y,z}$
$0 \subseteq \mathbb{Z}$	$(2;z)$	0	0	1	1	0	0	0	1	1	0	$\mathrm{e}^{(8)}_{2;z}$
$\mathbb{Z}_2 \subseteq \mathbb{Z}_2$	$(2;z)'$	2	2	0	0	0	2	2	0	0	0	$4\mathrm{e}^{(8)}_{2;z}$

TABLE C.13. Band labels of three-dimensional superconductors in tenfold-way class D with point group C_4 and representations $\Theta = A$ or $\Theta = B$.

$\mathcal{K}_i'' \subseteq \mathcal{K}_i' \subseteq \mathcal{K}_i$	Phase	BL $(0,0,0)$ $\mathfrak{p}_{\frac{1}{2}}$	BL $(0,0,0)$ $\mathfrak{p}_{\frac{5}{2}}$	BL $(0,0,0)$ $\mathfrak{N}_{\frac{3}{2}}$	BL $(\pi,0,0)$ $\mathfrak{p}_{\frac{1}{2}}$	BL $(\pi,0,0)$ $\mathfrak{p}_{\frac{3}{2}}$	BL $(\pi,\pi,0)$ $\mathfrak{p}_{\frac{1}{2}}$	BL $(\pi,\pi,0)$ $\mathfrak{p}_{\frac{5}{2}}$	BL $(\pi,\pi,0)$ $\mathfrak{N}_{\frac{3}{2}}$	BL $(0,0,\pi)$ $\mathfrak{p}_{\frac{1}{2}}$	BL $(0,0,\pi)$ $\mathfrak{p}_{\frac{5}{2}}$	BL $(0,0,\pi)$ $\mathfrak{N}_{\frac{3}{2}}$	BL $(\pi,0,\pi)$ $\mathfrak{p}_{\frac{1}{2}}$	BL $(\pi,0,\pi)$ $\mathfrak{p}_{\frac{3}{2}}$	BL (π,π,π) $\mathfrak{p}_{\frac{1}{2}}$	BL (π,π,π) $\mathfrak{p}_{\frac{5}{2}}$	BL (π,π,π) $\mathfrak{N}_{\frac{3}{2}}$	SI $\mathbb{Z}_2^4\times\mathbb{Z}_4$
-	$\mathbf{x}=(0,0),\ j=\frac{1}{2}$	1	0	0	1	0	1	0	0	1	0	0	1	0	1	0	0	0
-	$\mathbf{x}=(0,0),\ j=\frac{5}{2}$	0	1	0	1	0	0	1	0	0	1	0	1	0	0	1	0	0
-	$\mathbf{x}=(0,0),\ j=\frac{3}{2}$	0	0	1	0	1	0	0	1	0	0	1	0	1	0	0	1	0
-	$\mathbf{x}=(\frac{1}{2},\frac{1}{2}),\ j=\frac{1}{2}$	1	0	0	0	1	0	1	0	1	0	0	0	1	0	1	0	0
-	$\mathbf{x}=(\frac{1}{2},\frac{1}{2}),\ j=\frac{5}{2}$	0	1	0	0	1	1	0	0	0	1	0	0	1	1	0	0	0
-	$\mathbf{x}=(\frac{1}{2},\frac{1}{2}),\ j=\frac{3}{2}$	0	0	1	1	0	0	0	-1	0	0	1	1	0	0	0	-1	0
-	$\mathbf{x}=(\frac{1}{2},0),\ j=\frac{1}{2}$	1	1	0	1	1	0	0	0	1	1	0	1	1	0	0	0	0
-	$\mathbf{x}=(\frac{1}{2},0),\ j=\frac{3}{2}$	0	0	0	1	1	1	1	0	0	0	0	1	1	1	1	0	0
$\mathbb{Z}_2$	$(1,\frac{1}{2};x,y)$	1	0	0	1	0	1	0	0	0	0	0	0	0	0	0	0	$\mathrm{e}^{(2)}_{1,\frac{1}{2};x,y}$
$\mathbb{Z}_2$	$(1,\frac{5}{2};x,y)$	0	1	0	1	0	0	1	0	0	0	0	0	0	0	0	0	$\mathrm{e}^{(2)}_{1,\frac{5}{2};x,y}$
$0 \subseteq \mathbb{Z}$	$(2;z)$	0	0	0	1	1	1	0	1	0	0	0	1	1	1	0	1	$\mathrm{e}^{(4)}_{2;z}$
$\mathbb{Z}_2 \subseteq \mathbb{Z}_2$	$(2;x,y)'$	0	0	1	1	0	1	1	1	1	1	1	0	1	1	1	1	$\mathrm{e}^{(2)}_{2;x,y}$

TABLE C.14. Topological band labels of three-dimensional superconductors in tenfold-way class D with point group C_4 and representation $\Theta =^1 E$ or $\Theta =^2 E$.

$\mathcal{K}_i'' \subseteq \mathcal{K}_i' \subseteq \mathcal{K}_i$	Phase	BL $\mathfrak{p}^{(0,0,0)}$	$\mathfrak{p}^{(\pi,0,0)}$	$\mathfrak{p}^{(0,\pi,0)}$	$\mathfrak{p}^{(\pi,\pi,0)}$	$\mathfrak{p}^{(0,0,\pi)}$	$\mathfrak{p}^{(\pi,0,\pi)}$	$\mathfrak{p}^{(0,\pi,\pi)}$	$\mathfrak{p}^{(\pi,\pi,\pi)}$	SI $\mathbb{Z}_2^7$
	$\mathbf{x} = (0,0,0)$	1	1	1	1	1	1	1	1	0
	$\mathbf{x} = (\frac{1}{2},0,0)$	1	1	1	1	1	1	1	1	0
	$\mathbf{x} = (0,\frac{1}{2},0)$	1	1	1	1	1	1	1	1	0
	$\mathbf{x} = (\frac{1}{2},\frac{1}{2},0)$	1	1	1	1	1	1	1	1	0
$\mathbb{Z}_2$	$(1;y,z)$	1	0	1	0	1	0	1	0	$\mathrm{e}^{(2)}_{1;y,z}$
$\mathbb{Z}_2$	$(1;x,z)$	1	1	0	0	1	1	0	0	$\mathrm{e}^{(2)}_{1;x,z}$
$\mathbb{Z}_2$	$(1;x,y)$	1	1	1	1	0	0	0	0	$\mathrm{e}^{(2)}_{1;x,y}$
$\mathbb{Z}_2 \subseteq \mathbb{Z}_2$	$(2,+;z)'$	1	0	0	0	1	0	0	0	$\mathrm{e}^{(2)}_{2;z}$
$\mathbb{Z}_2 \subseteq \mathbb{Z}_2$	$(2,-;z)'$	1	0	0	0	1	0	0	0	$\mathrm{e}^{(2)}_{2;z}$
$0 \subseteq \mathbb{Z}$	$(2;y)$	1	0	1	0	0	0	0	0	$\mathrm{e}^{(2)}_{2;y}$
$0 \subseteq \mathbb{Z}$	$(2;x)$	1	1	0	0	0	0	0	0	$\mathrm{e}^{(2)}_{2;x}$
$0 \subseteq \mathbb{Z} \subseteq \mathbb{Z}$	$(3,+)'$	1	0	0	0	0	0	0	0	$\mathrm{e}^{(2)}_{3}$
$0 \subseteq \mathbb{Z} \subseteq \mathbb{Z}$	$(3,-)'$	1	0	0	0	0	0	0	0	$\mathrm{e}^{(2)}_{3}$

TABLE C.15. Topological band labels and symmetry-based indicators for three-dimensional superconductors in tenfold-way class D with point group C_{2v} and representation $\Theta = A_2$.

$\mathcal{K}_i'' \subseteq \mathcal{K}_i' \subseteq \mathcal{K}_i$	Phase	BL $\mathfrak{p}^{(0,0,0)}$	$\mathfrak{p}^{(\pi,0,0)}$	$\mathfrak{p}^{(0,\pi,0)}$	$\mathfrak{p}^{(\pi,\pi,0)}$	$\mathfrak{p}^{(0,0,\pi)}$	$\mathfrak{p}^{(\pi,0,\pi)}$	$\mathfrak{p}^{(0,\pi,\pi)}$	$\mathfrak{p}^{(\pi,\pi,\pi)}$	SI $\mathbb{Z}_2^3$
	$\mathbf{x} = (0,0,0)$	1	1	1	1	1	1	1	1	0
	$\mathbf{x} = (\frac{1}{2},0,0)$	1	1	1	1	1	1	1	1	0
	$\mathbf{x} = (0,\frac{1}{2},0)$	1	1	1	1	1	1	1	1	0
	$\mathbf{x} = (\frac{1}{2},\frac{1}{2},0)$	1	1	1	1	1	1	1	1	0
$\mathbb{Z}_2$	$(1;x,z)$	1	1	0	0	1	1	0	0	$\mathrm{e}^{(2)}_{1;x,z}$
$\mathbb{Z}_2$	$(1;x,y)$	1	1	1	1	0	0	0	0	$\mathrm{e}^{(2)}_{1;x,y}$
$\mathbb{Z}_2 \subseteq \mathbb{Z}_2$	$(2;y)'$	0	0	0	0	0	0	0	0	0
$0 \subseteq \mathbb{Z}$	$(2;x)$	1	1	0	0	0	0	0	0	$\mathrm{e}^{(2)}_{2;x}$
$0 \subseteq \mathbb{Z} \subseteq \mathbb{Z}$	$(3)'$	0	0	0	0	0	0	0	0	0

TABLE C.16. Topological band labels of three-dimensional superconductors in tenfold-way class D with point group C_{2v} and representation $\Theta = B_2$.

[1] S. Ono, H. C. Po, and H. Watanabe, Science Advances **6** (2020), 10.1126/sciadv.aaz8367.
[2] A. Kitaev, AIP Conference Proceedings **1134**, 22 (2009).
[3] A. P. Schnyder, S. Ryu, A. Furusaki, and A. W. W. Ludwig, AIP Conference Proceedings **1134**, 10 (2009).
[4] K. Shiozaki and M. Sato, Phys. Rev. B **90**, 165114 (2014).
[5] L. Trifunovic and P. W. Brouwer, Phys. Rev. X **9**, 011012 (2019).
[6] C.-K. Chiu, H. Yao, and S. Ryu, Phys. Rev. B **88**, 075142 (2013).
[7] T. Morimoto and A. Furusaki, Phys. Rev. B **88**, 125129 (2013).
[8] L. Trifunovic and P. W. Brouwer, Phys. Rev. B **96**, 195109 (2017).
[9] E. Cornfeld and A. Chapman, Phys. Rev. B **99**, 075105 (2019).
[10] K. Shiozaki, (2019), arXiv:1907.09354.
[11] M. Geier, L. Trifunovic, M. Hoskam, and P. W. Brouwer, Phys. Rev. B **97**, 205135 (2018).
[12] C. W. Groth, M. Wimmer, A. R. Akhmerov, and X. Waintal, New J. Phys. **16**, 063065 (2014).
[13] J. C. Y. Teo and C. L. Kane, Phys. Rev. B **82**, 115120 (2010).

CURRICULUM VITAE

Der Lebenslauf ist in der Online-Version aus Gründen des Datenschutzes nicht enthalten.